frontiers | Research Topics

Toxicity profiling of natural products and druggable compounds: Where are we now?

Edited by
Fareeha Anwar, Sarfraz Ahmad, Muhammad Furqan Akhtar, Tariq Ismail, Fawad Ali Shah and Arshad Mahmood

Published in
Frontiers in Pharmacology

FRONTIERS EBOOK COPYRIGHT STATEMENT

The copyright in the text of individual articles in this ebook is the property of their respective authors or their respective institutions or funders. The copyright in graphics and images within each article may be subject to copyright of other parties. In both cases this is subject to a license granted to Frontiers.

The compilation of articles constituting this ebook is the property of Frontiers.

Each article within this ebook, and the ebook itself, are published under the most recent version of the Creative Commons CC-BY licence. The version current at the date of publication of this ebook is CC-BY 4.0. If the CC-BY licence is updated, the licence granted by Frontiers is automatically updated to the new version.

When exercising any right under the CC-BY licence, Frontiers must be attributed as the original publisher of the article or ebook, as applicable.

Authors have the responsibility of ensuring that any graphics or other materials which are the property of others may be included in the CC-BY licence, but this should be checked before relying on the CC-BY licence to reproduce those materials. Any copyright notices relating to those materials must be complied with.

Copyright and source acknowledgement notices may not be removed and must be displayed in any copy, derivative work or partial copy which includes the elements in question.

All copyright, and all rights therein, are protected by national and international copyright laws. The above represents a summary only. For further information please read Frontiers' Conditions for Website Use and Copyright Statement, and the applicable CC-BY licence.

ISSN 1664-8714
ISBN 978-2-8325-2236-3
DOI 10.3389/978-2-8325-2236-3

About Frontiers

Frontiers is more than just an open access publisher of scholarly articles: it is a pioneering approach to the world of academia, radically improving the way scholarly research is managed. The grand vision of Frontiers is a world where all people have an equal opportunity to seek, share and generate knowledge. Frontiers provides immediate and permanent online open access to all its publications, but this alone is not enough to realize our grand goals.

Frontiers journal series

The Frontiers journal series is a multi-tier and interdisciplinary set of open-access, online journals, promising a paradigm shift from the current review, selection and dissemination processes in academic publishing. All Frontiers journals are driven by researchers for researchers; therefore, they constitute a service to the scholarly community. At the same time, the *Frontiers journal series* operates on a revolutionary invention, the tiered publishing system, initially addressing specific communities of scholars, and gradually climbing up to broader public understanding, thus serving the interests of the lay society, too.

Dedication to quality

Each Frontiers article is a landmark of the highest quality, thanks to genuinely collaborative interactions between authors and review editors, who include some of the world's best academicians. Research must be certified by peers before entering a stream of knowledge that may eventually reach the public - and shape society; therefore, Frontiers only applies the most rigorous and unbiased reviews. Frontiers revolutionizes research publishing by freely delivering the most outstanding research, evaluated with no bias from both the academic and social point of view. By applying the most advanced information technologies, Frontiers is catapulting scholarly publishing into a new generation.

What are Frontiers Research Topics?

Frontiers Research Topics are very popular trademarks of the *Frontiers journals series*: they are collections of at least ten articles, all centered on a particular subject. With their unique mix of varied contributions from Original Research to Review Articles, Frontiers Research Topics unify the most influential researchers, the latest key findings and historical advances in a hot research area.

Find out more on how to host your own Frontiers Research Topic or contribute to one as an author by contacting the Frontiers editorial office: frontiersin.org/about/contact

Toxicity profiling of natural products and druggable compounds: Where are we now?

Topic editors

Fareeha Anwar — Riphah International University (Lahore), Pakistan
Sarfraz Ahmad — University of Malaya, Malaysia
Muhammad Furqan Akhtar — Riphah International University (Lahore), Pakistan
Tariq Ismail — COMSATS University Islamabad, Abbottabad Campus, Pakistan
Fawad Ali Shah — Riphah International University, Pakistan
Arshad Mahmood — Al Ain University, United Arab Emirates

Citation

Anwar, F., Ahmad, S., Akhtar, M. F., Ismail, T., Shah, F. A., Mahmood, A., eds. (2023). *Toxicity profiling of natural products and druggable compounds: Where are we now?* Lausanne: Frontiers Media SA. doi: 10.3389/978-2-8325-2236-3

Table of contents

06 Preclinical safety evaluation of *Macleaya Cordata* extract: A re-assessment of general toxicity and genotoxicity properties in rodents
Zhen Dong, Shu-Sheng Tang, Xiao-Lan Ma, Chang-Hong Li, Zhao-Shan Tang, Zi-Hui Yang and Jian-Guo Zeng

22 Effect of *Rumex dentatus* on Gastrointestinal Protection and Toxicology in Rodents *via* Investigating H^+/K^+-ATPase, Calcium Channels, and PDE Mediated Signaling
Neelam Gul Qazi, Arif-ullah Khan, Sumra Wajid Abbasi, Imran Malik and Komal Naeem

43 *Acacia sieberiana* (Fabaceae) attenuates paracetamol and Bile Duct Ligation-Induced hepatotoxicity *via* modulation of biochemical and oxidative stress biomarkers
Miriam Watafua, Jane I. Ejiofor, Aminu Musa and Mubarak Hussaini Ahmad

57 The molecular pathogenesis of triptolide-induced hepatotoxicity
Yeqing Hu, Qiguo Wu, Yulin Wang, Haibo Zhang, Xueying Liu, Hua Zhou and Tao Yang

70 Toxicological safety evaluation of Qin-Zhi-Zhu-Dan formula in rats during the treatment and recovery periods
Wenxiu Xu, Dan Chen, Zehan Zhang, Shuling Liu, Congai Chen, Chunyan Sun, Wenchao Ni, Xiangdong Kang, Guojiao Shang, Xueqian Wang, Fafeng Cheng and Qingguo Wang

87 Effect of iodoacetic acid on the reproductive system of male mice
Yun Liang, Xinshuang Huang, Li Fang, Mingjie Wang, Chunxiao Yu and Qingbo Guan

98 Cytotoxic effects of extracts and isolated compounds from *Ifloga spicata* (forssk.) sch. bip against HepG-2 cancer cell line: Supported by ADMET analysis and molecular docking
Sajid Hussain, He Liufang, Syed Majid Shah, Fawad Ali, Saeed Ahmad Khan, Fawad Ali Shah, Jing Bo Li and Shupeng Li

110 The microbiome-product colibactin hits unique cellular targets mediating host–microbe interaction
Walaa K. Mousa

124 Elucidation of the binding mechanism of astragaloside IV derivative with human serum albumin and its cardiotoxicity in zebrafish embryos
You-Jiao Wu, Zhan-Hua Li, Jiu-Yan Li, Yan Zhou, Run-Yue Wang, Xiao-Yi Chen, Lin-Sen Qing and Pei Luo

142 Phytochemical and toxicological evaluation of Zephyranthes citrina
Muhammad Haseeb Ur Rehman, Uzma Saleem, Bashir Ahmad and Memoona Rashid

157 Macrophage malfunction in Triptolide-induced indirect hepatotoxicity
Tingting Qin, Muhammad Hasnat, Yang Zhou, Ziqiao Yuan and Wenzhou Zhang

171 Toxicity evaluation induced by single and 28-days repeated exposure of withametelin and daturaolone in Sprague Dawley rats
Muhammad Waleed Baig, Muhammad Majid, Bakht Nasir, Syed Shams ul Hassan, Simona Bungau and Ihsan-ul Haq

187 Acute, chronic, and genotoxic studies on the protopine total alkaloids of the *Macleaya cordata* (willd.) R. Br. in rodents
Zhen Dong, Shu-sheng Tang, Xiao-lan Ma, Bin Tan, Zhao-shan Tang, Chang-hong Li, Zi-hui Yang and Jian-guo Zeng

202 Anti-arthritic and toxicological evaluation of ethanolic extract of *Alternanthera bettzickiana* in rats
Maria Manan, Uzma Saleem, Bashir Ahmad, Nosheen Aslam, Asifa Anwar and Aimen Zafar

215 Pharmacological basis of bergapten in gastrointestinal diseases focusing on H^+/K^+ ATPase and voltage-gated calcium channel inhibition: A toxicological evaluation on vital organs
Huma Aslam, Arif-ullah Khan, Neelum Gul Qazi, Fawad Ali, Syed Shams ul Hassan and Simona Bungau

236 Metals-triggered compound CDPDP exhibits anti-arthritic behavior by downregulating the inflammatory cytokines, and modulating the oxidative storm in mice models with extensive ADMET, docking and simulation studies
Syed Shams ul Hassan, Syed Qamar Abbas, Ishaq Muhammad, Jia-Jia Wu, Shi-Kai Yan, Fawad Ali, Muhammad Majid, Hui-Zi Jin and Simona Bungau

262 Hypertension related toxicity of chloroquine explains its failure against COVID-19: Based on rat model
Junqi Wang, Xian Jing, Lizhong Hua, Yuling Zheng, Shiheng Hu, Jing Xiao, Dawei Guo, Wenda Wu, Hui Ji, Lin Peng, Shanxiang Jiang and Xiuge Gao

280 Nephroprotective potential of *Polyalthia longifolia* roots against vancomycin-induced renal toxicity in experimental animals
Kuntal Das, A. Muthukumar, Mansour Almuqbil, Mohd. Imran, Ali A. Rabaan, Muhammad A. Halwani, Mohammed Garout, Abdulmonem A. Alsaleh, Mohammed Alissa, Ameen S. S. Alwashmi, Ahmad A. Alshehri, Ahmed Alsayyah, Keserla Bhavani, Swati Mittal, R. Gayathri, Nasser Fawzan Alomar, Syed Imam Rabbani and Syed Mohammed Basheeruddin Asdaq

288 Fenchone, a monoterpene: Toxicity and diuretic profiling in rats
Asifa Bashir, Muhammad Naveed Mushtaq, Waqas Younis and Irfan Anjum

298 Pharmacological screening of silibinin for antischizophrenic activity along with its acute toxicity evaluation in experimental animals
Qurat Ul Ain, Uzma Saleem, Bashir Ahmad and Iqra Khalid

frontiers | Frontiers in Pharmacology

TYPE Original Research
PUBLISHED 12 August 2022
DOI 10.3389/fphar.2022.980918

Check for updates

OPEN ACCESS

EDITED BY
Fareeha Anwar,
Riphah International University (Lahore), Pakistan

REVIEWED BY
Muhamamd Haseeb,
Akhtar Saeed Medical and Dental College, Pakistan
Ayesha Shafi,
Riphah International University (Lahore), Pakistan

*CORRESPONDENCE
Zi-Hui Yang,
yangzihui_2006@163.com
Jian-Guo Zeng,
zengjianguo@hunau.edu.cn

SPECIALTY SECTION
This article was submitted to Predictive Toxicology, a section of the journal Frontiers in Pharmacology

RECEIVED 29 June 2022
ACCEPTED 20 July 2022
PUBLISHED 12 August 2022

CITATION
Dong Z, Tang S-S, Ma X-L, Li C-H, Tang Z-S, Yang Z-H and Zeng J-G (2022), Preclinical safety evaluation of Macleaya Cordata extract: A re-assessment of general toxicity and genotoxicity properties in rodents. *Front. Pharmacol.* 13:980918. doi: 10.3389/fphar.2022.980918

COPYRIGHT
© 2022 Dong, Tang, Ma, Li, Tang, Yang and Zeng. This is an open-access article distributed under the terms of the Creative Commons Attribution License (CC BY). The use, distribution or reproduction in other forums is permitted, provided the original author(s) and the copyright owner(s) are credited and that the original publication in this journal is cited, in accordance with accepted academic practice. No use, distribution or reproduction is permitted which does not comply with these terms.

Preclinical safety evaluation of *Macleaya Cordata* extract: A re-assessment of general toxicity and genotoxicity properties in rodents

Zhen Dong[1,2], Shu-Sheng Tang[3], Xiao-Lan Ma[4], Chang-Hong Li[5], Zhao-Shan Tang[5], Zi-Hui Yang[1,2]* and Jian-Guo Zeng[1,2]*

[1]College of Veterinary Medicine, Hunan Agricultural University, Changsha, China, [2]Key Laboratory of Chinese Veterinary Medicine in Hunan Province, Hunan Agricultural University, Changsha, China, [3]College of Veterinary Medicine, China Agricultural University, Beijing, China, [4]College of Veterinary Medicine, Shanxi Agricultural University, Jinzhong, China, [5]Hunan MICOLTA Biological Resources Co., Ltd., Changsha, China

Macleaya cordata extract (MCE) is widely used for its diverse pharmacological actions and beneficial effects on farm animals. Modern pharmacological studies have shown that it has anti-inflammatory, anti-cancer, and anti-bacterial activities, and is gradually becoming a long-term additive veterinary drug used to improve animal intestinal health and growth performance. Although some evidence points to the DNA mutagenic potential of sanguinarine (SAN), a major component of MCE, there is a lack of sufficient basic toxicological information on the oral route, posing a potential safety risk for human consumption of food of animal origin. In this study, we assessed the acute oral toxicity, repeated 90-day oral toxicity and 180-day chronic toxicity of MCE in rats and mice and re-evaluated the genotoxicity of MCE using a standard combined *in vivo* and *ex vivo* assay. In the oral acute toxicity test, the LD_{50} for MCE in rats and mice was 1,564.55 mg/kg (95% confidence interval 1,386.97–1,764.95 mg/kg) and 1,024.33 mg/kg (95% confidence interval 964.27–1,087.30 mg/kg), respectively. The dose range tested had no significant effect on hematology, clinical chemistry, and histopathological findings in rodents in the long-term toxicity assessment. The results of the bacterial reverse mutation, sperm abnormality and micronucleus test showed negative results and lack of mutagenicity and teratogenicity; the results of the rat teratogenicity test showed no significant reproductive or embryotoxicity. The results indicate that MCE was safe in the dose range tested in this preclinical safety assessment. This study provides data to support the further development of maximum residue limits (MRLs) for MCE.

KEYWORDS

***Macleaya cordata*, extract, rodent, acute toxicity, long-term toxicity, genotoxicity, teratogenicity**

Introduction

The *Papaveraceae* Juss. has about 38 genera and 700 species worldwide, mainly in the north temperate zone, especially in the Mediterranean region, West Asia, Central Asia to East Asia and southwestern North America (Zhang et al., 2020). Some of these species are used as medicines, especially *Corydalis yanhusuo* W. T. Wang in the genus *Corydalis* (Liu et al., 2021; Wu et al., 2021). However, a variety of plants in this family have obvious toxicity, such as *Papaver somniferum* L., *Macleaya cordata* (Willd.) R. Br., and *Chelidonium majus* L. Symptoms of poisoning manifest as depression of the central nervous system, liver damage, circulatory disorders, and gastrointestinal irritation (Moro et al., 2009; Günaydın et al., 2015; Lin et al., 2018). Because of its severe toxicity for human when taken orally, as documented in Tang Dynasty medical texts, *M. cordata* (Willd.) R. Br. (*M. cordata*) has been restricted to external use in China (Chen and Shang, 2002).

A variety of isoquinoline alkaloids have been identified in *M. cordata* (e.g., sanguinarine, dihydrosanguinarine, chelerythrine, dihydrochelerythrine, 6-cyano-dihydrochelerythrine, protopine, allocryptopine, berberine, etc.) (Ye et al., 2009; Qing et al., 2014, Qing et al., 2016a, Qing et al., 2016b; Lin et al., 2020), phenolic acids (ferulic acid, eugenol, p-hydroxybenzoic acid, and p-coumaric acid) and sterols (stigmasterol), etc. (Zou et al., 2016). Among them, alkaloids have the greatest advantage in terms of biological activity (Cai et al., 2020; Liu et al., 2022b).

Sanguinarine (SAN) and chelerythrine (CHE) are the most abundant alkaloids in *M. cordata*, which are also distributed in other plants of the poppy family, such as *Chelidonium majus* L., *Eomecon chionantha* Hance, etc. (Warowicka et al., 2019; Lu et al., 2020). They have a wide range of pharmacological activities, such as anti-inflammatory (Danielewski et al., 2022), anti-cancer (Zhu et al., 2020; Prabhu et al., 2021), antibacterial (Falchi et al., 2021; Lu et al., 2022), antifungal (Anjago et al., 2021), anthelmintic (Li et al., 2022), and immune enhancing (Liu et al., 2022a), etc. The biggest application of *M. cordata* is in livestock production, where studies have shown that MCE can provide a slight bitter taste in feed to increase animal intake (Chin, 2008; Wang et al., 2018). The main active ingredient of *M. cordata*, SAN, was included in the Chinese feed additive species list in 1999 (Ministry of Agriculture Announcement No. 105) and classified as a flavoring agent and spice management; SAN was approved as a flavoring agent by the European Union in 2004 and is on the feed additive list (Council of the European Union and European Parliament, 2008). Meanwhile, the standardized MCE product Sangrovit® is approved for use in animal feeds as a plant-derived feed additive as an alternative to feeding growth-promoting antibiotics (AGPs) to promote animal growth and improve feed conversion (Juskiewicz et al., 2011). MCE is well tolerated in animals such as pigs, chickens, sheep and reindeer, and has been shown to significantly improve animal intestinal health, reduce oxidative stress damage, enhance innate immunity and disease resistance, and thus improve growth performance (Juskiewicz et al., 2011; Aguilar-Hernández et al., 2016; Chen et al., 2018; Chen et al., 2020; Bussabong et al., 2021). MCE does not induce the spread of antibiotic resistance genes and has a lower ecological risk (Zhang et al., 2021). In view of the obvious "antibiotic" nature of SAN, the 2008 edition of the "Feed Additive Species List" (Ministry of Agriculture Announcement No. 1126) issued by the Chinese Ministry of Agriculture and Rural Development removed SAN and transferred it to the veterinary medicine department for management. A growing body of research evidence demonstrating the benefits of MCE as a farm input for animal health and antibiotic resistance control has raised public and governmental concerns about the safety of MCE. Although some reports point out the risks associated with SAN, such as intraperitoneal injection of SAN can induce hepatotoxicity through oxidation of the protein thiol (Choy et al., 2008); In a zebrafish model, SAN can trigger cardiotoxicity by inducing extracellular Ca^{2+} influx and MAPK pathway (Hu et al., 2005; Wang et al., 2022); In addition, studies have shown the damaging effects of SAN on oocytes of mice fertilized *in vitro* and the increased embryonic resorption and reduced fetal weight after embryo transfer into the body (Chan, 2011, 2015). However, the concerns about toxicity of SAN were mainly attributed to the 1998 outbreak in New Delhi, India, of a disease known collectively as "epidemic dropsy" caused by contamination or adulteration of *Argemone mexicana* seed oil (AO) (Vaidya et al., 2001; Sharma et al., 2002). Numerous studies have shown evidence of a correlation between AO and genotoxicity (Ansari et al., 2006; Ghosh and Mukherjee, 2016). SAN is considered to be a major contributor to AO toxicity, and *in vitro* tests have shown that SAN can be embedded in DNA, and *in vivo* tests have shown the potential of SAN to damage DNA in blood and bone marrow cells in mice (Ansari et al., 2005). Zdarilova et al. (2008) evaluated the use of MCE as a feed additive in rats fed 600 mg per kg of feed for 90 days without any significant risk of organismal damage or genotoxicity (Stiborova et al., 2008). In addition, MCE was declared a veterinary drug for long-term use in China and its safety needs to be re-evaluated due to a change in use, with the EU removing MCE from the list of feed additives in May 2021 (Directorate-General for Health and Food Safety, 2021). Since the predominant route of exposure to exogenous compounds is oral, however, oral safety data for MCE are still vacant. In this study, we systematically evaluated the acute, long-term toxicity (repeated oral toxicity and chronic toxicity) of MCE in rodents. Given the risk of genotoxicity of SAN, we also conducted a series of standardized genetic toxicology tests, including the murine *Salmonella* revertant mutation (Ames) test, the mouse sperm aberration test, and the mouse bone marrow micronucleus test, to reassess the genotoxicity of MCE. In addition to this, a rat teratogenicity test was carried out to assess the embryotoxicity of MCE. Our

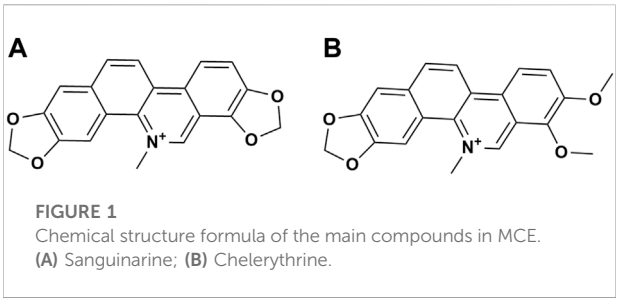

FIGURE 1
Chemical structure formula of the main compounds in MCE.
(A) Sanguinarine; **(B)** Chelerythrine.

findings provide data to support a comprehensive understanding of the potential risks of oral exposure to MCE.

Materials and methods

Test drugs and reagents

MCE, was provided by Hunan MICOLTA Biological Resources Co., Ltd. (Changsha, China). MCE is a standardized extract prepared by a series of processes, including heated sulfuric acid percolation, sodium hydroxide precipitation, filtration, drying, alcohol extraction, salt formation, and crushing. The total content of SAN (Figure 1A) and CHE (Figure 1B) in MCE is greater than 60%, with SAN ≥ 40% and CHE ≥ 20%, and the remaining trace components have been qualitatively characterized (Dong et al., 2021). The samples were kept at the Veterinary Drug Safety Supervision, Inspection and Testing Center of the Ministry of Agriculture and Rural Affairs, China Agricultural University (Beijing, China). Reagents for hematological and serum biochemical assays were purchased from Mindray Biomedical Electronics Co., Ltd. (Shenzhen, China). Other reagents were purchased from Sinopharm Chemical Reagent Co., Ltd. (Shanghai, China).

Animals

SPF-grade SD rats and ICR mice were purchased from Beijing Vital River Laboratory Animal Technology Co., Ltd. (Beijing, China) and housed in a China Ministry of Agriculture and Rural Affairs certified GLP animal rearing room at the Veterinary Drug Safety Supervision, Inspection and Testing Center, Ministry of Agriculture and Rural Affairs, China Agricultural University, with controlled environmental parameters Conditions were as follows: temperature 25 ± 2°C, relative humidity 50% ± 20%, 12-h light/dark cycle, and ventilation 8–15 times/hour. All animals had free access to maintenance diets (crude protein ≥18%, crude fat ≥4%, crude fiber ≤5%, Beijing Keao Xieli Feed Co., Ltd.) and reverse osmosis water. All animal experiments were approved by the Animal Ethics Committee of China Agricultural University (Experiment approval number: WTPJ20090001-1~7) and strictly followed the Chinese Guide for Ethical Review of Laboratory Animal Welfare (GB/T 35892, 2018).

TABLE 1 Oral acute toxicity dosing regimens in rats and mice.

Animals	Dose (mg/kg)	Animals	Dose (mg/kg)
Rats	2,500.00	Mice	1,750.00
Rats	2,000.00	Mice	1,400.00
Rats	1,600.00	Mice	1,120.00
Rats	1,280.00	Mice	896.00
Rats	1,024.00	Mice	716.80
Rats	819.20	Mice	573.44

Oral acute toxicity in rats and mice

Sixty healthy SD rats (weighing 180–200 g) and ICR mice (18–22 g) were housed adaptively for 5 days. The oral acute toxicity test of MCE was carried out on rats and mice with reference to the half lethal dose method in the Compendium of Technical Guidelines for Veterinary Drug Research and the Guidelines for the acute toxicity (LD_{50} determination) of veterinary drugs (Ministry of Agriculture and Rural Affairs of PRC, 2009f; Veterinary Drug Assessment Centre of the Ministry of Agriculture of the and People's Republic of China, 2012). The dose ranges were obtained from 2,500.00 to 879.20 mg/kg (rats) and 1750 to 573.44 mg/kg (mice) by pretesting, and the rats and mice were grouped separately (n = 10, half were males and the other half were females) using the complete randomization method, and the MCE was mixed in 1% CMCC-Na solution and transfused into rodents by oral gavage. The volume of the oral solution was 2 ml/100 g (rats) and 0.2 ml/100 g (mice) according to the protocol in Table 1. The rodents were observed for general behavior, signs of poisoning and mortality after poisoning.

Repeated dose 90-day oral toxicity test in rats

Repeated Dose 90-Day Oral Toxicity test was conducted with reference to the Guidelines for 30-Day and 90-Day Feeding Tests for Veterinary Drugs (Ministry of Agriculture and Rural Affairs of PRC, 2009a). SD rats of 80–100 g (n = 20/group, half males, and the other half females) were divided into four groups and pellets were

TABLE 2 Oral acute toxicity mortality in rats and mice at different doses of MCE.

Dosage (mg/kg)	Numbers	Number of deaths	Mortality rate (%)	Survival rate (%)
Rats				
2,500.00	10	10	100	0
2,000.00	10	7	70	30
1,600.00	10	5	50	50
1,280.00	10	3	30	70
1,024.00	10	1	10	90
819.20	10	0	0	100
1,750.00	10	10	100	0
Mice				
1,400.00	10	8	80	20
1,120.00	10	6	60	40
896.00	10	4	40	60
716.80	10	1	10	90
573.44	10	0	0	100

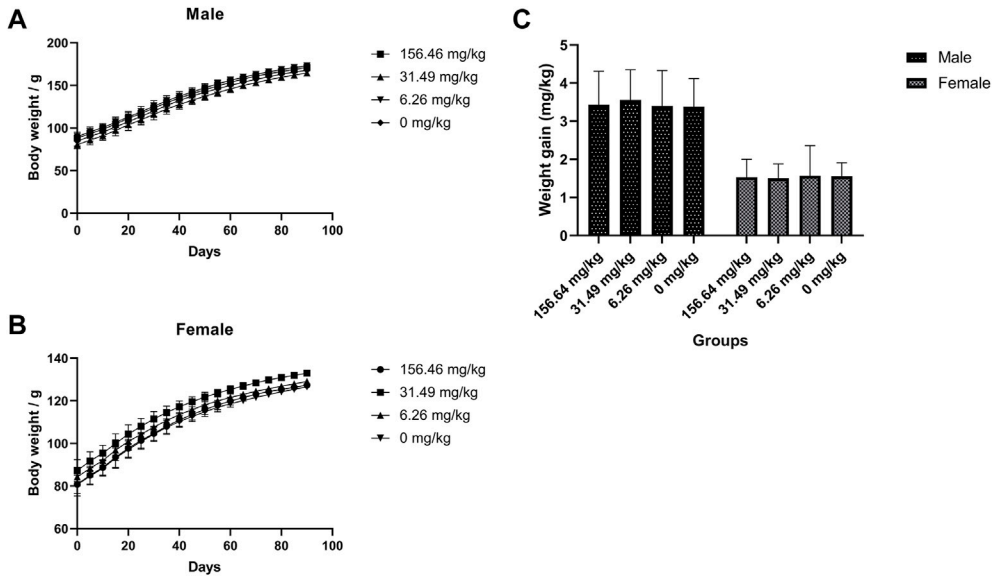

FIGURE 2
No effect of MCE on body weight gain in SD rats during 90 days of feeding. Male and female rats were orally administered 156.46, 31.49, 6.26, and 0 mg/kg (n = 10 rats/gender). **(A)** Body weight of male rats at 90 days; **(B)** Body weight of female rats at 90 days; **(C)** Body weight gain of male and female rats for 90 days.

made at 156.46 (1/10 LD_{50}), 31.49 (1/50 LD_{50}), 6.26 (1/250 LD_{50}) and 0 mg/kg of MCE added to the feed and given by *ad libitum* feeding for 90 days. At the end of 90 days, all surviving rats were anesthetized, heart blood was collected and executed.

Chronic toxicity test in rats

The 180-day chronic toxicity test was conducted with reference to the Guidelines for Chronic Toxicity and Carcinogenicity Testing of Veterinary Drugs (Ministry of

TABLE 3 Effect of feeding MCE for 90 and 180 days on hematological parameters in rats.

Groups	Hematological parameters (Mean ± SD)							
	Hg (g/L)		RBC (M/mm^3)		WBC (th/mm^3)		PLT (th/mm^3)	
	M	F	M	F	M	F	M	F
90 days								
156.46 mg/kg	140.00 ± 4.34	140.40 ± 3.88	7.74 ± 0.15	7.26 ± 0.15	9.18 ± 0.71	7.64 ± 0.30	360.20 ± 29.05	351.00 ± 15.59
31.29 mg/kg	142.00 ± 2.83	145.20 ± 3.01	7.69 ± 0.20	7.14 ± 0.08	9.06 ± 0.48	7.36 ± 0.44	352.40 ± 40.29	344.60 ± 15.17
6.26 mg/kg	140.80 ± 3.43	145.40 ± 5.75	7.81 ± 0.38	7.31 ± 0.09	8.93 ± 1.18	7.58 ± 0.26	367.00 ± 29.46	360.00 ± 28.16
0.00 mg/kg	139.60 ± 2.73	139.40 ± 4.22	7.52 ± 0.21	6.99 ± 0.33	10.22 ± 1.23	7.86 ± 0.30	353.40 ± 16.27	350.20 ± 17.23
180 days								
78.23 mg/kg	140.40 ± 6.80	140.40 ± 6.80	6.44 ± 0.29	7.04 ± 1.49	10.85 ± 0.60	8.58 ± 0.33	245.60 ± 15.52	247.60 ± 12.62
15.65 mg/kg	140.40 ± 5.13	139.40 ± 3.36	6.66 ± 0.93	6.95 ± 0.22	10.01 ± 0.66	8.69 ± 0.42	244.80 ± 23.89	244.20 ± 8.70
3.13 mg/kg	141.60 ± 3.58	139.20 ± 4.49	6.61 ± 0.29	7.13 ± 0.17	10.02 ± 0.89	8.60 ± 0.74	245.40 ± 15.84	246.20 ± 12.19
0.00 mg/kg	141.00 ± 6.20	140.60 ± 4.83	6.63 ± 0.13	6.91 ± 0.48	10.52 ± 0.73	8.62 ± 0.89	248.00 ± 22.26	246.40 ± 17.33

Note: Hg, Hemoglobin; RBC, Red Blood Count; WBC, White Blood Count; PLT, Platelet Count.

Agriculture and Rural Affairs of PRC, 2009c). Based on the results of 90-day subchronic toxicity, SD rats of 60–80 g (n = 50/group, half males, and the other half females) were divided into four groups and pellets were made at 78.23 (1/20 LD_{50}), 15.65 (1/100 LD_{50}), 3.13 (1/500 LD_{50}) and 0 mg/kg of MCE added to the feed and given by *ad libitum* feeding for 180 days. At the end of 180 days, all surviving rats were anesthetized, heart blood was collected and executed.

Hematology and serum biochemical tests

Blood from rats taken via the heart was tested separately in 90-day and 180-day long-term toxicity tests. Whole blood stored in vacuum EDTA-K2 anticoagulation tubes was examined on a BC-2800 Vet Animal Blood Cell Analyzer (Mindray Biomedical Electronics Co., Ltd., Shenzhen, China) for hemoglobin (Hg), red blood cell count (RBC), white blood cell count (WBC), and platelet count (PLT). Blood preserved in ordinary vacuum blood collection tubes without additives is separated by centrifugation to obtain serum. The serum alanine aminotransferase (ALT), aspartate aminotransferase (AST), urea nitrogen (BUN), creatinine (CR), glucose (GLU), albumin (ALB), total protein (TP), and total cholesterol (TCH) were measured using a BS-180 automated biochemical analyzer (Mindray Biomedical Electronics Co., Ltd., Shenzhen, China).

Gross autopsy and histopathological examination

The major organs of rats anesthetized and executed in 90-day and 180-day long-term toxicity tests were removed from the surface blood and weighed after visual detection of tissue damage. All organs were preserved in 10% neutral buffered formalin solution for more than 3 days. The fixed tissues were washed with water, dehydrated in gradient ethanol, and treated with xylene before paraffin embedding. The prepared paraffin tissue block was sectioned and stained with hematoxylin & eosin (H&E) and then glued and stored. According to the requirements of veterinary drug declaration, if no toxicity-related histopathological changes are found, the relevant results are not required, so the histopathological picture results are not reflected in this report.

Salmonella typhimurium revert mutation (Ames) test

Ames tests are conducted in accordance with the Guidelines for Ames Tests of Veterinary Drugs (Ministry of Agriculture and Rural Affairs of PRC, 2009b). Four test strains, TA97, TA98, TA100, and TA102, were tested by spot test and plate incorporation method using 100, 20, 4, 0.8, and 0.16 μg/ml of MCE, respectively. Additional solvent control, DMSO and

TABLE 4 Effect of feeding MCE for 90 and 180 days on serum biochemical parameters in rats.

Serum biochemical parameters (Mean ± SD)

Groups	ALT (U/L)		AST (U/L)		BUN (μmoL/L)		CR (μmoL/L)		GLU (mmoL/L)		ALB (mmoL/L)		TP (G/L)		TCH (mmoL/L)	
	M	F	M	F	M	F	M	F	M	F	M	F	M	F	M	F
90 days																
156.46 mg/kg	59.20 ± 3.71	59.20 ± 3.92	159.80 ± 3.71	157.40 ± 2.58	6.78 ± 0.17	7.68 ± 0.25	80.82 ± 4.04	89.12 ± 3.96	6.70 ± 0.55	6.22 ± 0.17	32.98 ± 1.35	39.40 ± 1.01	69.88 ± 3.84	78.74 ± 3.28	1.88 ± 0.16	1.94 ± 0.08
31.29 mg/kg	59.80 ± 3.54	60.80 ± 2.86	163.40 ± 6.72	158.40 ± 1.62	6.84 ± 0.65	7.56 ± 0.22	79.48 ± 2.72	90.32 ± 2.18	6.64 ± 0.41	6.24 ± 0.19	32.70 ± 1.30	38.30 ± 0.63	72.04 ± 4.06	78.81 ± 2.61	1.86 ± 0.10	1.82 ± 0.07
6.26 mg/kg	58.20 ± 2.32	59.00 ± 1.41	159.80 ± 5.64	158.60 ± 4.76	6.76 ± 0.60	7.58 ± 0.31	78.90 ± 3.25	90.44 ± 2.18	6.70 ± 0.32	6.32 ± 0.23	33.32 ± 1.14	38.22 ± 3.62	70.22 ± 2.31	78.20 ± 2.30	1.84 ± 0.10	1.86 ± 0.10
0.00 mg/kg	55.80 ± 5.91	60.00 ± 4.15	159.00 ± 5.73	158.40 ± 3.64	6.58 ± 0.40	7.62 ± 0.33	79.56 ± 4.16	91.58 ± 2.24	6.50 ± 0.58	6.34 ± 0.22	32.60 ± 1.31	39.50 ± 1.09	64.44 ± 14.19	79.50 ± 2.77	1.86 ± 0.30	2.04 ± 0.12
180 days																
78.23 mg/kg	58.20 ± 4.21	73.40 ± 3.21	173.20 ± 3.42	188.60 ± 1.14	8.86 ± 0.37	9.72 ± 0.45	76.70 ± 4.43	74.80 ± 2.16	7.52 ± 0.59	8.04 ± 0.18	32.88 ± 1.14	27.72 ± 1.13	72.28 ± 0.64	68.30 ± 0.71	1.52 ± 0.08	1.44 ± 0.15
15.65 mg/kg	58.40 ± 4.72	72.60 ± 4.51	173.40 ± 3.58	189.20 ± 5.07	8.94 ± 0.59	9.71 ± 0.14	77.82 ± 2.34	75.00 ± 0.71	7.56 ± 0.42	7.94 ± 0.52	32.42 ± 2.49	27.38 ± 0.92	73.06 ± 1.80	68.84 ± 2.04	1.60 ± 0.07	1.42 ± 0.11
3.13 mg/kg	58.00 ± 1.87	73.20 ± 3.11	173.00 ± 3.39	188.20 ± 5.07	8.92 ± 0.37	9.78 ± 0.25	77.06 ± 2.00	74.66 ± 1.67	7.50 ± 0.12	8.20 ± 0.59	32.60 ± 1.15	27.94 ± 0.34	72.96 ± 0.79	68.92 ± 1.64	1.58 ± 0.08	1.42 ± 0.08
0.00 mg/kg	58.20 ± 2.28	72.40 ± 8.91	173.20 ± 2.41	185.00 ± 6.11	8.82 ± 0.59	9.76 ± 0.27	77.30 ± 3.14	74.46 ± 1.56	7.54 ± 0.43	7.98 ± 0.45	32.74 ± 0.42	27.44 ± 1.13	77.92 ± 4.02	68.80 ± 1.30	1.58 ± 0.08	1.46 ± 0.11

Note: ALT, Alanine aminotransferase; AST, Aspartate aminotransferase; BUN, Blood urea nitrogen; CR, Creatinine; GLU, Glucose; ALB, Albumin; TP, Total protein; TCH, Total cholesterol.

10.3389/fphar.2022.980918

10.3389/fphar.2022.980918

TABLE 5 Effect of feeding MCE for 90 and 180 days on organ coefficients in rats.

Groups	Liver		Kidney		Spleen		Stomach and intestines		Lung		Heart		Testicles	Ovaries
	M	F	M	F	M	F	M	F	M	F	M	F		
156.46 mg/kg	3.22 ± 0.10	3.80 ± 0.12	0.64 ± 0.04	0.69 ± 0.06	0.14 ± 0.01	0.21 ± 0.02	6.74 ± 0.41	8.89 ± 0.57	0.46 ± 0.03	0.72 ± 0.06	0.31 ± 0.01	0.34 ± 0.04	0.64 ± 0.02	0.04 ± 0.01
31.29 mg/kg	2.98 ± 0.28	3.83 ± 0.13	0.65 ± 0.03	0.73 ± 0.04	0.13 ± 0.01	0.21 ± 0.01	6.21 ± 0.63	9.00 ± 0.35	0.46 ± 0.03	0.72 ± 0.03	0.30 ± 0.02	0.35 ± 0.02	0.64 ± 0.02	0.04 ± 0.00
6.26 mg/kg	3.19 ± 0.06	3.86 ± 0.08	0.66 ± 0.02	0.71 ± 0.01	0.13 ± 0.01	0.21 ± 0.01	6.35 ± 0.91	8.69 ± 0.33	0.46 ± 0.01	0.65 ± 0.16	0.30 ± 0.01	0.35 ± 0.02	0.63 ± 0.01	0.04 ± 0.00
0.00 mg/kg	3.21 ± 0.08	3.76 ± 0.12	0.64 ± 0.04	0.69 ± 0.07	0.14 ± 0.01	0.21 ± 0.02	6.73 ± 0.37	8.81 ± 0.60	0.46 ± 0.03	0.69 ± 0.05	0.31 ± 0.01	0.34 ± 0.01	0.64 ± 0.02	0.04 ± 0.00
78.23 mg/kg	3.05 ± 0.19	3.02 ± 0.19	0.56 ± 0.02	0.56 ± 0.05	0.15 ± 0.01	0.17 ± 0.01	6.34 ± 0.31	7.02 ± 1.40	0.45 ± 0.03	0.62 ± 0.01	0.26 ± 0.03	0.24 ± 0.01	0.61 ± 0.01	0.03 ± 0.01
15.65 mg/kg	2.92 ± 0.11	2.99 ± 0.08	0.59 ± 0.04	0.59 ± 0.04	0.15 ± 0.02	0.17 ± 0.01	6.20 ± 0.30	6.94 ± 0.34	0.44 ± 0.02	0.62 ± 0.02	0.28 ± 0.02	0.25 ± 0.01	0.59 ± 0.04	0.03 ± 0.00
3.13 mg/kg	3.06 ± 0.09	2.85 ± 0.10	0.62 ± 0.07	0.68 ± 0.01	0.14 ± 0.02	0.15 ± 0.01	6.40 ± 0.39	7.61 ± 0.74	0.59 ± 0.05	0.60 ± 0.11	0.26 ± 0.03	0.29 ± 0.03	0.59 ± 0.05	0.03 ± 0.00
0.00 mg/kg	3.00 ± 0.05	2.91 ± 0.07	0.57 ± 0.01	0.59 ± 001	0.15 ± 0.01	0.16 ± 0.01	6.12 ± 0.25	7.14 ± 0.38	0.44 ± 0.02	0.61 ± 0.01	0.26 ± 0.00	0.24 ± 0.02	0.61 ± 0.02	0.02 ± 0.00

Note: Organ coefficient = (organ weight/body weight) x 100%.

positive control groups were set up. Positive drugs were selected as follows: 2 mg/ml of 2-aminofluorene (2-AF) was used for TA97, TA98, TA100, and TA102 for the point test plus S9. Without S9, TA97, TA98, TA100, and TA102 were all treated with 1 mg/ml of diquat. In the plate incorporation test, TA97, TA98, TA100, and TA102 used 100 μg/ml of 2-AF when S9 was added; TA97 used 50 μg/ml of acriflavine; TA98 used 200 μg/ml of 2,7-diaminofluorene (2,7-AF); TA100 used 15 μg/ml of sodium azide (NaN_3) when S9 was not added; TA102 used 5 μg/ml of mitomycin; and TA97, TA98, TA100, and TA102 used 5 μg/ml of NaN_3. TA100 used 15 μg/ml of NaN_3; TA102 used 5 μg/ml of mitomycin C. The test was repeated twice and the number of revertant colonies formed in each test strain plate was counted after 48 h of incubation at 37°C. The test strains were purchased from China Veterinary Culture Collection Centre and approved for use by the Biosafety Committee of China Agricultural University.

Mice bone marrow cell micronucleus test

Bone marrow cell micronucleus testing in mice according to the Guidelines for Bone Marrow Cell Micronucleus Testing in Veterinary Mice (Ministry of Agriculture and Rural Affairs of PRC, 2009g). ICR mice from 25 to 30 g were housed for 1 week for environmental adaptation. With reference to the results obtained for oral acute toxicity in mice, three MCE groups were set up in the test at concentrations of 512.17, 256.08, and 128.04 mg/kg, a positive control group (40 mg/kg, cyclophosphamide monohydrate, Reagent grade, 97.0%–103.0%, Beyotime Biotechnology Shanghai, China) and negative control group (distilled water, homemade) (n = 20, male and female). The drug was administered by gavage at 0.2 ml/10 g. The drug was administered twice with an interval of 24 h between doses. Mice were euthanized by cervical dislocation 6 h after the second administration, and bone marrow cells were harvested from mouse femurs using FBS, coated on slides, oven-dried, fixed in methanol, stained with Giemsa working solution (Beyotime Biotechnology, Shanghai, China) for 30 min, rinsed in distilled water, and air-dried for examination. The number of polychromatic erythrocytes (PCE), micronucleated polychromatic erythrocytes and mature erythrocytes (RBC) were counted by double-blind light microscopic examination. PCE micronucleus rate and PCE/RBC values were calculated for female and male mice in each test group, and the respective standard deviations were also calculated. The formula is as follows: PCE micronucleus rate = number of PCE containing micronucleus/number of PCE examinations × 100%; PCE/RBC ratio = number of PCE examinations/number of RBCs.

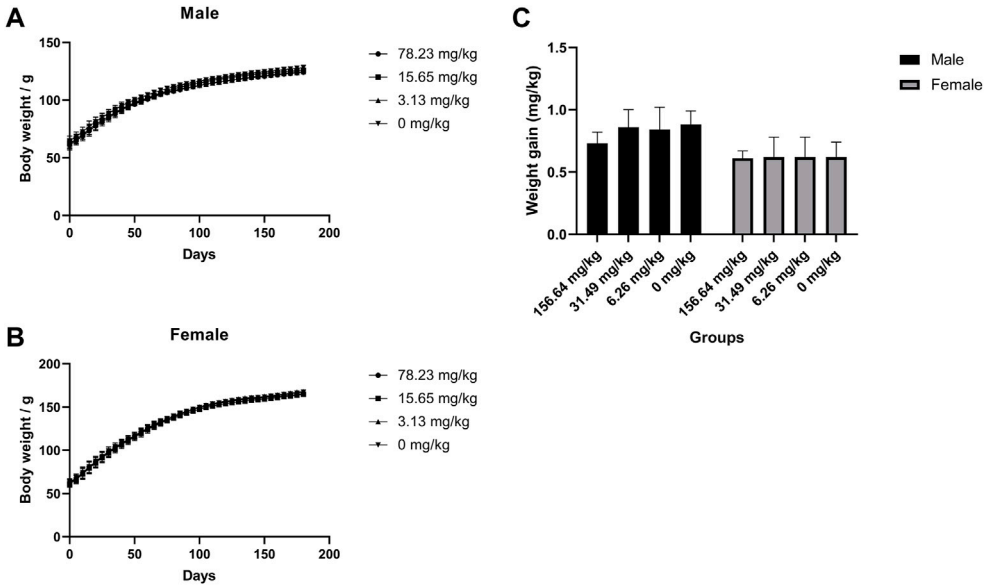

FIGURE 3
No effect of MCE on body weight gain in SD rats during 180 days of feeding. Male and female rats were orally administered 78.23, 15.65, 3.13, and 0 mg/kg (n = 25 rats/gender). **(A)** Body weight of male rats at 180 days; **(B)** Body weight of female rats at 180 days; **(C)** Body weight gain of male and female rats for 180 days.

TABLE 6 Ames test results for MCE (Mean ± SD).

Groups	TA_{97}		TA_{98}		TA_{100}		TA_{102}	
	−S9	+S9	−S9	+S9	−S9	+S9	−S9	+S9
100 μg/ml	123.7 ± 10.7	131.7 ± 3.5	34.3 ± 2.5	32.0 ± 1.0	151.3 ± 1.5	160.0 ± 6.2	269.0 ± 8.5	252.3 ± 8.5
	125.3 ± 5.1	130.0 ± 7.7	40.0 ± 4.6	41.0 ± 2.6	159.7 ± 8.5	171.7 ± 6.1	285.3 ± 9.5	262.7 ± 4.7
20 μg/ml	126.7 ± 5.5	134.3 ± 10.7	36.0 ± 3.6	39.0 ± 2.6	156.7 ± 2.1	157.7 ± 5.5	279.3 ± 7.4	262.0 ± 6.1
	130.7 ± 13.3	129.7 ± 2.3	44.7 ± 5.9	41.0 ± 3.6	167.0 ± 2.6	166.3 ± 10.3	281.7 ± 14.5	274.0 ± 7.9
4 μg/ml	120.3 ± 10.0	127.7 ± 5.5	32.3 ± 2.1	34.7 ± 4.0	154.3 ± 1.5	146.0 ± 2.6	264.3 ± 4.2	250.0 ± 2.6
	131.7 ± 11.6	143.7 ± 10.7	39.7 ± 8.1	41.7 ± 4.6	162.0 ± 8.7	161.7 ± 6.8	283.7 ± 17.4	262.7 ± 17.0
0.8 μg/ml	113.7 ± 9.3	138.3 ± 2.1	36.3 ± 2.3	36.0 ± 3.0	166.3 ± 3.8	147.0 ± 1.7	288.3 ± 6.0	246.3 ± 4.2
	120.3 ± 6.5	122.0 ± 4.4	37.0 ± 6.6	42.0 ± 6.6	170.7 ± 18.1	159.0 ± 7.0	280.7 ± 3.5	271.0 ± 1.0
0.16 μg/ml	137.7 ± 4.5	126.0 ± 11.0	39.0 ± 2.0	40.7 ± 1.2	160.7 ± 4.0	148.7 ± 3.5	272.3 ± 5.0	260.3 ± 5.0
	123.3 ± 6.0	132.3 ± 8.4	38.7 ± 7.1	41.3 ± 6.1	166.0 ± 9.5	159.0 ± 7.0	280.7 ± 3.5	271.0 ± 1.0
Solvent control	129.0 ± 9.6	127.0 ± 7.5	33.3 ± 1.5	33.3 ± 3.1	160.3 ± 6.8	145.3 ± 5.7	275.3 ± 10.5	261.3 ± 6.7
	124.3 ± 5.1	127.0 ± 13.5±	40.3 ± 7.5	40.0 ± 6.2	170.7 ± 8.7	156.0 ± 3.5	272.0 ± 1.0	273.3 ± 7.2
DMSO	132.0 ± 9.6	129.7 ± 4.9	37.0 ± 2.0	33.3 ± 2.1	149.0 ± 3.6	162.7 ± 6.0	279.7 ± 5.1	259.0 ± 8.7
	136.0 ± 9.5	132.3 ± 3.8	42.0 ± 2.6	37.7 ± 5.1	165.0 ± 4.4	172.0 ± 10.4	270.3 ± 10.7	271.3 ± 6.7
Positive control	579.3 ± 14.0	874.7 ± 15.0	283.7 ± 13.2	560.7 ± 10.0	758.0 ± 12.2	779.7 ± 12.2	1,148.0 ± 20.5	932.3 ± 23.2
	564.3 ± 12.3	873.3 ± 13.3	564.3 ± 12.3	569.0 ± 14.5	564.3 ± 12.3	795.7 ± 6.4	1,197.7 ± 49.5	935.7 ± 8.5
	Acriflavine (5 μg)	2-AF (10 μg)	2,7-AF (20 μg)	2-AF (10 μg)	NaN_3 (1.5 μg)	2-AF (10 μg)	MMC (0.5 μg)	2-AF (10 μg)

Note: NaN_3—Sodium azide; 2-AF, 2-Aminofluorene; 2,7-AF, 2,7-Diaminofluorene; MMC, Mitomycin C.

TABLE 7 Results of the micronucleus test in mouse bone marrow cells with MCE.

Groups	PCE/RBC		PCE micronucleus rate (%)	
	F (n = 5)	M (n = 5)	F (n = 5)	M (n = 5)
512.17 mg/kg	1.19 ± 0.21	0.96 ± 0.09	1.40 ± 0.56	1.20 ± 0.24
256.08 mg/kg	1.02 ± 0.43	1.00 ± 0.14	1.00 ± 0.20	1.19 ± 0.08
128.04 mg/kg	1.03 ± 0.32	1.09 ± 0.28	1.40 ± 0.40	1.60 ± 0.42
Negative control	1.10 ± 0.38	1.06 ± 0.14	1.20 ± 0.62	1.19 ± 0.09
CTX	1.30 ± 0.79	1.58 ± 0.49	22.60 ± 1.87*	17.8 ± 2.35*

Note: CTX, Cyclophosphamide; * indicates $p < 0.05$ compared to negative control group.

Mice sperm abnormality test

Sperm deformity test for mice was conducted according to the Guidelines for Sperm Deformity Test for Veterinary Mice (Ministry of Agriculture and Rural Affairs of PRC, 2009e). Three MCE dose groups of 204.87 (1/5 LD_{50}), 102.43 (1/10 LD_{50}), and 51.22 mg/kg (1/20 LD_{50}), a negative control group (distilled water, homemade) and a positive control group (40 mg/kg, cyclophosphamide, Reagent grade, 97.0%–103.0%, Beyotime Biotechnology, Shanghai, China) (n = 10, males). The drug was administered by gavage at 0.2 ml/10 g once a day for 5 days at 24 h intervals. On the 35th day after the first poisoning, the mice were executed by cervical dislocation and the epididymis was removed from both sides. Sperm solution was obtained using saline, and synthetic fiber blood mesh bags were filtered, and the filtrate was aspirated to make sperm smears. After air-drying, the smears were fixed with methanol for 10 min, dried and stained with 2% eosin (Solarbio Science & Technology Co., Ltd., Beijing, China) for 1 h, lightly rinsed with water and dried. Normal and abnormal spermatozoa (hookless, banana-shaped, fat-headed, amorphous, tail-folded, double-headed, double-tailed, etc.) were examined and counted under the microscope in the same field of view.

Traditional teratogenicity test in rats

Referring to the Guidelines for Traditional Teratogenicity Tests on Veterinary Drugs in Rats with some modifications, we conducted a traditional teratogenicity test in rats (Ministry of Agriculture and Rural Affairs of PRC, 2009d) and made some modifications. Based on the results of oral acute toxicity tests in rats, 391.15 (1/4 LD_{50}), 97.79 (1/16 LD_{50}), and 24.45 mg/kg (1/64 LD_{50}) and a negative control group (distilled water, homemade) were selected. Due to the instability of positive drug teratogenicity, a positive control group was not established for this test. The number of unmated young female rats in each group was 20 and the number of male rats was 10. Only female rats were used for gavage administration in the experiment, and males were used only for mating behavior. After the sexually mature male and female rats were caged together at 2:1, the females were checked daily to ensure that they had mated, and the mated females were used as the test rats, and the day of conception was taken as day zero. Repeated mating in the same cage was done until the number of rats detected that met the test conditions was sufficient for the test. The drug was administered from the 7th to the 16th day of conception, once/day for 10 consecutive days. The feeding, drinking and weight gain of pregnant rats were examined and recorded during the test period, and the general behavioral performance, poisoning and death of pregnant rats were observed. The pregnant rats were weighed on the 20th day of gestation, decapitated, and the ovaries and uterus were removed by dissection to check the number of corpus luteum, the number of absorbed fetuses, the number of stillbirths, the number of live fetuses, the male to female ratio of live fetuses, and the weight of ovaries and uterus. The live fetal rats were examined for weight, body length, tail length, and cosmetic abnormalities. Half of the live fetuses from each litter were fixed in 95% ethanol for 3 weeks, and the fixed fetuses were rinsed in water for several minutes and then placed in 2% potassium hydroxide solution for 72 h. The fetuses were then stained in alizarin red (sodium 3,4-dihydroxy anthraqinone-2-sulfonate) application solution (Beyotime Biotechnology, Shanghai, China) for 48 h and gently shaken twice a day until the skulls were stained red. The fetal rats were then removed and placed in transparent solution A (glycerol 20 ml, 2% potassium hydroxide solution 3 ml, add distilled water to 100 ml) for 2 days and in transparent solution B (glycerol 50 ml, 2% potassium hydroxide solution 3 ml, add distilled water to 100 ml) for 3 days, and the bones were left to stain red while the soft tissues were basically discolored. The stained fetal mouse specimens were observed under a stereomicroscope using a transmission light source, and

10.3389/fphar.2022.980918

TABLE 8 Sperm abnormality test for MCE in mice.

Groups	Number of animals	Sperm count	Abnormal sperm count	Sperm abnormality rate (%)	Percentage of deformed sperm species (%)						
					No hook	Banana-shaped	Amorphism	Fat head	Folded tail	Double heads	Double tails	Other
204.87 mg/kg	5	5 × 1,000	130	2.60	35.38	3.08	30.77	16.92	12.31	1.54	0	0
102.43 mg/kg	5	5 × 1,000	132	2.64	31.82	3.79	34.85	13.64	14.39	1.52	0	0
51.22 mg/kg	5	5 × 1,000	126	2.52	30.16	4.76	31.06	14.29	12.07	3.97	1.59	0
Negative control	5	5 × 1,000	138	2.56	20.88	8.09	28.99	13.04	20.29	5.07	2.17	0
Positive control	5	5 × 1,000	495*	9.90*	38.99	3.06	40.81	7.27	1.82	3.84	1.21	0

Note: * indicates $p < 0.05$ compared to negative control group.

then the skeleton was gradually examined for abnormalities. The other half of the fetal rats from each litter were placed in Bouin's fluid (Solarbio Science & Technology Co., Ltd., Beijing, China) and fixed for 2 weeks for visceral examination.

Statistical analysis

Data generated from the experiments were saved and organized by Microsoft Excel (Microsoft, Redmond, United States). Data were processed for appropriate statistical analysis such as *t* Test, One-way ANOVA and Chi-Squared Test using SPSS 19.0 (International Business Machines Corporation, Armonk, United States). Data are expressed as Mean ± SD and percentages. Image production was done by GraphPad prism 7.0 (GraphPad Software, San Diego, United States). *p*-values less than 0.05 and 0.01 were considered statistically significant and highly significant.

Results

Acute toxicity test in rats and mice

Acute oral toxicity tests were performed on SD rats and ICR mice, and the mortality of each dose group is shown in Table 2. The oral LD_{50} of MCE was calculated using Kärber's method (Mantel, 1967) to be 1,564.55 mg/kg (95% confidence interval 1,386.97–1764.95 mg/kg) and 1,024.33 mg/kg (95% confidence interval 964.27–1,087.93) for rats and mice, respectively. mg/kg). Rats and mice showed signs of intoxication with erect back hair, arching of the back, and slow movement, and death occurred about 3 h after administration (Table 2). No obvious pathological organ damage was found at necropsy. Referring to the GHS acute toxicity classification criteria, MCE was found to be grade 4 (United Nations, 2015).

Repeated 90-day oral toxicity test in rats

The rats were given MCE at three doses of 156.46, 31.29, and 6.26 mg/kg for 90 days by *ad libitum* feeding, and the general behavior of the rats was normal during the observation period, with no significant differences in feeding, drinking and weight gain (Figure 2) compared to the blank control group ($p > 0.05$). There was no poisoning or death in each group. There were no significant differences in hematology (Table 3), serum biochemistry (Table 4), organ coefficients (Table 5), and histopathological examination in each test group compared with the control group ($p > 0.05$).

TABLE 9 Effect of MCE on the reproductive performance of pregnant rats.

Groups	Number of pregnant rats	Weight gain	Ovarian weight	Number of corpus luteum	Number of nidation	Uterine weight	Average number of live births
391.15 mg/kg	12	2.47 ± 0.29	0.13 ± 0.01	16.33 ± 0.82	187	5.12 ± 0.17	15.50
97.79 mg/kg	12	2.59 ± 0.34	0.13 ± 0.01	16.50 ± 0.92	194	5.27 ± 0.18	16.08
24.45 mg/kg	12	2.15 ± 0.37	0.12 ± 0.01	16.42 ± 0.85	191	5.21 ± 0.13	15.75
Negative control	12	2.13 ± 0.36	0.12 ± 0.01	15.92 ± 0.71	185	5.18 ± 0.14	15.25

Chronic toxicity in rats

The potential chronic toxicity risk is of particular concern because MCE has been added to feed for long periods of time for clinical use. The rats were fed at 78.23, 15.65, and 3.13 mg/kg for 180 days and did not exhibit any significant abnormalities or die during the observation period in all dose groups. Similarly, MCE did not produce a significant effect ($p > 0.05$) on the desire to eat and drink and weight gain of the rats (Figure 3). Further hematological (Table 3), serum biochemical (Table 4), organ coefficients (Table 5) and histopathological examinations also did not observe significant changes compared to the control group ($p > 0.05$).

Ames test

Four test strains of *S. typhimurium* grew normally, and each strain in the positive control group reacted satisfactorily. MCE was in the range of 100–0.16 μg/dish, and the mean number of revertant colonies per dish for all four test bacteria in the presence or absence of the metabolic activation system (S9) was within twice that of the solvent (sterilized distilled water) control, and no dose-response relationship was seen, and the results of the two tests were consistent. It was shown that MCE was not mutagenic to *S. typhimurium* for the test. The results of the two replicate tests are shown in Table 6.

Mouse bone marrow cell micronucleus test

Due to the solid evidence of the reported mutagenic effect of SAN on bone marrow cell DNA *in vivo*, we conducted a mouse bone marrow cell micronucleus assay. The results showed that the positive control group (cyclophosphamide) contained a significantly higher rate of micronucleated PCEs than the negative control group ($p < 0.01$), in contrast, the values of PCE/RBC were within the normal range in all dose groups. The PCE rates of bone marrow cells in female and male mice in each dose group of MCE were not significantly different from solvent controls ($p > 0.05$), indicating the lack of mutagenicity of MCE in mice (Table 7).

Mice sperm abnormality test

Subsequently, we tested whether MCE can cause sperm cell aberrations *in vivo* using a mouse sperm deformation assay. The sperm malformation rate of mice in each dose group of MCE did not show significant differences from the negative control group after five doses of exposure. In contrast to the significant increase in sperm malformations caused by cyclophosphamide-treated group, sperm abnormality rates in mice remained essentially unchanged at any of the MCE doses tested (Table 8), indicating that MCE is not teratogenic in mice.

Traditional teratogenicity test in rats

Because of the previously reported risk of embryotoxicity of SAN (Chan, 2015), we further investigated the potential embryotoxicity of MCE using a conventional teratogenic assay in rats. The results showed that MCE did not produce maternal toxicity in pregnant rats in the dose range of 24.45–391.15 mg/kg, and the pregnant rats showed normal behavior, no poisoning and death, and no significant differences in drinking, feeding and weight gain compared with the negative control group ($p > 0.05$) (Table 9). There was no significant difference in ovarian weight, number of corpus luteum, number of implantations, uterine weight and number of live fetuses between the dose groups compared to the negative control group ($p > 0.05$) (Table 9). No teratogenic effect of MCE on fetal rats was also found in the examination of fetal rats (stillbirth, appearance, viscera, and bones) (Tables 10, 11). The test results showed that MCE had no significant reproductive toxicity or embryotoxicity to rats.

Discussion

M. cordata is a commonly used topical drug in traditional Asian ethnomedicine and its use has been restricted due to

TABLE 10 Teratogenic effects of MCE in pregnant rats.

Groups	Number of pregnant rats	Malformed appearance			Malformed bones			Malformed viscera		
		Number of fetal rats examined	The incidence of malformed fetuses (%)	Maternal malformation rate (%)	Number of fetal rats examined	The incidence of malformed fetuses (%)	Maternal malformation rate (%)	Number of fetal rats examined	The incidence of malformed fetuses (%)	Maternal malformation rate (%)
391.15 mg/kg	12	186	0	0	96	5.20	33.33	90	0	0
97.79 mg/kg	12	193	0	0	95	7.37	50.00	98	0	0
24.45 mg/kg	12	189	0	0	997	6.18	41.67	92	0	0
Negative control	12	183	0	0	94	7.44	50.00	89	0	0

Note: The incidence of malformed fetuses (%) = (numbers of malformed fetuses/numbers of fetal rats examined) × 100%; maternal malformation rate (%) = (numbers of pregnant rats with malformed fetuses/numbers of pregnant rats examined) × 100%.

transoral toxicity. Modern research has revealed that its main component, SAN, has a variety of biological activities and is used extensively in animal husbandry as a farming input to provide animal performance. Due to the long-term use in food animals and the potential toxicity risk of SAN, the safety information of MCE as a plant extract that can be added for a long time is of concern. Previous risk assessments of SAN were mostly based on intraperitoneal injections, whereas the most important route for the risk of ingestion of exogenous substances is via the oral route. Therefore, in this study, we systematically evaluated the safety of MCE by performing acute toxicity and long-term oral toxicity studies (subchronic and chronic toxicity) in rodents, while reassessing genotoxicity and developmental toxicity. This is the first systematic report on the safety of MCE after it was developed as a veterinary drug in China. In this report, MCE lacks long-term oral toxicity in rodents as well as mutagenic potential. In conclusion, our study provides important information for the rational use of MCE and subsequent residual safety assessment through general toxicity in rodents as well as genotoxicity assessment.

In acute toxicity studies in SD rats and ICR mice, the LD_{50} of MCE was 1,564.55 and 1,024.33 mg/kg, respectively, which were classified as low toxic substances in the acute toxicity classification of GHS and WHO compounds. The oral acute toxicity results of MCE in rats were similar to those previously obtained with alkaloid extracts of SAN and *Sanguinaria canadensis* L. (Becci et al., 1987). In the subsequent repeated 90-day oral toxicity test, the highest dose of 156.46 mg/kg did not affect body weight gain or other physiological factors for 90 days, and no toxicity-related clinical manifestations were observed during this period. No abnormalities associated with MCE were also found in the hematological, serum biochemical, profiling, and histopathological examinations, and the no observed adverse effect level (NOEAL) of the subchronic toxicity test was determined to be 156.46 mg/kg. In a previous 90-day oral toxicity study of a mixture of quaternary benzo[c] phenanthridine alkaloids of *M. cordata* in rats, 600 mg/kg was considered a safe dose with no significant difference from the negative control (Zdarilova et al., 2008). In addition, in a 90-day feeding trial in pigs, a daily intake of 5 mg/kg of the combined SA/CHE extract was considered safe (Kosina et al., 2004). There may be differences in the proportion of ingredients in the extract as much as possible, but this seems to improve the safety range of MCE. Nevertheless, since the toxicity of a mixture can be influenced by the type and proportion of constituents in it, safety inferences need to be made with caution until the other components of *M. cordata* alkaloid extracts have been subjected to a definitive risk assessment. Similarly, no signs of toxicity associated with MCE were found in further chronic toxicity studies in rats, and the NOEAL was 78.23 mg/kg.

TABLE 11 Effect of MCE on fetal rats.

Groups	Fetal resorption rate (%)	Fetal death rate (%)	Live fetus rate (%)	Female/ male ratio	Average placental weight	Average fetal rat weight	Average body length of fetal rats(cm)	Average tail length of fetal rats (cm)
391.15 mg/kg	0.53	0	99.47	91/95	0.45 ± 0.26	3.65 ± 0.23	3.55 ± 0.06	1.13 ± 0.04
97.79 mg/kg	0.52	0	99.48	91/102	0.43 ± 0.02	3.64 ± 0.07	3.54 ± 0.05	1.13 ± 0.05
24.45 mg/kg	1.05	0	98.85	99/90	0.43 ± 0.02	3.65 ± 0.09	3.55 ± 0.06	1.13 ± 0.05
Negative control	1.08	0	98.92	94/89	0.43 ± 0.03	3.65 ± 0.08	3.55 ± 0.06	1.13 ± 0.05

SAN has been reported to form DNA adducts *in vitro* and to increase the level of DNA single-strand breaks in mouse erythrocytes and bone marrow cells after intraperitoneal injection (Stiborová et al., 2002; Ansari et al., 2005; Kaminskyy et al., 2008). In the current study of the genotoxicity of MCE, the number of revertant colonies in all tested strains did not increase at the highest dose of 100 μg/dish. showed agreement with the results of a previous SAN trial in the *E. coli* PQ37 genotoxicity assay (SOS chromosome) (Kevekordes et al., 1999). Similarly, MCE showed a lack of mutagenic potential in the mouse sperm deformation test and micronucleus test. In another 90-day rat study, a mixture of 120 mg SAN and CHE per kg of feed was also shown to lack evidence of genotoxicity (Stiborova et al., 2008). In addition, some studies have shown toxic effects of SAN on oocytes *in vitro* and developmental risk after embryo transfer (Chan, 2011; Chan, 2015), but in the present study, the results of the conventional teratogenic test in rats were not consistent with this. Within the dose range tested, MCE did not exhibit significant maternal damaging effects or fetal developmental toxicity in pregnant rats. In conclusion, the experimental results in this study contradict the previously reported results, and the reasons for this are related to the nature of the SAN itself. Early risk assessments of SAN used almost exclusively intraperitoneal injections, ignoring the interaction between the gastrointestinal tract and SAN. Previous studies tested the stability of SAN and CHE in an artificially simulated gastrointestinal environment and showed that SAN and CHE were stable in an acidic solution, but the average recoveries of SAN and CHE were only 60.53% and 87.89% in an alkaline environment at pH = 8 (Zhang et al., 2017). The mRNA expression of CYP1A1 and CYP1A2 was increased in porcine intestinal epithelial cells after the administration of 5 and 50 μg/ml SAN (Palócz et al., 2019). Current evidence suggests that CYP1A1 and CYP1A2 play an important role in the conversion of SAN to dihydrosanguinarine (DHSA, the first metabolite of SAN metabolic transformation) (Psotová et al., 2006; Deroussent et al., 2010; Sandor et al., 2018) and this is considered to be a possible detoxification process for SANs (Vrba et al., 2004). Degradation and metabolism in the intestine may be one of the reasons for the low bioavailability of SAN. Although DHSA has also recently been reported to have anti-inflammatory (Xiang et al., 2022) and analgesic (Gaona-Tovar et al., 2022) properties, whether it can regulate intestinal flora still needs to be elucidated. Several pharmacokinetic studies explain that SAN and CHE have low gastrointestinal absorption and bioavailability, and are rapidly metabolized *in vivo* (Vecera et al., 2007; Hu et al., 2019; Wu et al., 2020; Zhao et al., 2021). Another toxicity test on the alkaloids of *Chelidonium majus* L. (CAL) yielded similar inferences (Gao et al., 2019). *In vitro* metabolism studies have shown that SAN may be metabolized in the intestine to DHSA, which has been shown to be much less toxic than SAN (Vecera et al., 2007; Vrublova et al., 2008; Sandor et al., 2016). The accumulation coefficients for SAN and DHSA after multiple oral administrations were 1.21 and 1.11, respectively, which seems to explain the low toxicity exhibited by long-term addition of SAN at reasonable doses (Wu et al., 2020).

Conclusion

We systematically evaluated the general and genetic developmental toxicity of MCE. In this study, MCE was found to exhibit hypotoxic properties in acute exposure to SD rats and ICR mice. The corresponding toxicity risk was also not demonstrated in long-term exposure tests. In addition, the results of systematic mutagenicity and teratogenicity tests showed a lack of evidence of genotoxicity by oral ingestion of MCE at the doses tested. The results of this study provide preliminary and more holistic risk assessment information for MCE in the context of veterinary clinical and human food safety. It is important to note that the results of this study are based on standardized MCE test substances manufactured in GMP

production plants. Caution should be exercised when using other *M. cordata* products that are different from MCE, as the difference in toxicity of the mixture depends mainly on the composition and proportions involved.

Data availability statement

The original contributions presented in the study are included in the article/supplementary material, further inquiries can be directed to the corresponding authors.

Ethics statement

The animal study was reviewed and approved by the Animal Ethics Committee of China Agricultural University.

Author contributions

Conceptualization, ZD and J-GZ; methodology, ZD and S-ST; software, ZD; validation, ZD and Z-HY; formal analysis, ZD and X-LM; resources, C-HL and J-GZ; data curation, ZD; writing—original draft preparation, ZD; writing—review and editing, ZD and S-ST; visualization, ZD; supervision, C-HL and Z-ST; project administration, Z-HY; All authors have read and agreed to the published version of the manuscript.

Funding

This research did not receive any specific grant from funding agencies in the public, commercial, or not-for-profit sectors.

Conflict of interest

C-HL and Z-ST were employed by Hunan MICOLTA Biological Resources Co., Ltd.

The remaining authors declare that the research was conducted in the absence of any commercial or financial relationships that could be construed as a potential conflict of interest.

Publisher's note

All claims expressed in this article are solely those of the authors and do not necessarily represent those of their affiliated organizations, or those of the publisher, the editors and the reviewers. Any product that may be evaluated in this article, or claim that may be made by its manufacturer, is not guaranteed or endorsed by the publisher.

References

Aguilar-Hernández, J. A., Urías-Estrada, J. D., López-Soto, M. A., Barreras, A., Plascencia, A., Montaño, M., et al. (2016). Evaluation of isoquinoline alkaloid supplementation levels on ruminal fermentation, characteristics of digestion, and microbial protein synthesis in steers fed a high-energy diet. *J. Anim. Sci.* 94, 267–274. doi:10.2527/jas.2015-9376

Anjago, W. M., Zeng, W., Chen, Y., Wang, Y., Biregeya, J., Li, Y., et al. (2021). The molecular mechanism underlying pathogenicity inhibition by sanguinarine in Magnaporthe oryzae. *Pest Manag. Sci.* 77, 4669–4679. doi:10.1002/ps.6508

Ansari, K. M., Dhawan, A., Khanna, S. K., and Das, M. (2005). *In vivo* DNA damaging potential of sanguinarine alkaloid, isolated from argemone oil, using alkaline comet assay in mice. *Food Chem. Toxicol.* 43, 147–153. doi:10.1016/j.fct.2004.09.005

Ansari, K. M., Dhawan, A., Khanna, S. K., and Das, M. (2006). Protective effect of bioantioxidants on argemone oil/sanguinarine alkaloid induced genotoxicity in mice. *Cancer Lett.* 244, 109–118. doi:10.1016/j.canlet.2005.12.014

Becci, P. J., Schwartz, H., Barnes, H. H., and Southard, G. L. (1987). Short-term toxicity studies of sanguinarine and of two alkaloid extracts of Sanguinaria canadensis L. *J. Toxicol. Environ. Health* 20, 199–208. doi:10.1080/15287398709530972

Bussabong, P., Rairat, T., Chuchird, N., Keetanon, A., Phansawat, P., Cherdkeattipol, K., et al. (2021). Effects of isoquinoline alkaloids from macleaya cordata on growth performance, survival, immune response, and resistance to Vibrio parahaemolyticus infection of Pacific white shrimp (Litopenaeus vannamei). *PLoS One* 16, e0251343. doi:10.1371/journal.pone.0251343

Cai, Q., Meng, J., Ge, Y., Gao, Y., Zeng, Y., Li, H., et al. (2020). Fishing antitumor ingredients by G-quadruplex affinity from herbal extract on a three-phase-laminar-flow microfluidic chip. *Talanta* 220, 121368. doi:10.1016/j.talanta.2020.121368

Chan, W.-H. (2011). Embryonic toxicity of sanguinarine through apoptotic processes in mouse blastocysts. *Toxicol. Lett.* 205, 285–292. doi:10.1016/j.toxlet.2011.06.018

Chan, W.-H. (2015). Hazardous effects of sanguinarine on maturation of mouse oocytes, fertilization, and fetal development through apoptotic processes. *Environ. Toxicol.* 30, 946–955. doi:10.1002/tox.21969

Chen, T., and Shang, Z. (2002). *Commentary on supplement to medica*. Hefei: Anhui Science and Technology Press.

Chen, J., Kang, B., Zhao, Y., Yao, K., and Fu, C. (2018). Effects of natural dietary supplementation with Macleaya cordata extract containing sanguinarine on growth performance and gut health of early-weaned piglets. *J. Anim. Physiol. Anim. Nutr.* 102, 1666–1674. doi:10.1111/jpn.12976

Chen, K., Liu, Y., Cheng, Y., Yan, Q., Zhou, C., He, Z., et al. (2020). Supplementation of lactobacillus plantarum or Macleaya cordata extract alleviates oxidative damage induced by weaning in the lower gut of young goats. *Animals.* 10, E548. doi:10.3390/ani10040548

Chin, C.-K. (2008). "Plant cell culture as a source of valuable chemicals," in *Biotechnology in flavor production* (Hoboken, United States: John Wiley & Sons), 104–117. doi:10.1002/9781444302493.ch4

Choy, C.-S., Cheah, K.-P., Chiou, H.-Y., Li, J.-S., Liu, Y.-H., Yong, S.-F., et al. (2008). Induction of hepatotoxicity by sanguinarine is associated with oxidation of protein thiols and disturbance of mitochondrial respiration. *J. Appl. Toxicol.* 28, 945–956. doi:10.1002/jat.1360

Council of the European Union and European Parliament (2008). Regulation (EC) No 882/2004 of the European Parliament and of the Council of 29 April 2004 on official controls performed to ensure the verification of compliance with feed and food law, animal health and animal welfare rules. *OJEU* L191, 1–52.

Danielewski, M., Zielińska, S., Matuszewska, A., Słupski, W., Włodarczyk, M., Jęśkowiak, I., et al. (2022). Sanguinarine-chelerythrine fraction of coptis chinensis exerts anti-inflammatory activity in carrageenan paw oedema test in rats and reveals reduced gastrotoxicity. *Oxid. Med. Cell. Longev.* 2022, 1504929. doi:10.1155/2022/1504929

Deroussent, A., Ré, M., Hoellinger, H., and Cresteil, T. (2010). Metabolism of sanguinarine in human and in rat: characterization of oxidative metabolites produced by human CYP1A1 and CYP1A2 and rat liver microsomes using liquid chromatography-tandem mass spectrometry. *J. Pharm. Biomed. Anal.* 52, 391–397. doi:10.1016/j.jpba.2009.09.014

Directorate-General for Health and Food Safety (2021). *European Union register of feed additives pursuant to Regulation (EC) No 1831/2003.Annex I, List of additives (Released date 21.09.2021)*. LU: Publications Office of the European Union. Available at: https://data.europa.eu/doi/10.2875/434313 (Accessed July 15, 2022).

Dong, Z., Liu, M., Zhong, X., Ou, X., Yun, X., Wang, M., et al. (2021). Identification of the impurities in bopu Powder® and Sangrovit® by LC-MS combined with a screening method. *Molecules* 26, 3851. doi:10.3390/molecules26133851

Falchi, F. A., Borlotti, G., Ferretti, F., Pellegrino, G., Raneri, M., Schiavoni, M., et al. (2021). Sanguinarine inhibits the 2-ketogluconate pathway of glucose utilization in *Pseudomonas aeruginosa*. *Front. Microbiol.* 12, 744458. doi:10.3389/fmicb.2021.744458

Gao, L., Schmitz, H.-J., Merz, K.-H., and Schrenk, D. (2019). Characterization of the cytotoxicity of selected chelidonium alkaloids in rat hepatocytes. *Toxicol. Lett.* 311, 91–97. doi:10.1016/j.toxlet.2019.04.031

Gaona-Tovar, E., Estrada-Soto, S., González-Trujano, M. E., Martínez-Vargas, D., Hernandez-Leon, A., Narváez-González, F., et al. (2022). Antinociceptive and gastroprotective activities of Bocconia arborea S. Watson and its bioactive metabolite dihydrosanguinarine in murine models. *J. Ethnopharmacol.* 296, 115492. doi:10.1016/j.jep.2022.115492

Ghosh, I., and Mukherjee, A. (2016). Argemone oil induces genotoxicity in mice. *Drug Chem. Toxicol.* 39, 407–411. doi:10.3109/01480545.2015.1135339

Günaydın, Y. K., Dündar, Z. D., Çekmen, B., Akıllı, N. B., Köylü, R., and Cander, B. (2015). Intoxication due to papaver rhoeas (corn poppy): five case reports. *Case Rep. Med.* 2015, 321360. doi:10.1155/2015/321360

Hu, C. M., Cheng, Y. W., Liao, J. W., Cheng, H. W., and Kang, J. J. (2005). Induction of contracture and extracellular Ca2+ influx in cardiac muscle by sanguinarine: a study on cardiotoxicity of sanguinarine. *J. Biomed. Sci.* 12, 399–407. doi:10.1007/s11373-005-3007-y

Hu, N.-X., Chen, M., Liu, Y.-S., Shi, Q., Yang, B., Zhang, H.-C., et al. (2019). Pharmacokinetics of sanguinarine, chelerythrine, and their metabolites in broiler chickens following oral and intravenous administration. *J. Vet. Pharmacol. Ther.* 42, 197–206. doi:10.1111/jvp.12729

Juskiewicz, J., Gruzauskas, R., Zdunczyk, Z., Semaskaite, A., Jankowski, J., Totilas, Z., et al. (2011). Effects of dietary addition of macleaya cordata alkaloid extract on growth performance, caecal indices and breast meat fatty acids profile in male broilers. *J. Anim. Physiol. Anim. Nutr.* 95, 171–178. doi:10.1111/j.1439-0396.2010.01037.x

Kaminskyy, V., Lin, K. W., Filyak, Y., and Stoika, R. (2008). Differential effect of sanguinarine, chelerythrine and chelidonine on DNA damage and cell viability in primary mouse spleen cells and mouse leukemic cells. *Cell Biol. Int.* 32, 271–277. doi:10.1016/j.cellbi.2007.09.004

Kevekordes, S., Mersch-Sundermann, V., Burghaus, C. M., Spielberger, J., Schmeiser, H. H., Arlt, V. M., et al. (1999). SOS induction of selected naturally occurring substances in *escherichia coli* (SOS chromotest). *Mutat. Res.* 445, 81–91. doi:10.1016/s1383-5718(99)00141-2

Kosina, P., Walterová, D., Ulrichová, J., Lichnovský, V., Stiborová, M., Rýdlová, H., et al. (2004). Sanguinarine and chelerythrine: Assessment of safety on pigs in ninety days feeding experiment. *Food Chem. Toxicol.* 42, 85–91. doi:10.1016/j.fct.2003.08.007

Li, J.-Y., Huang, H.-B., Pan, T.-X., Wang, N., Shi, C.-W., Zhang, B., et al. (2022). Sanguinarine induces apoptosis in eimeria tenella sporozoites via the generation of reactive oxygen species. *Poult. Sci.* 101, 101771. doi:10.1016/j.psj.2022.101771

Lin, L., Liu, Y.-C., Huang, J.-L., Liu, X.-B., Qing, Z.-X., Zeng, J.-G., et al. (2018). Medicinal plants of the genus macleaya (macleaya cordata, macleaya microcarpa): a review of their phytochemistry, pharmacology, and toxicology. *Phytother. Res.* 32, 19–48. doi:10.1002/ptr.5952

Lin, L., Li, X.-Y., Liu, S.-S., Qing, Z.-X., Liu, X.-B., Zeng, J.-G., et al. (2020). Systematic identification of compounds in macleaya microcarpa by high-performance liquid chromatography/quadrupole time-of-flight tandem mass spectrometry combined with mass spectral fragmentation behavior of macleaya alkaloids. *Rapid Commun. Mass Spectrom.* 34, e8715. doi:10.1002/rcm.8715

Liu, T., Li, T., Chen, X., Zhang, K., Li, M., Yao, W., et al. (2021). A network-based analysis and experimental validation of traditional Chinese medicine Yuanhu Zhitong Formula in treating neuropathic pain. *J. Ethnopharmacol.* 274, 114037. doi:10.1016/j.jep.2021.114037

Liu, F., Wang, H., Zhu, X., Jiang, N., Pan, F., Song, C., et al. (2022a). Sanguinarine promotes healthspan and innate immunity through a conserved mechanism of ROS-mediated PMK-1/SKN-1 activation. *iScience* 25, 103874. doi:10.1016/j.isci.2022.103874

Liu, Z.-H., Wang, W.-M., Zhang, Z., Sun, L., and Wu, S.-C. (2022b). Natural antibacterial and antivirulence alkaloids from Macleaya cordata against methicillin-resistant *Staphylococcus aureus*. *Front. Pharmacol.* 13, 813172. doi:10.3389/fphar.2022.813172

Lu, M., Li, K., He, H., Cheng, Y., and Yang, P. (2020). Systematic characterization of alkaloids in eomecon chionantha hance using ultrahigh-performance liquid chromatography-tandem quadrupole exactive orbitrap mass spectrometry with a four-step screening strategy. *Rapid Commun. Mass Spectrom.* 34, e8880. doi:10.1002/rcm.8880

Lu, C., Zhang, N., Kou, S., Gao, L., Peng, B., Dai, Y., et al. (2022). Sanguinarine synergistically potentiates aminoglycoside-mediated bacterial killing. *Microb. Biotechnol.* 15, 2055–2070. doi:10.1111/1751-7915.14017

Mantel, N. (1967). Adaptation of Kärber–s method for estimating the exponential parameter from quantal data, and its relationship to birth, death, and branching processes. *Biometrics* 23, 739–746.

Ministry of Agriculture and Rural Affairs of PRC (2009a). Guidelines for 30-day and 90-day feeding trials of veterinary drugs. *Notice No. 442 of the Ministry of Agriculture of the people's Republic of China*, 1–6.

Ministry of Agriculture and Rural Affairs of PRC (2009b). Guidelines for Ames testing of veterinary drugs. *Notice No. 442 of the Ministry of Agriculture of the people's Republic of China*, 1–17.

Ministry of Agriculture and Rural Affairs of PRC (2009c). Guidelines for chronic toxicity and carcinogenicity testing of veterinary drugs. *Notice No. 442 of the Ministry of Agriculture of the people's Republic of China*, 1–6.

Ministry of Agriculture and Rural Affairs of PRC (2009d). Guidelines for classical teratogenicity tests on veterinary drugs in rats, 1–9.

Ministry of Agriculture and Rural Affairs of PRC (2009e). Guidelines for sperm abnormality tests in veterinary mice. *Notice No. 442 of the Ministry of Agriculture of the people's Republic of China*, 1–4.

Ministry of Agriculture and Rural Affairs of PRC (2009f). Guidelines for the acute toxicity (LD50 determination) of veterinary drugs. *Notice No. 442 of the Ministry of Agriculture of the people's Republic of China*, 1–18.

Ministry of Agriculture and Rural Affairs of PRC (2009g). Guidelines for the veterinary mouse bone marrow cell staining aberration test. *Notice No. 442 of the Ministry of Agriculture of the people's Republic of China*, 1–7.

Moro, P. A., Cassetti, F., Giugliano, G., Falce, M. T., Mazzanti, G., Mennini-Ippolito, F., et al. (2009). Hepatitis from greater celandine (chelidonium majus L.): review of literature and report of a new case. *J. Ethnopharmacol.* 124, 328–332. doi:10.1016/j.jep.2009.04.036

Palócz, O., Szita, G., and Csikó, G. (2019). Alteration in inflammatory responses and cytochrome P450 expression of porcine jejunal cells by drinking water supplements. *Mediat. Inflamm.* 2019, 5420381. doi:10.1155/2019/5420381

Prabhu, K. S., Bhat, A. A., Siveen, K. S., Kuttikrishnan, S., Raza, S. S., Raheed, T., et al. (2021). Sanguinarine mediated apoptosis in non-small cell lung cancer via generation of reactive oxygen species and suppression of JAK/STAT pathway. *Biomed. Pharmacother.* 144, 112358. doi:10.1016/j.biopha.2021.112358

Psotová, J., Klejdus, B., Vecera, R., Kosina, P., Kubán, V., Vicar, J., et al. (2006). A liquid chromatographic-mass spectrometric evidence of dihydrosanguinarine as a first metabolite of sanguinarine transformation in rat. *J. Chromatogr. B Anal. Technol. Biomed. Life Sci.* 830, 165–172. doi:10.1016/j.jchromb.2005.10.030

Qing, Z.-X., Cheng, P., Liu, X.-B., Liu, Y.-S., Zeng, J.-G., and Wang, W. (2014). Structural speculation and identification of alkaloids in macleaya cordata fruits by high-performance liquid chromatography/quadrupole-time-of-flight mass spectrometry combined with a screening procedure. *Rapid Commun. Mass Spectrom.* 28, 1033–1044. doi:10.1002/rcm.6874

Qing, Z., Xu, Y., Yang, P., Yu, K., Peng, Y., Zuo, Z., et al. (2016a). Study on alkaloids of fruit from macleaya cordata. *Zhong Yao Cai* 39, 312–314. doi:10.13863/j.issn1001-4454.2016.02.018

Qing, Z.-X., Xu, Y.-Q., Yang, P., Yu, K., Cheng, P., and Zeng, J.-G. (2016b). Mass spectrometry-guided isolation of two new benzoquinoline alkaloids from Macleaya cordata. *Nat. Prod. Res.* 30, 1030–1035. doi:10.1080/14786419.2015.1101695

Sandor, R., Midlik, A., Sebrlova, K., Dovrtelova, G., Noskova, K., Jurica, J., et al. (2016). Identification of metabolites of selected benzophenanthridine alkaloids and their toxicity evaluation. *J. Pharm. Biomed. Anal.* 121, 174–180. doi:10.1016/j.jpba.2016.01.024

Sandor, R., Slanina, J., Midlik, A., Sebrlova, K., Novotna, L., Carnecka, M., et al. (2018). Sanguinarine is reduced by NADH through a covalent adduct. *Phytochemistry* 145, 77–84. doi:10.1016/j.phytochem.2017.10.010

Sharma, B. D., Bhatia, V., Rahtee, M., Kumar, R., and Mukharjee, A. (2002). Epidemic dropsy: observations on pathophysiology and clinical features during the Delhi epidemic of 1998. *Trop. Doct.* 32, 70–75. doi:10.1177/004947550203200204

Stiborová, M., Simánek, V., Frei, E., Hobza, P., and Ulrichová, J. (2002). DNA adduct formation from quaternary benzo[c]phenanthridine alkaloids sanguinarine and chelerythrine as revealed by the 32P-postlabeling technique. *Chem. Biol. Interact.* 140, 231–242. doi:10.1016/s0009-2797(02)00038-8

Stiborova, M., Vostalova, J., Zdarilova, A., Ulrichova, J., Hudecek, J., Tschirner, K., et al. (2008). Macleaya cordata extract and sangrovit genotoxicity. Assessment *in vivo*. *Biomed. Pap. Med. Fac. Univ. Palacky. Olomouc Czech. Repub.* 152, 35–39. doi:10.5507/bp.2008.005

United Nations (2015). *Globally harmonized system of classification and labelling of chemicals (GHS)*. 6th revised edition. New York: United Nations.

Vaidya, A. D., Pandita, N., Godse, C., and Meshram, M. (2001). Argemone mexicana and epidemic dropsy: phytopharmacology and putative sequelae and therapy. *J. Assoc. Physicians India* 49, 1041–1042.

Vecera, R., Klejdus, B., Kosina, P., Orolin, J., Stiborová, M., Smrcek, S., et al. (2007). Disposition of sanguinarine in the rat. *Xenobiotica.* 37, 549–558. doi:10.1080/00498250701230542

Veterinary Drug Assessment Centre of the Ministry of Agriculture of the, and People's Republic of China (2012). *Compilation of technical uidelines for veterinary drug research*. Beijing: Chemical Industry Press.

Vrba, J., Kosina, P., Ulrichová, J., and Modrianský, M. (2004). Involvement of cytochrome P450 1A in sanguinarine detoxication. *Toxicol. Lett.* 151, 375–387. doi:10.1016/j.toxlet.2004.03.005

Vrublova, E., Vostalova, J., Vecera, R., Klejdus, B., Stejskal, D., Kosina, P., et al. (2008). The toxicity and pharmacokinetics of dihydrosanguinarine in rat: a pilot study. *Food Chem. Toxicol.* 46, 2546–2553. doi:10.1016/j.fct.2008.04.013

Wang, W., Dolan, L. C., von Alvensleben, S., Morlacchini, M., and Fusconi, G. (2018). Safety of standardized macleaya cordata extract in an eighty-four-day dietary study in dairy cows. *J. Anim. Physiol. Anim. Nutr.* 102, e61–e68. doi:10.1111/jpn.12702

Wang, X., Yang, X., Wang, J., Li, L., Zhang, Y., Jin, M., et al. (2022). Cardiotoxicity of sanguinarine via regulating apoptosis and MAPK pathways in zebrafish and HL1 cardiomyocytes. *Comp. Biochem. Physiol. C. Toxicol. Pharmacol.* 252, 109228. doi:10.1016/j.cbpc.2021.109228

Warowicka, A., Popenda, Ł., Bartkowiak, G., Musidlak, O., Litowczenko-Cybulska, J., Kuźma, D., et al. (2019). Protoberberine compounds extracted from chelidonium majus L. as novel natural photosensitizers for cancer therapy. *Phytomedicine* 64, 152919. doi:10.1016/j.phymed.2019.152919

Wu, Y., Zhao, N.-J., Cao, Y., Sun, Z., Wang, Q., Liu, Z.-Y., et al. (2020). Sanguinarine metabolism and pharmacokinetics study *in vitro* and *in vivo*. *J. Vet. Pharmacol. Ther.* 43, 208–214. doi:10.1111/jvp.12835

Wu, L., Yang, Y., Mao, Z., Wu, J., Ren, D., Zhu, B., et al. (2021). Processing and compatibility of corydalis yanhusuo: phytochemistry, pharmacology, pharmacokinetics, and safety. *Evid. Based. Complement. Altern. Med.* 2021, 1271953. doi:10.1155/2021/1271953

Xiang, Y., Zhang, H., Xu Zhang, Z., Yang Qu, X., and Xia Zhu, F. (2022). Dihydrosanguinarine based RNA-seq approach couple with network pharmacology attenuates LPS-induced inflammation through TNF/IL-17/PI3K/AKT pathways in mice liver. *Int. Immunopharmacol.* 109, 108779. doi:10.1016/j.intimp.2022.108779

Ye, F., Feng, F., and Liu, W. (2009). Alkaloids from Macleaya cordata. *Zhongguo Zhong Yao Za Zhi* 34, 1683–1686.

Zdarilova, A., Vrublova, E., Vostalova, J., Klejdus, B., Stejskal, D., Proskova, J., et al. (2008). Natural feed additive of Macleaya cordata: safety assessment in rats a 90-day feeding experiment. *Food Chem. Toxicol.* 46, 3721–3726. doi:10.1016/j.fct.2008.09.054

Zhang, H., Chen, M., Liu, Y., Tang, Z., Zeng, J., and Liu, Z. (2017). Stability analysis of major alkaloids in macleaya cordata under simulated gastrointestinal environment. *Mod. Chin. Med.* 19, 1387–1390. doi:10.13313/j.issn.1673-4890.2017.10.007

Zhang, R., Guo, Q., Kennelly, E. J., Long, C., and Chai, X. (2020). Diverse alkaloids and biological activities of fumaria (papaveraceae): an ethnomedicinal group. *Fitoterapia* 146, 104697. doi:10.1016/j.fitote.2020.104697

Zhang, Q., Zhang, Z., Zhou, S., Jin, M., Lu, T., Cui, L., et al. (2021). Macleaya cordata extract, an antibiotic alternative, does not contribute to antibiotic resistance gene dissemination. *J. Hazard. Mat.* 412, 125272. doi:10.1016/j.jhazmat.2021.125272

Zhao, N.-J., Wang, L.-L., Liu, Z.-Y., Wang, Q., Liu, L., Sun, Z.-L., et al. (2021). Pharmacokinetics of chelerythrine and its metabolite after oral and intramuscular administrations in pigs. *Xenobiotica.* 51, 1264–1270. doi:10.1080/00498254.2021.1882714

Zhu, M., Gong, Z., Wu, Q., Shi, X., Su, Q., and Zhang, Y. (2020). Sanguinarine suppresses migration and metastasis in colorectal carcinoma associated with the inversion of EMT through the Wnt/β-catenin signaling. *Clin. Transl. Med.* 10, 1–12. doi:10.1002/ctm2.1

Zou, H., Fu, S., Zhang, Y., Li, L., Zhang, Y., Liu, B., et al. (2016). Non-alkaloid chemical constituents from Macleaya cordata. *Zhong Yao Cai* 39, 559–561. doi:10.13863/j.issn1001-4454.2016.03.023

frontiers | Frontiers in Pharmacology

ORIGINAL RESEARCH
published: 16 August 2022
doi: 10.3389/fphar.2022.936161

Effect of *Rumex dentatus* on Gastrointestinal Protection and Toxicology in Rodents *via* Investigating H^+/K^+-ATPase, Calcium Channels, and PDE Mediated Signaling

Neelam Gul Qazi[1], *Arif-ullah Khan*[1]*, *Sumra Wajid Abbasi*[2], *Imran Malik*[1] and *Komal Naeem*[3]

[1]Riphah Institute of Pharmaceutical Sciences, Riphah International University, Islamabad, Pakistan, [2]Nums Department of Biological Sciences, National University of Medical Sciences Rawalpindi, Rawalpindi, Pakistan, [3]University of Northern British Columbia, Prince George, BC, Canada

OPEN ACCESS

Edited by:
Fareeha Anwar,
Riphah International University, Pakistan

Reviewed by:
Irum Shahzadi,
COMSATS University Islamabad, Pakistan
Aslam Khan,
King Saud bin Abdulaziz University for Health Sciences, Saudi Arabia
Atta Ur Rehman,
Forman Christian College, Pakistan

***Correspondence:**
Arif-ullah Khan
arif.ullah@riphah.edu.pk

Specialty section:
This article was submitted to Predictive Toxicology, a section of the journal Frontiers in Pharmacology

Received: 04 May 2022
Accepted: 01 June 2022
Published: 16 August 2022

Citation:
Qazi NG, Khan A-u, Abbasi SW, Malik I and Naeem K (2022) Effect of Rumex dentatus on Gastrointestinal Protection and Toxicology in Rodents via Investigating H^+/K^+-ATPase, Calcium Channels, and PDE Mediated Signaling. Front. Pharmacol. 13:936161. doi: 10.3389/fphar.2022.936161

This present study aims to delineate *Rumex dentatus* crude extract (Rd.Cr), n-Hexane, ethyl acetate, aqueous fractions (Rd.n-Hex, Rd.ETAC, and Rd.Aq), and emodin for antidiarrheal, antisecretory effects, anti-spasmodic, gastrointestinal transient time, anti-*H. pylori*, antiulcer effects, and toxicology. Plant extracts attributed dose-dependent protection against castor oil-induced diarrhea and dose-dependently inhibited intestinal fluid secretions in mice. They decreased the distance transverse by charcoal in the gastrointestinal transit model in rats. In rabbit jejunum preparations, it causes a concentration-dependent relaxation of both spontaneous and K^+ (80 mM)-induced contraction, Rd.n-Hex and verapamil were relatively potent against K^+-induced contractions and shifted the Ca^{2+} concentration-response curves (CRCs) to the right, Rd.Cr and Rd.ETAC shifted the isoprenaline-induced inhibitory CRCs to the left, showing potentiating effect similar to papaverine. Rd.n-Hex showed anti-*H. pylori* effect. Extracts and emodin also show an inhibitory effect against H^+/K^+-ATPase. *Rumex dentatus* showed a gastroprotective and antioxidant effect. Histopathological evaluation showed improvement in cellular architecture and decrease in the expression of inflammatory markers such as cyclooxygenase (COX2), tumor necrosis factor (TNF-α), and phosphorylated nuclear factor kappa B (p-NFkB), validated through immunohistochemistry, ELISA, and western blot techniques. In RT-PCR, it decreases H^+/K^+-ATPase mRNA levels. *Rumex dentatus* was analyzed for certain safety aspects and exhibited a relative safety profile as no impairment was observed in kidneys, heart, liver, and brain further assisted by biochemical and hematological analysis. Docking studies revealed that emodin against H^+/K^+-ATPase pump and voltage gated L-type calcium channel showed E-value of –7.9 and –7.4 kcal/mol, respectively. MD simulations and molecular mechanics Poisson Boltzmann surface area and molecular mechanics Generalized Born surface area MMPBSA/GBSA findings are consistent with the *in-vitro, in-vivo,* and docking results. In conclusion, *Rumex dentatus* extracts and its phytoconstituent could be considered a potent antioxidant and anti-inflammatory drug candidates that possess anti-diarrheal, anti-secretary, antispasmodic, anti-*H. pylori,* and

anti-ulcer potential. Toxicity studies were done according to OECD standards 425. It belongs to group 5 (LD50 > 2000 mg/kg), which suggests that it is in the lower toxicity class.

Keywords: Rumex dentatus, anti-oxidant, anti-inflammatory, anti-ulcer, H/K$^+$-ATPase, calcium channel

INTRODUCTION

Many advances have been made in the world of medicine, yet there is no optimal cure for gastrointestinal diseases. This area of medicine has a lot of untapped potential for research. Furthermore, current treatment options provide relief for a shorter period of time, but medicinal plant extracts are considered a safer therapeutic option that also improves GI disorders for a longer period of time. Natural drug compounds and herbal extracts form the major proportion of drugs available around the globe and are considered a major part of modern medicine, that is, 61% (Khan and Gilani, 2009).

Gastrointestinal tract (GIT) performs various functions including secretions and contracting movements. Several pathologies of GIT possibly will amend the rate of motility and contractions of muscles, therefore, it leads to various GI diseases for instance diarrhea, constipation, and delay in emptying of stomach, etc. (Ohama et al., 2007).

Psychological conditions including emotions, the health state of an individual, and bulk content of intestine are some of the aspects that can alter the motility of gut. Bulk content of intestine can leads to the activation of sensory receptors present in mucosal lining of intestine and it enhance the propulsive peristalsis of intestine. Motility of intestine can also be altered due to some other factors including hyperactivity of thyroid glands, certain tumors, dystrophy of muscles, piles, diabetes, IBS and other inflammatory diseases, infection, and some drugs such as iron supplements, tricyclic antidepressants, antacids, and opioids (Hasler et al., 2010).

There are several signal transduction mechanisms (Muscuranic receptor, PGE2, Gastrin & Histamine) involved in the gastric parietal cells, which are linked to the $H^{+/}K^+$-ATPase. It is catalyzed by the interchange of intracellular H^+ and extracellular K^+, and cytoplasmic ATP hydrolysis. It is responsible for the crucial factor that causes gastric acid secretion. An imbalance between defensive and offensive agents causes a stomach ulcer, which directly compromises the integrity of the gastric mucosal barrier. Excess gastric acid, on the other hand, is one of the most offensive elements that lead to all types of gastric ulcer illnesses. Literature indicates that ethanol and nonsteroidal anti-inflammatory drugs (NSAIDs), such as aspirin, ibuprofen, and indomethacin, can promote gastric acid secretion, damage the gastric mucosa and disrupt the gastric mucosal barrier. All of the above, however, are linked to H^+/K^+-ATPase malfunction (Mishra, 2016). In the clinic, inhibiting the activity of the H^+/K^+-ATPase becomes a significant treatment for gastric ulcers.

Medicinal plants have been used to treat many diseases for centuries. Phytotherapy is getting more popular as the World Health Organization (WHO) advocates appropriate ethnomedicinal use and certifies the safety of herbal medications. The FDA and WHO underlines the importance of conducting scientific research to validate the efficacy and safety of herbal medicines (Saleem et al., 2017). The second genera of the family Polygonaceae are Rumex which contains approximately 150 species broadly scattered around the ecosphere. In China, there are 26 species. *Rumex dentatus* commonly known as dentate dock, Indian Dock, and Toothed Dock, is extensively distributed throughout China and Pakistan. This traditional plant has been used to heal different types of bacterial and fungal infections, including dysentery, enteritis, acariasis, and eczema (Zhang et al., 2012). Rumex and Rheum share several chemical components, such as chrysophanol, emodin, aloe-emodin, and physcion, since they are in the same family. Other important chemical components in Rumex include flavonoids, diphenylethenes, and naphthalenes (Shafiq et al., 2017). Emodin, chrysophanol, physcion, rumejaposides, cassialoin, and carotene have all been revealed through phytochemical analysis. It was previously used as a molluscicide, diuretic, anti-inflammatory, anti-tumor, anti-dermatitis, cholagogue, tonic, and laxative agent (Fatima et al., 2009).

In-silico and *in-vivo* assessment of extracts obtained from plants aids to sort out novel bioactive compounds and their additional indulgence lead to advanced therapeutic options. Furthermost and appropriate healing properties can be attained with purified form of isolated bioactive elements that can be formulated into an appropriate dosage form along with a prescription regime. Various chronic ailments have been treated by herbal preparations. Researchers have explored the role of plant extracts which have property to treat GI conditions (Ansari et al., 2019).

The purpose of this study was to discover *Rumex dentatus* extracts and its phytoconstituent for antidiarrheal effects, antisecretory effects, effects on motility of isolated tissue preparations, gastrointestinal transient time, anti-*H. pylori*, antiulcer potential, and toxicology. Another aim of this study is to demonstrate whether *Rumex dentatus* exerts a gastroprotective role in ethanol-induced ulcer *via* H^+/K^+ATPase-dependent pathway.

MATERIALS AND METHODS

Chemicals

Castor oil was acquired from KCL Pharma, Karachi, Pakistan. Acetylcholine, ethyl acetate, activated charcoal, omeprazole, ethanol, loperamide, papaverine, methanol, n-Hexane, atropine sulfate, potassium chloride, isoprenaline, verapamil hydrochloride (Sigma Chemicals Co, St Louis, MO, United States), and emodin (Carbosynth limited, Berkshire. United Kingdom) were used.

Animals

Experiments were performed in compilation with rules of the Research and Ethics Committee of Riphah Institute Of Pharmaceutical Sciences (Ref. no. REC/RIPS/2019/14) along with the guidelines of "Principles of Laboratory Animal care". Rabbits (1.0–2.0 kg) albino mice (20–25 g), and Sprague-Dawley rats (150–250 g) of either gender were used in the experimentation procedure, housed in animal house of the Riphah Institute of Pharmaceutical Sciences (RIPS) Islamabad provided with a controlled environment (20–25°C).

Plant Material

The *Rumex dentatus* plant was collected from hilly area of Batkhela, KPK, Pakistan. After the collection plant was authenticated by Dr. Mushtaq Ahmad, a taxonomist at Department of Plant Sciences, Quaid-a-Azam University Islamabad, and the voucher/specimen number (ISL-B-21) was collected after submitting the sample of the specimen to the herbarium at same Department. The plant was dried under shade (air-dried). The dried materials were powdered and then soaked in aqueous methanol (70% methanol) for 15 days at room temperature. The hydro methanolic extract (500 g) was collected and filtered. This process was repeated 2 more times and under reduced pressure, the filtrates were dried through a rotary evaporator. Semi-solid mass obtained, was further processed for fractionation in different solvents according to their polarity order (n-Hexane–Ethyl acetate–Methanol–Aqueous). Fractions of (n-Hex) n-hexane (50 g) (ETAC) ethyl acetate (100 g), and (Aq) aqueous (35 g) were obtained and stored for analysis.

Phytochemical Screening

The phytochemical screening was performed to determine the phytoconstituents (Alkaloids, anthraquinones, cardiac glycosides, coumarins, flavonoids, tannins, and saponins) present in the crude extract and all the fractions of *Rumex dentatus* by following the protocols reported in the literature (Okunlola et al., 2007).

Gas Chromatography Mass Spectrometry Analysis

A gas chromatography mass spectrometry (GC-MS; QP-2010 Plus Shimadzu, Japan) with a DB-5MS capillary column (30 m × 0.25 mm I.D, 0.25 μm film thicknesses, Shimadzu, Japan) was used. The inlet temperature was maintained at 250°C. The oven temperature was initially at 50°C, programmed to 220°C at 5°C/min, and then programmed to 300°C at 10°C/min holding for 15 min. Helium was used as carrier gas at a constant flow rate of 1.0 ml/min. The injection volume is 1 μl. The samples were analyzed by GC–MS with the pulsed split less injection mode. The ion source was set to 280°C and the MS transfer line was set to 280°C. Ionization was carried out in electron impact ionization (EI) mode at 70 eV. The mass spectra were recorded within 50–500 amu in full scan mode to collect the total ion current (TIC) (Dai et al., 2018).

Castor-Oil Induced Diarrhea

Mice were randomly assigned to one of 17 groups (n = 5) and fasted for 24 h (08:00–08:00). Animals were kept in separate cages with absorbent paper lining the floor. Loperamide hydrochloride (2 mg/kg) was given to the positive control group, while the negative control group was given an equal volume of saline (10 ml/kg) and after 1 h of treatment, mice were given castor oil (10 ml/kg p.o.). Diarrhea was induced with castor oil (10 ml/kg, p.o.) after administration of 50, 100, and 300 mg/kg doses of Rd.Cr, Rd.n-Hex, Rd.ETAC, Rd.Aq, and emodin, respectively. The animals were separated into white paper-lined cages. The onset of diarrhea, frequency of defecation, and weight of fecal output (wet and total feces in Gram) for each mouse were recorded throughout a 4-h period. The percentages of diarrheal inhibition and fecal output weight were calculated using **Formulas 1–3** (Sisay et al., 2017):

$$\% \text{ of inhibition} = \text{Average number of WFC} - \text{Average number of WFT/Average number of WFC X 100, where WFC} = \text{wet feces in the control; WFT} = \text{wet feces in the test group} \quad (1)$$

$$\text{Percentage of wet fecal output/WWFO} = \text{Mean weight of wet feces of each group/Mean weight of wet feces of control X 100} \quad (2)$$

$$\text{Percentage of total fecal output/WTFO} = \text{Mean weight of total feces of each group/Mean weight of total feces of control X 100} \quad (3)$$

Assessment of Intestinal Fluid Accumulation

The method described was used to determine the amount of fluid in the intestine. Mice that had been fasted for 24 h (08:00–08:00) were separated into 18 cages, each with five mice. Normal saline (10 ml/kg) and castor oil (10 ml/kg, p.o.) were given to groups I and II, respectively. The remaining groups received 50, 100, and 300 mg/kg intraperitoneally of Rd.Cr, Rd.n-Hex, Rd.ETAC, Rd.Aq, and emodin, respectively. A group was given the standard drug atropine at a dose of 0.1 mg/kg 1 h before induction with castor oil (10 ml/kg, p.o.). After 30 min, the mice were sacrificed and their intestines were removed and weighed. The results were written as (Pi/Pm) × 1,000, where Pi is the intestine's weight (g) and Pm is the animal's weight (Sisay et al., 2017).

Charcoal Meal Transit Time

A charcoal meal inhibitory activity in rats was calculated. The rats were fasted for 24 h but were allowed to drink freely. Rd.Cr, Rd.n-Hex, Rd.ETAC, Rd.Aq, and emodin were given in doses of 50, 100, and 300 mg/kg body weight in the test groups, while atropine sulfate (0.1 mg/kg, i.p.) was given to the positive control group. The negative control group received normal saline (10 ml/kg, p.o.) and 1 h after the pre-treatment period marker (25 mg/kg) (10 percent charcoal suspension in 5 percent gum acacia) was given to all groups. Animals have sacrificed 30 min after all treatments. The small intestine was

removed and the distance traveled by charcoal meal through the organ was calculated as a percentage of the small intestine's length using the formula below (Ansari et al., 2021).

$$\text{Peristaltic index (PI\%)} = \left(\text{Distance moved by charcoal meal/ total length of intestine}\right)(\text{cm}) \times 100$$

For further evaluation of % inhibition, peristaltic index is used.

$$\%\ \text{inhibition} = (\text{PIC} - \text{PIT})/\ \text{PIC X } 100$$

where PIC is the peristaltic index of control and PIT is the peristaltic index of test group.

Effect of Extracts and Emodin on the Motility of Isolated Tissue Preparations

The rabbits were fasted for 24 h (08:00–08:00) before the experiment but had free access to water. The jejunal section was isolated and cleaned with Tyrode's solution after cervical dislocation, about 10–12 cm after the stomach. After the instrument was calibrated, a 2 cm long jejunal segment was placed in a tissue bath containing Tyrode's solution for 30 min to equilibrate with the environment while having a proper supply of oxygen (95% O_2) and 5% CO_2 (carbogen). A 0.3 M concentration of ACh was used to stabilize each preparation. A force-displacement transducer (model FT-03) was used in conjunction with a bridge amplifier and power Lab 4/25 data collection equipment connected to a computer running Lab-Chart 6 software to collect responses (AD Instrument, Sydney Australia). The extracts were examined for percent change in jejunum contractions at various concentrations (Astudillo et al., 2004). To determine the calcium channel blocking activity, high K^+ (80 mM) depolarizes the preparations for smooth muscle contractions by opening voltage-dependent Ca^{2+} channels, allowing extracellular Ca^{2+} to the influx, resulting in a contractile effect, and a substance that inhibits high K^+ induced contraction is considered a blocker of Ca^{2+} influx through L-type Ca^{2+} channels. After the generated contraction had reached a plateau (typically within 7–10 min), test dosages were added in a cumulative manner to get concentration-dependent inhibitory responses. The tissue was allowed to stabilize in normal Tyrode's solution for 30 min before being replaced with Ca^{2+}–free Tyrode's solution containing EDTA (0.1 mM) to validate the test substance's Ca^{2+} antagonist effect. Furthermore, tissue was immersed in a K + -rich, Ca^{2+}–free Tyrode's solution with the following concentrations (mM): NaCl 91.03, NaHCO3 11.9, NaH2PO4.2H2O 0.32, EDTA-Na2.2H2O 0.1, KCl 50, MgCl2.6H2O 0.50, and glucose 5.05. Control concentration-response curves (CRCs) of Ca^{2+} were produced after a 30-min incubation period. The tissue was pretreated with test dose for 1 h after the control Ca^{2+} CRCs were confirmed super-imposable (typically after two cycles). The potential PDE inhibitory effect was investigated indirectly by constructing isoprenaline-induced inhibitory CRCs against CCh-induced contractions in the absence and presence of the plant extract (Gilani et al., 2005).

Anti-*Helicobacter pylori* Activity

The *H. pylori* clinical isolates with resistance profiles were obtained from Breath MAT Lab, Pakistan Institute of Nuclear Science and Technology, Islamabad, Pakistan. They were identified by microaerophilic growth (at 37°C), colony morphology, Gram staining, catalase oxidase, and urease tests (Ullah et al., 2019). Antibacterial effect of Rd.Cr, Rd.nHex, Rd.ETAC, Rd.Aq, and emodin was analyzed by disc diffusion method, measuring the zone of inhibition in mm using 5 mg of extract per disc. The *H. pylori* clinical isolate SJ 2013 10^8 cfu/ml resistant to commonly used antibiotics such metronidazole, clarithromycin, and amoxycillin were inoculated on Columbia blood agar (CM 0331B, Oxoid, United Kingdom) enriched with 5% defibrinated sheep blood. The dried extract impregnated discs were applied and incubated at 37°C for 72 h under microaerophilic conditions by using a gas generating kit, that is, *Campylobacter* gas generating kit (BR 0056A, Oxoid, United Kingdom). After 72 h, the zones of inhibition were measured by determining their diameters. The concentrations of minimum inhibitory (MIC) were assessed for the most potent extracts and compounds by microdilution using brain heart infusion (BHI) broth. The extracts and compound were serially diluted by two folds in BHI broth with serum. The final concentrations of extracts were 0.625–5.0 mg/ml. The concentration with no visual growth or turbidity was considered as MIC.

Ethanol-Induced Ulcer

Rats weighing (250–280 g) of either sex were randomly allocated to groups and fasted for 24 h (09:00–09:00). Group 1 was given normal saline as a negative control (10 ml/kg of body weight), the remaining groups received 50, 100, and 300 mg/kg (p.o.) of Rd.Cr, Rd.nHex, Rd.ETAC, Rd.Aq, and emodin. The last group received 20 mg/kg (p.o.) omeprazole as standard drug. After 1 h of treatment, all of the animals were given 1 ml/100 g of ethanol (p.o.) to produce gastric ulcers. One hour after ethanol treatment, animals were sacrificed by cervical dislocation. The stomachs were removed and cleansed in normal saline before the lesion index was calculated by measuring each lesion in millimeters along its larger curvature. Each lesion's surface area was measured and a score was assigned (Noor et al., 2017). The ulcer index was calculated as the mean ulcer score for each gastrointestinal lesion (US) The ulcer index was calculated by adding the lengths (mm) of all lesions for each gastric injury (UI). The gastroprotective evaluation was expressed as an inhibition percentage (I%), which was calculated using the formula:

$$\%\ \text{Inhibition} = \frac{(\text{USc} - \text{USt})}{\text{USc}} \text{X } 100$$

where USc is the ulcer surface area of control and USt is the ulcer surface area of test drug group.

For additional proteomic screening, the stomach tissues were preserved in a bio freezer (−80°C).

H^+/K^+-ATPase Inhibitory Activity

The inhibitory effect of extracts on rat gastric H^+/K^+-ATPase was analyzed by using the colorimetric method. The commercially available colorimetric H^+/K^+-ATPase activity assay screening kit (catalog No. E-BC-K122-S, Elabscience United States) was used for analysis. Stomach tissues kept at bio freezer (−80°C) for

storage were homogenized at 15,000 using SilentCrusher M (Heidolph), and the homogenate was then centrifuged at 3,500 rpm for 10 min and supernatant was collected. Resulting supernatant was analyzed for the release of inorganic phosphate after ATP hydrolysis spectrophotometrically at 660 nm. 1 ATPase activity unit is defined as 1 μmol of inorganic phosphorus released by ATP hydrolysis by ATPase of 1 mg of tissue protein per hour and results were expressed as μmol Pi/mg prot/hour (He et al., 2019).

Determination of Oxidative Stress Markers

The isolated rat gastric tissues were homogenized and centrifuged at 1,500 rpm for 30 min to separate the supernatant. The supernatants were analyzed for glutathione (GSH), glutathione-S-transferase (GST), catalase, and lipid peroxidation (LPO) levels. The GSH level was determined by oxidizing GSH and DTNP, which produced a yellow end product called 2-nitro-5-thiobenzoic acid. A microplate reader was used to measure absorbance at 412 nm. GSH concentrations are expressed in μmole/mg of protein. The level of GST was determined by forming a CDNB conjugate and measuring its absorbance at 340 nm. GST activity is calculated using the extinction coefficient of the product formed and is expressed as μmoles of CDNB conjugate/min/mg of proteins. In the presence of catalase, the degradation of H_2O_2 was measured. A microplate reader was used to measure absorbance at 340 nm. Catalase activity is measured in moles H_2O_2/min/mg of protein. Malondialdehyde, the end product of LPO, was used to assess its level (MDA). At 532 nm, absorbance was measured using a microplate reader. LPO values are given in TBARS nmoles/min/mg protein (Ali et al., 2020).

Hematoxylin and Eosin Staining and Immunohistochemistry

For morphological analysis, five rats were used in each group. Stomach tissues were fixed in 4% paraformaldehyde and embedded in paraffin, till further analysis. Subsequently, the tissues were sectioned at 5 μm by means of a rotary microtome and were stained with hematoxylin and eosin (H&E). According to (Ali et al., 2020), the stomach tissues were examined using an optical microscope, and photographs were taken. Immunohistochemical staining was carried out. Tissue sections on slides were deparaffinized with three different absolute xylenes and rehydrated with ethyl alcohol in varying concentrations (from 100% [absolute] to 70%). After that, the slides were washed with distilled water and maintained for 10 min in 0.01 M phosphate-buffered saline (PBS). Following the antigen retrieval step, the slides were incubated overnight with primary antibody, followed by 2 h of treatment with appropriate biotinylated secondary antibodies, and finally, 1 h of treatment with Avidin-biotin complex (ABC) reagents (Standard Vectastain ABC Elite Kit; Vector Laboratories, Burlingame, CA, United States) at optimum room temperature. The sections were washed in PBS and stained with 3,3′-Diaminobenzidine (DAB) solution as a chromogen, they were then washed in distilled water, dehydrated in graded ethanol solutions (70, 95, and 100%), fixed in xylene, then cover-slipped with a mounting media and allowed to air dry. A light microscope (Olympus, Japan) was used to examine the results, which was coupled to a high-quality digital photo-microscopy system. A light microscope was used to obtain immunohistochemical TIF images (5 images per plate). Phosphorylated nuclear factor-kappa β (SC-271908 Santa Cruz Biotechnology, Dallas, Tx, United States), tumor necrosis factor α (SC-52B83 Santa Cruz Biotechnology, Dallas, Tx, United States), and COX-2 (SC-514489 Santa Cruz Biotechnology, Dallas, Tx, United States) antibodies were quantified using ImageJ software.

Enzyme-Linked Immunosorbent Assay

Tumor necrotic factor (TNF-α), prostaglandin-E_2 (PGE_2), interleukin-8 (IL-8), and phosphorylated nuclear factor kappa B (p-NF-κB) detection was conducted according to the manufacturer's instructions (Elabscience). The stomach tissues (n = 3) were kept in bio freezer (−80°C) for storage, homogenize at 15 rpm × 1,000 using SilentCrusher M (Heidolph) and supernatant was collected after centrifugation (at 1,350 × g for 1 h). Supernatant was then analyzed for TNF-α (Catalog No: E-EL-R0019), PGE_2 (Catalog No: E-EL-0034), IL-8 (Catalog No: EKF57830), and p-NF-ƙb (Catalog No: E-EL-R0674) quantification through Elabscience Rat ELISA kit.

Western Blot

Western blot analysis technique was used to determine the expression of inflammatory mediators which play role in ulcer progression. Sample proteins (n = 3) from each experimental group were prepared by addition of Laemmle buffer, vertexed, and incubated for 10 min at 96°C temps. Samples were then placed in ice for another 10 min after incubation and then vertexed. Gels were prepared and after preparation protein samples were loaded in polyacrylamide gels separated by SDS/PAGE. In gel electrophoresis proteins' separation is based on their charge. SDS has negative charge and was used for protein denaturation and polyacrylamide permits the protein movement at different speeds. Proteins from gel were then transferred to polyvinylidene fluoride membrane for trans blot operation. Membranes were washed and blocked for non-specific binding using 5% skimmed milk solution prepared in TBST buffer. Primary antibodies phosphorylated nuclear factor-kappa β (SC-271908 Santa Cruz Biotechnology, Dallas, Tx, United States), tumor necrosis factor α (SC-52B83 Santa Cruz Biotechnology, Dallas, Tx, United States), and COX-2 (SC-514489 Santa Cruz Biotechnology, Dallas, Tx, United States) were applied and membranes were incubated for 16 h at 4°C. Membranes were then washed for 10 min in TBST buffer and an anti-mouse secondary antibody was applied for 3–4 h at room temperature. Secondary antibody detects target proteins by binding with primary antibody. The PVDF membrane was then again washed in TBST and proteins on the PVDF membrane were transferred to X-ray sheet. Band density was measured and was standardized to β-actin (Irshad et al., 2021).

Real Time-Polymerase Chain Reaction

After homogenization of gastric tissues (n = 3), trizol method was used to extract total ribonucleic acid (RNA) following the manufacturer's instructions. Using 1–2 μg of total RNA, cDNA was synthesized by reverse transcriptase enzyme, and cDNA was then amplified by real-time PCR (RT-PCR) using a thermocycler. The mRNA expression was normalized to expression levels of Beta-actin. The relative gene expression was determined by $2^{\Delta\Delta-CT}$ method for real-time quantitative PCR (Irshad et al., 2021). Primers sequences for β-actin and H^+/K^+-ATPase are as follows:

Rat-BetaActin-Forward: CCCGCGAGTACAACCTTCT.
Rat-BetaActin-Reverse: CGTCATCCATGGCGAACT.
H^+/K^+-ATPase Forward: TATGAATTGTACTCAGTGGA.
H^+/K^+-ATPase Reverse: TGGTCTGGTACTTCTGCT.

Acute Toxicity Assay

A total of 10 non-pregnant, nulliparous female rats were used in this study to determine acute toxicity of plant extract. They were placed into two groups, each with five females: the control group and the treatment group. Only one was given the limited oral dose of 2,000 mg/kg in accordance with OECD standards 425 (Saleem et al., 2017) and they were deprived of food and water overnight. The rat was monitored for 24 h and if it survived, the same approach was used on the other rats in the therapy group. The animals were closely observed for the first 30 min, then for 4, 24, and 48 h for signs of distress, mortality and then daily for 14 days for various signs of toxicity such as squinting eyes, writhing, salivation, tremors, convulsions, loss of fur, change in overall behavior, stress, and mortality. Blood samples were taken from animals *via* cardiac puncture on the 15th day for various biochemical and hematological analyses. After killing rats by cervical dislocation, vital organs were excised; organ weights were recorded and preserved in 10% formalin for histopathological evaluation and antioxidant profile.

Biochemical Analysis

Urea, uric acid, creatinine, cholesterol, triglyceride, high-density lipoprotein (HDL), low-density lipoprotein (LDL), very low-density lipoprotein (VLDL), bilirubin, alanine aminotransferase (ALT), aspartate aminotransferase (AST), alkaline phosphate (ALP), and total protein were measured by using Randox kits.

Hematological Analysis

For hematological analysis, blood samples from animals (both treatment and control groups) were obtained in EDTA-containing tubes. CBC parameters, hemoglobin (Hb), total RBC, packed cell volume (PVC), mean corpuscular volume (MCV), mean corpuscular hemoglobin (MCH), mean corpuscular hemoglobin concentration (MCHC), platelet count, white blood cells (WBC) count, neutrophils (N), lymphocytes (L), monocytes (M), and eosinophils (E) were determined with humalyzer.

Histopathological Study

The vital organs of sacrificed mice were fixed in 10% formalin and then embedded in paraffin wax after processing. Hematoxylin and eosin were used to stain 5 mm paraffin sections. Under a light microscope, the slides were examined, and magnified images of tissue structure were taken for further analysis.

In-Silico Studies

The docking studies of emodin were carried out through Auto Dock Vina and PyRX software against H^+/K^+ATPase (PDB ID: 4ux2) and calcium channel (PDB ID:1t3s). All the targets were downloaded from the protein data bank (http://www.rcsb.org/pdb/home/home.do) in PDB format purified through the "Discovery Studio Visualizer" (DSV). 3D structure of standard drugs, that is, omeprazole (PubChem CID 4594) and verapamil (PubChem CID 2520) were downloaded from PubChem database and then converted to PDBQT format by Auto Dock tools. The results were analyzed as the binding affinities/E-values (kcal/mol) and best binding pose. Post docking analysis *via* Biovia Discovery Studio Client 2016 was carried out using one best pose with the lowest energy value. 2D and 3D images were evaluated to determine the interactions between amino acid residues and ligands with the receptor (Ansari et al., 2019).

Molecular Dynamic Simulations

All of the top-ranked docked complexes were subjected to molecular dynamics simulations using Amber 18. The simulations were based on docked structures of the protein with an inhibitor. For 50 nano seconds (ns), simulations were run in a periodic water box with the ff03. r1 force field. The topologies of the study proteins were recorded using the Leap module in Amber 18 tools. To neutralize the systems, sodium (Na^+) ions were added. The neutralized systems were then solvated with a distance of 8.0 utilizing the water molecules box (TIP3PBOX). The protonation status of the histidine residues in the proteins has been determined. Before running a production run of molecular dynamic (MD) simulations, the solvated systems were completely reduced. For the first 1,500 interations, the steepest descent method utilizing the SANDER module was used, followed by 1,000 steps of the conjugate gradient. These 2,500 energy minimization cycles were designed to alleviate adverse protein structural conflicts. Every run began with a 100 ps heating session that progressed from 0 to 300 K while maintaining a pressure of 1 atm. First round of 100 ps of equilibration at a steady temperature of 300 K is required prior to the production phase. An interchange of kinetic and potential energy occurred during the equilibration phase. Total energy remained nearly constant throughout the equilibration, whereas potential and kinetic energies differed. In order to acquire statistically precise results, equilibration was followed by a production run of 50 ns for both natural and mutant proteins. To limit all atoms covalently linked to a hydrogen atom, the SHAKE algorithm was used. Periodic boundary conditions with canonical ensemble were utilized in the simulation box. The temperature was kept constant using the Berendsen coupling integration procedure with a non-bonded cutoff of 8.0. The Ewald summation method was used to do MD simulations. Chimera and QtGrace were used to conduct post-simulation studies (root-mean-square deviation (RMSD) and secondary structure timeline analyses) (Abbasi et al., 2016). Molecular mechanics Poisson Boltzmann surface area and molecular mechanics Generalized Born surface area MMGB/PBSA techniques were used to calculate the binding free energy for both

TABLE 1 | Effect of *Rumex dentatus* crude extract (Rd.Cr) and fractions: n-hexane (Rd.n-Hex), ethyl acetate (Rd.ETAC), aqueous (Rd.Aq), emodin, and loperamide against castor-oil induced diarrhea in mice.

Treatment (mg/kg)	No of wet feces	Total No of feces	Average weight of wet feces (gm)	Average weight of total feces (gm)	% inhibition of defecation	% WWFO	% WTFO
Saline (10 ml/kg) + Castor-oil (10 ml/kg)	7.2 ± 0.3	8.4 ± 0.24	0.44 ± 0.05	0.5 ± 0.01	0	0	0
Rd.Cr (50 mg/kg) + Castor-oil (10 ml/kg)	5.7 ± 0.09	7.2 ± 0.37	0.37 ± 0.01	0.44 ± 0.05	20*	84.09	88
Rd.Cr (100 mg/kg) + Castor-oil (10 ml/kg)	2.4 ± 0.24	5.5 ± 0.1	0.13 ± 0.03	0.35 ± 0.05	66.6***	29.54	70
Rd.Cr (300 mg/kg) + Castor-oil (10 ml/kg)	1.6 ± 0.15	4.8 ± 0.19	0.08 ± 0.06	0.31 ± 0.06	77.7***	18.18	62
Rd.n-Hex (50 mg/kg) + Castor-oil (10 ml/kg)	4 ± 0.2	6.8 ± 0.2	0.24 ± 0.05	0.39 ± 0.01	44.44**	54.5	78
Rd.n-Hex (100 mg/kg) + Castor-oil (10 ml/kg)	3 ± 0.21	5.5 ± 0.18	0.16 ± 0.05	0.32 ± 0.03	58.33***	36.36	64
Rd.n-Hex (300 mg/kg) + Castor-oil (10 ml/kg)	1.5 ± 0.0	4 ± 0.02	0.06 ± 0.0	0.23 ± 0.04	79.16***	13.6	46
Rd.ETAC (50 mg/kg) + Castor-oil (10 ml/kg)	4.7 ± 0.2	6.2 ± 0.30	0.29 ± 0.08	0.4 ± 0.05	34.7**	65.9	80
Rd.ETAC (100 mg/kg) + Castor-oil (10 ml/kg)	2.4 0.24	5.3 ± 0.16	0.14 ± 0.04	0.31 ± 0.01	66.66***	31.81	62
Rd.ETAC (300 mg/kg) + Castor-oil (10 ml/kg)	0 ± 0.0	2.8 ± 0.03	0 ± 0.0	0.15 ± 0.02	100***	0	30
Rd.Aq (50 mg/kg) + Castor-oil (10 ml/kg)	7.2 ± 0.12	8.2 ± 0.2	0.44 ± 0.21	0.49 ± 0.03	0	100	98
Rd.Aq (100 mg/kg) + Castor-oil (10 ml/kg)	6.9 ± 0.2	7.4 ± 0.05	0.39 ± 0.32	0.45 ± 0.06	4.1	88.6	90
Rd.Aq (300 mg/kg) + Castor-oil (10 ml/kg)	6.7 ± 0.04	7.2 ± 0.04	0.37 ± 0.15	0.43 ± 0.16	6.94	84.09	86
Emodin (10 mg/kg) + Castor-oil (10 ml/kg)	7.2 ± 0.21	8.3 ± 0.25	0.44 ± 0.01	0.49 ± 0.26	0	100	98
Emodin (30 mg/kg) + Castor-oil (10 ml/kg)	7.31 ± 0.09	8.4 ± 0.29	0.43 ± 0.21	0.48 ± 0.31	1.38	97.7	96
Emodin (50 mg/kg) + Castor-oil (10 ml/kg)	6.66 ± 0.11	7.5 ± 0.31	0.41 ± 0.32	0.45 ± 0.22	7.5	93.1	90
Loperamide (2 mg/kg) + Castor-oil (10 ml/kg)	0 ± 0.0	2.2 ± 0.2	0 ± 0.0	0.11 ± 0.03	100***	0	22

Values expressed as mean ± SEM (n = 5). One-way ANOVA, with post-hoc *Tukey's test.* $^{###}p < 0.001$ *vs. saline group*, $^{*}p < 0.05$, $^{**}p < 0.01$, $^{***}p < 0.001$ *vs. castor oil group.*

protein–inhibitor docked complexes. To compute the binding free energy differences, 1,000 snapshots were taken during the MD simulation trajectory using the same methods as before (Kollman et al., 2000).

Statistical Analysis

Data was expressed as Mean ± SEM (n = 5) and median effective concentrations (EC_{50}) having 95% confidence intervals. Statistical analysis of the results was analyzed using one-way ANOVA followed by *post-hoc* Tukey's test. Non-linear regression using the Graph Pad program (GraphPAD, SanDiego, CA-United States) was used to analyze the concentration-response curves.

RESULTS

Phytochemical Analysis

The phytochemical analysis of *Rumex dentatus* showed different categories of phytoconstituents (**Supplementary Table S1**) and shows different peaks in GC-MS chromatogram (**Supplementary Figure S1**, **Supplementary Table S2**).

Effect on Castor Oil-Induced Diarrhea

In the castor oil-induced diarrheal model, the Rd.Cr and fractions significantly prolonged the onset of diarrhea and reduced the frequency and weight of fecal outputs at doses of 50–300 mg/kg as compared to the control. Data revealed that the percent inhibition of defecation for Rd.Cr at the dose of 50, 100, and 300 mg/kg were 20, 66.6, and 77.7%, respectively. Coming to solvent fractions both Rd.n-Hex and Rd.ETAC has significant results. The diarrheal inhibition obtained as compared to control were 44.44, 58.33, and 79.16% at dose 50–300 mg/kg Rd.nHex, respectively. At dose of 50–300 mg/kg the inhibition for Rd.ETAC was 34.7, 66.66, and 100%, respectively. Loperamide at dose of 2 mg/kg has 100% inhibition. All of them also showed a significant reduction in weight of both wet and total fecal outputs at all doses. Rd.Aq and emodin have a weak antidiarrheal effect (**Table 1**).

TABLE 2 | Effect of *Rumex dentatus* crude extract (Rd.Cr) and fractions: n-hexane (Rd.n-Hex), ethyl acetate (Rd.ETAC), aqueous (Rd.Aq), emodin, and atropine against castor-oil induced fluid accumulation in mice.

N0	Treatment (mg/kg)	% Inhibition
1	Saline (10 ml/kg)	89.7
2	Castor-oil (10 ml/kg)	126.8$^{###}$
3	Rd.Cr (50 mg/kg) + Castor-oil (10 ml/kg)	121.6
4	Rd.Cr (100 mg/kg) + Castor-oil (10 ml/kg)	112*
5	Rd.Cr (300 mg/kg) + Castor-oil (10 ml/kg)	91***
6	Rd.n-Hex (50 mg/kg) + Castor-oil (10 ml/kg)	119*
7	Rd.n-Hex (100 mg/kg) + Castor-oil (10 ml/kg)	95***
8	Rd.n-Hex (300 mg/kg) + Castor-oil (10 ml/kg)	82***
8	Rd.ETAC (50 mg/kg) + Castor-oil (10 ml/kg)	122
9	Rd.ETAC (100 mg/kg) + Castor-oil (10 ml/kg)	117*
10	Rd.ETAC (300 mg/kg) + Castor-oil (10 ml/kg)	107**
11	Rd.Aq (50 mg/kg) + Castor-oil (10 ml/kg)	126
12	Rd.Aq (100 mg/kg) + Castor-oil (10 ml/kg)	123
13	Rd.Aq (300 mg/kg) + Castor-oil (10 ml/kg)	119*
14	Emodin (10 mg/kg) + Castor-oil (10 ml/kg)	127
15	Emodin (30 mg/kg) + Castor-oil (10 ml/kg)	124
16	Emodin (50 mg/kg) + Castor-oil (10 ml/kg)	122
17	Atropine (0.1 mg/kg) + Castor-oil (10 ml/kg)	74.10***

Values expressed as mean ± SEM (n = 5). One-way ANOVA, with post-hoc *Tukey's test.* $^{###}p < 0.001$ *vs. saline group*, *p < 0.05, **p < 0.01, ***p < 0.001 *vs. castor oil group.*

Effect on Intestinal Fluid Accumulation

In castor oil-induced intestinal fluid accumulation assay, Rd.Cr, Rd.n-Hex, Rd.ETAC exhibited a dose-dependent (50–300 mg/kg) anti-secretory effect. Intestinal fluid accumulation in the saline-treated group was 89.7 ± 0.93 (mean ± SEM, n = 5), whereas in the castor oil-treated group it was raised to 126.8 ± 0.73. The Fluid accumulation was significantly decreased by Rd.Cr, Rd.n-Hex and Rd.ETAC at dose of 50–300 mg/kg to 121.6, 112, 91, 119, 95, 82, 122, 117, and 107, respectively. Rd.Aq and emodin have week anti-secretary effects. Atropine at the dose of 0.1 mg/kg decreased the intestinal fluid accumulation to 74.10 ± 0.42 (**Table 2**).

Effect on Charcoal Meal Transit Time

Rd.Cr and fractions delay the charcoal meal to travel through the small intestine in a dose-dependent manner. Percent inhibition in charcoal meal transit by Rd.Cr, Rd.n-Hex, Rd.ETAC, and Rd.Aq at 50, 100, and 300 mg/kg dose and emodin (10–50 mg/kg) is 1.85, 4.8, 14.9, 9.37, 15.4, 33.05, 26.70, 41.09, 70.03, 3.08, 6.1, 13.18, 4.11, 15.4, and 48.6, respectively. Atropine (0.1 mg/kg, i.p.) shows an inhibitory effect of 81.40% (**Table 3**).

Effect of Extracts and Emodin on the Motility of Isolated Tissue Preparations

Figure 1 shows the inhibitory effect of the plant extract, papaverine, and verapamil against spontaneous and K^+ (80 mM) induced contractions. Rd.Cr was found to be equally effective against spontaneous and K^+ (80 mM) induced contractions with EC values of 0.19 mg/ml (0.149–0.264) and 0.15 (0.0942–0.242), respectively, as shown in **Figure 1A**. Similarly, papaverine also showed a similar pattern of nonspecific inhibitory response (**Figure 1G**) with respective EC50 values of 0.4 μM (0.22–0.81, n = 4) in spontaneous and 0.6 (0.31–1.32, n = 4) in high K^+ (80 mM) induced contractions, whereas verapamil was found more potent against K^+ (80 mM) induced contractions with EC50 value of 0.04 μM (0.031–0.062, n = 4), as compared to spontaneous contractions (0.12 μM (0.10–0.20, n = 3)), as shown in **Figure 1F**. Ethyl acetate fraction (Rd.ETAC) produced similar nonspecific inhibitory response as papaverine with EC50 value of 0.0884 mg/ml (0.0013–0.042) against spontaneous and 0.585 mg/ml (0.267–1.28) against K^+ induced contractions **Figure 1C**, hexane fraction (Rd.n-Hex) shows verapamil like response with EC50 values of 0.8641 mg/ml (0.458–1.629) against spontaneous contractions and 0.249 mg/ml (0.11–0.583) against K^+ induced contractions **Figure 1B** whereas aqueous fraction (Rh.Aq) and emodin shows weak response against

TABLE 3 | Effect of *Rumex dentatus* crude extract (Rd.Cr) and fractions: n-hexane (Rd.n-Hex), ethyl acetate (Rd.ETAC), aqueous (Rd.Aq), emodin, and atropine on charcoal meal transit time in rats.

Treatment (mg/kg)	Mean length of intestine (cm)	Distance moved by charcoal (cm)	Peristaltic index (PI) (%)	% Inhibition
Saline (10 ml/kg) + Charcoal (25 mg/kg)	92.6	90	97.1	0
Rd.Cr (50 mg/kg) + Charcoal (25 mg/kg)	94.4	90	95.3	1.85
Rd.Cr (100 mg/kg) + Charcoal (25 mg/kg)	97.8	90.4	92.4	4.8
Rd.Cr (300 mg/kg) + Charcoal (25 mg/kg)	91	75.2	82.63	14.9*
Rd.n-Hex (50 mg/kg) + Charcoal (25 mg/kg)	98	86.6	88	9.37
Rd.n-Hex (100 mg/kg) + Charcoal (25 mg/kg)	96	78.8	82.08	15.4*
Rd.n-Hex (300 mg/kg) + Charcoal (25 mg/kg)	98	63.7	65	33.05**
Rd.ETAC (50 mg/kg) + Charcoal (25 mg/kg)	94	66.9	71.17	26.70**
Rd.ETAC (100 mg/kg) + Charcoal (25 mg/kg)	95	54.4	57.2	41.09**
Rd.ETAC (300 mg/kg) + Charcoal (25 mg/kg)	96	28	29.1	70.03***
Rd.Aq (50 mg/kg) + Charcoal (25 mg/kg)	92	86.6	94.1	3.08
Rd.Aq (100 mg/kg) + Charcoal (25 mg/kg)	95	86.6	91.1	6.1
Rd.Aq (300 mg/kg) + Charcoal (25 mg/kg)	94.6	79.8	84.3	13.18*
Emodin (10 mg/kg) + Charcoal (25 mg/kg)	93	86.6	93.1	4.11
Emodin (30 mg/kg) + Charcoal (25 mg/kg)	96	78.8	82.08	15.4*
Emodin (50 mg/kg) + Charcoal (25 mg/kg)	92.1	46	49.9	48.6**
Atropine (0.1 mg/kg, i.p.) + Charcoal (25 mg/kg)	90.8	16.4	18.06	81.40***

Values expressed as mean ± SEM (n = 5). One-way ANOVA, with post-hoc *Tukey's test.* $^{###}p < 0.001$ *vs. saline group*, *p < 0.05, **p < 0.01, ***p < 0.001 *vs. charcoal group.*

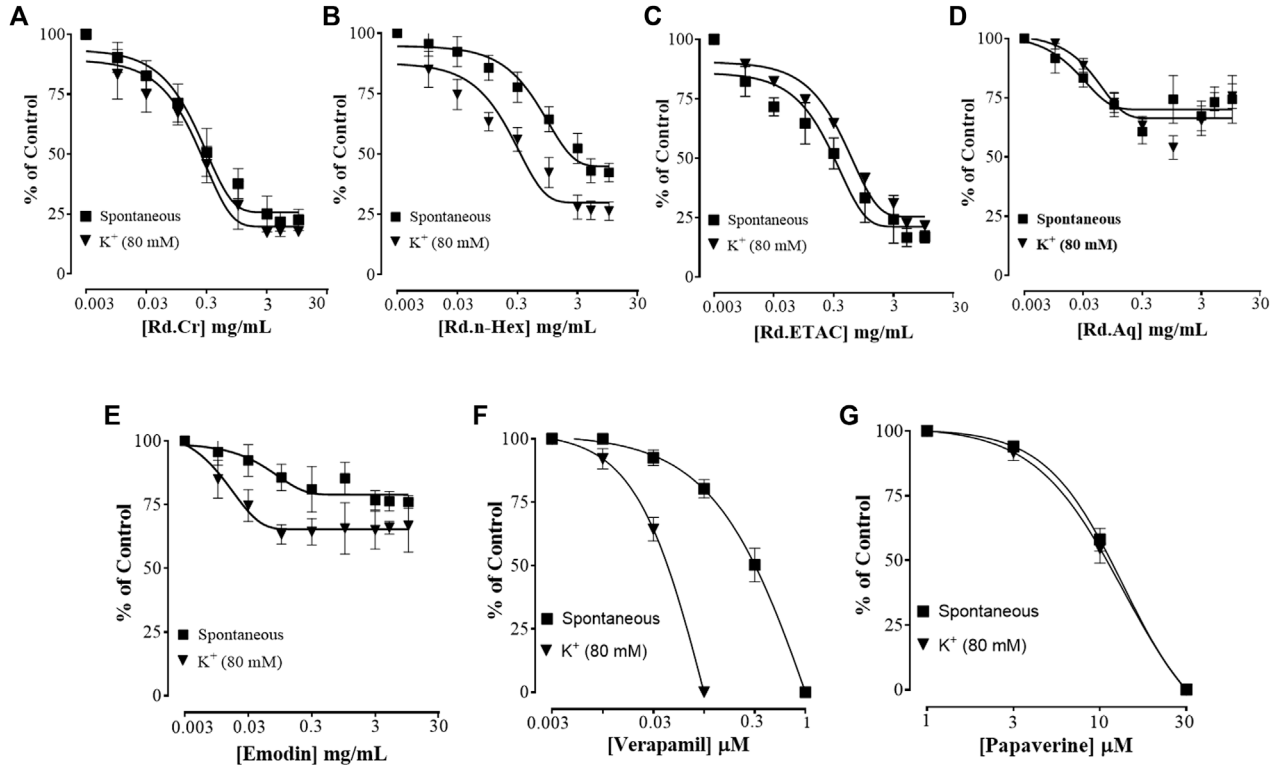

FIGURE 1 | Concentration-dependent inhibitory effect on spontaneous and K^+ (80 mM) induced contractions of **(A)** *Rumex dentatus* crude extract (Rd.Cr) and fractions: **(B)** n-hexane (Rd.n-Hex), **(C)** ethyl acetate (Rd.ETAC), **(D)** aqueous (Rd.Aq), **(E)** emodin **(F)**, verapamil, and **(G)** papaverine in isolated rabbit jejunum preparations. Values are expressed as mean ± SEM (n = 4–5).

both contractions **Figures 1D,E**. When tested for its possible interaction with calcium channels, except Rd.Aq and emodin, caused rightward shift in the Ca^{2+} CRCs, similar to that produced by papaverine or verapamil (**Figure 2**). When tested for possible interaction with isoprenaline, pretreatment of the tissue with Rd.Cr (0.3–1 mg/ml) and Rd.ETAC (0.1–0.3 mg/ml) shifted the isoprenaline-induced inhibitory CRCs to the left, showing potentiating effect. Papaverine also caused a similar concentration-dependent leftward shift in the CRCs of isoprenaline, while pretreatment of tissue with verapamil did not alter the inhibitory response to isoprenaline (**Figure 3**).

Anti *H.pylori* Effect

Zone of inhibition and MIC values were assessed against *H. pylori* isolate which showed more sensitivity by disc diffusion method for the most potent fraction. Rd.n-Hex showed 20 ± 0.62, zone of inhibition against isolate. The MIC value of Rd.n-Hex was 2.5 mg/ml.

Effect on Ethanol-Induced Ulcer

Rd.Cr, fractions, and emodin in dose-dependent manner (50–300 mg/kg) exhibited an antiulcer effect. Rd.Cr, Rd.n-Hex, Rd.ETAC, and Rd.Aq at 50, 100, and 300 mg/kg dose and emodin (10–50 mg/kg) caused 56, 76, 92.6, 57, 77, 95, 55.8, 95, 100, 0, 3.9, 4.9, 58, 80, and 92% inhibition, respectively (**Table 4**). Omeprazole (20 mg/kg) exhibited 96.2% inhibitory effect. Macroscopic observation showed the gastric mucosa of rats (**Figure 4**).

H^+/K^+-ATPase Inhibition

Abnormal activity of H^+/K^+ATPase is closely related to gastric ulcers. In ethanol-treated group (1 ml/100 g) the H^+/K^+ATPase activity was significantly increased. Treatment with Rd.Cr, Rd.n-Hex, Rd.ETAC (300 mg/kg), emodin (10–50 mg/kg) and omeprazole (20 mg/kg) considerably reduced the activity (**Figure 5**).

Antioxidant Profile

The activity of GST, GSH, and catalase was significantly reduced while LPO has increased in ethanol-induced ulcer gastric tissues. Rd.Cr, Rd.n-Hex, Rd.ETAC (300 mg/kg), emodin (50 mg/kg) and omeprazole (20 mg/kg) treated groups restored GST, GSH, catalase, and considerably reduced LPO. Rd.Aq (300 mg/kg) treated group has a weak effect on oxidative stress markers (**Figure 6**).

Histopathological Examination

Figure 7 indicates the H&E staining performed on the gastric tissue. The gastric cells were evaluated for cellular changes or being intact in a normal state. Saline group (10 ml/kg) indicated

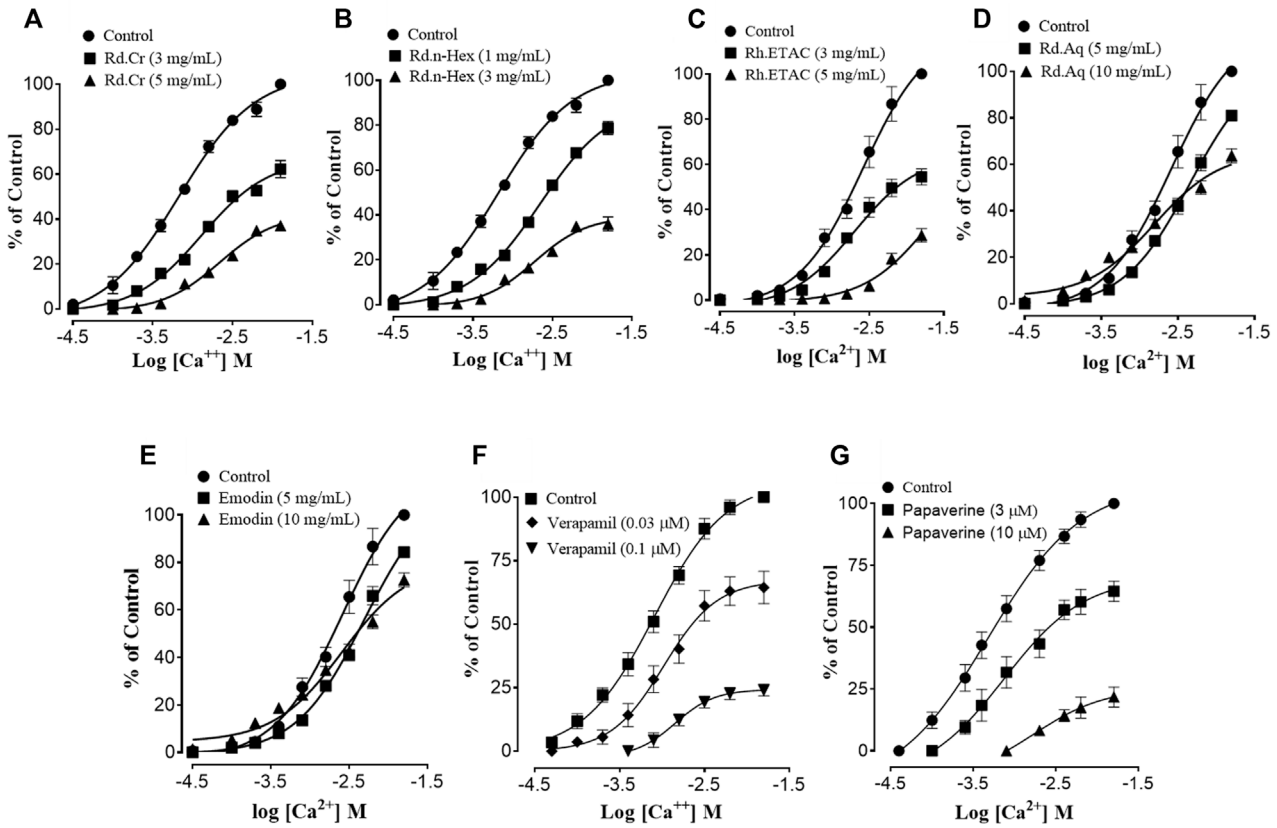

FIGURE 2 | Concentration-response curves of Ca^{2+} in the absence and presence of the increasing concentrations of **(A)** *Rumex dentatus* extract (Rd.Cr) and fractions: **(B)** n-hexane (Rd.n-Hex), **(C)** ethyl acetate (Rd.ETAC), **(D)** aqueous (Rd.Aq), **(E)** emodin, **(F)** verapamil, and **(G)** papaverine in isolated rabbit jejunum preparations. Values are expressed as mean ± SEM (n = 4–5).

intact shape, size, and stain of the gastric cells, ethanol group (1 ml/100 g) indicates vigorous cellular changes as necrotic cells and hemorrhage can be observed with disruption of the morphological cell boundaries. Comparatively, the Rd.Cr, Rd.n-Hex, Rd.ETAC (300 mg/kg), emodin (50 mg/kg), and omeprazole (20 mg/kg) treatment groups revealed relatively intact cell boundaries and cell morphological features as size, shape, vacuolation, and staining. Rd.Aq (300 mg/kg) treated group has relatively weak effects in restoring the cell morphological features.

IHC Analysis

Ethanol (1ml/100 g) treated group revealed hyper-expression of COX-2, TNFα, and p-NFkB in gastric tissues. In Rd.Cr, Rd.n-Hex, Rd.ETAC (300 mg/kg), emodin (50 mg/kg) and omeprazole (20 mg/kg) treated groups their expression reduced (**Figures 8**, **9**).

Effect on Inflammatory Markers

The levels of IL-8 in ethanol (1 ml/100 g) treated group were raised to 862.53 pg/ml. The IL-8 expression was significantly decreased in Rd.Cr, Rd.n-Hex, Rd.ETAC (300 mg/kg), and emodin (50 mg/kg) treated groups to 427.5, 305, 540, and 315 pg/ml, respectively. Omeprazole (20 mg/kg) decreased the expression up to 259.8 pg/m. Rd.Aq (300 mg/kg) treated group shows weak effect on expression of IL-8, that is, 790 pg/ml (**Figure 10A**). The levels of PGE_2 in ethanol (1 ml/100 g) treated group was 825 pg/ml. The PGE2 expression was significantly increased in Rd.Cr, Rd.n-Hex, Rd.ETAC (300 mg/kg), and emodin (50 mg/kg) treated groups was found to be 1,535, 1,157.5, 1,490, and 1,730 pg/ml, respectively. Omeprazole (20 mg/kg) raised the levels up to 1,760 pg/ml. Rd.Aq (300 mg/kg) treated group didn't show any significant results as compared to the control group, that is, 775 pg/ml (**Figure 10B**). The levels of p-NFkB in ethanol (1 ml/100 g) treated group was 3,802.5 pg/ml p-NFkB expression was significantly decreased in Rd.Cr, Rd.n-Hex, Rd.ETAC (300 mg/kg), and emodin (50 mg/kg) treated groups to 2,856, 2,995, 2,137.5, and 1,570 pg/ml, respectively. Omeprazole (20 mg/kg) decreased the levels to 536.15 pg/ml p-NFkB expression in Rd.Aq (300 mg/kg) treated was 3,754.5 pg/ml (**Figure 10C**). TNFα levels in ethanol (1 ml/100 g) treated group were raised to 3,896.37 pg/ml. Expression of TNFα was significantly decreased in Rd.Cr, Rd.n-Hex, Rd.ETAC (300 mg/kg), and emodin (50 mg/kg) treated groups to 2,435, 1,580, 2,200, and 1,280 pg/ml, respectively. Omeprazole (20 mg/kg) reduced the levels to 1,422.67 pg/ml. Rd.Aq (300 mg/kg) treated

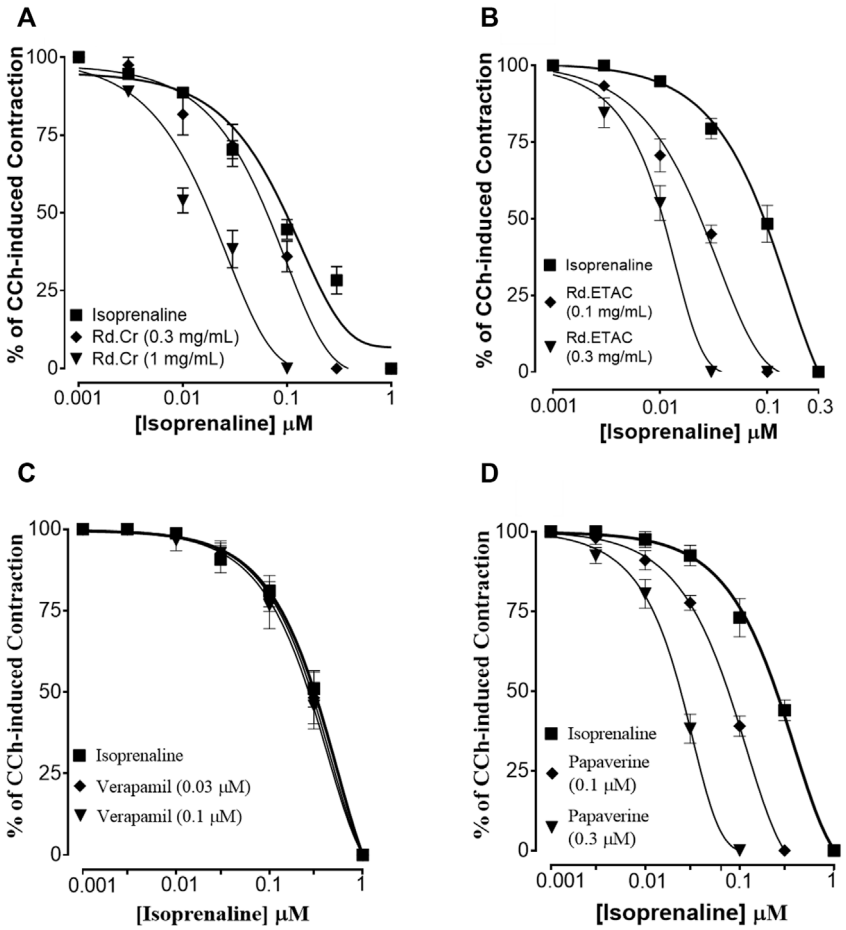

FIGURE 3 | Concentration-response curves of isoprenaline against carbachol (CCh)-induced contractions in the presence of different concentrations of **(A)** *Rumex dentatas* extract crude (Rd.Cr), **(B)** ethyl acetate fraction (Rd.ETAC), **(C)** verapamil, and **(D)** papaverine in isolated rabbit jejunum preparations. Values are expressed as mean ± SEM (n = 4–5).

group shows less effect on TNFα expression, that is, 3685 pg/ml (**Figure 10D**).

Western Blot Analysis

Western blot analysis (gastric tissues) confirmed COX-2, TNFα, and p-NFκB levels were increased in ethanol-treated group, but Rd.Cr, Rd.n-Hex, Rd.ETAC (300 mg/kg), emodin (50 mg/kg), and omeprazole (20 mg/kg) treated groups showed a decrease in expression levels as compared to a negative control group (**Figure 11**).

Quantification of mRNA Levels

RT-PCR determined the fold expression of H^+/K^+-ATPase in ethanol-induced gastric ulcer model. The ethanol (1 ml/100 g) administered group indicates increased expression of H^+/K^+-ATPase mRNA levels. Rd.Cr, Rd.ETAC (300 mg/kg), and emodin (50 mg/kg) caused a significant decrease in expression levels. Omeprazole (20 mg/kg) also reduced the expression compared to the negative control group (**Figure 12**).

Toxicity Studies

The OECD guidelines 425 were used to evaluate the safety profile of *Rumex dentatus*. No mortality was observed. All results are as follows:

Behavioral Pattern and Body Weight

After receiving 2000 mg/kg of extract the body weights of test animals in both the control and extract treatment groups increased gradually during the study period. Behavioral observations show that fur and skin, eyes, salivation, fecal consistency, urine color, breathing, mucous membrane, and sleep pattern were all normal. There were no symptoms of convulsions or distress in any group of animals (**Supplementary Table S3**).

Effects on Organs Weight

On examining the weight of organs no significant variation was found in drug-treated animals as compared to control group (**Table 5**).

TABLE 4 | Effect of *Rumex dentatus* crude extract (Rd.Cr) and fractions: n-hexane (Rd.n-Hex), ethyl acetate (Rd.ETAC), aqueous (Rd.Aq), emodin, and omeprazole against ethanol-induced ulcer in rats.

Treatment (mg/kg)	Ulcer index	% Inhibition
Saline (10 ml/kg)	0.0 ± 0.2	100
Ethanol (1 ml/100 g)	10.2 ± 0.2$^{###}$	0
Rd.Cr (50 mg/kg) + ethanol (1 ml/100 g)	4.6 ± 0.09***	56
Rd.Cr (100 mg/kg) + ethanol (1 ml/100 g)	2.6 ± 0.06***	76
Rd.Cr (300 mg/kg) + ethanol (1 ml/100 g)	0.94 ± 0.05***	92.6
Rd.n-Hex (50 mg/kg) + ethanol (1 ml/100 g)	4.5 ± 0.13***	57
Rd.n-Hex (100 mg/kg) + ethanol (1 ml/100 g)	2.5 ± 0.22***	77
Rd.n-Hex (300 mg/kg) + ethanol (1 ml/100 g)	0.7 ± 0.06***	95
Rd.ETAC (50 mg/kg) + ethanol (1 ml/100 g)	4.5 ± 0.20***	55.8
Rd.ETAC (100 mg/kg) + ethanol (1 ml/100 g)	0.5 ± 0.07***	95
Rd.ETAC (300 mg/kg) + ethanol (1 ml/100 g)	0.0 ± 0.00	100
Rd.Aq (50 mg/kg) + ethanol (1 ml/100 g)	10.5 ± 0.21	0
Rd.Aq (100 mg/kg) + ethanol (1 ml/100 g)	9.8 ± 0.5	3.9
Rd.Aq (300 mg/kg) + ethanol (1 ml/100 g)	9.7 ± 0.23	4.9
Emodin (10 mg/kg) + ethanol (1 ml/100 g)	4.4 ± 0.16***	58
Emodin (30 mg/kg) + ethanol (1 ml/100 g)	2.2 ± 0.2***	80
Emodin (50 mg/kg) + ethanol (1 ml/100 g)	1 ± 0.06***	92
Omeprazole (20 mg/kg) + ethanol (1 ml/100 g)	0.58 ± 0.04***	96.2

Values expressed as mean ± SEM (n = 5). One-way ANOVA, with post-hoc *Tukey's test* $^{###}p < 0.001$ *vs. saline group*, ***$p < 0.001$ *vs. ethanol group.*

Biochemical Analysis and Antioxidant Profile

There were normal LFTs, RFTs, and lipid profiles (**Figure 13** and **Table 6**). There were no changes in antioxidant profiling (**Figure 13**).

Hematological Analysis

It can be seen that no significant changes were observed in hematological profile when compared to control group (**Table 6**).

Histopathological Study

Histopathological examination of vital organs such as the brain, liver, kidney, and heart revealed no evidence of vacuolation, dystrophy, or atrophy (**Figure 14**). *Rumex dentatus* was found to be safe to consume up to a dose of 2,000 mg/kg in a comprehensive toxicity profile.

Molecular Docking

In the present study, emodin exhibited variable binding affinities against different protein targets. emodin against H^+/K^+-ATPase pump and voltage-gated L-type calcium channel showed E-value of −7.9, and −7.4 kcal/mol, respectively. Omeprazole against H^+/K^+-ATPase pump exhibited E-value of −7.8 kcal/mol. Verapamil against voltage-gated L-type calcium channel showed E-value of −6.2 kcal/mol. **Supplementary Table S4** shows the atomic energy/E-values (kcal/mol), hydrogen bonding, and residues involved in H-bonding with best-docked poses of drug-protein complex. **Supplementary Figures S2, S3** illustrates 2D-view of interactions of emodin and standard drug with their protein targets.

Molecular Dynamic Simulations

The structural flexibility of targeted proteins and the stability of docked complexes were investigated using molecular dynamics (MD) simulation. The selected best-docked poses for the

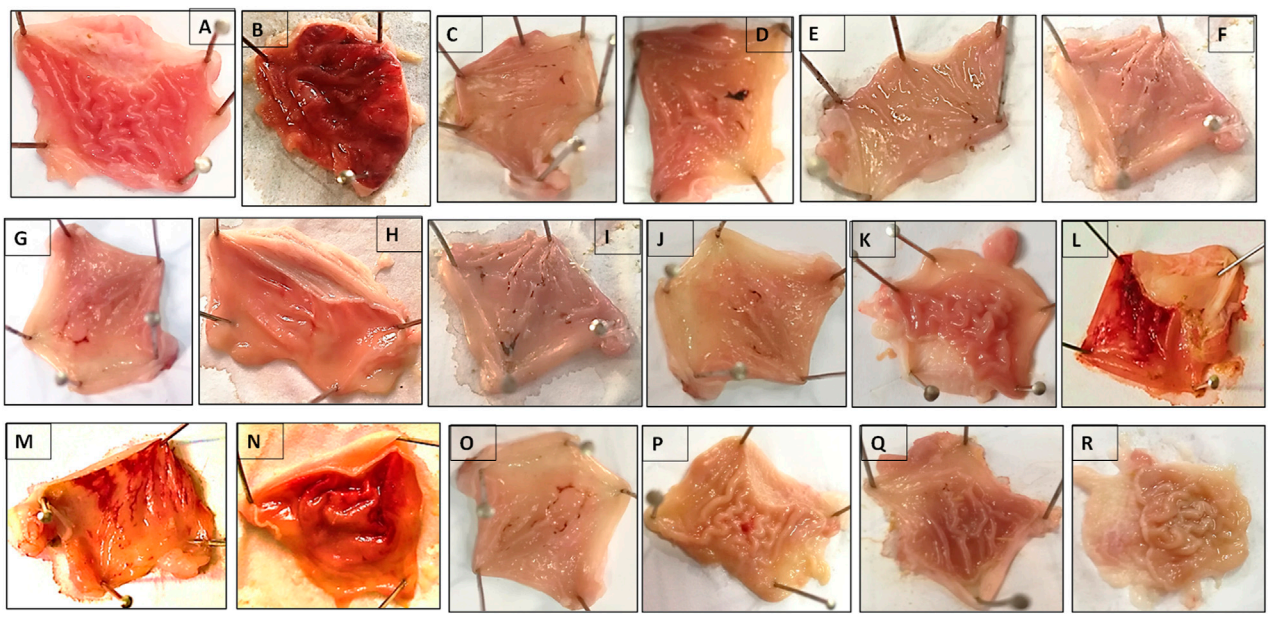

FIGURE 4 | Gross-appearance of gastric mucosa in rats: Pretreated with **(A)** saline (10 ml/kg), **(B)** ethanol (1 ml/100 g) severe injuries are seen, as ethanol produced excessive hemorrhagic necrosis of gastric mucosa, pretreated with **(C)** *Rumex dentatus* crude extract (Rd.Cr 50 mg/kg), **(D)** Rd.Cr 100 mg/kg, **(E)** Rd.Cr 300 mg/kg and fractions: **(F)** ethyl acetate (Rd.ETAC 50 mg/kg), **(G)** Rd.ETAC 100 mg/kg, **(H)** Rd.ETAC 300 mg/kg, **(I)** n-Hexane (Rd.n-Hex 50 mg/kg), **(J)** Rd.n-Hex 100 mg/kg, **(K)** Rd.n-Hex 300 mg/kg, (L) aqueous (Rd.Aq 50 mg/kg), **(M)** Rd.Aq 100 mg/kg, **(N)** Rd.Aq 300 mg/kg, **(O)** emodin 10 mg/kg, **(P)** emodin 30 mg/kg, **(Q)** emodin 50 mg/kg, and **(R)** omeprazole 20 mg/kg.

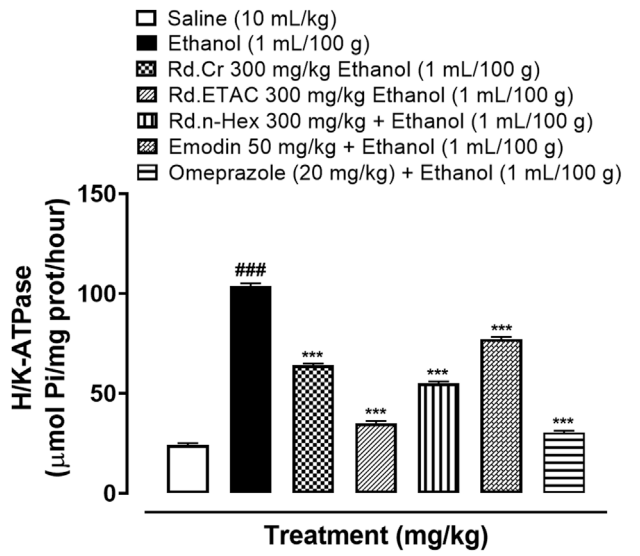

FIGURE 5 | Effect of *Rumex dentatus* crude extract (Rd.Cr), n-hexane (Rd.n-Hex), ethyl acetate (Rd.ETAC) fraction, emodin, and omeprazole against H^+/K^+-ATPase in ethanol treated rats' gastric tissues. Values expressed as mean ± SEM (n = 3). One-way ANOVA with *post-hoc* Tukey's test. $^{###}p < 0.001$ vs. saline group, $^{***}p < 0.001$ vs. Ethanol group.

complexes were used to initiate the simulation process for the period of 50 ns. The dynamic stabilities of the systems were calculated and plotted using root-mean square deviation (RMSD) analysis. For the emodin-H^+/K^+ATPase and emodin-voltage gated L-type calcium channel top-ranked docked complex, trajectories analysis using RMSD plot confirms the stability of protein backbone atoms throughout the simulation run (50 ns) with an average RMSD value of 4.118 Å and 4.185 Å, respectively **Supplementary Figures S4A, S5A**. The emodin trajectory analysis reveals a nearly constant RMSD throughout the simulation process. A constant ligand RMSD, with an average RMSD of 0.380 Å (emodin- H^+/K^+ATPase) and 0.236 Å (emodin-voltage gated L-type calcium channel), indicates that the ligand did not flip or move during simulations (**Supplementary Figures S4B, S5B**). The RMSF plot revealed that the residues involved in binding were more stable than the rest of the protein's residues. The average RMSF value was estimated to be 29.925 Å (emodin-H^+/K^+ATPase) and 23.068 Å (emodin-voltage gated L-type calcium channel) which also highlighted the high degree of flexibility of protein due to loop regions (**Supplementary Figures S4C, S5C**). All of the energy values were calculated as the average of 150 snapshots from the MD trajectories of the last 10 ns. The total free energies (ΔTOTAL) calculated for emodin- H^+/K^+ATPase docked complex in the case of MMGBSA and MMPBSA were −21.2321 and −22.6338 kcal mol^{-1}, respectively (**Supplementary Table S5**). On the other hand, the MMGBSA and MMPBSA values estimated for emodin-voltage gated L-type calcium channel were −14.2361 kcal mol^{-1} and −13.5124 kcal mol^{-1}, respectively, (**Supplementary Table S6**). The overall estimated energy values were found to be within

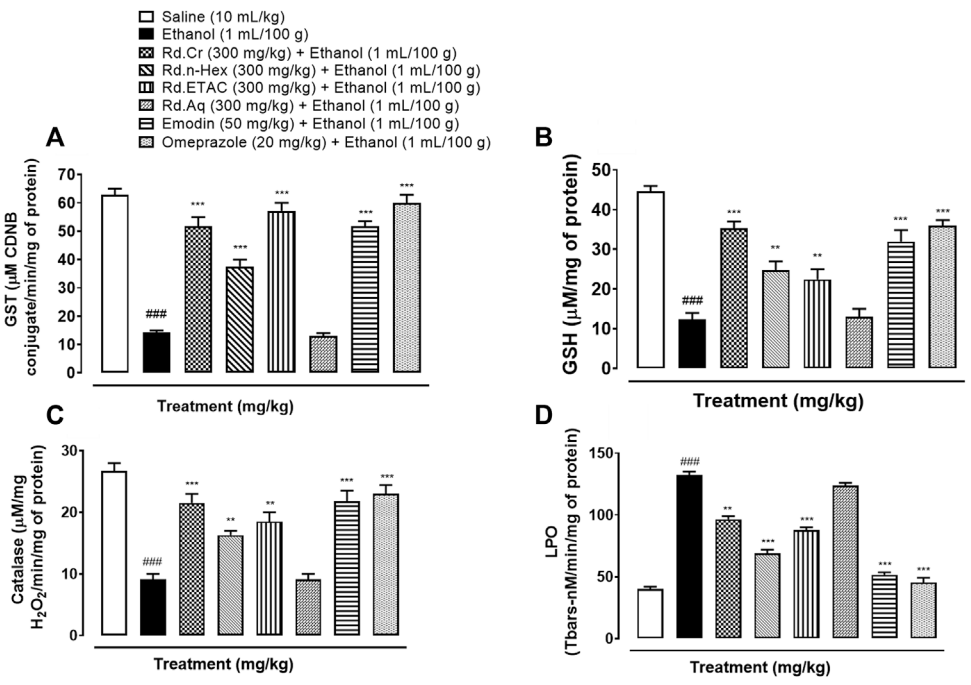

FIGURE 6 | Effect of *Rumex dentatus* crude extract (Rd.Cr), n-hexane (Rd.n-Hex), ethyl acetate (Rd.ETAC), aqueous fraction (Rd.Aq), emodin, and omeprazole groups against **(A)** glutathione-S-transferase (GST), **(B)** reduced glutathione (GSH), **(C)** catalase, and **(D)** lipid peroxidation (LPO) in ethanol-treated rats' gastric tissues. Values expressed as mean ± SEM (n = 3). One-way ANOVA with *post-hoc* Tukey's test. $^{###}p < 0.001$ vs. saline group.

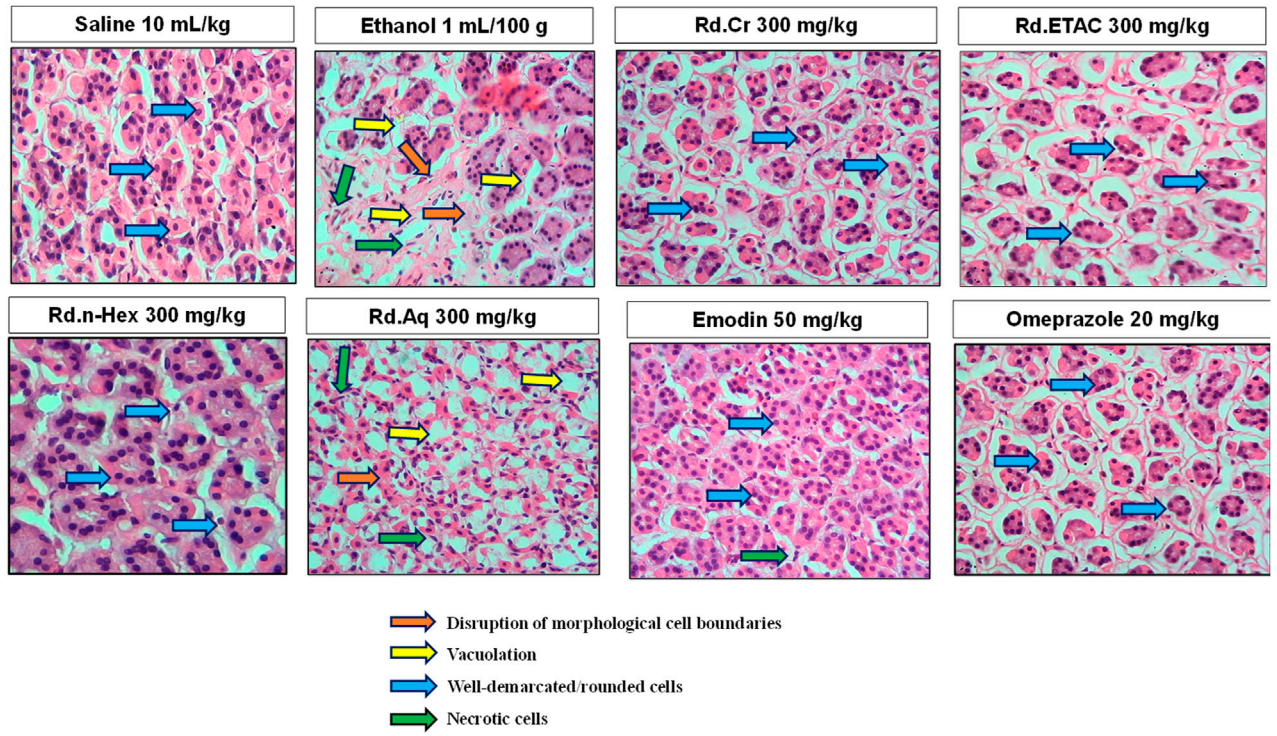

FIGURE 7 | Histopathological slides showing the effect of *Rumex dentatus* crude extract (Rd.Cr), n-hexane (Rd.n-Hex), ethyl acetate (Rd.ETAC), aqueous fraction (Rd.Aq), emodin, and omeprazole in ethanol-treated rats gastric tissues using hematoxylin and eosin staining histopathological technique. Bar 50 μm, magnification ×40.

an acceptable range and confirming the docked complexes' stability. Overall the MD simulation findings and MMPBSA/GBSA calculations are consistent with the *in-vitro, in-vivo,* and docking results.

DISCUSSION

Multiple disorders are involved in GIT as it is expanded in various body organs and covers a larger area. The prevalence of GIT disorders are increasing around the globe. IBS, gastric and peptic ulcers, colorectal cancers, constipation, diarrhea, GERD, and *H. pylori* infection are some of the GIT disorders that are prevalent worldwide (Jones et al., 2017). Based on *Rumex dentatus* ethnopharmacological use in gastrointestinal problems such as dysentery, gastritis, inflammation, and wound healing (Zhang et al., 2012). The antidiarrheal, antisecretory, antispasmodic, charcoal meal gastrointestinal motility, antiulcer effects, and toxicity of *Rumex dentatus* crude extract, fractions, and one of the primary phytoconstituents were studied. To rationalize the plant's aforementioned ethnomedicinal uses, *in-silico, in-vitro, in-vivo,* and molecular approaches were used to elucidate possible underlying mechanism(s). Alkaloids, anthraquinones, cardiac glycosides, coumarins, flavonoids, saponins, tannins, and terpenoids are among the phytoconstituents found in *Rumex dentatus* extract. GC-MS analysis revealed the presence of different compound peaks. Amongst compound peaks oleic acid, phthalic acid, octanoic acid, 6-octadecenoic acid, certain glycosides polysaccharides, and other compounds obtained are reported to have effect as anti-inflammatory, anti-ulcer, and in other gastrointestinal diseases (Cipriani et al., 2008; Kaithwas and Majumdar, 2010; Nassar et al., 2013; Boniface et al., 2020). The obtained effectiveness in GI ailments can be attributed to the phytochemical profile of this plant. Spectral analysis of *Rumex dentatus* in literature reveals the presence of emodin as one of the main phytoconstituents. HPLC and LCMS data indicating the presence of emodin are available (Jeelani et al., 2017). Emodin has been examined for its effectiveness in gastrointestinal ailments. Therefore, we examined different fractions of *Rumex dentatus* along with emodin for its pharmacological efficacy in GIT up to the molecular level. Rd.Cr, Rd.ETAC and Rd.n-Hex showed protective effects against castor oil-induced diarrhea, similar to loperamide, a standard medicine, and its likely underlying mechanism was determined using isolated tissue preparations that were also linked to a reduction in gastrointestinal motility. In mice, these extracts were found to protect against castor oil-induced intestinal fluid secretion. Antidiarrheal and antisecretory actions are mediated by a gut relaxant constituent found in *Rumex dentatus.* Rd.Aq fraction and emodin on the other hand did not show potent antidiarrheal and antisecretory effects. In test doses, Rd.n-Hex, Rd.ETAC, and emodin in the small intestine suppress the propulsion of charcoal marker, similar to the standard medicine atropine sulfate (Ansari et al., 2021), which has a strong anticholinergic activity on intestinal transit. A decrease in GIT motility tone increases the retention of substances in the intestine, allowing for improved water

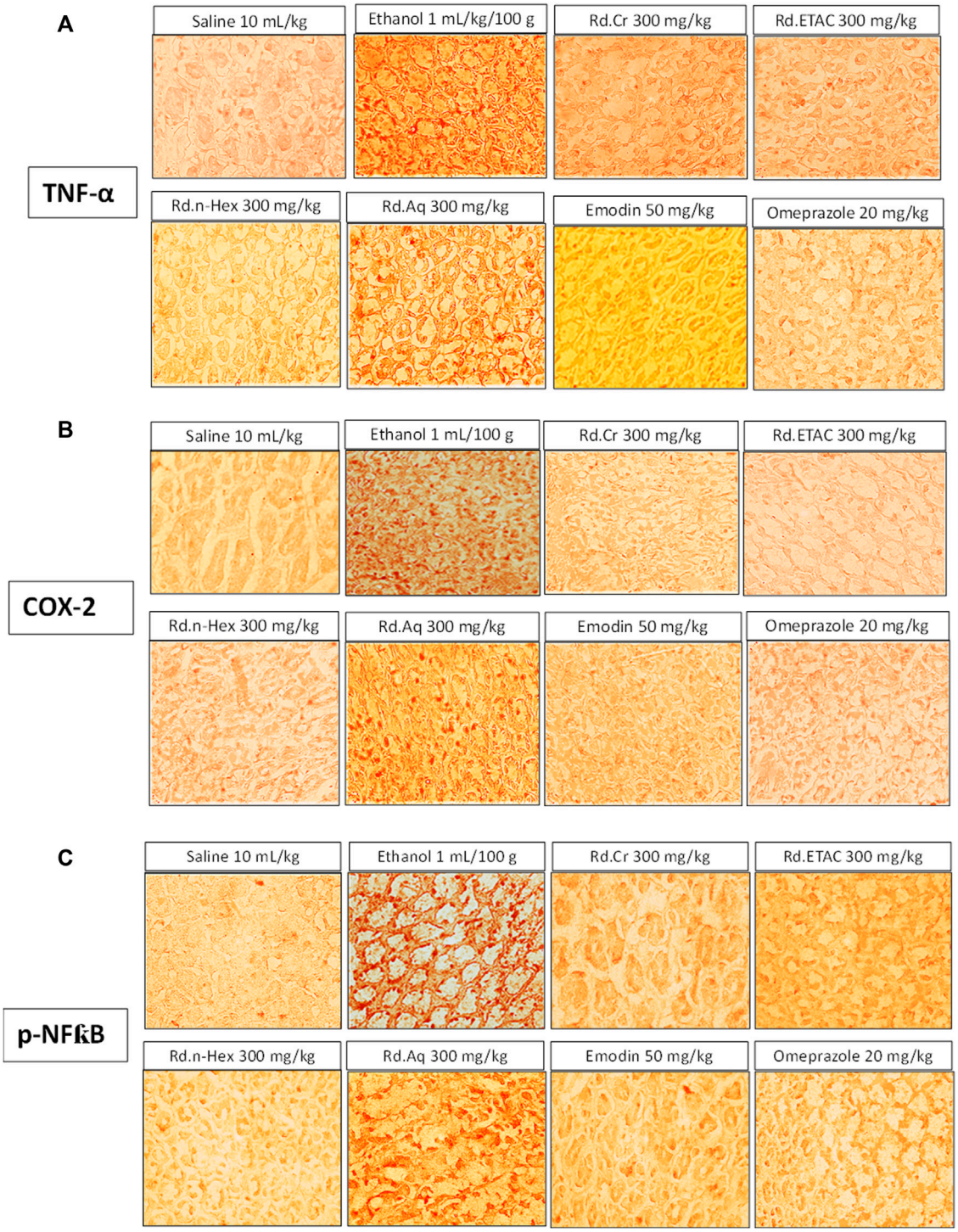

FIGURE 8 | Effect of *Rumex dentatus* crude extract (Rd.Cr), n-hexane (Rd.n-Hex), ethyl acetate (Rd.ETAC), aqueous fraction (Rd.Aq), emodin, and omeprazole on apoptotic markers. **(A)** Tumor necrosis factor-alpha (TNF-α), **(B)** cyclooxygenase 2 (COX-2), and **(C)** phosphorylated-nuclear factor-kappa B (p-NFκB) in ethanol-treated rats gastric tissues using immunohistochemical technique. Bar 50 μm, magnification ×40.

absorption. Rd.Cr and Rd.Aq didn't show much potent effect. These findings suggested that the plant had an antimotility effect *via* altering the peristaltic movement of the gut. The importance of many physiological mediators, such as acetylcholine, histamine, substance P-cholecystokinins, prostaglandins, and 5-hydroxytryptamine, as well as some ion channels, such as

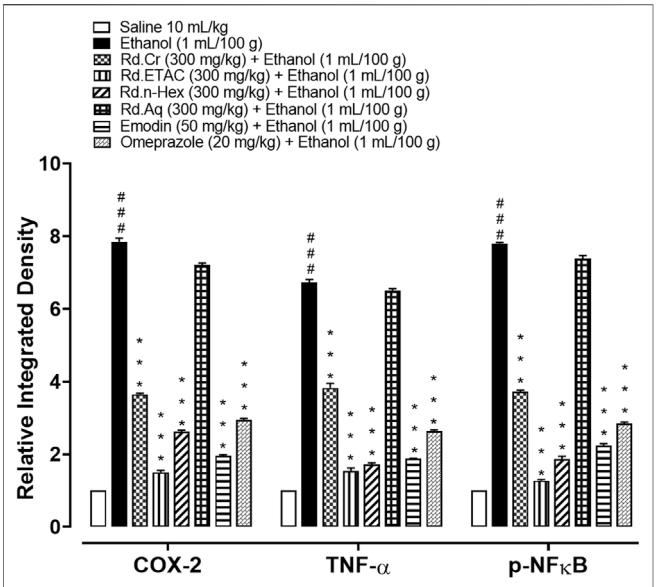

FIGURE 9 | Inhibitory effect of *Rumex dentatus* crude extract (Rd.Cr), n-hexane (Rd.n-Hex), ethyl acetate (Rd.ETAC), aqueous fraction (Rd.Aq), emodin, and omeprazole against cyclooxygenase 2 (COX-2), tumor necrosis factor-alpha (TNF-α) and phosphorylated-nuclear factor-kappa B (p-NFkB) expression in ethanol-treated rats' gastric tissues, using immunohistochemical technique. Values expressed as mean ± SEM (n = 3). One-way ANOVA with *post-hoc* Tukey's test. $^{###}p < 0.001$ vs. saline group, $^{***}p < 0.001$ vs. ethanol group.

K^+ or Ca^{++}, in gastrointestinal system regulation, is well recognized. Furthermore, most spasmolytic drugs have been shown to have therapeutic potential in diarrhea by relaxing the smooth muscle of the gut, which helps to keep luminal fluid in the bowl (Rehman et al., 2012). In spontaneously contracting rabbit jejunum preparations, the extracts were examined for their probable spasmolytic effect, Rd.Cr and Rd.ETAC suppressed both spontaneous and K^+-induced contractions with similar potency. Similarly, papaverine, a PDE and Ca^{++} influx inhibitor (Ansari et al., 2019), produced a similar pattern of inhibition with comparable potency against spontaneous and K^+-induced contractions, whereas Rd.n-Hex shows verapamil-like effect, a standard Ca^{++} antagonist (Mehmood et al., 2015), was relatively selective in its inhibitory effect on K^+-induced contractions. Pretreatment of the tissue with the extracts shifted the Ca^{++} CRCs to the right, similar to that generated by papaverine or verapamil, indicating the presence of calcium antagonist constituent(s). The fact that plant extract has a comparable inhibitory pattern to papaverine against spontaneous and K^+-induced contractions suggests that it may have another mechanism implicated in the spasmolytic effect, such as PDE inhibition. The PDE inhibitory-like effect was confirmed when the Rd.Cr and Rd.ETAC potentiated the isoprenaline-induced relaxant effect, which was similar to that produced by papaverine, whereas Rd.n-Hex, Rd.Aq, emodin, and verapamil had no such effect. Ulcer therapy's primary objectives are to treat pain, heal the ulcer, and prevent it from recurring. H^+/

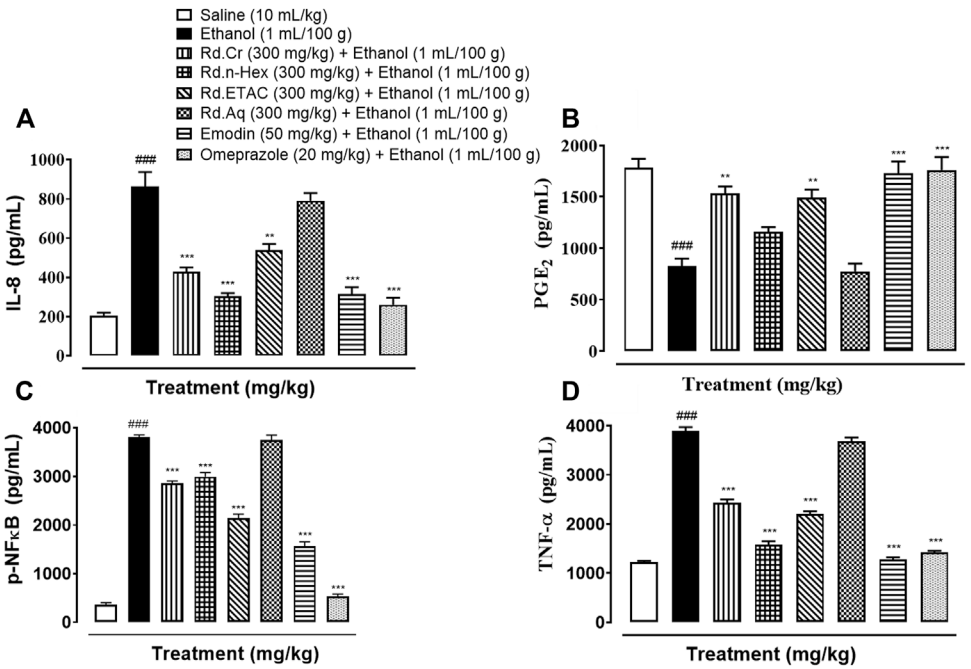

FIGURE 10 | Effect of *Rumex dentatus* crude extract (Rd.Cr), n-hexane (Rd.n-Hex), ethyl acetate (Rd.ETAC), aqueous fraction (Rd.Aq), emodin, and omeprazole groups against **(A)** interleukin 8 (IL-8), **(B)** prostaglandin E2 (PGE2), **(C)** phosphorylated-nuclear factor kappa B (p-NFkB), and **(D)** tumor necrosis factor alpha (TNF-α) in ethanol treated rats gastric tissues, measured by enzyme-linked immunosorbent assay (ELISA) technique. Values expressed as mean ± SEM (n = 3). One-way ANOVA with *post-hoc* Tukey's test. $^{###}p < 0.001$ vs. saline group, $^{**}p < 0.01$, $^{***}p < 0.001$ vs. Ethanol group.

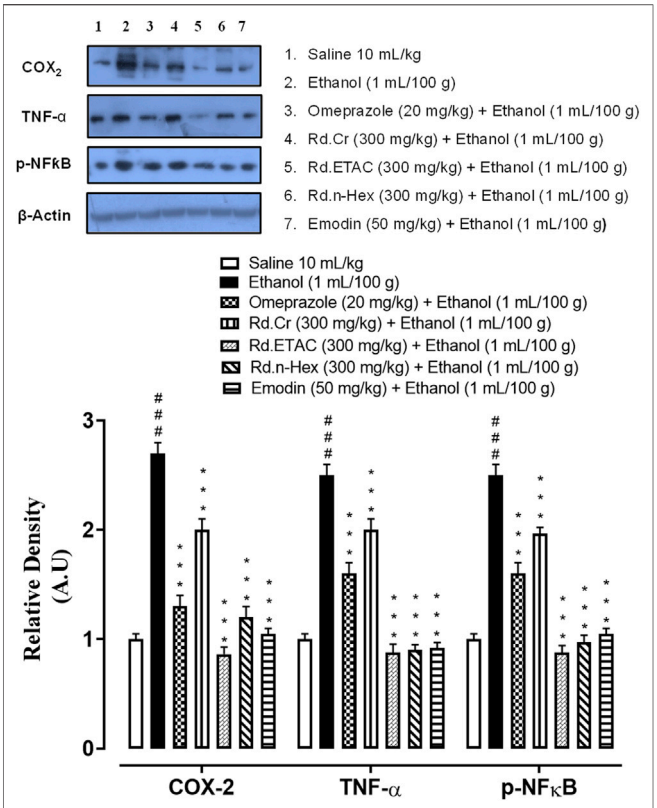

FIGURE 11 | Inhibitory effect of *Rumex dentatus* crude extract (Rd.Cr), ethyl acetate (Rd.ETAC), n-hexane fraction (Rd.n-Hex), emodin, and omeprazole against cyclooxygenase 2 (COX-2), tumor necrosis factor-alpha (TNF-α), phosphorylated-nuclear factor-kappa B (p-NFkB) and β-actin expression in ethanol-treated rats' gastric tissues, using western blot technique. Values expressed as mean ± SEM (n = 3). One-way ANOVA with *post-hoc* Tukey's test. $^{###}p < 0.001$ vs. saline group, $^{***}p < 0.001$ vs. Ethanol group.

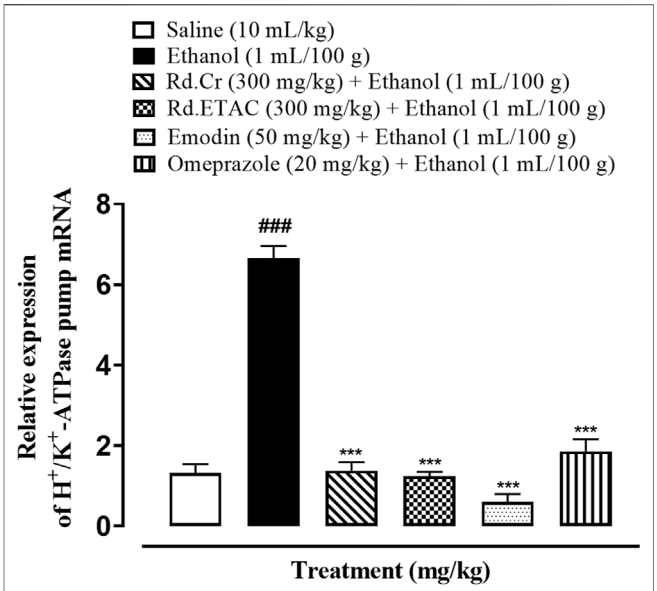

FIGURE 12 | Inhibitory effect of *Rumex dentatus* crude extract (Rd.Cr), n-hexane (Rd.n-Hex) fraction, emodin, and omeprazole against mRNA of H^+/K^+ATPase expression in ethanol-treated rats' gastric tissues, using real-time-polymerase chain reaction (RT-PCR) technique. Values expressed as mean ± SEM (n = 3). One-way ANOVA with *post-hoc* Tukey's test. $^{###}p < 0.001$ vs. saline group, $^{***}p < 0.001$ vs. ethanol group.

TABLE 5 | Effects on organs weight of rats in extract (at limit dose 2000 mg/kg b.w. p.o.) treated and control groups.

Organs	Control	Rd.Cr (2,000 mg/kg)
Heart	0.34 ± 0.2 g	0.41 ± 0.4 g
Kidney	1.2 ± 0.1 g	1.15 ± 0.3 g
Liver	6.4 ± 0.3 g	6.9 ± 0.2 g
Brain	1.42 ± 0.2 g	1.49 ± 0.1 g

K^+ ATPase is a proton pump involved in gastric acid secretion and the only major common pathway for hydrochloric acid secretion in the stomach. Because of the key mechanistic significance of gastric acid regulation in the GIT, it was evident that inhibiting proton transport into the stomach by interfering with the proton pump mechanism was the ideal target for the development of new anti-ulcer medications as well as relief from GERD symptoms (Mishra, 2016). Consequently, in the present experiment Rd.Cr, Rd.ETAC, Rd.n-Hex, and emodin is being analyzed for an *in-vitro* H^+/K^+-ATPase inhibitory assay, Rd.n-Hex and Rd.ETAC shows proton pump inhibitory action equivalent to that of the standard medicine omeprazole, an irreversible proton pump inhibitor. RT-PCR study revealed that the expression levels of H^+/K^+-ATPase in Rd.Cr, Rd.ETAC, and emodin were dramatically reduced, indicating that the anti-ulcer mechanism of the plant is displayed through proton pump inhibition pathway at the molecular level. As a result, RT-PCR research confirmed that *Rumex dentatus* exerts its gastroprotective action through a proton pump inhibitory mechanism. Various aggressive (acid, pepsin, and *Helicobacter pylori* infection) and protective (mucin secretion, prostaglandin, epidermal growth factors, and bicarbonate) factors play a key role in the production and release of acids in the gastrointestinal tract. Disturbance in these variables causes the mucosal barrier to break down, exposing the gastric lining to various enzyme and acid productions, resulting in ulcers (Ansari et al., 2019). The plant's beneficial effect was investigated using an ethanol-induced gastric model, which stimulated ulcers through a variety of mechanisms such as free radicals OH, NO production, mucus exhaustion, mucosal damage, and the release of superoxide anion, which ultimately prolonged tissue oxidative stress and numerous studies have suggested that proinflammatory mediators such as interleukin-8 (IL-8), TNF-α, COX-2 upregulation, and NF-ƙB activation, play a role in inflammatory cascades (Khan et al., 2011). The etiology of gastric ulcers is complicated by oxidative stress (Sisay et al., 2017). Rd.Cr, Rd.ETAC, Rd.n-Hex, and emodin reduced gastric lipid peroxidation and increased GSH, GST, and catalase levels, implying that the plant's anti-ulcerogenic properties are linked to its antioxidant profile. The antiulcer activity of extract may

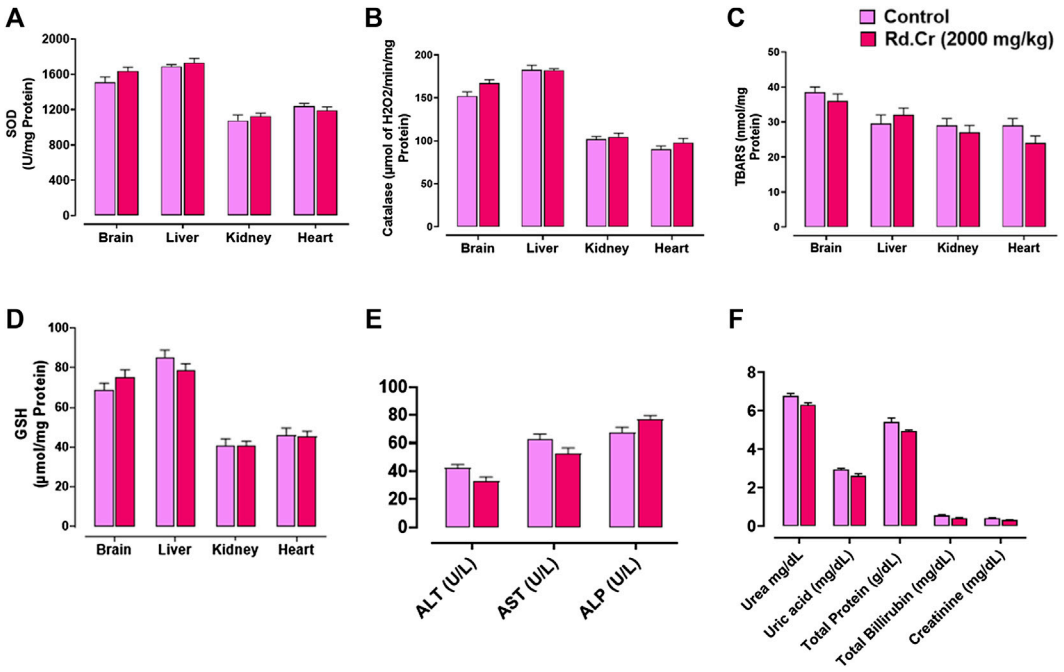

FIGURE 13 | Effect of *Rumex dentatus* crude extract (Rd.Cr) on **(A)** superoxide dismutase (SOD), **(B)** catalase, **(C)** lipid peroxidation (LPO), **(D)** reduced glutathione (GSH), **(E)** liver function tests (LFTs), and **(F)** renal function tests (RFTs) in rats' tissues.

TABLE 6 | Effects of the extract (at limit dose 2,000 mg/kg b.w. p.o) and control groups on lipid profile and complete blood count (CBC) in rats.

Parameters	unit	Control	Rd.Cr (2,000 mg/kg)
Cholesterol	mg/dl	155 ± 1.5	170 ± 1.8
Triglycerides	mg/dl	130 ± 1	145 ± 1.2
H.D.L (cholesterol)	mg/dl	27 ± 0.68	31 ± 0.53
L.D.L (cholesterol)	mg/dl	107 ± 1.24	115 ± 0.78
V.L.D.L	mg/dl	30 ± 0.45	25 ± 1.2
Hb	g/dL	11 ± 0.08	11.9 ± 0.13
Total RBC	$*10^6$/uL	5.02 ± 0.2	5.5 ± 0.06
HCT	%	30.2 ± 0.8	37.5 ± 0.6
MCV	Fl	53 ± 0.05	46.5 ± 1.15
MCHC	g/dL	33 ± 0.32	29.5 ± 1.16
Platelets	$*10^5$/uL	290 ± 2.5	245 ± 1.9
WBC count (TLC)	$*10^3$/uL	2.2 ± 0.11	3.5 ± 0.2
Neutrophils	%	10 ± 0.053	10.6 ± 0.04
Lymphocytes	%	82 ± 1.8	86 ± 0.9
Monocytes	%	4 ± 0.12	3 ± 0.08
Eosinophils	%	2 ± 0.11	1 ± 0.04
MCH	pg	15.7 ± 0.6	16 ± 0.018

refer to its mechanism similar to CCB, as Ca^{+2} antagonist is known for such effects as explored earlier (Alican et al., 1994). Monitoring inflammatory mediators may potentially be a useful tool for preventing gastric lesions (Ansari et al., 2021). The protein expression of IL-8, TNF-α, PGE-2, and p-NF-kB was measured using an ELISA method. Rd.Cr, Rd.ETAC, Rd.n-Hex, and emodin cause a considerable reduction in the expression of IL-8, TNF-α, and p-NF-ƙB. The anti-inflammatory profile of the plant was validated by Western blot analysis and comparable findings were revealed with reduced expression of COX2, TNF-α, p-NF-KB, and increased expression of PGE2 in the treated groups. Hence, the plant's protective action could be attributable to its anti-inflammatory properties. These results are further supported by immunohistochemistry screening of gastric tissues. By lowering the expression of the inflammatory markers COX-2, TNF-α, and p-NF-KB and enhancing the expression of PGE2, the plant protects the gastric tissues. Finally, histological analysis of gastric tissues revealed that the extracts-treated groups had improved cellular infiltration and cell morphology. Dealing with multidrug-resistant (MDR) microorganisms is a key issue in the chemotherapeutic management of infectious diseases, thus researchers are focused on natural products to discover novel antibacterial, antifungal, and anti-parasitic medicines. Plant-based medicines are a rich source of safe and effective treatments that have been employed in crude form as well as pure isolated substances throughout history (Ullah et al., 2019). We used the disc diffusion method to test the antibacterial potential of *Rumex dentatus* against *H. pylori* in this investigation. The results revealed that Rd.n-Hex has substantial antibacterial potential, however, the effect of the remaining fractions and emodin was insignificant. The above-mentioned substances' potent antibacterial effect was also confirmed by determining their MIC. *H. pylori* is the most common cause of peptic ulcers, which are caused by erosion of the gastric and duodenal mucosa. R. Aq on the other hand didn't show promising results in the aforementioned activities that can be justified by the absence of the active phytoconstituent required for effectiveness in GI diseases. Therefore, due to being in an active fraction it was not evaluated further for detailed

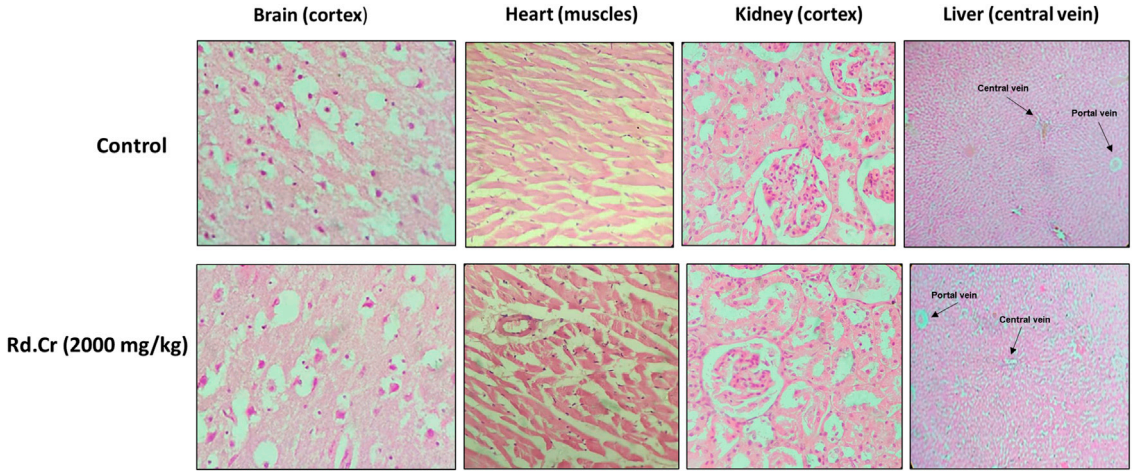

FIGURE 14 | Histopathological slides showing the effect of *Rumex dentatus* crude extract (Rd.Cr) on vital organs of rats using hematoxylin and eosin staining histopathological technique. Bar 50 μm, magnification ×40.

molecular studies. To ensure the safety of herbal drugs, a preliminary toxicological examination is required. Despite the fact that *Rumex dentatus* have valuable pharmacological effects, there has been a lack of knowledge about its toxicity potential. As a result, the current study was carried out in an animal model to assess the acute toxicity of *Rumex dentatus* crude extract, in accordance with OECD guidelines 425 (Saleem et al., 2017), as an acute oral toxicity study is required to determine the safer dose range to manage the drugs' clinical signs and symptoms. Chemicals are classified into five classes based on their LD50 (Persson et al., 2017) according to a globally harmonized classification method. *Rumex dentatus* belongs to group 5 (LD50 > 2,000 mg/kg), which suggests that it is in the lower toxicity class. The preliminary findings suggested that the herb's safety should be further investigated for long-term use and repeated dose effects. Molecular docking was used to evaluate the ligand's affinity for calcium channels and H^+/K^+-ATPase. Docking is now used as a preliminary step to confirm the interaction of a ligand with its target (Faheem et al., 2018). The positive docking results in the form of binding affinities and hydrogen bonds were the reason for molecular dynamics (MD) simulations to confirm the interaction of emodin with calcium channels and H^+/K^+ATPase. Researchers working on drug development and discovery are becoming more interested in MD simulations. This technique can be used to assess conformational changes, atomic structure positioning, identify the mutation, protonation, phosphorylation, and most importantly, the interactions of any atom, target, or ligand with its environment (Karplus and McCammon, 2002). The MD simulation was initially used in 1970 and it later attracted a large number of scientists, who use it to test their newly developed/discovered compounds. Many researchers have used it to compare and correlate results from animal studies (McCammon et al., 1977). We also run a 50ns MD simulations of two complexes. Complexes were evaluated for stability using the Amber 18 software package for 50 nanoseconds. The complexes were found to be stable, with RMSF and RMSD values that were within a range and a favorable interaction that determined the ligands' affinity for their targets.

CONCLUSION

In conclusion, our experimental findings provide substantial evidence that *Rumex dentatus* extracts and its phytoconstituent could be considered as a potent antioxidant and anti-inflammatory drug candidates that possess anti-diarrheal, anti-secretary, antispasmodic, anti-*H. pylori,* and anti-ulcer potential. Furthermore, we demonstrated the involvement of the H^+/K^+-ATPase pathway in the gastroprotective activity. It elevates the level of protective GST, GSH, catalase, and down-regulates oxidative stress marker (LPO). It reverses the ethanol-induced pathological changes, confirmed by H&E staining and IHC staining of gastric tissues. We also analyzed certain safety aspects of *Rumex dentatus* and it exhibited a relative safety profile as no impairment was observed in kidneys, heart, liver, and brain further assisted by biochemical and hematological analysis. Due to multi effective properties, it may reduce polypharmacy, be economically cost-effective, decrease medication error, drug-drug interactions, and effective in gastrointestinal disorders (**Supplementary Figure S6**).

DATA AVAILABILITY STATEMENT

The original contributions presented in the study are included in the article/Supplementary Material, further inquiries can be directed to the corresponding authors.

ETHICS STATEMENT

The animal study was reviewed and approved by Research and Ethics Committee of Riphah Institute Of Pharmaceutical Sciences (Ref. no. REC/RIPS/2019/14) along with the guidelines of "Principles of Laboratory Animal care".

AUTHOR CONTRIBUTIONS

Conceptualization, NQ and A-UK, methodology, NQ; Experimentation, formal analysis, investigation, NQ, IM, and KN; resources, A-UK; writing-original draft preparation, NQ; MD Simulations, S-UK; writing-review and editing, A-UK and NQ; supervision, A-UK. All authors have read and agreed to publish a version of the manuscript.

ACKNOWLEDGMENTS

We are thankful to Higher Education Commission for facilitating us in our research work.

SUPPLEMENTARY MATERIAL

The Supplementary Material for this article can be found online at: https://www.frontiersin.org/articles/10.3389/fphar.2022.936161/full#supplementary-material

REFERENCES

Abbasi, S., Raza, S., Azam, S. S., Liedl, K. R., and Fuchs, J. E. (2016). Interaction Mechanisms of a Melatonergic Inhibitor in the Melatonin Synthesis Pathway. *J. Mol. Liq.* 221, 507–517. doi:10.1016/j.molliq.2016.06.034

Ali, A., Shah, F. A., Zeb, A., Malik, I., Alvi, A. M., Alkury, L. T., et al. (2020). NF-κB Inhibitors Attenuate MCAO Induced Neurodegeneration and Oxidative Stress-A Reprofiling Approach. *Front. Mol. Neurosci.* 13, 33. doi:10.3389/fnmol.2020.00033

Alican, I., Toker, F., Arbak, S., Yegen, B. C., Yalçin, A. S., and Oktay, S. (1994). Gastric Lipid Peroxidation, Glutathione and Calcium Channel Blockers in the Stress-Induced Ulcer Model in Rats. *Pharmacol. Res.* 30, 123–135. doi:10.1016/1043-6618(94)80004-9

Ansari, S. F., Khan, A. U., Qazi, N. G., Shah, F. A., and Naeem, K. (2019). *In Vivo*, Proteomic, and In Silico Investigation of Sapodilla for Therapeutic Potential in Gastrointestinal Disorders. *Biomed. Res. Int.* 2019, 4921086–4921119. doi:10.1155/2019/4921086

Ansari, S. F., Khan, A.-u., Qazi, N. G., Shah, F. A., and Naeem, K. (2021). Proteomic Analysis and *In Vivo* Studies Reveal the Potential Gastroprotective Effects of CHCl3 and Aqueous Extracts of Ficus Palmata. *Evidence-Based Complementary Altern. Med.* 2021, 1–11. doi:10.1155/2021/6613140

Astudillo, A., Hong, E., Bye, R., and Navarrete, A. (2004). Antispasmodic Activity of Extracts and Compounds of Acalypha Phleoides Cav. *Phytother. Res.* 18, 102–106. doi:10.1002/ptr.1414

Boniface, M. T., Ngozi, O. E., Eiza, Y. P., Mathew, A. O., and Adejoh, I. P. (2020). Gas Chromatography-Mass Spectrometry (GC-MS) Profiling and Anti-ulcer Activity of the Aqueous Extract of Lophira Lanceolata Leaves. *Int. J. Adv. Res. Biol. Sci.* 7, 48–55.

Cipriani, T. R., Mellinger, C. G., de Souza, L. M., Baggio, C. H., Freitas, C. S., Marques, M. C. A., et al. (2008). Acidic Heteroxylans from Medicinal Plants and Their Anti-ulcer Activity. *Carbohydr. Polym.* 74, 274–278. doi:10.1016/j.carbpol.2008.02.012

Dai, H., Chen, Z., Shang, B., and Chen, Q. (2018). Identification and Quantification of Four Anthraquinones in Rhubarb and its Preparations by Gas Chromatography-Mass Spectrometry. *J. Chromatogr. Sci.* 56, 195–201. doi:10.1093/chromsci/bmx103

Faheem, M., Khan, A-U., Nadeem, H., and Ali, F. J. F. (2018). Computational and Pharmacological Evaluation of Heterocyclic 1,3,4-Oxadiazole and Pyrazoles Novel Derivatives for Toxicity Assessment, Tumour Inhibition, Antioxidant, Analgesic and Anti-inflammatory Actions. *Farmacia* 66, 909–919. doi:10.31925/farmacia.2018.5.24

Fatima, N., Zia, M., Rehman, R., Rizvi, Z. F., Ahmad, S., Mirza, B., et al. (2009). Biological Activities of Rumex Dentatus L: Evaluation of Methanol and Hexane Extracts. *Afr. J. Biotechnol.* 8, 24.

Gilani, A. H., Khan, A. U., Subhan, F., and Khan, M. (2005). Antispasmodic and Bronchodilator Activities of St John's Wort Are Putatively Mediated through Dual Inhibition of Calcium Influx and Phosphodiesterase. *Fundam. Clin. Pharmacol.* 19, 695–705. doi:10.1111/j.1472-8206.2005.00378.x

Hasler, W. L., Parkman, H. P., Wilson, L. A., Pasricha, P. J., Koch, K. L., Abell, T. L., et al. (2010). Psychological Dysfunction Is Associated with Symptom Severity but Not Disease Etiology or Degree of Gastric Retention in Patients with Gastroparesis. *Am. J. Gastroenterol.* 105, 2357–2367. doi:10.1038/ajg.2010.253

He, H., Li, X., Yu, H., Zhu, S., He, Y., Komatsu, K., et al. (2019). Gastroprotective Effect of Araloside A on Ethanol- and Aspirin-Induced Gastric Ulcer in Mice: Involvement of H^+/K^+-ATPase and Mitochondrial-Mediated Signaling Pathway. *J. Nat. Med.* 73, 339–352. doi:10.1007/s11418-018-1256-0

Irshad, N., Khan, A.-u., Alamgeer, M. S., Khan, S.-U. -D., and Iqbal, M. S. (2021). Antihypertensive Potential of Selected Pyrimidine Derivatives: Explanation of Underlying Mechanistic Pathways. *Biomed. Pharmacother.* 139, 111567. doi:10.1016/j.biopha.2021.111567

Jeelani, S. M., Farooq, U., Gupta, A. P., and Lattoo, S. K. (2017). Phytochemical Evaluation of Major Bioactive Compounds in Different Cytotypes of Five Species of Rumex L. *Industrial Crops Prod.* 109, 897–904. doi:10.1016/j.indcrop.2017.09.015

Jones, N. L., Koletzko, S., Goodman, K., Bontems, P., Cadranel, S., Casswall, T., et al. (2017). Joint ESPGHAN/NASPGHAN Guidelines for the Management of *Helicobacter pylori* in Children and Adolescents (Update 2016). *J. Pediatr. Gastroenterol. Nutr.* 64, 991–1003. doi:10.1097/MPG.0000000000001594

Kaithwas, G., and Majumdar, D. K. (2010). Evaluation of Antiulcer and Antisecretory Potential of Linum usitatissimum Fixed Oil and Possible Mechanism of Action. *Inflammopharmacology* 18, 137–145. doi:10.1007/s10787-010-0037-5

Karplus, M., and McCammon, J. A. (2002). Molecular Dynamics Simulations of Biomolecules. *Nat. Struct. Biol.* 9, 646–652. doi:10.1038/nsb0902-646

Khan, A., ur Rehman, N., AlKharfy, K. M., and Gilani, A. H. (2011). Antidiarrheal and Antispasmodic Activities of Salvia Officinalis Are Mediated through Activation of K+ Channels. *Bangladesh J. Pharmacol.* 6, 111–116. doi:10.3329/bjp.v6i2.9156

Khan, A.-u., and Gilani, A. H. (2009). Antidiarrheal, Antisecretory, and Bronchodilatory Activities ofHypericum Perforatum. *Pharm. Biol.* 47, 962–967. doi:10.1080/13880200902960206

Kollman, P. A., Massova, I., Reyes, C., Kuhn, B., Huo, S., Chong, L., et al. (2000). Calculating Structures and Free Energies of Complex Molecules: Combining Molecular Mechanics and Continuum Models. *Acc. Chem. Res.* 33, 889–897. doi:10.1021/ar000033j

McCammon, J. A., Gelin, B. R., and Karplus, M. (1977). Dynamics of Folded Proteins. *Nature* 267, 585–590. doi:10.1038/267585a0

Mehmood, M. H., Munir, S., Khalid, U. A., Asrar, M., and Gilani, A. H. (2015). Antidiarrhoeal, Antisecretory and Antispasmodic Activities of Matricaria Chamomilla Are Mediated Predominantly through K(+)-channels Activation. *BMC Complement. Altern. Med.* 15, 75–79. doi:10.1186/s12906-015-0595-6

Mishra, V. (2016). Potent Gastroprotective Effect Chrysophanol and Emodin from Rehum Emodi via H+/K+atpase Inhibition and Increasing the PGE2 Level in Rats. *Nat. Products:An Indian J.* 12, 1–12.

Nassar, M. I., Mohamed, T. K., Elshamy, A. I., El-Toumy, S. A., Abdel Lateef, A. M., and Farrag, A. R. (2013). Chemical Constituents and Anti-ulcerogenic Potential of the Scales of Cynara Scolymus (Artichoke) Heads. *J. Sci. Food Agric.* 93, 2494–2501. doi:10.1002/jsfa.6065

Noor, A., Qazi, N. G., Nadeem, H., Khan, A. U., Paracha, R. Z., Ali, F., et al. (2017). Synthesis, Characterization, Anti-ulcer Action and Molecular Docking Evaluation of Novel Benzimidazole-Pyrazole Hybrids. *Chem. Cent. J.* 11, 85–13. doi:10.1186/s13065-017-0314-0

Ohama, T., Hori, M., and Ozaki, H. (2007). Mechanism of Abnormal Intestinal Motility in Inflammatory Bowel Disease: How Smooth Muscle Contraction Is Reduced? *J. Smooth Muscle Res.* 43, 43–54. doi:10.1540/jsmr.43.43

Okunlola, A., Adewoyin, B. A., and Odeku, O. A. (2007). Evaluation of Pharmaceutical and Microbial Qualities of Some Herbal Medicinal Products in South Western Nigeria. *Trop. J. Pharm. Res.* 6, 661–670. doi:10.4314/tjpr.v6i1.14644

Persson, L., Karlsson-Vinkhuyzen, S., Lai, A., Persson, Å., and Fick, S. (2017). The Globally Harmonized System of Classification and Labelling of Chemicals—Explaining the Legal Implementation Gap. *Sustainability* 9 (12), 2176. doi:10.3390/su9122176

Rehman, N. U., Mehmood, M. H., Alkharfy, K. M., and Gilani, A. H. (2012). Studies on Antidiarrheal and Antispasmodic Activities of Lepidium Sativum Crude Extract in Rats. *Phytother. Res.* 26, 136–141. doi:10.1002/ptr.3642

Saleem, U., Amin, S., Ahmad, B., Azeem, H., Anwar, F., and Mary, S. (2017). Acute Oral Toxicity Evaluation of Aqueous Ethanolic Extract of Saccharum Munja Roxb. Roots in Albino Mice as Per OECD 425 TG. *Toxicol. Rep.* 4, 580–585. doi:10.1016/j.toxrep.2017.10.005

Shafiq, N., Saleem, M., Kousar, S., Sahar, M., Mahboob, S., and Jabeen, F. (2017). Investigation of Genus Rumex for Their Biologically Active Constituents. *Pharm. Chem. Sci.* 2, 148–165.

Sisay, M., Engidawork, E., and Shibeshi, W. (2017). Evaluation of the Antidiarrheal Activity of the Leaf Extracts of Myrtus Communis Linn (Myrtaceae) in Mice Model. *BMC Complement. Altern. Med.* 17, 103–111. doi:10.1186/s12906-017-1625-3

Ullah, I., Khan, M., Khan, A., Akhlaq, M., Mukhtiar, M., and Rasheed, F. (2019). Chemical Identification, Antibacterial Effect and Synergistic Potential of Mentha Arvensis with 5-Fluorouracil against HCT-116 Colon Cancer Cell Line. *Lat. Am. J. Pharm.* 38, 762–770.

Zhang, H., Guo, Z., Wu, N., Xu, W., Han, L., Li, N., et al. (2012). Two Novel Naphthalene Glucosides and an Anthraquinone Isolated from *Rumex dentatus* and Their Antiproliferation Activities in Four Cell Lines. *Molecules* 17, 843–850. doi:10.3390/molecules17010843

Conflict of Interest: The authors declare that the research was conducted in the absence of any commercial or financial relationships that could be construed as a potential conflict of interest.

Publisher's Note: All claims expressed in this article are solely those of the authors and do not necessarily represent those of their affiliated organizations, or those of the publisher, the editors, and the reviewers. Any product that may be evaluated in this article, or claim that may be made by its manufacturer, is not guaranteed or endorsed by the publisher.

Copyright © 2022 Qazi, Khan, Abbasi, Malik and Naeem. This is an open-access article distributed under the terms of the Creative Commons Attribution License (CC BY). The use, distribution or reproduction in other forums is permitted, provided the original author(s) and the copyright owner(s) are credited and that the original publication in this journal is cited, in accordance with accepted academic practice. No use, distribution or reproduction is permitted which does not comply with these terms.

frontiers | Frontiers in Pharmacology

TYPE Original Research
PUBLISHED 19 August 2022
DOI 10.3389/fphar.2022.959661

Check for updates

OPEN ACCESS

EDITED BY
Fareeha Anwar,
Riphah International University (Lahore), Pakistan

REVIEWED BY
Hafiz Muhammad Asif,
Islamia University of Bahawalpur, Pakistan
Asifa Bashir,
Riphah International University (Lahore), Pakistan

*CORRESPONDENCE
Miriam Watafua,
miriamwatafua@unimaid.edu.ng
Mubarak Hussaini Ahmad,
mubarakhussainiahmad@gmail.com

SPECIALTY SECTION
This article was submitted to Predictive Toxicology, a section of the journal Frontiers in Pharmacology

RECEIVED 01 June 2022
ACCEPTED 29 June 2022
PUBLISHED 19 August 2022

CITATION
Watafua M, Ejiofor JI, Musa A and Ahmad MH (2022), Acacia sieberiana (Fabaceae) attenuates paracetamol and Bile Duct Ligation-Induced hepatotoxicity via modulation of biochemical and oxidative stress biomarkers.
Front. Pharmacol. 13:959661.
doi: 10.3389/fphar.2022.959661

COPYRIGHT
© 2022 Watafua, Ejiofor, Musa and Ahmad. This is an open-access article distributed under the terms of the Creative Commons Attribution License (CC BY). The use, distribution or reproduction in other forums is permitted, provided the original author(s) and the copyright owner(s) are credited and that the original publication in this journal is cited, in accordance with accepted academic practice. No use, distribution or reproduction is permitted which does not comply with these terms.

Acacia sieberiana (Fabaceae) attenuates paracetamol and Bile Duct Ligation-Induced hepatotoxicity *via* modulation of biochemical and oxidative stress biomarkers

Miriam Watafua[1,2]*, Jane I. Ejiofor[2], Aminu Musa[2] and Mubarak Hussaini Ahmad [2]*

[1]Department of Biochemistry, Faculty of Science, University of Maiduguri, Maiduguri, NG, Nigeria, [2]Department of Pharmacology and Therapeutics, Ahmadu Bello University, Zaria, KD, Nigeria

Background: The plant *Acacia sieberiana* (Fabaceae) is traditionally used to manage hepatitis. This research work aims to investigate the hepatoprotective effectiveness of root bark extract of *Acacia sieberiana* (ASE) against paracetamol (PCM) and bile duct ligation (BDL)-induced hepatotoxicity. The phytochemical and median lethal dose (LD_{50}) investigations were conducted. The rats were pre-treated with the ASE (250, 750, and 1,500 mg/kg) once daily via oral route for 7 consecutive days. On the 8th day, liver injury was initiated by PCM administration (2 g/kg). Similarly, in the BDL-induced liver injury, the animals were administered ASE (125, 250, and 380 mg/kg) intraperitoneally for 7 consecutive days. After 24 h, blood samples and hepatic tissues were obtained for biochemical and histopathological investigations.

Results: Phytocomponents determination revealed glycosides, triterpenes, glycosides, saponins, tannins, flavonoids and alkaloids. The oral and intraperitoneal LD_{50} values of the ASE were >5,000 and 1,300 mg/kg, respectively. The ASE efficiently ($p < 0.05$) decreased the alanine transaminase (ALT) and aspartate transaminase (AST) levels and elevated the albumin and total protein (TP) levels. The direct bilirubin effectively ($p < 0.05$) decreased at 750 mg/kg. Besides, the extract efficiently elevated the glutathione peroxidase (GPx), superoxide dismutase (SOD), and catalase (CAT) in relation to the PCM hepatotoxic group. Also, the malondialdehyde (MDA) concentration was reduced by the ASE. Meanwhile, in the BDL–induced liver injury, the ASE remarkably ($p < 0.05$) declined the AST, ALP, bilirubin,and MDA. Besides, there was effective ($p < 0.05$) elevation in SOD, GPx and CAT in the ASE-treated groups. The morphology of liver tissue was preserved at 125 and 250 mg/kg ASE groups from BDL-induced necrosis and vascular congestion.

Conclusion: The study shows that the ASE has hepatoprotective actions against liver damage by possible modulation of biochemical and oxidative stress biomarkers.

KEYWORDS

hepatoprotective effects, medicinal plants, biochemical biomarkers, oxidative stress, *Acacia sieberiana* var. woodii

1 Introduction

The liver is the largest and one of the most essential organs in the human body, weighing approximately 2%–3% of the average body weight (Pingili et al., 2019; Yue et al., 2020). It participates in a lot of physiological activities to keep the normal body system in healthy conditions, such as carbohydrate, lipids and protein metabolism; removal of toxic agents and pathogens; immunological, digestive, nutritional, and storage functions (Duncan et al., 2009; Protzer et al., 2012; Khan et al., 2019; Elmasry, 2021). Besides, the liver is the most important location for the biotransformation of exogenous and endogenous chemical compounds (Khan et al., 2019). It also participates in key biochemical processes in the body such as growth, energy production, reproduction, maintaining blood glucose level in the fasting stage by gluconeogenesis and glycogenolysis; supply of energy to muscle and brain during starvation; and synthesis of blood clotting factors (Khan et al., 2011; Pingili et al., 2019).

As a result of its diverse functions, the liver is frequently vulnerable to both direct and indirect toxic agents (Uzunhisarcikli and Aslanturk, 2019). Hepatic disorders, including cirrhosis, hepatitis, fibrosis and hepatocellular carcinoma, are among the main health care obstacles globally (Elufioye and Habtemariam, 2019). Some factors associated with the pathogenesis of liver disease include lipid peroxidation, reactive oxygen species (ROS), complement factors and pro-inflammatory mediators (chemokines and cytokines) (Elufioye and Habtemariam, 2019). Although the liver has a natural capability to regenerate its lost tissues, certain hepatic injuries or diseases sometimes tend to progress beyond this ability and may result in liver failure or death (Michalopoulos, 2017). Generally, the undiagnosed or unmanaged hepatic injury may progress from acute hepatitis of mere inflammatory reactions to chronic fibrosis, cirrhosis or liver failure (Tag et al., 2015). Besides, it eventually affects the biological functions of body organs (Younossi et al., 2011). Acute or chronic liver disorders lead to high morbidity and cause about 2 million global deaths annually (Asrani et al., 2019). The development and progression of hepatic diseases could be implicated by viruses (hepatitis A, B, and C), excessive alcohol intake, malnutrition, and metabolic disorders (Miltonprabu et al., 2016; Lin et al., 2017). Besides, drug-induced hepatic damage serves as the second leading cause of the acute hepatic disorder (Bernal et al., 2010). Some common drugs implicated in liver diseases include paracetamol (PCM), anti-infective agents, anticonvulsants and anti-inflammatory agents (Elufioye and Habtemariam, 2019). Despite the advancement in orthodox medical practice, no effective medications absolutely protect the liver against damage, stimulate its functions, or enhance its hepatic cell regeneration (Madrigal-santillán et al., 2014). Therefore, it is vital to investigate more effective and less toxic alternative therapies to manage liver diseases (Abenavoli et al., 2018; Ma et al., 2020).

Herbal preparations have gained attention in traditional practice against many diseases (Usman et al., 2021). Approximately 75% of the global personalities use herbal preparations for their basic health needs (Muhammad et al., 2021). The biological screening of medicinal plants has motivated the discovery of noble and effective agents against various disorders (Ahmad et al., 2020). About one-third of the medicinal products used in modern medicine were obtained from medicinal plants (Usman et al., 2021). Besides, herbal preparations have gained popularity in traditional practice for their therapeutic uses against hepatic diseases, which stimulates interest in exploring complementary and alternative medicine to develop therapeutically effective compounds against hepatic disorders (Miltonprabu et al., 2016; Ali et al., 2019). Biological investigations have validated the liver protective effect of medicinal plants (Park et al., 2019; Anyasor et al., 2020). Similarly, natural antioxidant compounds have gained attention for utilization against hepatic ailments by virtue of the role played by oxidative stress in the pathogenesis of hepatic disease (Rašković et al., 2014).

The plant *Acacia sieberiana* var Woodii (Fabaceae) is a tree of 3–25 m in height and 0.6–1.8 m in diameter (Ngaffo et al., 2020). The bark is yellowish in colour and rough with gummy exudates. The leaves are sparse and hairy, while the flowers are cream, white or pale yellow (Dawurung et al., 2012). The plant possesses dehiscent shiny brown fruits of approximately 1.3 cm in thickness, 9–21 cm in length and 1.7–3.5 cm in diameter (Dawurung et al., 2012). It is frost and drought resistant and grows in the savannah area with many botanical structures throughout the Sahel and other African nations (Ameh and Eddy, 2014). It is commonly distributed in Ethiopia, Benin, Chad, Gambia, Cameroon, Ghana, Kenya, Liberia, Zimbabwe, South Africa, Mozambique, Senegal, Mali, Mauritania, Namibia, Sierra Leone, Swaziland, Sudan, Nigeria, Portugal, Tanzania, Uganda, Zambia, Togo, and India (Ameh and Eddy, 2014). In Nigeria, the plant is available as an economic tree in the Northern regions, including Yobe, Jigawa, and Sokoto States (Ameh and Eddy, 2014). It is commonly referred to as umbrella thorn/white thorn/paperback thorn/flat-topped thorn or paperback in English, *Farar kaya* in Hausa, *Aluki* or *Sie* in Yoruba, *Siyi* in Igbo, *Daneji* in Fulfulde languages (Ameh and Eddy, 2014; Salisu et al., 2014).

Previous studies on the phytochemical contents in the *Acacia* sieberiana resulted in isolation of gallic acid, kaempferol, ellagic acid, quercetin, isoferulic acid, kaempferol 3-α-$_{L}$-arabinoside and quercetin 3-O-β-$_{D}$-glucoside (Abdelhady, 2013). Other secondary metabolites including luteolin-*7*-O-rutinoside, chrysoeriol-*7*-O-rutinoside, apigenin-*7*-O-β-$_{D}$-glucopyranoside,

chrysoeriol-7-O-β-$_D$-glucopyranoside, luteolin, luteolin-3′,4′-dimethoxylether-7-O-β-$_D$-glucoside and sitosterol-3-O-β-$_D$-glucoside, were isolated from the leaves of the plant (Ngaffo et al., 2020). The stem and leaves of *Acacia* sieberiana contains dihydroacacipetalin and acacipetalin (Seigler et al., 1975).

The root decoction of *Acacia sieberiana* is utilized in Nigeria to treat hepatic diseases (Ohemu et al., 2014). The bark and stem of the *Acacia sieberiana* are also used to manage jaundice (Dawurung et al., 2012). Despite the ethnomedicinal applications of the *Acacia sieberiana* in folk medicine to manage liver diseases, no study in the literature scientifically documents its ameliorative actions against liver damage. Hence, the current study evaluates the effect of the methanol root bark extract of *Acacia sieberiana* on PCM- and bile duct ligation-induced liver injuries.

2 Materials and methods

2.1 Plant collection

The plant *Acacia sieberiana* was obtained from Samaru, Kaduna State, Nigeria. It was identified and validated by Mallam Namadi Sanusi at the herbarium unit of Biological Sciences Department, Ahmadu Bello University (ABU), Zaria, Nigeria (Specimen number = 16,136).

2.2 Animals

Adult Wistar rats (males and females) ranging from 120 to 200 g were sourced from the Animal Facility of the Department of Pharmacology and Therapeutics, ABU, Zaria, Nigeria. They were maintained in well-ventilated animal cages (temperature 22 ± 3°C, relative humidity of 30%–70%) and provided with sufficient animal feed (Vital feed, Jos, Nigeria). Sufficient water was supplied to the animals *ad libitum*. The rats acclimatized to the laboratory environment for two weeks before the research work commenced. The study was conducted in accordance with the ABU Ethical Committee on Animal Use and Care Research Policy (ABUCAUC/2016/049) and ARRIVE (Animal Research: Reporting of *In Vivo* Experiments) guidelines. On completing the experiment, the rats were anaesthetized, euthanized by cervical dislocation and buried as per the ABU's guideline for appropriate disposal of experimental animals remain.

2.3 Extraction

The fresh root barks of *Acacia sieberiana* were air-dried in a shaded environment to a uniform weight and size reduced with mortar and pestle. Then 2,500 g of the powdered material was soaked in 10 L of 70%$^{v}/_{v}$ methanol in a conical flask for 72-h with frequent shaking. The mixture was filtered with Whatman filter paper (No. 1). The filtrate was concentrated on a water bath maintained at 50°C to obtain the extract, packaged and labeled as *Acacia sieberiana* extract (ASE). The mixture of the ASE was prepared freshly for each experiment with distilled water.

Then the extractive value of the extract was obtained as follows:

$$\text{Extractive value } (\%) = \frac{\text{Weight of the crude ASE (g)}}{\text{Weight of the size reduced plant (g)}} \times 100$$

2.4 Phytochemical determination

Preliminary phytochemical determination of the ASE was conducted using an appropriate procedure (Sofowora, 1993).

2.5 Acute toxicity evaluation

The intraperitoneal (*i. p*) and oral acute toxicity determination on the ASE were determined in rats in two phases (Lorke, 1983). In the 1st stage, 9 animals were categorized into 3 different groups (n = 3), administered the ASE *via* oral route at 10, 100 and 1,000 mg/kg and then observed for 24-h for signs of harmful effects or loss of life. In the 2nd stage, 3 rats were categorized into 3 groups (n = 1 rat per group) administered with the higher doses of the extract orally (600, 2,900, and 5,000 mg/kg) and observed for possible signs of harmful effects and mortality. The same procedure was followed to determine the *i. p* acute toxicity. The estimated oral and *i. p* median lethal doses (LD_{50}) were estimated by taking the geometric mean of the highest non-lethal and the lowest lethal doses as follows:

$$LD_{50} = \sqrt{(\text{maximum non} - \text{lethal dose} \times \text{minimum lethal dose})}$$

2.6 Hepatoprotective effects

2.6.1 Paracetamol-induced hepatotoxicity in rats

The procedure previously described by (Mahmood et al., 2014) was used. The rats were randomly categorised into 6 various groups (n = 5) and treated as follows:

Group 1: Distilled water (1 ml/kg, *p. o*) once daily for 7 days
Group 2: Distilled water (1 ml/kg, *p. o*) once daily for 7 days
Group 3: Silymarin (50 mg/kg, *p. o*) once daily for 7 days
Group 4: ASE (250 mg/kg, *p. o*) once daily for 7 days

TABLE 1 Effects of ASE on liver biomarkers of rats in paracetamol-induced liver injury.

Liver biomarkers	Treatment groups (per kg)					
	D/W (1 ml)	D/W (1 ml)+ PCM (2 g)	Sily (50 mg)+ PCM (2 g)	ASE (250 mg)+ PCM (2 g)	ASE (750 mg)+ PCM (2 g)	ASE (1,500 mg)+ PCM (2 g)
ALT (IU/L)	11.33 ± 0.88	30.33 ± 2.03[a]	17.00 ± 1.15[a,b]	16.33 ± 1.45[a,b]	17.00 ± 2.65[a,b]	26.33 ± 3.76[a]
AST (IU/L	38.67 ± 3.48	45.33 ± 0.40[a]	41.00 ± 3.79[b]	37.33 ± 1.45[b]	38.33 ± 4.63[b]	41.35 ± 4.61
ALP (IU/L)	12.49 ± 1.18	13.58 ± 0.53	14.55 ± 1.05	14.05 ± 1.16	11.70 ± 1.03[a]	12.64 ± 1.05
Total Protein (g/dL)	9.37 ± 0.53	8.05 ± 0.09[a]	9.14 ± 0.19[b]	8.86 ± 0.17[b]	10.16 ± 0.91[b]	10.14 ± 0.95[b]
Albumin (g/dL)	3.85 ± 0.81	2.64 ± 0.27[a]	3.03 ± 0.56	3.25 ± 0.18[b]	3.46 ± 0.19[b]	3.00 ± 0.12[b]
Direct bilirubin (mmol/L)	3.03 ± 0.44	4.24 ± 0.68[a]	3.23 ± 0.21[b]	3.56 ± 0.43	3.18 ± 0.26[b]	4.07 ± 1.19
Total bilirubin (mmol/L)	5.30 ± 0.35	5.78 ± 0.41	5.33 ± 0.43	5.45 ± 0.30	5.16 ± 0.97	5.69 ± 0.46

N = 5; The parameters are expressed as mean ± SEM; One Way ANOVA followed by Bonferroni post hoc test.
[a]$p < 0.05$ significant compared to the D/
[b]$p<0.05$ significant compared to the D/W + PCM group. Sily = Silymarin; D/W = Distilled water; PCM = PCM; ALT = alanine aminotransferase; AST = aspartate aminotransferase; ALP = alkaline phosphatase; ASE = *Acacia sieberiana* extract.

Group 5: ASE (750 mg/kg, *p. o*) once daily for 7 days
Group 6: ASE (1,500 mg/kg, *p. o*) once daily for 7 days

Following the administration in the above groups (except group 1), liver damage was induced by the PCM (2 g/kg) administration (8th day). The rats were anaesthetised with chloroform soaked in cotton, put into an inhalational chamber, and euthanized by cervical dislocation. The blood samples were obtained from the various groups in bottles and centrifuged at 3,000 revolutions per minute (rpm) for 10 min. The obtained sera were assayed for biochemical biomarkers such as alanine transaminase (ALT), aspartate transaminase (AST), alkaline phosphatase (ALP), albumin, total protein (TP), total bilirubin (TB) and direct bilirubin (DB). The oxidative stress markers, namely; catalase (CAT), glutathione peroxidase (GPx), superoxide dismutase (SOD), and malondialdehyde (MDA), were also analysed. The livers were excised and placed in 10% formalin for histopathological examination.

2.6.2 Bile duct ligation-induced liver injury

The method reported by (Tag et al., 2015) was employed. A total of fifty (50) male animals were anaesthetized with thiopental sodium (40 mg/kg, *i. p*). The abdominal furs of the rats were shaved off, and a short incision of about 2 cm was made below the xiphoid process of the abdomen to expose the bile duct region. Double ligation was placed at the common bile duct of forty-four 44) of the rats such that the bile did not flow. The incisions were then sutured, and the animals were kept to recover (fully awake and active). Thirty (30) out of the 44 double ligated rats that were fully awake and active within 24-h were selected and categorized into 5 groups of 6 rats each, while the 6 non-ligated rats served as a negative control for the study and were treated as follows:

Group 1 (non-ligated): Distilled water (1 ml/kg, *p. o*) once daily for 7 days
Group 2: Distilled water (1 ml/kg, *p. o*) once daily for 7 days
Group 3: Silymarin (50 mg/kg, *p. o*) once daily for 7 days
Group 4: ASE (125 mg/kg, *i. p*) once daily for 7 days
Group 5: ASE (250 mg/kg, *i. p*) once daily for 7 days
Group 6: ASE (380 mg/kg, *i. p*) once daily for 7 days

Then 24-h post-treatment, the animals were anaesthetised with chloroform and euthanized. The blood samples were obtained from the various groups in bottles and centrifuged at 3,000 rpm. The obtained sera were assayed for biochemical biomarkers such as ALT, AST, ALP, TP, Albumin, TB, and DB. The antioxidant markers namely; SOD, CAT, GPx, and MDA, were also assayed. The livers were obtained for histopathological examination.

2.7 Data analysis

The values obtained were expressed as mean ± standard error of the mean (SEM) in tables. We used the one way analysis of variance (ANOVA) to analyse the parameters, followed by the Bonferonni post hoc test. The $p \leq 0.05$ was taken as significant.

3 Results

3.1 Extractive value

A sticky dark-brown solid residue of 115.78 g (4.63%$^{w}/_{w}$) with a mild sweet smell was obtained from the 2,500 g powdered sample of the crude root bark of *A. sieberiana*.

TABLE 2 Effects of the ASE on oxidative stress biomarkers of rats in paracetamol-induced liver injury.

Treatment groups (per kg)	Oxidative stress biomarkers			
	SOD (ng/mL)	CAT (ng/mL)	MDA (nmol/mL)	GPx (ng/mL)
D/W (1 ml)	9.47 ± 1.64	40.94 ± 1.45	13.71 ± 0.65	92.39 ± 4.42
D/W (1 ml) + PCM	6.58 ± 0.74[a]	41.31 ± 2.39	27.00 ± 3.60[a]	89.62 ± 5.80
Sily (50 mg) + PCM	11.45 ± 1.61[b]	48.90 ± 6.64[a]	14.17 ± 1.19[b]	99.92 ± 1.61[a,b]
ASE (250) + PCM	10.71 ± 0.81[b]	45.58 ± 1.26[a,b]	12.28 ± 0.50[b]	99.88 ± 9.81
ASE (750) + PCM	12.55 ± 0.81[a,b]	53.91 ± 3.17[a,b]	11.93 ± 0.96[b]	97.06 ± 4.62
ASE (1,500) + PCM	13.22 ± 0.97[a,b]	40.82 ± 3.07	12.11 ± 0.65[b]	94.59 ± 9.77

$N = 5$; parameters are expressed as mean ± SEM; One Way ANOVA followed by Bonferroni post hoc test.
[a]$p < 0.05$ significant compared to the D/W.
[b]$p < 0.05$ significant compared to the D/W + PCM. Sily = silymarin; D/W = Distilled water; PCM = PCM; SOD = Superoxide dismutase; CAT = Catalase; MDA = Malondialdehyde; GPx = glutathione peroxidise; ASE = *Acacia sieberiana* extract.

3.2 Phytocomponents

The phytocomponents analysis on the ASE indicated cardiac glycosides, saponins, tannins, triterpenes, flavonoids, and alkaloids. The steroids and anthraquinones were not present.

3.3 Acute toxicity

Acute oral administration of ASE showed no death and behavioural signs of toxicity at 5,000 mg/kg, and thus, the oral LD_{50} of the ASE was determined to be ≥ 5,000 mg/kg. For the *i. p* acute toxicity study, mortality was not recorded in the first phase of the ASE treatments. However, the rats at all the increased doses (1,600, 2,900 and 5,000 mg/kg) in the second phase died. Hence, the *i. p* LD_{50} was about 1,300 mg/kg.

3.4 Paracetamol-elicited hepatic injury

3.4.1 Effects of *Acacia sieberiana* on liver biomarkers of rats in paracetamol-elicited hepatic injury

The liver of the PCM intoxicated group reflected a remarkable ($p < 0.05$) upsurge in ALT, AST, and DB and an efficient decrease ($p < 0.05$) in TP and albumin when related to the healthy group. The group treated with silymarin and ASE (250 and 750 mg/kg) remarkably reduced the PCM-induced elevated ALT and AST concentrations in relation to the hepatotoxic control group. Besides, the silymarin and ASE at all doses abolished the significant ($p < 0.05$) reduction in TP caused by the PCM intoxication. In addition, the extract at all doses efficiently ($p < 0.05$) increased the albumin level, while the silymarin pre-treatment showcased a non-significant increase. There was a remarkable ($p < 0.05$) decline in the PCM-caused DB elevation in the silymarin and ASE (750 mg/kg) treated groups. The effects of the ASE on the hepatic biomarkers of rats in PCM-elicited liver injury are presented in Table 1.

3.4.2 Effects of *Acacia sieberiana* on oxidative stress biomarkers in paracetamol-elicited liver injury

This result showed that the PCM-elicited hepatic damage significantly reduced ($p < 0.05$) the SOD level in relation to the healthy rats. However, the groups treated with the silymarin and ASE at all doses efficiently ($p < 0.05$) and dose-dependently elevated SOD plasma concentration related to the PCM-hepatotoxic group. The concentration of the CAT was not affected by the PCM intoxication. However, the CAT level significantly increased ($p < 0.05$) in the categories that received the ASE at 250 and 750 mg/kg compared to the distilled water healthy and hepatotoxic groups. The PCM intoxicated group elicited significant ($p < 0.05$) elevation in the MDA concentration, which was reversed effectively ($p < 0.05$) by the silymarin and ASE at all doses. The PCM-induced injury slightly and insignificantly reduced the GPx concentration. However, its serum concentration was increased in all the ASE pre-treated groups in relation to the distilled water healthy group. There was an effective ($p < 0.05$) increase in the GPx in the silymarin pre-treated group in relation to the PCM-intoxicated category. The actions of the ASE on the oxidative stress biomarkers of rats in PCM-induced liver injury are presented in Table 2.

3.4.3 Effects of *Acacia sieberiana* on the liver histology in the paracetamol-elicited liver injury

The histopathological results of the rats' livers after PCM-induced liver injuries showed that the PCM produced intense hepatocellular necrosis with sinusoid and vascular congestion. At the same time, the group pre-treated with the standard drug silymarin exhibited slight focal necrosis, lymphocyte hyperplasia and vascular congestion. There was slight

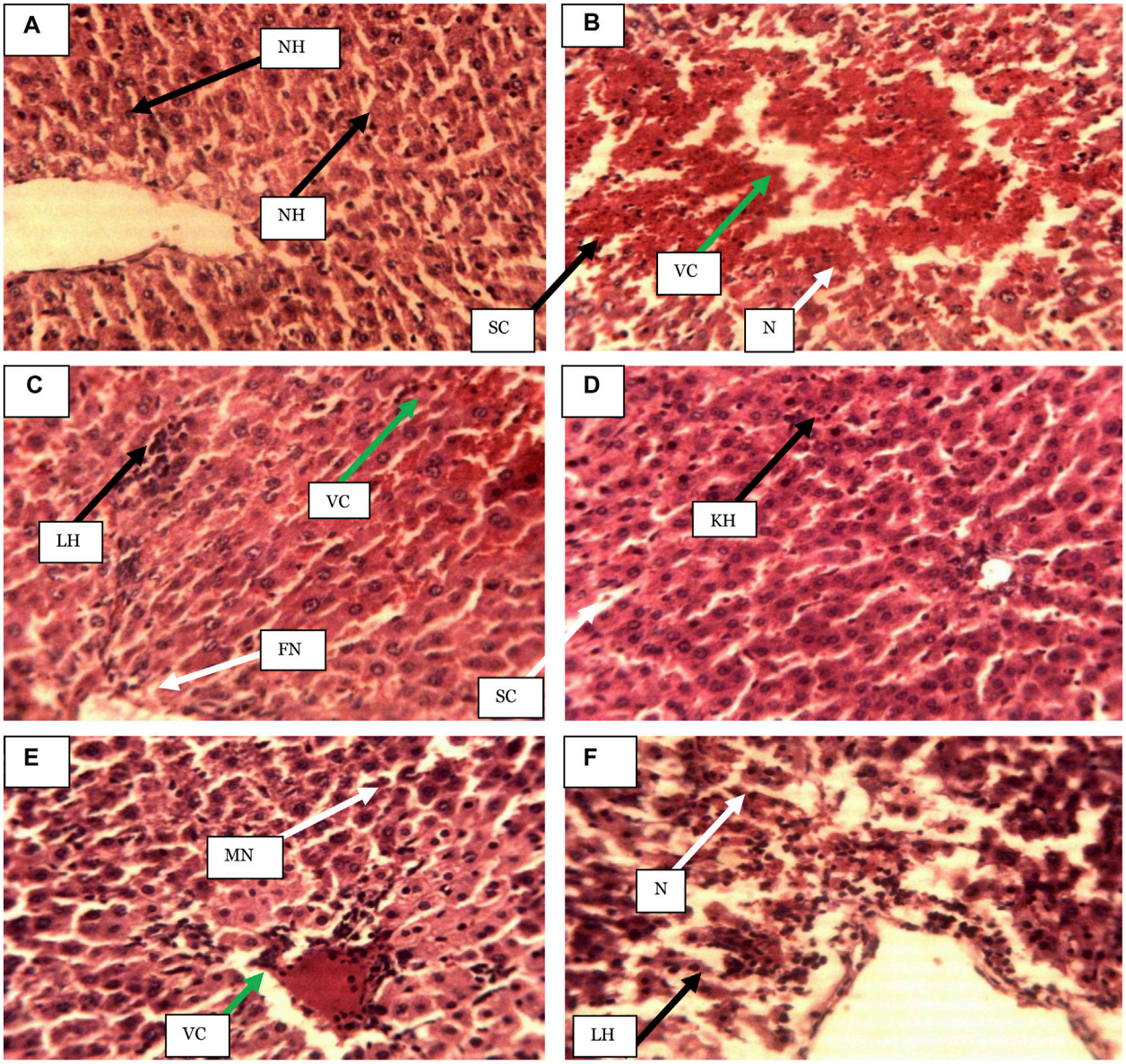

FIGURE 1
Photomicrographs of hepatic sections of rats after 7-days of ASE pre-treatment in the paracetamol-induced liver injury (Haematoxylin and eosin-stained at ×250 magnification). **(A)** Distilled water (1 ml/kg), **(B)** Distilled water (1 ml/kg) + PCM), **(C)** Sily (50 mg/kg) + PCM), **(D)** ASE (250 mg/kg) + PCM), **(E)** ASE (750 mg/kg) + PCM), **(F)** ASE (1,500 mg/kg) + PCM), NH = Normal hepatocytes, N= Necrosis, SC = Sinusoid congestion, VC = Vascular congestion, FN = Focal necrosis, LH = Lymphocytes hyperplasia, KH = Kupffer cell hyperplasia, SC = slight sinusoidal congestion, MN = Moderate necrosis, ASE = *Acacia sieberiana* extract.

kupffer cell hyperplasia and slight sinusoidal congestion in the group that received ASE at 250 mg/kg, while the group pre-treated with the ASE at 750 mg/kg showed vascular congestion and slight vacuolation and necrosis. However, the group pre-treated with 1,500 mg/kg of ASE showed intense hepatocellular necrosis and lymphocyte hyperplasia. The actions of the ASE on the hepatic histology of rats in PCM-produced liver injury are shown in Figure 1.

3.5 Bile duct ligation-elicited hepatic injury

3.5.1 Effects of *Acacia sieberiana* on hepatic biomarkers of rats in bile duct ligation-induced liver injury

All the liver biomarkers in the BDL-induced hepatic injured group were elevated, which were significant ($p < 0.05$) for ALP,

TABLE 3 Effects of ASE on liver biomarkers of rats in bile duct ligation-induced liver injury.

Liver biomarkers	Treatment groups (per kg)					
	Non-ligated + D/W (1 ml)	BDL + D/W (1 ml)	BDL + sily (50 mg)	BDL + ASE (125 mg)	BDL + ASE (250 mg)	BDL + ASE (380 mg)
ALT (IU/L)	7.67 ± 0.88	8.33 ± 1.45	9.02 ± 1.00	6.67 ± 0.33[c]	7.00 ± 1.0 2	7.67 ± 1.45
AST (IU/L)	9.00 ± 1.15	24.67 ± 4.17[a]	20.00 ± 3.58[a]	12.05 ± 2.08[b,c]	10.50 ± 0.50[b,c]	19.67 ± 1.76[a]
ALP (IU/L)	12.87 ± 2.04	16.23 ± 0.84[a]	13.32 ± 2.18	15.93 ± 0.38[a]	12.57 ± 0.26[b]	13.93 ± 1.21[b]
Total Protein (g/dL)	5.98 ± 0.09	6.35 ± 0.90	6.78 ± 1.16	5.39 ± 0.60	5.59 ± 0.50	5.62 ± 0.64
Albumin (g/dL)	1.88 ± 0.37	1.43 ± 0.38	2.20 ± 0.16[b]	1.42 ± 0.31	1.64 ± 0.30	1.91 ± 0.13
Direct bilirubin (mmol/L)	0.33 ± 0.13	2.83 ± 0.08[a]	0.39 ± 0.08[b]	0.27 ± 0.04[b]	0.23 ± 0.10[b]	0.27 ± 0.04[b]
Total bilirubin (mmol/L)	0.56 ± 0.17	2.86 ± 0.08[a]	1.18 ± 0.23[a,b]	0.82 ± 0.27[b]	0.58 ± 0.10[b]	1.53 ± 0.10[a,b]

$N = 6$; The parameters expressed as mean ± SEM; One Way ANOVA followed by Bonferroni post hoc test.
[a]$p < 0.05$ significant compared to the Non-ligated + D/W.
[b]$p < 0.05$ significant compared to the BDL + D/W.
[c]$p < 0.05$ significant compared to the BDL + Sily; Sily = silymarin; D/W = Distilled water; BDL = Bile duct ligation; ALT = alanine aminotransferase; AST = aspartate aminotransferase; ALP = alkaline phosphatise; ASE = *Acacia sieberiana* extract.

AST, and bilirubins in relation to the non-ligated control group. However, the BDL produced a non-significant reduction in the albumin level related to the non-ligated control group. The ASE non-significantly declined the ALT and total protein levels at all doses compared to the BDL-treated control group. The ASE also produced a remarkable ($p < 0.05$) reduction in the AST (125 and 250 mg/kg), ALP (250 and 380 mg/kg), direct and total bilirubin levels at all doses. However, the ASE at higher doses (250 and 380 mg/kg) produced a non-significant increase in the plasma albumin concentration. The standard agent silymarin increased the ALT, total protein, and albumin related to the BDL-ligated control category. However, the ALP and AST declined insignificantly in the category pre-treated with the silymarin in relation to the BDL-ligated control group. Also, the direct and total bilirubin reduced ($p < 0.05$) in the silymarin administered group. The effects of the ASE on the hepatic biomarkers of rats in BDL-induced liver injury are showcased in Table 3.

3.5.2 Effects of *Acacia sieberiana* on oxidative stress biomarkers in bile duct ligation-induced liver injury

The SOD and CAT concentration effectively ($p < 0.05$) reduced in the BDL-induced liver injured group related to the non-ligated control class. The MDA level was increased significantly ($p < 0.05$) in the BDL-induced liver injured group. In addition, the GPx level was slightly elevated in the BDL-ligated group. The standard drug (silymarin) and ASE (125 and 250 mg/kg) showed a remarkable ($p < 0.05$) upsurge in the serum SOD concentration in comparison to the BDL-treated control group. Similarly, the silymarin and extract elicited dose-dependent and significant elevation in the CAT level. Also, an efficient ($p < 0.05$) increase in the GPx was observed in all the extract-treated groups. The standard agent (silymarin) and ASE (125 mg/kg) showed a remarkable ($p < 0.05$) reduction in the MDA serum concentration related to the BDL-treated control group. The effects of the ASE on the oxidative stress biomarkers of rats in BDL-induced liver injury are presented in Table 4.

3.5.3 Effects of *Acacia sieberiana* on the liver histology in the bile duct ligation-induced liver injury

The hepatocytes of the operated, non-ligated control group were intact with normal structures. However, the BDL-injured group showed moderate hepatic necrosis and vascular congestion, which was slightly reversed in the group that received the ASE at 125 mg/kg. The group treated with the extract at 250 mg/kg showed lymphocyte hyperplasia. The ASE at the highest dose (380 mg/kg) revealed Kupffer cell hyperplasia and vascular congestion. The effects of the ASE on the liver histology are shown in Figure 2.

4 Discussion

The liver is often exposed to diverse endogenous and exogenous toxic xenobiotics, drugs, metabolic waste products, and viral or bacterial agents which traverse it for detoxification or excretion (Zhou et al., 2019). This predisposes the liver to the harmful effects of drugs and other toxicants (Ramirez et al., 2018). Therapeutic agents used against hepatic disorders possess limited therapeutic efficacy. Hence, it has become imperative to develop new, effective, safe drugs to manage liver disorders (Jin et al., 2021). The use of abundant medicinal plants and formulas with hepatoprotective efficacy to manage hepatic disorders has gained considerable attention (Jadeja et al., 2015; Ilyas et al., 2016). For example, the flavonoids extract of *Silybum marianum* plant, currently standardised as silymarin has been reported to be

TABLE 4 Effects of ASE on oxidative stress biomarkers in bile duct ligation-induced liver injury.

Treatment groups (per kg)	Oxidative stress biomarkers			
	SOD (ng/mL)	CAT (ng/mL)	MDA (nmol/mL)	GPx (ng/mL)
Non-ligated + D/W (1 ml)	5.47 ± 0.65	40.94 ± 1.45	36.71 ± 1.54	95.06 ± 4.05
BDL + D/W (1 ml)	1.27 ± 0.18[a]	32.48 ± 8.27[a]	68.61 ± 6.09[a]	99.61 ± 1.02
BDL + Sily (50 mg)	2.01 ± 0.13[a,b]	61.38 ± 5.30[a,b]	47.30 ± 9.44[b]	105.28 ± 7.40
BDL + ASE (125 mg)	2.35 ± 0.40[a,b]	45.06 ± 3.24[b,c]	52.45 ± 3.91[a,b]	112.62 ± 8.31[a,b]
BDL + ASE (250 mg)	2.61 ± 0.31[a,b]	49.11 ± 4.95[a,b,c]	67.45 ± 7.45[a]	116.50 ± 7.50[a,b]
BDL + ASE (380 mg)	1.65 ± 0.37[a]	53.70 ± 3.75[a,b]	68.23 ± 6.23[a]	113.54 ± 7.54[a,b]

$N = 6$; The values are expressed as mean ± SEM; one way ANOVA followed by bonferroni post hoc test.
[a]$p < 0.05$ compared to the Non-ligated + D/W.
[b]$p < 0.05$ compared to the BDL + D/W.
[c]$p < 0.05$ compared to the BDL + Sily group. Sily = Silymarin; D/W = Distilled water; BDL = Bile duct ligation; CAT = Catalase; SOD = Superoxide dismutase; GPx = Glutathione peroxidise; MDA = Malondialdehyde; ASE = *Acacia sieberiana* extract.

an effective hepatoprotective agent ((Vargas-mendoza et al., 2014; Papackova et al., 2018; Mukhtar et al., 2021). This informed the rationale for the current experiment to evaluate the effectiveness of the methanol root bark of *Acacia sieberiana* in the PCM and BDL-induced rat models of liver injury with altered biochemical parameters, oxidative stress biomarkers and liver histopathological alterations to validate its folkloric use in liver diseases.

The acute toxicity evaluation is important in checking the potentially noxious effects of chemical agents after acute administration. Besides, it helps in the LD_{50} determination of new bioactive compounds for biological screening (Musila et al., 2017; Kpemissi et al., 2020). The lack of toxic indications and death in animals following the acute administration of the compound at a dose of 5,000 mg/kg after a 14-days observation period showcases that the LD_{50} of the said compound could be higher than the 5 g/kg (Qin et al., 2009). Thus, the oral LD_{50} of the ASE in the current experiment might be greater than 5,000 mg/kg, and it could be safe at that dose *via* oral administration. However, mortality was observed following the *i. p* administration of the ASE 1,600 mg/kg resulting in a calculated *i. p* LD_{50} of 1,300 mg/kg, as an indication that it could be relatively safe at the dose after acute *i. p*. Administration.

Paracetamol is among the hepatotoxic therapeutic agents that cause acute hepatic failure at a high dose (Sinaga et al., 2021). Approximately one-fourth of the administered PCM binds to plasma protein and is partially biotransformed by the hepatic microsomal enzymes. It can also be metabolized by conjugation with glucuronic acid in the liver (Sinaga et al., 2021). The cytochrome P450 changes about 5%–15% of PCM within the therapeutic range to a highly reactive product N-acetyl-p-benzoquinonymin (NAPBQI), which is easily nullified by glutathione conjugation (Ohba et al., 2016). Following the PCM intoxication, the NAPBQI targets the mitochondrial protein and interferes with the energy production, generating ROS, which leads to oxidative stresses and subsequently generates hepatotoxicity (Yoon et al., 2016; Tsai et al., 2018).

The AST, ALT, and ALP are parameters that reveal the hepatic metabolic activities (El Kabbaoui et al., 2017). The AST and ALT have been particularly elevated in conditions that cause hepatocellular damage that eventually causes leakage of these enzymes into the blood in liver injuries (Ahmad et al., 2022; Li et al., 2019). The ALP level increases in case of bile duct obstruction and indicates liver or bone disorder (Sinaga et al., 2021). The effective decline in the ALT and AST levels by the ASE after the PCM hepatotoxic injury in the current work at the 250 and 750 mg/kg may be associated with its hepatoprotective efficacy. Sometimes, the toxic injury had been reported not to affect the ALP concentration, and this seemed to be confirmed in this study in that the PCM toxic injury did not significantly increase the ALP activity, unlike the ALT and AST.

The reduction in the total protein and albumin plasma concentration and the elevated levels of total and direct bilirubin in the hepatotoxic rats showcases interference of the hepatic cellular integrity and function as a result of paracetamol intoxication (Yoon et al., 2016). The ASE at all doses in this research increased the concentrations of the total protein and albumin efficiently, suggestive of its hepatoprotective activity. Besides, the ASE reduced the PCM-induced elevated bilirubin level, which was significant only in the 750 mg/kg ASE-treated group for the direct bilirubin.

The pathogenesis of hepatotoxicity is mostly related to the metabolic changes of xenobiotics to ROS, which eventually result in oxidative stress and damage to the hepatic cellular contents (Zhang et al., 2018). The antioxidant enzymes (SOD, CAT, and GPx) produce defensive mechanisms against ROS. Therefore, the imbalance between the generated ROS and antioxidant enzyme activity is responsible for the mechanisms of hepatic diseases, including hepatitis, cirrhosis, necrotic hepatitis and hepatocellular carcinoma

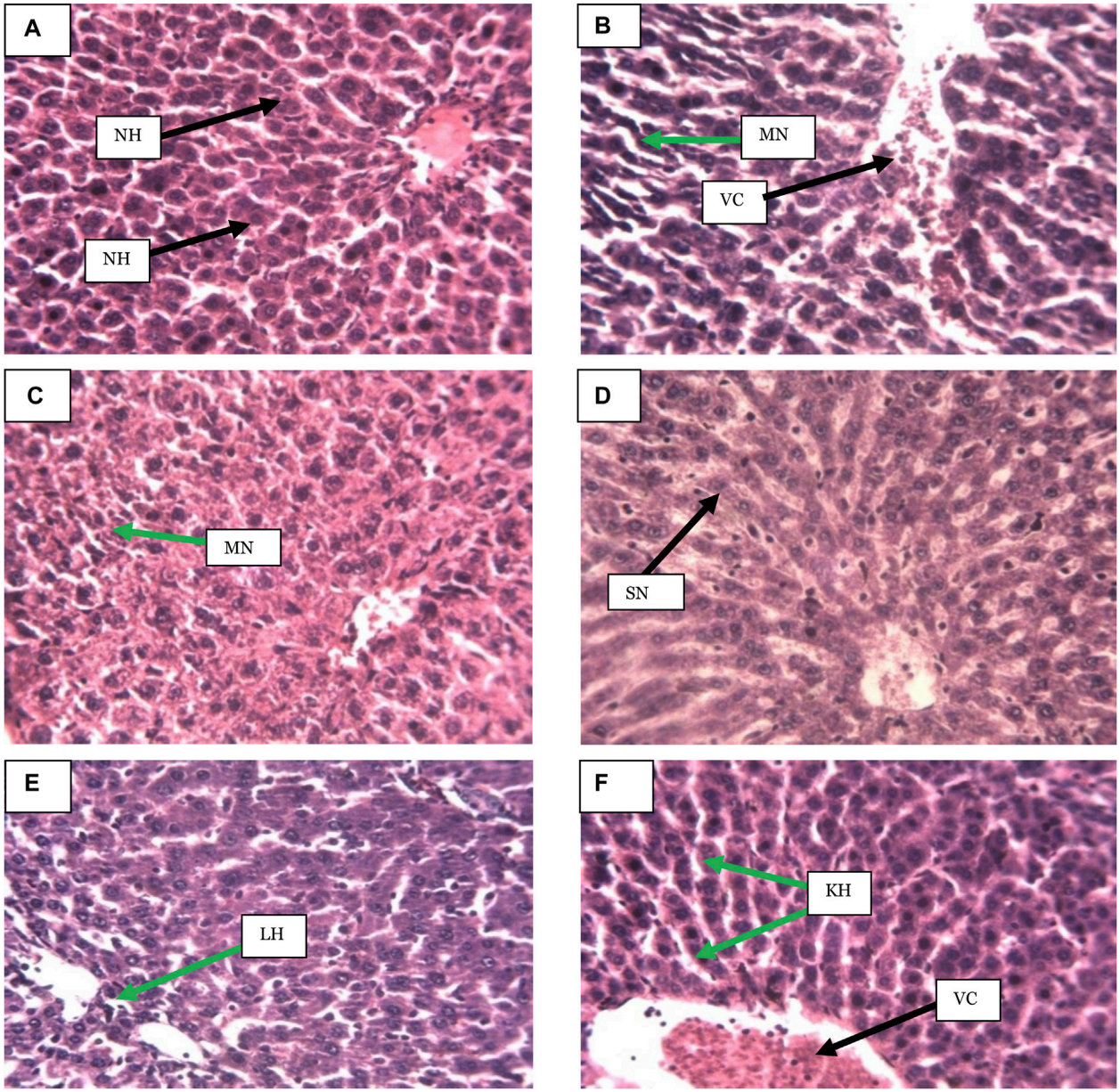

FIGURE 2
(A) Distilled water (1 ml/kg), **(B)** BDL + Distilled water (1 ml/kg), **(C)** BDL + Sily (50 mg/kg), **(D)** BDL + ASE (125 mg/kg), **(E)** BDL + ASE (250 mg/kg), **(F)** BDL + ASE (380 mg/kg), NH = Normal hepatocytes, VC = Vascular congestion, MN = Moderate necrosis, SN = Slight necrosis, LH = Lymphocytes hyperplasia, KH = Kupffer cell hyperplasia, ASE = *Acacia sieberiana* extract.

(Banerjee et al., 2020). The SOD enzyme converts superoxide radicals to an oxygen molecule and hydrogen peroxide to maintain a steady oxygen state (Palanivel et al., 2008). CAT and GPx often convert the hydrogen peroxide into water to complete the SOD's scavenging activity (Li et al., 2015). In this process, the toxic species (superoxide radical and hydrogen peroxide) are modified to the harmless water. Therefore, the reduction in the SOD level as seen in the PCM hepatotoxic group in this study suggests hepatocellular damage, which was efficiently attenuated in all the ASE-treated groups as an indication of protection against the PCM toxic injury. Although the PCM toxic injury did not affect the CAT concentration, ASE at 250 and 750 mg/kg as with silymarin elevated its level to indicate its hepatic boosting ability. The ASE ameliorated the injury from the PCM-induced reduction in GPx at all doses, almost to the same extent as the standard

agent. It was also obvious that the PCM-induced hepatic damage results in lipid peroxidation, as evident with the enhanced MDA level in the current research. The MDA generated as a result of lipid peroxidation tend to amplify cellular damage, thus, are often used as biomarkers of oxidative liver damage (Wang et al., 2019). Hence, oxidative hepatic damage could be alleviated by inhibiting the lipid peroxidation and MDA production (Liu et al., 2015). The reduction in the MDA concentration in both the silymarin and ASE administered groups in the current work further explained the ameliorative effects of the extract against the hepatic lipid peroxidation, free radicals and cellular damage.

The reduction in the PCM-induced intense necrosis and congestion in the silymarin and ASE treated groups further indicated the hepatoprotective activity resulting probably by increasing the activity of the antioxidant system in the body, thereby preventing liver damage. This protection seemed better with the lower ASE doses than 1,500 mg/kg.

The BDL is an animal model used to induce extrahepatic cholestasis in rats accompanied by fibrosis and oxidative stress (Pereira et al., 2009). Cholestasis can result from abnormal bile secretion by the hepatic and bile duct cells or by the blockade of bile ducts (Moslemi et al., 2021). The increased concentrations of ALT, ALP, and AST, total protein and bilirubin serve as sensitive markers of cholestasis to indicate bile acid degradation (Qiao et al., 2019). Generally, AST, ALT, and ALP elevations are associated with hepatic damage, necrosis, and bile salts accumulation, respectively (Aryal et al., 2019; Moslemi et al., 2021). The BDL-elicited liver damage in this study seemed to suggest milder toxicity than in the PCM-induced model. Similar to the PCM-induced model, the ASE in the current experiment demonstrated ameliorative effects in the BDL-induced hepatotoxicity. All the extract groups reduced the elevated ALT concentration. However, the reduced ALT level at the lowest extract dose, which showed more of the reduction, was not significant to the BDL-injury. The BDL-injury elevated AST was also reduced in all the extract groups, but only the lower extract doses were significantly reduced. However, ALP which was also reduced in all the treatment groups, was only significant at the higher extract doses. The better result exhibited by the lower doses of the extract for ALT and AST seemed to suggest its liver protection.

The effect of ligation was slight for both total protein (which increased) and albumin (decreased slightly). The ASE at the higher doses increased the albumin level, but total protein slightly decreased in all the ASE doses, which were insignificant. The direct and total bilirubin elevated with the BDL injury were significantly reduced in all the extract-treated groups, which could be related to the enhanced bilirubin uptake or its conjugation by the extract (Zhu et al., 2018). Therefore, the ASE in the present work might have increased the bile formation as part of its hepatoprotective efficacy.

Oxidative stress is the major pathogenesis in cholestasis, resulting from an imbalance between the antioxidant and oxidative systems (Moslemi et al., 2021). Some enzymes, such as CAT, SOD, and GPx, are antioxidants (Moslemi et al., 2021). The decrease in SOD from BDL-injury was prevented in the lower ASE doses (125 and 250 mg/kg) better than the silymarin. Although the SOD level was increased in all the treatment groups, the level was still significantly below that of the normal control. A dose-dependent increase in the CAT concentration also occurred with all the ASE-treated groups, and in this case, the increase at the 380 mg/kg extract dose was more and was not significantly different from the silymarin group unlike the lower extract doses. In both the PCM- and BDL-induced injury, the GPx concentration was not significantly reduced, but it was increased in all the treatment groups of both the standard drug and ASE dose groups. GPx is an enzyme that protects haemoglobin from oxidative degradation in the red blood cells. The enzyme has been reported to be over-expressed to protect cells against oxidative damage and apoptosis induced by hydrogen peroxide. It was also evident that the lowest ASE dose reduced the BDL-induced elevated MDA level, suggesting protection against the oxidative free radical, hepatic lipid peroxidation, and hepatocellular injury.

The moderate necrosis and vascular congestion observed with the BDL-produced liver damage were reversed by the 125 mg/kg extract group. Besides, milder effects were observed in the higher ASE dose groups (250 and 380 mg/kg). These effects could suggest some level of liver protection and regenerative potential of the extract.

The therapeutic potentials of the medicinal plant are usually a direct function of the bioactive components in the plant, which could serve as a lead to develop hepatoprotective compounds (Girish et al., 2009). The present experiment showcased that glycosides, triterpenes, saponins, tannins, flavonoids, and alkaloids could be available in the ASE. These compounds mostly act as antioxidants to abolish free radical generation and eventually prevent hepatic damage (Ramadan et al., 2013). For instance, flavonoids compounds such as catechin and kaempferol fight against free radicals and inhibit liver disease pathogenesis (Okaiyeto et al., 2018). Also, glycosides act as an antioxidant to provide hepatoprotective efficacy (Siddiqui et al., 2018; Asaad et al., 2021). Besides, (Huang et al., 2014), reported the hepatic protection of triterpenoids and saponins. A previous study by (Jan et al., 2017) has shown that alkaloids reduced biochemical biomarkers (ALT, AST, and ALP), attenuated hepatic inflammation, and elevated the antioxidant enzyme concentration in liver damage. Hence, the hepatic protective potentials of the ASE observed in the current research could be related to the presence of these phytocomponents.

5 Conclusion

The research findings have shown that the root bark extract of *Acacia sieberiana* ameliorates chemically-induced and cholestatic liver damages, possibly *via* modulating the biochemical and oxidative stress biomarkers, which justifies its ethnomedicinal value against hepatic disorders.

Data availability statement

The raw data supporting the conclusions of this article will be made available by the authors, without undue reservation.

Ethics statement

The animal study was reviewed and approved by Ahmadu Bello University Ethical Committee on Animal Use and Care Research Policy (ABUCAUC) of Ahmadu Bello University Zaria, Nigeria.

Author contributions

MW: Conceptualization, resources, investigation, writing original draft, data curation, review, editing, and data analysis. JIE: Supervision, validation, review, and project administration. AM: Investigation, review, and editing. MHA: Investigation, writing the original draft, revised and edit the entire manuscript. All the authors read and approved the final version of the manuscript.

Acknowledgments

The authors appreciate the entire staff of the Department of Pharmacology and Therapeutics, ABU, Zaria, Nigeria, for their support throughout the period of the experiment.

Conflict of interest

The authors declare that the research was conducted in the absence of any commercial or financial relationships that could be construed as a potential conflict of interest.

Publisher's note

All claims expressed in this article are solely those of the authors and do not necessarily represent those of their affiliated organizations, or those of the publisher, the editors and the reviewers. Any product that may be evaluated in this article, or claim that may be made by its manufacturer, is not guaranteed or endorsed by the publisher.

References

Abdelhady, M. I. (2013). A novel polyphenolic compound isolated from *Acacia sieberiana*. *Org. Chem.* 9 (6), 236–238.

Abenavoli, L., Izzo, A. A., Natasa, M., Cicala, C., Santini, A., Capasso, R., et al. (2018). Milk thistle (*Silybum marianum*): A concise overview on its chemistry, pharmacological, and nutraceutical uses in liver diseases. *Phytother. Res.* 32, 2202–2213. doi:10.1002/ptr.6171

Ahmad, M. H., Zezi, A. U., Bola, A. S., Alhassan, Z., Mohammed, M., Danraka, R. N., et al. (2020). Mechanisms of antidiarrhoeal activity of methanol leaf extract of *Combretum hypopilinum* Diels (Combretaceae): Involvement of opioidergic and (α1 and β)-adrenergic pathways. *J. Ethnopharmacol.* 269, 113750. doi:10.1016/j.jep.2020.113750

Ahmad, M. H., Zezi, A. U., Sherifat, B. A., Alshargi, O. Y., Mohammed, M., Mustapha, S., et al. (2022). Sub-acute toxicity study on hydromethanolic leaves extract of *Combretum hypopilinum* (Combretaceae) Diels in Wistar rats. *Toxicol. Res.* 38, 1–16. doi:10.1007/s43188-022-00133-5

Ali, S. A., Sharief, N. H., and Mohamed, Y. S. (2019). Hepatoprotective activity of some medicinal plants in Sudan. *Evidence-Based Complementary Altern. Med.* 2196315, 1–16. doi:10.1155/2019/2196315

Ameh, P. O., and Eddy, N. O. (2014). Characterisation of Acacia sieberiana (AS) gum and their corrosion inhibition potentials for zinc in sulphuric acid medium. *Int. J. Nov. Res. Phys. Chem. Math.* 1 (1), 25–36.

Anyasor, G. N., Moses, N., and Kale, O. (2020). Hepatoprotective and hematological effects of *Justicia secunda* Vahl leaves on carbon tetrachloride-induced toxicity in rats. *Biotech. Histochem.* 00 (00), 349–359. doi:10.1080/10520295.2019.1700430

Aryal, S., Adhikari, B., Panthi, K., Aryal, P., Sharifi-rad, J., and Koirala, N. (2019). Antipyretic, antinociceptive, and anti-Inflammator Activities from *Pogostemon benghalensis* leaf extract in experimental wister rats. *Medicines* 6, 96. doi:10.3390/medicines6040096

Asaad, G. F., Mohammed, H., Abdallah, I., Mohammed, H. S., and Nomier, Y. A. (2021). Hepatoprotective effect of kaempferol glycosides isolated from *Cedrela odorata* L. leaves in albino mice: Involvement of raf/MAPK pathway. *Res. Pharm. Sci.* 16 (4), 370–380. doi:10.4103/1735-5362.319575

Asrani, S. K., Devarbhavi, H., Eaton, J., and Kamath, P. S. (2019). Burden of liver diseases in the world. *J. Hepatol.* 70 (1), 151–171. doi:10.1016/j.jhep.2018.09.014

Banerjee, A., Das, D., Paul, R., Roy, S., Bhattacharjee, A., Ug, P., et al. (2020). Altered composition of high-lipid diet may generate reactive oxygen species by disturbing the balance of antioxidant and free radicals. *J. Basic Clin. Physiol. Pharmacol.* 31, 20190141. doi:10.1515/jbcpp-2019-0141

Bernal, W., Auzinger, G., Dhawan, A., and Wendon, J. (2010). Acute liver failure. *Lancet* 376 (9736), 190–201. doi:10.1016/S0140-6736(10)60274-7

Dawurung, C. J., Elisha, I. L., Offiah, N. V., Gotep, J. G., Oladipo, O. O., Makoshi, M. S., et al. (2012). Antidiarrheal evaluation of aqueous and ethanolic leaf extracts of *Acacia sieberiana* DC. (Fabaceae) in albino rats. *Asian J. Exp. Biol. Sci.* 4 (4), 799–803.

Duncan, A. W., Dorrell, C., and Grompe, M. (2009). Stem cells and liver regeneration. *Gastroenterology* 137 (2), 466–481. doi:10.1053/j.gastro.2009.05.044

El Kabbaoui, M., Chda, A., El-Akhal, J., Azdad, O., Mejrhit, N., Aarab, L., et al. (2017). Acute and sub-chronic toxicity studies of the aqueous extract from leaves of *Cistus ladaniferus* L. in mice and rats. *J. Ethnopharmacol.* 209, 147–156. doi:10.1016/j.jep.2017.07.029

Elmasry, S., and Moawad, M. (2021). The hepatoprotective effect of gooseberry and black mulberry extracts against carbon tetrachloride-induced liver injury in rats. *JoBAZ.* 82 (33), 33. doi:10.1186/s41936-021-00224-z

Elufioye, T. O., and Habtemariam, S. (2019). Hepatoprotective effects of rosmarinic acid: Insight into its mechanisms of action. *Biomed. Pharmacother. J.* 112, 108600. doi:10.1016/j.biopha.2019.108600

Girish, C., Koner, B. C., Jayanthi, S., Rao, K. R., Rajesh, B., Pradhan, S. C., et al. (2009). Hepatoprotective activity of picroliv, curcumin and ellagic acid compared to silymarin on paracetamol induced liver toxicity in mice. *Fundam. Clin. Pharmacol.* 23, 735–745. doi:10.1111/j.1472-8206.2009.00722.x

Huang, B., Fu, H., Chen, W., Luo, Y., and Ma, S. (2014). Hepatoprotective triterpenoid saponins from *Callicarpa nudiflora*. *Chem. Pharm. Bull.* 62 (July), 695–699. doi:10.1248/cpb.c14-00159

Ilyas, U., Katare, D. P., Aeri, V., and Naseef, P. P. (2016). A review on hepatoprotective and immunomodulatory herbal plants. *Pharmacogn. Rev.* 10 (19), 66–70. doi:10.4103/0973-7847.176544

Jadeja, R., Devkar, R. V., and Nammi, S. (2015). Hepatoprotective potential of herbal medicine. *Evid. Based. Complement. Altern. Med.* 2015, 536564. doi:10.1155/2015/536564

Jan, N. U., Ahmad, B., Ali, S., Adhikari, A., Ali, A., Jahan, A., et al. (2017). Steroidal alkaloids as an emerging therapeutic alternative for investigation of their immunosuppressive and hepatoprotective potential. *Front. Pharmacol.* 8, 114. doi:10.3389/fphar.2017.00114

Jin, S. E., Shin, H., and Ha, H. (2021). Hepatoprotective effects of Gamisoyo-san against acetaminophen-induced liver injuries. *Integr. Med. Res.* 10 (1), 100466. doi:10.1016/j.imr.2020.100466

Khan, A., ur-Rehman, N.Alkharfy, K. M., and Gilani, A. H. (2011). Antidiarrheal and antispasmodic activities of *Salvia officinalis* are mediated through activation of K + channels. *Bangladesh J. Pharmacol.* 6 (2), 111–116. doi:10.3329/bjp.v6i2.9156

Khan, H., Ullah, H., and Nabavi, S. M. (2019). Mechanistic insights of hepatoprotective effects of curcumin: Therapeutic updates and future prospects. *Food Chem. Toxicol.* 124, 182–191. doi:10.1016/j.fct.2018.12.002

Kpemissi, M., Metowogo, K., Melila, M., Veerapur, V. P., Negru, M., Taulescu, M., et al. (2020). Acute and subchronic oral toxicity assessments of *Combretum micranthum* (Combretaceae) in Wistar rats. *Toxicol. Rep.* 7, 162–168. doi:10.1016/j.toxrep.2020.01.007

Li, S., Tan, H., Wang, N., Zhang, Z., Lao, L., Wong, C., et al. (2015). The role of oxidative stress and antioxidants in liver diseases. *Int. J. Mol. Sci.* 16 (11), 26087–26124. doi:10.3390/ijms161125942

Li, Y., Kandhare, A. D., Mukherjee, A. A., and Bodhankar, S. L. (2019). Acute and sub-chronic oral toxicity studies of hesperidin isolated from orange peel extract in Sprague Dawley rats. *Regul. Toxicol. Pharmacol.* 105 (1), 77–85. doi:10.1016/j.yrtph.2019.04.001

Lin, S., Wang, Y., Chen, W., Liao, S., Chou, S., Yang, C., et al. (2017). Hepatoprotective activities of rosmarinic acid against extrahepatic cholestasis in rats. *Food Chem. Toxicol.* 108, 214–223. doi:10.1016/j.fct.2017.08.005

Liu, J., Lu, J., Wen, X., Kan, J., and Jin, C. (2015). Antioxidant and protective effect of inulin and catechin grafted inulin against CCl 4 -induced liver injury. *Int. J. Biol. Macromol.* 72, 1479–1484. doi:10.1016/j.ijbiomac.2014.09.066

Lorke, D. (1983). A new approach to practical acute toxicity testing. *Arch. Toxicol.* 54, 275–287. doi:10.1007/BF01234480

Ma, X., Jiang, Y., Zhang, W., Wang, J., Wang, R., Wang, L., et al. (2020). Natural products for the prevention and treatment of cholestasis: A review. *Phytother. Res.* 34 (6), 1291–1309. doi:10.1002/ptr.6621

Madrigal-santillán, E., Madrigal-bujaidar, E., Álvarez-gonzález, I., Sumaya-martínez, M. T., Gutiérrez-salinas, J., Bautista, M., et al. (2014). Review of natural products with hepatoprotective effects. *World J. Gastroenterol.* 20 (40), 14787–14804. doi:10.3748/wjg.v20.i40.14787

Mahmood, N. D., Mamat, S. S., Kamisan, F. H., Yahya, F., Kamarolzaman, M. F. F., Nasir, N., et al. (2014). Amelioration of paracetamol-induced hepatotoxicity in rat by the administration of methanol extract of *Muntingia calabura* L . Leaves. *Biomed. Res. Int.* 2014 (695678). doi:10.1155/2014/695678

Michalopoulos, G. K. (2017). Hepatostat: Liver regeneration and normal liver tissue maintenance. *Hepatology* 65 (4), 1384–1392. doi:10.1002/hep.28988

Miltonprabu, S., Tomczyk, M., Skalicka-Woźniak, K., Rastrelli, L., Daglia, M., Nabavi, S. F., et al. (2016). Hepatoprotective effect of quercetin: From chemistry to medicine. *Food Chem. Toxicol.* 108, 365–374. doi:10.1016/j.fct.2016.08.034

Moslemi, Z., Bahrami, M., Hosseini, E., Mansourian, M., Daneshyar, Z., Eftekhari, M., et al. (2021). *Portulaca oleracea* methanolic extract attenuate bile duct ligation-induced acute liver injury through hepatoprotective and anti-inflammatory effects. *Heliyon* 7, e07604. doi:10.1016/j.heliyon.2021.e07604

Muhammad, S. L., Wada, Y., Mohammed, M., Ibrahim, S., Musa, K. Y., Olonitola, O. S., et al. (2021). Bioassay-guided identification of bioactive compounds from *Senna alata* L . against methicillin-resistant *Staphylococcus aureus*. *Appl. Microbiol.* 1, 520–536. doi:10.3390/applmicrobiol1030034

Mukhtar, S., Xiaoxiong, Z., Qamer, S., Saad, M., Mubarik, M. S., Mohammed, A. H., et al. (2021). Hepatoprotective activity of silymarin encapsulation against hepatic damage in albino rats. *Saudi J. Biol. Sci.* 28 (1), 717–723. doi:10.1016/j.sjbs.2020.10.063

Musila, M. N., Ngai, D. N., Mbiri, J. W., Njagi, S. M., Mbinda, W. M., Ngugi, M. P., et al. (2017). Acute and sub-chronic oral toxicity study of methanolic extract of *Caesalpinia volkensii* (harms). *J. Drug Metab. Toxicol.* 08 (01), 1–8. doi:10.4172/2157-7609.1000222

Ngaffo, C. M. N., Tchangna, R. S. V., Mbaveng, A. T., Kamga, J., Harvey, F. M., Ngadjui, B. T., et al. (2020). Botanicals from the leaves of *Acacia sieberiana* had better cytotoxic effects than isolated phytochemicals towards MDR cancer cells lines. *Heliyon* 6, e05412. doi:10.1016/j.heliyon.2020.e05412

Ohba, H., Kanazawa, M., Kakiuchi, T., and Tsukada, H. (2016). Effects of acetaminophen on mitochondrial complex I activity in the rat liver and kidney: A PET study with 18 F-BCPP-BF. *EJNMMI Res.* 682, 82. doi:10.1186/s13550-016-0241-4

Ohemu, T. L., Agunu, A., Olotu, P. N., Ajima, U., Dafam, D. G., and Azila, J. J. (2014). Ethnobotanical survey of medicinal plants used in the traditional treatment of viral infections in Jos, Plateau state, Nigeria. *Int. J. Med. Aromatic Plants* 4 (2), 74–81.

Okaiyeto, K., Nwodo, U. U., Mabinya, L. V., and Okoh, A. I. (2018). A review on some medicinal plants with hepatoprotective effects. *Pharmacogn. Rev.* 12 (24), 186. doi:10.4103/phrev.phrev_52_17

Palanivel, M. G., Rajkapoor, B., Kumar, R. S., Einstein, J. W., Kumar, E. P., Kumar, M. R., et al. (2008). Hepatoprotective and antioxidant effect of *Pisonia aculeata* L. Against CCl4-induced hepatic damage in rats. *Sci. Pharm.* 76 (2), 203–215. doi:10.3797/scipharm.0803-16

Papackova, Z., Heczkova, M., Dankova, H., Sticova, E., Lodererova, A., Bartonova, L., et al. (2018). Silymarin prevents acetaminophen-induced hepatotoxicity in mice. *PLoS ONE* 13 (1), e0191353. doi:10.1371/journal.pone.0191353

Park, H., Jo, E., Han, J., Jung, S., Lee, D., Park, I., et al. (2019). Hepatoprotective effects of an *Acer tegmentosum* Maxim extract through antioxidant activity and the regulation of autophagy. *J. Ethnopharmacol.* 239, 111912. doi:10.1016/j.jep.2019.111912

Pereira, F. A., Facincan, I., Jorgetti, V., Ramalho, L. N. Z., Volpon, J. B., Reis Dos, L. M., et al. (2009). Etiopathogenesis of hepatic osteodystrophy in wistar rats with cholestatic liver disease. *Calcif. Tissue Int.* 85 (1), 75–83. doi:10.1007/s00223-009-9249-3

Pingili, R. B., Pawar, A. K., Challa, S. R., Kodali, T., Koppula, S., Toleti, V., et al. (2019). A comprehensive review on hepatoprotective and nephroprotective activities of chrysin against various drugs and toxic agents. *Chem. Biol. Interact.* 308, 51–60. doi:10.1016/j.cbi.2019.05.010

Protzer, U., Maini, M. K., and Knolle, P. A. (2012). Living in the liver: Hepatic infections. *Nat. Rev. Immunol.* 12 (3), 201–213. doi:10.1038/nri3169

Qiao, J., Li, H., Liu, F., Li, Y., Tian, S., and Cao, L. (2019). Effects of *Portulaca oleracea* extract on acute alcoholic liver injury of rats. *Molecules* 24 (16), 2887. doi:10.3390/molecules24162887

Qin, Y., Wu, X., Huang, W., Gong, G., Li, D., He, Y., et al. (2009). Acute toxicity and sub-chronic toxicity of steroidal saponins from *Dioscorea zingiberensis* C . H . Wright in rodents. *J. Ethnopharmacol.* 126, 543–550. doi:10.1016/j.jep.2009.08.047

Ramadan, M. M., Abd-algader, N. N., El-kamali, H. H., Ghanem, K. Z., and Farrag, A. R. (2013). Volatile compounds and antioxidant activity of the aromatic herb *Anethum graveolens*. *J. Arab. Soc. Med. Res.* 8 (2), 79. doi:10.4103/1687-4293.123791

Ramirez, T., Strigun, A., Verlohner, A., Huener, H.-A., Peter, E., Herold, M., et al. (2018). Prediction of liver toxicity and mode of action using metabolomics *in vitro* in HepG2 cells. *Arch. Toxicol.* 92 (2), 893–906. doi:10.1007/s00204-017-2079-6

Rašković, A., Milanovi, I., Pavlović, N., Ćebović, T., Vukmirović, S., Mikov, M., et al. (2014). Antioxidant activity of rosemary (*Rosmarinus officinalis* L.) essential oil and its hepatoprotective potential. *BMC Complement. Altern. Med.* 14 (225), 225. doi:10.1186/1472-6882-14-225

Salisu, A., Ogbadu, G. H., Onyenekwe, P. C., Olorode, O., Ndana, R. W., Segun, O., et al. (2014). Evaluating the nutritional potential of *Acacia sieberiana* seeds (dc) growing in north west of Nigeria. *J. Biol. Life Sci.* 5 (2), 25. doi:10.5296/jbls.v5i2.4860

Seigler, D. S., Butterfield, C. S., Dunn, J. E., and Conn, E. E. (1975). Dihydroacacipetalin–a new cyanogenic glucoside from *Acacia sieberiana* var. *Woodi.* Phytochem. 14, 1419–1420. doi:10.1016/s0031-9422(00)98641-2

Siddiqui, M. A., Ali, Z., Chittiboyina, A. G., and Khan, I. A. (2018). Hepatoprotective effect of steroidal glycosides from *Dioscorea villosa* on hydrogen peroxide-induced hepatotoxicity in HepG2 cells. *Front. Pharmacol.* 9, 797. doi:10.3389/fphar.2018.00797

Sinaga, E., Fitrayadi, A., Asrori, A., Rahayu, S. E., Suprihatin, S., Prasasty, V. D., et al. (2021). Hepatoprotective effect of *Pandanus odoratissimus* seed extracts on paracetamol-induced rats induced rats. *Pharm. Biol.* 59 (1), 31–39. doi:10.1080/13880209.2020.1865408

Sofowora, A. (1993). *Medicinal plants and traditional medicine in Africa*. 2nd Editio. Ibadan: Spectrum Books Ltd.

Tag, C. G., Sauer-lehnen, S., Weiskirchen, S., Borkham-kamphorst, E., Tolba, R. H., Tacke, F., et al. (2015). Bile duct ligation in mice: Induction of inflammatory liver injury and fibrosis by obstructive cholestasis. *J. Vis. Exp.* 96 (e52438), 1–11. doi:10.3791/52438

Tsai, M.-S., Wang, Y.-H., Lai, Y.-Y., Tsou, H., Liou, G., Ko, J., et al. (2018). Kaempferol protects against propacetamol-induced acute liver injury through CYP2E1 inactivation, UGT1A1 activation, and attenuation of oxidative stress, inflammation and apoptosis in mice. *Toxicol. Lett.* 290, 97–109. doi:10.1016/j.toxlet.2018.03.024

Usman, A. M., Danjuma, N. M., Ya'u, J., Ahmad, M. M., Alhassan, Z., Abubakar, Y. M., et al. (2021). Antidiarrhoeal potentials of methanol bark extract of *Hymenocardia Acida* Tul (Euphorbiaceae) in laboratory animals. *Bull. Natl. Res. Cent.* 45 (118), 118. doi:10.1186/s42269-021-00575-1

Uzunhisarcikli, M., and Aslanturk, A. (2019). Hepatoprotective effects of curcumin and taurine against bisphenol A-induced liver injury in rats. *Environ. Sci. Pollut. Res. Int.* 26 (36), 37242–37253. doi:10.1007/s11356-019-06615-8

Vargas-mendoza, N., Madrigal-santillán, E., Morales-González, Á., Esquivel-soto, J., Esquivel-chirino, C., González-rubio, M. G., et al. (2014). Hepatoprotective effect of silymarin. *World J. Hepatol.* 6 (3), 144–149. doi:10.4254/wjh.v6.i3.144

Wang, Y. A. O., Chen, Q., Shi, C., Jiao, F., and Gong, Z. (2019). Mechanism of glycyrrhizin on ferroptosis during acute liver failure by inhibiting oxidative stress. *Mol. Med. Rep.* 20, 4081–4090. doi:10.3892/mmr.2019.10660

Yoon, E., Babar, A., Choudhary, M., Kutner, M., and Pyrsopoulos, N. (2016). Acetaminophen-induced hepatotoxicity: A comprehensive update. *J. Clin. Transl. Hepatol.* 4 (2), 131–142. doi:10.14218/JCTH.2015.00052

Younossi, Z. M., Stepanova, M., Afendy, M., Fang, Y., Younossi, Y., Mir, H., et al. (2011). Changes in the prevalence of the most common causes of chronic liver diseases in the United States from 1988 to 2008. *Clin. Gastroenterol. Hepatol.* 9 (6), 524–530. doi:10.1016/j.cgh.2011.03.020

Yue, S., Xue, N., Li, H., Huang, B., Chen, Z., Wang, X., et al. (2020). Hepatoprotective effect of apigenin against liver injury via the non-canonical NF- κ B pathway *in Vivo* and *in vitro*. *Inflammation* 43 (5), 1634–1648. doi:10.1007/s10753-020-01238-5

Zhang, C., Wang, N., Xu, Y., Tan, H., Li, S., Feng, Y., et al. (2018). Molecular mechanisms involved in oxidative stress-associated liver injury induced by Chinese herbal medicine : An experimental evidence-based literature review and network Pharmacology study. *Int. J. Mol. Sci.* 19 (9), 2745. doi:10.3390/ijms19092745

Zhou, H., Wang, H., Shi, K., Li, J., Zong, Y., Du, R., et al. (2019). Hepatoprotective effect of baicalein against acetaminophen-induced acute liver injury in mice. *Molecules* 24 (1), 131. doi:10.3390/molecules24010131

Zhu, L., Wang, L., Cao, F., Liu, P., Bao, H., Yan, Y., et al. (2018). Modulation of transport and metabolism of bile acids and bilirubin by chlorogenic acid against hepatotoxicity and cholestasis in bile duct ligation rats: Involvement of SIRT1-mediated deacetylation of FXR and PGC-1α. *J. Hepatobiliary. Pancreat. Sci.* 25 (3), 195–205. doi:10.1002/jhbp.537

Glossary

ABU Ahmadu Bello University

ABUCAUC ABU Ethical Committee on Animal Use and Care Research Policy

ALP Alkaline phosphatase

ALT Alanine transaminase

ANOVA Analysis of variance

ARRIVEAnimal Research: Animal Research:Reporting of *In Vivo* Experiments

ASE *Acacia sieberiana* extract

AST aspartate transaminase

BDL Bile duct ligation

CAT Catalase

DB Direct bilirubin

DW Distilled water

FN Focal necrosis

GPx Glutathione peroxidase

i. p ntraperitoneal

KH Kupffer cell hyperplasia

LD50 Medial lethal dose

LH Lymphocytes hyperplasia

MDA Malondialdehyde

MN Moderate necrosis.

N Necrosis

NAPBQI N-acetyl-p-benzoquinonymin

NH Normal hepatocytes

PCM Paracetamol

ROS Reactive oxygen species

rpm Revolutions per minute

SC Sinusoid congestionslight sinusoidal congestion

SC Sinusoid congestionslight sinusoidal congestion

SEM Standard error of the mean

SN Slight necrosis

SOD Superoxide dismutase

TB Total bilirubin

TP Total protein

VC Vascular congestion

frontiers | Frontiers in Pharmacology

TYPE Review
PUBLISHED 24 August 2022
DOI 10.3389/fphar.2022.979307

Check for updates

OPEN ACCESS

EDITED BY
Fareeha Anwar,
Riphah International University, Pakistan

REVIEWED BY
Ling Fu,
Arthur Riggs Diabetes and Metabolism Research Institute, United States
Rongtao Li,
Kunming University of Science and Technology, China
Yuan Wei,
Jiangsu University, China

*CORRESPONDENCE
Tao Yang,
yangtao@shutcm.edu.cn
Hua Zhou,
zhouhua@shutcm.edu.cn

SPECIALTY SECTION
This article was submitted to Predictive Toxicology, a section of the journal Frontiers in Pharmacology

RECEIVED 27 June 2022
ACCEPTED 02 August 2022
PUBLISHED 24 August 2022

CITATION
Hu Y, Wu Q, Wang Y, Zhang H, Liu X, Zhou H and Yang T (2022), The molecular pathogenesis of triptolide-induced hepatotoxicity.
Front. Pharmacol. 13:979307.
doi: 10.3389/fphar.2022.979307

COPYRIGHT
© 2022 Hu, Wu, Wang, Zhang, Liu, Zhou and Yang. This is an open-access article distributed under the terms of the Creative Commons Attribution License (CC BY). The use, distribution or reproduction in other forums is permitted, provided the original author(s) and the copyright owner(s) are credited and that the original publication in this journal is cited, in accordance with accepted academic practice. No use, distribution or reproduction is permitted which does not comply with these terms.

The molecular pathogenesis of triptolide-induced hepatotoxicity

Yeqing Hu[1,2,3], Qiguo Wu[4], Yulin Wang[1,2,3], Haibo Zhang[1,2,3], Xueying Liu[1,2,3], Hua Zhou[1,2,3]* and Tao Yang[1,2,3,5]*

[1]Institute of Cardiovascular Disease, Shuguang Hospital Affiliated to Shanghai University of Traditional Chinese Medicine, Shanghai, China, [2]Institute of Cardiovascular Disease of Integrated Traditional Chinese Medicine and Western Medicine, Shuguang Hospital Affiliated to Shanghai University of Traditional Chinese Medicine, Shanghai, China, [3]Shuguang Hospital Affiliated to Shanghai University of Traditional Chinese Medicine, Branch of National Clinical Research Center for Chinese Medicine Cardiology, Shanghai, China, [4]Department of Pharmacy, Anqing Medical College, Anqing, China, [5]Shanghai Key Laboratory of Traditional Chinese Clinical Medicine, Shanghai, China

Triptolide (TP) is the major pharmacologically active ingredient and toxic component of *Tripterygium wilfordii* Hook. f. However, its clinical potential is limited by a narrow therapeutic window and multiple organ toxicity, especially hepatotoxicity. Furthermore, TP-induced hepatotoxicity shows significant inter-individual variability. Over the past few decades, research has been devoted to the study of TP-induced hepatotoxicity and its mechanism. In this review, we summarized the mechanism of TP-induced hepatotoxicity. Studies have demonstrated that TP-induced hepatotoxicity is associated with CYP450s, P-glycoprotein (P-gp), oxidative stress, excessive autophagy, apoptosis, metabolic disorders, immunity, and the gut microbiota. These new findings provide a comprehensive understanding of TP-induced hepatotoxicity and detoxification.

KEYWORDS

triptolide, hepatotoxicity, CYP450s, oxidative stress, immunity

1 Introduction

Tripterygium wilfordii Hook. F (*Tw*HF), the dried root or root xylem of *Tripterygium wilfordii* Hook. f. *Tw*HF and its preparations, have been widely used to treat autoimmune and inflammatory diseases because of its significant anti-inflammatory and immunosuppressive effects (Luo et al., 2019). Triptolide (TP) is a diterpene triepoxide, which is the major pharmacologically active ingredient and toxic component of *Tw*HF (Xi et al., 2017). TP has attracted the attention of researchers because of its high potential for clinical application, such as its anti-inflammatory, anti-cancer, anti-immune, and anti-oxidant effects (Guo et al., 2016; Yu et al., 2021; Gao et al., 2022; Song et al., 2022). However, its clinical potential is limited by a narrow therapeutic window and multiple organ toxicity, especially hepatotoxicity (Zhou et al., 2012; Xi et al., 2017).

The data on adverse reactions (ADRs) of *Tw*HF preparations containing TP released by the National Adverse Drug Reaction Monitoring Center of China shows that 839 cases of ADRs caused by *Tw*HF preparations from 2004 to September 2011, mainly manifested as drug-induced hepatitis and renal insufficiency. Furthermore, there are 472 cases of

ADRs were reported in *Tripterygium wilfordii* polyglycosides from 1 September 2014 to 31 August 2019 and 54 cases (11.44%) of which were abnormal liver function. It was reported that the distribution concentration of TP in rat liver was more than three times that of other tissues, which might be the reason for the significant hepatotoxicity among the multi-organ toxicities (Mei et al., 2012). Clinically, the hepatotoxicity caused by *Tw*HF and its preparations containing TP is mainly manifested as acute hepatitis, with symptoms such as nausea, fatigue, anorexia, increased serum alanine transaminase (ALT)and aspartate aminotransferase (AST) levels, and obvious cholestasis (Yang et al., 2018). Focal necrosis, inflammatory cell infiltration, cell degeneration, apoptosis, and bile duct hyperplasia are the common pathological manifestations in TP-induced hepatotoxicity (Wang X. Z. et al., 2018; Zou et al., 2020).

The hepatotoxicity mechanisms of TP are quite complex and show significant inter-individual variability. Researchers have explored the mechanism of TP-induced hepatotoxicity. Therefore, this review will provide a comprehensive analysis of the toxicological mechanism of TP to promote our understanding of TP-induced hepatotoxicity and detoxification.

2 The mechanisms of TP-induced hepatotoxicity

2.1 CYP450s and P-gp mediated hepatotoxicity

TP, an active electrophile containing three epoxide groups, can bind covalently to a 90-kda protein, XPB (Xeroderma pigmentosum, complementation group B), thereby inhibiting XPB's ATPase activity, which might be the underlying reason for the toxicity of TP (Titov et al., 2011). Opening the epoxide ring of TP can reduce its toxicity (Zhang and Li, 2004). Clinically, the therapeutic dose of ,*TW*HF tablets is about 4-6 tablets/d,

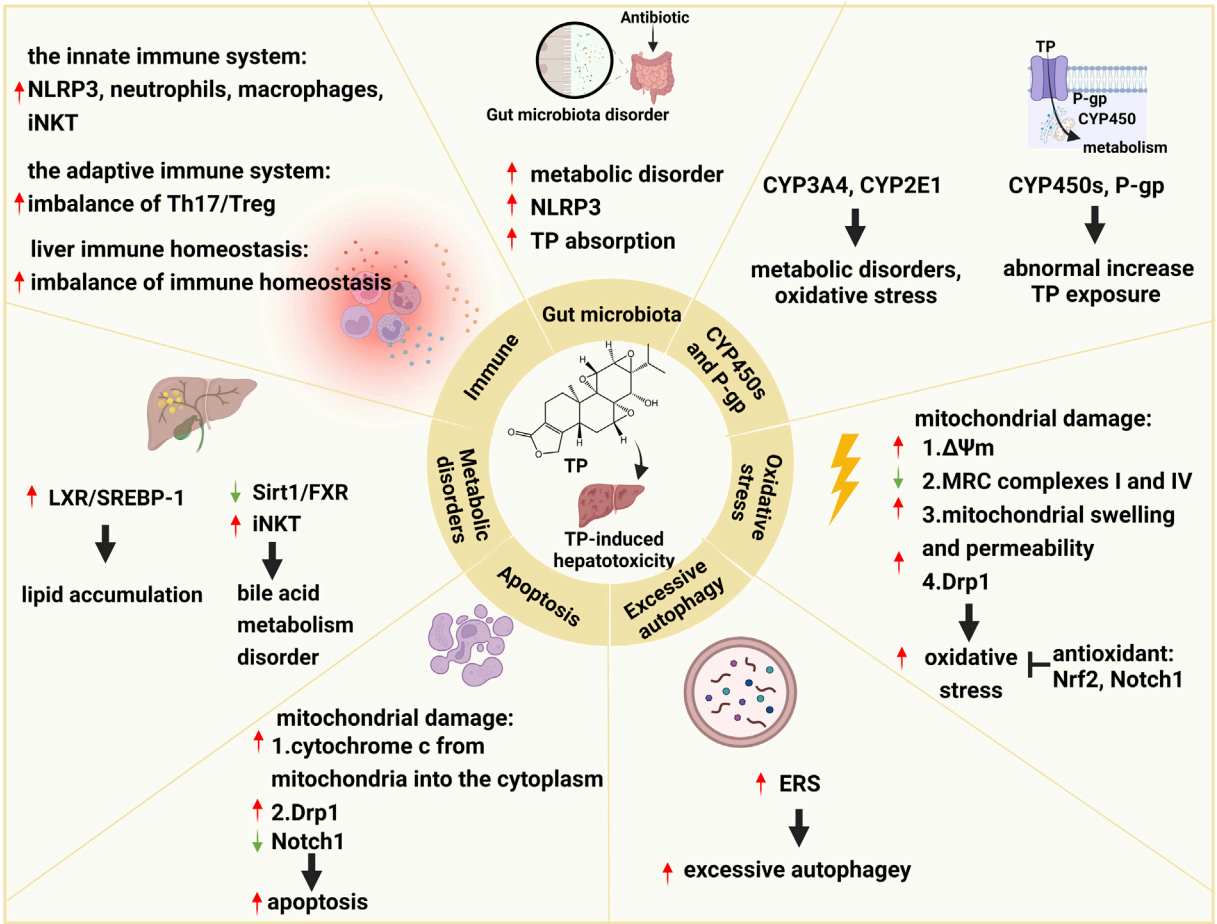

FIGURE 1
Schematic diagram of molecular pathogenesis of TP-induced hepatotoxicity. This figure shows that TP-induced hepatotoxicity is mainly related to CYP450s, P-gp, oxidative stress, excessive autophagy, apoptosis, metabolic disorders, immunity, and the gut microbiota. ↑: upregulation; ↓: downregulation; ⊤: inhibition.

which is equal to 400–600 μg/d TP (Qu et al., 2015). In addition, the effective dose of TP could reach 400 μg/kg administered continuously for 40 days in the animal experiments (Pan et al., 2017). However, the acute toxicity study showed that administration of 500 μg/kg in mice could cause liver injury (Wang et al., 2016), and the acute toxicity dose converted into 60 kg of human is 2,400 μg. These data implicate a narrow therapeutic window of TP and a slight excess of TP can lead to the risk of hepatotoxicity. Furthermore, studies have demonstrated that TP-induced hepatotoxicity is dose- and time-dependent (Yuan et al., 2019a; Zhao J. et al., 2020). In addition, cytochrome P450 (CYP) enzymes are involved in TP metabolism and P-glycoprotein (P-gp) is involved in TP transport, which affects the *in vivo* processing of TP (Xue et al., 2011; Zhang et al., 2016). Therefore, the abnormal increase TP exposure caused by CYP450s and P-gp, which leads to the increase of TP's direct hepatotoxicity, is an important factor for its hepatotoxicity.

2.1.1 CYP450s

2.1.1.1 Abnormal metabolism of CYP450 enzyme systems

CYP450s, a superfamily of enzymes, catalyze phase I oxidation and reduction of endogenous and xenobiotics substances (Nebert and Dalton, 2006). Studies have demonstrated that CYP450-mediated phase I metabolism of TP is the major pathway for reducing hepatotoxicity. Glutathione (GSH)-conjugated phase II metabolism induces mild detoxification and plays a minor role in TP-induced hepatotoxicity (Du et al., 2014; Li et al., 2015). Comparing liver-specific CYP450 reductase knockout mice and wild-type mice, the inactivation of hepatic CYP450 could significantly increase TP bioavailability and levels in liver tissue, leading to increased hepatotoxicity (Xue et al., 2011). Similarly, the CYP450 enzyme inhibitor 1-aminobenzotriazole or the CYP450 enzyme activator phenobarbital could increase or decrease the TP level, thereby modulating TP-induced primary rat hepatocyte toxicity (Jin et al., 2019). However, compared with wild-type mice, there were no significant differences in hepatotoxicity and pharmacokinetics in mice with low levels of extrahepatic CYP450 reductase, demonstrating that extrahepatic CYP450 has no effect on TP-induced hepatotoxicity (Wei et al., 2018). These studies confirmed the important role of hepatic CYP450 enzyme-mediated TP metabolism in TP-induced hepatotoxicity.

CYP450 isoforms make different contributions to TP metabolism and hepatotoxicity. CYP3A4 and CYP2C19 are involved in the metabolism of TP in male human liver microsomes, and CYP3A4 is the main isoform responsible for its hydroxylation (Li et al., 2008). Dexamethasone, a CYP3A inducer, increases TP metabolism and reduces TP-induced hepatotoxicity in rats (Ye et al., 2010). Another *in vitro* experiment confirmed that CYP3A-mediated TP metabolism can modulate TP-induced hepatotoxicity (Shen et al., 2014).

TP has been investigated to inhibit CYP450s. It was reported that TP exposure has a weak and time-dependent inhibitory effect on CYP3A in rat liver microsomes and hepatocytes (Shen et al., 2014). Likewise, TP inhibited the activity of human hepatic CYP1A2 and CYP3A4, but not other CYP450 isoforms, such as CYP2A6, 2E1, 2D6, 2C9, 2C19, and 2C8 (Zhang et al., 2017). Furthermore, long-term oral administration of TP could significantly inhibit the expression and activity of CYP3A4 in rats (Zhang et al., 2014). Researchers further investigated the effect of TP on the six major subtypes of CYP450 (1A2, 2C9, 2C19, 2D6, 2E1, and 3A). The result showed that continuous gavage of TP for 28 days could inhibit the activity and expression of CYP450 isoforms 3A, 2C9, 2C19, and 2E1 and cause hepatotoxicity in rats (Lu et al., 2017). In addition, TP could inhibit the transcriptional activation of the pregnane X receptor (PXR), thereby inhibiting the expression and function of metabolic detoxification enzymes, especially CYP3A4, which ultimately led to reduced metabolic elimination of TP and increased hepatotoxicity (Zheng et al., 2021). From the above studies, we speculated that the inhibitory effect of TP on CYP450s can cause alterations in TP metabolism and hepatotoxicity. However, whether TP inhibits CYP2E1 and CYP2C9 remains controversial.

Besides, studies have shown that CYP450s are also involved in endogenous substance metabolism and reactive oxygen species (ROS) production. A metabolomic study showed that TP treatment induced metabolic disorders, such as changes in carnitine, lysophosphatidylcholine (LPC), and a series of amino acids in female mice, and regulating the activity of CYP3A4 can modulate LPC levels, amino acid levels, the glutathione (GSH)/Glutathione disulfide (GSSG) ratio, and oxidative stress, thereby altering TP-induced hepatotoxicity (Xiao et al., 2020). Moreover, the TP-induced increase in CYP2E1 expression induces hepatic oxidative stress (Jiang et al., 2021). In C57 mice and IHHA-1 cell models, CYP2E1 expression was upregulated after TP exposure, which not only directly increased ROS levels, but also increased the expression of nuclear factor kappa B (NF-κB) (p65) to mediate oxidative stress and inflammatory responses (Jiang et al., 2021).

2.1.1.2 Sex differences, genetic polymorphisms and circadian rhythms

A significant difference in the hepatotoxicity of TP was found between different sexes in rats. The expression of CYP3A2, which is involved in TP metabolism, is higher in male rats than in female rats, a factor that makes females more susceptible to TP-induced hepatotoxicity (Liu et al., 2010). Inhibiting the expression and activity of CYP3A2 in male neonatal rats could eliminate the sex-dependent differences in TP metabolism (Liu et al., 2011).

Synonymous nucleotide polymorphisms can affect gene expression and function. Chen et al. established stable HepG2 cells with lentiviral vectors expressing either *CYP2E1-1263C/wt* or *CYP2E1-1263T/mt* constructs to investigate the effect of synonymous SNP rs2515641 on *CYP2E1* expression, and found that both the mRNA and protein expression levels of CYP2E1 were significantly decreased, and the ALT level of CYP2E1-1263T/mt recombinant cells was increased compared with that in the CYP2E1-1263C/wt recombinant cells after TP treatment for 48 h, indicating that synonymous mutation rs2515641 induced susceptibility to TP-induced hepatotoxicity by affecting CYP2E1 mRNA and protein expression (Chen et al., 2020).

Clock proteins affect drug metabolism and drug detoxification by regulating CYP450s (Zhao et al., 2019). A pharmacokinetic experiment showed that gavage with *TwHF* at Zeitgeber time 2 (ZT2) generated higher plasma concentrations of TP and more severe liver injury compared with ZT14 dosing, which was associated with circadian expression of hepatic CYP3A11 regulated by the circadian clock (Zhao H. et al., 2020). Likewise, the core clock gene *Bmal1* (encoding brain and muscle ARNT-like 1) controls the circadian rhythm of CYP3A11 by regulating D-box binding PAR BZIP transcription factor (DBP)/ hepatocyte nuclear factor 4 alpha (HNF4α), TP-induced hepatotoxicity exhibited more severe daytime (ZT2/8) than nighttime (ZT14/20) toxicity (Lin et al., 2019).

2.1.2 P-gp

P-gp, an efflux transporter, attenuates intestinal absorption, limits penetration of the blood-brain barrier, and mediates biliary and urinary excretion of substrate drugs (Zamek-Gliszczynski et al., 2021). The bidirectional transport of TP across Caco-2 cells was investigated *in vitro*, which showed that the transport of TP in Caco-2 cells was significantly increased in the basolateral to the apical direction and was abolished in the presence of the P-gp inhibitor, verapamil, indicating that P-gp is involved in intestinal absorption of TP (Gong et al., 2015). A Rhodamine-123 uptake assay confirmed that TP did not affect the activity of P-gp in Caco-2 Cells (Zhang et al., 2017). Therefore, P-gp protein activity does not change when TP is used alone, and the absorption of TP might not be altered. However, when TP is combined with drugs that interfere with P-gp activity, the absorption of TP, which might lead to changes in hepatotoxicity.

TP is mainly secreted in bile (Liu et al., 2014). A recent study showed that P-gp is involved in TP clearance and detoxification in a Sandwich-cultured rat hepatocyte model, and identified TP as a P-gp substrate using a rat *Mdr1* (the gene responsible for encoding the P-gp protein) membrane ATPase assay (Zhuang et al., 2013). Small interfering RNA (siRNA) and the specific inhibitor tariquidar were used to downregulate hepatic P-gp levels, which significantly increased the plasma and hepatic exposure of TP in mice, resulting in severe hepatotoxicity (Kong et al., 2015). The above research indicates that hepatic P-gp regulates TP-induced hepatotoxicity by affecting its clearance.

2.2 Oxidative stress mediated hepatotoxicity

Oxidative stress (OS) is caused by an imbalance between oxidation and antioxidants. OS causes lipid and DNA damage, leading to organelle dysfunction and damage (Pole et al., 2016; Campbell and Colgan, 2019). Numerous *in vivo* and *in vitro* studies have found that administration of TP causes an increase in ROS and malondialdehyde (MDA), and a decrease in superoxide dismutase (SOD), catalase (CAT), glutathione-S-transferase (GST) and GSH (Li et al., 2014; Jiang et al., 2021). Thus, TP-induced hepatotoxicity is associated with oxidative stress.

2.2.1 Mitochondrial oxidative stress

Mitochondria are important sites for biosynthetic processes that regulate stress responses (Vakifahmetoglu-Norberg et al., 2017). TP increased the mitochondrial membrane transmembrane potential ($\Delta\Psi m$) in a concentration-dependent manner in HepG2 and HL7702 cells, which increased oxidative stress (Fu et al., 2011; Fu et al., 2013). In addition, TP inhibited the activity of mitochondrial respiratory chain complexes I and IV in a concentration-dependent manner, leading to obstruction of electron flow, causing the accumulation of electrons in the upstream respiratory chain complex, which reacts with oxygen through the upstream complex to form superoxide anion radical (O^{2-}), thereby increasing ROS and inducing oxidative stress (Fu et al., 2011). Moreover, in mice, inhibition of the mitochondrial respiratory chain by TP induced secondary β-oxidative damage, microvesicular steatosis, increased lactate and ROS, and decreased GSH, resulting in liver injury (Fu et al., 2011). Moreover, TP caused mitochondrial dysfunction by inducing mitochondrial swelling and permeability in female rat liver mitochondria (Fu et al., 2013). Notably, in a rat model of TP-induced hepatotoxicity, TP upregulated the expression of the mitochondrial fission-related, dynamin-related protein 1 (Drp1), leading to disturbances in mitochondrial dynamics and mitochondrial dysfunction, such as increased ROS, DNA membrane depolarization, decreased ATP production, and decreased mitochondrial DNA copy number (Hasnat et al., 2019; Hasnat et al., 2020). Taken together, these studies proved the importance of mitochondrial oxidative stress in TP-induced hepatotoxicity.

2.2.2 Imbalance of antioxidant

In addition to oxidative stress caused by TP-induced mitochondrial dysfunction, oxidative stress caused by TP-induced imbalance of cellular antioxidant protect systems is also an important mechanism of TP-induced hepatotoxicity.

Nuclear factor erythroid 2-related factor 2 (Nrf2) is a redox-sensitive transcription factor that regulates cellular oxidative stress (Lee et al., 2005). Upregulating *NRF2* expression can reduce TP-induced HepG2 cytotoxicity, whereas silencing *NRF2* can raised oxidative stress and aggravated triptolide-induced cytotoxicity in HepG2 and L02 cells (Li et al., 2014; Zhou et al., 2017). Also, treatment with the canonical Nrf2 agonist sulforaphane (SFN) attenuated TP-induced hepatotoxicity by reducing oxidative stress in mice (Li et al., 2014). *In vitro*, TP enhanced *NRF2* expression, induced Nrf2 nuclear translocation, increased Nrf2 adenine-uridine rich element (ARE)-binding activity, increased heme oxygenase 1 (HO-1) and NAD(P)H quinone dehydrogenase 1 (NQO1) expression in L-02 and HepG2 cells (Zhou et al., 2017). MicroRNA-155 (miR-155), an endogenous non-coding small RNA, was upregulated in a TP concentration-dependent manner, resulting in downregulation of the Nrf2 signaling pathway, and inhibition of miR-155 reversed the downregulation of the Nrf2 signaling pathway by TP and alleviated TP-induced hepatotoxicity (Li et al., 2021). Furthermore, TP treatment can inhibit the endogenous peroxisome proliferator-activated receptor alpha (PPARα) signaling pathway, leading to increased long-chain acylcarnitines in mouse serum, which in turn activated the Notch-Nrf2 pathway to protect against TP-induced hepatotoxicity (Hu et al., 2019). According to the above research, there is controversy regarding whether TP inhibits or upregulates Nrf2. What is clear, however, is that activation of Nrf2 protects can against TP-induced hepatotoxicity.

Activation of the Notch1 signaling pathway has been shown to reduce oxidative stress in injured tissues (Cai et al., 2022). The thioredoxin (TRX) system is a key antioxidant system against oxidative stress (Lu and Holmgren, 2014). A study demonstrated that TP could inhibit Notch1 expression, impaired the antioxidant activity of TRX through the phosphatase and tensin homolog (PTEN)/protein kinase B (AKT)/thioredoxin interacting protein (Txnip) signaling pathway, and caused oxidative damage (Shen et al., 2019).

Taken together, oxidative stress is involved in TP-induced hepatotoxicity, and regulation of Drp1, or activation of Nrf2 and Notch1 can alleviate oxidative stress and TP-induced hepatotoxicity.

2.3 Excessive autophagy-mediated hepatotoxicity

Autophagy is a lysosomal degradation pathway through which cellular contents, such as damaged organelles and proteins, are recycled (Xie and Klionsky, 2007). A study showed that TP-induced oxidative stress led to a time- and dose-dependent increase in autophagy-related proteins Beclin1 and membrane-bound microtubule-associated protein light chain 3 (LC3II). The study identified the presence of autophagosomes by transmission electron microscopy, and inhibition of autophagy decreased cell viability and enhanced apoptosis in a TP-induced HL7702 cytotoxicity model (Wei et al., 2019). This indicated that autophagy plays a protective role in TP-induced hepatotoxicity. Yet, in another *in vitro* experiment, it was shown that TP exposure led to excessive autophagy induced by endoplasmic reticulum stress (ERS) through the PERK-ATF4-CHOP pathway. Co-treatment with the autophagy agonist RAPA increased TP-induced cytotoxicity and apoptosis, while co-treatment with the autophagy inhibitor 3-MA decreased TP-induced cytotoxicity and apoptosis (Zhang et al., 2022b). This may due to the unclarified role that autophagy plays in the TP-induced hepatotoxicity. Appropriate autophagy can protect TP-induced hepatotoxicity, while excessive autophagy aggravates TP-induced hepatotoxicity.

Besides, electron microscopy showed obvious mitophagy in TP-treated rat liver tissue, and mitophagy was related to the disturbance of mitochondrial function and dynamics caused by the TP-induced increase in Drp1 (Hasnat et al., 2019). However, that study did not further verify the role of mitophagy in TP-induced hepatotoxicity. Furthermore, another study found that TP-induced ERS could induce excessive mitophagy in HepaRG cells. Co-treatment with Mdivi-1, a specific inhibitor of mitophagy could alleviate TP-induced HepaRG cytotoxicity (Zhang et al., 2022c).

Collectively, TP-induced ERS lead to excessive autophagy, and modulation of autophagy can alleviate TP-induced hepatotoxicity.

2.4 Apoptosis-mediated hepatotoxicity

Apoptosis is a programmed death process that is mainly triggered by two basic pathways: The death receptor pathway and the mitochondrial pathway, both of which ultimately lead to the activation of caspases (Dara and Kaplowitz, 2017; Galluzzi et al., 2018). Using transcriptomic techniques, among apoptosis-related genes, 46 genes were upregulated and 43 genes were downregulated in TP-induced hepatotoxicity in Wistar rats (Wang et al., 2013). In another transcriptomics study, TP-induced apoptosis through regulating the phosphatidylinositol-4,5-bisphosphate 3-kinase (PI3K)/AKT signaling pathway, the tumor necrosis factor alpha (TNFα) signaling pathway, the mitogen-activated protein kinase (MAPK) signaling pathway, and the P53 signaling pathway; however, these pathways have not been further validated (Zhao J. et al., 2020). These studies indicated that apoptosis is associated with TP-induced hepatotoxicity.

TP exposure caused loss of mitochondrial membrane potential and the release of cytochrome c from mitochondria into the cytoplasm, which leads to downregulation of the level of the anti-apoptotic protein, B-cell CLL/lymphoma 2 (Bcl-2),

upregulation of the level of the pro-apoptotic protein BCL2 associated X (Bax) and the tumor suppressor protein P53, and an increase in the activity of caspase 9 and caspase 3, ultimately causing apoptosis in L-02 cells (Yao et al., 2008). An in-depth study showed that TP treatment induced dysfunction and altered dynamics of mitochondria by causing the translocation of Drp1 from the cytoplasm to the mitochondrial outer membrane, with concomitant release of cytochrome c from mitochondria into the cytoplasm, which activated caspase 3, leading to apoptosis (Hasnat et al., 2020). TP caused an increase in ROS by inhibiting Notch1, which ultimately induced apoptosis, and upregulating the expression of Notch1 can reduce apoptosis and alleviate TP-induced hepatotoxicity (Shen et al., 2019). In general, TP-induced mitochondrial damage and oxidative stress are important factors in triggering apoptosis.

2.5 Hepatotoxicity mediated by metabolic disorders

Bile duct hyperplasia and lipid accumulation were observed in the histological manifestations of TP-induced hepatotoxicity (Fu et al., 2011; Jin et al., 2015), which indicated that metabolic disorders are involved in TP-induced hepatotoxicity.

2.5.1 Bile acid metabolism

The farnesoid X receptor (FXR) is a ligand-activated transcription factor that activates certain genes involved in phases II and III of xenobiotic metabolism, protecting the liver from toxic metabolites and xenobiotics (Lee et al., 2010). Pretreatment with the FXR activator, GW4046, has been shown to maintain metabolism homeostasis and attenuate TP-induced hepatotoxicity by increasing gene expression related to phase II and phase III xenobiotic metabolism (Jin et al., 2015). Besides, FXR also plays a key role in maintaining hepatic bile acid homeostasis (Molinaro and Marschall, 2022). Additionally, sirtuin 1 (Sirt1) regulates FXR activation, and depletion of hepatic Sirt1 reduces FXR signaling (García-Rodríguez et al., 2014). TP suppressed the Sirt1/FXR signaling pathway by inhibiting Sirt1 activity, which led to a decrease in the expression of the bile salt export pump (BSEP), an increase in the expression of bile acid synthesis rate-limiting enzyme CYP7A, and a decrease in the expression of gluconeogenesis proteins glucose-6-phosphatase catalytic subunit (G6PC) and phosphoenolpyruvate carboxykinase 2, mitochondrial (PEPCK), resulting in the destruction of bile acid homeostasis and gluconeogenesis, thus causing liver injury in rats (Yang et al., 2017). Zhou et al. (Zou et al., 2020) found that TP induced the activation of iNKT cells, which in turn led to decreased expression of the cholestasis-related nuclear receptor FXR, transporter organic anion-transporting polypeptide 1b2 (OATP1B2), and CYP450 enzymes, which was also responsible for aggravating cholestatic liver injury.

2.5.2 Lipid metabolism

A study suggests that sex differences in TP-induced hepatotoxicity might be related to dyslipidemia. Continuous gavage of TP resulted in significant upregulation of the liver X receptor-alpha (LXR)/sterol regulatory element binding transcription factor 1 (SREBP-1) signaling axis in females, while male rats showed only slight changes, resulting in more lipid droplets in TP-treated female rats than in TP-treated male rats, which might be a factor in the sex differences in TP-induced hepatotoxicity (Jiang et al., 2016). In addition, targeted fatty acids analysis showed that TP exposure induced significant changes in fatty acid levels in the livers of rats and mice (Li et al., 2017; Liu et al., 2021).

2.5.3 Other metabolisms

Moreover, several untargeted metabolomics studies showed that a variety of metabolic pathway disorders can be found in TP-induced hepatotoxicity, including glutathione metabolism, purine metabolism, and glycerophospholipid metabolism (Zhao J. et al., 2020; Yang et al., 2022). Additionally, targeted amino acid and sphingolipid analysis revealed that TP exposure induced changes in amino acid and sphingolipid metabolism profiles (Qu et al., 2015; Hu et al., 2021). However, no in-depth research has been carried out.

2.6 Immune-mediated hepatotoxicity

As an immune organ, the liver is enriched with a large number of innate immune cells, such as neutrophils, Kupffer cells (KCs), dendritic cells (DCs), and natural killer cells (NKs), as well as adaptive immune cells, such as T cells and B cells. Evidence demonstrates that the immune response is closely linked to the development of drug-induced liver injury (DILI) (Jiang et al., 2020; Nguyen et al., 2022).

2.6.1 The innate immune system

NLR family pyrin domain containing 3 (NLRP3), a multi-protein complex assembled in response to the activation of intracellular pattern recognition receptors (PRRs), is an important component of the innate immune system. NLRP3 can be activated by damage-related molecular patterns (DAMPs) produced by damaged cells and pathogen-related molecular patterns (PAMPs) generated by enterohepatic axis pathogens (Kanneganti et al., 2007; Yu et al., 2022). Activation of the NLRP3 inflammasome releases inflammatory factors IL-1β and IL-18, which initiate an inflammatory cascade (Baroja-Mazo et al., 2014; Bruchard et al., 2015; Tsai et al., 2017). Research has shown that activation of the TLR4-MYD88 innate immune signal transduction adaptor (Myd88)-NF-κB pathway and oxidative

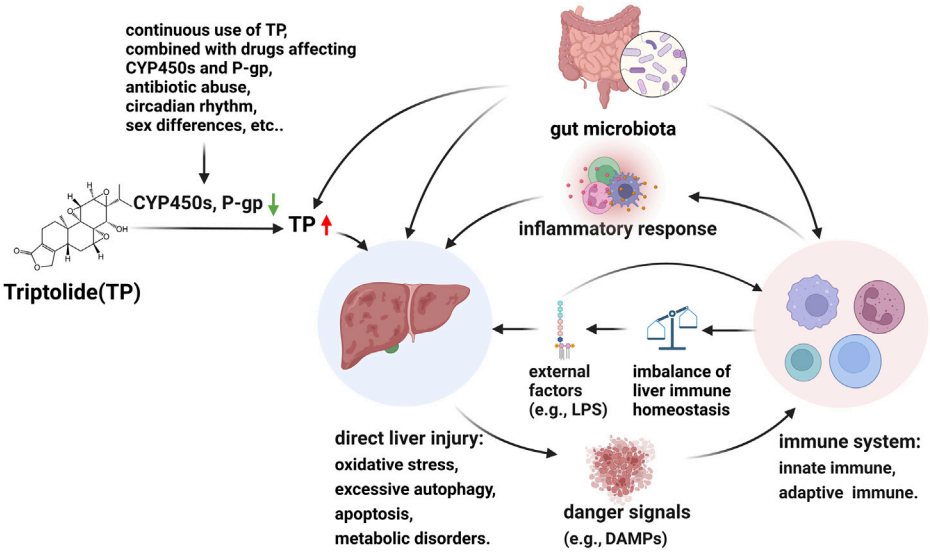

FIGURE 2
Hypothesis of molecular pathogenesis of TP-induced hepatotoxicity. CYP450 enzymes are involved in TP metabolism and P-gp is involved in TP transport. Some factors such as the continuous use of TP, combined with drugs affecting CYP450s and P-gp, antibiotic abuse, circadian rhythm, and sex differences, should affect the level of TP in the liver. TP itself is hepatotoxic and direct liver toxicity due to excessive exposure to TP, such as oxidative stress, excessive autophagy, apoptosis, metabolic disorders, etc. Cell damage caused by direct hepatotoxicity releases danger signals, such as DAMPs, which can activate the innate and adaptive immune systems, and then a large number of pro-inflammatory factors will be released. The inflammatory response further aggravates liver injury by promoting cell death, inducing excessive autophagy and metabolic disorders, etc. In addition, the imbalance of hepatic immune homeostasis caused by changes in immune cells makes the liver sensitive to external factors, such as LPS, then aggravates hepatotoxicity. Furthermore, gut microbiota mediates the hepatotoxicity of TP by affecting TP *in vivo* exposure, metabolic homeostasis, and immunity. ↓: downregulation of CYP450s and p-gp; ↑: abnormal increase TP exposure.

stress by TP are involved in the overactivation of the NLRP3 inflammasome, which releases a large amount of IL-1β and increases the recruitment of neutrophils and macrophages, thereby aggravating liver injury (Yuan et al., 2019a). A single dose of Ac-Yvad-Cmk (a Caspase 1 inhibitor) injected before TP administration could effectively protect against TP-induced hepatotoxicity (Yuan et al., 2019a).

Hepatic macrophages are the most abundant hepatic immune cells which play a vital role in maintaining hepatic homeostasis and contribute to the progression of DILI (Tsuji et al., 2020). Several studies have shown that TP inhibited the phagocytosis of macrophages, increased the number of macrophages, and modulated the polarization of macrophages in mice (Wang L. et al., 2018; Liu L. et al., 2022). what's more, in a study of TP-induced acute hepatotoxicity, researchers found that depletion of macrophages using clodronate liposomes pretreatment could suppress the inflammatory response and alleviated TP-induced hepatotoxicity (Zhao, 2018).

Neutrophils, the innate immune cells, are the most abundant leukocytes in mammals (Tang et al., 2021). It has been found that neutrophils increasingly infiltrate the liver following TP treatment because of activation of the NLRP3 inflammasome, induction of the TLR4 and TLR9 signaling pathway, release of inflammatory factors, or activation of other immune cells (Wang X.z. et al., 2018; Wang X. Z. et al., 2018; Yuan et al., 2019a). A study showed that neutrophil infiltration had little effect on TP-induced hepatotoxicity, because depletion of neutrophils only showed mild protection against TP-induced hepatotoxicity (Wang X. Z. et al., 2018).

Natural Killer T (NKT) cells express both NK and T cell surface markers, linking innate and adaptive immunity (Kaer et al., 2011). Among them, invariant NKT (iNKT) cells are a subset of cells that cause liver inflammation and play a pathogenic role (Maricic et al., 2018; Marrero et al., 2018; Nong et al., 2020). NKT, especially iNKT, cells are increasingly activated in the liver after TP administration, resulting from the upregulation of the Toll-like receptor (TLR) signaling pathway, which mainly releases the Th1 cytokine interferon gamma (IFN-γ), recruits neutrophils and macrophages, and causes hepatotoxicity (Wang X.z. et al., 2018). Further research demonstrated that TP-activated iNKT cells released significantly increased levels of the Th2 cytokine, IL-4, thereby inhibiting type 2 NKT cells and promoting the expression of C-X-C motif chemokine ligand 10 (CXCL10), intercellular adhesion molecule 1 (ICAM-1), and early growth response 1 (Egr-1),

resulting in downregulated expression levels of liver nuclear receptor FXR, bile acid transporter organic anion-transporting polypeptide 2b1 (OATP2B1), and CYP450 enzymes, ultimately exacerbating TP-induced cholestatic liver injury (Zou et al., 2020).

2.6.2 The adaptive immune system

The balance of T helper cell 17 (Th17)/regulatory T cell (Treg) in adaptive immune cells is crucial to maintain immune homeostasis (Liu et al., 2018; Lee et al., 2021). Tregs have anti-inflammatory effects that suppress immune responses. In contrast, Th17s have pro-inflammatory effects to promote immune responses. Increased levels of Th17s and their related cytokine IL-17, but decreased levels of Treg cells and their related cytokine IL-10, were observed in TP-induced hepatotoxicity (Wang et al., 2014a). Another study found the number of Tres was reduced by TP-mediated upregulation of suppressor of cytokine signaling (SOCS) and Notch signaling, resulting in a Th17/Treg imbalance and aggravated TP-induced hepatotoxicity (Wang et al., 2016). Furthermore, in mice, IL-17 produced by Th17s contributed to TP-induced hepatotoxicity (Wang et al., 2014b).

2.6.3 Liver immune homeostasis

Mild bacterial-derived lipopolysaccharide (LPS) in the gut could enter the liver through the portal vein. Under physiological conditions, the hepatic immune system protects the host from the adverse effects of low-dose LPS, while mice that were gavaged daily with TP for 7 days showed disrupted liver immune homeostasis, evidenced by the liver's inability to detoxify the harmful response induced by a non-hepatotoxic dose of LPS (Yuan et al., 2019b). Researchers further found that the imbalance of hepatic immune homeostasis was caused by TP-induced inhibition of NF-κB-dependent transcriptional activity and CASP8 and FADD like apoptosis regulator (CFLAR, also known as FLIP) production (Yuan et al., 2020). Furthermore, TP inhibited the phagocytic function of macrophages, increased the number of macrophages, and regulated

TABLE 1 Detoxification strategies for TP.

Drug	Model	Treatment	Effector Mechanisms	References
Arctiin	BALB/C mice	pretreatment with Arctiin (500 mg/kg i.g. 12), TP (0.6 mg/kg, i.g. 24 h)	Nrf2	Zhou et al. (2020)
	HepG2 cells	pretreatment with Arctiin (50 μM, 12 h), TP (50 nM, 12 h)		
Catalpol	HepaRG cells	pretreatment with Catalpol (40 μg/L 12 h), TP (20 μg/L 12 h)	inhibit excessive autophagy	Zhang et al. (2022b)
Catalpol	Female SD Rats	TP (1.2 mg/kg) + Catalpol (2.4, 24, 240 mg/kg) i.g. 14d	regulate phase I and II detoxification enzymes of TP	Fu et al. (2020)
	L-02 cells	pretreated with Catalpol (2 μg/ml, 10 μg/ml, 50 μg/ml, and 250 μg/ml 12 h). TP (20 μg/ml 36 h)		
	HepG2 cells	pretreated with Catalpol (0.4 μg/ml, 2 μg/ml, and 10 μg/ml, 12 h), TP (40 μg/ml, 36 h)		
Chlorogenic acid	Male Kunming mice	pretreatment with Chlorogenic acid (10,20 and 40 mg/kg, i.g. 7 d), TP (1 mg/kg, i.g. 24 h)	Nrf2	Wang et al. (2018a)
Epigallocatechin-3-gallate	Female C57BL/6 mice	pretreated with Epigallocatechin-3-gallate (5 mg/kg, i.g. 10d), TP (0.5 mg/kg, i.g. 22 h)	Th17/Treg balance	Yu et al. (2016)
Isoliquiritigenin	Male ICR mice	pretreatment with Isoliquiritigenin (25 and 50 mg/kg i.g. 7 d), TP (1.0 mg/kg, i.p. 24 h))	Nrf2, bile acid metabolic homeostasis	Hou et al. (2018)
	L-02 cells	pretreatment with Isoliquiritigenin (2.5,5.0, 7.5 μM 12 h); TP (50 nM, 24 h)		
Isoliquiritigenin	Male ICR mice	pretreatment with Isoliquiritigenin (50 mg/kg i.g. 7d), TP (1.0 mg/kg, i.p. 6 h), Isoliquiritigenin (50 mg/kg i.g. 18 h)	Nrf2	Cao et al. (2016)
Licorice root extract	Male Wistar rats	pretreatment with Licorice root extract (120,240 and 480 mg/kg, i.g. 7 d), TP (0.6 mg/kg, i.g. 18 h)	Nrf2	Tan et al. (2018)
	L-02 cells	pretreatment with Licorice root extract (30, 60, and 90 μg/ml, 24 h), TP (80 nM, 18 h)		
magnesium isoglycyrrhizinate	Male Wistar rats	pretreatment with magnesium isoglycyrrhizinate (13.5 mg/kg, i.g. 7 d), TP (0.6 mg/kg, i.g. 18 h)	Nrf2	Tan et al. (2018)
	L-02 cells	pretreatment with magnesium isoglycyrrhizinate (30 μg/ml, 24 h), TP (80 nM, 18 h)		
Quercetin	Female C57BL/6 mice	pretreatment Quercetin (20, 50 and 80 mg/kg i.g. 10 d), TP (0.5 mg/kg, i.g. 22 h)	Th17/Treg balance	Wei et al. (2017)
Vitamin C	Male C57/BL6 mice	pretreatment Vitamin C (250 mg/kg i.g. 12 and 24 h), TP (1.0 mg/kg, i.p. 24 h)	mitigation of oxidative stress	Xu et al. (2019)

macrophages polarization in the mouse liver, resulting in an amplification of the inflammatory response to a non-hepatotoxic dose of LPS and exacerbated hepatotoxicity (Wang L. et al., 2018; Liu L. et al., 2022). Recently, it was found that the immune disorder caused by a TP-induced Th17/Treg imbalance was also the cause of liver intolerance to a non-hepatotoxic dose of LPS in TP-induced acute hepatotoxicity (Zhang H. et al., 2022). Hence, TP treatment led to an imbalance of immune homeostasis in the liver, making the liver susceptible to external factors, such as LPS, thereby aggravating liver damage.

2.7 Gut microbiota mediated hepatotoxicity

The close connection between the liver and the gut, such as the "gut-liver axis" and "enterohepatic circulation" means that the gut microbiota has an important impact on the efficacy and toxicity of drugs (Kashyap et al., 2017; Wilson and Nicholson, 2017; Andrade et al., 2019). Enzymes or metabolites derived from the gut microbiota alter DILI by affecting the *in vivo* processing of drugs (Gong et al., 2018; Yip et al., 2018; Li et al., 2019). Moreover, the gut microbiota and its metabolites can regulate liver injury by influencing immunity and the gut barrier (Sun et al., 2020; Yan et al., 2022).

In recent years, researchers have focused on the association between the gut microbiota and TP-induced hepatotoxicity. An *in vitro* experiment on SD rat colon contents demonstrated that TP could be metabolized by the gut microbiota and the content of TP showed a downward trend over time, with a decrease of 3% at 6 h, 16% at 12 h, and 45% at 24 h (Peng et al., 2020). In mice, TP injection after antibiotic depletion of the gut microbiota increased TP-induced hepatotoxicity, and the mechanism was related to metabolic disorders. Gut microbiota-derived propionate was reported to defend against TP-induced hepatotoxicity through metabolic intervention (Huang et al., 2020). Considering that most TP-containing drugs are delivered orally, our study further demonstrated that gut microbiota disturbances induced by antibiotic pretreatment exacerbated oral TP-induced hepatotoxicity, which is associated with an aggravated NLRP3-mediated inflammatory response and increased TP absorption (Liu Y. T. et al., 2022).

3 Conclusion

The pathogenesis of TP-induced hepatotoxicity is complicated, and the occurrence of TP-induced hepatotoxicity is the result of the interaction of multiple factors. In summary, the mechanisms of TP-induced hepatotoxicity are mainly related to CYP450s, P-gp, oxidative stress, excessive autophagy, apoptosis, metabolic disorders, immunity, and the gut microbiota (Figure 1).

In this section, we propose an overall hypothesis for a possible mechanism of TP-induced hepatotoxicity. TP-induce hepatotoxicity is dose-dependently (Yuan et al., 2019a; Zhao J. et al., 2020). Therefore, hepatic CYP450s and P-gp, which affect TP exposure, play a vital role in TP-induced hepatotoxicity. Some factors such as the continuous use of TP, combined with drugs affecting CYP450s and P-gp, antibiotic abuse, circadian rhythm, and sex differences, should affect the level of TP in the liver. TP itself is hepatotoxic (Titov et al., 2011), and direct liver toxicity due to excessive exposure to TP, such as oxidative stress, excessive autophagy, apoptosis, metabolic disorders, etc. Cell damage caused by direct hepatotoxicity releases danger signals, such as DAMPs, which can activate the innate and adaptive immune systems, such as activation of NLRP3, recruitment of macrophages, Th17s, etc., and then a large number of pro-inflammatory factors will be released. The inflammatory response further aggravates liver injury by promoting cell death, inducing excessive autophagy and metabolic disorders, etc. In addition, the imbalance of hepatic immune homeostasis caused by changes in immune cells makes the liver sensitive to external factors, such as LPS, then aggravates hepatotoxicity. Furthermore, gut microbiota mediates the hepatotoxicity of TP by affecting TP *in vivo* exposure, metabolic homeostasis, and immunity (Figure 2).

Moreover, a comprehensive analysis of the toxicological mechanisms of TP could advance our understanding of the detoxification effect of TP. Increasing the expression of hepatic CYP450s and P-gp, activating Nrf2, Notch1, FXR, inhibiting excessive autophagy, regulating mitochondrial fission protein Drp1, and suppressing immune hyperactivation, are expected to become key strategies for TP detoxification. Studies show that there are variety of drugs, such as chlorogenic acid (Wang J. M. et al., 2018), and Catalpol (Zhang et al., 2022b), etc., alleviated TP-induced hepatotoxicity by modulating key targets or biological processes such as Nrf2, and autophagy (Table 1).

However, research on the mechanism of TP-induced hepatotoxicity lacks depth. For example, studies have found that the role of autophagy in a model of TP-induced hepatotoxicity is controversial. It seems that proper autophagy protects TP-induced hepatotoxicity, yet excessive autophagy increases TP-induced hepatotoxicity (Wei et al., 2019; Zhang et al., 2022b). However, there is currently no clear indicator to determine the extent of autophagy in TP-induced hepatotoxicity, and it cannot tell us how to regulate autophagy. Therefore, it is necessary to develop appropriate experimental models to clarify the role of autophagy in TP-induced hepatotoxicity and look for the key indicators or biomarkers. Furthermore, multiple mechanisms have been demonstrated to be involved in TP-induced hepatotoxicity while reduce the expression of these targets does not seem to significantly

alleviate TP-induced hepatotoxicity. This suggests that TP-induced hepatotoxicity is caused by the interaction of multiple factors and the key pathogenesis of TP-induced hepatotoxicity has not yet been identified. Thus, key pathogenic mechanisms need to be discovered and validated for detoxification strategies for TP-induced hepatotoxicity.

Author contributions

YH and QW drafted the manuscript and edited the manuscript. YW, HZ, and XL participated in preparing the figures and collected the literatures. TY and HZ revised the draft. All authors read and approved the submitted version.

Funding

This work was supported by the Three-year Action Plan of Shanghai Shenkang Medical Development Center (grant numbers SHDC2020CR1053B and SHDC2020CR6012-003), the Science and Technology Support Project of Shanghai Science and Technology Commission (grant numbers 20S21901800, 18401900700 and 18401932800), and Three-Year Action Plan for Development of TCM in Shanghai (ZY3-CCCX-2-1003).

Conflict of interest

The authors declare that the research was conducted in the absence of any commercial or financial relationships that could be construed as a potential conflict of interest.

Publisher's note

All claims expressed in this article are solely those of the authors and do not necessarily represent those of their affiliated organizations, or those of the publisher, the editors and the reviewers. Any product that may be evaluated in this article, or claim that may be made by its manufacturer, is not guaranteed or endorsed by the publisher.

References

Andrade, R. J., Chalasani, N., Bjornsson, E. S., Suzuki, A., Kullak-Ublick, G. A., Watkins, P. B., et al. (2019). Drug-induced liver injury. *Nat. Rev. Dis. Prim.* 5 (1), 58. doi:10.1038/s41572-019-0105-0

Baroja-Mazo, A., Martín-Sánchez, F. G. A. I., Martínez, C. M. A.-I., Compan, J., Barberà-Cremades, M., et al. (2014). The NLRP3 inflammasome is released as a particulate danger signal that amplifies the inflammatory response. *Nat. Immunol.* 15 (8), 738–748. doi:10.1038/ni.2919

Bruchard, M., Rebé, C., Derangère, V., Togbé, D., Ryffel, B., Boidot, R., et al. (2015). The receptor NLRP3 is a transcriptional regulator of TH2 differentiation. *Nat. Immunol.* 16 (8), 859–870. doi:10.1038/ni.3202

Cai, W., Shen, K., Ji, P., Jia, Y., Han, S., Zhang, W., et al. (2022). The Notch pathway attenuates burn-induced acute lung injury in rats by repressing reactive oxygen species. *Burns Trauma* 10, tkac008. doi:10.1093/burnst/tkac008

Campbell, E. L., and Colgan, S. P. (2019). Control and dysregulation of redox signalling in the gastrointestinal tract. *Nat. Rev. Gastroenterol. Hepatol.* 16 (2), 106–120. doi:10.1038/s41575-018-0079-5

Cao, L., Yan, M., Ma, Y. X., Zhang, B. K., Fang, P. F., Xiang, D. X., et al. (2016). Isoliquiritigenin protects against triptolide-induced hepatotoxicity in mice through Nrf2 activation. *Pharmazie* 71 (7), 394–397. doi:10.1691/ph.2016.6535

Chen, K., Guo, R., and Wei, C. (2020). Synonymous mutation rs2515641 affects CYP2E1 mRNA and protein expression and susceptibility to drug-induced liver injury. *Pharmacogenomics* 21 (7), 459–470. doi:10.2217/pgs-2019-0151

Dara, L., and Kaplowitz, N. (2017). "Cell death in drug-induced liver injury," in *Cellular injury in liver diseases* (Berlin, Germany: Springer), 1–35.

Du, F., Liu, Z., Li, X., and Xing, J. (2014). Metabolic pathways leading to detoxification of triptolide, a major active component of the herbal medicine Tripterygium wilfordii. *J. Appl. Toxicol.* 34 (8), 878–884. doi:10.1002/jat.2906

Fu, L., Zhou, L., Geng, S., Li, M., Lu, W., Lu, Y., et al. (2020). Catalpol coordinately regulates phase I and II detoxification enzymes of Triptolide through CAR and NRF2 pathways to reduce Triptolide-induced hepatotoxicity. *Biomed. Pharmacother.* 129, 110379. doi:10.1016/j.biopha.2020.110379

Fu, Q., Huang, X., Shu, B., Xue, M., Zhang, P., Wang, T., et al. (2011). Inhibition of mitochondrial respiratory chain is involved in triptolide-induced liver injury. *Fitoterapia* 82 (8), 1241–1248. doi:10.1016/j.fitote.2011.08.019

Fu, Q., Jiang, Z. Z., and Zhang, L. Y. (2013). Impairment of triptolide on liver mitochondria in isolated liver mitochondria and HL7702 cell line. *Chin. J. Integr. Med.* 19 (9), 683–688. doi:10.1007/s11655-012-1265-x

Galluzzi, L., Vitale, I., Aaronson, S. A., Abrams, J. M., Adam, D., Agostinis, P., et al. (2018). Molecular mechanisms of cell death: Recommendations of the nomenclature committee on cell death 2018. *Cell Death Differ.* 25 (3), 486–541. doi:10.1038/s41418-017-0012-4

Gao, J., Liang, Z., Zhao, F., Liu, X., and Ma, N. (2022). Triptolide inhibits oxidative stress and inflammation via the microRNA-155-5p/brain-derived neurotrophic factor to reduce podocyte injury in mice with diabetic nephropathy. *Bioengineered* 13 (5), 12275–12288. doi:10.1080/21655979.2022.2067293

García-Rodríguez, J., Barbier-Torres, L., Fernández-Álvarez, S., Gutiérrez-de Juan, V., Monte, M., Halilbasic, E., et al. (2014). SIRT1 controls liver regeneration by regulating bile acid metabolism through farnesoid X receptor and mammalian target of rapamycin signaling. *Hepatology* 59 (5), 1972–1983. doi:10.1002/hep.26971

Gong, S., Lan, T., Zeng, L., Luo, H., Yang, X., Li, N., et al. (2018). Gut microbiota mediates diurnal variation of acetaminophen induced acute liver injury in mice. *J. Hepatol.* 69 (1), 51–59. doi:10.1016/j.jhep.2018.02.024

Gong, X., Chen, Y., and Wu, Y. (2015). Absorption and metabolism characteristics of triptolide as determined by a sensitive and reliable LC-MS/MS method. *Molecules* 20 (5), 8928–8940. doi:10.3390/molecules20058928

Guo, X., Xue, M., Li, C., Yang, W., Wang, S., Ma, Z., et al. (2016). Protective effects of triptolide on TLR4 mediated autoimmune and inflammatory response induced myocardial fibrosis in diabetic cardiomyopathy. *J. Ethnopharmacol.* 193, 333–344. doi:10.1016/j.jep.2016.08.029

Hasnat, M., Yuan, Z., Naveed, M., Khan, A., Raza, F., Xu, D., et al. (2019). Drp1-associated mitochondrial dysfunction and mitochondrial autophagy: A novel mechanism in triptolide-induced hepatotoxicity. *Cell Biol. Toxicol.* 35 (3), 267–280. doi:10.1007/s10565-018-9447-8

Hasnat, M., Yuan, Z., Ullah, A., Naveed, M., Raza, F., Baig, M., et al. (2020). Mitochondria-dependent apoptosis in triptolide-induced hepatotoxicity is associated with the Drp1 activation. *Toxicol. Mech. Methods* 30 (2), 124–133. doi:10.1080/15376516.2019.1669247

Hou, Z., Chen, L., Fang, P., Cai, H., Tang, H., Peng, Y., et al. (2018). Mechanisms of triptolide-induced hepatotoxicity and protective effect of combined use of isoliquiritigenin: Possible roles of Nrf2 and hepatic transporters. *Front. Pharmacol.* 9, 226. doi:10.3389/fphar.2018.00226

Hu, C., Li, H., Wu, L., Ke, J., Yu, X., Xiong, Y., et al. (2021). Metabolic profiling of 19 amino acids in triptolide-induced liver injured rats by gas chromatography-triple quadrupole mass spectrometry. *Hum. Exp. Toxicol.* 40 (10), 1685–1697. doi:10.1177/09603271211006167

Hu, D. D., Zhao, Q., Cheng, Y., Xiao, X. R., Huang, J. F., Qu, Y., et al. (2019). The protective roles of PPARα activation in triptolide-induced liver injury. *Toxicol. Sci.* 171, 1–12. doi:10.1093/toxsci/kfz146

Huang, J. F., Zhao, Q., Dai, M. Y., Xiao, X. R., Zhang, T., Zhu, W. F., et al. (2020). Gut microbiota protects from triptolide-induced hepatotoxicity: Key role of propionate and its downstream signalling events. *Pharmacol. Res.* 155, 104752. doi:10.1016/j.phrs.2020.104752

Jiang, H. Y., Bao, Y. N., Lin, F. M., and Jin, Y. (2021). Triptolide regulates oxidative stress and inflammation leading to hepatotoxicity via inducing CYP2E1. *Hum. Exp. Toxicol.* 40 (12), S775–S787. doi:10.1177/09603271211056330

Jiang, W., Dai, T., Xie, S., Ding, L., Huang, L., and Dai, R. (2020). Roles of diclofenac and its metabolites in immune activation associated with acute hepatotoxicity in TgCYP3A4/hPXR-humanized mice. *Int. Immunopharmacol.* 86, 106723. doi:10.1016/j.intimp.2020.106723

Jiang, Z., Huang, X., Huang, S., Guo, H., Wang, L., Li, X., et al. (2016). Sex-related differences of lipid metabolism induced by triptolide: The possible role of the lxrα/SREBP-1 signaling pathway. *Front. Pharmacol.* 7, 87. doi:10.3389/fphar.2016.00087

Jin, C., Wu, Z., Wang, L., Kanai, Y., and He, X. (2019). CYP450s-Activity relations of celastrol to interact with triptolide reveal the reasons of hepatotoxicity of Tripterygium wilfordii. *Molecules* 24 (11), E2162. doi:10.3390/molecules24112162

Jin, J., Sun, X., Zhao, Z., Wang, W., Qiu, Y., Fu, X., et al. (2015). Activation of the farnesoid X receptor attenuates triptolide-induced liver toxicity. *Phytomedicine* 22 (10), 894–901. doi:10.1016/j.phymed.2015.06.007

Kaer, L. V., Parekh, V. V., and Wu, L. (2011). Invariant natural killer T cells: Bridging innate and adaptive immunity. *Cell Tissue Res.* 343 (1), 43–55. doi:10.1007/s00441-010-1023-3

Kanneganti, T. D., Lamkanfi, M., and Nunez, G. (2007). Intracellular NOD-like receptors in host defense and disease. *Immunity* 27 (4), 549–559. doi:10.1016/j.immuni.2007.10.002

Kashyap, P. C., Chia, N., Nelson, H., Segal, E., and Elinav, E. (2017). Microbiome at the frontier of personalized medicine. *Mayo Clin. Proc.* 92 (12), 1855–1864. doi:10.1016/j.mayocp.2017.10.004

Kong, L. L., Zhuang, X. M., Yang, H. Y., Yuan, M., Xu, L., and Li, H. (2015). Inhibition of P-glycoprotein gene expression and function enhances triptolide-induced hepatotoxicity in mice. *Sci. Rep.* 5, 11747. doi:10.1038/srep11747

Lee, F. Y., de Aguiar Vallim, T. Q., Chong, H. K., Zhang, Y., Liu, Y., Jones, S. A., et al. (2010). Activation of the farnesoid X receptor provides protection against acetaminophen-induced hepatic toxicity. *Mol. Endocrinol.* 24 (8), 1626–1636. doi:10.1210/me.2010-0117

Lee, J. M., Li, J., Johnson, D. A., Stein, T. D., Kraft, A. D., Calkins, M. J., et al. (2005). Nrf2, a multi-organ protector? *FASEB J. official Publ. Fed. Am. Soc. Exp. Biol.* 19 (9), 1061–1066. doi:10.1096/fj.04-2591hyp

Lee, S. K., Park, M. J., Jhun, J. Y., Beak, J. A., Choi, J. Y., Rye, J. Y., et al. (2021). Combination treatment with metformin and tacrolimus improves systemic immune cellular homeostasis by modulating Treg and Th17 imbalance. *Front. Immunol.* 11, 581728. doi:10.3389/fimmu.2020.581728

Li, J., Shen, F., Guan, C., Wang, W., Sun, X., Fu, X., et al. (2014). Activation of Nrf2 protects against triptolide-induced hepatotoxicity. *PLoS One* 9 (7), e100685. doi:10.1371/journal.pone.0100685

Li, M., Hu, T., Tie, C., Qu, L., Zheng, H., and Zhang, J. (2017). Quantitative proteomics and targeted fatty acids analysis reveal the damage of triptolide in liver and kidney. *Proteomics* 17 (22), 1700001. doi:10.1002/pmic.201700001

Li, W., Liu, Y., He, Y. Q., Zhang, J. W., Gao, Y., Ge, G. B., et al. (2008). Characterization of triptolide hydroxylation by cytochrome P450 in human and rat liver microsomes. *Xenobiotica.* 38 (12), 1551–1565. doi:10.1080/00498250802503359

Li, X. X., Du, F. Y., Liu, H. X., Ji, J. B., and Xing, J. (2015). Investigation of the active components in Tripterygium wilfordii leading to its acute hepatotoxicty and nephrotoxicity. *J. Ethnopharmacol.* 162, 238–243. doi:10.1016/j.jep.2015.01.004

Li, Y., Guo, L., Hou, Z., Gong, H., Yan, M., and Zhang, B. (2021). Role of MicroRNA-155 in triptolide-induced hepatotoxicity via the nrf2-dependent pathway. *J. Ethnopharmacol.* 281, 114489. doi:10.1016/j.jep.2021.114489

Li, Y., Pan, H., Li, X., Jiang, N., Huang, L., Lu, Y., et al. (2019). Role of intestinal microbiota-mediated genipin dialdehyde intermediate formation in geniposide-induced hepatotoxicity in rats. *Toxicol. Appl. Pharmacol.* 377, 114624. doi:10.1016/j.taap.2019.114624

Lin, Y., Wang, S., Zhou, Z., Guo, L., Yu, F., and Wu, B. (2019). Bmal1 regulates circadian expression of cytochrome P450 3a11 and drug metabolism in mice. *Commun. Biol.* 2, 378. doi:10.1038/s42003-019-0607-z

Liu, J., Li, W., Zhu, W., He, W., Zhao, H., Xiang, Y., et al. (2018). Chronic intermittent hypoxia promotes the development of experimental non-alcoholic steatohepatitis by modulating Treg/Th17 differentiation. *Acta Biochim. Biophys. Sin.* 50, 1200–1210. doi:10.1093/abbs/gmy131

Liu, J., Zhou, X., Chen, X. Y., and Zhong, D. F. (2014). Excretion of [3H]triptolide and its metabolites in rats after oral administration. *Acta Pharmacol. Sin.* 35 (4), 549–554. doi:10.1038/aps.2013.192

Liu, L., Jiang, Z., Huang, X., Liu, J., Zhang, J., Xiao, J., et al. (2011). Disappearance of sexual dimorphism in triptolide metabolism in monosodium glutamate treated neonatal rats. *Arzneimittelforschung.* 61 (2), 98–103. doi:10.1055/s-0031-1296174

Liu, L., Jiang, Z., Liu, J., Huang, X., Wang, T., Liu, J., et al. (2010). Sex differences in subacute toxicity and hepatic microsomal metabolism of triptolide in rats. *Toxicology* 271 (1-2), 57–63. doi:10.1016/j.tox.2010.03.004

Liu, L., Zhang, X., Xing, X., Mohammed, I., Xu, X. T., Jiang, Z. Z., et al. (2022a). Triptolide induces liver injury by regulating macrophage recruitment and polarization via the Nrf2 signaling pathway. *Oxid. Med. Cell. Longev.* 2022, 1492239. doi:10.1155/2022/1492239

Liu, X., Hu, C., Li, H., Wu, L., Xiong, Y., Tang, X., et al. (2021). Metabolic profiling of fatty acids in Tripterygium wilfordii multiglucoside- and triptolide-induced liver-injured rats. *Open Life Sci.* 16 (1), 184–197. doi:10.1515/biol-2021-0016

Liu, Y. T., Hu, Y. Q., Wang, Y. L., Huang, K., Chen, G. F., Zhou, H., et al. (2022b). Antibiotic pretreatment promotes orally-administered triptolide absorption and aggravates hepatotoxicity and intestinal injury in mice. *J. Ethnopharmacol.* 292, 115224. doi:10.1016/j.jep.2022.115224

Lu, J., and Holmgren, A. (2014). The thioredoxin antioxidant system. *Free Radic. Biol. Med.* 66, 75–87. doi:10.1016/j.freeradbiomed.2013.07.036

Lu, Y., Xie, T., Zhang, Y., Zhou, F., Ruan, J., Zhu, W., et al. (2017). Triptolide Induces hepatotoxicity via inhibition of CYP450s in Rat liver microsomes. *BMC Complement. Altern. Med.* 17 (1), 15. doi:10.1186/s12906-016-1504-3

Luo, D., Zuo, Z., Zhao, H., Tan, Y., and Xiao, C. (2019). Immunoregulatory effects of Tripterygium wilfordii Hook F and its extracts in clinical practice. *Front. Med.* 13 (5), 556–563. doi:10.1007/s11684-018-0649-5

Maricic, I., Marrero, I., Eguchi, A., Nakamura, R., Johnson, C. D., Dasgupta, S., et al. (2018). Differential activation of hepatic invariant NKT cell subsets plays a key role in progression of nonalcoholic steatohepatitis. *J. Immunol.* 201 (10), 3017–3035. doi:10.4049/jimmunol.1800614

Marrero, I., Maricic, I., Feldstein, A. E., Loomba, R., Kumar, V., Rivera-Nieves, J., et al. (2018). Complex network of NKT cell subsets controls immune homeostasis in liver and gut. *Front. Immunol.* 9, 2082. doi:10.3389/fimmu.2018.02082

Mei, X. A., Yan, Z. A., Xjl, A., Zzj, B., Liang, Z. C., Shl, A., et al. (2012). Comparison of toxicokinetic and tissue distribution of triptolide-loaded solid lipid nanoparticles vs free triptolide in rats. *Eur. J. Pharm. Sci.* 47 (4), 713–717. doi:10.1016/j.ejps.2012.05.012

Molinaro, A., and Marschall, H. (2022). Bile acid metabolism and FXR-mediated effects in human cholestatic liver disorders. *Biochem. Soc. Trans.* 50 (1), 361–373. doi:10.1042/bst20210658

Nebert, D. W., and Dalton, T. P. (2006). The role of cytochrome P450 enzymes in endogenous signalling pathways and environmental carcinogenesis. *Nat. Rev. Cancer* 6 (12), 947–960. doi:10.1038/nrc2015

Nguyen, N., Umbaugh, D., Sanchez-Guerrero, G., Ramachandran, A., and Jaeschke, H. (2022). Kupffer cells regulate liver recovery through induction of chemokine receptor CXCR2 on hepatocytes after acetaminophen overdose in mice. *Arch. Toxicol.* 96 (1), 305–320. doi:10.1007/s00204-021-03183-0

Nong, C., Zou, M., Xue, R., Bai, L., Liu, L., Jiang, Z., et al. (2020). The role of invariant natural killer T cells in experimental xenobiotic-induced cholestatic hepatotoxicity. *Biomed. Pharmacother.* 122, 109579. doi:10.1016/j.biopha.2019.109579

Pan, Y., Meng, M., Zheng, N., Cao, Z., Yang, P., Xi, X., et al. (2017). Targeting of multiple senescence-promoting genes and signaling pathways by triptonide induces complete senescence of acute myeloid leukemia cells. *Biochem. Pharmacol.* 126, 34–50. doi:10.1016/j.bcp.2016.11.024

Peng, R., Ma, S. R., Fu, J., Han, P., Pan, L. B., Zhang, Z. W., et al. (2020). Transforming of triptolide into characteristic metabolites by the gut microbiota. *Molecules* 25 (3), 606. doi:10.3390/molecules25030606

Pole, A., Dimri, M., and Dimri, G. P. (2016). Oxidative stress, cellular senescence and ageing. *AIMS Mol. Sci.* 3 (3), 300–324. doi:10.3934/molsci.2016.3.300

Qu, L., Qu, F., Jia, Z., Wang, C., Wu, C., and Zhang, J. (2015). Integrated targeted sphingolipidomics and transcriptomics reveal abnormal sphingolipid metabolism

as a novel mechanism of the hepatotoxicity and nephrotoxicity of triptolide. *J. Ethnopharmacol.* 170, 28–38. doi:10.1016/j.jep.2015.05.010

Shen, F., Xiong, Z., Kong, J., Wang, L., Cheng, Y., Jin, J., et al. (2019). Triptolide impairs thioredoxin system by suppressing Notch1-mediated PTEN/Akt/Txnip signaling in hepatocytes. *Toxicol. Lett.* 300, 105–115. doi:10.1016/j.toxlet.2018.10.024

Shen, G., Zhuang, X., Xiao, W., Kong, L., Tan, Y., and Li, H. (2014). Role of CYP3A in regulating hepatic clearance and hepatotoxicity of triptolide in rat liver microsomes and sandwich-cultured hepatocytes. *Food Chem. Toxicol.* 71, 90–96. doi:10.1016/j.fct.2014.05.020

Song, X., He, H., Zhang, Y., Fan, J., and Wang, L. (2022). Mechanisms of action of triptolide against colorectal cancer: Insights from proteomic and phosphoproteomic analyses. *Aging* 14 (7), 3084–3104. doi:10.18632/aging.203992

Sun, J., Zhao, F., Lin, B., Feng, J., Wu, X., Liu, Y., et al. (2020). Gut microbiota participates in antithyroid drug induced liver injury through the lipopolysaccharide related signaling pathway. *Front. Pharmacol.* 11, 598170. doi:10.3389/fphar.2020.598170

Tan, Q. Y., Hu, Q., Zhu, S. N., Jia, L. L., Xiao, J., Su, H. Z., et al. (2018). Licorice root extract and magnesium isoglycyrrhizinate protect against triptolide-induced hepatotoxicity via up-regulation of the Nrf2 pathway. *Drug Deliv.* 25 (1), 1213–1223. doi:10.1080/10717544.2018.1472676

Tang, J., Yan, Z., Feng, Q., Yu, L., and Wang, H. (2021). The roles of neutrophils in the pathogenesis of liver diseases. *Front. Immunol.* 12, 625472. doi:10.3389/fimmu.2021.625472

Titov, D. V., Gilman, B., He, Q. L., Bhat, S., Low, W. K., Dang, Y., et al. (2011). XPB, a subunit of TFIIH, is a target of the natural product triptolide. *Nat. Chem. Biol.* 7 (3), 182–188. doi:10.1038/nchembio.522

Tsai, Y. L., Hua, K. F., Chen, A., Wei, C. W., Chen, W. S., Wu, C. Y., et al. (2017). NLRP3 inflammasome: Pathogenic role and potential therapeutic target for IgA nephropathy. *Sci. Rep.* 7, 41123. doi:10.1038/srep41123

Tsuji, Y., Kuramochi, M., Golbar, H. M., Izawa, T., Kuwamura, M., and Yamate, J. (2020). Acetaminophen-induced rat hepatotoxicity based on M1/M2-macrophage polarization, in possible relation to damage-associated molecular patterns and autophagy. *Int. J. Mol. Sci.* 21 (23), E8998. doi:10.3390/ijms21238998

Vakifahmetoglu-Norberg, H., Ouchida, A., and Norberg, E. (2017). The role of mitochondria in metabolism and cell death. *Biochem. Biophys. Res. Commun.* 482 (3), 426–431. doi:10.1016/j.bbrc.2016.11.088

Wang, J., Jiang, Z., Ji, J., Wang, X., Wang, T., Zhang, Y., et al. (2013). Gene expression profiling and pathway analysis of hepatotoxicity induced by triptolide in Wistar rats. *Food Chem. Toxicol.* 58, 495–505. doi:10.1016/j.fct.2013.04.039

Wang, J. M., Chen, R. X., Zhang, L. L., Ding, N. N., Liu, C., Cui, Y., et al. (2018a). *In vivo* protective effects of chlorogenic acid against triptolide-induced hepatotoxicity and its mechanism. *Pharm. Biol.* 56 (1), 626–631. doi:10.1080/13880209.2018.1527370

Wang, L., Xu, D., Li, L., Xing, X., Liu, L., Ismail Abdelmotalab, M., et al. (2018b). Possible role of hepatic macrophage recruitment and activation in triptolide-induced hepatotoxicity. *Toxicol. Lett.* 299, 32–39. doi:10.1016/j.toxlet.2018.08.017

Wang, X., Jiang, Z., Cao, W., Yuan, Z., Sun, L., and Zhang, L. (2014a). Th17/Treg imbalance in triptolide-induced liver injury. *Fitoterapia* 93, 245–251. doi:10.1016/j.fitote.2014.01.006

Wang, X., Jiang, Z., Xing, M., Fu, J., Su, Y., Sun, L., et al. (2014b). Interleukin-17 mediates triptolide-induced liver injury in mice. *Food Chem. Toxicol.* 71, 33–41. doi:10.1016/j.fct.2014.06.004

Wang, X., Sun, L., Zhang, L., and Jiang, Z. (2016). Effect of adoptive transfer or depletion of regulatory T cells on triptolide-induced liver injury. *Front. Pharmacol.* 7, 99. doi:10.3389/fphar.2016.00099

Wang, X. z., Xue, R. f., Zhang, S. y., Zheng, Y. t., Zhang, L. y., and Jiang, Z. z. (2018c). Activation of natural killer T cells contributes to triptolide-induced liver injury in mice. *Acta Pharmacol. Sin.* 39 (12), 1847–1854. doi:10.1038/s41401-018-0084-9

Wang, X. Z., Zhang, S. Y., Xu, Y., Zhang, L. Y., and Jiang, Z. Z. (2018d). The role of neutrophils in triptolide-induced liver injury. *Chin. J. Nat. Med.* 16 (9), 653–664. doi:10.1016/s1875-5364(18)30105-5

Wei, C. B., Tao, K., Jiang, R., Zhou, L. D., Zhang, Q. H., and Yuan, C. S. (2017). Quercetin protects mouse liver against triptolide-induced hepatic injury by restoring Th17/Treg balance through Tim-3 and TLR4-MyD88-NF-κB pathway. *Int. Immunopharmacol.* 53, 73–82. doi:10.1016/j.intimp.2017.09.026

Wei, Y. M., Luan, Z. H., Liu, B. W., Wang, Y. H., Chang, Y. X., Xue, H. Q., et al. (2019). Autophagy in triptolide-mediated cytotoxicity in hepatic cells. *Int. J. Toxicol.* 38 (5), 436–444. doi:10.1177/1091581819864518

Wei, Y., Wang, D., Chen, M., Ouyang, Z., Wang, S., and Gu, J. (2018). Extrahepatic cytochrome P450s play an insignificant role in triptolide-induced toxicity. *Chin. Med.* 13, 23. doi:10.1186/s13020-018-0179-8

Wilson, I. D., and Nicholson, J. K. (2017). Gut microbiome interactions with drug metabolism, efficacy, and toxicity. *Transl. Res.* 179, 204–222. doi:10.1016/j.trsl.2016.08.002

Xi, C., Peng, S., Wu, Z., Zhou, Q., and Zhou, J. (2017). Toxicity of triptolide and the molecular mechanisms involved. *Biomed. Pharmacother.* 90, 531–541. doi:10.1016/j.biopha.2017.04.003

Xiao, X., Zhang, T., Huang, J., Zhao, Q., and Li, F. (2020). Effect of CYP3A4 on liver injury induced by triptolide. *Biomed. Chromatogr.* 34 (8), e4864. doi:10.1002/bmc.4864

Xie, Z., and Klionsky, D. (2007). Autophagosome formation: Core machinery and adaptations. *Nat. Cell Biol.* 9 (10), 1102–1109. doi:10.1038/ncb1007-1102

Xu, P., Li, Y., Yu, Z., Yang, L., Shang, R., and Yan, Z. (2019). Protective effect of vitamin C on triptolide-induced acute hepatotoxicity in mice through mitigation of oxidative stress. *An. Acad. Bras. Cienc.* 91 (2), e20181257. doi:10.1590/0001-3765201920181257

Xue, X., Gong, L., Qi, X., Wu, Y., Xing, G., Yao, J., et al. (2011). Knockout of hepatic P450 reductase aggravates triptolide-induced toxicity. *Toxicol. Lett.* 205 (1), 47–54. doi:10.1016/j.toxlet.2011.05.003

Yan, M., Zhao, C., Lu, S., Cui, J., Sun, Z., Liu, X., et al. (2022). Trimethylamine N-oxide exacerbates acetaminophen-induced liver injury by interfering with macrophage-mediated liver regeneration. *J. Cell. Physiol.* 237 (1), 897–910. doi:10.1002/jcp.30568

Yang, J., Sun, L., Wang, L., Hassan, H. M., Wang, X., Hylemon, P. B., et al. (2017). Activation of Sirt1/FXR signaling pathway attenuates triptolide-induced hepatotoxicity in rats. *Front. Pharmacol.* 8, 260. doi:10.3389/fphar.2017.00260

Yang, T., Wang, Y. L., Zhang, Y. L., Liu, Y. T., Tao, Y. Y., Zhou, H., et al. (2022). The protective effect of Capparis spinosa fruit on triptolide-induced acute liver injury: A metabolomics-based systematic study. *J. Funct. Foods* 90, 104989. doi:10.1016/j.jff.2022.104989

Yang, T., Zhang, Y., Zhu, T., Xing, L., Liu, Y. t., and Liu, C. h. (2018). A preliminary study on clinical characteristics and Toxicology mechanism of Tripterygium wilfordii induced liver injury. *Mod. Traditional Chin. Med. Materia Medica-World Sci. Technol.* 20 (11), 2027–2032. doi:10.11842/wst.2018.11.021

Yao, J., Jiang, Z., Duan, W., Huang, J., Zhang, L., Hu, L., et al. (2008). Involvement of mitochondrial pathway in triptolide-induced cytotoxicity in human normal liver L-02 cells. *Biol. Pharm. Bull.* 31 (4), 592–597. doi:10.1248/bpb.31.592

Ye, X., Li, W., Yan, Y., Mao, C., Cai, R., Xu, H., et al. (2010). Effects of cytochrome P4503A inducer dexamethasone on the metabolism and toxicity of triptolide in rat. *Toxicol. Lett.* 192 (2), 212–220. doi:10.1016/j.toxlet.2009.10.028

Yip, L. Y., Aw, C. C., Lee, S. H., Hong, Y. S., Ku, H. C., Xu, W. H., et al. (2018). The liver-gut microbiota axis modulates hepatotoxicity of tacrine in the rat. *Hepatology* 67 (1), 282–295. doi:10.1002/hep.29327

Yu, G., Zhou, L., Zeng, B., Huang, J., and She, X. (2021). The antioxidant effect of triptolide contributes to the therapy in a collagen-induced arthritis rat model. *Redox Rep.* 26 (1), 197–202. doi:10.1080/13510002.2021.2004047

Yu, L., Hong, W., Lu, S., Li, Y., Guan, Y., Weng, X., et al. (2022). The NLRP3 inflammasome in non-alcoholic fatty liver disease and steatohepatitis: Therapeutic targets and treatment. *Front. Pharmacol.* 13, 780496. doi:10.3389/fphar.2022.780496

Yu, S. J., Jiang, R., Mazzu, Y. Z., Wei, C. B., Sun, Z. L., Zhang, Y. Z., et al. (2016). Epigallocatechin-3-gallate prevents triptolide-induced hepatic injury by restoring the Th17/treg balance in mice. *Am. J. Chin. Med.* 44 (6), 1221–1236. doi:10.1142/S0192415X16500683

Yuan, Z., Hasnat, M., Liang, P., Yuan, Z., Zhang, H., Sun, L., et al. (2019a). The role of inflammasome activation in Triptolide-induced acute liver toxicity. *Int. Immunopharmacol.* 75, 105754. doi:10.1016/j.intimp.2019.105754

Yuan, Z., Yuan, Z., Hasnat, M., Zhang, H., Liang, P., Sun, L., et al. (2020). A new perspective of triptolide-associated hepatotoxicity: The relevance of NF- kappa B and NF- kappa B-mediated cellular FLICE-inhibitory protein. *Acta Pharm. Sin. B* 10 (5), 861–877. doi:10.1016/j.apsb.2020.02.009

Yuan, Z., Zhang, H., Hasnat, M., Ding, J., Chen, X., Liang, P., et al. (2019b). A new perspective of triptolide-associated hepatotoxicity: Liver hypersensitivity upon LPS stimulation. *Toxicology* 414, 45–56. doi:10.1016/j.tox.2019.01.005

Zamek-Gliszczynski, M. J., Patel, M., Yang, X., Lutz, J. D., Chu, X., Brouwer, K. L. R., et al. (2021). Intestinal P-gp and putative hepatic OATP1B induction: International

transporter consortium perspective on drug development implications. *Clin. Pharmacol. Ther.* 109 (1), 55–64. doi:10.1002/cpt.1916

Zhang, f., and Li, Y. c. (2004). Progress in structure modification of Triptolide. *Acta Pharm. Sin.* 39 (10), 857–864. doi:10.16438/j.0513-4870.2004.10.020

Zhang, H., Ya, G., and Rui, H. (2017). Inhibitory effects of triptolide on human liver cytochrome P450 enzymes and P-glycoprotein. *Eur. J. Drug Metab. Pharmacokinet.* 42 (1), 89–98. doi:10.1007/s13318-016-0323-8

Zhang, H., Yuan, Z., Zhu, Y., Yuan, Z., Wang, J., Nong, C., et al. (2022a). Th17/Treg imbalance mediates hepatic intolerance to exogenous lipopolysaccharide and exacerbates liver injury in triptolide induced excessive immune response. *J. Ethnopharmacol.* 295, 115422. doi:10.1016/j.jep.2022.115422

Zhang, L., Li, C., Fu, L., Yu, Z., Xu, G., Zhou, J., et al. (2022b). Protection of catalpol against triptolide-induced hepatotoxicity by inhibiting excessive autophagy via the PERK-ATF4-CHOP pathway. *PeerJ* 10, e12759. doi:10.7717/peerj.12759

Zhang, L., Zhou, J., Feng, Z., Jiang, B., Li, C., Zhou, L., et al. (2022c). Qingluo tongbi formula alleviates hepatotoxicity induced by Tripterygium wilfordii Hook. F. By regulating excessive mitophagy through the PERK-ATF4 pathway. *Front. Pharmacol.* 13, 918466. doi:10.3389/fphar.2022.918466

Zhang, X. F., Liu, J., Ye, F., Ji, S. G., Zhang, N., Cao, R. S., et al. (2014). Effects of triptolide on the pharmacokinetics of cyclophosphamide in rats: A possible role of cytochrome P3A4 inhibition. *Chin. J. Integr. Med.* 20 (7), 534–539. doi:10.1007/s11655-014-1710-0

Zhang, Y., Li, J., Lei, X., Zhang, T., Liu, G., Yang, M., et al. (2016). Influence of verapamil on pharmacokinetics of triptolide in rats. *Eur. J. Drug Metab. Pharmacokinet.* 41 (4), 449–456. doi:10.1007/s13318-015-0275-4

Zhao, H., Tong, Y., Lu, D., and Wu, B. (2020a). Circadian clock regulates hepatotoxicity of Tripterygium wilfordii through modulation of metabolism. *J. Pharm. Pharmacol.* 72 (12), 1854–1864. doi:10.1111/jphp.13299

Zhao, J. (2018). *Study on the mechanism of triptolide-induced liver injury*. China, Hebei, Shijiazhuang: Ph. D., Hebei Medical University.

Zhao, J., Xie, C., Wang, K., Takahashi, S., Krausz, K. W., Lu, D., et al. (2020b). Comprehensive analysis of transcriptomics and metabolomics to understand triptolide-induced liver injury in mice. *Toxicol. Lett.* 333, 290–302. doi:10.1016/j.toxlet.2020.08.007

Zhao, M., Zhao, H., Deng, J., Guo, L., and Wu, B. (2019). Role of the CLOCK protein in liver detoxification. *Br. J. Pharmacol.* 176 (24), 4639–4652. doi:10.1111/bph.14828

Zheng, N., Wei, A., Wu, T., Long, L., Yang, H., Li, H., et al. (2021). Triptolide and atorvastatin synergistically promote hepatotoxicity in cultured hepatocytes and female Sprague-Dawley rats by inhibiting pregnane X receptor-mediated transcriptional activation of CYP3A4. *Toxicol. Lett.* 342, 85–94. doi:10.1016/j.toxlet.2021.02.008

Zhou, L. L., Zhou, C., Liang, X. W., Feng, Z., Liu, Z. P., Wang, H. L., et al. (2017). Self-protection against triptolide-induced toxicity in human hepatic cells via Nrf2-ARE-NQO1 pathway. *Chin. J. Integr. Med.* 23 (12), 929–936. doi:10.1007/s11655-017-2546-6

Zhou, Y., Xia, L., Yao, W., Han, J., and Wang, G. (2020). Arctiin antagonizes triptolide-induced hepatotoxicity via activation of Nrf2 pathway. *Biomed. Res. Int.* 2020, 2508952. doi:10.1155/2020/2508952

Zhou, Z. L., Yang, Y. X., Ding, J., Li, Y. C., and Miao, Z. H. (2012). Triptolide: Structural modifications, structure-activity relationships, bioactivities, clinical development and mechanisms. *Nat. Prod. Rep.* 29 (4), 457–475. doi:10.1039/c2np00088a

Zhuang, X. M., Shen, G. L., Xiao, W. B., Tan, Y., Lu, C., and Li, H. (2013). Assessment of the roles of P-glycoprotein and cytochrome P450 in triptolide-induced liver toxicity in sandwich-cultured rat hepatocyte model. *Drug Metab. Dispos.* 41 (12), 2158–2165. doi:10.1124/dmd.113.054056

Zou, M., Nong, C., Yu, Z., Cai, H., Jiang, Z., Xue, R., et al. (2020). The role of invariant natural killer T cells and associated immunoregulatory factors in triptolide-induced cholestatic liver injury. *Food Chem. Toxicol.* 146, 111777. doi:10.1016/j.fct.2020.111777

frontiers | Frontiers in Pharmacology

TYPE Original Research
PUBLISHED 25 August 2022
DOI 10.3389/fphar.2022.987997

Check for updates

OPEN ACCESS

EDITED BY
Fareeha Anwar,
Riphah International University (Lahore), Pakistan

REVIEWED BY
Muhammad Tayyab Imtiaz,
Riphah International University (Lahore), Pakistan
Aslam Khan,
King Saud bin Abdulaziz University for Health Sciences, Saudi Arabia

*CORRESPONDENCE
Xueqian Wang,
shirlyding@163.com
Fafeng Cheng,
fafengcheng@gmail.com
Qingguo Wang,
wangqg8558@163.com

†These authors have contributed equally to this work and share first authorship

SPECIALTY SECTION
This article was submitted to Predictive Toxicology, a section of the journal Frontiers in Pharmacology

RECEIVED 06 July 2022
ACCEPTED 27 July 2022
PUBLISHED 25 August 2022

CITATION
Xu W, Chen D, Zhang Z, Liu S, Chen C, Sun C, Ni W, Kang X, Shang G, Wang X, Cheng F and Wang Q (2022), Toxicological safety evaluation of Qin-Zhi-Zhu-Dan formula in rats during the treatment and recovery periods. *Front. Pharmacol.* 13:987997. doi: 10.3389/fphar.2022.987997

COPYRIGHT
© 2022 Xu, Chen, Zhang, Liu, Chen, Sun, Ni, Kang, Shang, Wang, Cheng and Wang. This is an open-access article distributed under the terms of the Creative Commons Attribution License (CC BY). The use, distribution or reproduction in other forums is permitted, provided the original author(s) and the copyright owner(s) are credited and that the original publication in this journal is cited, in accordance with accepted academic practice. No use, distribution or reproduction is permitted which does not comply with these terms.

Toxicological safety evaluation of Qin-Zhi-Zhu-Dan formula in rats during the treatment and recovery periods

Wenxiu Xu[1†], Dan Chen[1†], Zehan Zhang[1], Shuling Liu[1], Congai Chen[2], Chunyan Sun[2], Wenchao Ni[2], Xiangdong Kang[1], Guojiao Shang[1], Xueqian Wang[1*], Fafeng Cheng[1*] and Qingguo Wang[1*]

[1]School of Traditional Chinese Medicine Department, Beijing University of Chinese Medicine, Beijing, China, [2]Dongzhimen Hospital, Beijing University of Chinese Medicine, Beijing, China

Background: Qinzhi Zhudan Formula (QZZD), optimized from Angong Niuhuang Wan, consists of *Radix Scutellariae*, *Fructus Gardeniae* and *Pulvis Fellis Suis*. We had investigated the neuroprotective effects of QZZD and its active components, and demonstrated that it could treat cerebral ischemia and dementia through multiple pathways and mechanisms. Nevertheless, toxicological data on this formula still remains limited. In the study, we sought to examine the toxicological effects of QZZD during the treatment and recovery periods.

Methods: We investigated potential toxicities of QZZD in Sprague-Dawley (SD) rats *via* 28-day gavage administration. SD rats were randomly divided into control group and treatment groups of A (0.5 g/kg/d QZZD), B (1.5 g/kg/d QZZD), and C (5.0 g/kg/d QZZD). The 56-day course includes treatment period (administration with water or QZZD once a day for 28 consecutive days) and recovery period (28 days). The rats received daily monitoring of general signs of toxicity and mortality, as well as weekly determination of body weight and food consumption. Moreover, the complete blood cell count, biochemistry, coagulation, and urine indicators, organ weights, and histopathological report were analyzed respectively at the end of the treatment and recovery periods.

Results: There was no death related to the active pharmaceutical ingredients of QZZD during the treatment period. The maximum no observed adverse effect level (NOAEL) was 0.5 g/kg/d, which is approximately 16.7 times of the equivalent dose of clinical dose in rats. In group TB (1.5 g/kg/d QZZD) and TC (5.0 g/kg/d QZZD), there were adverse effects of blue coloring of tail skin, weight loss, a significant increase of total bilirubin (TBIL), blackening of liver and kidney in gross examination, hyperplasia of bile duct and karyomegaly of hepatocytes in histopathological examination. Besides, in females rats, the food consumption was reduced, while in male rats, there was decrease in triglycerides (TG) and slight increase in white blood cell (WBC) count and neutrophils. In group TC (5.0 g/kg/d QZZD), the indicators of red blood cell (RBC) count, hemoglobin (HGB) and hematocrit (HCT) were decreased slightly,

while the platelet count (PLT) was increased. However, these changes were not considered to be toxicologically significant because they resolved during the recovery period.

Conclusion: Overall, QZZD exhibited a good safety profile. The maximum no observed adverse effect level was 0.5 g/kg/d, and no target organs toxicity were identified. The present findings might confirm the safety of QZZD in clinical practices.

KEYWORDS

sub-chronic toxicity, scutellaria baicalensis extract, gardenia extract, pulvis fellis suis, reversibility study, organ coefficient, biochemical

Introduction

Traditional Chinese medicine (TCM) has been widely utilized worldwide for thousands of years. TCM is well-recognized for its ability to treat multiple ailments and promote health (Alam et al., 2016). In recent years, natural products have received increasing attention given their low toxicity and high efficacy (Gao et al., 2018; Qi et al., 2020). Chinese herbs and extracts have become a research hotspot for their therapeutic and cytoprotective characteristics for treating neurodegenerative diseases in human beings (Gaire et al., 2014), especially in treating the etiology and pathogenesis of vascular dementia. Overwhelming evidence substantiates the pharmacological activities of the three components (at a ratio of 10:6:1.5) of QZZD: *Radix Scutellariae*, *Fructus Gardeniae* and *Pulvis Fellis Suis* (Gaire et al., 2014; Zhang et al., 2017; Ma et al., 2020; Rui et al., 2020).

Radix Scutellariae is the most widely used herb for neuroprotection in TCM. The major phytochemicals isolated from S. baicalensis are flavonoids, glycosides and their glucuronides, such as baicalin, baicalein, and wogonin (Gaire et al., 2014), with good safety and therapeutic effect against cerebral ischemia. *Radix Scutellariae* generally listed in treatment of cerebral ischemia's traditional formulas including NiuHuangQingXinWan, Angong Niuhuang Boluses, and Huanglian jiedu decoction, and is also the core component of QZZD. Modern studies have shown that *Radix Scutellariae* has antagonistic effects on neuronal cell death and neurodegeneration due to glutamate toxicity, oxidative cascade, inflammation, and apoptosis (Gaire et al., 2014). Furthermore, we found that baicalin could inhibit cerebral ischemia-induced activation of the NFκB/CCL2/CCR2 pathway via targeting NFκB activation and CCL2/CCR2 interaction. *In vitro*, baicalin significantly inhibited the secretion of NO, IL6, TNFα, and CCL2 in macrophages and promoted the secretion of IL13, IFN -γ, and IL-1α (Xu et al., 2022).

Fructus Gardeniae (FG) is the dried fruit of *Gardenia jasminoides Ellis* (GjE), which belongs to the family Rubiaceae and is an outstanding traditional medicinal plant used for medicine and food. FG is a traditional Chinese medicine that has been originally recorded in the "Shennong Bencao Jing" and listed in each version of "Chinese Pharmacopoeia", with the effects of "discharging fire, eliminating vexation, reducing fever and causing diuresis", cooling blood to remove pathogenic heat. (Chinese Pharmacopoeia Commission, 2010). Approximately 162 chemical compounds have been isolated and identified from FG. Previous studies have reported various pharmacological properties, including beneficial effects on the nervous, cardiovascular and digestive systems, hepatoprotective activity, antidepressant activity, and anti-inflammatory activity (Chen et al., 2020). Studies have shown that *Gardenia jasminoides* extract (GJE) may play a protective effect in improving chronic cerebral ischemia based on its antioxidant properties by scavenging free radicals, reducing NO toxicity and AChE activity in brain neurons (Zhang et al., 2017).

Pulvis Fellis Suis (PFS), named "Zhu Danfen" in China, was first listed in the 2000 version of "Chinese Pharmacopoeia" (Shi et al., 2018). According to the Chinese Pharmacopoeia 2020, PFS has a bitter taste and cold nature and belongs to the liver, gallbladder, lung and large intestine channels. It has the functions of clearing heat, moistening dryness, relieving cough, relieving asthma and detoxifying (Chinese Pharmacopoeia Commission, 2020). PFS is rich in substances, including bile acids, bile pigments, mucoproteins, lipids and inorganic substances (He et al., 2017). Modern pharmacological research indicates that these compounds exert diverse biological activities, such as antitussive, anti-inflammatory, antibacterial, cholagogic, antibacterial, anti-tumor and other pharmacological effects (He et al., 2017; Chen et al., 2021), and are clinically used to treat whooping cough, asthma, hepatitis, vaginitis, intrahepatic bile duct stones, intestinal diseases, etc. (He et al., 2011). Our previous study showed that cholalic acid components have a good anti-cerebral ischemic effect. For instance, cholic acid (CA) exerted protective effects on the neurovascular unit (NVU), mediated by increased release of BDNF and further

stimulating the BDNF-TrkB-PI3K/Akt and BDNF-TrkB-MAPK/Erk signaling pathways during OGD/R-induced injury (Li et al., 2020).

Our previous research also showed that QZZD could significantly improve learning memory and spatial exploration disorders in Alzheimer's and vascular dementia rat models (Liu et al., 2022). Additionally, QZZD could reduce neuroinflammation by regulating the TNF Receptor1-ERK1/2-NF-κBp65 pathway and reducing the expression of the β-amyloid protein in APP/PS1 double-transgenic AD mice (unpublished data). Repeated dose toxicity studies play an indispensable role in preclinical evaluation of safety, whose purpose is to predict possible toxicities in human body. It can help to determine no observed adverse effect level (NOAEL) and first-in-human (FIH) dose, which will provide a safe dose range for subsequent application of QZZD in clinical trials (Gua et al., 2014) However, few studies have hitherto investigated QZZD toxicological safety, emphasizing a lack of evidence for further clinical translation.

In the present study, we aimed to evaluate the subchronic toxicity of QZZD. Rats were administered with 0.5, 1.5, and 5.0 g/kg/d of QZZD for 4 weeks, followed by 4 weeks of recovery, and all relative parameters were monitored during these 8 weeks. Collectively, our findings provide the foothold for applying QZZD in clinical therapy and reliable experimental data for its rational and safe application.

Materials and methods

Preparation of qinzhi zhudan formula

QZZD was provided by the China Academy of Chinese Medical Sciences and accredited by expert pharmacognosists. The three medicinals (*Radix Scutellaria*, *Fructus Gardeniae* and *Pulvis Fellis Suis*) were mixed at a ratio of 10:6:1.5. The extraction process and quality control were implemented according to our previous study. *Radix Scutellaria* was decocted with water 12 times of its volume twice, 1 h each time. The decoctions were combined and filtered. The filtrate was concentrated to a relative density of 1.05–1.10, and 2 mol/L hydrochloric acid solution is added at 80°C to adjust the pH value to 1.0–2.0. It was then kept warm for 30 min before centrifuged at 4000 rpm for 10 min. The sediment was washed with a small amount of 50% ethanol that was then evaporated. Then it was dried under 60°C under reduced pressure before use. *Fructus Gardeniae* was grinded and extracted at room temperature for 3 times with 75% ethanol 10 times of its volume, 8 h each time. The solution was combined before ethanol recovery at reduced pressure below 60°C. Then the concentrated solution is spray dried before use. *Pulvis Fellis Suis* was mixed with the above two extracts and kept refrigerated at −20°C until use. Chromatography with tandem mass spectrometry (LC-MS-MS) was used in a previous study to analyze the composition of the QZZD and identified baicalin, geniposide, cholic acid, hyodeoxycholic acid, and chenodeoxycholic acid. The results of QZZD-UHPLC-QE-MS are shown in Supplementary Tables S1, S2.

Chemicals and agents

Radix Scutellariae and Fructus Gardeniae were purchased from Anxing Chinese Herbal Medicine Co., Ltd. (No. 200901, China). *Pulvis Fellis Suis* was purchased from Shengtai Chinese Herbal Medicine Co., Ltd. (No. 190901, China). Xylazine Hydrochloride Injection was purchased from Jilin Hualu Mu Animal Health Products Co., Ltd. (No. 20201118). Zolelil ®50 was obtained from Virbac Co., Ltd. (No.7XDYA). Tropicamide was supplied by Shandong Doctor Renfreida Pharmaceutical Co., Ltd. (No.20073001/20102901, Jinan, Shandong province, China).

Animals

A total of 144 Sprague-Dawley (SD) rats of both sexes (specific pathogen-free (SPF) grade) (males weighing 273.4–333.2 g and females 184.2–233.8 g) were purchased from Beijing WeiTongLiHua Laboratory Animal Technology Co., Ltd. The rats were fed with a standard rodent diet (SPF grade, supplied by Beijing Keao Xieli Feed Co. Ltd., Beijing, China) and water (Conform to GB14925-2010, GB5749-2006 standards) *ad libitum* in a Good Laboratory Practice (GLP) center, approved by the China Food and Drug Administration (CFDA) under controlled conditions [temperature (23 ± 3°C) with a relative humidity of 40.10%–76.89%, and maintained under a 12/12-h light/dark cycle]. The cage beddings and water bottles were cleaned daily. The animals were allowed 1 week of acclimatization before the beginning of experimental procedures. The standards of the feeding environment were based on the People's Republic of China national standard (GB14925-2010), and the Honeywell EBI R430.1 automatic control system was used.

Grouping and drug administration

An ear tag was attached to each rat with a unique identification number. Cage cards were made according to the animal numbers in Table 1. The determination of dose of QZZD in this study was in accordance with Technical Guidelines for Repeated Dose Toxicity Studies (2014) issued by China Food and Drug Administration (CFDA). To ensure animal welfare and the feasibility of gavage, 5.0 g/kg/d was regarded as a high-dose concentration, and the maximum concentration for gavage was set to 250 mg/ml QZZD. The animals were randomly divided into a control group (CN) and three experimental groups (TA, TB, and TC) according to the QZZD dosage.

TABLE 1 Group grouping and identification of test animals.

Group number	Group	Number		Animal number		Cage number		Necropsy time	Cage card color
		♀	♂	♀	♂	♀	♂		
1	CN	18	18	1101–1112 1113–1118	1201–1212 1213–1218	1–4 5, 6	7–10 11, 12	end of administration end of the recovery period	white
2	TA	18	18	2101–2112 2113–2118	2201–2212 2213–2218	13–16 17, 18	19–22 23, 24	end of administration end of the recovery period	green
3	TB	18	18	3101–3112 3113–3118	3201–3212 3213–3218	25–28 29, 30	31–34 35, 36	end of administration end of the recovery period	yellow
4	TC	18	18	4101–4112 4113–4118	4201–4212 4213–4218	37–40 41, 42	43–46 47, 48	end of administration end of the recovery period	red

Animal numbers 4110 and 4111 were dead at D15 and D9, respectively.

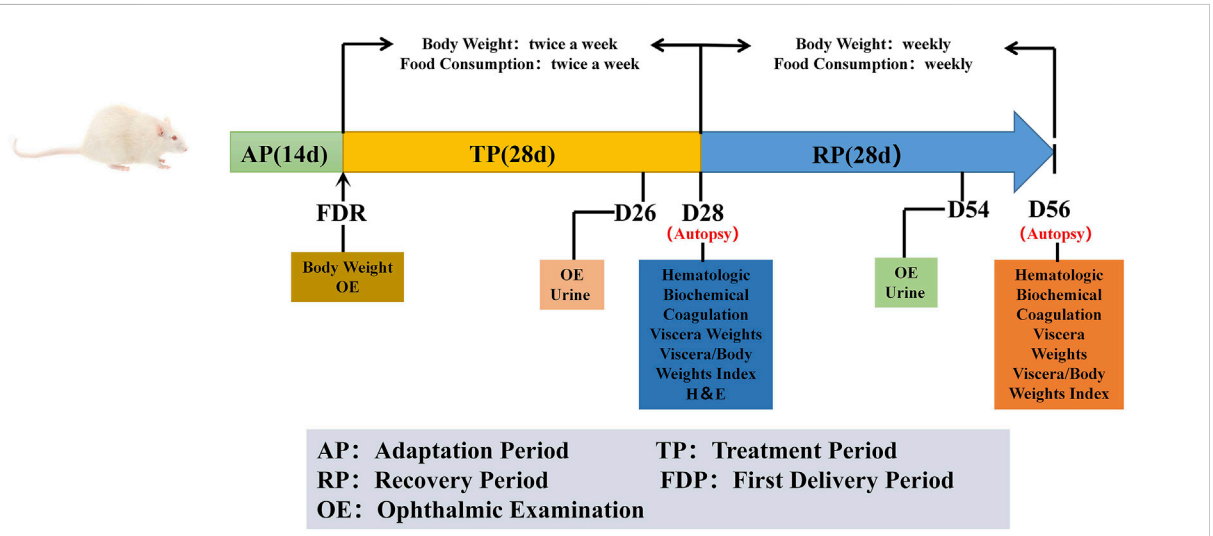

FIGURE 1
Representative experimental scheme. 'AP' indicates 14 days of suitability rearing before the experiment; 'FDR' was defined as trial day 1 (D1), body weight and ophthalmic examinations were performed. The whole experiment lasted for 56 days, it was divided into treatment period (TP) and recovery period (RP). During the trial, cage observation daily; detailed clinical signs observation, body weight and food consumption were performed weekly. Ophthalmic examination and urine examination are performed before the end of the treatment and the recovery periods (D26 and D54). Hematologic, biochemical and coagulation examinations were tested at the end of the treatment period and the recovery period (D28 and D56), and necropsy, organ weight and histopathological examination were performed after the animals were euthanized.

There were 18 female and 18 male rats in each group. Rats in the TA, TB, and TC groups were administered with 0.5 g/kg/d, 1.5 g/kg/d, and 5.0 g/kg/d QZZD, hence termed as low, middle, and high-dose groups, respectively. The experimental group's dosage was 20 ml/kg, and the control group received the same volume of double distilled water.

At the end of the treatment period, 12 male and 12 female rats from each group were sacrificed for analyses of the complete blood count, biochemistry, and urine indicators, major organ weights, and histopathology of reproductive organs. The remaining rats in each group, including six females and six males, were given free access to food and water for another 4 weeks (5–8 weeks, named recovery period) until the end of the experiment. They were sacrificed at the end of the recovery period, and the above-mentioned parameters were assessed. A representative experimental scheme is shown in Figure 1.

Clinical signs observation

Cage-side observations for apparent signs of toxicity or injury (behavior, mental status, gland secretion, feces characteristics, genitals, and death) were conducted twice a day after daily drug exposure, and once experimental animals developed toxic symptoms, the observation frequency was increased. During the recovery period, the observation was performed once a day.

Detailed clinical observations were made before grouping and once a week during administration until the end of the trial. If the detailed clinical observation coincided with the cage-side observation time, the detailed clinical observation replaced the cage-side observation in this period.

Body weight and food consumption

The body weight in all groups was measured once during the adaptation period (when grouping) and then measured twice per week (D3, D7, D10, D14, D17, D21, D24, D28) during the treatment period and then measured weekly (D35, D42, D49, D56) during the recovery period. Food consumption was measured once or twice weekly over a 24-h period. When food consumption was assayed, 200 g of animal feed was delivered; the remaining portions were measured at the same time on the second day, and the food consumption was calculated. Specifically, the food intake was measured twice weekly during the treatment period (D2, D6, D9, D13, D16, D20, D23, and D27) and then measured weekly (D34, D41, D48, D55) during the recovery period.

Ophthalmic examination

During adaptation and at the end of treatment period (D26) and recovery (D54) periods, tropicamide was applied to the mydriasis, cornea, conjunctiva, iris, pupil, crystalline lens, anterior/atria chamber, and fundus oculi of all animals, and they were examined using a binocular indirect ophthalmoscope (Cat. #YZ25C, 6-6 VISION TECH Co., Ltd., Suzhou, Jiangsu province, China).

CBC, biochemical, and coagulation examination

At the end of treatment period (D28) and recovery (D56), aorta blood (6 ml) was collected from all animals after fasting for 12 h.

For the complete blood count assay, 2 ml of blood was anticoagulated by ethylenediamine tetraacetic acid (EDTA). Hematological parameters, including red blood cells (RBC), white blood cells (WBC), hemoglobin (HGB), hematocrit (HCT), platelets (PLT), mean corpuscular volume (MCV), mean corpuscular hemoglobin (MCH), mean corpuscular hemoglobin concentration (MCHC), reticulocyte (RET%, RET#), neutrophils (NEUT%, NEUT#), lymphocytes (LYMPH %, LYMPH#), monocytes (MONO%, MONO#), eosinophils (EOS%, EOS#) and basophils (BASO%, BASO#) were detected by the Automatic Blood Analyzer (XT-2000IV, SYSMEX, Japan).

For biochemical examination, 2 ml of blood was centrifuged (3000 rpm, 10 min, RT), and serum was prepared for analysis. Parameters, including alanine aminotransferase (ALT), aspartate aminotransferase (AST), alkaline phosphatase (ALP), creatine phosphokinase (CK), total bilirubin (TBIL), glucose (GLU), urea (Urea), creatinine (Crea), triglyceride (TG), cholesterol total (TC), troponin (TP), albumin (ALB), globulin (GLOB), sodium (Na^+), potassium (K^+), and chloride ion (Cl^-) and albumin/globulin (A/G), were detected by Automatic Blood Biochemical Analyzer (Hitachi 7180, Hitachi Hi-Tech, Japan).

1.8 ml of blood was anticoagulated by sodium citrate to detect clotting indexes, and the plasma was separated for examination by centrifugation at 3000 rpm for 10 min at room temperature (RT). Blood coagulation indexes, including prothrombin time (PT), activated partial thromboplastin time (APTT), and fibrinogen (FIB), were detected by an automatic Hemagglutination Analyzer (CA-1500, SYSMEX, Japan).

Urine examination

Urine examinations were conducted once on day 26 and before the end of the recovery period (D54). Urine parameters, including specific gravity (SG), glucose (GLU), protein (PRO), bilirubin (BIL), urobilinogen (URO), pH, ketones (KET), specific gravity (SG), occult blood (BLO), nitrogen (NIT), turbidity (TURB), WBC and pigment, were detected by Urine Analyzer (Zhongke Meiling Cryogenics Co., Ltd., Hefei, Anhui province, China).

Bone marrow examination

Given that the hematological indexes of the animals indicated normal bone marrow hematopoiesis, a bone marrow smear was not required.

Necropsy and organ weight

Necropsy was conducted at the end of treatment period (on day 29, twelve rats per group) and the remaining rats were autopsied during the recovery period. Prior to dissection, all rats fasted overnight and were euthanized after intraperitoneal injection of sutai and serrazine hydrochloride mixture. A detailed

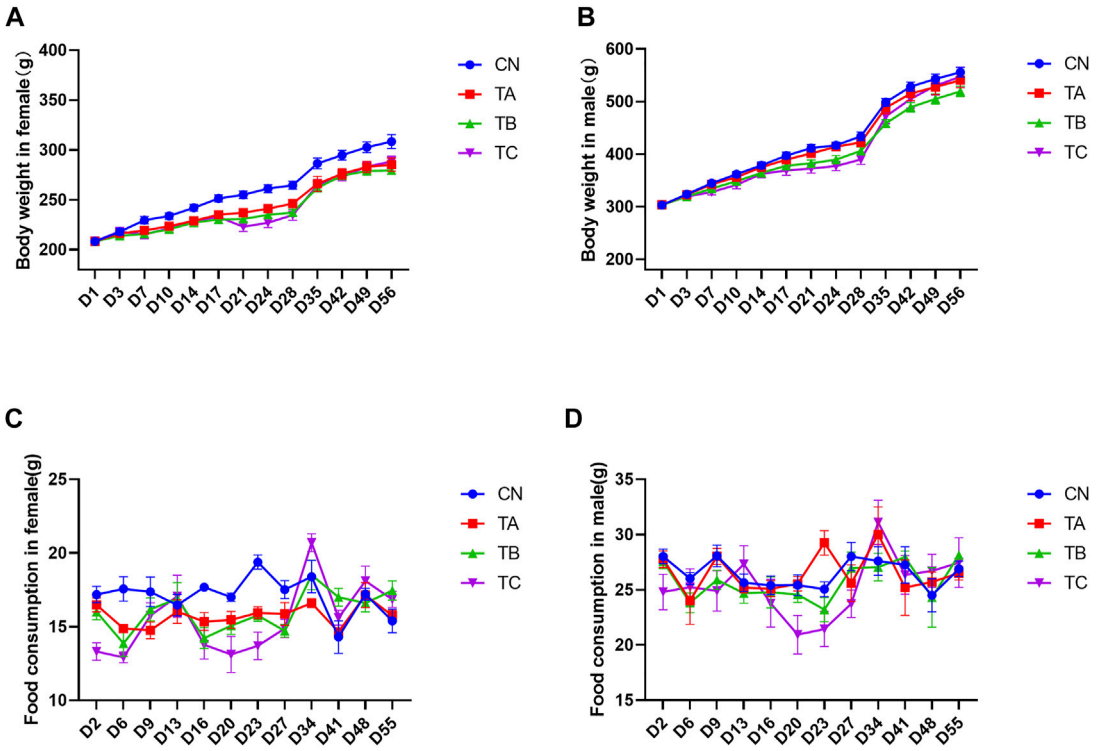

FIGURE 2
Effects of different doses of QZZD on the body weight in female **(A)** or male **(B)** rats and food consumption in female **(C)** or male **(D)** rats. In the treatment period, $n = 18$ in each group, and two female rats (4110 and 4111) death caused by faulty gavage operation, the total number was 16 ($n = 16$) in TC female group. In the recovery period, $n = 6$ in each group for female or male.

macroscopic examination was performed on the systemic organs and tissues. The wet weight of the following organs was measured, and the organ coefficients and organ brain coefficients were calculated separately: the brain, spleen, thymus, heart, liver, testis (bilateral)/ovaries (bilateral), epididymis (bilateral), kidneys (bilateral), adrenal glands (bilateral), and uterus (including the cervix) were separated and weighed. For paired organs, the weights of both organs were added together.

Histopathological examination

The following organs and tissues were extracted from the rats and fixed in 10% neutral buffered formalin: the brain, heart, aorta, pituitary, thyroid, parathyroid, lung including bronchi, liver, trachea, spleen, kidney, adrenal glands, salivary glands (submandibular), esophagus, stomach, duodenum, jejunum, ileum, cecum, colon, rectum, pancreas, epididymis, prostate, seminal vesicle, ovary, uterus (including the cervix), vagina, urinary bladder, submandibular lymph node, mesenteric lymph node, mammary gland (female and male), mammary gland skin, sternum (including bone marrow), femur (including bone marrow), skeletal muscle (biceps flexor cruris), nervi ischiadicus, spinal cord (neck, chest and waist) and abnormal tissues and tissue masses were visually observed. The testes, eyeballs, optic nerve and the harderian gland were fixed with Davidson's fixative.

All tissues/organs were fixed, and tissue slides were prepared by a standardized process, including dehydration, paraffin embedding, trimming, sectioning by microtome, and staining with hematoxylin-eosin (H&E). A histopathological examination was performed on the toxic target organs of dissected animals. The photomicroscopic assessment and the histopathology slides were viewed at various magnifications (×100 and ×400) to detect pathological lesions using a BX60 photomicroscope (Olympus, Tokyo, Japan). We invited pathologist Yingyong from the Shandong Academy of Pharmaceutical Sciences to peer review the sections.

Statistical analysis

Data were calculated and analyzed with SPSS (version 20.0, IBM, Armonk, NY). All values were presented as mean ± standard

TABLE 2 Effect of QZZD on hematological parameters in the sub-chronic oral toxicity study.

Parameter (mean ± SD)	Treatment period (n = 12)				Recovery period (n = 6)			
	CN	TA	TB	TC	CN	TA	TB	TC
Female								
WBC(10^9/L)	4.87 ± 1.38	4.61 ± 1.66	6.12 ± 2.04	5.20 ± 1.27	4.53 ± 1.04	4.54 ± 1.29	4.53 ± 1.32	5.40 ± 1.51
RBC(10^{12}/L)	7.24 ± 0.22	7.25 ± 0.38	6.95 ± 0.50	6.74 ± 0.50*	7.58 ± 0.33	7.83 ± 0.27	7.68 ± 0.27	7.66 ± 0.18
HGB (g/L)	140.33 ± 6.01	140.17 ± 7.00	136.17 ± 7.69	135.50 ± 5.48	146.83 ± 5.23	151.00 ± 5.62	148.67 ± 4.76	151.17 ± 3.71
PLT (10^9/L)	1164.92 ± 123.32	1171.25 ± 97.27	1181.08 ± 113.10	1505.40 ± 139.32*	1105.00 ± 80.38	1008.33 ± 81.16	1075.33 ± 68.60	1002.33 ± 147.20
HCT (%)	36.74 ± 1.40	36.62 ± 1.28	35.89 ± 1.80	36.21 ± 1.45	38.70 ± 1.59	39.93 ± 1.23	40.08 ± 1.24	40.77 ± 1.17
MCV(fL)	50.77 ± 1.61	50.58 ± 1.90	51.75 ± 2.15	53.85 ± 2.59*	51.08 ± 1.00	51.00 ± 1.19	52.22 ± 1.86	53.28 ± 1.49*
MCH(pg)	19.38 ± 0.50	19.35 ± 0.63	19.62 ± 0.56	20.14 ± 0.86*	19.38 ± 0.32	19.28 ± 0.28	19.35 ± 0.46	19.77 ± 0.53
MCHC(g/L)	381.92 ± 6.72	382.83 ± 8.29	379.33 ± 6.41	374.30 ± 6.78*	379.50 ± 4.59	378.17 ± 6.31	371.00 ± 9.34	370.67 ± 2.80
NEUT% (%)	17.76 ± 7.12	20.01 ± 8.14	21.23 ± 11.06	23.99 ± 12.02	17.53 ± 3.43	20.43 ± 8.36	15.73 ± 6.03	15.37 ± 4.86
LYMPH % (%)	78.39 ± 7.42	75.81 ± 8.03	75.68 ± 11.37	71.95 ± 12.66	77.42 ± 3.23	74.45 ± 8.32	78.25 ± 6.21	80.53 ± 5.03
MONO% (%)	2.68 ± 1.25	2.86 ± 0.76	2.30 ± 1.05	3.26 ± 1.23	3.72 ± 0.75	3.52 ± 0.55	4.60 ± 4.04	3.33 ± 0.94
EO% (%)	1.18 ± 0.60	1.33 ± 0.64	0.79 ± 0.36	0.80 ± 0.33	1.33 ± 0.24	1.60 ± 0.88	1.42 ± 0.54	0.77 ± 0.28
BASO% (%)	0.00 ± 0.00	0.00 ± 0.00	0.00 ± 0.00	0.00 ± 0.00	0.00 ± 0.00	0.00 ± 0.00	0.00 ± 0.00	0.00 ± 0.00
NEUT#(10^9/L)	0.83 ± 0.37	0.95 ± 0.67	1.35 ± 0.94	1.21 ± 0.66	0.80 ± 0.25	1.00 ± 0.66	0.70 ± 0.28	0.79 ± 0.23
LYMPH#(10^9/L)	3.86 ± 1.31	3.47 ± 1.18	4.59 ± 1.55	3.78 ± 1.21	3.51 ± 0.83	3.32 ± 0.69	3.54 ± 1.12	4.39 ± 1.39
MONO#(10^9/L)	0.13 ± 0.08	0.13 ± 0.06	0.14 ± 0.06	0.17 ± 0.07	0.17 ± 0.04	0.16 ± 0.06	0.22 ± 0.22	0.18 ± 0.08
EO#(10^9/L)	0.05 ± 0.02	0.06 ± 0.03	0.05 ± 0.02	0.04 ± 0.02	0.06 ± 0.01	0.07 ± 0.03	0.06 ± 0.02	0.04 ± 0.02
BASO#(10^9/L)	0.00 ± 0.00	0.00 ± 0.00	0.00 ± 0.00	0.00 ± 0.00	0.00 ± 0.00	0.00 ± 0.00	0.00 ± 0.00	0.00 ± 0.00
RET#(10^{12}/L)	0.2389 ± 0.0400	0.2670 ± 0.0419	0.3392 ± 0.0657*	0.5621 ± 0.1479*	0.2068 ± 0.0541	0.2032 ± 0.0242	0.2078 ± 0.0408	0.2156 ± 0.0282
RET%	3.301 ± 0.542	3.693 ± 0.627	4.901 ± 1.020*	8.373 ± 2.083*	2.715 ± 0.601	2.595 ± 0.300	2.712 ± 0.548	2.823 ± 0.421
Male								
WBC(10^9/L)	7.41 ± 1.56	8.53 ± 2.92	9.29 ± 1.78	9.97 ± 1.55*	7.34 ± 1.54	6.78 ± 1.10	6.63 ± 0.67	6.62 ± 1.25
RBC(10^{12}/L)	8.16 ± 0.33	8.09 ± 0.20	7.91 ± 0.49	7.46 ± 0.40*	8.38 ± 0.56	8.25 ± 0.18	8.27 ± 0.20	8.38 ± 0.35
HGB (g/L)	155.67 ± 6.17	153.58 ± 4.62	149.08 ± 9.37	139.67 ± 6.83*	152.67 ± 7.50	152.67 ± 4.37	153.00 ± 8.32	158.50 ± 4.68
PLT (10^9/L)	1163.92 ± 96.90	1130.67 ± 139.77	1272.83 ± 187.87	1466.42 ± 118.05*	1126.33 ± 167.22	1140.00 ± 98.81	1055.00 ± 123.94	1095.17 ± 68.36
HCT (%)	40.76 ± 1.67	40.29 ± 1.35	39.40 ± 2.31	37.18 ± 1.85*	40.20 ± 1.76	40.13 ± 1.26	41.52 ± 2.01	42.28 ± 1.51
MCV(fL)	50.02 ± 1.86	49.84 ± 2.05	49.82 ± 1.54	49.92 ± 2.63	48.10 ± 1.91	48.65 ± 1.43	50.22 ± 2.51	50.50 ± 1.95
MCH(pg)	19.08 ± 0.50	19.00 ± 0.64	18.84 ± 0.42	18.74 ± 0.72	18.25 ± 0.47	18.53 ± 0.31	18.50 ± 0.98	18.95 ± 0.63
MCHC(g/L)	382.00 ± 7.50	381.33 ± 6.49	378.50 ± 10.96	375.83 ± 8.22	379.83 ± 5.81	380.50 ± 8.26	368.33 ± 4.27*	374.83 ± 2.71
NEUT% (%)	12.91 ± 3.26	13.46 ± 4.41	20.01 ± 9.35*	17.53 ± 6.77	18.60 ± 2.36	16.20 ± 3.45	18.10 ± 5.22	16.80 ± 3.49
LYMPH % (%)	83.46 ± 3.88	82.63 ± 5.05	76.35 ± 10.08	79.23 ± 7.03	74.27 ± 3.53	76.75 ± 3.29	75.48 ± 5.10	76.63 ± 4.66
MONO% (%)	2.68 ± 0.78	3.23 ± 0.89	2.91 ± 1.12	2.75 ± 0.59	5.67 ± 2.04	5.72 ± 0.82	5.22 ± 1.22	5.43 ± 1.30
EO% (%)	0.95 ± 0.42	0.68 ± 0.19	0.73 ± 0.33	0.49 ± 0.21*	1.47 ± 0.88	1.33 ± 0.19	1.20 ± 0.33	1.13 ± 0.46
BASO% (%)	0.00 ± 0.00	0.00 ± 0.00	0.00 ± 0.00	0.00 ± 0.00	0.00 ± 0.00	0.00 ± 0.00	0.00 ± 0.00	0.00 ± 0.00
NEUT#(10^9/L)	0.94 ± 0.26	1.11 ± 0.49	1.91 ± 1.12*	1.70 ± 0.61*	1.36 ± 0.27	1.08 ± 0.16	1.20 ± 0.37	1.12 ± 0.35
LYMPH#(10^9/L)	6.21 ± 1.45	7.09 ± 2.65	7.04 ± 1.50	7.95 ± 1.75	5.45 ± 1.21	5.23 ± 1.03	5.00 ± 0.61	5.07 ± 1.00
MONO#(10^9/L)	0.20 ± 0.06	0.27 ± 0.13	0.27 ± 0.13	0.27 ± 0.05*	0.43 ± 0.19	0.39 ± 0.07	0.35 ± 0.10	0.35 ± 0.07
EO#(10^9/L)	0.07 ± 0.03	0.06 ± 0.02	0.07 ± 0.02	0.05 ± 0.02	0.11 ± 0.07	0.09 ± 0.03	0.08 ± 0.03	0.08 ± 0.03

(Continued on following page)

TABLE 2 (*Continued*) Effect of QZZD on hematological parameters in the sub-chronic oral toxicity study.

Parameter (mean ± SD)	Treatment period (n = 12)				Recovery period (n = 6)			
	CN	TA	TB	TC	CN	TA	TB	TC
BASO#(10^9/L)	0.00 ± 0.00	0.00 ± 0.00	0.00 ± 0.00	0.00 ± 0.00	0.00 ± 0.00	0.00 ± 0.00	0.00 ± 0.00	0.00 ± 0.00
RET#(10^{12}/L)	0.2789 ± 0.0356	0.3100 ± 0.0421	0.3863 ± 0.0717*	0.5739 ± 0.1246*	0.2997 ± 0.0210	0.2617 ± 0.0176*	0.2538 ± 0.0630	0.2329 ± 0.0200*
RET%	3.413 ± 0.356	3.830 ± 0.482*	4.915 ± 1.100*	7.685 ± 1.585*	3.585 ± 0.243	3.173 ± 0.212*	3.070 ± 0.765	2.780 ± 0.211*

Compared with control group, $p \leq 0.05$.

QZZD, 5.0 g/kg group, two female rats (4110 and 4111) death caused by faulty gavage operation in treatment period, resulting in animal sample reduction, the total number was 10 (n = 10).

TA, (treatment group A, 0.5 g/kg/day QZZD); TB, (treatment group B, 1.5 g/kg/day QZZD); TC, (treatment group C, 5.0 g/kg/day QZZD); CN, (control group, 20 ml/kg pure water); WBC, white blood cell; RBC, red blood cell; HGB, hemoglobin; PLT, Platelet; HCT%, hematocrit percentage; MCV, mean corpuscular volume; MCH, mean corpuscular hemoglobin; MCHC, mean corpuscular hemoglobin concentration; NEUT%, neutrophil percentage; LYMPH%, lymphocyte percentage; MONO%, monocyte percentage; EO%, eosinophil percentage; BASO%, basophil percentage; NEUT#,neutrophil; LYMPH#, lymphocyte; MONO#, monocyte; EO#, eosinophil; BASO#, basophil; RET #, reticulocytes; RET %, reticulocytes percentage.

deviation. Quantitative indicators were statistically tested by one-way analysis of variance (ANOVA). Levene's homogeneity of variance was conducted to assess the homogeneity of variance. When the variance was heterogeneous ($p \leq 0.05$), the Kruskal–Wallis H rank-sum test (K-W method) was used, When the difference was statistically significant ($p \leq 0.05$), the Mann-Whitney U rank-sum test (M-W method) was used to compare the group differences. When variance was homogeneous ($p > 0.05$) and one-way analysis of variance (ANOVA) was statistically significant ($p \leq 0.05$), differences between groups were compared using the Dunnett method.

Comparisons of differences were performed among groups CN, TA, TB, and TC, and all statistical tests were two-sided (α = 0.05). Statistical analysis was performed using SPSS, and male and female data calculations and statistical analysis were performed separately. Ophthalmic examination results were not counted and expressed as individual data.

Results

Death of animals

There were two deaths of female rats (rat numbers: 4110 and 4111) in group TC (5.0 g/kg/d QZZD) before administration on D15 and D9, with no significant abnormalities in weight, food intake and clinical symptoms. A gross necropsy revealed yellow liquid around the lips and enlarged lungs in both rat. The histopathological report showed mild congestion of the heart, liver, kidney, thyroid, adrenal gland, and ovary, moderate pulmonary congestion, edema, and emphysema in rat 4110, while in rat 4111, there were mild congestion of the heart, liver, kidney, pituitary, and ovary, as well as moderate pulmonary congestion and emphysema.

It was thus concluded that the deaths were attributed to improper administration. No other deaths were observed until the end of the experiment.

Clinical signs observation

There were no abnormal symptoms in group CN and group TA (0.5 g/kg/d QZZD) during the experiment. In group TB (1.5 g/kg/d QZZD) from D20 to D30, there was blue coloring of part of the tail skin of some rats, and the bedding and feces in the cage also turned blue. In group TC (5.0 g/kg/d QZZD) rats exhibited partial blue staining of the tail skin from D15 to D52, and part of the bedding and feces in the cage turned blue from D16 to D38. After the recovery period, the above symptoms disappeared.

Body weight and food consumption

Changes in body weight are widely acknowledged as an important indicator of adverse effects of herbs. During the experiment, there was significant body weight decrease of female rats from D14 to D56 in group TA (0.5 g/kg/d QZZD), while no significant differences were observed in male rats. In group TB (1.5 g/kg/d QZZD), the body weight of female rats was decreased from D7 to D56 and that of male rats was decreased from D21 to D24. In group TC (5.0 g/kg/d QZZD), body weight decrease was observed from D7 to D49 in females and from D17 to D28 in males. During the drug administration period, weight decrease exhibited a good dose-response relationship and time-response relationship. Therefore, it may be attributed to the tested formula. The female rats in group TA (0.5 g/kg/d QZZD) showed smaller body decrease and exhibited normal behavior with no significant organ injury. Detailed analysis is shown in Figures 2A,B.

During drug administration, the average food intake was decreased on D6 and D23 in females ($p < 0.05$) and was increased on D23 in males ($p < 0.05$) in group TA (0.5 g/kg/d QZZD). Group TB (1.5 g/kg/d QZZD) witnessed decrease in females on D6, D16, D23 and D27 ($p < 0.05$), while there was no significant difference in males. Group TC (5.0 g/kg/d QZZD) showed

TABLE 3 Effect of QZZD on biochemical and coagulation parameters in the sub-chronic oral toxicity study.

Parameter (mean ± SD)	Treatment period (n = 12)				Recovery period (n = 6)			
	CN	TA	TB	TC	CN	TA	TB	TC
Female								
ALT (U/L)	40.48 ± 5.19	40.39 ± 9.83	39.95 ± 8.74	37.50 ± 14.61	44.92 ± 7.39	40.00 ± 6.81	47.78 ± 3.00	41.33 ± 4.50
AST (U/L)	140.59 ± 25.16	116.68 ± 23.99	127.78 ± 33.45	140.86 ± 36.80	139.58 ± 21.98	132.97 ± 31.63	147.72 ± 36.54	117.48 ± 21.48
TP (g/L)	61.08 ± 3.65	62.43 ± 3.11	59.85 ± 2.15	63.39 ± 3.80	68.85 ± 4.09	64.92 ± 2.95	64.20 ± 1.97	67.85 ± 5.95
ALB (g/L)	29.47 ± 1.57	30.44 ± 1.88	29.13 ± 1.48	30.06 ± 1.21	32.85 ± 2.15	30.48 ± 1.95	31.13 ± 1.11	32.45 ± 3.05
TBIL (mmol/L)	1.78 ± 0.36	2.56 ± 0.75*	3.84 ± 1.80*	7.98 ± 4.20*	1.79 ± 0.43	1.39 ± 0.44	1.02 ± 0.31*	1.11 ± 0.44*
ALP(U/L)	93.00 ± 16.03	85.67 ± 16.39	94.83 ± 17.68	120.30 ± 37.46	72.50 ± 31.28	67.00 ± 11.51	91.33 ± 22.66	83.50 ± 8.73
GLU (mmol/L)	7.68 ± 1.23	7.95 ± 1.33	7.87 ± 1.09	7.86 ± 1.17	8.39 ± 1.73	7.89 ± 1.00	9.33 ± 1.33	10.25 ± 2.66
Urea (mmol/L)	5.85 ± 1.07	5.25 ± 1.06	5.65 ± 0.72	8.63 ± 5.24*	6.65 ± 1.50	6.01 ± 1.48	6.55 ± 1.08	7.20 ± 1.37
Crea (mmol/L)	31.47 ± 4.88	31.57 ± 5.57	27.15 ± 3.67	31.25 ± 10.31	34.97 ± 4.11	33.55 ± 3.46	40.93 ± 6.22	29.78 ± 4.27
TC (mmol/L)	1.59 ± 0.29	1.56 ± 0.31	1.50 ± 0.19	1.91 ± 0.53	1.87 ± 0.38	1.68 ± 0.40	1.75 ± 0.35	1.82 ± 0.37
TG (mmol/L)	0.41 ± 0.10	0.44 ± 0.09	0.35 ± 0.13	0.40 ± 0.13	0.74 ± 0.40	0.58 ± 0.18	0.45 ± 0.14	0.56 ± 0.31
CK(U/L)	956.83 ± 311.83	751.58 ± 318.33	931.75 ± 385.25	1146.10 ± 533.25	970.17 ± 199.83	924.00 ± 306.83	960.00 ± 530.28	802.83 ± 160.32
K^+(mmol/L)	4.54 ± 0.22	4.56 ± 0.27	4.44 ± 0.24	4.87 ± 0.31*	4.50 ± 0.18	4.32 ± 0.23	4.55 ± 0.52	4.48 ± 0.24
Na^+(mmol/L)	141.92 ± 0.90	142.42 ± 1.83	142.08 ± 1.31	141.40 ± 1.51	141.50 ± 1.05	141.83 ± 0.41	141.83 ± 1.94	141.50 ± 0.55
Cl^-(mmol/L)	106.58 ± 1.51	105.83 ± 1.95	105.50 ± 1.17	102.20 ± 3.16*	103.67 ± 1.03	103.33 ± 1.37	102.67 ± 2.07	102.33 ± 1.21
GLOB(g/L)	31.62 ± 2.67	31.98 ± 1.74	30.73 ± 1.61	33.33 ± 2.95	36.00 ± 2.14	34.43 ± 1.76	33.07 ± 2.04	35.40 ± 3.33
A/G	0.94 ± 0.07	0.95 ± 0.06	0.95 ± 0.07	0.91 ± 0.06	0.92 ± 0.04	0.89 ± 0.06	0.95 ± 0.08	0.92 ± 0.06
PT (sec)	15.16 ± 0.37	15.28 ± 0.47	15.65 ± 0.36*	16.65 ± 1.06*	8.17 ± 0.05	8.22 ± 0.12	8.13 ± 0.31	8.28 ± 0.44
APTT (sec)	11.82 ± 0.93	11.74 ± 0.77	11.74 ± 0.97	13.23 ± 1.47*	12.07 ± 1.19	11.17 ± 0.55	11.58 ± 0.97	12.12 ± 0.85
Fbg (g/L)	1.98 ± 0.23	1.93 ± 0.16	1.89 ± 0.14	2.08 ± 0.30	1.74 ± 0.08	1.87 ± 0.20	1.60 ± 0.17	1.70 ± 0.14
Male								
ALT (U/L)	48.56 ± 7.96	41.11 ± 8.49	39.25 ± 7.96	43.44 ± 9.72	46.00 ± 7.56	42.60 ± 11.50	43.57 ± 3.51	43.15 ± 5.17
AST (U/L)	148.18 ± 50.12	129.25 ± 43.52	128.49 ± 42.27	125.30 ± 47.06	132.75 ± 34.89	117.33 ± 21.41	100.07 ± 14.56	123.58 ± 27.49
TP (g/L)	59.88 ± 2.77	59.64 ± 2.89	58.72 ± 3.82	59.12 ± 3.51	63.13 ± 2.78	62.53 ± 1.86	62.55 ± 2.68	62.25 ± 3.31
ALB (g/L)	26.69 ± 0.83	26.98 ± 0.95	27.09 ± 1.21	27.17 ± 1.07	27.63 ± 0.49	27.15 ± 0.94	26.93 ± 1.31	27.83 ± 0.80
TBIL (mmol/L)	1.74 ± 0.26	2.15 ± 0.44*	2.29 ± 0.64*	7.43 ± 3.01*	1.50 ± 0.21	1.47 ± 0.38	1.37 ± 0.38	1.16 ± 0.26
ALP(U/L)	183.25 ± 40.33	178.00 ± 29.01	180.67 ± 46.38	236.17 ± 97.25	133.17 ± 22.24	119.33 ± 31.45	121.33 ± 20.19	145.33 ± 35.03
GLU (mmol/L)	9.03 ± 1.51	8.12 ± 1.48	7.97 ± 1.07	8.91 ± 2.05	8.26 ± 1.08	8.60 ± 1.92	8.58 ± 1.54	9.28 ± 1.54
Urea (mmol/L)	5.67 ± 0.74	4.84 ± 1.07	5.18 ± 0.63	6.38 ± 1.29	5.65 ± 1.04	6.05 ± 1.56	5.66 ± 0.71	5.75 ± 1.08
Crea (mmol/L)	25.41 ± 2.04	24.38 ± 4.43	26.11 ± 7.27	26.02 ± 2.86	25.35 ± 3.22	25.92 ± 3.47	26.22 ± 3.51	24.63 ± 4.29
TC (mmol/L)	1.47 ± 0.29	1.45 ± 0.24	1.31 ± 0.30	1.53 ± 0.41	1.66 ± 0.22	1.58 ± 0.12	1.65 ± 0.23	1.40 ± 0.28
TG (mmol/L)	0.53 ± 0.20	0.42 ± 0.13	0.38 ± 0.11*	0.28 ± 0.13*	0.83 ± 0.07	0.73 ± 0.31	0.60 ± 0.18	0.77 ± 0.25
CK(U/L)	1161.75 ± 714.29	822.42 ± 640.61	768.33 ± 494.33	909.75 ± 587.29	944.33 ± 518.88	786.83 ± 360.22	555.00 ± 201.42	760.17 ± 347.95
K^+(mmol/L)	5.00 ± 0.30	5.03 ± 0.23	5.53 ± 0.97	5.39 ± 0.22*	4.87 ± 0.30	4.88 ± 0.17	4.77 ± 0.12	4.83 ± 0.28

(Continued on following page)

TABLE 3 (*Continued*) Effect of QZZD on biochemical and coagulation parameters in the sub-chronic oral toxicity study.

Parameter (mean ± SD)	Treatment period (n = 12)				Recovery period (n = 6)			
	CN	TA	TB	TC	CN	TA	TB	TC
Na^+(mmol/L)	143.25 ± 1.22	142.92 ± 1.16	143.25 ± 1.29	143.17 ± 1.34	142.00 ± 0.89	142.00 ± 1.10	143.17 ± 1.17	143.00 ± 0.89
Cl^-(mmol/L)	105.67 ± 1.50	105.83 ± 1.34	105.33 ± 2.15	103.00 ± 1.54*	103.50 ± 1.38	101.83 ± 1.72	103.00 ± 1.67	102.67 ± 1.03
GLOB(g/L)	33.18 ± 2.47	32.66 ± 2.24	31.63 ± 2.92	31.95 ± 2.64	35.50 ± 2.46	35.38 ± 1.53	35.62 ± 2.06	34.42 ± 2.93
A/G	0.81 ± 0.06	0.83 ± 0.05	0.86 ± 0.06	0.85 ± 0.04	0.78 ± 0.05	0.77 ± 0.04	0.76 ± 0.05	0.82 ± 0.06
PT (sec)	15.38 ± 0.45	15.29 ± 0.41	15.75 ± 0.52	17.15 ± 0.77*	8.77 ± 0.34	9.47 ± 1.10	9.08 ± 0.66	9.08 ± 0.47
APTT (sec)	13.56 ± 0.72	13.24 ± 1.13	12.24 ± 1.14	13.06 ± 1.63	12.95 ± 0.96	13.40 ± 0.79	14.08 ± 0.88	13.35 ± 1.31
Fbg (g/L)	2.35 ± 0.14	2.36 ± 0.12	2.36 ± 0.18	2.49 ± 0.55	2.01 ± 0.06	2.03 ± 0.07	2.15 ± 0.10*	1.97 ± 0.10

Compared with control group, $p \leq 0.05$.

QZZD, 5.0 g/kg group, two female rats (4110 and 4111) death caused by faulty gavage operation in treatment period, resulting in animal sample reduction, the total number was 10 (n = 10). TA, (treatment group A, 0.5 g/kg/day QZZD); TB, (treatment group B, 1.5 g/kg/day QZZD); TC, (treatment group C, 5.0 g/kg/day QZZD); CN, (control group, 20 ml/kg pure water); ALT, alanine aminotransferase; AST, aspartate aminotransferase; TP, total protein; ALB, albumin; TBIL, total bilirubin; ALP, alkaline phosphatase; GLU, glucose; Crea, Creatinine; TC, total cholesterol; TG, triglyceride; CK, creatine kinase; K, potassium; Na, Sodium; Cl, Chloride; GLOB, Globulin; A/G,Albumin/globulin; PT, Partial Thromboplastin time; APTT, Activated partial thromboplastin time; Fbg, Fasting blood glucose.

decrease of the average food intake on D2, D6, D16, D20, D23, and D27 in females ($p < 0.05$) and in males on D20 ($p < 0.05$). During the recovery period, the food intake of all groups returned to normal. The decrease of food intake and duration in females of the above groups showed a good dose-response relationship, which was considered to be related to the tested formula. Although fluctuations were observed in few males, the overall food intake remained relatively stable. In group TA (0.5 g/kg/d QZZD), females exhibited less variations in average food intake, the abnormal food intake were scattered in time, and the duration was shorter. It can be concluded that the overall food intake in group TA (0.5 g/kg/d QZZD) was relatively stable and normal. More detailed analysis is shown in Figures 2C,D.

Ophthalmologic examination

Ophthalmic examination of animals during the experiment showed no significant abnormalities. Individual data are shown in Supplementary Table S3.

Complete blood count results

Hematological parameters, including the Complete Blood Count, are sensitive indicators of toxicity and serves as an important index of health status for humans and animals (Ding et al., 2021). At the end of administration, there was no significant difference in hematological indexes of female between group TA (0.5 g/kg/d QZZD) and group CN, while the RET% of males in group TA (0.5 g/kg/d QZZD) was significantly increased ($p < 0.05$). In group TB (1.5 g/kg/d QZZD), RET# and RET% were increased in females ($p < 0.05$), while NEUT#, NEUT%, RET# and RET% were increased in males ($p < 0.05$). In group TC (5.0 g/kg/d QZZD), RBC and MCHC were significantly decreased in female rats ($p < 0.05$), while PLT, MCV, MCH, RET#, and RET% were significantly increased ($p < 0.05$); in males, the RBC, HGB, HCT, and EO% were significantly decreased ($p < 0.05$), while WBC, PLT, NEUT#, MONO#, RET# and RET% were increased ($p < 0.05$).

At the end of the recovery period, there were no significant differences in CBC parameters of females between group TA (0.5 g/kg/d QZZD) and group CN, while the RET# and RET% of males in group TA (0.5 g/kg/d QZZD) were significantly decreased ($p < 0.05$). In group TB (1.5 g/kg/d QZZD), there were no significant differences in hematological indexes of females, while the MCHC of males was significantly decreased ($p < 0.05$). In group TC (5.0 g/kg/d QZZD), the MCV of females was significantly increased ($p < 0.05$), while RET# and RET% of males was decreased ($p < 0.05$). The red blood cell count in the recovery stage returned to normal, and no significant changes in RET#, RET%, MCHC and MCV were observed. Detailed analysis is shown in Table 2.

Blood biochemical and coagulation indicators assessment

It is well-acknowledged that serum biochemical parameters and coagulation indexes play an important part during toxicological evaluation. Data of the biochemical parameters in rats at the end of the treatment and recovery periods are shown in Table 3. At the end of the treatment period, there was significant increase of TBIL in both females and males in group TA (0.5 g/kg/d QZZD) compared with group CN ($p < 0.05$). In

TABLE 4 Effect of QZZD on urine parameters in the sub-chronic oral toxicity study. (results were presented as number).

Index (mean ± SD)	Treatment period (n = 12)				Recovery period (n = 6)			
	CN	TA	TB	TC	CN	TA	TB	TC
Female								
Appearance	**Colorless/Light Yellow/Yellow (n/n)**							
	1/11/0	0/10/2	0/10/2	1/7/2	0/5/1	0/2/4	0/5/1	0/4/2
PH	7.58 ± 0.46	7.5 ± 0.52	7.62 ± 0.31	7.25 ± 0.54	8.25 ± 0.27	8.16 ± 0.4	8.25 ± 0.41	8 ± 0.44
S.G.	1.011 ± 0.002	1.009 ± 0.001	1.01 ± 0.004	1.012 ± 0.004	1.012 ± 0.002	1.013 ± 0.002	1.012 ± 0.002	1.014 ± 0.002
GLU	**0/2.8 (mmol/L,n/n)**							
	12/0	12/0	12/0	10/0	5/1	6/0	6/0	6/0
PRO	**0/0.1/0.2/0.3/0.5 (g/L,n/n)**							
	12/0/0/0/0	12/0/0/0/0	12/0/0/0/0	10/0/0/0/0	5/1/0/0/0	3/2/1/0/0	6/0/0/0/0	3/2/1/0/0
BIL	**Negative/Positive (n/n)**							
	12/0	12/0	12/0	10/0	6/0	6/0	6/0	6/0
URO	**Negative/Positive(n/n)**							
	12/0	12/0	12/0	10/0	6/0	6/0	6/0	6/0
BLD	**Negative/Positive (n/n)**							
	9/3	9/3	11/1	10/0	6/0	6/0	6/0	6/0
KET	**Negative/Positive (n/n)**							
	12/0	12/0	12/0	10/0	6/0	6/0	6/0	6/0
NIT	**Negative/Positive(n/n)**							
	4/8	3/9	5/7	10/0	4/2	3/3	3/3	4/2
LEU	**0/25/75(Leu/ul,n/n)**							
	12/0/0	12/0/0	11/1/0	7/2/1	6/0	6/0	6/0	6/0
TURB	**Negative/Positive(n/n)**							
	11/1	11/1	11/1	10/0	0/6	0/6	0/6	0/6
Male								
Appearance	**Colorless/Light Yellow/Yellow (n/n)**							
	1/8/3	0/10/2	0/11/1	0/9/3	0/2/4	0/2/4	0/3/3	0/5/1
PH	7.91 ± 0.28	8 ± 0.21	7.87 ± 0.22	7.81 ± 0.4	8.33 ± 0.25	8.33 ± 0.25	8.25 ± 0.27	8.5 ± 0
S.G.	1.012 ± 0.003	1.014 ± 0.007	1.011 ± 0.002	1.013 ± 0.004	1.012 ± 0.002	1.013 ± 0.002	1.013 ± 0.002	1.011 ± 0.001
GLU	**0/2.8 (mmol/L,n/n)**							
	12/0	12/0	12/0	12/0	6/0	6/0	5/1	6/0
PRO	**0/0.1/0.2/0.3/0.5 (g/L,n/n)**							
	7/3/1/1/0	5/4/2/0/1	9/2/1/0/0	10/1/1/0/0	0/3/2/1/0	2/0/4/0/0	0/3/2/1/0	
BIL	**Negative/Positive (n/n)**							
	12/0	12/0	12/0	12/0	6/0	6/0	6/0	6/0
URO	**Negative/Positive (n/n)**							
	12/0	12/0	12/0	12/0	6/0	6/0	6/0	6/0
BLD	**Negative/Positive (n/n)**							
	12/0	11/1	12/0	10/2	5/1	6/0	6/0	6/0
KET	**Negative/Positive (n/n)**							
	11/1	10/2	12/0	12/0	6/0	5/1	6/0	6/0
NIT	**Negative/Positive (n/n)**							
	4/8	7/5	11/1	11/1	3/3	5/1	2/4	4/2
LEU	**0/25/75 (Leu/ul,n/n)**							
	9/3/0	8/4/0	11/1/0	3/8/1	6/0	6/0	5/1	6/0
TURB	**Negative/Positive (n/n)**							
	10/2	6/6	9/3	10/2	0/6	0/6	0/6	0/6

QZZD, 5.0 g/kg group, two female rats (4110 and 4111) death caused by faulty gavage operation in treatment period, resulting in animal sample reduction, the total number was 10 (n = 10). TA, (treatment group A, 0.5 g/kg/day QZZD); TB, (treatment group B, 1.5 g/kg/day QZZD); TC, (treatment group C, 5.0 g/kg/day QZZD); CN, (control group, 20 ml/kg pure water); PH, potential of hydrogen; S.G., specific gravity; GLU, glucose; PRO, protein; BIL, bilirubin; URO, urbilinogen; BLD, blood; KET, ketone; NIT, nitrite; LEU, leucocyte; TURB, turbidity.

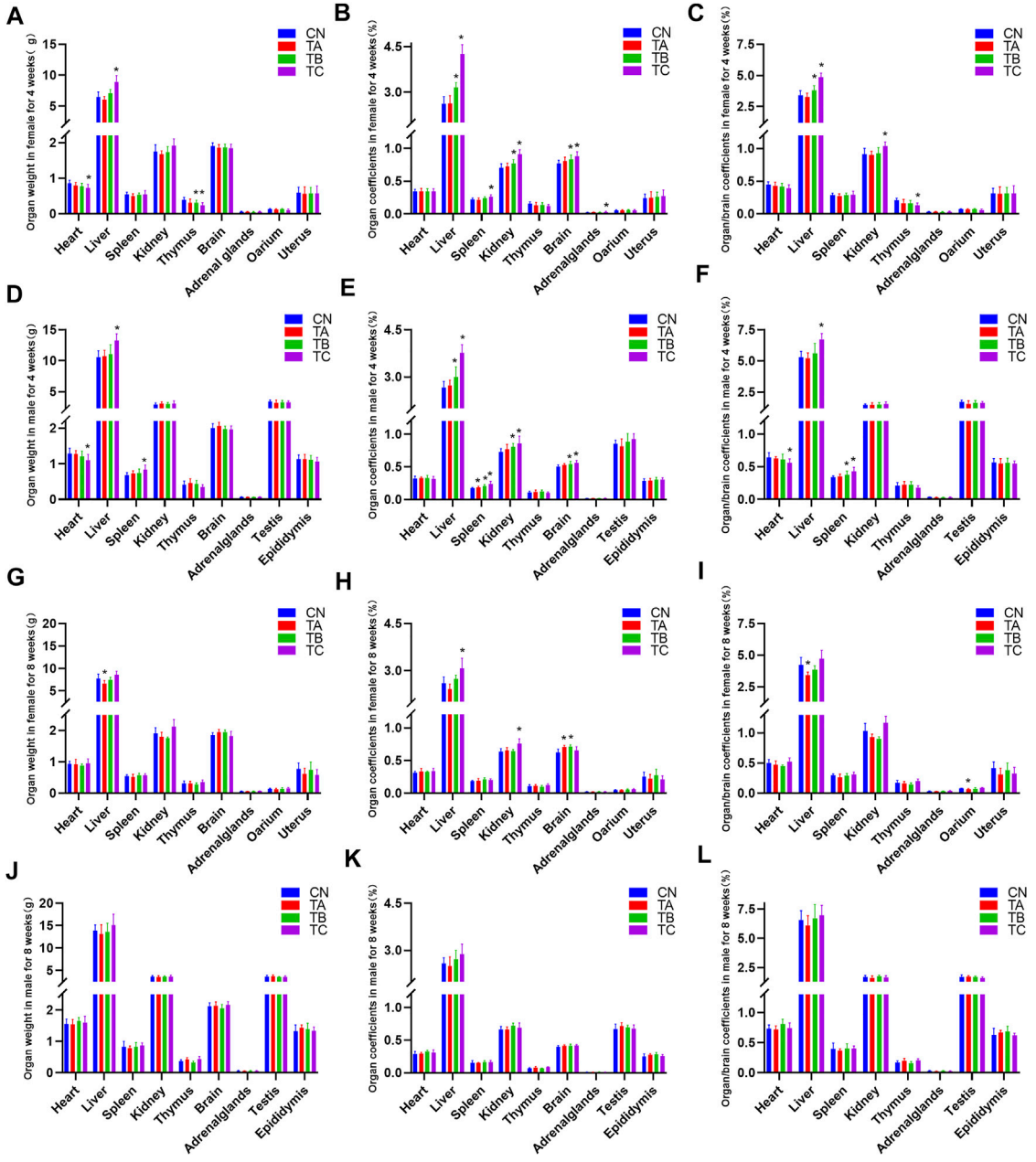

FIGURE 3
Effects of three different doses of QZZD on absolute organ weights, organ coefficients and organ/brain coefficients in male or female rats at the end of the treatment period or recovery period. In the treatment period, $n = 12$ in female group ($n = 10$ in TC) **(A–C)**, and $n = 12$ in male group **(D–F)**. In the recovery period, $n = 6$ in each group, including six females **(G–I)** and six males **(J–L)**. Compare with the control group *$p < 0.05$.

group TB (1.5 g/kg/d QZZD), there was increase of TBIL in males, while in females there were decrease of TG and increase of TBIL ($p < 0.05$). In group TC (5.0 g/kg/d QZZD), TBIL, Urea, and K+ were significantly increased and CL-was decreased in females, while TBIL and K+ were increased and TG and CL-decreased in males ($p < 0.05$).

At the end of the recovery period, TBIL of female rats in group TB (1.5 g/kg/d QZZD) and group TC (5.0 g/kg/d QZZD) was decreased compared with that of group CN. However, TBIL in the two groups were within the normal range. Besides, there were no other significant differences of serum biochemical

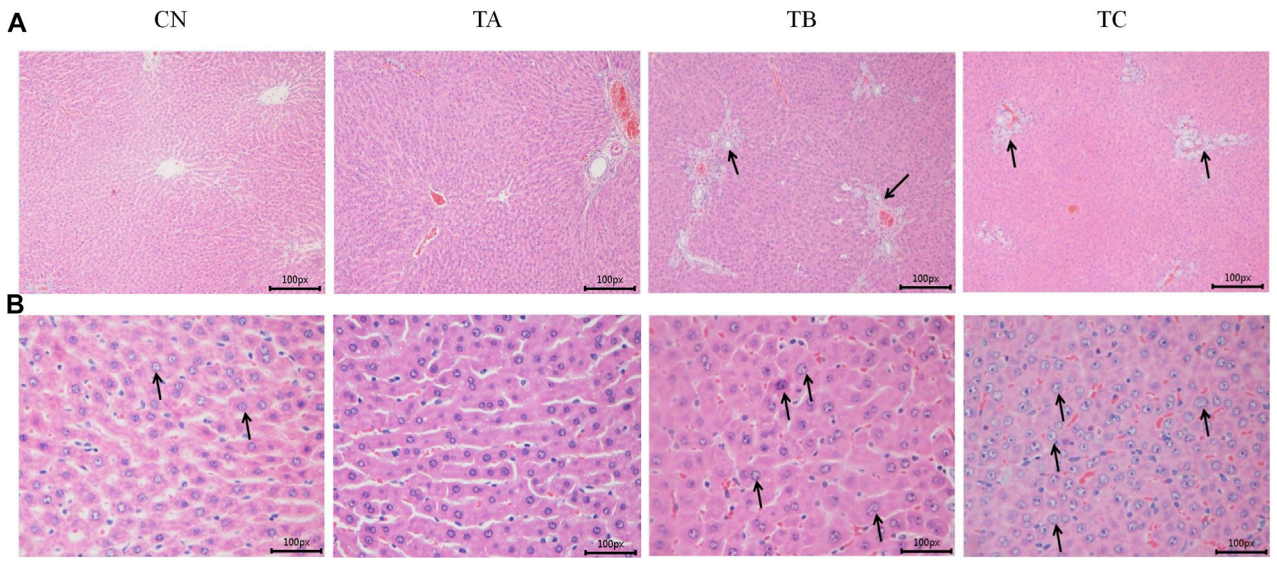

FIGURE 4
The representative histopathological sections of rat liver at the end of the treatment period. **(A)** The CN and TA rats liver showing normal hepatocytes and hepatic vasculature; The TB and TC rats liverr showing bile duct proliferation and karyomegaly of hepatocytes (×100 magnification). **(B)** The CN and TA rats liver showing normal hepatocytes and hepatic vasculature; The TB and TC rats liver showing bile duct proliferation and karyomegaly of hepatocytes (×400 magnification).

indexes between males and females in all groups except for those mentioned above.

At the end of treatment, there was no significant difference between group TA (0.5 g/kg/d QZZD) and group CN in both genders. In group TB (1.5 g/kg/d QZZD), PT was significantly increased in females ($p < 0.05$), but there was no significant difference in males. In group TC (5.0 g/kg/d QZZD), there was increase of PT and APTT in females ($p < 0.05$), and increase of PT in males ($p < 0.05$). The increase of PT and APTT mentioned above were within the normal range and were not considered to be related to the formula.

At the end of the recovery period, there was a slight increase of Fbg of male rats in group TB (1.5 g/kg/d QZZD) compared with group CN, which was within the normal range ($p < 0.05$). Given that no significant dose-response relationship was observed, it was not considered related to the tested formula. In addition, all groups exhibited no significant differences in coagulation indexes. Detailed analysis is shown in Table 3.

Urine examination

It is widely acknowledged that urinary indices can reflect the metabolic status of the body (Lu et al., 2014). As shown in Table 4, all urinary parameters from each group were within the normal physiological range throughout the experimental period, and no significant abnormal changes associated with the tested formula were observed.

Organ weights, organ coefficients and organ/brain coefficients

The organ-to-body weight ratio (organ coefficients) is another sensitive index for toxicity evaluation. Generally, changes in organ coefficient occur before morphological changes (Piao et al., 2013). At the end of the treatment period, there was no significant change of the weight and organ coefficients of female rats, while the organ-body ratio of spleen in male rats was increased in group TA (0.5 g/kg/d QZZD) compared with group CN ($p < 0.05$). In group TB (1.5 g/kg/d QZZD), the wet weight of the thymus was decreased, the organ-body ratio of liver, kidney and brain was increased, and the organ-brain ratio of the liver was increased in females ($p < 0.05$); while in males, the organ-body ratio of liver, kidney, spleen and brain was increased, and the organ-brain ratio of spleen was increased ($p < 0.05$). For females in group TC (5.0 g/kg/d QZZD), the wet weight of the heart and thymus was decreased ($p < 0.05$) while that of the liver was increased ($p < 0.05$); the organ-body ratio of liver, spleen, kidney, brain and adrenal gland was increased ($p < 0.05$), the organ-brain ratio of liver and kidney was increased ($p < 0.05$), and the organ-brain ratio of thymus was decreased ($p < 0.05$), For males in group TC (5.0 g/kg/d QZZD), the wet weight of the heart was decreased ($p < 0.05$), and the wet weight of liver and spleen was increased ($p < 0.05$); there was also an increase in organ-body ratio of liver, spleen, kidney and brain, and in organ-brain ratio of liver and spleen ($p <$

0.05), while the organ-brain ratio of heart was decreased ($p < 0.05$).

In group TA (0.5 g/kg/d QZZD), there was a decrease in the wet weight and organ-brain ratio of liver and an increase in the organ-body ratio of brain, and the ovary/brain coefficient was decreased at the end of the recovery period ($p < 0.05$). The organ-body ratio of brain in female rats of group TB (1.5 g/kg/d QZZD) was increased ($p < 0.05$). Moreover, the organ coefficients of liver and kidney of females in group TC (5.0 g/kg/d QZZD) was increased ($p < 0.05$). There were no significant differences in weight and organ coefficient of males in each group. Detailed analysis is shown in Figure 3.

Pathological examination

Macroscopic observation of morphological characteristics and histopathological examination were performed on tissues/organs at the end of the treatment and recovery period, respectively. The macroscopic examination revealed darkening of livers and kidneys in group TB (1.5 g/kg/d QZZD) and group TC (5.0 g/kg/d QZZD) after the treatment period. At the end of the recovery period, the liver and kidneys of all the rats in group TC (5.0 g/kg/d QZZD) turned black. The pathological examination showed normal staining of liver and kidney tissues with no pigmentation or other organic changes. Individual data of macroscopic morphological observation are shown in Supplementary Table S4.

In group TB (1.5 g/kg/d QZZD), histopathological examination at the end of the treatment period exhibited minimal biliary hyperplasia ($n = 5$) and minimal karyomegaly of hepatocytes ($n = 5$). In group TC (5.0 g/kg/d QZZD), there were mild-to-moderate biliary hyperplasia ($n = 11$), and the severity of karyomegaly of hepatocytes ranged from minimal to mild ($n = 11$). After 28 days of drug withdrawal, related lesions recovered completely. The representative histopathological changes after treatment period are shown in Figure 4.

Furthermore, in the experiment period, tissues/organs of SD rats exhibited pathological changes, including basophilic tubules and interstitial mononuclear cell infiltration in the kidney, myocardial cell necrosis and mononuclear cell infiltration in cardiac tissue. These were considered background lesions of SD rats due to their low incidence, mild degree severity and absence of a significant dose-response relationship.

Discussion

Over the years, the use of herbal medicines has become popular around the world (Wu et al., 2018). The efficacy of herbal medicines is well-established in treating various diseases, being used in traditional and non-traditional forms of medicine for thousands of years (Wang et al., 2019). Meanwhile, much emphasis has been placed on the safety profile of herbal medicine in recent years. Indeed, the low safety profile accounts for the rejection of compounds with druggable profiles in early clinical trials. QZZD is derived from a traditional Chinese medicinal formula, Angong Niuhuang Wan; the efficiency of QZZD has been demonstrated in rat models of VD (Liu et al., 2022). However, the administered doses were not high enough to ensure the clinical safety of QZZD. Therefore, a systematic toxicology study of QZZD in animals is essential to ensure its safety as a therapeutic agent for VD prior to progressing to clinical translation.

It is widely thought that QZZD, composed of *Radix Scutellariae*, *Fructus Gardeniae*, and *Pulvis Fellis Suis*, has heat-clearing and detoxification effects. Current evidence suggests that these components are safe and non-toxic. A toxicity study by Jing et al. found that geniposide did not influence animal mortality, the general condition of the animals, body weights or food consumption. After 4 weeks of treatment, no significant toxicity was observed (Tian et al., 2018). Another study showed that *Radix Scutellariae* exerted no significant adverse effects on the clinical signs, hematology, biochemistry, necropsy, organ weight, and histopathology throughout subacute toxicity tests in rats (Wang et al., 2017). These are consistent with our experimental results.

During the 28-day repeated oral dose toxicity study, QZZD at doses of 0.5, 1.5, and 5.0 g/kg/day caused no death and no treatment-related adverse effects on food consumption, organ weight, ophthalmologic, urinalysis, and hematological parameters. Two female rats in group TC (5.0 g/kg/d QZZD) died during the experiment. Based on our macroscopic and microscopic examination findings, we speculate that the direct cause of death was the incorrectly oral gavage procedure. During the 28-day repeated oral dose toxicity study, QZZD at doses of 0.5, 1.5, and 5.0 g/kg/day caused no death and no treatment-related adverse effects on food consumption, organ weight, ophthalmologic, urinalysis, and hematological parameters. Importantly, some treatment-related changes, including clinical signs (blue-colored stool and tail), body weight (weight loss), serum biochemistry (decreased TG level and increased TBIL level), necropsy findings (liver and kidneys turn black), and histopathological findings (liver bile duct hyperplasia and hepatocyte nuclei hypertrophy), were observed. However, these changes were resolved during the recovery period.

The clinical symptoms of animals is an important indicator to measure the toxicity of the tested drug (Hardisty et al., 2020). During the experiment, the tail skin of rats from the medium and high-dose group turned blue and the bluish coloration of the bedding and feces exhibited a dose-response relationship. The liver and kidney of the medium and high-dose groups turned black, and the clinical signs and macroscopic observations showed good physiological consistency, and these abnormalities disappeared at the end of the recovery period. These abnormalities may be attributed to the pigments in QZZD or its metabolites (Tang et al., 2020).

Body weight and food consumption are used to evaluate the adverse effects caused by the tested drug. And body weight and food consumption are usually correlated and need comprehensive analysis (Dziwenka et al., 2020). Compared with the control group, the female body weight and food consumption of the medium and high dose group was reduced, which had a good dose correlation. In addition, the female rats show variations in body weight and food consumption as compared to male rats. These may be due to high dose and administration volume will contribute to the decrease of gastric volume of rats. The female rats have lower weight and smaller gastric volume compared with the male rats, which predisposes them to gastric volume decrease. Therefore, the food consumption and weight increase in female rats was smaller than that in male rats. In terms of safety evaluation, the fluctuations of body weight and food consumption are small, which fall into the category of physiological fluctuations.

Hematological tests are commonly used to observe the treatment effect and determine whether treatment should be continued or not (Guo et al., 2022). WBC, RBC, HGB, and PLT are the most sensitive indicators in CBC, which are sensitive in response to pathological changes (Mukinda and Eagles, 2010). In the present study, the main indicators RBC, HGB and HCT were moderately reduced in group TC (5.0 g/kg/d QZZD) but remained within the normal physiological reference range; a certain dose-response relationship was observed. Accordingly, these changes were related to the test drug. The increase in RET# and RET% formed part of the adaptive compensatory reaction caused by decreased RBC. The PLT of male and female rats in group TC (5.0 g/kg/d QZZD) was significantly increased, and the coagulation index PT of the animals in the group was increased. Combined with the results of coagulation function, it was believed that the increase in PLT was a compensatory reaction, not secondary to the direct toxicity of the test drug. Combined with the statistical results and individual animal data, it was found that WBC and NEUT# in male animals of the medium- and high-dose groups exhibited an increasing trend, which was believed to be correlated with the test drug. However, the WBC, NEUT#, NEUT%, MONO# and EO% mentioned above were all variations of leukocytes and their classification indexes, which fluctuated slightly within the normal physiological reference range, and the composition proportion of each classification index of leukocyte was also at the normal physiological level. Therefore, they were attributed to physiological fluctuations instead of toxicity-induced injury.

The serum clinical chemistry analysis is highly relevant for the determination of target organs of toxicologic pathology (Weingand et al., 1996). And biochemical indicators are important to evaluate tested drugs for its toxic effect on the liver and kidney functions (Travlos et al., 1996). The TBIL index increased in all treatment groups mentioned above, and a significant increase was observed in group TC (5.0 g/kg/d QZZD), indicating a significant dose-response relationship, which was believed to be related to the test drug. The decrease of TG in medium-dose and high-dose groups male rats exhibited a certain dose correlation, which was thought to be related to the test drug. The variations for K^+ and CL^- indexes were small and fluctuated within the normal physiological reference range, which was not considered abnormal toxicity changes. The increase in Urea levels was caused by exaggerated individual values and was not considered toxicity-induced.

On the organ weights, there was a good dose correlation between the wet weight of the liver, the organ coefficients and organ/brain coefficients at the end of drug administration. Combined with the histological results, it was believed that the variation in the above indexes corresponded to the liver's adaptive changes during the test drug's continuous metabolism *in vivo*. The change in other organ indexes was non-significant, and no obvious histopathological abnormalities were found, indicating physiological changes and no obvious toxicity. At the end of the recovery period, the liver wet weight and organ-brain ratio decreased in group TA (0.5 g/kg/d QZZD), although the reduction was not significant, with no histopathological abnormality and no significant dose correlation, which were not attributed to the test drug. Abnormal values were observed for the organ/body ratio or organ/brain ratio, although the difference was not statistically significant and could not be attributed to the test drug.

Anatomical examination and histopathological findings are usually the main sources of toxicities. Observable lesions in the gross anatomy and histopathological examination results might help to determine the possible target organs of toxicities (Olayode et al., 2020). Our study found that QZZD at doses of 1.5 g/kg/d and 5.0 g/kg/d caused bile duct hyperplasia and karyomegaly of hepatocytes in SD rats in the drug treatment group, and the incidence and severity of the lesions were significantly dose-related. Accordingly, the liver lesions in experimental animals were related to drug-reduced. Importantly, these liver lesions fully recovered after 4 weeks of drug withdrawal. The bile duct hyperplasia and karyomegaly of hepatocytes were not seen in recovery groups at the end of the 28-day recovery period indicating these liver lesions were reversible.

Taken together, the repeated administration of QZZD did not cause any toxic effects in rats at doses of up to 0.5 g/kg/d, which corresponds to approximately 16.7 times the proposed dose administered in the clinical trial. The findings of this study substantiate that QZZD has a good safety profile, suitable for the long-term treatment of dementia. And further provide reliable experimental data for rational and safe clinical application of QZZD preparations.

Conclusion

In conclusion, the present toxicity studies clearly suggest the QZZD has a broad range of safety profiles. QZZD has no systemic toxicity through oral administration. The oral no-observed-adverse-effect-level of QZZD from the 28-day repeated oral dose toxicity study is 0.5 g/kg/d, and no target organ toxicity was identified. Together, the observations from the

present study raise no toxicity concern and affirm a broad-spectrum safety of QZZD.

Data availability statement

The original contributions presented in the study are included in the article/Supplementary Material, further inquiries can be directed to the corresponding authors.

Ethics statement

The animal study was reviewed and approved by the Ethics Review Committee for Animal Experimentation of New Drug Evaluation Center of Shandong Academy of Pharmaceutical Science(IACUC-2021020PD-02R).

Author contributions

QW, FC, and XW contributed to the conception and design of the study and approved the final version to be submitted. WX, DC, and ZZ contributed to drafting the article. SL and CC performed data analysis and interpretation. CS, WN, XK, and GS contributed to animal experiments. All authors have read and approved the final manuscript.

Funding

The present study was supported by grants from the National Natural Science Foundation of China (Nos.U21A20400 and 81973789) and the Major Science and Technology Project for "Significant New Drugs Creation" New Drugs Creation (Grant No. 2019ZX09301-173).

Acknowledgments

The authors acknowledge the Beijing University of Chinese Medicine University and New Drug Evaluation Center of Shandong Academy of Pharmaceutical Sciences for providing the research assistance and the Editorial Department of HOME for Researchers for proofreading the manuscript.

Conflict of interest

The authors declare that the research was conducted in the absence of any commercial or financial relationships that could be construed as a potential conflict of interest.

Publisher's note

All claims expressed in this article are solely those of the authors and do not necessarily represent those of their affiliated organizations, or those of the publisher, the editors and the reviewers. Any product that may be evaluated in this article, or claim that may be made by its manufacturer, is not guaranteed or endorsed by the publisher.

Supplementary material

The Supplementary Material for this article can be found online at: https://www.frontiersin.org/articles/10.3389/fphar.2022.987997/full#supplementary-material

References

Alam, A., Ferdosh, S., Ghafoor, K., Hakim, A., Juraimi, A. S., Khatib, A., et al. (2016). Clinacanthus nutans: a review of the medicinal uses, pharmacology and phytochemistry. *Asian Pac. J. Trop. Med.* 9 (4), 402–409. doi:10.1016/j.apjtm.2016.03.011

Chen, L., Li, M., Yang, Z., Tao, W., Wang, P., Tian, X., et al. (2020). Gardenia jasminoides Ellis: ethnopharmacology, phytochemistry, and pharmacological and industrial applications of an important traditional Chinese medicine. *J. Ethnopharmacol.* 257, 112829. doi:10.1016/j.jep.2020.112829

Chen, X. L., Su, S. L., Liu, R., Qian, D. W., Chen, L. L., Qiu, L. P., et al. (2021). Chemical constituents and pharmacological action of bile acids from animal: a review. *Zhongguo Zhong Yao Za Zhi* 46 (19), 4898–4906. doi:10.19540/j.cnki.cjcmm.20210630.201

Ding, J., Gao, X., Zhang, F., Zhou, Y., Li, S., Lu, Y., et al. (2021). Toxicological safety evaluation of Qiguiyin formula in rats at the treatment phase and recovery phase. *J. Ethnopharmacol.* 279, 114364. doi:10.1016/j.jep.2021.114364

Dziwenka, M., Coppock, R., Alexander, M., Palumbo, E., Ramirez, C., and Lermer, S. (2020). Safety assessment of a hemp extract using genotoxicity and oral repeat-dose toxicity studies in sprague-dawley rats. *Toxicol. Rep.* 7, 376–385. doi:10.1016/j.toxrep.2020.02.014

Gaire, B. P., Moon, S. K., and Kim, H. (2014). Scutellaria baicalensis in stroke management: nature's blessing in traditional eastern medicine. *Chin. J. Integr. Med.* 20 (9), 712–720. doi:10.1007/s11655-014-1347-9

Gao, S. M., Liu, J. S., Wang, M., Cao, T. T., Qi, Y. D., Zhang, B. G., et al. (2018). Traditional uses, phytochemistry, pharmacology and toxicology of codonopsis: a review. *J. Ethnopharmacol.* 219, 50–70. doi:10.1016/j.jep.2018.02.039

Gua, H., Hang, L., and Wang, Q. (2014). Interpretations on the content of the guidance for repetitive dose toxicity testing. *Chin. J. Clin. Pharmacol.* 30 (08), 744–745. doi:10.13699/j.cnki.1001-6821.2014.08.028

Guo, X., Weng, L., Yi, L., and Geng, D. (2022). Toxicological safety evaluation in acute and 21-day studies of ethanol extract from solanum lyratum thunb. *Evid. Based. Complement. Altern. Med.* 2022, 8518324. doi:10.1155/2022/8518324

Hardisty, J. F., Harris, S. B., Hayes, W. A., and Weber, K. (2020). Oral repeated-dose toxicity studies of BIA 10-2474 in beagle dogs. *Regul. Toxicol. Pharmacol.* 111, 104555. doi:10.1016/j.yrtph.2019.104555

He, J., Liang, J., Zhu, S., Li, J., Zhang, Y., and Sun, W. (2011). Anti-inflammatory effects of Pulvis Fellis Suis extract in mice with ulcerative colitis. *J. Ethnopharmacol.* 138 (1), 53–59. doi:10.1016/j.jep.2011.08.019

He, J., Lv, L., Wang, Z., Huo, C., Zheng, Z., Yin, B., et al. (2017). Pulvis Fellis Suis extract attenuates ovalbumin-induced airway inflammation in murine model of asthma. *J. Ethnopharmacol.* 207, 34–41. doi:10.1016/j.jep.2017.06.016

Li, C., Wang, X., Yan, J., Cheng, F., Ma, X., Chen, C., et al. (2020). Cholic acid protects *in vitro* neurovascular units against oxygen and glucose deprivation-induced injury through the BDNF-TrkB signaling pathway. *Oxid. Med. Cell. Longev.* 2020, 1201624. doi:10.1155/2020/1201624

Liu, S., Cheng, F., Ren, B., Xu, W., Chen, C., Ma, C., et al. (2022). Qinzhi Zhudan formula improves memory and alleviates neuroinflammation in vascular dementia rats partly by inhibiting the TNFR1-mediated TNF pathway. *J. Traditional Chin. Med. Sci.* 9, 298–310. doi:10.1016/j.jtcms.2022.06.011

Lu, Y., Hajifathalian, K., Ezzati, M., Woodward, M., Rimm, E. B., and Danaei, G. (2014). Metabolic mediators of the effects of body-mass index, overweight, and obesity on coronary heart disease and stroke: a pooled analysis of 97 prospective cohorts with 1·8 million participants. *Lancet* 383 (9921), 970–983. doi:10.1016/s0140-6736(13)61836-x

Ma, C., Wang, X., Xu, T., Zhang, S., Liu, S., Zhai, C., et al. (2020). An integrative pharmacology-based analysis of refined qingkailing injection against cerebral ischemic stroke: a novel combination of baicalin, geniposide, cholic acid, and hyodeoxycholic acid. *Front. Pharmacol.* 11, 519. doi:10.3389/fphar.2020.00519

Mukinda, J. T., and Eagles, P. F. (2010). Acute and sub-chronic oral toxicity profiles of the aqueous extract of Polygala fruticosa in female mice and rats. *J. Ethnopharmacol.* 128 (1), 236–240. doi:10.1016/j.jep.2010.01.022

Olayode, O. A., Daniyan, M. O., and Olayiwola, G. (2020). Biochemical, hematological and histopathological evaluation of the toxicity potential of the leaf extract of Stachytarpheta cayennensis in rats. *J. Tradit. Complement. Med.* 10 (6), 544–554. doi:10.1016/j.jtcme.2019.05.001

Piao, Y., Liu, Y., and Xie, X. (2013). Change trends of organ weight background data in sprague dawley rats at different ages. *J. Toxicol. Pathol.* 26 (1), 29–34. doi:10.1293/tox.26.29

Qi, H., Liu, R., Zheng, W., Zhang, L., Ungvari, G. S., Ng, C. H., et al. (2020). Efficacy and safety of traditional Chinese medicine for tourette's syndrome: a meta-analysis of randomized controlled trials. *Asian J. Psychiatr.* 47, 101853. doi:10.1016/j.ajp.2019.101853

Rui, W., Li, S., Xiao, H., Xiao, M., and Shi, J. (2020). Baicalein attenuates neuroinflammation by inhibiting NLRP3/caspase-1/GSDMD pathway in MPTP induced mice model of Parkinson's disease. *Int. J. Neuropsychopharmacol.* 23 (11), 762–773. doi:10.1093/ijnp/pyaa060

Shi, Y., Wei, F., and Ma, S. (2018). Medicinal research progress on pig bile and overview of its quality control. *China J. Chin. Materia Medica* 43 (04), 637–644. doi:10.19540/j.cnki.cjcmm.20180104.012

Tang, X., Wang, Y., Yang, W., Zheng, Y., Liu, C., Qu, M., et al. (2020). Acute and subchronic oral toxicity study of gardenia yellow E500 in sprague-dawley rats. *Int. J. Environ. Res. Public Health* 17 (2), E531. doi:10.3390/ijerph17020531

Tian, J., Yi, Y., Zhao, Y., Li, C., Zhang, Y., Wang, L., et al. (2018). Oral chronic toxicity study of geniposide in rats. *J. Ethnopharmacol.* 213, 166–175. doi:10.1016/j.jep.2017.11.008

Travlos, G. S., Morris, R. W., Elwell, M. R., Duke, A., Rosenblum, S., and Thompson, M. B. (1996). Frequency and relationships of clinical chemistry and liver and kidney histopathology findings in 13-week toxicity studies in rats. *Toxicology* 107 (1), 17–29. doi:10.1016/0300-483x(95)03197-n

Wang, J., Wang, L., Lou, G. H., Zeng, H. R., Hu, J., Huang, Q. W., et al. (2019). Coptidis rhizoma: a comprehensive review of its traditional uses, botany, phytochemistry, pharmacology and toxicology. *Pharm. Biol.* 57 (1), 193–225. doi:10.1080/13880209.2019.1577466

Wang, L., Liu, Y., Chai, J., Du, T., Hu, J., and Zhu, R. (2017). Acute and subacute toxicity trials of tetraploid skullcap D20. *J. Traditional Chin. Veterinary Med.* 36 (03), 11–14. doi:10.13823/j.cnki.jtcvm.2017.03.003

Weingand, K., Brown, G., Hall, R., Davies, D., Gossett, K., Neptun, D., et al. (1996). Harmonization of animal clinical pathology testing in toxicity and safety studies. *Toxicol. Sci.* 29 (2), 198–201. doi:10.1093/toxsci/29.2.198

Wu, R., Xiao, Z., Zhang, X., Liu, F., Zhou, W., and Zhang, Y. (2018). The cytochrome P450-mediated metabolism alternation of four effective lignans from schisandra chinensis in carbon tetrachloride-intoxicated rats and patients with advanced hepatocellular carcinoma. *Front. Pharmacol.* 9, 229. doi:10.3389/fphar.2018.00229

Xu, T., Wang, X., Ma, C., Ji, J., Xu, W., Shao, Q., et al. (2022). Identification of potential regulating effect of baicalin on NFκB/CCL2/CCR2 signaling pathway in rats with cerebral ischemia by antibody-based array and bioinformatics analysis. *J. Ethnopharmacol.* 284, 114773. doi:10.1016/j.jep.2021.114773

Zhang, H., Lai, Q., Li, Y., Liu, Y., and Yang, M. (2017). Learning and memory improvement and neuroprotection of Gardenia jasminoides (Fructus gardenia) extract on ischemic brain injury rats. *J. Ethnopharmacol.* 196, 225–235. doi:10.1016/j.jep.2016.11.042

frontiers | Frontiers in Pharmacology

TYPE Original Research
PUBLISHED 26 August 2022
DOI 10.3389/fphar.2022.958204

Check for updates

OPEN ACCESS

EDITED BY
Tariq Ismail,
COMSATS University Islamabad,
Abbottabad Campus, Pakistan

REVIEWED BY
Irum Shahzadi,
COMSATS University Islamabad,
Pakistan
Romana Khan,
COMSATS University Islamabad,
Abbottabad Campus, Pakistan

*CORRESPONDENCE
Chunxiao Yu,
yuchx08@163.com
Qingbo Guan,
doctorguanqingbo@163.com

SPECIALTY SECTION
This article was submitted to Predictive Toxicology,
a section of the journal
Frontiers in Pharmacology

RECEIVED 31 May 2022
ACCEPTED 28 July 2022
PUBLISHED 26 August 2022

CITATION
Liang Y, Huang X, Fang L, Wang M, Yu C and Guan Q (2022), Effect of iodoacetic acid on the reproductive system of male mice.
Front. Pharmacol. 13:958204.
doi: 10.3389/fphar.2022.958204

COPYRIGHT
© 2022 Liang, Huang, Fang, Wang, Yu and Guan. This is an open-access article distributed under the terms of the Creative Commons Attribution License (CC BY). The use, distribution or reproduction in other forums is permitted, provided the original author(s) and the copyright owner(s) are credited and that the original publication in this journal is cited, in accordance with accepted academic practice. No use, distribution or reproduction is permitted which does not comply with these terms.

Effect of iodoacetic acid on the reproductive system of male mice

Yun Liang[1,2,3,4,5], Xinshuang Huang[1,2,3,4,5], Li Fang[1,2,3,4,5], Mingjie Wang[6,7], Chunxiao Yu[2,3,4,5,6]* and Qingbo Guan[2,3,4,5,6]*

[1]Shandong University of Traditional Chinese Medicine, Jinan, China, [2]Shandong Provincial Hospital, Shandong University, Jinan, China, [3]Shandong Clinical Research Center of Diabetes and Metabolic Diseases, Shandong Provincial Hospital, Jinan, China, [4]Shandong Laboratory of Endocrinology and Lipid Metabolism, Shandong Provincial Hospital, Jinan, China, [5]Shandong Prevention and Control Engineering Laboratory of Endocrine and Metabolic Diseases, Shandong Provincial Hospital, Jinan, China, [6]Shandong Provincial Hospital, Shandong University, Jinan, China, [7]Department of Endocrinology, Affiliated Hospital of Inner Mongolia Medical University, Inner Mongolia Medical University, Inner Mongolia, China

Iodoacetic acid (IAA) is one of the most common water disinfection byproducts (DBPs). Humans and animals are widely and continuously exposed to it. Many species of water DBPs are harmful to the reproductive system of organisms. Nevertheless, the potential effects of IAA exposure on testosterone and spermatogenesis *in vivo* remain ambiguous. Spermatogenous cells are the site of spermatogenesis, Leydig cells are the site of testosterone synthesis, and Sertoli cells build the blood–testis barrier (BTB), providing a stable environment for the aforementioned important physiological functions in testicular tissue. Therefore, we observed the effects of IAA on spermatogenic cells, Leydig cells, and Sertoli cells in the testis. In this study, we found that oral administration of IAA (35 mg/kg body weight per day for 28 days) in male mice increased serum LH levels and reduced sperm motility, affecting average path velocity and straight line velocity of sperm. In addition, IAA promoted the expression of γH2AX, a marker for DNA double-strand breaks. Moreover, IAA downregulated the protein expression of the scavenger receptor class B type 1 (SRB1), and decreased lipid droplet transport into Leydig cells, which reduced the storage of testosterone synthesis raw materials and might cause a drop in testosterone production. Furthermore, IAA did not affect the function of BTB. Thus, our results indicated that IAA exposure affected spermatogenesis and testosterone synthesis by inducing DNA damage and reducing lipid droplet transport.

KEYWORDS

iodoacetic acid, testis, sperm, testosterone, γH2AX, SRB1

Introduction

In recent years, male fertility has generally shown a downward trend (Agarwal et al., 2021), and the effect of endocrine disruptors is one of the reasons (Kahn et al., 2020). There are many types of endocrine disruptors, and water disinfection by-products (DBPs) are one of them. DBPs are chemical contaminants formed by the reaction between organic

matter and disinfectants. Research proves that water DBPs disrupt ovarian function and spermatogenesis, and produce adverse reproductive outcomes (Gonsioroski et al., 2020a) because many species of these are cytotoxic, neurotoxic, genotoxic, carcinogenic, and teratogenic (Kali et al., 2021).

Haloacetic acid disinfection by-products (HAA-DBPs) are a class of water DBPs. Iodoacetic acid (IAA) is one type of HAA-DBPs. It is also used in the research of organic synthesis, dye industry, and plant resources, where people are exposed to a large dose of poisoning environment. Research has shown that IAA is the most genotoxic of all HAA-DBPs studied to date (Dong et al., 2019), which was more cytotoxic and genotoxic than their chlorinated and brominated analogues in primary human lymphocytes (Escobar-Hoyos et al., 2013). After inoculation into BALB/C nude mice, IAA transformed NIH3T3 cells into tumorigenic lines and formed aggressive fibro sarcomas, which demonstrated that it had a biological activity consistent with a carcinogen (Wei et al., 2013). IAA potentially disrupted the thyroid endocrine system by down-regulating the mRNA and protein expression levels of the thyrotropin receptor (TSHR) and the sodium/iodide symporter (NIS) (Xia et al., 2018). Moreover, IAA reduced cell viability significantly in the mouse primary hepatocytes (Wang et al., 2018).

For the adult female mice, IAA, as a hypothalamic–pituitary–gonadal axis toxicant, affected the pituitary directly and increased mRNA levels of kisspeptin (Kiss1) significantly in the arcuate nucleus (Gonzalez et al., 2021). Research demonstrated that IAA had reproductive and developmental toxicity (Long et al., 2021). Another study reported that IAA exhibited the most potent estrogenic activity (Kim et al., 2020). *In vivo*, IAA altered estrous cyclicity, ovarian gene expression, and estradiol levels in mice (Gonsioroski et al., 2021). Meanwhile, IAA inhibited follicle growth, decreased cell proliferation, and altered steroidogenesis *in vitro* (Jeong et al., 2016; Gonsioroski et al., 2020b). In the Comet assay, IAA resulted in DNA damage in sperm (Ali et al., 2014). However, the effect of IAA on the testis *in vivo* is not yet fully understood. Particularly, its effect on spermatogenesis and testosterone synthesis has not been elucidated.

To observe the effects of IAA on the male reproductive system and to test the mechanism, we constructed a model of IAA exposure by gavage and observed several common indicators of Leydig cells, Sertoli cells, and spermatogenic cells from the gene expression and protein levels. For spermatogenic cells, γH2AX, DAZL, and VASA were observed; for Leydig cells, scavenger receptor class B type 1 (SRB1), steroidogenic acute regulatory protein (STAR), P450 side-chain cleavage enzyme (CYP11A1), and cytochrome P450 17A1 (CYP17A1) were detected; and for Sertoli cells, WT-1, N-cadherin, and β-catenin were recorded. In addition, the levels of FSH, LH, and testosterone in the mouse serum were also determined.

Materials and methods

Materials and reagents

IAA was purchased from Sigma-Aldrich (Shanghai Warehouse, China). Antibodies for STAR (8449s) and CYP11A1 (14217s) were procured from Cell Signaling Technology, Inc. Antibody for CYP17A1 (14447-1-AP) was purchased from Wuhan SANYING Proteintech (Wuhan Warehouse, China). The other antibodies were obtained from Abcam (Shanghai, China) including DAZL (ab34139), VASA (ab13840), γH2AX (ab81299), SRB1 (ab217318), Wilms tumor-1 (WT-1) (ab89901), N-cadherin (ab18203), β-catenin (ab16051), and tubulin (ab7291).

Animals and treatments

All animals used in the experiment were male 8 -week-old C57BL/6 mice, purchased from Vital River Laboratory Animal Technology Co., Ltd. (Beijing, China). They were randomly divided into two groups, with free access to water and food. After 1 week of acclimatization, the control group (8 mice) received treatment *via* gavage with a matching volume of double distilled H_2O, and the experiment group (10 mice) was administered IAA at 35 mg/kg *via* oral gavage daily. The dosage and duration of IAA were referred to the previous literature (Xia et al., 2018). All mice were adapted to a 12-h light/dark cycle at 22–25°C. They were weighed twice a week, and doses were adjusted according to their bodyweight. After treatment for 28 days, all the mice were anesthetized, the blood was collected, and the caudal part of the epididymis was used for the evaluation of sperm parameters. Then the testis samples were removed quickly for the subsequent analyses. One testis was fixed in Bouin's solution for the histopathological examination and immunofluorescent staining, and the other testis was frozen in liquid nitrogen and stored at −80°C until used for the assessment of mRNA and protein expression.

All animal experiments were approved by the Animal Ethics Committee of Shandong Provincial Hospital and performed according to the Shandong Provincial Hospital Animal Care and Use Committee.

Sex hormone analysis

The level of luteinizing hormone (LH) in the serum was measured by the ELISA kit from CLOUD-CLONE CORP. (Wuhan, China). Testosterone and follicle stimulating hormone (FSH) in the serum were measured by the ELISA kit from Cusabio (Wuhan, China). The operating procedure was strictly in accordance with the kit instructions.

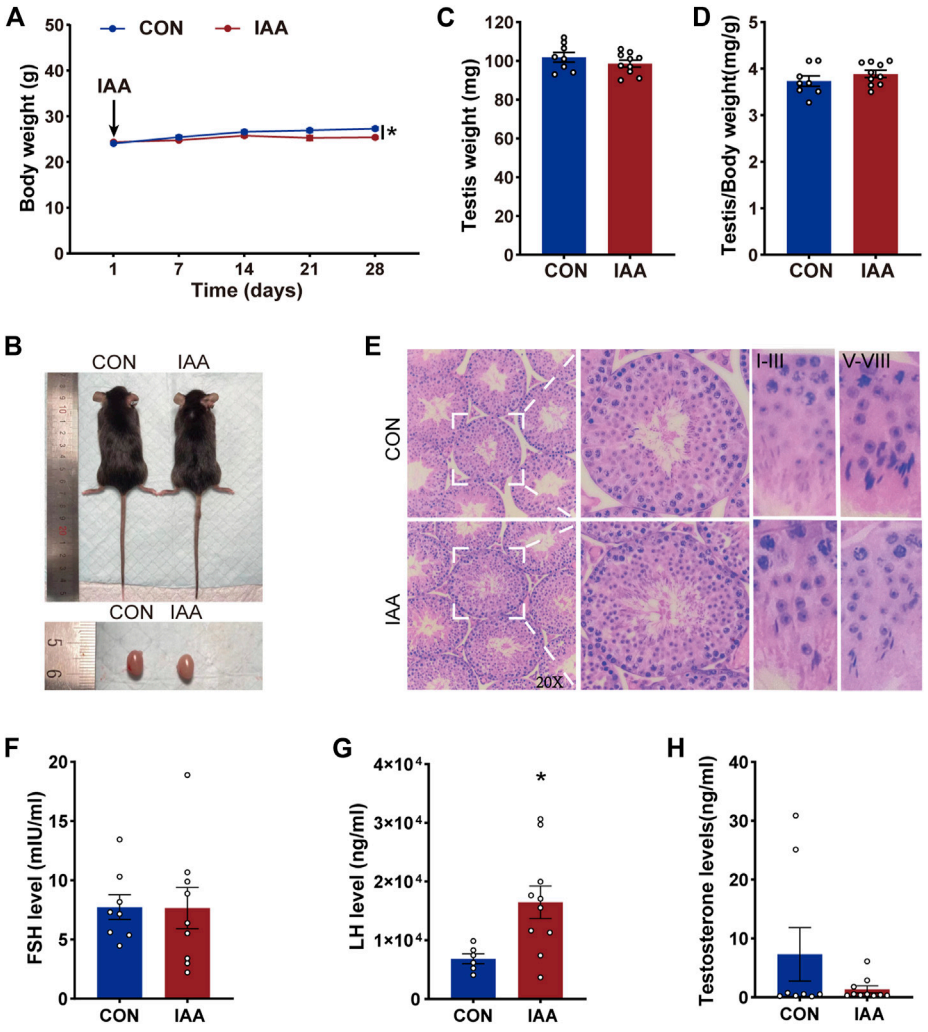

FIGURE 1
Effects of IAA exposure on general condition and serum hormone levels in mice. During the IAA exposure, the body weights of the mice were recorded twice a week. Only weekly values are shown in the graph **(A)**. Pictures of mice and testis **(B)**, testicular weight **(C)**, and the relative weight of testis **(D)** between the two groups were recorded after sacrifice. Hematoxylin-eosin (H&E) sections of testicular tissue of mice were also recorded and the pathological morphology was observed **(E)**. After IAA exposure, serum FSH, LH, and testosterone levels of mice were detected by ELISA **(F–H)**. Data are presented as the mean ± SEM. * Significant differences compared to control ($p < 0.05$).

Sperm quality

The cauda part of the right epididymis of each mouse was collected and cut into pieces with scissors to release sperms into an M199 culture medium (containing 1% BSA). The cultures were maintained in a humidified chamber (37°C, 5% CO_2 incubator) for 5 min. A total of one hundred microliters of each sample was taken and diluted four times. Then thirty microliters of the sample were used for the following assay. Five pictures were taken per sample. Then the data were quantified by computer-aided sperm analysis (CASA, Hamilton-Thorne, Shanghai, China), and the appurtenant software was used to assess sperm concentration, motility, progressive, quantity, average path velocity, straight line velocity, and curvilinear velocity.

Hematoxylin-eosin staining

The testis was immersed in Bouin's fluid fixative for 24 h, transferred to 70% ethanol, and placed into an automated tissue processor for gradient ethanol dehydration. The samples were embedded in paraffin wax and cut into 3 μm sections. Then the testicular specimens were deparaffinized with xylene and ethanol, stained with hematoxylin and eosin, dehydrated, and mounted. Afterward, the morphological changes of the testis were observed

TABLE 1 Sperm parameters.

	CON	IAA	*p* value
VAP (μm/s)	87.10 ± 4.40	80.65 ± 7.12	0.040*
VSL (μm/s)	63.94 ± 5.27	57.79 ± 5.91	0.035*
VCL (μm/s)	184.93 ± 9.50	177.69 ± 16.19	0.281
ALH (μm)	8.98 ± 0.51	9.03 ± 0.51	0.822
BCF (Hz)	36.09 ± 0.71	35.91 ± 1.21	0.719
LIN (%)	36.62 ± 2.92	35.40 ± 2.37	0.340
STR (%)	70.75 ± 3.45	69.70 ± 2.58	0.471
Concentration (M/ml)	9.63 ± 1.92	8.21 ± 1.69	0.116
Motile (%)	53.63 ± 9.50	56.00 ± 11.10	0.638
Progressive (%)	20.00 ± 4.57	17.80 ± 5.35	0.369
Rapid sperm (%)	11.63 ± 5.40	39.70 ± 6.57	0.621
Medium sperm (%)	41.13 ± 5.09	15.50 ± 8.06	0.262
Slow sperm (%)	0.65 ± 0.26	0.95 ± 0.41	0.097
Static sperm (%)	46.38 ± 9.50	44.00 ± 11.10	0.638

*Significant differences compared to the control ($p < 0.05$).

under a microscope to complete the image collection and analysis.

RNA extraction and real-time PCR

Total RNA was extracted from testicular tissue (10 mg) with TRIzol reagent (Takara, Tokyo, Japan) according to the manufacturer's instructions. A Prime-Script RT Reagent Kit (Takara, Japan) was used to reverse-transcribe RNA into cDNA, and SYBR Premix Ex Taq (Takara, Japan) was used to perform a quantitative real-time polymerase chain reaction (PCR) utilizing a Thermal Cycler Dice Real-Time System (Takara, Japan). The program used to analyze the abundance of different genes was 95°C for 5 min, 40 cycles of 95°C for 10 s, 60°C for 10 s, and 72°C for 10 s, followed by a melting curve from 95 to 60°C, and cool to 37°C for 10 s. β-actin was employed as an endogenous control to normalize the data, and the 2-ΔΔCt calculation method was employed to analyze them. The qPCR primers used are listed in Supplementary Table S1.

Western blotting

Mouse testicular fragments were lysed with ice-cold radioimmunoprecipitation assay buffer (RIPA buffer) supplemented with protease and phosphatase inhibitors (Shenergy Biocolor Bioscience & Technology Company, Shanghai, China), subjected to ultrasound pyrolysis, and centrifuged at 15,000 g for 15 min. Total protein was quantified using the BCA protein assay. After denaturation, proteins were separated by sodium dodecyl sulphate-polyacrylamide gel electrophoresis (SDS-PAGE) on 10%–12% polyacrylamide gels under reducing conditions. Separated proteins were electro transferred onto a polyvinylidene difluoride membrane (Millipore, Billerica, MA, United States) and blocked-in with 5% non-fat powdered milk containing 0.1% Tween 20 for 1 h. Next, to detect γH2AX, VASA, DAZL, SRB1, STAR, CYP17A1, CYP11A1, WT-1, N-cadherin, and β-catenin proteins (antibodies listed in Supplementary Table S2), the membrane was incubated with the respective primary antibodies at 4°C overnight. Thereafter, the membranes were washed briefly with TBST, incubated in the anti-rabbit or anti-mouse IgG secondary antibody conjugated to horseradish peroxidase (1:5000) for 1 h at room temperature, and visualized by a HyGLO HRP detection kit (Denville, NJ, United States). Protein expression levels were quantified with Fluor Chem Q SA software.

Immunofluorescence

For fluorescent microscopy, paraffin sections of the testis were deparaffinized with xylene, hydrated with a series of alcohol solutions, and washed three times in phosphate-buffered saline (PBS). The specimens were immersed in EDTA antigen repair buffer and heated in a microwave oven for 25 min. Then they were cooled for 60 min, washed three times with PBS, and incubated with 5% donkey serum for 60 min at room temperature. Afterward, the slides were incubated with their respective primary antibodies overnight. The next day, the sections were washed three times with PBST and then incubated with FITC-conjugated donkey anti-rabbit IgG (1:1000; Thermo Fisher) for 1 h at room temperature. After a final wash in PBST, nuclei were stained with DAPI, the slides were visualized under a fluorescence microscope, and the photos were taken and analyzed.

Statistical analysis

All data were analyzed with SPSS 25.0 and were expressed as the mean ± standard error of the mean (SEM). Outliers were removed by the ROUT's test using GraphPad outlier calculator software. Means were compared using unpaired Student's t-test for comparisons between two groups, and a two-tailed value of $p < 0.05$ was considered statistically significant.

Results

Effects of iodoacetic acid on testicular morphology and hypothalamus pituitary gonadal axis hormones

Compared with the control group, a slight decrease in body weight was observed after the IAA exposure for 28 days (Figures

1A,B). The relative weight of testis was calculated by testes weight (mg)/body weight (g), but there were no significant reductions in the testis weight and its relative weight between two groups (Figures 1C,D). As shown in Figure 1E, no evidence of atrophy and vacuoles was seen in the experimental group. The testis tissue presented a normal testicular morphology and complete seminiferous tubules, and also possessed different stages of spermatogonium, spermatocyte, and spermatozoa in the seminiferous tubules. IAA did not alter the pathology and morphology of the testicular tissues. To clarify the effect of IAA exposure on sex hormones, serum FSH, LH, and testosterone levels were detected. There was no significant difference in the FSH level between the two groups (Figure 1F). However, a significant increase in the LH level was observed versus control ($p = 0.020$, Figure 1G). Although there was no significant reduction in the testosterone level, a descending trend was observed compared with the control group ($p = 0.166$, Figure 1H).

Effects of iodoacetic acid exposure on sperm motility

To observe the effect of IAA exposure on sperm motility, various indicators of sperm motility and concentration were tested (as listed in Table 1). As observed in our results, there were no significant changes in the following sperm parameters, such as sperm concentration, motile, progressive, and curvilinear velocity (VCL). But the average path velocity (VAP) and straight line velocity (VSL) of sperm decreased significantly compared with the control group. We also tested the sperm ratios as rapid, medium, slow, and static. There were no statistical differences in these indicators between the two groups; however, there was a clear increasing trend in the proportion of slow motile sperm.

Effects of iodoacetic acid exposure on markers of spermatogenic cells

Spermatogenesis is an important physiological function of testicular tissue. To observe the effects of IAA exposure on spermatogenic cells, the gene expression and protein levels of relevant indicators during spermatogenesis were examined. As shown in Figure 2A, no significant changes were observed in the spermatogenesis indicators Dazl, Vasa, Plzf, c-Kit, Stra8, Sycp1, Sycp3, Tnp2, and Piwil1 at the mRNA level between the two groups. But IAA treatment significantly increased γH2AX expression compared to no treatment. All seminiferous tubules contain γH2AX spermatocytes at respective steps in development. Meanwhile, γH2AX is a marker of the DNA damage response and replication stress. Although IAA exposure did not change the protein levels of VASA and DAZL compared to the control (Figures 2B,C,F,G), the protein level of γH2AX was observed increasingly by Western Blot (WB) and immunofluorescence staining experiments (Figures 2B–E).

Effects of iodoacetic acid on cholesterol transport and testosterone synthesis-related enzymes

To evaluate the effect of IAA exposure on testosterone synthesis, changes in gene expression, protein levels of these enzymes and LDs were examined. The results demonstrated that IAA exposure decreased LD storage in Leydig cells (Figures 3A,B). SRB1, as a high-density lipoprotein receptor, is responsible for the transport of LDs. In our study, although the gene expression did not change between the two groups (Figure 3C), there was a decrease in the protein level (Figures 3D–G). Compared with the control group, a mild decrease in Cyp11a1 mRNA expression was observed, as shown in Figure 3C. However, its protein level showed no significant difference between the two groups (Figures 3D,E,H,I). The steroidogenic acute regulatory (STAR), as a key enzyme in testosterone synthesis, tended to decrease in the experiment group, but the differences failed to reach statistical significance (Figures 3D,E). In the immunofluorescence staining experiment, it showed no difference *versus* control (Supplement Figures 1A,B). Also, no changes were observed in the gene expression of Cyp17a1, Cyp19a1, 3β-hsd, and Lhcgr between the two groups (Figure 3C).

Effects of iodoacetic acid on blood–testis barrier function in Sertoli cells

To assess the effect of IAA exposure on Sertoli cells, changes in genes and proteins of WT-1 and some indicators of tight junctions were examined. As shown in Figure 4A, there were no differences at the genetic level between the two groups on Wt-1, Claudin-11, Nectin-2, Zo-2, β-catenin, Jam-A, N-cadherin, and Connexin-43. The protein levels of WT-1, N-cadherin, and β-catenin also did not perform a statistical difference compared with control (Figures 4B–E).

Discussion

It is well known that endocrine disruptors have a direct impact on gonads and long-term reproductive health (Delbes et al., 2022). IAA has a negative influence on the female reproductive system, while the effects on the male reproductive system have not been systematically studied. From the perspective of the physiological structure of the testis, the male reproductive system mainly includes spermatogenic cells, Leydig cells, and Sertoli cells (Mäkelä

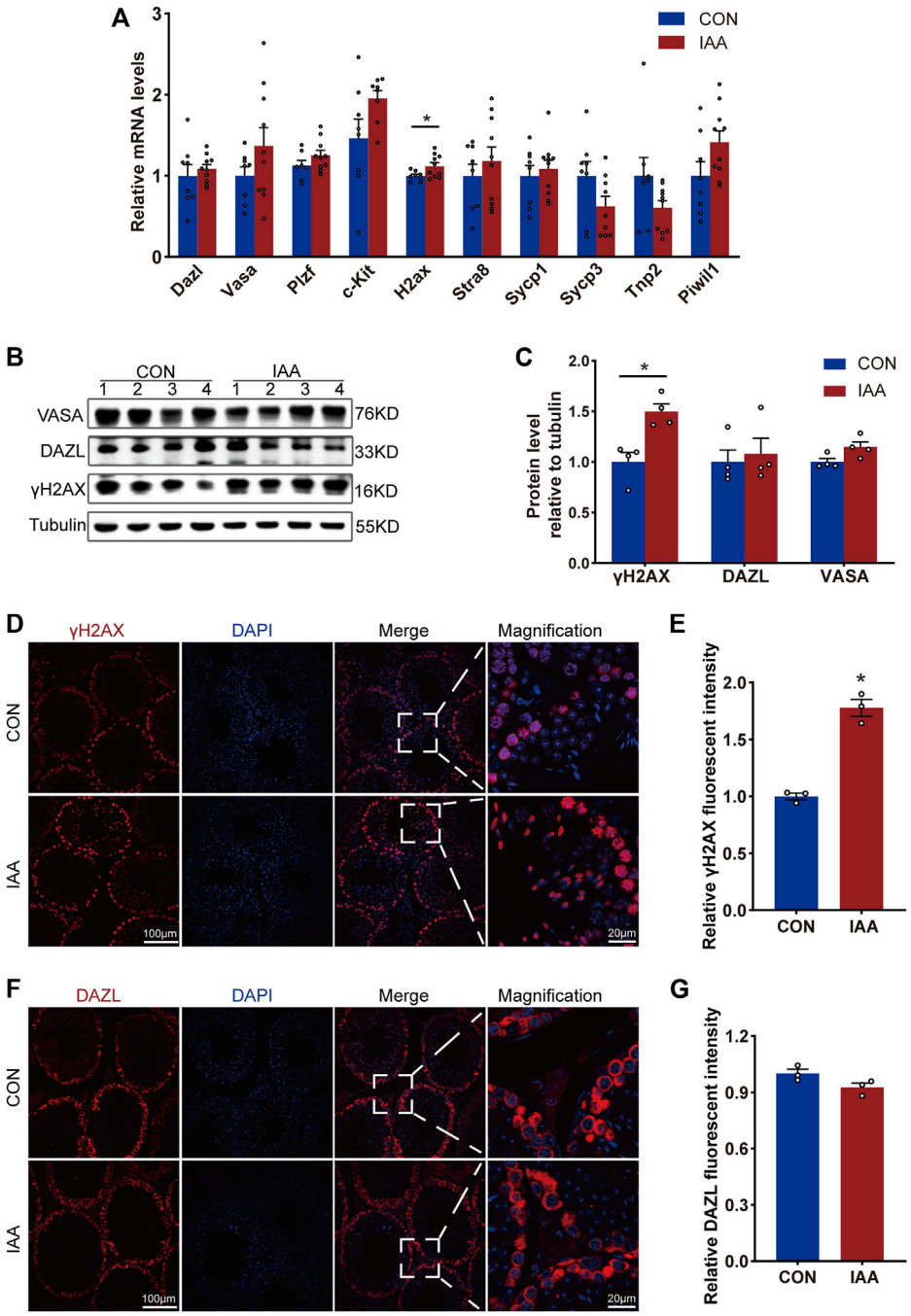

FIGURE 2
Changes of spermatogenesis-related indexes were observed from gene expression and protein level, respectively. The expression of the following genes, such as Dazl, Vasa, Plzf, c-Kit, H2ax, Stra8, Sycp1, Sycp3, Tnp2, and Piwil1, in the testis tissue of the two groups were detected by real-time PCR (qRT-PCR) technology **(A)**. Also, the changes of protein levels such as VASA, DAZL, and γH2AX between the two groups of mice were observed by Western Blot **(B,C)** and immunofluorescence staining experiments **(D–G)**. * Significant differences compared to the control ($p < 0.05$).

et al., 2019). Therefore, we mainly observed the effect of IAA on its function from these three aspects. In our study, IAA exposure had no apparent effect on Sertoli cell function, but it exacerbated DNA damage in spermatogenic cells and reduced cholesterol storage in Leydig cells by reducing the protein expression of SRB1. In addition, IAA also affected sperm motility, slowing

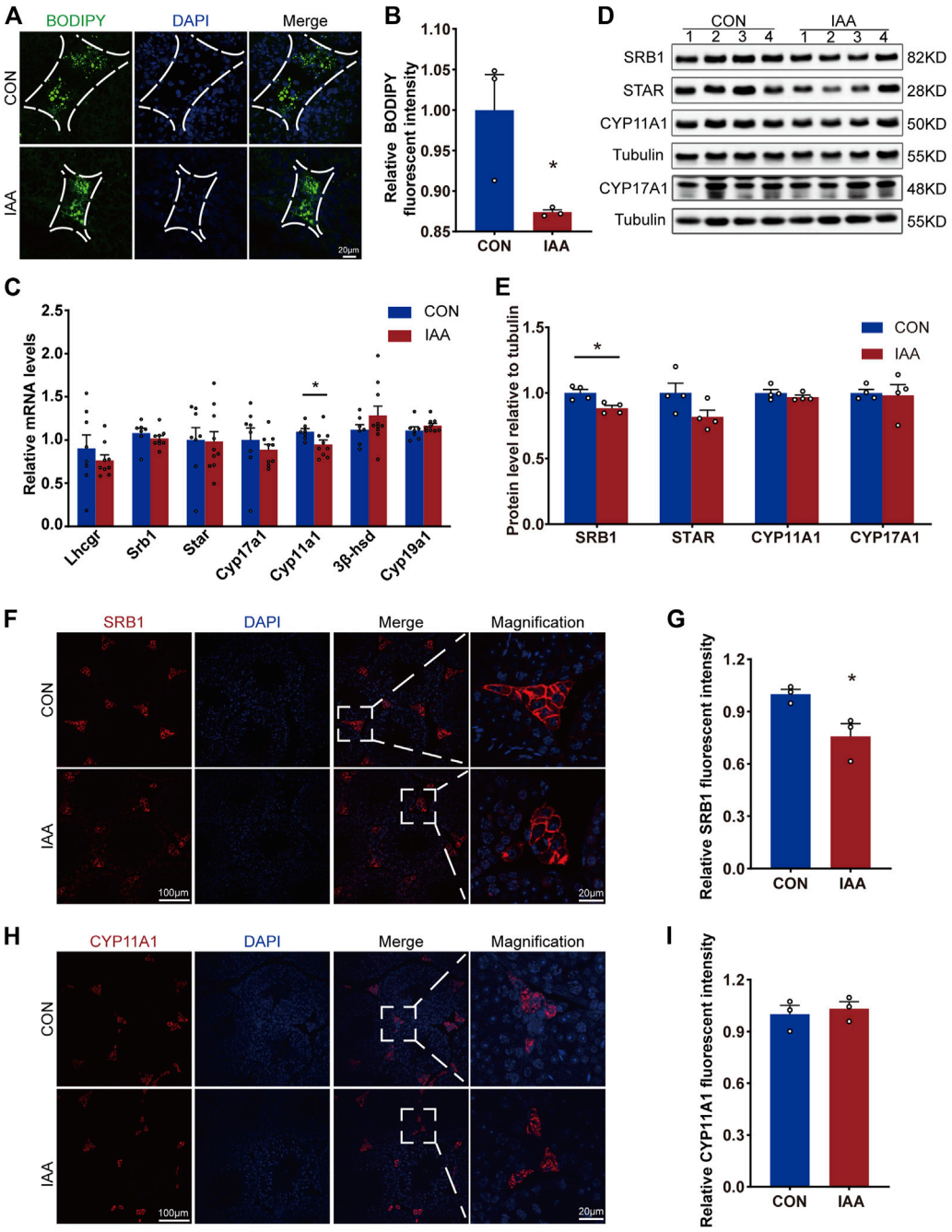

FIGURE 3
Lipid droplet storage in Leydig cells and changes in testosterone synthase from gene expression and protein levels were examined. Cholesterol storage in Leydig cells between the two groups was visualized by BODIPY staining **(A,B)**. The relative mRNA levels of the following indicators, Lhcgr, Srb1, Star, Cyp17a1, Cyp11a1, 3β-hsd, and Cyp19a1, were detected by qRT-PCR **(C)**. Also, the protein levels of cholesterol transporter SRB1 and testosterone synthase STAR, CYP11A1, and CYP17A1 were observed by Western Blot **(D,E)** and immunofluorescence staining experiments **(F–I)**.
* Significant differences compared to the control ($p < 0.05$).

down VAP and VSL. Furthermore, it caused dysfunction of the hypothalamic–pituitary–gonadal axis, especially the increase in LH in serum.

We found that the body weight in the experimental group showed a slight decrease. This may be mainly due to the effect of IAA on gastric acid secretion (Cheng et al., 2001), which finally

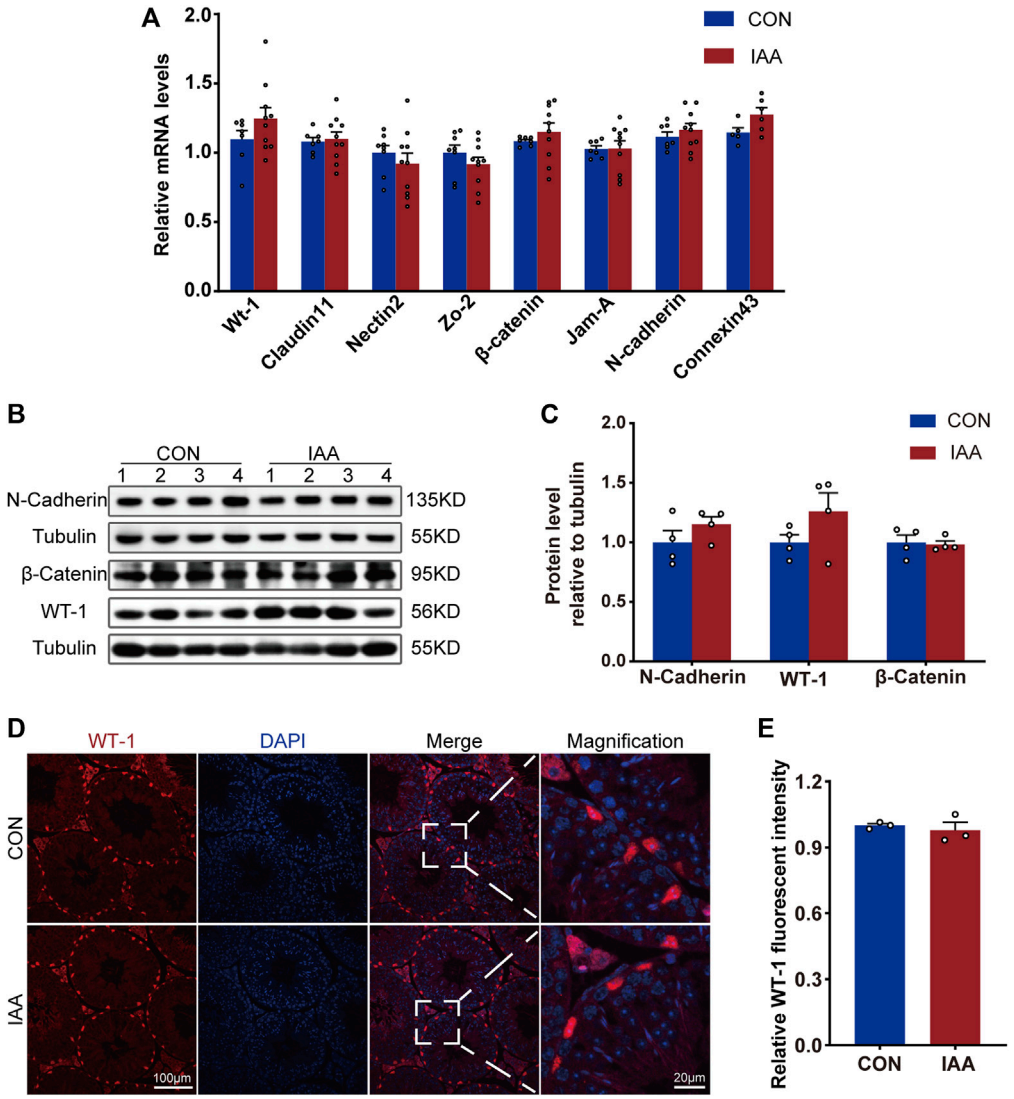

FIGURE 4
Changes of BTB-related indexes were detected from gene expression and protein level. Relative mRNA levels between the two groups, Wt-1, Claudin-11, Nectin-2, Zo-2, β-catenin, Jam-A, N-cadherin and Connexin-43, were observed **(A)**. The protein levels of WT-1, N-cadherin, and β-catenin were also observed by Western Blot **(B,C)** and immunofluorescence staining experiments **(D,E)**. * Significant differences compared to the control ($p < 0.05$).

caused the mice to lose weight. To observe the effect of IAA on sex hormones *in vivo*, we measured the levels of FSH, LH, and testosterone in the serum. In our study, FSH did not change compared to the control group, but LH showed a significant increase *versus* control. Research showed that in adult female mice, IAA did not alter LHβ expression, while it reduced FSHβ-positive cell number and FSHβ mRNA expression at a dose of 10 mg/kg *in vivo* (Gonzalez et al., 2021). The inconsistent results might be due to the difference in dosage and time of medication. Given that testosterone varies widely between individuals, we did not remove outliers. Although there was no difference in testosterone between the two groups, there was a descending trend in the experimental group. We inferred that IAA exposure caused a decrease in testosterone but increased LH through negative feedback, thus maintaining normal levels of testosterone.

To observe the effect of IAA on sperm, we examined changes in relevant sperm parameters, such as sperm concentration, motility, progressiveness, VAP, VSL, VCL, ALH, and BCF. Among them, VAP and VSL showed a significant decrease compared to the control group. We deduced that was because IAA inhibited the glyceraldehyde-

3-phosphate dehydrogenase (GAPDH), which was the key target of IAA (Hall et al., 2020) and one of the key enzymes in glycolysis, reduced cellular ATP levels (Dad et al., 2018), and ultimately slowed down sperm motility.

Sperm production is one of the most important functions of the testis. Spermatogenesis is a complex developmental process that consists of three stages: mitosis, meiosis, and spermiogenesis (Zhao J. et al., 2021). To observe the effect of IAA on spermatogenesis, protein levels of DAZL, VASA, γH2AX, and related gene expression changes were detected. Phosphorylated histone H2AX (γH2AX) is a hallmark of chromatin remodeling in male meiosis (Abe et al., 2020). Meanwhile, it is a sensitive marker for DNA double-strand breaks (DSBs) (Arnould et al., 2021), and a number of studies have regarded it as a marker of DNA damage (Guo et al., 2021; Zhang et al., 2021; Wang et al., 2022). Increased expression of γH2AX levels at the gene expression and protein level are detected, indicating that DNA damage is exacerbated after IAA exposure. DAZL, which is crucial for normal spermatogenesis, plays an important role in primordial germ cell formation, and genetic loss of DAZL causes infertility in both sexes of mice (Li et al., 2019). In our study, changes in DAZL gene and protein levels were not observed. VASA (DDX4/MVH), as the hallmark of meiotic cells at the stage from pachytene spermatocytes to round spermatids, is essential for male gametogenesis (Lin et al., 2017). It also showed no difference between the two groups in our study. Plzf and Kit are essential in maintaining spermatogonial stem cell proliferation (Mao et al., 2017; Yu et al., 2022). Stra8 (Sun et al., 2022), Sycp1 and Sycp3 (Dunce et al., 2018), and Tnp2 (Gustafson et al., 2020) play important roles in different stages of meiosis. Also, knockout of the Piwi gene in mice and human causes sterility (Gou et al., 2017). Fortunately, with the exception of H2AX, IAA exposure did not cause changes in the other genes described previously.

The second important function of the testis is testosterone biosynthesis. In order to observe the effect of IAA on testosterone, we focused on the changes in cholesterol and key enzymes in cholesterol transport and testosterone synthesis. SRB1 is a cell surface HDL receptor that mediates HDL-cholesteryl ester (CE) uptake, and it promotes the transport of CEs to Leydig cells and stores them as lipid droplets (LDs), which are used for the synthesis of testosterone in testis tissue (Shen et al., 2018). In our study, the content of cholesterol in Leydig cells decreased in the IAA-exposed group. This was because IAA affected LD transport by reducing the protein expression of SRB1, although IAA did not alter the gene expression of it. We infer that IAA causes changes in SRB1 protein levels through post-transcriptional translation or epigenetic modification, which, of course, requires further experimental validation. At the same time, we also detected a series of key enzymes in testosterone synthesis, such as STAR, CYP11A1, CYP17A1, and 3β-HSD. Except for the decrease of Cyp11a1 at the gene level, other indicators did not show significant differences both in gene expression and at the protein level. However, STAR, one of the most critical enzymes regulating testosterone synthesis (Zhao L. et al., 2021), showed a significant downward trend at the protein level, which further corroborated our conclusion that testosterone had declined during the medication. In Leydig cells, LHCGR acts as an LH receptor to sense the control of testosterone synthesis by the hypothalamic–pituitary–testicular axis (Holota et al., 2020). Gene expression of Lhcgr did not change between the two groups. In addition, the gene level of Cyp19a1, a key enzyme that converts testosterone to estrogen, was examined, and did not change compared to control. This means IAA does not influence the conversion of testosterone to estrogen in male mice.

An important function of Sertoli cells is to form the BTB, which forms the microenvironment for spermatogenesis and protects spermatogenic cells from autoimmune reactions. To assess the function of the BTB, we examined the expression of WT-1, N-cadherin, and β-catenin. WT-1, expressed in all Sertoli cells, is essential for germ cell survival and spermatogenesis (Gupta et al., 2021). N-Cadherin is a protein with greater connection flexibility, which is highly expressed in testis tissue (Verón et al., 2021). At the same time, in other tissues, it is often regarded as highly correlated with tissue migration, and is even used as one of the indicators of tumor aggressiveness (He et al., 2021). β-Catenin is also a characteristic protein of the BTB, and its abnormal accumulation can lead to impaired testicular junction integrity, which can lead to abnormal structures and functions of the BTB (Lei et al., 2021). In our study, the gene expression and protein levels of WT-1, N-cadherin, and β-catenin were not different between the two groups. As important components of tight junctions, such as claudin11 (She et al., 2021), Nectin-2 (Bronson et al., 2017), Zo-2 (Otani et al., 2019), Jam-A (Ebnet, 2017), and Connexin 43 (Liang et al., 2019), they all play a key role in maintaining the integrity of the BTB. Fortunately, there were no statistically significant differences in their gene levels.

In conclusion, in male mice, IAA reduced sperm motility, exacerbated DNA damage, and decreased storage of LDs, the raw material for testosterone synthesis. Of course, a deeper mechanism is needed in further research. At present, the adverse health consequences of endocrine disruptors have been known to all sectors of society (La Merrill et al., 2020), and various countries are also formulating some corresponding regulatory measures (Kassotis et al., 2020). However, little attention has been paid to water DBPs such as IAA. It not only affects the health of frontline workers producing such materials but also has long-term human contact in the form of water DBPs. Given that these endocrine disruptors have toxic effects on humans and even transmit their toxic effects to offspring in a genetic or

epigenetic manner (Lombó and Herráez, 2021), laws and regulations on the control of them should be formulated as soon as possible. Also, we should try to find other healthier disinfection methods to replace chlorine-containing disinfectants to reduce their harm to the reproductive system and even human health.

Data availability statement

The original contributions presented in the study are included in the article/Supplementary Material; further inquiries can be directed to the corresponding authors.

Ethics statement

The animal study was reviewed and approved by the Animal Ethics Committee of Shandong Provincial Hospital.

Author contributions

YL was responsible for the completion of molecular biology experiments and the draft of the article. XH completed the collection and arrangement of the experimental data. LF and MW completed the production of the chart. CY was responsible for the design, guidance of the experimental techniques, and manuscript correction. QG completed the overall thinking and supervision of the project.

Funding

This work was supported by grants from the National Natural Science Foundation (81770860 and 81641030) and the Key Research and Development Plan of Shandong Province (2017CXGC1214).

Conflict of interest

The authors declare that the research was conducted in the absence of any commercial or financial relationships that could be construed as a potential conflict of interest.

Publisher's note

All claims expressed in this article are solely those of the authors and do not necessarily represent those of their affiliated organizations, or those of the publisher, the editors, and the reviewers. Any product that may be evaluated in this article, or claim that may be made by its manufacturer, is not guaranteed or endorsed by the publisher.

Supplementary material

The Supplementary Material for this article can be found online at: https://www.frontiersin.org/articles/10.3389/fphar.2022.958204/full#supplementary-material

References

Abe, H., Alavattam, K. G., Hu, Y. C., Pang, Q., Andreassen, P. R., Hegde, R. S., et al. (2020). The initiation of meiotic sex chromosome inactivation sequesters DNA damage signaling from autosomes in mouse spermatogenesis. *Curr. Biol.* 30 (3), 408–420. e5. doi:10.1016/j.cub.2019.11.064

Agarwal, A., Baskaran, S., Parekh, N., Cho, C. L., Henkel, R., Vij, S., et al. (2021). Male infertility. *Lancet* 397 (10271), 319–333. doi:10.1016/s0140-6736(20)32667-2

Ali, A., Kurzawa-Zegota, M., Najafzadeh, M., Gopalan, R. C., Plewa, M. J., and Anderson, D. (2014). Effect of drinking water disinfection by-products in human peripheral blood lymphocytes and sperm. *Mutat. Res.* 770, 136–143. doi:10.1016/j.mrfmmm.2014.08.003

Arnould, C., Rocher, V., Finoux, A. L., Clouaire, T., Li, K., Zhou, F., et al. (2021). Loop extrusion as a mechanism for formation of DNA damage repair foci. *Nature* 590 (7847), 660–665. doi:10.1038/s41586-021-03193-z

Bronson, R., Mikhailik, A., Schwedes, J., Gnatenko, D., and Hatchwell, E. (2017). Detection of candidate nectin gene mutations in infertile men with severe teratospermia. *J. Assist. Reprod. Genet.* 34 (10), 1295–1302. doi:10.1007/s10815-017-0985-4

Cheng, A. M., Morrison, S. W., Yang, D. X., and Hagen, S. J. (2001). Energy dependence of restitution in the gastric mucosa. *Am. J. Physiol. Cell Physiol.* 281 (2), C430–C438. doi:10.1152/ajpcell.2001.281.2.C430

Dad, A., Jeong, C. H., Wagner, E. D., and Plewa, M. J. (2018). Haloacetic acid water disinfection byproducts affect pyruvate dehydrogenase activity and disrupt cellular metabolism. *Environ. Sci. Technol.* 52 (3), 1525–1532. doi:10.1021/acs.est.7b04290

Delbes, G., Blázquez, M., Fernandino, J. I., Grigorova, P., Hales, B. F., Metcalfe, C., et al. (2022). Effects of endocrine disrupting chemicals on gonad development: Mechanistic insights from fish and mammals. *Environ. Res.* 204, 112040. doi:10.1016/j.envres.2021.112040

Dong, H., Qiang, Z., and Richardson, S. D. (2019). Formation of iodinated disinfection byproducts (I-DBPs) in drinking water: emerging concerns and current issues. *Acc. Chem. Res.* 52 (4), 896–905. doi:10.1021/acs.accounts.8b00641

Dunce, J. M., Dunne, O. M., Ratcliff, M., Millán, C., Madgwick, S., Usón, I., et al. (2018). Structural basis of meiotic chromosome synapsis through SYCP1 self-assembly. *Nat. Struct. Mol. Biol.* 25 (7), 557–569. doi:10.1038/s41594-018-0078-9

Ebnet, K. (2017). Junctional adhesion molecules (JAMs): cell adhesion receptors with pleiotropic functions in cell physiology and development. *Physiol. Rev.* 97 (4), 1529–1554. doi:10.1152/physrev.00004.2017

Escobar-Hoyos, L. F., Hoyos-Giraldo, L. S., Londoño-Velasco, E., Reyes-Carvajal, I., Saavedra-Trujillo, D., Carvajal-Varona, S., et al. (2013). Genotoxic and clastogenic effects of monohaloacetic acid drinking water disinfection by-products in primary human lymphocytes. *Water Res.* 47 (10), 3282–3290. doi:10.1016/j.watres.2013.02.052

Gonsioroski, A., Meling, D. D., Gao, L., Plewa, M. J., and Flaws, J. A. (2021). Iodoacetic acid affects estrous cyclicity, ovarian gene expression, and hormone levels in mice. *Biol. Reprod.* 105 (4), 1030–1042. doi:10.1093/biolre/ioab108

Gonsioroski, A., Meling, D. D., Gao, L., Plewa, M. J., and Flaws, J. A. (2020). Iodoacetic acid inhibits follicle growth and alters expression of genes that regulate apoptosis, the cell cycle, estrogen receptors, and ovarian steroidogenesis in mouse ovarian follicles. *Reprod. Toxicol.* 91, 101–108. doi:10.1016/j.reprotox.2019.10.005

Gonsioroski, A., Mourikes, V. E., and Flaws, J. A. (2020). Endocrine disruptors in water and their effects on the reproductive system. *Int. J. Mol. Sci.* 21 (6), 1929. doi:10.3390/ijms21061929

Gonzalez, R. V. L., Weis, K. E., Gonsioroski, A. V., Flaws, J. A., and Raetzman, L. T. (2021). Iodoacetic acid, a water disinfection byproduct, disrupts hypothalamic, and pituitary reproductive regulatory factors and induces toxicity in the female pituitary. *Toxicol. Sci.* 184 (1), 46–56. doi:10.1093/toxsci/kfab106

Gou, L. T., Kang, J. Y., Dai, P., Wang, X., Li, F., Zhao, S., et al. (2017). Ubiquitination-deficient mutations in human Piwi cause male infertility by impairing histone-to-protamine exchange during spermiogenesis. *Cell* 169 (6), 1090–1104. doi:10.1016/j.cell.2017.04.034

Guo, H., Ouyang, Y., Wang, J., Cui, H., Deng, H., Zhong, X., et al. (2021). Cu-induced spermatogenesis disease is related to oxidative stress-mediated germ cell apoptosis and DNA damage. *J. Hazard. Mat.* 416, 125903. doi:10.1016/j.jhazmat.2021.125903

Gupta, A., Mandal, K., Singh, P., Sarkar, R., and Majumdar, S. S. (2021). Declining levels of miR-382-3p at puberty trigger the onset of spermatogenesis. *Mol. Ther. Nucleic Acids* 26, 192–207. doi:10.1016/j.omtn.2021.07.001

Gustafson, E. A., Seymour, K. A., Sigrist, K., Rooij, D. G. D. E., and Freiman, R. N. (2020). ZFP628 is a TAF4b-interacting transcription factor required for mouse spermiogenesis. *Mol. Cell. Biol.* 40 (7), e00228–19. doi:10.1128/MCB.00228-19

Hall, D. R., Yeung, K., and Peng, H. (2020). Monohaloacetic acids and monohaloacetamides attack distinct cellular proteome thiols. *Environ. Sci. Technol.* 54 (23), 15191–15201. doi:10.1021/acs.est.0c03144

He, J., Chu, Z., Lai, W., Lan, Q., Zeng, Y., Lu, D., et al. (2021). Circular RNA circHERC4 as a novel oncogenic driver to promote tumor metastasis via the miR-556-5p/CTBP2/E-cadherin axis in colorectal cancer. *J. Hematol. Oncol.* 14 (1), 194. doi:10.1186/s13045-021-01210-2

Holota, H., Thirouard, L., Monrose, M., Garcia, M., De Haze, A., Saru, J. P., et al. (2020). FXRα modulates leydig cell endocrine function in mouse. *Mol. Cell. Endocrinol.* 518, 110995. doi:10.1016/j.mce.2020.110995

Jeong, C. H., Gao, L., Dettro, T., Wagner, E. D., Ricke, W. A., Plewa, M. J., et al. (2016). Monohaloacetic acid drinking water disinfection by-products inhibit follicle growth and steroidogenesis in mouse ovarian antral follicles *in vitro*. *Reprod. Toxicol.* 62, 71–76. doi:10.1016/j.reprotox.2016.04.028

Kahn, L. G., Philippat, C., Nakayama, S. F., Slama, R., and Trasande, L. (2020). Endocrine-disrupting chemicals: Implications for human health. *Lancet Diabetes Endocrinol.* 8 (8), 703–718. doi:10.1016/S2213-8587(20)30129-7

Kali, S., Khan, M., Ghaffar, M. S., Rasheed, S., Waseem, A., Iqbal, M. M., et al. (2021). Occurrence, influencing factors, toxicity, regulations, and abatement approaches for disinfection by-products in chlorinated drinking water: a comprehensive review. *Environ. Pollut.* 281, 116950. doi:10.1016/j.envpol.2021.116950

Kassotis, C. D., Vandenberg, L. N., Demeneix, B. A., Porta, M., Slama, R., and Trasande, L. (2020). Endocrine-disrupting chemicals: economic, regulatory, and policy implications. *Lancet. Diabetes Endocrinol.* 8 (8), 719–730. doi:10.1016/S2213-8587(20)30128-5

Kim, D. H., Park, C. G., and Kim, Y. J. (2020). Characterizing the potential estrogenic and androgenic activities of two disinfection byproducts, monohaloacetic acids and haloacetamides, using *in vitro* bioassays. *Chemosphere* 242, 125198. doi:10.1016/j.chemosphere.2019.125198

La Merrill, M. A., Vandenberg, L. N., Smith, M. T., Goodson, W., Browne, P., Patisaul, H. B., et al. (2020). Consensus on the key characteristics of endocrine-disrupting chemicals as a basis for hazard identification. *Nat. Rev. Endocrinol.* 16 (1), 45–57. doi:10.1038/s41574-019-0273-8

Lei, W. L., Li, Y. Y., Meng, T. G., Ning, Y., Sun, S. M., Zhang, C. H., et al. (2021). Specific deletion of protein phosphatase 6 catalytic subunit in Sertoli cells leads to disruption of spermatogenesis. *Cell Death Dis.* 12 (10), 883. doi:10.1038/s41419-021-04172-y

Li, H., Liang, Z., Yang, J., Wang, D., Wang, H., Zhu, M., et al. (2019). DAZL is a master translational regulator of murine spermatogenesis. *Natl. Sci. Rev.* 6 (3), 455–468. doi:10.1093/nsr/nwy163

Liang, J., Wang, N., He, J., Du, J., Guo, Y., Li, L., et al. (2019). Induction of Sertoli-like cells from human fibroblasts by NR5A1 and GATA4. *Elife* 8, e48767. doi:10.7554/eLife.48767

Lin, Z., Hsu, P. J., Xing, X., Fang, J., Lu, Z., Zou, Q., et al. (2017). Mettl3-/Mettl14-mediated mRNA N6-methyladenosine modulates murine spermatogenesis. *Cell Res.* 27 (10), 1216–1230. doi:10.1038/cr.2017.117

Lombó, M., and Herráez, P. (2021). The effects of endocrine disruptors on the male germline: an intergenerational health risk. *Biol. Rev. Camb. Philos. Soc.* 96 (4), 1243–1262. doi:10.1111/brv.12701

Long, K., Sha, Y., Mo, Y., Wei, S., Wu, H., Lu, D., et al. (2021). Androgenic and teratogenic effects of iodoacetic acid drinking water disinfection byproduct *in vitro* and *in vivo*. *Environ. Sci. Technol.* 55 (6), 3827–3835. doi:10.1021/acs.est.0c06620

Mäkelä, J. A., Koskenniemi, J. J., Virtanen, H. E., and Toppari, J. (2019). Testis development. *Endocr. Rev.* 40 (4), 857–905. doi:10.1210/er.2018-00140

Mao, A. P., Ishizuka, I. E., Kasal, D. N., Mandal, M., and Bendelac, A. (2017). A shared Runx1-bound Zbtb16 enhancer directs innate and innate-like lymphoid lineage development. *Nat. Commun.* 8 (1), 863. doi:10.1038/s41467-017-01780-1

Otani, T., Nguyen, T. P., Tokuda, S., Sugihara, K., Sugawara, T., Furuse, K., et al. (2019). Claudins and JAM-A coordinately regulate tight junction formation and epithelial polarity. *J. Cell Biol.* 218 (10), 3372–3396. doi:10.1083/jcb.201812157

She, J., Feng, N., Zheng, W., Zheng, H., Cai, P., Zou, H., et al. (2021). Zearalenone exposure disrupts blood-testis barrier integrity through excessive Ca2+-mediated autophagy. *Toxins* 13 (12), 875. doi:10.3390/toxins13120875

Shen, W. J., Azhar, S., and Kraemer, F. B. (2018). SR-B1: a unique multifunctional receptor for cholesterol influx and efflux. *Annu. Rev. Physiol.* 80, 95–116. doi:10.1146/annurev-physiol-021317-121550

Sun, S., Jiang, Y., Zhang, Q., Pan, H., Li, X., Yang, L., et al. (2022). Znhit1 controls meiotic initiation in male germ cells by coordinating with Stra8 to activate meiotic gene expression. *Dev. Cell* 57 (7), 901–913. e4. doi:10.1016/j.devcel.2022.03.006

Verón, G. L., Veiga, M. F., Cameo, M., Marín-Briggiler, C. I., and Vazquez-Levin, M. H. (2021). Epithelial and neural cadherin in mammalian fertilization: studies in the mouse model. *Cells* 11 (1), 102. doi:10.3390/cells11010102

Wang, J., Jia, R., Zheng, X., Sun, Z., Liu, R., and Zong, W. (2018). Drinking water disinfection byproduct iodoacetic acid interacts with catalase and induces cytotoxicity in mouse primary hepatocytes. *Chemosphere* 210, 824–830. doi:10.1016/j.chemosphere.2018.07.061

Wang, W., Peng, M., Yuan, H., Liu, C., Zhang, Y., Fang, Y., et al. (2022). Studying the mechanism of sperm DNA damage caused by folate deficiency. *J. Cell. Mol. Med.* 26 (3), 776–788. doi:10.1111/jcmm.17119

Wei, X., Wang, S., Zheng, W., Wang, X., Liu, X., Jiang, S., et al. (2013). Drinking water disinfection byproduct iodoacetic acid induces tumorigenic transformation of NIH3T3 cells. *Environ. Sci. Technol.* 47 (11), 5913–5920. doi:10.1021/es304786b

Xia, Y., Mo, Y., Yang, Q., Yu, Y., Jiang, M., Wei, S., et al. (2018). Iodoacetic acid disrupting the thyroid endocrine system *in vitro* and *in vivo*. *Environ. Sci. Technol.* 52 (13), 7545–7552. doi:10.1021/acs.est.8b01802

Yu, S., Zhou, C., He, J., Yao, Z., Huang, X., Rong, B., et al. (2022). BMP4 drives primed to naïve transition through PGC-like state. *Nat. Commun.* 13 (1), 2756. doi:10.1038/s41467-022-30325-4

Zhang, X. Y., Wang, B., Xu, S., Wang, J., Gao, L., Song, Y. P., et al. (2021). Reactive oxygen species-evoked genotoxic stress mediates arsenic-induced suppression of male germ cell proliferation and decline in sperm quality. *J. Hazard. Mat.* 406, 124768. doi:10.1016/j.jhazmat.2020.124768

Zhao, J., Lu, P., Wan, C., Huang, Y., Cui, M., Yang, X., et al. (2021). Cell-fate transition and determination analysis of mouse male germ cells throughout development. *Nat. Commun.* 12 (1), 6839. doi:10.1038/s41467-021-27172-0

Zhao, L., Zhang, J., Yang, L., Zhang, H., Zhang, Y., Gao, D., et al. (2021). Glyphosate exposure attenuates testosterone synthesis via NR1D1 inhibition of StAR expression in mouse Leydig cells. *Sci. Total Environ.* 785, 147323. doi:10.1016/j.scitotenv.2021.147323

frontiers | Frontiers in Pharmacology

TYPE Original Research
PUBLISHED 09 September 2022
DOI 10.3389/fphar.2022.986456

Check for updates

OPEN ACCESS

EDITED BY
Ahmed A. Al-Karmalawy,
Horus University, Egypt

REVIEWED BY
Osama G. Mohamed,
University of Michigan, United States
Wagdy Mohamed Eldehna,
Kafrelsheikh University, Egypt

*CORRESPONDENCE
Jing Bo Li,
lijb_003@163.com

SPECIALTY SECTION
This article was submitted to Predictive Toxicology,
a section of the journal
Frontiers in Pharmacology

RECEIVED 05 July 2022
ACCEPTED 15 August 2022
PUBLISHED 09 September 2022

CITATION
Hussain S, Liufang H, Shah SM, Ali F, Khan SA, Shah FA, Li JB and Li S (2022), Cytotoxic effects of extracts and isolated compounds from Ifloga spicata (forssk.) sch. bip against HepG-2 cancer cell line: Supported by ADMET analysis and molecular docking.
Front. Pharmacol. 13:986456.
doi: 10.3389/fphar.2022.986456

COPYRIGHT
© 2022 Hussain, Liufang, Shah, Ali, Khan, Shah, Li and Li. This is an open-access article distributed under the terms of the Creative Commons Attribution License (CC BY). The use, distribution or reproduction in other forums is permitted, provided the original author(s) and the copyright owner(s) are credited and that the original publication in this journal is cited, in accordance with accepted academic practice. No use, distribution or reproduction is permitted which does not comply with these terms.

Cytotoxic effects of extracts and isolated compounds from *Ifloga spicata* (forssk.) sch. bip against HepG-2 cancer cell line: Supported by ADMET analysis and molecular docking

Sajid Hussain[1], He Liufang[2], Syed Majid Shah[1], Fawad Ali[1], Saeed Ahmad Khan[1], Fawad Ali Shah[3], Jing Bo Li[4]* and Shupeng Li[5]

[1]Department of Pharmacy, Kohat University of Science and Technology, Kohat, Pakistan, [2]Pediatrics Department, Shenzhen University General Hospital, Shenzhen University, Shenzhen, China, [3]Riphah Institute of Pharmaceutical Sciences, Riphah International University, Islamabad, Pakistan, [4]Shenzhen University Clinical Research Center for Neurological Diseases, Health Management Center, Shenzhen University General Hospital, Shenzhen University Clinical Medical Academy, Shenzhen University, Shenzhen, China, [5]State Key Laboratory of Oncogenomics, School of Chemical Biology and Biotechnology, Shenzhen Graduate School, Peking University, Shenzhen, China

The purpose of this study was to determine the anticancer potential of *Ifloga spicata* (*I. spicata*) against HepG-2 cell line. To assess *I. spicata* cytoxicity, brine shrimp lethality and MTT assays were performed. In the brine shrimp bioassay, the ethyl acetate fraction had a significant impact with an IC_{50} of 10 µg/ml. The ethyl acetate and chloroform fractions inhibited HepG-2 cell line effectively (IC_{50} values 5.54 and 6.52 µg/ml, respectively). The isolated compound, heptadecyl benzoate inhibited growth significantly (IC_{50}, 8.92 µg/ml) while methyl dihydroxybenzoate had modest activity (25.66 µg/ml) against the cell line. Both compounds displayed acceptable pharmacokinetic parameters in the ADME study. In the docking study, the methyl dihydroxybenzoate was involved in two hydrogen bonds with two different residues Thr830 and Asp831. The heptadecyl benzoate carbonyl oxygen exhibited a single hydrogen bond with Lys692. Both showed good interactions with the active site of the (EGFR) tyrosine kinase. Our findings suggest that *I. spicata* might be a viable source of anticancer natural agents. This discovery raises the prospect of the future development of a new medication for the treatment of liver cancer.

KEYWORDS

Ifloga spicata, brine shrimp lethality, MTT assay, tyrosine kinase, molecular docking

Introduction

Cancer is the world's second greatest cause of mortality, after cardiovascular illnesses, with approximately 10 million deaths in 2020 (Sung et al., 2021). Despite recent advancements in cancer therapy, this figure is anticipated to double in the next 10 years (N'guessan et al., 2021; Ferlay et al., 2019). Liver cancer is the principal reason of death associated with cancer across the globe. Liver cancer is the 5th and 9th most common cancer among men and females, respectively, and the 2nd cause of mortality across the globe (Ferlay et al., 2015). According to the published data, the annual number of reported cases of liver cancer is 600,000–800,000, accounting for about 5.6% of all cancers. It was also expected that the number of cases will be about 100,0000 by 2030 (Alqahtani et al., 2019).

Medicinal herbs have a long history of being used to cure a variety of illnesses, including cancer (Khan et al., 2019; Xiao et al., 2020). More than 60% of cancer medications, such as doxorubicin and bleomycin, are derived from natural sources, such as plants and microbes (Cragg and Newman, 2005). Many plant-derived natural agents have potential value as chemotherapeutic agents (Pezzuto, 1997). Several useful anticancer agents in clinical use are obtained from plants like vinblastine and vincristine obtained from *C. roseus,* etoposide from lignans of Podophyllum spp, paclitaxel isolated from the bark of the Pacific yew and camptothecin derivatives, like topotecan, isolated from *Camptotheca acuminate* (Newman et al., 2003; Basili and Moro, 2009).

Tyrosine kinases (TKs) are useful in the development of cancer-targeting drugs (Paul and Mukhopadhyay, 2004). For both external and internal stimuli, TKs are required for several biological operations like apoptosis, growth and migration, differentiation, and metabolism (Vlahovic and Crawford, 2003). TKs are enzymes that start the phosphorylation process for certain tyrosine residues with the help of ATP. Following biosynthesis, protein covalent and enzymatic modification is a crucial aspect of maintaining normal cellular communication and homeostasis (Hussain et al., 2019).

I. spicata is an annual herb used to treat skin problems and heart disorders (Abouri et al., 2012). *I. spicata* has been shown to have anti-leishmanial properties. Furthermore, the anticancer activity of *I. spicata* against lung cancer has been scientifically proven. (Shah et al., 2019a; Shah et al., 2019b). The current study aimed to evaluate the pharmacokinetic profile, tyrosine kinase receptor sensitivity and the anticancer effects of fractions and isolated compounds of *I. spicata* using brine shrimp lethality and MTT assays.

Materials and methods

Chemicals and equipment

The extraction solvents (ethyl acetate, chloroform, *n-hexane*, and methanol) were acquired from Daejung Korea. Sigma Chemicals Co. MTT dye and dimethyl sulfoxide were obtained from Sigma Chemicals Co. (St. Louis, United States). The standards etoposide (Cas number 33419-42-0) and doxorubicin (Cas number 25316-40-9) were purchased from Merck. Silica gel 60 F254 cards was purchased from Merck. Silica. gel, 70–230 mesh, obtained from Scharlau, Spain. ELISA reader (ELx800 BioTek) and Rota vapour 210 were used for recording the absorbance and concentrating the fractions respectively.

Preparation of crude extract and its subsequent fractions

The *I. spicata* was collected from District, Karak, Khyber Pakhtunkhwa, Pakistan in the month of April 2016. The plant material was identified by taxonomist Dr. Waheed Murad, Department of Botany, Kohat university of science and technology, Kohat. A voucher specimen with catalog no KUH-1002 was deposited in the herbarium of the Department of Botany, Kohat University of Science and Technology, Kohat. The plant material was shade-dried and crushed into coarse powder after being collected. The plant's coarse powder was macerated in methanol for 15 days after being shade dried. By using rotary evaporator, the filtrate was concentrated to get methanol extract. The methanolic extract of 500 g was dispersed in distilled water and sequentially extracted with organic solvents. *n-hexane*, chloroform, and ethyl acetate to get polarity-based fractions. All fractions were kept in the refrigerator until they were utilized in experiments.

Isolation scheme

The most bioactive ethyl acetate-soluble fraction was analyzed using column chromatography with a mobile phase of *n-hexane*/ethyl acetate and a stationary phase of flash silica gel. Column chromatography was performed with the help of a column (4.6 mm internal diameter and 30 cm in length). for the most bioactive ethyl acetate-soluble fraction using a mixture of n-*hexane*/ethyl acetate [Daejung CAS No.110-54-3, (Daejung CAS No.141-78-6)] as the mobile phase, and flash silica gel (230–400 mesh) as the stationary phase and eluted two sub fractions. The two eluted sub fractions were subject to repeated column chromatography using a pencil column (3.9 × 15). Methyl dihydroxybenzoate (15 mg) was obtained from fraction 1 using mobile phase n-hexane/ethyl acetate in the ratio 90:10, and Heptadecyl benzoate (12 mg) from fraction 2 using n-hexane/ethyl acetate in the ratio 94:6. Aluminum sheets precoated with silica gel 60 F2s4 (20 cm, 0.2 mm thick; E-Merck) were used for TLC and visualization of the TLC plates was carried out under UV at 254 and 366 nm and also by spraying ceric sulphate reagent with heating. Various

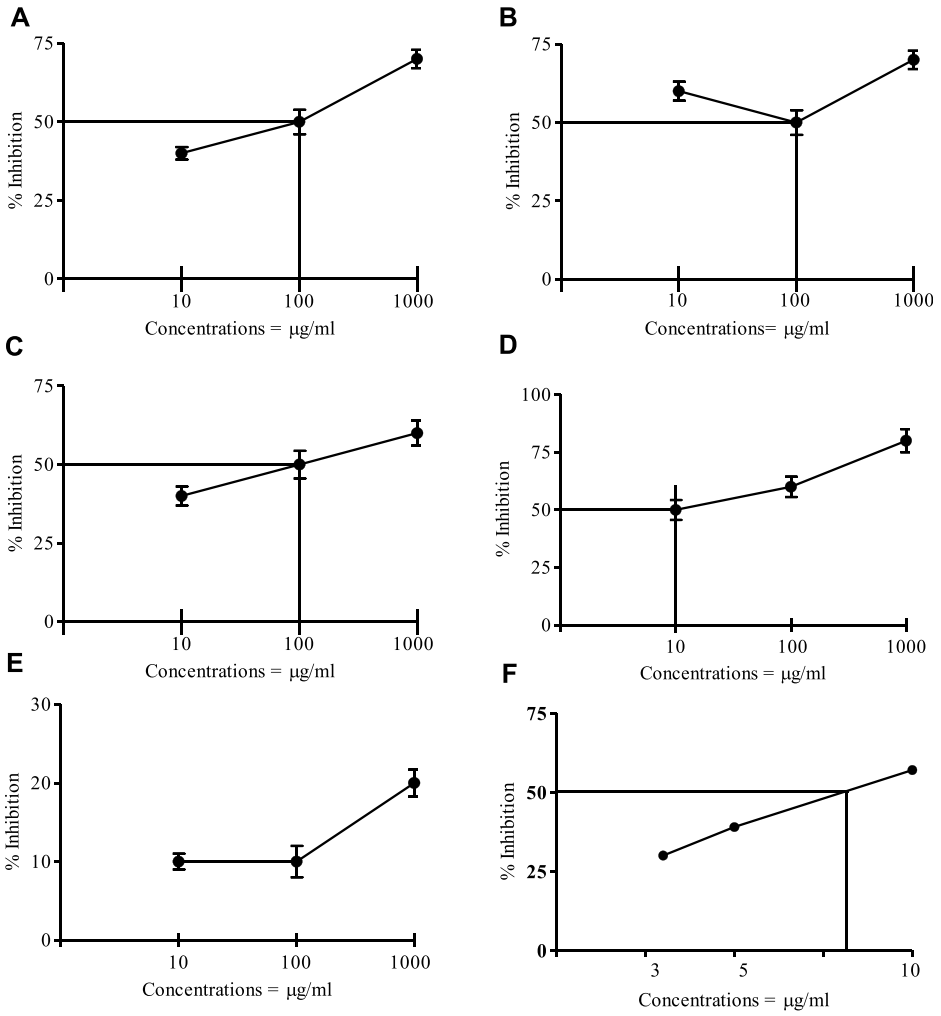

FIGURE 1
Brine shrimp cytotoxic effect of the crude and fractions of *I. spicata* at various Concentrations. **(A)** = Crude drug, **(B)** = Hexane fraction; **(C)** = Chloroform fraction; **(D)** = Ethyl acetate fraction; **(E)** = Water fraction; **(F)** = Etoposide, IC_{50} = 7.35 µg/ml. Data are mean ±SEM of three independent readings).

spectroscopic methods, such as ^{1}H and ^{13}C techniques, including homonuclear (COSY) and heteronuclear correlation tests (HSQC and HMBC), as well as a literature survey, were used to confirm the structure of the compounds (http://www.mdpi.com/2227-9717/7/4/208/s1) as previously published (Shah et al., 2019c).

Brine shrimp lethality assay

This assay was used to assess the toxicity of *I. spicata* crude extract and its subsequent fractions to brine shrimp. Brine shrimp eggs were hatched in a beaker containing seawater. Plant samples were dissolved in DMSO (Meyer et al., 1982; Mohtasheem et al., 2001). Plant extracts at a concentration range of 10–1000 µg/ml were used in the lethality assay. 30 live shrimps were added to each container containing 5 ml of simulated seawater (composition: sea salt 38 g/L of DW having pH 7.4). 100 µL of each plant extract was added to containers and incubated for 24 h. After incubation, the shrimps that survived were counted in each container. As a standard, etoposide (1000, 100. 10 µg/ml) was utilized. The negative control was DMSO. The percentage mortality of plant samples was calculated. The IC_{50} value for each extract of *I. spicata* was determined.

Cell culture

Cancer cells (HepG-2) were obtained from the National Centre of Excellence in Molecular Biology at the University of

TABLE 1 *I. spicata* fractions and compounds cytotoxicity against HepG-2 cell line.

Plant samples	Concentration (μg/ml)	Percent inhibition against HepG-2 cell lin	IC_{50} (μg/ml) against HepG-2 cell line
Crude extract	200	86.6 ± 1.1	17.82
	100	76.7 ± 1,2	
	50	65.2 ± 0.9	
	25	57.7 ± 0.6	
	12.5	44.6 ± 0.5	
	6.25	31.7 ± 0.8	
n-Hexane	200	77.7 ± 0.5	27.62
	100	72.4 ± 0.3	
	50	60.3 ± 0.3	
	25	50.8 ± 0.2	
	12.5	35.9 ± 0.2	
	6.25	25.5 ± 0.2	
Chloroform	200	81.5 ± 1.0	6.52
	100	78.8 ± 0.5	
	50	71.6 ± 0.9	
	25	69.6 ± 0.6	
	12.5	60.3 ± 0.7	
	6.25	44.5 ± 1.2	
Ethyl acetate	200	91.7 ± 0.5	5.54
	100	84.5 ± 0.6	
	50	75.7 ± 0.9	
	25	70.6 ± 0.2	
	12.5	61.7 ± 0.9	
	6.25	52.7 ± 0.6	
Aqueous	200	60.7 ± 0.4	71.81
	100	54.5 ± 0.2	
	50	46.7 ± 0.6	
	25	38.7 ± 0.9	
	12.5	30.9 ± 0.5	
	6.25	17.9 ± 0.4	
Methyl dihydroxybenzoate	200	78.6 ± 1.1	25.66
	100	69.9 ± 0.9	
	50	59.6 ± 0.7	
	25	49.8 ± 0.9	
	12.5	42.6 ± 0.4	
	6.25	26.5 ± 1.1	
Heptadecyl benzoate	200	89.6 ± 0.9	8.92
	100	78.5 ±0.3	
	50	69.5 ± 0,7	
	25	64.4 ± 0.9	
	12.5	53.4 ± 0.6	
	6.25	47.7 ± 0.3	

(Continued on following page)

TABLE 1 (*Continued*) *I. spicata* fractions and compounds cytotoxicity against HepG-2 cell line.

Plant samples	Concentration (μg/ml)	Percent inhibition against HepG-2 cell lin	IC_{50} (μg/ml) against HepG-2 cell line
Doxorubicin	200	90.1 ± 0.2	1.25
	100	84.4 ± 0.4	
	50	79.6 ± 0.3	
	25	74.8 ± 0.4	
	12.5	70.3 ± 0.3	
DMSO	0 μg/ml	NA	NA

Data are represented as mean ± S.E.M of three independent readings (n = 3). The reference standard, Doxorubicin, IC_{50} = 1.25 μg/ml. NA, Not active.

Punjab in Pakistan. Cancer and normal cells (Vero) were nurtured in DMEM. The cultured cells were preserved until they were utilized in research.

Cytotoxicity assay

The cytotoxicity of plant fractions and the compounds was determined by using a 3-(4,5-Dimethylthiazol)-diphenyl tetrazolium bromide (MTT) assay (Mosmann, 1983; Khorrami et al., 2018). The normal Vero and HepG2 cell lines were cultured in DMEM containing antibiotics (streptomycin/penicillin) and nutrients 10% fetal bovine serum. The normal and cancer cells were incubated in a CO_2 incubator for 24 h at 37°C. Both the cell lines were treated with different concentrations in a range of 6.25–200 μg/ml with the extracts and compounds and incubated for a further 1 day. Doxorubicin in a concentration range of 6.25–200 μg/ml and under same experimental conditions was used as standard. DMSO was used as negative control in this MTT assay. A 100 μL of MTT reagent (5 mg/ml in phosphate buffer saline) is added to each well and incubated for 4 h at 37°C in a 5% CO_2 atmosphere. Absorbance was measured at 570 nm using an ELISA reader. By using the following formula, the percentage of cytotoxicity was determined:

Cell viability % = absorbance of treated cells/absorbance of control cells × 100.

The experiments were done in triplicates. The IC_{50} values were calculated for each plant sample.

ADMET analysis

Swiss-ADME (http://www.swissadme.ch/index.php) tool was used for ADMET analysis (Absorption, distribution, metabolism, excretion and Toxicity) (DeLano, 2002). The ADMET analysis is considered too important for a molecule to be considered a drug candidate (Hassan et al., 2022). The pharmacokinetic scores of compounds were measured using the online database pkCSM (http://biosig.unimelb.edu.au/pkcsm/prediction).

Molecular docking study

The MOE-2016 software was used for the docking study of compounds 1 and 2 against the target enzyme, Epidermal Growth Factor Receptor (EGFR) tyrosine kinase domain (EC 2.7.10.1) having PDB ID: 1M17. The 3D structures of compounds and target enzymes were built and the energy of compounds was minimized up to 0.05 gradient using MMFF 94s forcefield (Mphahlele et al., 2017).

By using the Triangular Matching docking method, 10 different conformations for each compound were generated based on the binding of compounds with the active sites of receptor and binding energies were determined. The molecular interactions of ligand-protein complexes were noted. By using LigPlot 3D images were drawn.

Results

Brine shrimp lethality bioassay

Figure 1 represents the cytotoxicity of *I. spicata* crude and resulting fractions. The ethyl acetate component of the plant displayed a promising impact with an IC_{50} of 10 μg/ml. When compared to the control medication, etoposide, the mortality effects of crude extract, *n-hexane*, and chloro-form fractions were modest. The aqueous fraction was inactive.

In vitro cytotoxicity

An MTT assay was used to assess the cytotoxic activity of *I. spicata* extracts and isolated components. Table 1 summarizes the findings of the experiment. The ethyl acetate and chloroform fractions were regarded as the most potent fractions, with IC_{50} values of 5.54 and 6.52 μg/ml, respectively. The results indicated that the crude extract and *n-hexane* inhibited the cancer cell line effectively. In comparison to other plant fractions, the

TABLE 2 Physicochemical and lipophilicity properties of methyl dihydroxybenzoate and heptadecyl benzoate.

Properties	Parameters	Methyl dihydroxybenzoate	Heptadecyl benzoate
Physicochemical properties	MW[a] (g/mol)	152.15	360.57
	Rotatable bonds	2	18
	HBA[b]	3	2
	HBD[c]	1	0
	Fraction Csp3	0.12	0.71
	TPSA[d]	46.53	26.30
Lipophilicity Log $P_{o/w}$	iLOGP	1.63	5.68
	XLOGP3	1.96	10.58
	MLOGP	1.32	5.98
	Consensus	1.46	7.60

[a]Molecular weight
[b]Hydrogen bond acceptor
[c]Hydrogen bond donor
[d]Typological polar surface area

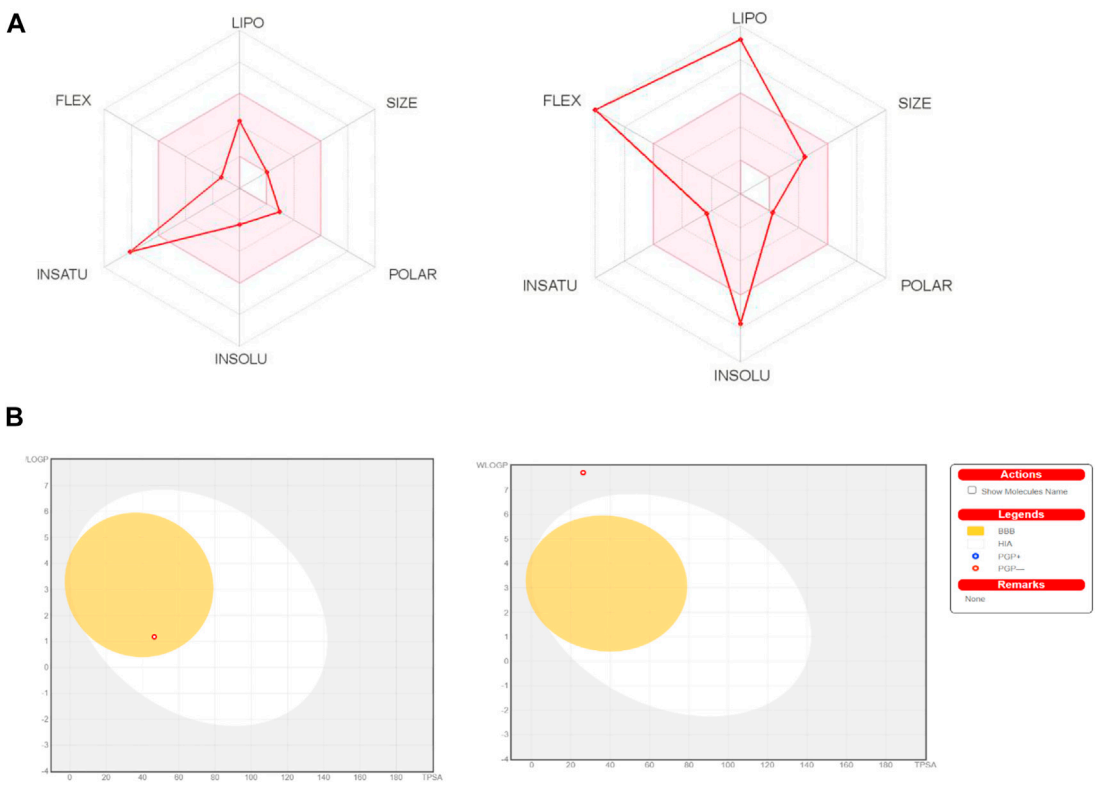

FIGURE 2
(A) Bioavailability radar chart for methyl dihydroxybenzoate and heptadecyl benzoate respectively. **(B)** Predicted BOILED-Egg plot from *swiss ADME* online web tool for methyl dihydroxybenzoate and heptadecyl benzoate respectively.

aqueous fraction's anticancer efficacy was modest. A significant inhibition of growth was recorded for heptadecyl benzoate with an IC_{50} value of 8.92 µg/ml. The plant extracts and compounds did show any inhibitory effect against the normal Vero cell line. The methyl dihydroxybenzoate had moderate anticancer activity.

TABLE 3 Predicted pharmacokinetics parameters of methyl dihydroxybenzoate and heptadecyl benzoate.

Properties	Parameters	Methyl dihydroxybenzoate	Heptadecyl benzoate
Absorption	Water solubility (log S(ESOL))	−1.695	−7.329
	GI[a] (gastrointestinal absorption)	High	Low
	Skin Permeability cm/s	−2.342	−2.676
	P-glycoprotein substrate	No	No
Distribution	VDss (volume of distribution at steady state, (human)	−0.165	0.677
	Fraction unbound (human)	0.448	0
	BBB permeability	Yes	No
	CNS permeability (Log PS)	−2.072	−1.152
	CYP1A2 inhibitor	Yes	Yes
	CYP2C19 inhibitor	No	Yes
	CYP2C9 inhibitor	No	No
	CYP2D6 inhibitor	No	No
	CYP3A4 inhibitior	No	No
Excretion	Total Clearance (log ml/min/kg)	0.73	1.95
	Renal OCT2 substrate	No	No

TABLE 4 Toxicity profile of methyl dihydroxybenzoate and heptadecyl benzoate.

Parameters	Methyl dihydroxybenzoate	Heptadecyl benzoate
AMES toxicity	No	No
Max. tolerated dose (human) (log mg/kg/day)	1.215	0.796
hERG I inhibitor	No	No
hERG II inhibitor	No	Yes
Oral Rat Toxicity (LD50) (mg/kg)	2.793	3.362
Hepatotoxicity	No	No
Skin Sensitization	No	Yes

ADMET analysis (pharmacokinetic and toxicological properties)

The physicochemical properties of the compounds are mentioned in Table 2. The physicochemical features were investigated and classified into six broad groups based on their oral bioavailability ranges. Both compounds' results are within the acceptable ranges.

The chemical absorption from the gastrointestinal absorption region (GI[a]) and the blood brain barrier (BBB) permeation are shown in the BOILED-EGG graph. Methyl dihydroxybenzoate has higher oral bioavailability, as seen in Figure 2A of the Bioavailability Radar Chart. Figure 2B shows that methyl dihydroxybenzoate is in the white zone, while heptadecyl benzoate is in the grey zone. Methyl dihydroxybenzoate had a high GI[a] and BBB permeability (Table 3), but heptadecyl benzoate had a low GI[a] and no BBB permeation. Methyl dihydroxybenzoate inhibits CYP1A2, whereas the heptadecyl benzoate inhibits two isoforms, CYP1A2 and CYP2C19, resulting in considerable pharmacological interaction with the substrates of these two isoforms. The clearance value for methyl dihydroxybenzoate was insufficient. Both compounds appear to be non-substrates of Organic Cation Transporter 2 (OCT2), and their interaction with an OCT2 inhibitor promotes unfavorable interactions Table 3.

Furthermore, the online database pKCSM was used to examine the toxicity profile of methyl dihydroxybenzoate and heptadecyl benzoate (Table 4). Methyl dihydroxybenzoate had a greater maximum tolerated dose (MTD) than heptadecyl benzoate. The MTD is a unit of measurement for a chemical's toxic dose threshold in humans. Both compounds did not reduce hERG I, however, only heptadecyl benzoate inhibited hERG II, according to our findings. Skin hypersensitive reaction is a possible adverse effect of the chemical, and heptadecyl benzoate has demonstrated skin allergies. Furthermore, both

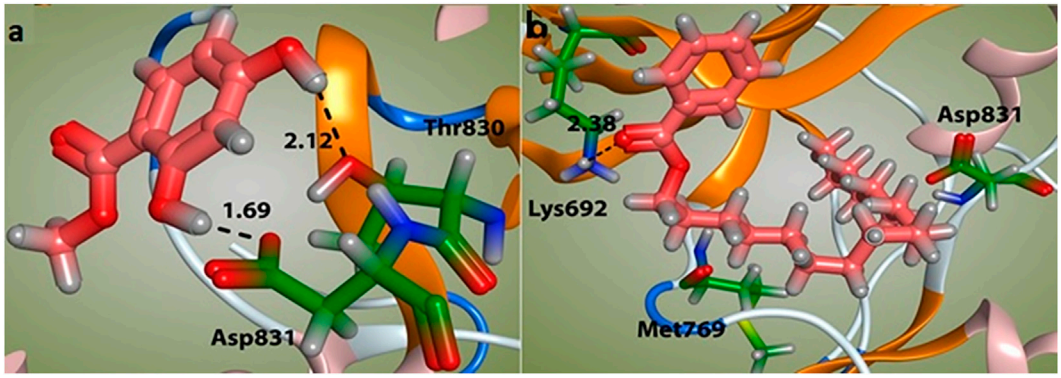

FIGURE 3
Binding mode of compounds methyl dihydroxybenzoate **(A)** and heptadecyl benzoate **(B)** with the target enzyme, (EGFR) tyrosine kinase. The ligands are shown as pink and residues as green.

TABLE 5 The structure and Lipinski's properties of ligands.

S.No	Compound	Structure	Properties
1	Methyl 2,4-dihydroxybenzoate	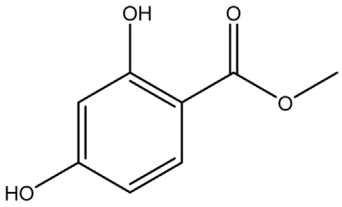	MW 168.15 g/mol, LogP 0.92, Don 2, Acc 3
2	Heptadecyl benzoate	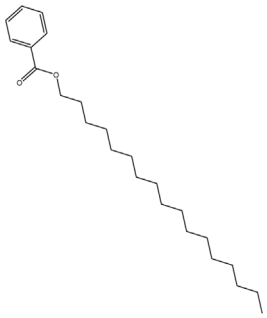	MW 360.58 g/mol, LogP 9.49, Don 0, Acc 1

substances have a low score level for calculating fatal dose (LD_{50}), i.e., 2.793 mg/kg and 3.362 mg/kg, and were classified as class 1.

Compound-target enzyme interactions

The docking study was conducted to investigate the binding poses of isolated compounds from *I. Spicta* in the active site of (EGFR) tyrosine kinase. The compounds fit best in the active site and have favorable interactions with the active site residues. The methyl dihydroxybenzoate was involved in two hydrogen bonds with two different residues Thr830 and Asp831. The heptadecyl benzoate carbonyl oxygen shows a single hydrogen bond with Lys692. The interactions shown by the compounds may be due to the presence of hydrogen bond donor and hydrogen bond acceptor groups. Figure 3 shows compound 3D interactions with (EGFR) tyrosine kinase active site residues. The drug-likeness properties, binding energies,

TABLE 6 Docking score, binding energies and Predicted interactions of compounds.

S.No	Docking score	Binding energy	Binding affinity	Interaction of compounds with the receptor
1	−4.759	−26.51	−5.07	Ligand Receptor Interaction Distance O 10 OG1 THR 830 H-donor 2.12 O 12 OD2 ASP 831 H-donor 1.69
2	−5.801	−33.45	−6.4	Ligand Receptor Interaction Distance O 63 NZ LYS 692 H-acceptor 2.38

docking score and interaction detail of compounds are summarized in Tables 5, 6.

Discussion

The brine shrimp lethality test is a commonly used bioassay for preliminary screening in the discovery of anticancer medicines (Ullah et al., 2013). The ethyl acetate exhibited a marked effect with IC_{50} of 10 µg/ml. In comparison to standard etoposide, crude extract, *n-hexane*, and chloroform fractions had a mild impact. For the aqueous fraction, no impact was seen. It demonstrates that cytotoxic plant components are higher concentrated in the ethyl acetate fraction. The cytotoxic effect of the plant organic fractions might be due to the active constituents present in the plant extracts Therefore, the cytotoxic effects of the tested samples indicate that they can be selected for further study against human cancer cell lines (Manilal et al., 2009). It is thus stated that plant *I. spicata* possess cytotoxic effects which are in accordance with the findings obtained earlier and can be used as a source of potential anticancer agents (Shah et al., 2015; Naher et al., 2019).

Polyphenols are a kind of phytochemical that has lately gained popularity due to their potential to prevent cancer cell development. Polyphenols have been shown to cause cell cycle arrest in malignancies such as gastric cancer, hepatoma, endometrial cancer, nasopharyngeal cancer, prostate cancer, breast cancer, pancreatic cancer, and lymphoma cancer. Resveratrol, a stilbene, and quercetin, a flavonol, are two polyphenols that limit cancer cell proliferation. As a result, their effects have been investigated in a variety of cancers, including breast, prostate, hepatoma, and colon cancer (Kampa et al., 2007). The MTT assay is the most commonly used technique to evaluate cell viability and proliferation (Table 1). The findings of this study are consistent with earlier studies that show similar effects are caused by the presence of various bioactive substances (Kumar and Pandey, 2013; Taiwo et al., 2020). The crude extract and *n-hexane* fractions showed concentration-dependent inhibition of HepG-2 cell line in tested concentration range of 6.25–200 µg/ml. In a previous study the anticancer activity of *I. spicata* against lung cancer has also been reported (Shah et al., 2019a). A new juglone analog, 2-ethoxystypandrone, derived from ethyl acetate extract of the roots of *Polygonum cuspidatum,* has been shown to have anticancer action against hepatocellular carcinoma (Shah et al., 2019c). The activity of aqueous extract was low as compared to other fractions of plant. A significant inhibition of growth was observed for heptadecyl benzoate with an IC_{50} value of 8.92 µg/mL. A moderate activity (IC_{50} = 25.66 µg/ml) was shown by methyl dihydroxybenzoate. In another study glycoalkaloids isolated from *Salanum melongena* demonstrated a significant antiproliferative effect against liver cancer cells (Fekry et al., 2019).

This study uses cytotoxicity, ADMET, and molecular docking approaches to assess the efficacy of extracts and isolated compounds of *I. spicata* as a putative biomolecule therapeutically active against HepG-2 Cancer Cells. The physicochemical features of compounds were studied. The results of both compounds fall within the limits, demonstrating their potential as drug candidates for clinical trials.

The BOILED-EGG graph indicates the compound absorption from the GI^a and the BBB permeation. The white area is for GI^a showing the compound absorption region, and the yellow zone (yolk) is for the BBB diffusion. While if the compound occurs in the grey geographical zone, it suggests that the compound has neither GI absorption nor it crosses BBB (Daina and Zoete, 2016). GI^a and CNS absorption are crucial factors examined for every single drug candidate prior to its access to drug formulation (Chen et al., 2020). The Blood-brain barrier penetration is necessary for the compound to have actions on the central nervous system (Cruz et al., 2018). In Bioavailability radar chart, methyl dihydroxybenzoate showed better oral bioavailability. The methyl dihydroxybenzoate has presented a high GI^a with BBB permeability than Heptadecyl benzoate, indicating that

heptadecyl benzoate low occurrence for CNS side effects. Both are not P-gp (P-glycoprotein) substrate hence they are not prone to the efflux mechanism of P-gp, as many cancer lines exploited that mechanism as a source of drug resistance (Binkhathlan and Lavasanifar, 2013). Furthermore, the methyl dihydroxybenzoate showed less skin permeation, as more the negative Log Kp valve of the molecule results in less skin permeability (DeLano, 2002).

Furthermore, the most common cytochromes isoforms were analyzed against these compounds as these enzymes have a significant part in drug excretion. Inhibition of these isoforms results in drug interaction (Chen et al., 2020). The heptadecyl benzoate inhibits more isoforms, causing significant drug interaction. Calculation of drug clearance of a compound is critical for a molecule to find steady-state concentrations. The methyl dihydroxybenzoate clearance value was inadequate. Both compounds showed as non-substrate of Organic Cation Transporter 2 (OCT2).

Drug toxicity profiling is necessary before a drug enters into the clinical trials or in the pre-formulation stage [25]. Therefore compounds have been assessed for toxicities i.e., human, oral and rat. The AMES toxicity test normally estimates the mutagenic ability of a compound. In this study, we found that both compounds were characterized as non-Ames risky, representing no carcinogenic ability. The maximum tolerated dose (MTD) for methyl dihydroxybenzoate was higher than heptadecyl benzoate. The MTD is a quantity of a chemical's harmful dosage threshold in humans. In our findings, hERG I was not suppressed by both compounds but hERG II was inhibited only by heptadecyl benzoate, hERG-encoded potassium channels inhibition consequence in ventricular arrhythmia by QT prolongation (Robertson and Morais-Cabral, 2020). The isolated compounds were also predicted as non-hepatotoxic, therefore considered as a safe drug in terms of drug-induced liver adverse effects (Hoitsma et al., 1991). A probable side effect of a molecule is a skin hypersensitivity reaction, heptadecyl benzoate has shown skin allergies.

The docking analysis was used to identify the binding poses of the isolated compounds in the active site of (EGFR) tyrosine kinase. In docking tests, both agents demonstrated a high binding affinity (Docking score −4.759, binding energy −26.51 and binding affinity −5.07 for methyl dihydroxybenzoate. Docking score −5.801, binding energy −33.45 and binding affinity −6.4 for heptadecyl benzoate). The docking results supported the *in vitro* results against the cancer cells. Our findings are consistent with previous studies (Galal et al., 2014). In our previous study, a novel compound, 3-hydroxyoctyl-5, trans-docosenoate, isolated from the plant, *Anchusa arvensis* has exhibited significant interaction with tyrosine kinase enzyme (Hussain et al., 2019). Therefore, it could be assumed that these two compounds might have anticancer effects through tyrosine kinase. However, it will require further experimental confirmation.

Conclusion

The current study provides new understanding of the anticancer potential of *I. spicata* against liver cancer. The ethyl acetate fraction had a significant effect in the brine shrimp mortality experiment, with an IC_{50} of 10 µg/mL. A significant effect was exhibited by heptadecyl benzoate. Both compounds exhibited acceptable pharmacokinetic properties except in absorption of heptadecyl benzoate in ADME analysis. Both isolated compounds showed a safer profile in toxicity assessment. Furthermore, both compounds showed marked binding affinity towards (EGFR) tyrosine kinase, supporting the *in-vitro* effects. Our results suggest that *I. spicata* has bioactive compounds with promising anticancer potential. Therefore, it can be further used for the development of drugs for liver cancer treatment.

Data availability statement

The original contributions presented in the study are included in the article/Supplementary Materials, further inquiries can be directed to the corresponding authors.

Author contributions

The experimental work and data collection were performed SH, SK, HL, and FS. SS and FA were performed. Data were evaluated by SH, JL, and SL. Computational studies were performed by FA. SH and JL was involved in the literature search and manuscript preparation. SH, SL, JL, and HL, refined the manuscript for publication. HL, JL, and SL financially supported the research work. All authors contributed to data analysis, drafting and revising the article, gave final approval of the version to be published, and agree to be accountable for all aspects of the work.

Acknowledgments

We are thankful to Higher Education Commission for facilitating us in our research work Acknowledgments. Authors are thankful to Researchers Supporting Project Natural Science Foundation of Shezhen University General Hospital No: SUGH2020QD015 and No: SUGH2019QD018 for financial support. The authors are also

thankful to the Department of Pharmacy, Kohat University of Science and Technology, for the provision of a laboratory.

Conflict of interest

The authors declare that the research was conducted in the absence of any commercial or financial relationships that could be construed as a potential conflict of interest.

Publisher's note

All claims expressed in this article are solely those of the authors and do not necessarily represent those of their affiliated organizations, or those of the publisher, the editors and the reviewers. Any product that may be evaluated in this article, or claim that may be made by its manufacturer, is not guaranteed or endorsed by the publisher.

References

Abouri, M., El Mousadik, A., Msanda, F., Boubaker, H., Saadi, B., and Cherifi, K. (2012). An ethnobotanical survey of medicinal plants used in the Tata Province, Morocco. *Int. J. Med. Plants Res.* 1 (7), 99

Alqahtani, A., Khan, Z., Alloghbi, A., S Said Ahmed, T., Ashraf, M., and M Hammouda, D. J. M. (2019). Hepatocellular carcinoma: Molecular mechanisms and targeted therapies. *Medicina* 55 (9), 526. doi:10.3390/medicina55090526

Basili, S., and Moro, S. (2009). Novel camptothecin derivatives as topoisomerase I inhibitors. *Expert Opin. Ther. Pat.* 19 (5), 555–574. doi:10.1517/13543770902773437

Binkhathlan, Z., and Lavasanifar, A. (2013). P-Glycoprotein inhibition as a therapeutic approach for overcoming multidrug resistance in cancer: Current status and future perspectives. *Curr. Cancer Drug Targets* 13 (3), 326–346. doi:10.2174/15680096113139990076

Chen, Y., Tian, Y., Gao, Y., Wu, F., Luo, X., Ju, X., et al. (2020). *In silico* design of novel HIV-1 NNRTIs based on combined modeling studies of Dihydrofuro [3, 4-d] pyrimidines. *Front. Chem.* 8, 164. doi:10.3389/fchem.2020.00164

Cragg, G. M., and Newman, D. J. (2005). Plants as a source of anti-cancer agents. *J. Ethnopharmacol.* 100 (1-2), 72–79. doi:10.1016/j.jep.2005.05.011

Cruz, J. V., Serafim, R. B., da Silva, G. M., Giuliatti, S., Rosa, J. M., Neto, M. F. A., et al. (2018). Computational design of new protein kinase 2 inhibitors for the treatment of inflammatory diseases using QSAR, pharmacophore-structure-based virtual screening, and molecular dynamics. *J. Mol. Model.* 24 (9), 225–316. doi:10.1007/s00894-018-3756-y

Daina, A., and Zoete, V. (2016). A boiled-egg to predict gastrointestinal absorption and brain penetration of small molecules. *ChemMedChem* 11 (11), 1117–1121. doi:10.1002/cmdc.201600182

DeLano, W. L. (2002). Pymol: An open-source molecular graphics tool. *CCP4 Newsl. protein Crystallogr.* 40 (1), 82

Fekry, M. I., Ezzat, S. M., Salama, M. M., Alshehri, O. Y., and Al-Abd, A. M. (2019). Bioactive glycoalkaloides isolated from Solanum melongena fruit peels with potential anticancer properties against hepatocellular carcinoma cells. *Sci. Rep.* 9 (1), 1746–1811. doi:10.1038/s41598-018-36089-6

Ferlay, J., Colombet, M., Soerjomataram, I., Mathers, C., Parkin, D. M., Piñeros, M., et al. (2019). Estimating the global cancer incidence and mortality in 2018: GLOBOCAN sources and methods. *Int. J. Cancer* 144 (8), 1941–1953. doi:10.1002/ijc.31937

Ferlay, J., Soerjomataram, I., Dikshit, R., Eser, S., Mathers, C., Rebelo, M., et al. (2015). Cancer incidence and mortality worldwide: Sources, methods and major patterns in GLOBOCAN 2012. *Int. J. Cancer* 136 (5), E359–E386. doi:10.1002/ijc.29210

Galal, S. A., Khairat, S. H., Ragab, F. A., Abdelsamie, A. S., Ali, M. M., Soliman, S. M., et al. (2014). Design, synthesis and molecular docking study of novel quinoxalin-2 (1H)-ones as anti-tumor active agents with inhibition of tyrosine kinase receptor and studying their cyclooxygenase-2 activity. *Eur. J. Med. Chem.* 86, 122–132. doi:10.1016/j.ejmech.2014.08.048

Hassan, S. S. U., Zhang, W.-D., Jin, H.-z., Basha, S. H., and Priya, S. (2022). *In-silico* anti-inflammatory potential of guaiane dimers from Xylopia vielana targeting COX-2. *J. Biomol. Struct. Dyn.* 40 (1), 484–498. doi:10.1080/07391102.2020.1815579

Hoitsma, A. J., Wetzels, J. F., and Koene, R. A. (1991). Drug-induced nephrotoxicity. Aetiology, clinical features and management. *Drug Saf.* 6 (2), 131–147. doi:10.2165/00002018-199106020-00004

Hussain, S., Ullah, F., Ayaz, M., Shah, S. A. A., Shah, A.-u.-H. A., Shah, S. M., et al. (2019). *In silico*, cytotoxic and antioxidant potential of novel ester, 3-hydroxyoctyl-5-trans-docosenoate isolated from anchusa arvensis (L.) m. bieb. against hepg-2 cancer cells. *Drug Des. devel. Ther.* 13, 4195–4205. doi:10.2147/DDDT.S228971

Kampa, M., Nifli, A.-P., Notas, G., and Castanas, E. (2007). Polyphenols and cancer cell growth. *Rev. Physiol. Biochem. Pharmacol.* 159, 79–113. doi:10.1007/112_2006_0702

Khan, I., Abbas, T., Anjum, K., Abbas, S. Q., Shagufta, B. I., Ali Shah, S. A., et al. (2019). Antimicrobial potential of aqueous extract of Camellia sinensis against representative microbes. *Pak. J. Pharm. Sci.* 32 (2), 631

Khorrami, S., Zarrabi, A., Khaleghi, M., Danaei, M., and Mozafari, M. (2018). Selective cytotoxicity of green synthesized silver nanoparticles against the MCF-7 tumor cell line and their enhanced antioxidant and antimicrobial properties. *Int. J. Nanomedicine* 13, 8013–8024. doi:10.2147/IJN.S189295

Kumar, S., and Pandey, A. K. (2013). Chemistry and biological activities of flavonoids: An overview. *ScientificWorldJournal.* 2013, 162750. doi:10.1155/2013/162750

Manilal, A., Sujith, S., Kiran, G. S., Selvin, J., and Shakir, C. (2009). Cytotoxic potentials of red alga, laurencia brandenii collected from the Indian coast. *Glob. J. Pharmacol.* 3 (2), 90

Meyer, B., Ferrigni, N., Putnam, J., Jacobsen, L., Nichols, D. j., and McLaughlin, J. L. (1982). Brine shrimp: A convenient general bioassay for active plant constituents. *Planta Med.* 45 (05), 31–34. doi:10.1055/s-2007-971236

Mohtasheem, M., Ahmad, S. W., Iqbal, A., and Ali, M. S. (2001). Brine shrimp bioassay of phoenix sylvestris. *Pak. J. Pharm. Sci.* 14, 19–21.

Mosmann, T. (1983). Rapid colorimetric assay for cellular growth and survival: Application to proliferation and cytotoxic assay. *J. Immunol. Methods* 65, 55–63. doi:10.1016/0022-1759(83)90303-4

Mphahlele, M. J., Paumo, H. K., and Choong, Y. S. (2017). Synthesis and *in vitro* cytotoxicity of the 4-(halogenoanilino)-6-bromoquinazolines and their 6-(4-fluorophenyl) substituted derivatives as potential inhibitors of epidermal growth factor receptor tyrosine kinase. *Pharmaceuticals* 10 (4), 87. doi:10.3390/ph10040087

Naher, S., Aziz, M. A., Akter, M. I., Rahman, S. M., Sajon, S. R., and Mazumder, K. (2019). Anti-diarrheal activity and brine shrimp lethality bioassay of methanolic extract of Cordyline fruticosa (L.) A. Chev. leaves. *Clin. Phytosci.* 5 (1), 15–16. doi:10.1186/s40816-019-0109-z

Newman, D. J., Cragg, G. M., and Snader, K. M. (2003). Natural products as sources of new drugs over the period 1981– 2002. *J. Nat. Prod.* 66 (7), 1022–1037. doi:10.1021/np030096l

N'guessan, B. B., Asiamah, A. D., Arthur, N. K., Frimpong-Manso, S., Amoateng, P., Amponsah, S. K., et al. (2021). Therapies, Ethanolic extract of Nymphaea lotus L.(Nymphaeaceae) leaves exhibits *in vitro* antioxidant, *in vivo* anti-inflammatory and cytotoxic activities on Jurkat and MCF-7 cancer cell lines. *BMC Complementary Med. Ther.* 21 (1), 1–13. doi:10.1186/s12906-020-03195-w

Paul, M. K., and Mukhopadhyay, A. K. (2004). Tyrosine kinase–role and significance in cancer. *Int. J. Med. Sci.* 1 (2), 101–115. doi:10.7150/ijms.1.101

Pezzuto, J. M. (1997). Plant-derived anticancer agents. *Biochem. Pharmacol.* 53 (2), 121–133. doi:10.1016/s0006-2952(96)00654-5

Robertson, G. A., and Morais-Cabral, J. H. (2020). hERG function in light of structure. *Biophys. J.* 118 (4), 790–797. doi:10.1016/j.bpj.2019.10.010

Shah, S. M., Hussain, S., Khan, A.-u., Shah, A. U., Khan, H., Ullah, F., et al. (2015). Cytotoxic and phytotoxic actions of Heliotropium strigosum. *Toxicol. Ind. Health* 31 (5), 429–432. doi:10.1177/0748233712471706

Shah, S. M., Ullah, F., Ayaz, M., Sadiq, A., Hussain, S., Shah, A., et al. (2019). Benzoic acid derivatives of Ifloga spicata (Forssk.) Sch. Bip. as potential anti-

Leishmanial against Leishmania tropica. *Processes* 7 (4), 208. doi:10.3390/pr7040208

Shah, S. M., Ullah, F., Ayaz, M., Sadiq, A., Hussain, S., Shah, S. A. A., et al. (2019). β-Sitosterol from ifloga spicata (forssk.) sch. Bip. As potential anti-leishmanial agent against leishmania tropica: Docking and molecular insights. *Steroids* 148, 56–62. doi:10.1016/j.steroids.2019.05.001

Shah, S. M., Ullah, F., Ayaz, M., Wahab, A., and Shinwari, Z. K. (2019). Phytochemical profiling and pharmacological evaluation of ifloga spicata (FORSSK.) SCH. BIP. in leishmaniasis, lungs cancer and oxidative stress. *Pak. J. Bot.* 51 (6), 2143–2152. doi:10.30848/pjb2019-6(39)

Sung, H., Ferlay, J., Siegel, R. L., Laversanne, M., Soerjomataram, I., Jemal, A., et al. (2021). Global cancer statistics 2020: GLOBOCAN estimates of incidence and mortality worldwide for 36 cancers in 185 countries. *Ca. Cancer J. Clin.* 71 (3), 209–249. doi:10.3322/caac.21660

Taiwo, B. J., Popoola, T. D., van Heerden, F. R., and Fatokun, A. A. (2020). Pentagalloylglucose, isolated from the leaf extract of Anacardium occidentale L., could elicit rapid and selective cytotoxicity in cancer cells. *BMC Complement. Med. Ther.* 20 (1), 287–289. doi:10.1186/s12906-020-03075-3

Ullah, M. O., Haque, M., Urmi, K. F., Zulfiker, A. H. M., Anita, E. S., Begum, M., et al. (2013). Anti–bacterial activity and brine shrimp lethality bioassay of methanolic extracts of fourteen different edible vegetables from Bangladesh. *Asian pac. J. Trop. Biomed.* 3 (1), 1–7. doi:10.1016/S2221-1691(13)60015-5

Vlahovic, G., and Crawford, J. (2003). Activation of tyrosine kinases in cancer. *Oncologist* 8 (6), 531–538. doi:10.1634/theoncologist.8-6-531

Xiao, Y., Zhu, S., Wu, G., Xie, Y., Ishaq, M., Sun, Y., et al. (2020). Chemical constituents of vernonia parishii. *Chem. Nat. Compd.* 56 (1), 134–136. doi:10.1007/s10600-020-02963-x

frontiers | Frontiers in Pharmacology

TYPE Review
PUBLISHED 12 September 2022
DOI 10.3389/fphar.2022.958012

Check for updates

OPEN ACCESS

EDITED BY
Fareeha Anwar,
Riphah International University (Lahore), Pakistan

REVIEWED BY
Irum Shahzadi,
COMSATS University Islamabad, Pakistan
Jun-Seob Kim,
Incheon National University, South Korea

*CORRESPONDENCE
Walaa K. Mousa,
walaa.mousa@aau.ac.ae

SPECIALTY SECTION
This article was submitted to Predictive Toxicology, a section of the journal Frontiers in Pharmacology

RECEIVED 31 May 2022
ACCEPTED 18 August 2022
PUBLISHED 12 September 2022

CITATION
Mousa WK (2022), The microbiome-product colibactin hits unique cellular targets mediating host–microbe interaction. *Front. Pharmacol.* 13:958012. doi: 10.3389/fphar.2022.958012

COPYRIGHT
© 2022 Mousa. This is an open-access article distributed under the terms of the Creative Commons Attribution License (CC BY). The use, distribution or reproduction in other forums is permitted, provided the original author(s) and the copyright owner(s) are credited and that the original publication in this journal is cited, in accordance with accepted academic practice. No use, distribution or reproduction is permitted which does not comply with these terms.

The microbiome-product colibactin hits unique cellular targets mediating host–microbe interaction

Walaa K. Mousa[1,2]*

[1]College of Pharmacy, Al Ain University, Abu Dhabi, United Arab Emirates, [2]College of Pharmacy, Mansoura University, Mansoura, Egypt

The human microbiota produces molecules that are evolved to interact with the diverse cellular machinery of both the host and microbes, mediating health and diseases. One of the most puzzling microbiome molecules is colibactin, a genotoxin encoded in some commensal and extraintestinal microbes and is implicated in initiating colorectal cancer. The colibactin cluster was discovered more than 15 years ago, and most of the research studies have been focused on revealing the biosynthesis and precise structure of the cryptic encoded molecule(s) and the mechanism of carcinogenesis. In 2022, the Balskus group revealed that colibactin not only hits targets in the eukaryotic cell machinery but also in the prokaryotic cell. To that end, colibactin crosslinks the DNA resulting in activation of the SOS signaling pathway, leading to prophage induction from bacterial lysogens and modulation of virulence genes in pathogenic species. These unique activities of colibactin highlight its ecological role in shaping gut microbial communities and further consequences that impact human health. This review dives in-depth into the molecular mechanisms underpinning colibactin cellular targets in eukaryotic and prokaryotic cells, aiming to understand the fine details of the role of secreted microbiome chemistry in mediating host–microbe and microbe–microbe interactions. This understanding translates into a better realization of microbiome potential and how this could be advanced to future microbiome-based therapeutics or diagnostic biomarkers.

KEYWORDS

colibactin, phage induction, genotoxicity, human microbiome, colorectal cancer, inflammation, colitis, DNA damage

Introduction

Trillions of microbes reside in the human gut interacting with each other and the outcome of their interaction affects human health and diseases (Sharon et al., 2014; Dhanaraju and Rao 2022; de Vos et al., 2022). This interaction is mediated by evolved small molecules, of which the vast majority are still dark matter (Wilson, Zha, and Balskus 2017; Zha et al., 2022). A few examples of microbiome secreted products are reported, each with a unique activity such as the microbial genotoxin colibactin (Wernke et al., 2020). Colibactin is a hybrid

polyketide–non-ribosomal peptide product encoded in the genome of some Enterobacteriaceae that belong to the phylogenetic group B. Colibactin is implicated in causing colorectal cancer (CRC) by inducing a signature mutation in DNA. Isolation and structural elucidation of colibactin has challenged the scientific field for over 15 years because of its contact-dependent synthesis, minimal expression, and chemical instability. The bulk of the research study on colibactin is centered around revealing its structure, mainly through bioinformatic analysis, comparative metabolomics, and mutational studies (Tang et al., 2022). However, to appreciate the evolved function of colibactin(s) and other microbiome products, we must understand their ecological role in enhancing the competency and fitness of producers. There are some reports on the antimicrobial-like activity of colibactin, but most of the data come from observational or associational studies without revealing the underpinning mechanism of action (T. Faïs et al., 2016). In a pioneering study, the group of Dr. Balskus revealed that colibactin induces prophage activation on a wide scale in multiple phage–bacteria systems. This activity is mediated by its ability to damage DNA activating the SOS response. Moreover, induction of prophages affects prophage-encoded genes such as some bacterial toxins, which are crucial for their pathogenicity. This finding reveals another interesting role of colibactin in mediating microbe–microbe interaction and shaping the structure of gut microbes (Silpe et al., 2022; Tronnet et al., 2020).

Our knowledge of colibactin(s) is developing and there are previous reviews covering their prospective research period (Faïs et al., 2018; Bode 2015; Balskus 2015; Williams et al., 2020; Wernke et al., 2020; Tang et al., 2022). These reviews mainly focused on summarizing advances in understanding possible biosynthetic pathways, bioinformatic prediction of colibactin and precolibactin structures, and the mechanism of DNA mutation. In this review, we analyze the unique cellular targets of colibactin(s) mediating host–microbe interactions that shape gut microbiome structures and influence host's health. We discuss the molecular mechanisms underlying the evolved function of colibactin in hitting multiple targets in both the eukaryotic and prokaryotic cell machinery. We propose a mechanistic model for the series of events leading to colibactin-induced cancer. This knowledge is central to better advancing the use of microbiome secreted products or genes as diagnostic biomarkers or therapeutic interventions.

The latest development in understanding the biosynthesis and structure of colibactin(s)

Prevalence and significance of colibactin gene cluster in prokaryotes

The first report on the colibactin cluster is dated back to 2006 when Nougayrède et al. (2006) reported the discovery of *Escherichia coli* strains belonging to the phylogenetic group B2 that can block mitosis, leading to megalocytosis and eventually cell death. The authors linked this weird activity to a genomic island that encodes cryptic molecule(s), named at this time colibactin (Nougayrède et al., 2006). Interestingly, this gene cluster is prevalent in gut microbes, in particular Group B of human-associated strains of *E. coli* and Enterobacteriaceae, including commensal and probiotic strains such as *E. coli* Nissle 1917, a commercial probiotic (Mutaflor) used to improve gastrointestinal inflammatory conditions such as ulcerative colitis (Schultz 2008). The Colibactin cluster is also sequenced from other non-human associated microbes such as *Pseudovibrio* sp. JE062, isolated from a marine sponge (Bondarev et al., 2013) and a novel strain of *Erwina oleae* sp. isolated from olive tree nots caused by *Pseudomonas savastanoi* (Moretti et al., 2011). The *Frischella perrara* PEB0191 is a commensal gut microbe in honey bees. The Crawford group showed that *F. perrara* PEB0191 produces colibactin mimics and induces DNA breaks similar to human microbiome strains (Engel, Vizcaino, and Crawford 2015). This widespread prevalence of colibactin or its homologs indicates its potential role in a symbiotic relationship, which likely confers beneficial outcomes to the host.

Genomic organization of the colibactin cluster

The colibactin cluster encodes 54-kb hybrid nonribosomal peptide synthetase-polyketide synthase (NRPS-PKS) biosynthetic genes known as the *pks or clb* gene cluster (Figure 1). The cluster consisted of 19 genes, named alphabetically, clb A-S. These 19 genes encode three polyketide synthases (PKSs), three nonribosomal peptide synthases (NRPSs), two hybrids NRPS/PKS, MATE transporter, resistance gene, and other nine tailoring and accessory enzymes as per the latest update as reviewed (Tang et al., 2022). Intensive research reports confirm that all of these genes are essential for genotoxicity, except for clb M, S, and R (Nougayrède et al., 2006). Our current understanding of colibactin structure is shaped through understanding the organization of its biosynthetic genes, mutational studies, heterologous expression, and structure prediction using bioinformatics models. Over the last 16 years, there have been multiple hypotheses for the biosynthesis of colibactin, and the most recent is the prodrug activation theory (Figure 1) developed by the Balskus group (Brotherton and Balskus 2013; Balskus 2015). The genomic island of colibactin contains the *clbP* gene, which is a peptidase enzyme that shares structure/function homology with cleavage enzymes functioning in ribosomaly synthesized posttranslational modified peptides such as ZmaM in zwittermicin biosynthesis (Luo et al., 2011). This similarity is revealed by a plethora of confirmation analyses, including structure–activity relationship, crystallography, and

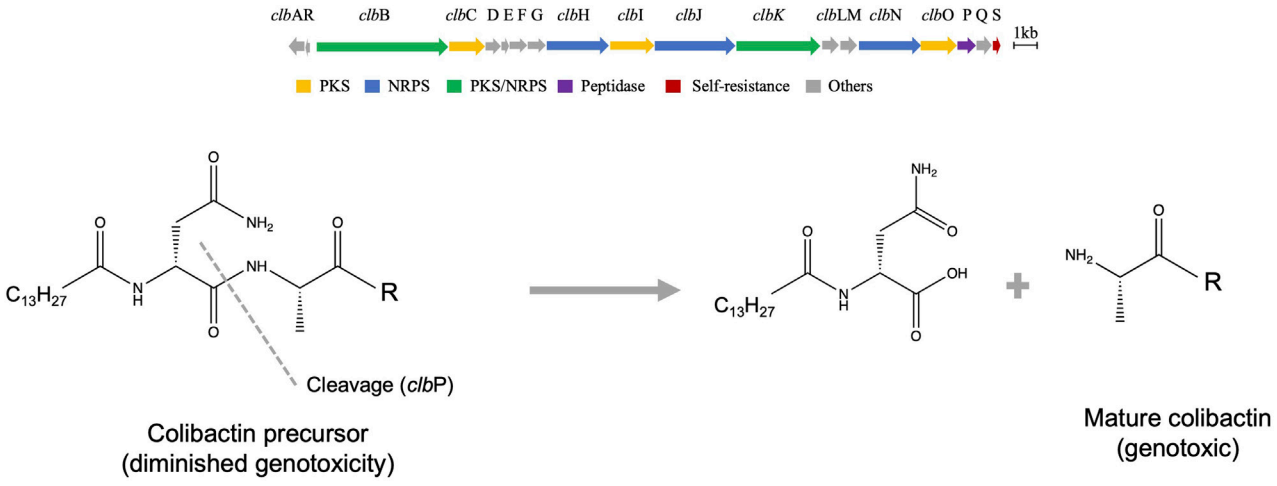

FIGURE 1
Genetic organization and possible biosynthesis of colibactin. **(A)** Organization of the biosynthetic genes cluster of colibactin. **(B)** Prodrug activation hypothesis overview shows the last required step for production of the genotoxin, which is catalyzed by peptidase enzyme.

mutagenesis (Cougnoux et al., 2012; Dubois et al., 2011). This fact leads Balskus and coworkers to hypothesize the prodrug activation theory for the biosynthesis of colibactin in which two NRPS modules (clbN and clbB) install the N-acyl-D-asparagine scaffold earlier in the biosynthesis, followed by clbP cleaving the amide bond and releasing the final active colibactin product (Brotherton and Balskus 2013). The Muller group added additional verification of the hypothesis by isolating the hypothesized prodrug from *E. coli*-Nissle 1917 (Bian et al., 2013). Further studies revealed that silencing of this peptidase enzyme (Δ clbP strain) facilitates the accumulation of precolibactins, which are more stable derivatives of the main genotoxic molecule. Δ clbP strains have a diminished genotoxic activity compared to wild type. Of note, we still lack more precise information on the genetic organization of colibactin-like clusters in other species and how the possible polymorphism might lead to functionally diverse molecules.

Revealing the structure of colibactin derivatives (precolibactins)

The precise structure of the colibactin molecule has remained unknown for over a decade. Purification of colibactin from native or heterologous hosts is challenging due to its minimal production upon fermentation, instability, and contact or inflammation-dependent gene expression. To overcome this challenge, several research groups developed alternative strategies to characterize the more stable derivatives or precursors of colibactin, named precolibactins (Vizcaino et al., 2014; Li et al., 2019; Vizcaino and Crawford 2015; Brotherton et al., 2015; Bian et al., 2015; Li et al., 2015; Li et al., 2016; Healy, Vizcaino, et al., 2016b). These strategies involve: 1) mutating the *clbP* gene, an essential enzyme required to produce active genotoxic colibactin molecules, and the generation of a series of other mutants; 2) heterologous expression of the mutated gene clusters; 3) comparative metabolomic analysis of mutants and wild-type strains; 4) tandem MS–MS fragmentation analysis coupled with isotopic feeding experiments; and 5) synthesis of potential precolibactin analogues. Following these approaches, around 40 precolibactins have been predicted, isolated, or synthesized. Some structurally unique examples of precolibactins are shown in Figure 2. Isolated or predicted precolibactins might be biosynthetically related, and for example, theoretically, precolibactin C could be biosynthesized from A via cyclodehydration as proposed (Healy 2017). Healy et al. proposed that precolibactins A-C may not be the precursors for colibactin as previously thought but rather alternative products produced only when the cibP is nonfunctional by a double cyclodehydration pathway (Healy et al., 2016a; Healy et al., 2016b). This hypothesis is based on some evidence that colibactin alkylates DNA by the formation of unsaturated imines, which could not be generated from the pyridone ring in precolibactins A-C (Healy et al., 2016a). Interestingly, some precolibactins share a structural similarity with yatakemycin and duramycin, mainly the aminocyclopropane moiety, which attacks DNA via nucleophilic ring-opening (Tichenor and Boger 2008). Precolibactin A weakly cross-links DNA *in vitro* while a precolibactin derivative lacking the spiro bicyclic structure was inactive (Vizcaino and Crawford 2015). Further evidence suggests that the two precolibactins isolated are products of the intact colibactin cluster.

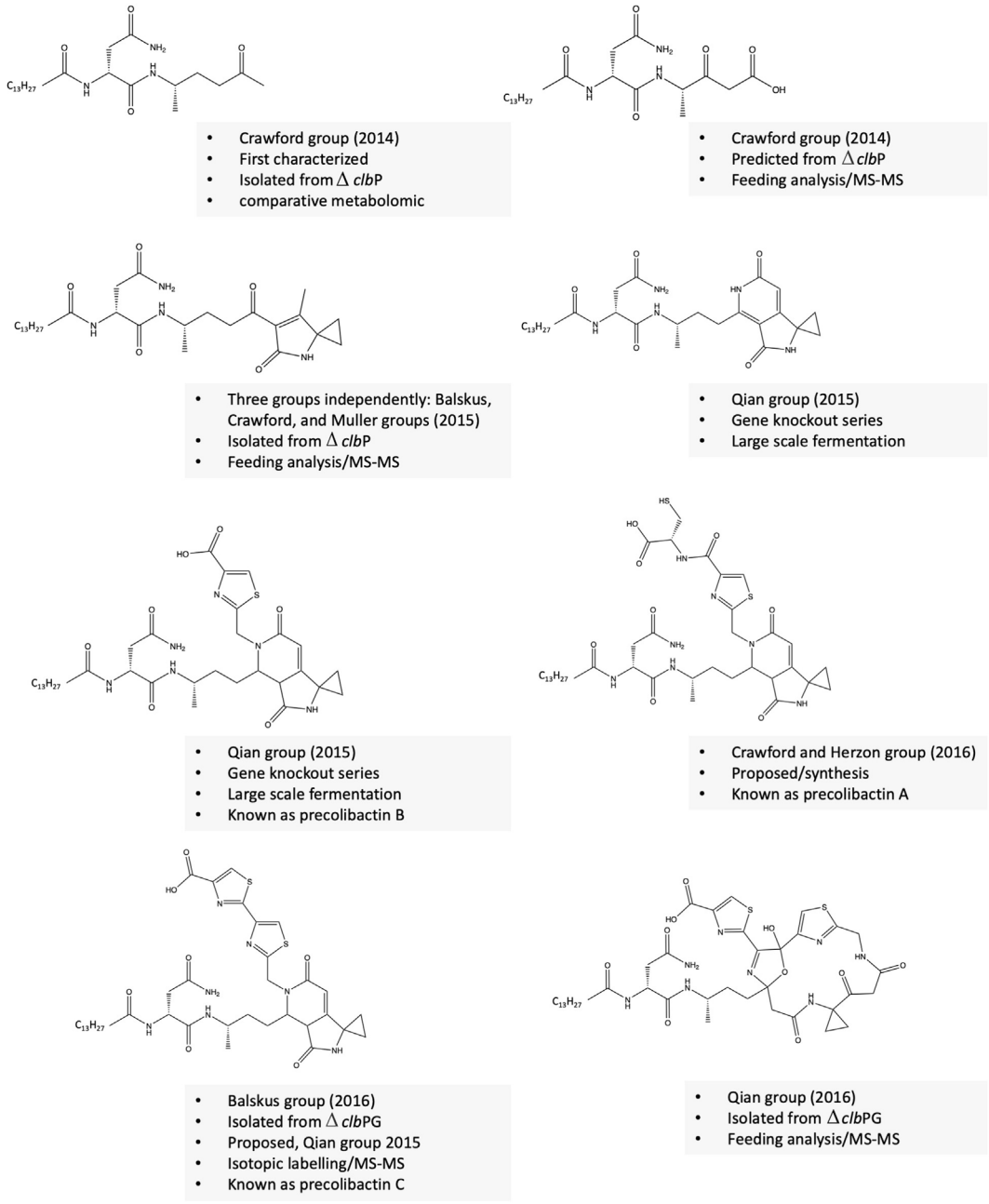

FIGURE 2
Selected examples of precolibactins with unique structures.

Revealing the structure of colibactin(s)

In 2019, the Qian group elucidated the structure of a colibactin molecule based on *in vitro* cleavage of an isolated precolibactin with an MWT of 969 to yield colibactin with an MWT of 645 (Li et al., 2019). Further evidence confirms that this structure is produced from the native PKS + strain. This evidence includes the presence of the product in the extract of native colibactin-harboring *E. coli* CFT073 as detected by MS–MS analysis and the ability of the compound to induce the characteristic DNA double-strand breaks (Li et al., 2019). In the same year, Crawford/Herzon and Balskus groups independently elucidated the structure of another colibactin molecule with an MWT of 770 and validated its

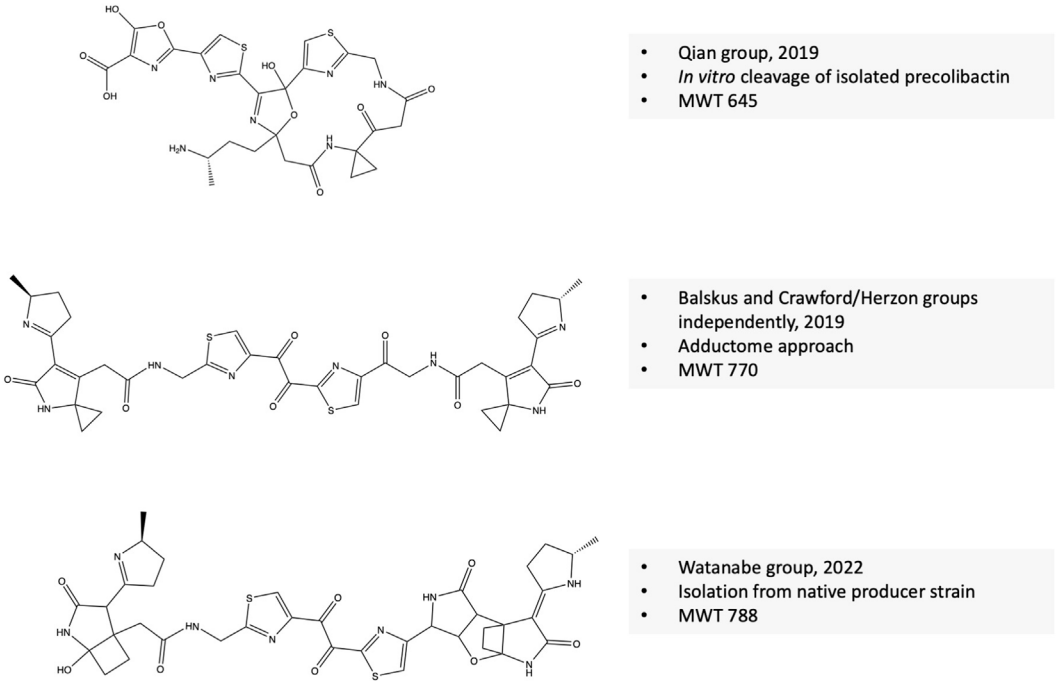

FIGURE 3
Confirmed structure of colibactin(s).

genotoxic activity (Xue et al., 2019; Jiang et al., 2019). Crawford/Herzon predicted the structure by a DNA adductome approach followed by total synthesis. The Balskus group predicted the structure by studying *clbP*/*clbL* double mutants, labeling experiments, and an adductome approach. The clbL is predicted to encode amidase functions by hydrolysis of an amide bond; however, the authors validated that this enzyme is rather the final step in the production of intact precolibactin (Jiang et al., 2019). In 2022, the Watanabe group isolated a colibactin molecule with an MWT of 788 from the *pks* + *E. coli* strain-50, a strain isolated from colorectal cancer tissues that produces 26-fold more colibactin than Nissle 1917 (Hirayama et al., 2019; Zhou et al., 2021). Of note, the same group has developed an activity-based fluorescent probe to identify high colibactin producers from clinical samples 3 years before elucidating the first-isolation-based structure of colibactin (Hirayama et al., 2019). At first, the authors obtained two fragments of the compound whose structures are suggestive of spontaneous hydrolysis of the candidate molecule at the 1,2-diketone moiety as previously described by the Herzon group (Healy et al., 2019). Next, they managed to protect the compound from hydrolysis by adding *o*-phenylenediamine to convert the 1,2-diketone moiety into quinoxaline, which is not subjected to hydrolysis and isolated a few micrograms of colibactin sufficient for further NMR spectroscopic analysis (Zhou et al., 2021). The three revealed structures of colibactin are shown in Figure 3.

Colibactin hits unique molecular targets in the eukaryotic cells

Our gut microbes secrete a plethora of molecules with diverse structures and functions. These molecules can either promote host health such as butyrate or trigger diseases. In addition to colibactin, several microbiome-derived molecules are noted as mediators of diseases, such as the autism-promoting molecule 4-ethylphenylsulfate and the gut genotoxin cyclomodulin (Hsiao et al., 2013; Buc et al., 2013). Colibactin might hit other targets in the eukaryotic machinery than what we currently appreciate. A study shows that some synthetic precolibactins exhibited antagonist activity on the mammalian brain receptors such as serotonin 5-hydroxytryptamine type 7 (5-HT7) *in vitro* (Vizcaino et al., 2014). Of note, 5-HT7 is expressed in dendritic cells. Studies show that 5-HT7 receptor antagonists such as SB-269970 decrease both acute and chronic inflammation in a mouse model of colitis (Kim et al., 2013). Synthetic precolibactin also showed antagonist activity against dopamine 5 receptors (Vizcaino et al., 2014). Dopamine receptors are reported to be located in the CNS and gut (Z. S. Li et al., 2006).

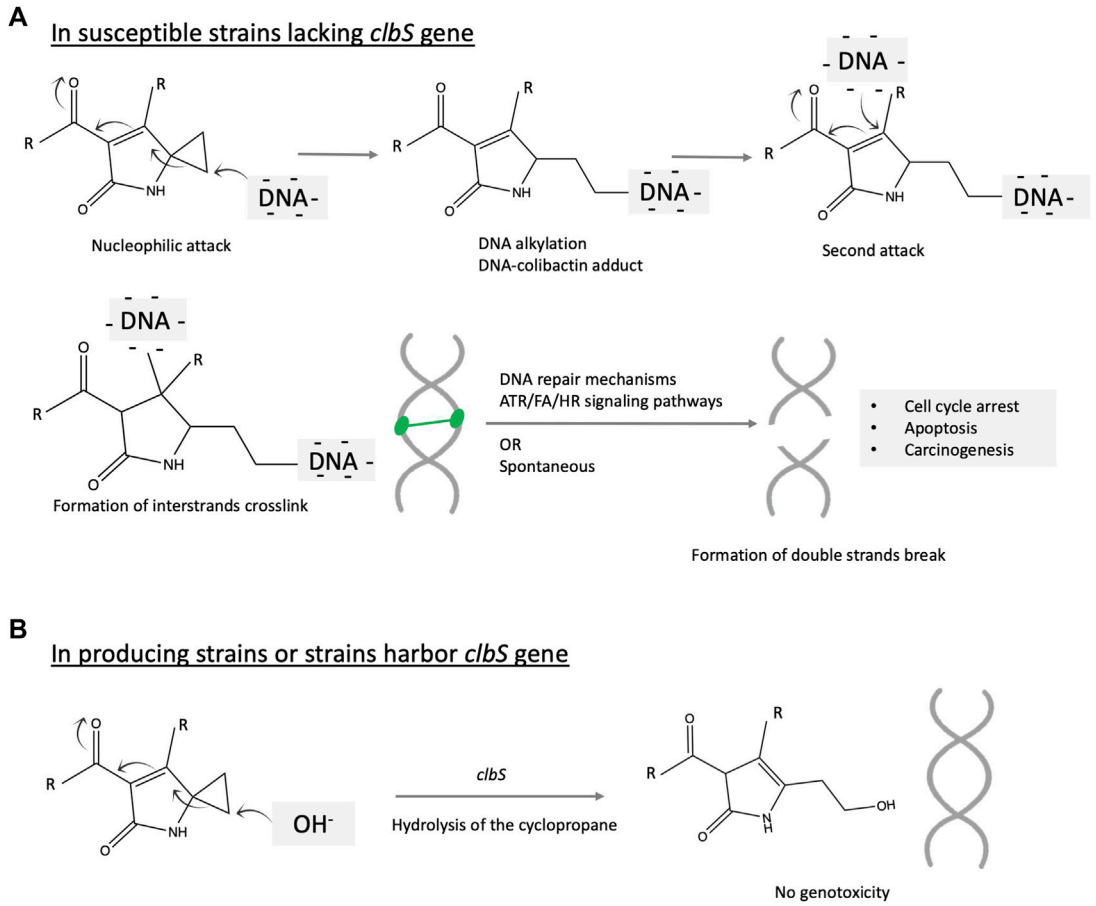

FIGURE 4
Illustration of the proposed mechanism of colibactin mutagenesis on the eukaryotic cell. The key structural scaffolds mediating this mechanism is the azospirobicyclic ring (warhead). The process is initiated by a nucleophilic attack on the electrophilic ring, which results in DNA alkylation and creates another electrophilic center subjected to a second alkylation reaction. Two alkylation events cross-link the DNA, which further activate multiple and complex DNA repair mechanisms including Ataxia telangiectasia mutated-and Rad3-related (ATR), Fanconi anemia (FA), homologous recombination (HR) signaling pathways. The DNA double strands break may be the product of the repair system or spontaneously formed. Accumulation of this mutation might initiate colorectal cancer.

Mechanistic insights into colibactin signature mutation

Colibactin alkylates DNA in the eukaryotic cell leading to colorectal cancer. Overall, colibactin causes an inter-strand DNA cross-link, leading to double-strand breaks in the DNA triggering cell-cycle arrest and further to CRC. The mechanism of colibactin mutation is detailed below and illustrated in Figure 4. DNA double-strand breaks are prevalent in more than half of the patients suffering from inflammatory bowel diseases and CRC (Buc et al., 2013). The colibactin-DNA signature adduct is detected in both human and animal cells and *in vivo* in experimental animals (Wilson et al., 2019). A study conducted on mouse models of invasive carcinoma revealed that inoculation with *pks*$^{+}$ *E. coli* NC101 increases tumor and enables metastasis (Arthur et al., 2012). This tumor-promoting activity is diminished with the deletion of the colibactin gene cluster. However, this deletion does not affect the inflammatory status (Arthur et al., 2012). The DNA alkylation or formation of the covalent bond between the electrophilic warhead of colibactin (azospiro 2,4 bicyclic ring) and the nucleophilic DNA results in the formation of a colibactin–DNA adduct and creates a second electrophilic center that further reacts with DNA to form a cross-link. DNA alkylation is mediated by the electrophilic cyclopropane moiety of colibactin. Initially, colibactin forms an unstable adduct, which is considered a biomarker signature for colibactin (Wilson et al., 2019).

Cross-linked DNA adducts trigger multiple DNA repair signaling pathways, leading to the formation of double-strand breaks and further carcinogenesis (Figure 4). Another research study proposed an alternative mechanism of formation of this characteristic DNA mutation involving cupper-mediated

oxidative damage (Li et al., 2019). DNA alkylating agents constitute a major class of chemotherapeutics that cause cytotoxic DNA damage and collateral mutagenic damage, leading to cell death. This damaging process is defended by several cellular mechanisms, including base excision repair, mismatch repair, and direct DNA damage reversal. The response to alkylating agents required delicate coordination between repair pathways and show much variability between cells and individuals as reviewed (Fu et al., 2012). Alkylating agents attack the nitrogen or oxygen atoms in the DNA nitrogenous base. Alkylating agents could be monofunctional if they only have one active moiety and can attack a single site on DNA or bifunctional if they have two reactive moieties and can bind to two separate bases and consequently crosslink DNA. In 2016, Healy et al. validated the hypothesis that colibactin alkylates the DNA by cyclopropane ring opening via the formation of unsaturated imines. The authors synthesized 13 structural mimics of colibactin and tested their DNA alkylation potential (Healy et al., 2016a). In 2019, Wilson et al. used chemical synthesis coupled with an untargeted DNA adductomic approach to reveal DNA alkylation in HeLa cell lines incubated with a colibactin-producing strain of *E. coli* (Wilson et al., 2019). The same reaction is observed *in vivo* in mice (Wilson et al., 2019). The authors reveal that this covalent DNA alkylation is mediated by the electrophilic cyclopropane moiety of colibactin (Wilson et al., 2019). Other data show that colibactin cross-links DNA. The study employed NMR spectroscopy and bioinformatics-guided isotopic labeling to characterize the colibactin warhead (Vizcaino and Crawford 2015). The synthetic colibactin mimic contains a spiro bicyclic structure and can cross-links duplex DNA *in vitro*. The authors proposed that colibactin alkylates DNA via a homo-Michael addition reaction, turning colibactin into a second Michael receptor. Thereafter, intramolecular Michael addition will generate a DNA cross-link (Vizcaino and Crawford 2015). This hypothesis is supported by pieces of evidence. First, is the observation that precolibactins do not form much of the higher molecular weight adduct product when reacting with linearized plasmid DNA. Second, synthetic colibactin inspired by the biosynthetic information showed that the cyclopropane ring could be a target for thiol nucleophile attack and is essential to shearing the DNA (Healy et al., 2016a). Further results based on gel electrophoresis reveal that, upon artificial dimerization, these colibactin mimics cross-link the DNA.

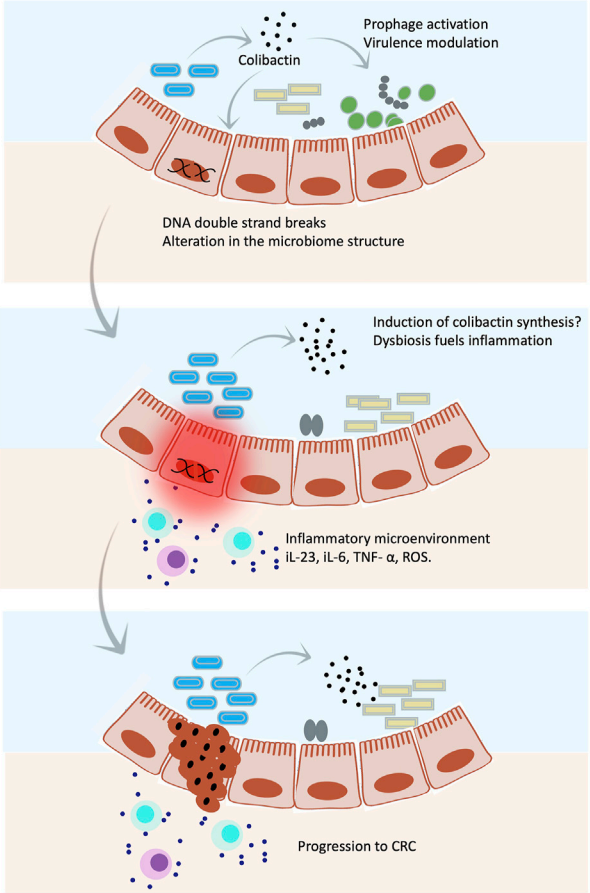

FIGURE 5
Colibactin hits targets in both eukaryotic and prokaryotic cells. Illustrations show an overall mechanism by which colibactin mediates host–microbe interaction. Colibactin shapes the gut microbial community by selective killing of some species through induction of prophages and/or stimulation of the virulence factor expression. Meanwhile, colibactin induces double strand breaks in host DNA. The altered microbial community together with the genetic abnormalities caused by colibactin triggers an inflammatory microenvironment, which might induce synthesis of more colibactin, leading to even greater damage that might result in CRC.

Colibactin-induced events leading to inflammation and cancer

The interplay between genotoxic molecules such as colibactin and inflammation is not clear. It is speculated that DNA damage initiates tumor formation while inflammatory cytokines and cells promote it by creating a microenvironment that enables more DNA damage (Balkwill and Mantovani 2001; Ullman and Itzkowitz 2011) by, for example, inducing gene expression of genotoxic molecules. Previous studies show that microbial colonization enhances the development of cancer in mice that are genetically susceptible to inflammation (Ullman and Itzkowitz 2011). A shift in gut microbes was observed during inflammation, with unknown directionality, characterized by enrichment in genera of *E. coli*, *Akkermansia*, *Shigella*, and *Bacteroides* and a sharp reduction in Lachnospiraceae, Muribaculaceae, and Lactobacilli (Lang et al., 2020). Another study suggested that the microbial shift is associated with inflammation in the first place and not with cancer in the colitis-susceptible $Il10^{-/-}$ mouse strain. Among the sifted species, *E. coli* showed a 100-fold increase in colitis (Ullman and Itzkowitz 2011). Additionally, *E. coli* NC101 causes profound colitis in germ-free mice with 80% of the subjects

developing adenocarcinoma (Ullman and Itzkowitz 2011), again questioning the directionality of the association. Another study used *in vitro* 3-D cell culture models to examine the host factors that might contribute to susceptibility to colibactin-induced cancer. The authors reported that the presence of the expression of mucin genes in forming the mucous layer that adheres to the intestinal epithelia decreased the genotoxic effect of colibactin. Moreover, the removal of the mucous layer in other models restored the genotoxicity (Reuter et al., 2018). Since inflammation is associated with degradation of the mucous layer and a decrease in the tight junction protein, also known as "leaky gut" that might be another factor to add to the colibactin–inflammation–cancer equation. Inflammation also allows leakage of microbes and other microbial products, not only colibactin, which flares up an even more intense immune response (Ahmad et al., 2017; Kidane et al., 2014). Of note is that the microbial composition in the presence of colibactin is altered, which might promote the abundance of pro-inflammatory bacteria. The interplay between colibactin-induced inflammation and cancer is illustrated in Figure 5.

Colibactin hits targets of the prokaryotic cells controlling microbiome structure

The genomic organization of the colibactin cluster suggests a potential antimicrobial activity

Microbes are known to produce microbial toxins such as antibiotics to kill competing microbes and gain significant ecological competency. To protect themselves, the toxin-producing strains mostly harbor self-resistance genes. The presence of a self-resistance gene in the colibactin cluster suggests that colibactin is not only affecting cellular target in the human cell but also the bacterial cell. The biosynthetic gene cluster of colibactin ends with a resistance gene encoding a 170-amino acid protein named *clbS*. *clbS* encodes a cyclopropane hydrolase, resulting in the ring-opening of the DNA alkylating scaffolds, conferring self-resistance to producing strains (Tripathi et al., 2017) (Figure 4B). This gene is not only present in colibactin-producing strains but also in some other strains that lack the entire colibactin cluster, suggesting that this gene is transferable within the bacterial community by horizontal gene transfer to gain an ecological advantage. *clbS*-like genes with at least 50% sequence similarity have been found in members of the human gut microbiome, namely, *Escherichia albertii*, *Kluyvera intestini*, and *Metakosakonia* sp. and the honeybee microbiome, namely, *Snodgrasella alvi* (Silpe et al., 2022). Heterologous expression of these four clbS-like genes resulted in attenuated DNA damage and phage lysis when co-cultured with a colibactin-producing strain, suggesting that acquisition of clbS provides immunity against colibactin-induceddamage. Interestingly, *clbS* protects against colibactin-specific induction of prophages but provides no protection against other inducing agents such as MMC. This resistance is intra-cellular and is not shared between cells (Silpe et al., 2022). Other studies show that deletion of the *clbS* gene does not kill the strain but its growth will be dependent on the DNA repair mechanism (Bossuet-Greif et al., 2016).

Molecular targets behind colibactin activity on prokaryotes

Colibactin belongs to the PKS/NRPS natural products, which include many antibiotics such as daptomycin and β-lactams (Walsh 2004). Earlier studies suggested that colibactin might have antibiotic-like activity but the precise mechanism was not clear. A study showed that *E. coli* harboring a colibactin cluster exhibits growth inhibition against multi-resistant *Staphylococcus aureus* in the agar diffusion method and growth competition assay. This activity is observed in 95% of the tested strains, while the ΔclbP *E. coli* lost this activity (T. Faïs et al., 2016). The authors reported that this activity requires live culture, suggesting it is an inducible trait. Another study reported that inoculation of pregnant mice with a colibactin harboring strain resulted in a decreased abundance of firmicutes and a significant alteration in microbial diversity in pups, especially after 35 days of birth (Tronnet et al., 2020). Interestingly, the authors reported increased activity in DNA repair pathways, suggesting that colibactin not only modulates the structure of gut microbes but also their function (Tronnet et al., 2020). Another research study shows that the colibactin biosynthetic gene (*clbA*) might affect siderophore biosynthesis enhancing its producer fitness (Martin et al., 2013).

In 2022, the Balskus group revealed an interesting mechanism beyond the observed activities of colibactin in shaping the microbial population (Silpe et al., 2022). They discovered that colibactin-induced damage activates SOS signaling pathways, leading to the induction of prophages exerting lethal action on their host bacteria. The authors show that the effect of colibactin on prophages extends to a wide range of phages residing in phylogenetically distinct bacteria, including *Salmonella typhimurium*, *Staphylococcus aureus*, *Citrobacter* rodentium, and *Enterococcus* faecium (Silpe et al., 2022). Interestingly, there is a significant increase in Shiga toxin production upon co-culture of *C. rodentium* (harboring Stx genes) with *pks* + *E. coli* (Silpe et al., 2022). Induction of prophages enables selective lethal action against other members of the microbial community, providing an elegant ecological advantage and enhancing the competitiveness of the producing strain.

Molecular mechanism of prophage induction following DNA damage in the host

Lytic activation of prophages in bacterial lysogens is normally induced by DNA damage, such as after exposure

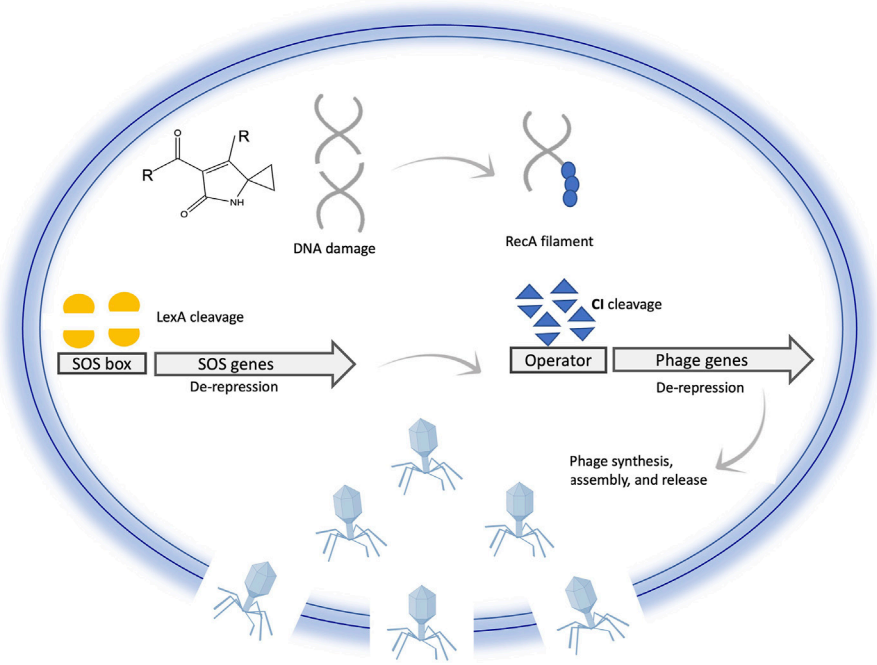

FIGURE 6
Illustration of prophage activation following DNA damage inside a bacterial cell. DNA damage induces cleavage of phage repressor genes mediated by SOS signaling. Cleavage of the phage repressor leads to exciton of prophage from the bacterial chromosome, synthesis of phage-related genes and proteins, assembly, cell lysis, and phage release. This illustration is simplified to communicate the main idea; for example CI binds to two distant regions and not only to one site as shown for simplicity of the illustration.

to UV radiation or DNA damaging agents such as mitomycin C (MMC) (Lee et al., 2006; Humphrey, Stanton, and Jensen 1995). In addition to DNA damage, other internal and external stimuli might lead to prophage induction, such as pH, heat, reactive oxygen species (ROS), or even spontaneous induction (Nanda, Thormann, and Frunzke 2015). Maintenance of lysogeny is tightly controlled by the activity of the λ CI repressor proteins. Two dimers of CI bind to the operator regions of phage genes and suppress their expression (Hochschild 2002; Little, Shepley, and Wert 1999). The CI protein is a molecular switch that controls lysogeny in lambda phages. CI binds to operator regions of phage genes and represses their expression while inducing its own expression. DNA damage activates the master regulator RecA, resulting in de-repression of SOS genes mediated by cleavage of their transcriptional repressor LexA (Gimble and Sauer 1989; Little and Michalowski 2010; Thomason et al., 2021). Activation of SOS genes and RecA leads to the cleavage of the CI protein resulting in the de-repression of phage genes to enter the lytic cycle (Hochschild 2002; Little, Shepley, and Wert 1999). This molecular mechanism is simply illustrated in Figure 6. Genetic mutations affecting dimerization of lambda repressor increase the rate of its cleavage, while repressor dimer stabilized by covalent disulfide bond resists cleavage (Gimble and Sauer 1989). An exception is the prophages in *Salmonella* genomes, which uses another inductive strategy based on the use of anti-repressor molecules that bind the dimer without cleavage, leading to its dissociation from the DNA. Production of these anti-repressors is under the direct control of LexA (Lemire, Figueroa-Bossi, and Bossi 2011).

Prophages contribute to the ecological fitness of harboring strains

Viral genes make up to 20% of microbial genomes, either as prophage-like elements, phage remnants, or fully prophages that could be induced into the lytic life cycle (Wang et al., 2010). These prophages contribute to the ecological fitness and virulence of the lysogens. Reports show that lysogens can use prophages as a survival strategy (Bossi et al., 2003; Gama et al., 2013). For example, in a mixed culture, *Salmonella enterica* induces its prophages, leading to the killing of some self-cells while the others are converted back to lysogens. The released prophages are then used as a weapon to kill competitors although it results in some self-destruction. This strategy will also benefit the phage by spreading its genes (Bossi et al., 2003; Gama et al.,

2013). Another example is the induction of prophages in *Streptococcus pneumoniae* to wipe off *S. aureus* via the production of hydrogen peroxide-inducing SOS genes. Induction of SOS leads to activation of prophages in *S. aureus*, which are mostly lysogens while S. *pneumoniae* are immune, giving S. *pneumoniae* an ecological advantage to dominate (Selva et al., 2009; Pericone et al., 2003). A study shows that deletion of nine cryptic prophages from *E-coli* suppresses fitness by rendering the bacteria more susceptible to sublethal concentrations of β-lactam and quinolone antibiotics. Moreover, this deletion rendered the bacteria less able to form biofilms and more prone to damage caused by acid or osmotic pressure (Wang et al., 2010). A study shows that prophages enable biofilm formation in *Pseudomonas aeruginosa*, contributing to its virulence and. when cells die in the biofilm, the prophage is converted to a super infective form (Rice et al., 2009). Biofilm is a group behavior in which bacterial cells adhere to one another and solid surfaces using a sticky matrix made of extracellular proteins, carbohydrates, and DNA molecules (Madsen et al., 2012). The formation of biofilm is a virulence strategy that helps enable bacteria to resist antibiotics and host immune defense. Prophage induction in a biofilm will lead to the accumulation of extracellular DNA promoting horizontal gene transfer and enhancing diversification of the microbial community within the biofilm (Molin and Tolker-Nielsen 2003). The role of prophages on biofilm formation and further consequences on host fitness is reviewed (Nanda, Thormann, and Frunzke 2015). The production of toxins is a crucial virulence trait for pathogens (Brown et al., 2006). Some toxins are encoded by bacteriophages, including cholera toxin (Ctx) and Shiga toxins (Stx), required for the virulence of *Vibrio cholerae* and *E. coli*, respectively (Waldor and Mekalanos 1996; Neely and Friedman 1998). For example, Shiga toxin (Stx) in enterohemorragic *E. coli* enables bacterial cells to attach and colonize the gut epithelia (Robinson et al., 2006). Similarly, some cells of *E. faecalis* V583 and *Streptococcus mitis* induce prophages to express phage genes to help the remaining cells adhere to human platelets, leading to systemic infection (Matos et al., 2013; Seo et al., 2010). This regulatory activity of microbiome-secreted molecules has been noted before. For example, quinolone antibiotics increase the production of Stx toxin via activation of prophages via SOS response (Pleguezuelos-Manzano et al., 2020). Co-culture of colibactin with *Citrobacter rodentium* increases the production of Stx (Silpe et al., 2022). Another interesting activity of colibactin was reported by Marcq et al. (2014). Driven by the association between pks$^+$ *E. coli* strains and septicemia, the authors investigated the effect of colibactin-harboring strains on lymphopenia and sepsis. The results show that colibactin-producing *E. coli* causes the characteristic double-strand break in the DNA of lymphocytes, leading to an exaggerated lymphopenia and subsequent low survival rate from bacteremia in mice (Marcq et al., 2014).

Conclusion

Colibactin demonstrates the potential of microbiome secreted chemistry to hit multiple targets spanning prokaryotic and eukaryotic cell machinery. It is interesting to speculate that colibactin gives the producing species an ecological advantage in occupying specific niches such as the human gut by controlling other competitive microbes. Understanding how precisely colibactin-producing strains alter gut microbiome composition and their further indirect impact on human health and diseases seems exciting. Of note, we still do not appreciate all the microbiome species that we host in our bodies or their cryptic genes and encoded chemistry. Revealing the microbiome products that exert microbial control and affect population dynamics will help to advance better strategies to tackle the antibiotic resistance crisis. Microbiome chemistry is certainly a new uncharted Frontier for understanding mediators of human conditions and developing innovative therapeutics or diagnostic biomarkers. For example, delivering colibactin mimics or genes to induce the lethal killing of a cancer cell or as an antimicrobial for life-threatening biofilm infection.

Is colibactin a harmful molecule?

Host-associated microbes produce molecules that help to increase their ecological fitness and competitiveness and to establish a long-term, mostly symbiotic, relationship with the host. From an ecological perspective, we can imagine colibactin as a beneficial microbial product that is produced to shape the microbial community and confer beneficial traits to the host, such as decreasing inflammation as long as the mutualistic relationship is established. Evidence for this hypothesis came from the research on Nissle 1917. The efficacy of probiotic *E-coli* Nissle 1917 in treating colitis and preventing further remission is even comparable to that of mesalazine, the gold standard drug in the treatment of colitis (Kruis et al., 2004). The mechanism of action involves modulation of cytokine expression. Interestingly, further investigation on Nissle 1917 activity suggests that its beneficial anti-inflammatory activity is dependent on the expression of the colibactin biosynthetic pathway (Olier et al., 2012). Knockout strains that lost the ability to express the colibactin cluster not only lost the anti-inflammatory activity but also resulted in more inflammation (Olier et al., 2012). Moreover, inflammation is thought to be a triggering signal for further expression of the colibactin gene cluster. Chronic inflammation and accumulation of DNA damage will eventually lead to cancer development. The question now is, do these microbiome strains, or more specifically colibactin, initiate cancer or evolved to combat cancer and act as an immunomodulin

based on the activity profile of *E. coli* Nissle 1917? One can postulate that it produces colibactin to kill transformative cells at the beginning of inflammation in a similar way to chemotherapeutic agents and more inflammation triggers more synthesis of the mysterious molecule(s). This bidirectional dependency is puzzling and poses an outstanding question on the directionality of microbiome diseases association and warns of the urgent need for a holistic deep understanding of the microbiome secreted chemistry evolved to hit multiple cellular targets under very tight and complex regulation resulting in a variety of negative and positive outcomes for the host. Another interesting hypothesis is that the colibactin biosynthetic cluster encodes or supplies precursor molecules with immunomodulatory activity as originally proposed (Olier et al., 2012). Support for this hypothesis comes from the strong association between colitis and microbial dysbiosis, so it is interesting to speculate on the role of colibactin in shaping microbiome structure and whether it may restore the balanced composition to the pre-colitis status. However, the members of Enterobacteriacea are often considered proinflammatory, and some reports show significant enrichment in Enterobacteriacea with the onset of gastrointestinal inflammatory conditions (Garrett et al., 2010) and the dominant presence of adherent-invasive strains of *E. coli* such as LF82 (Carvalho et al., 2008), belonging to the same phylogenetic group as Nissle 1917, although it lacks the colibactin genomic cluster. Taken together, our knowledge of microbiome mediators and their evolved function is still in its infancy. Despite the explosion of research on the microbiome, the diversity and richness in species of the microbiome, their cryptic genes, and secreted molecules are still a dark matter.

A proposed model for colibactin–microbe–host interaction and health outcome

Host-associated microbes produce toxic molecules with the primary function of killing competitors and gaining an ecological advantage to dominate a particular niche. However, these toxins might also hit molecular targets in the host. Considering that the priority function of colibactin is microbial related, we can propose that the reasonable order of events leading to CRC might be as follows: 1) colibactin shapes microbial composition in the gut to modulate inflammation, especially during microbial dysbiosis; 2) chronic dysbiosis triggers inflammation, which leads to leaky gut; 3) colibactin diffuses inside the eukaryotic cell and causes DNA damage eliciting the repair mechanism; 4) chronic inflammatory microenvironment further advances the microbial dysbiosis, and gut permeability resulted in more diffusion of colibactin to eukaryotic cells (or maybe an induction of its synthesis); and 5) under high load of colibactin, accumulation of DNA damage might occur leading to colorectal cancer (Figure 7). This situation gets worse with a genetic predisposition to inflammation or defect in the DNA repair pathways. Considering this model, chronic microbial dysbiosis and inflammation are crucial for colibactin-induced colorectal cancer and might serve as a risk factor to predicting CRC, especially if this is combined with genetic disorders in genes related to the DNA repair pathways or immune function. This understanding is not only helpful in predicting risks but also in taking preventative measures such as implementing an anti-inflammatory diet for high-risk groups to decrease the incidence of CRC.

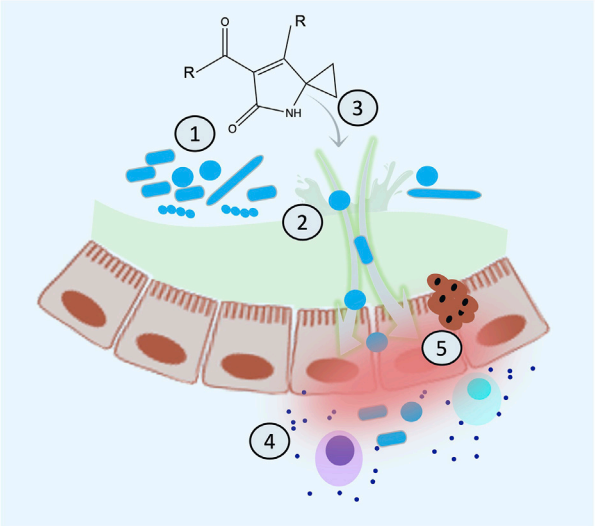

FIGURE 7
Proposed mechanistic model for the sequence of the events of colibactin-induced cancer. **(A)** Colibactin induces dysbiosis, **(B)** dysbiosis results in inflammation and leaky gut, **(C)** colibactin diffuses inside the cell resulting in DNA damage, **(D)** chronic inflammation increases the load of colibactin inside the cell and more DNA damage, and **(E)** accumulating DNA damage leads to CRC.

Author contributions

The author confirms being the sole contributor of this work and has approved it for publication.

Conflict of interest

The author declares that the research was conducted in the absence of any commercial or financial relationships that could be construed as a potential conflict of interest.

Publisher's note

All claims expressed in this article are solely those of the authors and do not necessarily represent those of their affiliated organizations, or those of the publisher, the editors, and the reviewers. Any product that may be evaluated in this article, or claim that may be made by its manufacturer, is not guaranteed or endorsed by the publisher.

References

Ahmad, R., Sorrell, M. F., Batra, S. K., Dhawan, P., Singh, A. B., and Dhawan, P. (2017). Gut permeability and mucosal inflammation: Bad, good or context dependent. *Mucosal Immunol.* 10 (2), 307–317. doi:10.1038/mi.2016.128

Arthur, Janelle C., Perez-Chanona, Ernesto, Mühlbauer, Marcus, Tomkovich, Sarah, Uronis, Joshua M., Fan, Ting-Jia, et al. (2012). Intestinal inflammation targets cancer-inducing activity of the microbiota. *Science* 338 (6103), 120–123. doi:10.1126/science.1224820

Balkwill, F., and Mantovani, A. (2001). Inflammation and cancer: Back to virchow? *Lancet (London, Engl.* 357 (9255), 539–545. doi:10.1016/S0140-6736(00)04046-0

Balskus, Emily P. (2015). Colibactin: Understanding an elusive gut bacterial genotoxin. *Nat. Prod. Rep.* 32 (11), 1534–1540. doi:10.1039/c5np00091b

Bian, Xiaoying, Fu, Jun, Plaza, Alberto, Herrmann, Jennifer, Pistorius, Dominik, Zhang, Youming, et al. (2013). *In vivo* evidence for a prodrug activation mechanism during colibactin maturation. *Chembiochem* 14 (10), 1194–1197. doi:10.1002/cbic.201300208

Bian, Xiaoying, Plaza, Alberto, Zhang, Youming, and Müller, Rolf (2015). Two more pieces of the colibactin genotoxin puzzle from Escherichia coli show incorporation of an unusual 1-aminocyclopropanecarboxylic acid moiety. *Chem. Sci.* 6 (5), 3154–3160. doi:10.1039/C5SC00101C

Bode, Helge B. (2015). The microbes inside us and the race for colibactin. *Angew. Chem. Int. Ed. Engl.* 54 (36), 10408–10411. doi:10.1002/anie.201505341

Bondarev, Vladimir, Richter, Michael, Romano, Stefano, Piel, Jörn, Schwedt, Anne, and Schulz-Vogt, Heide N. (2013). The genus Pseudovibrio contains metabolically versatile bacteria adapted for symbiosis. *Environ. Microbiol.* 15 (7), 2095–2113. doi:10.1111/1462-2920.12123

Bossi, Lionello, Fuentes, Juan A., Guido, Mora, and Figueroa-Bossi, Nara (2003). Prophage contribution to bacterial population dynamics. *J. Bacteriol.* 185 (21), 6467–6471. doi:10.1128/jb.185.21.6467-6471.2003

Bossuet-Greif, Nadège, Dubois, Damien, Petit, Claude, Tronnet, Sophie, Martin, Patricia, Bonnet, Richard, et al. (2016). Escherichia coli ClbS is a colibactin resistance protein. *Mol. Microbiol.* 99 (5), 897–908. doi:10.1111/mmi.13272

Brotherton, Carolyn A., and Balskus, Emily P. (2013). A prodrug resistance mechanism is involved in colibactin biosynthesis and cytotoxicity. *J. Am. Chem. Soc.* 135 (9), 3359–3362. doi:10.1021/ja312154m

Brotherton, Carolyn A., Wilson, Matthew, Byrd, Gary, and Balskus, Emily P. (2015). Isolation of a metabolite from the pks island provides insights into colibactin biosynthesis and activity. *Org. Lett.* 17 (6), 1545–1548. doi:10.1021/acs.orglett.5b00432

Brown, Nat F., Wickham, Mark E., Coombes, Brian K., and Finlay, B. Brett (2006). Crossing the line: Selection and evolution of virulence traits. *PLoS Pathog.* 2 (5), e42. doi:10.1371/journal.ppat.0020042

Buc, Emmanuel, Dubois, Damien, Sauvanet, Pierre, Raisch, Jennifer, Delmas, Julien, Darfeuille-Michaud, Arlette, et al. (2013). High prevalence of mucosa-associated E. Coli producing cyclomodulin and genotoxin in colon cancer. *PloS One* 8 (2), e56964. doi:10.1371/journal.pone.0056964

Carvalho, Frédéric A., Barnich, Nicolas, Sauvanet, Pierre, Darcha, Claude, Gelot, Agathe, and Darfeuille-Michaud, Arlette (2008). Crohn's disease-associated Escherichia coli LF82 aggravates colitis in injured mouse colon via signaling by flagellin. *Inflamm. Bowel Dis.* 14 (8), 1051–1060. doi:10.1002/ibd.20423

Cougnoux, Antony, Gibold, Lucie, Robin, Frederic, Dubois, Damien, Pradel, Nathalie, Darfeuille-Michaud, Arlette, et al. (2012). Analysis of structure-function relationships in the colibactin-maturating enzyme ClbP. *J. Mol. Biol.* 424 (3–4), 203–214. doi:10.1016/j.jmb.2012.09.017

de Vos, Willem M., Herbert, Tilg, Van Hul, Matthias, and Cani, Patrice D. (2022). Gut microbiome and health: Mechanistic insights. *Gut* 71 (5), 1020–1032. doi:10.1136/gutjnl-2021-326789

Dhanaraju, Rajkumar, and Rao, Desirazu N. (2022). The human microbiome: An acquired organ? *Reson.* 27 (2), 247–272. doi:10.1007/s12045-022-1312-7

Dubois, Damien, Baron, Olivier, Antony, Cougnoux, Delmas, Julien, Pradel, Nathalie, Boury, Michèle, et al. (2011). ClbP is a prototype of a peptidase subgroup involved in biosynthesis of nonribosomal peptides. *J. Biol. Chem.* 286 (41), 35562–35570. doi:10.1074/jbc.M111.221960

Engel, Philipp, Vizcaino, Maria I., and Crawford, Jason M. (2015). Gut symbionts from distinct hosts exhibit genotoxic activity via divergent colibactin biosynthesis pathways. *Appl. Environ. Microbiol.* 81 (4), 1502–1512. doi:10.1128/AEM.03283-14

Faïs, T., Cougnoux, A., Dalmasso, G., Laurent, F., Delmas, J., and Bonnet, R. (2016). Antibiotic activity of Escherichia coli against multiresistant Staphylococcus aureus. *Antimicrob. Agents Chemother.* 60 (11), 6986–6988. doi:10.1128/AAC.00130-16

Faïs, Tiphanie, Delmas, Julien, Barnich, Nicolas, Bonnet, Richard, and Dalmasso, Guillaume (2018). Colibactin: More than a new bacterial toxin. *Toxins* 10 (4), E151. doi:10.3390/toxins10040151

Fu, Dragony, Calvo, Jennifer A., and Samson, Leona D. (2012). Balancing repair and tolerance of DNA damage caused by alkylating agents. *Nat. Rev. Cancer* 12 (2), 104–120. doi:10.1038/nrc3185

Gama, João Alves, Reis, Ana Maria, Domingues, Iolanda, Mendes-Soares, Helena, Matos, Ana Margarida, and Dionisio, Francisco (2013). Temperate bacterial viruses as double-edged swords in bacterial warfare. *PloS One* 8 (3), e59043. doi:10.1371/journal.pone.0059043

Garrett, Wendy S., Gallini, Carey A., Yatsunenko, Tanya, Michaud, Monia, DuBois, Andrea, Delaney, Mary L., et al. (2010). Enterobacteriaceae act in concert with the gut microbiota to induce spontaneous and maternally transmitted colitis. *Cell Host Microbe* 8 (3), 292–300. doi:10.1016/j.chom.2010.08.004

Gimble, F. S., and Sauer, R. T. (1989). Lambda repressor mutants that are better substrates for RecA-mediated cleavage. *J. Mol. Biol.* 206 (1), 29–39. doi:10.1016/0022-2836(89)90521-4

Healy, Alan R., Herman, Nikolayevskiy, Patel, Jaymin R., Crawford, Jason M., and Herzon, Seth B. (2016a). A mechanistic model for colibactin-induced genotoxicity. *J. Am. Chem. Soc.* 138 (48), 15563–15570. doi:10.1021/jacs.6b10354

Healy, Alan R., Vizcaino, Maria I., Crawford, Jason M., and Herzon, Seth B. (2016b). Convergent and modular synthesis of candidate precolibactins. Structural revision of precolibactin A. *J. Am. Chem. Soc.* 138 (16), 5426–5432. doi:10.1021/jacs.6b02276

Healy, Alan R., Wernke, Kevin M., Kim, Chung Sub, Lees, Nicholas R., Crawford, Jason M., and Herzon, Seth B. (2019). Synthesis and reactivity of precolibactin 886. *Nat. Chem.* 11 (10), 890–898. doi:10.1038/s41557-019-0338-2

Hirayama, Yuichiro, Tsunematsu, Yuta, Yoshikawa, Yuko, Tamafune, Ryota, Matsuzaki, Nobuo, Iwashita, Yuji, et al. (2019). Activity-based probe for screening of high-colibactin producers from clinical samples. *Org. Lett.* 21 (12), 4490–4494. doi:10.1021/acs.orglett.9b01345

Hochschild, Ann. (2002). The λ switch: CI closes the gap in autoregulation. *Curr. Biol.* 12 (3), R87–R89. doi:10.1016/S0960-9822(02)00667-X

Hsiao, Elaine Y., McBride, Sara W., Hsien, Sophia, Gil, Sharon, Hyde, Embriette R., Tyler, McCue, et al. (2013). Microbiota modulate behavioral and physiological abnormalities associated with neurodevelopmental disorders. *Cell* 155 (7), 1451–1463. doi:10.1016/j.cell.2013.11.024

Humphrey, S. B., Stanton, T. B., and Jensen, N. S. (1995). Mitomycin C induction of bacteriophages from serpulina hyodysenteriae and serpulina innocens. *FEMS Microbiol. Lett.* 134 (1), 97–101. doi:10.1111/j.1574-6968.1995.tb07921.x

Jiang, Yindi, Stornetta, Alessia, Villalta, Peter W., Wilson, Matthew R., Boudreau, Paul D., Zha, L., et al. (2019). Reactivity of an unusual amidase may explain colibactin's DNA cross-linking activity. *J. Am. Chem. Soc.* 141 (29), 11489–11496. doi:10.1021/jacs.9b02453

Kidane, Dawit, Chae, Wook Jin, Czochor, Jennifer, Eckert, Kristin A., Glazer, Peter M., Bothwell, Alfred L. M., et al. (2014). Interplay between DNA repair and inflammation, and the link to cancer. *Crit. Rev. Biochem. Mol. Biol.* 49 (2), 116–139. doi:10.3109/10409238.2013.875514

Kim, Janice J., Bridle, Byram W., Ghia, Jean-Eric, Wang, Huaqing, Syed, Shahzad N., Manocha, Marcus M., et al. (2013). Targeted inhibition of serotonin type 7 (5-HT7) receptor function modulates immune responses and reduces the severity of

intestinal inflammation. *J. Immunol.* 190 (9), 4795–4804. doi:10.4049/jimmunol.1201887

Kruis, W., Fric, P., Pokrotnieks, J., Lukás, M., Fixa, B., Kascák, M., et al. (2004). Maintaining remission of ulcerative colitis with the probiotic Escherichia coli Nissle 1917 is as effective as with standard mesalazine. *Gut* 53 (11), 1617–1623. doi:10.1136/gut.2003.037747

Lang, Michaela, Baumgartner, Maximilian, Rożalska, Aleksandra, Frick, Adrian, Riva, Alessandra, Jarek, Michael, et al. (2020). Crypt residing bacteria and proximal colonic carcinogenesis in a mouse model of lynch syndrome. *Int. J. Cancer* 147 (8), 2316–2326. doi:10.1002/ijc.33028

Lee, Young-Ju, Park, Su-Jung, Ciccone, Samantha L. M., Kim, Chong-Rak, and Lee, Suk-Hee (2006). An *in vivo* analysis of MMC-induced DNA damage and its repair. *Carcinogenesis* 27 (3), 446–453. doi:10.1093/carcin/bgi254

Lemire, Sébastien, Figueroa-Bossi, Nara, and Bossi, Lionello (2011). Bacteriophage crosstalk: Coordination of prophage induction by trans-acting antirepressors. *PLoS Genet.* 7 (6), e1002149. doi:10.1371/journal.pgen.1002149

Li, Zhi Shan, Schmauss, Claudia, Cuenca, Abigail, Ratcliffe, Elyanne, and Gershon, Michael D. (2006). Physiological modulation of intestinal motility by enteric dopaminergic neurons and the D2 receptor: Analysis of dopamine receptor expression, location, development, and function in wild-type and knock-out mice. *J. Neurosci.* 26 (10), 2798–2807. doi:10.1523/JNEUROSCI.4720-05.2006

Li, Zhong-Rui, Li, Jie, Cai, Wenlong, Lai, Jennifer Y. H., McKinnie, Shaun M. K., Zhang, Wei-Peng, et al. (2019). Macrocyclic colibactin induces DNA double-strand breaks via copper-mediated oxidative cleavage. *Nat. Chem.* 11 (10), 880–889. doi:10.1038/s41557-019-0317-7

Li, Zhong-Rui, Li, Jie, Gu, Jin-Ping, Lai, Jennifer Y. H., Duggan, Brendan M., Zhang, Wei-Peng, et al. (2016). Divergent biosynthesis yields a cytotoxic aminomalonate-containing precolibactin. *Nat. Chem. Biol.* 12 (10), 773–775. doi:10.1038/nchembio.2157

Li, Zhong-Rui, Li, Yongxin, Lai, Jennifer Y. H., Tang, Jianqiang, Wang, Bin, Lu, Liang, et al. (2015). Critical intermediates reveal new biosynthetic events in the enigmatic colibactin pathway. *Chembiochem* 16 (12), 1715–1719. doi:10.1002/cbic.201500239

Little, John W., Shepley, Donald P., and Wert, David W. (1999). Robustness of a gene regulatory circuit. *EMBO J.* 18 (15), 4299–4307. doi:10.1093/emboj/18.15.4299

Little, John W., and Michalowski, Christine B. (2010). Stability and instability in the lysogenic state of phage lambda. *J. Bacteriol.* 192 (22), 6064–6076. doi:10.1128/JB.00726-10

Luo, Yi, Ruan, Li-Fang, Zhao, Chang-Ming, Wang, Cheng-Xian, Peng, Dong-Hai, and Sun, Ming (2011). Validation of the intact zwittermicin A biosynthetic gene cluster and discovery of a complementary resistance mechanism in Bacillus thuringiensis. *Antimicrob. Agents Chemother.* 55 (9), 4161–4169. doi:10.1128/AAC.00111-11

Madsen, Jonas Stenløkke, Burmølle, Mette, Hansen, Lars Hestbjerg, and Sørensen, Søren Johannes (2012). The interconnection between biofilm formation and horizontal gene transfer. *FEMS Immunol. Med. Microbiol.* 65 (2), 183–195. doi:10.1111/j.1574-695X.2012.00960.x

Marcq, Ingrid, Martin, Patricia, Payros, Delphine, Cuevas-Ramos, Gabriel, Boury, Michèle, Watrin, Claude, et al. (2014). The genotoxin colibactin exacerbates lymphopenia and decreases survival rate in mice infected with septicemic Escherichia coli. *J. Infect. Dis.* 210 (2), 285–294. doi:10.1093/infdis/jiu071

Martin, Patricia, Marcq, Ingrid, Magistro, Giuseppe, Penary, Marie, Garcie, Christophe, Payros, Delphine, et al. (2013). Interplay between siderophores and colibactin genotoxin biosynthetic pathways in Escherichia coli. *PLoS Pathog.* 9 (7), e1003437. doi:10.1371/journal.ppat.1003437

Matos, R. C., Lapaque, N., Rigottier-Gois, L., Debarbieux, L., Meylheuc, T., Gonzalez-Zorn, B., et al. (2013). Enterococcus faecalis prophage dynamics and contributions to pathogenic traits. *PLoS Genet.* 9 (6), e1003539. doi:10.1371/journal.pgen.1003539

Molin, Søren, and Tolker-Nielsen, Tim (2003). Gene transfer occurs with enhanced efficiency in biofilms and induces enhanced stabilisation of the biofilm structure. *Curr. Opin. Biotechnol.* 14 (3), 255–261. doi:10.1016/s0958-1669(03)00036-3

Moretti, C., Hosni, T., Vandemeulebroecke, K., Brady, C., De Vos, P., Buonaurio, R., et al. (2011). Erwinia Oleae sp. Nov., isolated from olive knots caused by Pseudomonas savastanoi pv. Savastanoi. *Int. J. Syst. Evol. Microbiol.* 61 (11), 2745–2752. doi:10.1099/ijs.0.026336-0

Nanda, Arun M., Thormann, Kai, and Julia, Frunzke (2015). Impact of spontaneous prophage induction on the fitness of bacterial populations and host-microbe interactions. *J. Bacteriol.* 197 (3), 410–419. doi:10.1128/jb.02230-14

Neely, Melody N., and Friedman, David I. (1998). Arrangement and functional identification of genes in the regulatory region of lambdoid phage H-19B, a carrier of a shiga-like toxin. *Gene* 223 (1–2), 105–113. doi:10.1016/s0378-1119(98)00236-4

Nougayrède, Jean-Philippe, Homburg, Stefan, Taieb, Frédéric, Boury, Michèle, Brzuszkiewicz, Elzbieta, Gottschalk, Gerhard, et al. (2006). Escherichia coli induces DNA double-strand breaks in eukaryotic cells. *Sci. (New York, N.Y.)* 313 (5788), 848–851. doi:10.1126/science.1127059

Olier, M., Marcq, I., Salvador-Cartier, C., Secher, T., Ulrich, D., Boury, M., et al. (2012). Genotoxicity of Escherichia coli Nissle 1917 strain cannot Be dissociated from its probiotic activity. *Gut Microbes* 3 (6), 501–509. doi:10.4161/gmic.21737

Pericone, Christopher D., Park, Sunny, James, A. Imlay, and Weiser, Jeffrey N. (2003). Factors contributing to hydrogen peroxide resistance in Streptococcus pneumoniae include pyruvate oxidase (SpxB) and avoidance of the toxic effects of the fenton reaction. *J. Bacteriol.* 185 (23), 6815–6825. doi:10.1128/jb.185.23.6815-6825.2003

Pleguezuelos-Manzano, Cayetano, Puschhof, Jens, Arne van HoeckWood, Henry M., Nomburg, Jason, Gurjao, Carino., et al. (2020). Mutational signature in colorectal cancer caused by genotoxic Pks+ E. Coli. *Nature* 580 (7802), 269–273. doi:10.1038/s41586-020-2080-8

Reuter, Christian, Alzheimer, Mona, Walles, Heike, and Oelschlaeger, Tobias A. (2018). An adherent mucus layer attenuates the genotoxic effect of colibactin. *Cell. Microbiol.* 20 (2), e12812. doi:10.1111/cmi.12812

Rice, Scott A., Tan, Chuan Hao, Kung, Vanderlene, Woo, Jerry, Tay, Martin, Hauser, Alan, et al. (2009). The biofilm life cycle and virulence of Pseudomonas aeruginosa are dependent on a filamentous prophage. *ISME J.* 3 (3), 271–282. doi:10.1038/ismej.2008.109

Robinson, Cory M., Sinclair, James F., Smith, Michael J., and O'Brien, Alison D. (2006). Shiga toxin of enterohemorrhagic Escherichia coli type O157: H7 promotes intestinal colonization. *Proc. Natl. Acad. Sci. U. S. A.* 103 (25), 9667–9672. doi:10.1073/pnas.0602359103

Schultz, Michael (2008). Clinical use of E. Coli Nissle 1917 in inflammatory bowel disease. *Inflamm. Bowel Dis.* 14 (7), 1012–1018. doi:10.1002/ibd.20377

Selva, Laura, Viana, David, Regev-Yochay, Gili, Trzcinski, Krzysztof, Lasa, Inigo, Novick, Richard P., et al. (2009). Killing niche competitors by remote-control bacteriophage induction. *Proc. Natl. Acad. Sci. U. S. A.* 106 (4), 1234–1238. doi:10.1073/pnas.0809600106

Seo, Ho Seong, Xiong, Yan Q., Mitchell, Jennifer, Seepersaud, Ravin, Bayer, Arnold S., and Sullam, Paul M. (2010). Bacteriophage lysin mediates the binding of Streptococcus mitis to human platelets through interaction with fibrinogen. *PLoS Pathog.* 6 (8), e1001047. doi:10.1371/journal.ppat.1001047

Sharon, Gil, Garg, Neha, Debelius, Justine, Knight, Rob, Dorrestein, Pieter C., and Mazmanian, Sarkis K. (2014). Specialized metabolites from the microbiome in health and disease. *Cell Metab.* 20 (5), 719–730. doi:10.1016/j.cmet.2014.10.016

Silpe, Justin E., Joel, W. H., Wong, Siân V. Owen, Balskus, Emily P., and Balskus, E. P. (2022). The bacterial toxin colibactin triggers prophage induction. *Nature* 603 (7900), 315–320. doi:10.1038/s41586-022-04444-3

Tang, Jian-Wei, Liu, Xin, Ye, Wei, Li, Zhong-rui, and Qian, Pei-Yuan (2022). Biosynthesis and bioactivities of microbial genotoxin colibactins. *Nat. Product. Rep.* 39 (5), 991–1014. doi:10.1039/D1NP00050K

Thomason, Lynn C., Schiltz, Carl J., Court, Carolyn, Hosford, Christopher J., Chappie, Myfanwy C. Adams, Joshua S., Court, Donald L., et al. (2021). Bacteriophage λ RexA and RexB functions assist the transition from lysogeny to lytic growth. *Mol. Microbiol.* 116 (4), 1044–1063. doi:10.1111/mmi.14792

Tichenor, Mark S., and Boger, Dale L. (2008). Yatakemycin: Total synthesis, DNA alkylation, and biological properties. *Nat. Prod. Rep.* 25 (2), 220–226. doi:10.1039/b705665f

Tripathi, Prabhanshu, Shine, Emilee E., Healy, Alan R., Kim, Chung Sub, Herzon, Seth B., Bruner, Steven D., et al. (2017). ClbS is a cyclopropane hydrolase that confers colibactin resistance. *J. Am. Chem. Soc.* 139 (49), 17719–17722. doi:10.1021/jacs.7b09971

Tronnet, Sophie, Floch, Pauline, Lucarelli, Laetitia, Gaillard, Deborah, Martin, Patricia, Serino, Matteo, et al. (2020). The genotoxin colibactin shapes gut microbiota in mice. *MSphere* 5 (4), e00589–20. doi:10.1128/mSphere.00589-20

Ullman, Thomas A., and Itzkowitz, Steven H. (2011). Intestinal inflammation and cancer. *Gastroenterology* 140 (6), 1807–1816. doi:10.1053/j.gastro.2011.01.057

Vizcaino, Maria I., and Crawford, Jason M. (2015). The colibactin warhead crosslinks DNA. *Nat. Chem.* 7 (5), 411–417. doi:10.1038/nchem.2221

Vizcaino, Maria I., Engel, Philipp, Trautman, Eric, Crawford, Jason M., and Crawford, J. M. (2014). Comparative metabolomics and structural characterizations illuminate colibactin pathway-dependent small molecules. *J. Am. Chem. Soc.* 136 (26), 9244–9247. doi:10.1021/ja503450q

Waldor, Matthew K., and Mekalanos, John J. (1996). Lysogenic conversion by a filamentous phage encoding cholera toxin. *Science* 272 (5270), 1910–1914. doi:10.1126/science.272.5270.1910

Walsh, Christopher T. (2004). Polyketide and nonribosomal peptide antibiotics: Modularity and versatility. *Sci. (New York, N.Y.)* 303 (5665), 1805–1810. doi:10.1126/science.1094318

Wang, Xiaoxue, Kim, Younghoon, Ma, Qun, Hong, Seok Hoon, Pokusaeva, Karina, Sturino, Joseph M., et al. (2010). Cryptic prophages help bacteria cope with adverse environments. *Nat. Commun.* 1 (1), 147–149. doi:10.1038/ncomms1146

Wernke, Kevin M., Xue, Mengzhao, Tirla, Alina, Kim, Chung Sub, Crawford, Jason M., and Herzon, Seth B. (2020). Structure and bioactivity of colibactin. *Bioorg. Med. Chem. Lett.* 30 (15), 127280. doi:10.1016/j.bmcl.2020.127280

Williams, Peyton C., Wernke, Kevin M., Tirla, Alina, and Herzon, Seth B. (2020). Employing chemical synthesis to study the structure and function of colibactin, a 'dark matter' metabolite. *Nat. Prod. Rep.* 37 (11), 1532–1548. doi:10.1039/d0np00072h

Wilson, Matthew R., Jiang, Yindi, Villalta, Peter W., Stornetta, Alessia, Boudreau, Paul D., Carrá, Andrea, et al. (2019). The human gut bacterial genotoxin colibactin alkylates DNA. *Science* 363 (6428), eaar7785. doi:10.1126/science.aar7785

Wilson, Matthew R., Zha, Li, and Balskus, Emily P. (2017). Natural product discovery from the human microbiome. *J. Biol. Chem.* 292 (21), 8546–8552. doi:10.1074/jbc.R116.762906

Xue, Mengzhao, Kim, Chung Sub, Healy, Alan R., Wernke, Kevin M., Wang, Zhixun, Frischling, Madeline C., et al. (2019). Structure elucidation of colibactin and its DNA cross-links. *Science* 365 (6457), eaax2685. doi:10.1126/science.aax2685

Zha, Yuguo, Chong, Hui, Yang, Pengshuo, and Kang, Ning (2022). Microbial dark matter: From discovery to applications. *Genomics Proteomics Bioinforma.* S1672-0229 (22), 00037–7. doi:10.1016/j.gpb.2022.02.007

Zhou, Tao, Hirayama, Yuichiro, Tsunematsu, Yuta, Suzuki, Nanami, Tanaka, Seiji, Uchiyama, Nahoko, et al. (2021). Isolation of new colibactin metabolites from wild-type Escherichia coli and *in situ* trapping of a mature colibactin derivative. *J. Am. Chem. Soc.* 143 (14), 5526–5533. doi:10.1021/jacs.1c01495

frontiers | Frontiers in Pharmacology

TYPE Original Research
PUBLISHED 23 September 2022
DOI 10.3389/fphar.2022.987882

Check for updates

OPEN ACCESS

EDITED BY
Fareeha Anwar,
Riphah International University, Pakistan

REVIEWED BY
Atanu Singha Roy,
National Institute of Technology Meghalaya, India
Rufeng Wang,
Beijing University of Chinese Medicine, China

*CORRESPONDENCE
Lin-Sen Qing,
qingls@cib.ac.cn
Pei Luo,
pluo@must.edu.mo

†These authors have contributed equally to this work

SPECIALTY SECTION
This article was submitted to Predictive Toxicology, a section of the journal Frontiers in Pharmacology

RECEIVED 06 July 2022
ACCEPTED 01 September 2022
PUBLISHED 23 September 2022

CITATION
Wu Y-J, Li Z-H, Li J-Y, Zhou Y, Wang R-Y, Chen X-Y, Qing L-S and Luo P (2022), Elucidation of the binding mechanism of astragaloside IV derivative with human serum albumin and its cardiotoxicity in zebrafish embryos.
Front. Pharmacol. 13:987882.
doi: 10.3389/fphar.2022.987882

COPYRIGHT
© 2022 Wu, Li, Li, Zhou, Wang, Chen, Qing and Luo. This is an open-access article distributed under the terms of the Creative Commons Attribution License (CC BY). The use, distribution or reproduction in other forums is permitted, provided the original author(s) and the copyright owner(s) are credited and that the original publication in this journal is cited, in accordance with accepted academic practice. No use, distribution or reproduction is permitted which does not comply with these terms.

Elucidation of the binding mechanism of astragaloside IV derivative with human serum albumin and its cardiotoxicity in zebrafish embryos

You-Jiao Wu[1†], Zhan-Hua Li[1†], Jiu-Yan Li[1], Yan Zhou[2], Run-Yue Wang[2], Xiao-Yi Chen[1], Lin-Sen Qing[2]* and Pei Luo[1]*

[1]State Key Laboratories for Quality Research in Chinese Medicines, Macau University of Science and Technology, Taipa, Macao, SAR, China, [2]Chengdu Institute of Biology, Chinese Academy of Sciences, Chengdu, China

LS-102 is a new derivative of astragaloside IV (AGS IV) that has been shown to possess potentially significant cardioprotective effects. However, there are no reports concerning its interaction with human serum albumin (HSA) and toxicology in vertebrates. The present investigation was undertaken to characterize the interaction of AGS IV and LS-102 with HSA using equilibrium dialysis and UHPLC-MS/MS methods, along with computational methods. Notably, the effects of AGS IV and LS-102 were studied *in vivo* using the zebrafish embryo model. Markers related to embryonic cardiotoxicity and thrombosis were evaluated. We showed that the plasma protein binding rate of AGS IV (94.04%–97.42%) was significantly higher than that of LS-102 (66.90%–69.35%). Through site marker competitive experiments and molecular docking, we found that AGS IV and LS-102 were located at the interface of subdomains IIA and IIIA, but the site I might be the primary binding site. Molecular dynamics revealed that AGS IV showed a higher binding free energy mainly due to the stronger hydrophobic and hydrogen bonding interactions. Moreover, the secondary structure implied no obvious effect on the protein structure and conformation during the binding of LS-102. LS-102 significantly ameliorated the astramizole-induced heart rate slowing, increased SV-BA spacing, and prevented arachidonic acid-induced thrombosis in zebrafish. To our knowledge, we are the first to reveal that LS-102 binds to HSA with reversible and moderate affinity, indicating its easy diffusion from the circulatory system to the target tissue, thereby providing significant insights into its pharmacokinetic and pharmacodynamic properties when spread in the human body. Our results also provide a reference for the rational clinical application of LS-102 in the cardiovascular field.

KEYWORDS

astragaloside IV derivative, drug-HSA interaction, equilibrium dialysis, UHPLC-MS/MS, molecular modeling, zebrafish

1 Highlights

A comparison between astragaloside IV and LS-102 on the interaction with HSA was performed.

Equilibrium dialysis and UHPLC–MS/MS combined with *in silico* approaches was established.

Preliminary elucidation the potential mechanism of cardiovascular toxicity caused by LS-102.

2 Introduction

Astragaloside IV (AGS IV, 3-*O*-β-D-xylopyranosyl-6-*O*-β-D-glucopyranosyl-cycloastragenol) is a cycloartane-type triterpenoid saponin that is considered the primary active ingredient of Astragali Radix, which is widely used in treating cardiovascular diseases in China (Ren et al., 2013). Unfortunately, AGS IV has limited efficacy, which is mainly due to its very low solubility in biological fluids, resulting in pharmacokinetic disadvantages after oral administration (Huang et al., 2006). Hence, a new water-soluble derivative of AGS IV, astragalosidic acid (LS-102), has been synthesized by our research group (Qing et al., 2017). LS-102 and AGS IV share a similar structure, except for a substitution of –COOH for $-CH_2OH$ on a glucose moiety (structure shown in Figure 1A). However, LS-102 demonstrated higher cardioprotective activity and bioavailability enhancement activities than AGS IV through *in vitro* and *in vivo* experiments. For instance, LS-102 exerted protective effects on cardiomyocyte damage induced by hypoxia/reoxygenation injury and alleviates myocardial ischemia reperfusion-induced injury in animal and cell models. Its cardioprotective mechanism has also been further illustrated (Chen et al., 2020). Additionally, LS-102 showed better transepithelial permeability and intestinal absorption in rodent pharmacokinetics studies, and showed no abnormalities or death in mice, even at high treatment doses (Qing et al., 2019; Sun et al., 2019). Increasing evidence indicates that LS-102 displays significant cardioprotective potential for further preclinical research. Despite the promising activities of LS-102 mentioned above, the molecular basis, cardiac function-improving effects and thromboprophylactic effects are unclear. Moreover, various other factors may influence the circulation of LS-102 in humans, including binding of the compound to plasma proteins (Lakhani, 2005).

Human serum albumin (HSA) is one of the most abundant plasma proteins available in blood and other interstitial fluids. HSA crystallographic data have revealed that it is a single polypeptide chain of 585 residues with a helical triple-domain structure. The principal function of HSA is to act as a carrier for drugs, fatty acids and metabolites to particular biological targets at its two primary binding sites (site I and site II) (Zsila et al., 2011; Wang et al., 2017). Therefore, the investigation of drug binding to HSA is crucial to understanding the pharmacodynamics and pharmacokinetic profile of a drug (Vallner, 1977). Due to the high concentration of HSA in plasma, the binding affinity of drugs to HSA is an important consideration when designing and developing new drugs (Yang et al., 2014). Additionally, the interaction of drugs that bind simultaneously to HSA can change the HSA binding behavior and potentially modulate the final therapeutic efficiency of the drugs (Tesseromatis and Alevizou, 2008). Generally, drugs with high affinity for HSA usually show a relatively slow distribution and clearance of drugs, which may extend the apparent half-life and lead to a high probability of various drug interactions (Lakhani, 2005). In contrast, the less bound a drug is, the more efficiently it can traverse cell membranes and diffuse (Benet and Hoener, 2002). To the best of our knowledge, despite the various biological effects of AGS IV, no previous study has performed an in-depth analysis of the interaction between AGS IV and HSA. Recently, XU *et al.* found that AGS IV had a very high degree of protein binding (up to 86.69%) with human plasma (Xu et al., 2016). Earlier reports demonstrated that the ratio of protein binding of drugs decreases accordingly with increasing polarity (Liang et al., 2013); thus, we raise the hypothesis that the chemical modification LS-102 will favor either the binding or release of HSA, thereby increasing its tissue distribution and ability to achieve suitable oral bioavailability in the human body. Further research on drug binding sites is needed to comprehensively understand the interaction of LS-102 with HSA, which may provide a structural basis for rationally designing drugs to use or exclude the impact of HSA on drug delivery (Petitpas et al., 2001).

Until now, various techniques have been implemented to probe the interaction of compounds on proteins *in vitro*, including fluorescence spectroscopy, (Ibrahim et al., 2010) circular dichroism spectroscopy (Yue et al., 2011), ultrafiltration, NMR (Ermakova et al., 2020), and isothermal titration calorimetry (Nevidalova et al., 2018). However, equilibrium dialysis, combined with highly sensitive assays, such as ultrahigh-performance liquid chromatography/tandem mass spectrometry (UHPLC-MS/MS), is the gold standard for investigating the direct interaction between HSA and drugs (Jiao et al., 2018). The working principle of equilibrium dialysis is that the drug can be separated from the protein solution through a semipermeable membrane. Free drug can pass through the semipermeable membrane until the dialysis reaches equilibrium, while the protein-drug complex is retained in the dialysis bag. Meanwhile, the binding rate with HSA can be calculated by the MS/MS technique to quantify the free drug concentration on both sides of the dialysis solution. This method is simple, practical, economical, and can eliminate the possible influence of nonspecific binding.

The zebrafish is a vertebrate with a high degree of genetic similarity to humans and comparable experimental results. The zebrafish model is less time consuming and less dose intensive than mammals such as rats, and the embryos are transparent and easy to observe. Additionally, zebrafish are highly reproductive, fast-growing and simple to administer. As a result, zebrafish embryos are now widely used for assessing acute and chronic

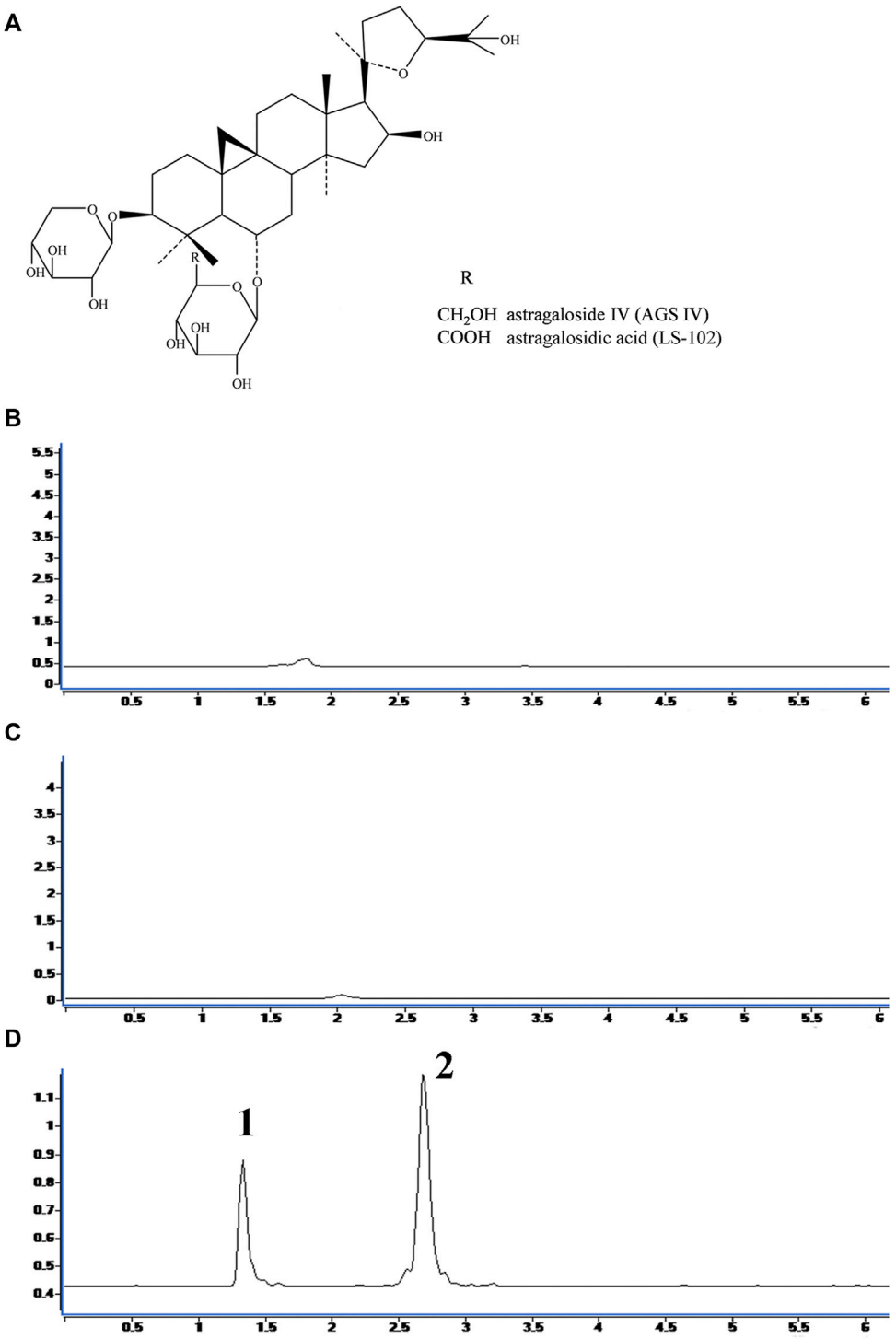

FIGURE 1
(A) Chemical structures of astragaloside IV (AGS IV) and astragalosidic acid (LS-102). The chromatograms for selectivity validation of LS-102. **(B)** Blank human plasma; **(C)** Blank external dialysate; **(D)** Human plasma (internal dialysate) sample from the protein binding assay; **(E)** Blank plasma spiked with LS-102 and internal standard; **(F)** External dialysate sample from the protein binding assay; **(G)** Blank external dialysate spiked with LS-102 and internal standard; 1, Digoxin; 2, LS-102.

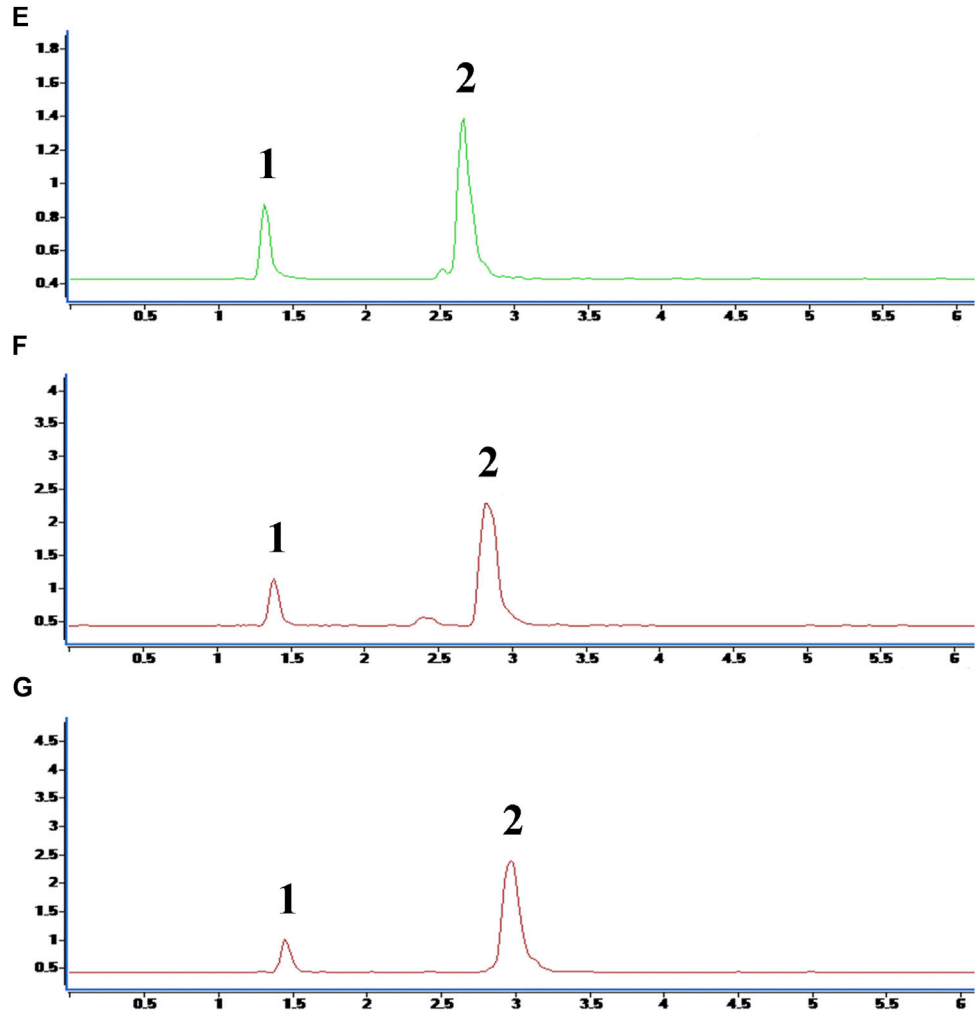

FIGURE 1
(Continued)

toxicity, cardiovascular disease, and many other diseases. (Bournele and Beis, 2016; Raftery et al., 2017).

In this study, we aimed to evaluate the binding properties of AGS IV and LS-102 with HSA and gain deeper insight into the mechanism. The combination of equilibrium dialysis and UHPLC-MS/MS was used to determine the plasma protein binding rates, as well as to explore the binding sites of HSA in the absence and presence of probes (warfarin for site I, ibuprofen for site II). Furthermore, to verify the experimental results and better understand the binding mechanism at the molecular level, molecular docking and molecular dynamics (MD) simulations were conducted to measure the binding mode and structural basis. Additionally, the effects of AGS IV and LS-102 on cardiotoxicity and thrombosis in zebrafish embryos were compared. The zebrafish heart function was viewed by measuring the heart rate, SV-BA spacing, and cardiac cystic edema, and the effect of thrombosis prevention was examined by calculating the red blood cell staining intensity and thrombus length. To the best of our knowledge, this is the first report using these effective approaches to simultaneously explore the plasma protein binding rate and competitive effect of AGS IV or its derivative, the results of which may provide more evidence for their clinical drug development.

3 Materials and methods

3.1 Regents and materials

Astragaloside IV (AGS IV) (>98%) was isolated from Astragali Radix, and its water-soluble derivative (LS-102) (>98%) was synthesized from AGS IV in our laboratory.

Digoxin (purity ≥98%, The Cat. No. D6003) purchased from Aldrich Chemical Co. (Milwaukee, United States) was utilized as an internal standard (IS). Warfarin (Cat. No. A2250), ibuprofen (Cat. No. I4883) and phosphate buffer saline (PBS) tablets (Cat. No. 524650) were purchased from Sigma. Human blood samples with K_2EDTA anticoagulant collected from healthy volunteers were provided by the Macau Blood Transfusion Centre. An equilibrium dialysis membrane with a molecular weight cutoff of 14,000 Da was purchased from Biosharp, China. MS grade methanol and acetonitrile were purchased from Anaqua (Boston, United States). Ultrapure water was generated with a Milli-Q system (Millipore, Bedford, MA, United States). Other reagents were of the highest grade commercially available.

3.2 Instruments and UHPLC-MS/MS conditions

UHPLC-MS/MS was performed on an Agilent 6460 series triple quadrupole mass spectrometer (Agilent, Santa Clara, California, United States) coupled with an Agilent 1290 UHPLC system. The separation was performed on a 2.1 × 100 mm Acuity UPLC Hass C_{18} column (1.8 μm particle size) equipped with elution with a mobile phase consisting of water (A) and acetonitrile (B), with gradient elution of 36% B at 0–5 min, 36%–95% min B at 5–5.1 min, 95% B at 5.1–7 min, 95%–36% min B at 7–7.1 min, and 36% B at 7.1–11 min for separation. The total run time for the analysis was 11 min (including equilibrium). The flow rate was 0.35 ml/min, and the injection volume of the sample was set as 1 μL. The column temperature was set to 30 °C, which could afford a more stabilized peak area and retention time. The triple quadrupole mass spectrometer was operated in a positive mode with a capillary voltage of 4 kV. Nitrogen served as the collision gas, and the gas temperature was set at 400 °C. The nebulizer pressure was set at 500 V. The fragment energy of 120 V and collision energy of 35 V were set for AGS IV, LS-102, and internal standard, digoxin. The quantitation of AGS IV and LS-102 was achieved in MRM mode with *m/z* transitions of 807.5 → 495.5 for AGS IV, 821.5 → 495.5 for LS-102, and 803.5 → 387.2 for digoxin.

3.3 Sample preparation

Following approval by the Clinical Research Ethics Committee of Macau University of Science and Technology, the human blood samples were centrifuged at 3000 × g for 10 min at 4°C, and then the supernatants were transferred into a centrifuge tube and stored at −80 °C before the protein binding experiment. Stock solutions of AGS IV and LS-102 (both 1 mg/ml) were prepared by dissolving the compounds in methanol and stored at 4 °C until they were required for the binding rate assay. Warfarin and ibuprofen were prepared in the same manner for the competitive experiment.

3.4 Treatment of dialysis membranes

The dialysis membranes were processed according to the guidelines provided by the supplier. Briefly, the membranes were cut into 10 cm long sections and then boiled and soaked in deionized water for 20 min. Subsequently, the membranes were soaked in 30% ethanol for 20 min and washed completely with deionized water. Following washing, the membranes were transferred into PBS (pH 7.4) solution to activate for 60 min and finally soaked in methanol solution for storage at 4°C.

3.5 Plasma protein binding study

The binding rate of AGS IV/LS-102 and HSA was determined using a slightly modified equilibrium dialysis method (Metsu et al., 2020). Briefly, three concentrations of AGS IV and LS-102 were prepared separately at 0.714, 0.476, and 0.238 mg/ml for the high, medium, and low drug groups, respectively. The stock solutions of HSA (0.5 ml) and drug group (0.5 ml) were placed in a dialysis membrane bag that was ligated at both ends and then immersed in a test tube filled with 50 ml of PBS solution for 72 h at 4 °C. After equilibrium, a 0.5-ml solution of outer dialysate and internal dialysate was collected into a 2-ml EP tube, and 10 μL IS (digoxin, 0.1 mg/ml) solution was added to each tube. Both samples were added to 1.5 ml of acetonitrile and vortexed for 3 min, and then the samples were separated via centrifugation at 18,000 × g for 20 min. The supernatants were transferred to another EP tube and dried under a nitrogen stream. The residue was redissolved in 1 ml methanol, sonicated for 2 min, vortexed for 3 min, and centrifuged at 18,000 × g for 10 min. The supernatant was filtered with a 0.22 μm microporous syringe filter in a 2 ml sample vial, and 1 μL was injected into the UHPLC-MS/MS system for analysis. The plasma protein binding rate was calculated according to the following formula (Talbert et al., 2002):

$$\textit{Plasma binding rate} = \frac{\textit{Internal drug concentration} - \textit{External drug concentration}}{\textit{Initial drug concentration}} \times 100\%$$

3.6 Method validation

The method validation for the plasma protein binding rate assay included linearity, accuracy, precision, selectivity, recovery, and stability, which were validated on 3 consecutive days. The linearity of the calibration curve for the external dialysate and plasma groups was assessed. The calibration curve was generated by taking the peak area of each standard solution sample to IS as

the ordinate (Y) and the mass concentration of each standard solution sample as the abscissa (X). The stock solutions of AGS IV and LS-102 were diluted with methanol into six increasing concentration groups as calibration curve standard solutions, with concentrations ranging from 0.02 to 0.17 mg/ml for plasma curves and 0.02–0.07 mg/ml for external dialysate curves. A 1 μl aliquot of sample for each group was analyzed after processing following the sample preparation procedure. The correlation coefficient, as a standard for evaluating the linearity, was considered acceptable at ≥ 0.990.

The accuracy and precision validation was evaluated via the determination of the quality control (QC) samples spiked with three concentrations of AGS IV and LS-102 (0.15 mg/ml, 0.10 mg/ml, and 0.06 mg/ml) for plasma and external dialysate. Specifically, six separately prepared QC samples at 3 concentrations were measured in 1 day for accuracy validation. One group of QC samples at three concentrations was measured six times for precision validation. The selectivity validation was evaluated by comparing the chromatograms of the blank human plasma, the blank human plasma spiked with AGS IV and the human plasma sample obtained from the plasma protein binding assay. The stability was assessed via determination of the relative standard deviation (RSD) value of QC samples spiked with three concentrations (0.15 mg/ml, 0.10 mg/ml, and 0.06 mg/ml) of AGS IV and LS-102 at different times (0, 2, 4, 8, and 12 h) stored at 4°C. Extraction recovery was determined by determining the peak area ratio of the plasma sample spiked with AGS IV and IS before the sample preparation procedure.

3.7 Data analysis

All chromatograms were evaluated with Mass Hunter version 1.1 software using the internal standard method and all peak area ratios of the analyte over internal standard for calculation.

3.8 Site marker competitive experiments

The site marker competitive experiments were performed using two classical site probes, warfarin and ibuprofen, which were selected as the markers of subdomain IIA (site I) and subdomain IIIA (site II) separately of HAS (Ghuman et al., 2005). The procedure was consistent with the method described in section *2.5*, except that the concentrations of AGS IV and LS-102 were both fixed at 0.476 mg/ml, while the external dialysis solution was changed to contain the probe with a final concentration of 0, 0.06, 0.3, 1.2 mg/ml PBS solution. Briefly, the AGS IV/LS-102 HSA mixture (0.5 ml drug and 0.5 ml HSA) was separately incubated with three different concentrations of probe to evaluate the effects of warfarin or ibuprofen on drug-protein binding influence. Three replicates of each concentration were prepared. After equilibrium dialysis, the internal and external dialysates were analyzed by UHPLC-MS/MS.

3.9 Molecular modeling

Molecular docking and MD simulations were applied to investigate the binding mode and stability between AGS IV/LS-102 and HSA. Docking calculations were performed using AutoDock Vina software (version 1.12) with the Lamarckian genetic algorithm (Morris et al., 1998; Xu et al., 2017). The 3D structures of AGS IV and LS-102 were optimized for energy minimization, and the crystal structure of HSA (PDB ID: 1H9Z) was obtained from the PDB BANK (http://www.rcsb.org/pdb). The ligands and water were removed from the protein using PyMOL software. Polar hydrogen atoms were added, and Geisteger charges were assigned to the receptor protein by means of AutoDock Tools version 1.5.6. A grid box was prepared for HSA to cover the binding site with a grid box size of 78 × 40 × 82 Å and a spacing of 1 Å centered at coordinates x, y, and z (25.033, 9.569, and 20.112, respectively). The saved file in the PDBQT format was used as an input in AutoDock Vina. To increase the docking accuracy, the value of exhaustiveness was set to 120, and the final number of conformations generated was set as 20. Differences between the accessible surface areas (ΔASA) of HSA before and after binding with AGS IV/LS-102 were calculated using the online server http://cib.cf.ocha.ac.jp/bitool/ASA (Warsi et al., 2021). The conformation with the lowest energy was used for post-docking analysis and subsequent MD simulations.

The MD simulations were conducted under the periodic boundary condition (PBC) using the GROMOS G54A7FF force field of the GROMACS 5.1.3 package (van Der Spoel et al., 2005; Kabiri et al., 2012). The topology parameters of AGS IV and LS-102 were built using the Automated Topology Builder (ATB) web server (Kim et al., 2016). The complex was immersed in a cubic box of extended simple point charge water molecules. The distance between the complexes and the edge of the box was set to 10 Å. Counterions (Na^+) were added to neutralize the system. Energy minimization was performed using the steepest descent method of 10,000 steps followed by the conjugate gradient method for 10,000 steps to release conflicting contacts. The position-restrained dynamics simulation (equilibration phase) (NVT and NPT) of the system was performed at 300 K for 100 ps followed by an MD production run for 50 ns, while the pressure was maintained at 1 bar using the Parinello-Rahman coupling algorithm. The short-range Columbic and Lennard–Jones interaction energies between compound 1 and the surroundings were monitored during the course of the productive simulation step. The visualization of protein–ligand complexes and MD trajectory analysis were conducted using VMD software. The MD trajectories were saved every 2000 ps. The stability and conformational changes in the complexes were assessed through the analysis of root-mean-square deviation (RMSD), root mean square fluctuations (RMSF), radius of gyration (Rg) and secondary structure calculations. The molecular mechanics Poisson Boltzmann surface area (MM/PBSA) analysis was performed using the

TABLE 1 The protein binding rates of AGS IV and LS-102 at different concentrations (n = 3).

Concentration (mg/ml)	Protein binding rate (%, Mean±SD)	
	AGS IV	LS-102
0.238	94.62 ± 2.70	68.24 ± 1.01**
0.476	97.42 ± 1.91	69.35 ± 0.97**
0.714	94.06 ± 1.02	68.57 ± 1.19**

**$p < 0.01$, vs. analytes AGS IV.

g_mmpbsa tool of GROMACS and was used to calculate the complex binding energies and a more precise prediction of binding modes from MD trajectories. All graphs were obtained using the Origin 85 software.

3.10 Animal embryos

The wild-type AB strain of zebrafish was bred by natural pair breeding, and embryos were collected 2 h and 3 days post fertilization (3 dpf), while zebrafish of the translucent Albino strain, which were mutant for the melanin allele, were bred by natural pair breeding, and embryos were collected 3 dpf. Embryos were maintained at 28°C in fish water (water quality: 200 mg of instant sea salt per 1 L of reverse osmosis water, conductivity 480–510 μS/cm; pH 6.9–7.2 and hardness 53.7–71.6 mg/L $CaCO_3$). The zebrafish facility at Hunter Biotechnology, Inc. is accredited by the Association for Assessment and Accreditation of Laboratory Animal Care (AAALAC) International. This study was approved by the Animal Ethics Committee of the State Key Laboratories for Quality Research in Chinese Medicines, Macau University of Science and Technology.

3.11 Maximum tolerated concentration of LS-102

Zebrafish embryos at 3 dpf were randomly selected and treated with LS-102 at concentrations of 1, 10, 100, 250 and 500 μg/ml in water, while the control group was left untreated. The mortality of zebrafish was recorded for each experimental group after 24 h of treatment.

3.12 Evaluation of the effects of LS-102 and AGS IV on the cardiotoxicity of astemizole-induced in zebrafish embryos

3.12.1 Evaluation of the effect of LS-102 and AGS IV on zebrafish morphology

A total of 270 wild-type AB zebrafish at 3 dpf were randomly selected, and 30 zebrafish were plated in each well of a six-well plates. The concentrations of LS-102 were 27.8, 83.3 and 250 μg/ml, AGS IV was 250 μg/mL. A normal control group (fish culture water) and a 4 μM astemizole model control group were also established. Ten zebrafish were randomly selected from each group, and the heart rate and venous sinus-to-arterial bulb distance (SV-BA) of zebrafish were observed under a dissecting microscope after 2 h, 6 h and 24 h of LS-102 and AGS IV treatment. Images were collected by photographing, and the ameliorative effect of LS-102 and AGS IV on astemizole-induced cardiotoxicity in zebrafish was evaluated by the statistical significance of the heart rate and the SV-BA interval index.

3.12.2 Evaluation of the effects of LS-102 and AGS IV on the development of zebrafish hearts

A total of 270 wild-type AB zebrafish at 2 h post-fertilization (2 hpf) were randomly selected, and 30 zebrafish were plated in each well of a six-well plates. The concentrations of LS-102 were 27.8, 83.3 and 250 μg/ml, while that of AGS IV was 250 μg/mL. A normal control group (fish culture water) and a 4 μM astemizole model control group were also established. After LS-102 and AGS IV were cotreated with astemizole for 48 h, zebrafish heart development was observed and photographed under a microscope to evaluate the ameliorative effect of LS-102 and AGS IV on astemizole-induced toxicity in zebrafish heart development.

3.13 Evaluation of the effects of LS-102 and AGS IV on arachidonic acid-induced thrombosis in zebrafish

A total of 270 melanin allele mutant translucent albino strain zebrafish at 3 dpf were randomly selected, with 30 zebrafish per well in six-well plates. The concentrations of LS-102 were 6.25, 12.5, 25, 50, and 100 μg/ml, while that of AGS IV was 100 μg/ml, and the positive control drug aspirin was 25 μg/ml. After treatment with LS-102 and AGS IV for 3 h, arachidonic acid aqueous solution was administered for 1.5 h to induce a thrombosis model in zebrafish in all experimental groups except the normal group. After staining with *o*-anisidine,

TABLE 2 Plasma protein binding of AGS IV and LS-102 plus site markers in HSA ($\bar{x} \pm s$, n = 3).

Analyte	Without site markers	With warfarin (mg/ml)			With ibuprofen (mg/ml)		
		0.06	0.3	1.2	0.06	0.3	1.2
AGS IV	96.67±1.14	94.90±1.95	91.10±1.06*	92.19±2.38*	92.82±1.44	93.87±2.26	97.19±1.37
LS-102	66.90±0.93	53.29±2.14**	58.93±0.98**	54.70±1.25**	63.22±0.72	75.16±1.99*	72.03±1.83*

*$p < 0.05$.
**$p < 0.01$, vs. analytes without site markers.

zebrafish were randomly selected from each experimental group and observed under a dissecting microscope and photographed. Data were collected to qualitatively evaluate thrombosis in zebrafish, and the intensity of cardiac erythrocyte staining (length of venous thrombus *vs.* number of cardiac erythrocytes) in zebrafish was analyzed and counted to establish, the preventive effect of LS-102 and AGS IV with aspirin on thrombosis in zebrafish. The formula was calculated as follows:

Thromboprophylactic effect (%) =

$$\frac{S\left(drug\ administration\ group\right) - S\left(model\ group\right)}{S\left(nomal\ control\ group\right) - S\left(model\ group\right)} \times 100\%$$

3.14 Statistical analysis

For zebrafish experiments, statistical analyses were performed in triplicate, and statistical treatments were expressed as mean ± standard deviation (SD). All statistical analyses were performed using GraphPad Prism 9.3.1 statistical software for ANOVA and Dunnett's *t*-test to determine significant differences ($p < 0.05$).

4 Result

4.1 Method validation

4.1.1 Optimization of equilibrium dialysis conditions

A temperature of 37°C and 4°C is usually necessary to achieve a steady state or equilibrium between bound and free concentrations in the equilibrium dialysis test (Metsu et al., 2020). However, the poor reproducibility of the test results when equilibrated at 37°C was experimentally investigated in this study, while the sample reached equilibrium after incubation for 72 h at 4°C with a relatively stable result. Therefore, a temperature of 4°C and a dialysis time of 72 h were used for all subsequent equilibrium dialysis experiments.

In the plasma protein binding rate study, plasma protein leakage into the external dialysate could occur due to improper operation of the experiment or other reasons, which will affect the determination of the research results. Therefore, the solution needs to be tested for leaks before sample processing. The turbidimetric method was used to determine whether protein leakage was present (Ruiter et al., 2012). After equilibrium, 1 ml of the external dialysate was collected in a transparent test tube, and then 0.5 ml of 20% trichloroacetic aid was added and observed in a dark background. If a white flocculent precipitate appeared, then protein leakage was considered to have occurred.

4.1.2 Linearity and selectivity

The regression equation and correlation coefficient for the internal and external dialysates of the AGS IV and LS-102 calibration curves are shown in Supplementary Table S1. All correlation coefficient values were >0.999, which indicates decent linearity for the calibration curves in a certain range. The selectivity validation was evaluated by comparing the chromatograms, which showed that there were no endogenous interfering substances in the matrix by comparing Figure 1B and Figure 1C. Furthermore, no exogenous interference was inspected in the result after analyzing the chromatograms of Figure 1D and Figure 1E. Similarly, no interference from external dialysate could be observed later in scrutinizing Figure 1F and Figure 1G.

4.1.3 Accuracy, precision, and extraction recovery

The precision, accuracy, and extraction recovery values of three QC samples with different concentrations of AGS IV and LS-102 are listed in Supplementary Table S2. The precision was measured by RSD, and the accuracy was expressed as the relative error (RE) (Lu et al., 2019). Supplementary Table S2 shows that the precision values range from 3.23% to 11.56%, and all accuracy values were within ±13.22%, suggesting that all precision and accuracy values are acceptable. The extraction recovery rate of AGS IV and LS-102 remained in the range of 85%–117%, and there was no orthogonal relationship between the recovery rate and concentration of each QC sample.

4.2 Plasma protein binding rate

The AGS IV/LS-102 HSA binding properties were studied by the equilibrium dialysis method. During incubation, components

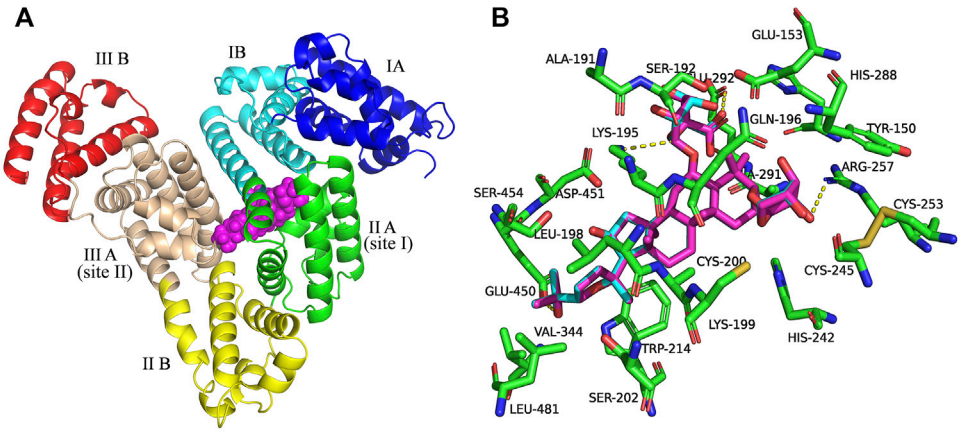

FIGURE 2
(A) Superposition of the structures of AGS IV and LS-102 (magenta spheres) within the active site pocket of human plasma albumin (HSA) (PDB ID: 1H9Z). Cartoon representation of HSA showing the six subdomains remarked with the following colors: IA, blue; IB, cyans; IIA, green; IIB, yellow; IIIA, wheat; IIIB, red. **(B)** The binding site was enlarged to show the superposition structures of AGS IV and LS102, with major amino acid residues (green sticks) surrounding ligands within 4 Å. The cyan structure stands for AGS IV and magentas is for LS-102, the yellow dotted lines indicating hydrogen bonds.

of the drug group could freely interact with HSA inside the dialysis bag, while the excess drugs could freely diffuse to the outside. Therefore, after equilibrium dialysis, the difference between the amounts of the external and internal drugs in the dialysis bag was detected to obtain the plasma binding rate (Zhang et al., 2012). As shown in Table 1, Student's *t* test proved no significant difference within the concentration groups of human plasma ($p > 0.05$). The binding rates were 94.62% ± 2.70%, 97.42% ± 1.91%, and 94.06% ± 1.02% for AGS IV and 68.24% ± 1.01%, 69.35% ± 0.97%, and 68.57% ± 1.19% for LS-102. The results showed that there was no drug concentration dependence between the binding process of both AGS IV and LS-102 with HSA, which provides an experimental basis for clinical medication.

Generally, albumin binding events play a vital role in the transport and distribution of drugs; only free drugs can act on target organs through biomembranes and are responsible for pharmacological activities, while bound drugs have no pharmacological effects. Theoretically, drugs with a high plasma protein binding rate require correspondingly higher doses to achieve an effective concentration *in vivo*, which are prone to safety problems. In other words, when combined with other strongly HSA-binding drugs, the exponentially increasing free drug concentration caused by changes in protein binding may have side effects or toxicity (Lombardo et al., 2002). Accordingly, the binding rate of AGS IV in HSA is always higher than 94% at the three concentrations, indicating that AGS IV could be easily stored and transported in the circulatory system by HSA, which is consistent with previous reports (Xu et al., 2016). In contrast, LS-102 binds moderately to HSA in the range of 68.24%–69.35%, which is significantly lower than that of AGS IV ($p < 0.01$), implying that an appropriate amount of unbound LS-102 remains in the blood circulatory system. Hence, the dissociative LS-102 can reach the target tissue to achieve the pharmacological effects of the drug.

In short, attention should be given to the variation in the free drug concentration caused by the drug combination or endogenous ligand binding. Detailed molecular information on HSA binding sites may help to evaluate the cooperative effects given that HSA has a limited number of high-affinity binding sites (Yang et al., 2014). However, as the binding sites of AGS IV and LS-102 on HSA were unclear, competitive displacement experiments were subsequently performed.

4.3 Competitive binding experiments using the equilibrium dialysis method coupled with UHPLC-MS/MS

Generally, HSA has two principal ligand-binding sites located in the hydrophobic cavity, namely, site I (termed the warfarin site) and site II (termed the ibuprofen site). In particular, triterpenoids such as saikosaponin C, glycyrrhetinic acid and oleanolic acid have been proven to bind to site I by fluorescence, site marker competitive or molecular docking research (Tang et al., 2006; Chen et al., 2016; Abboud et al., 2017). In this study, a simple and efficient modified equilibrium dialysis method coupled with UHPLC-MS/MS (Liu et al., 2013; Yang et al., 2014; Yu et al., 2016) was first used to identify the

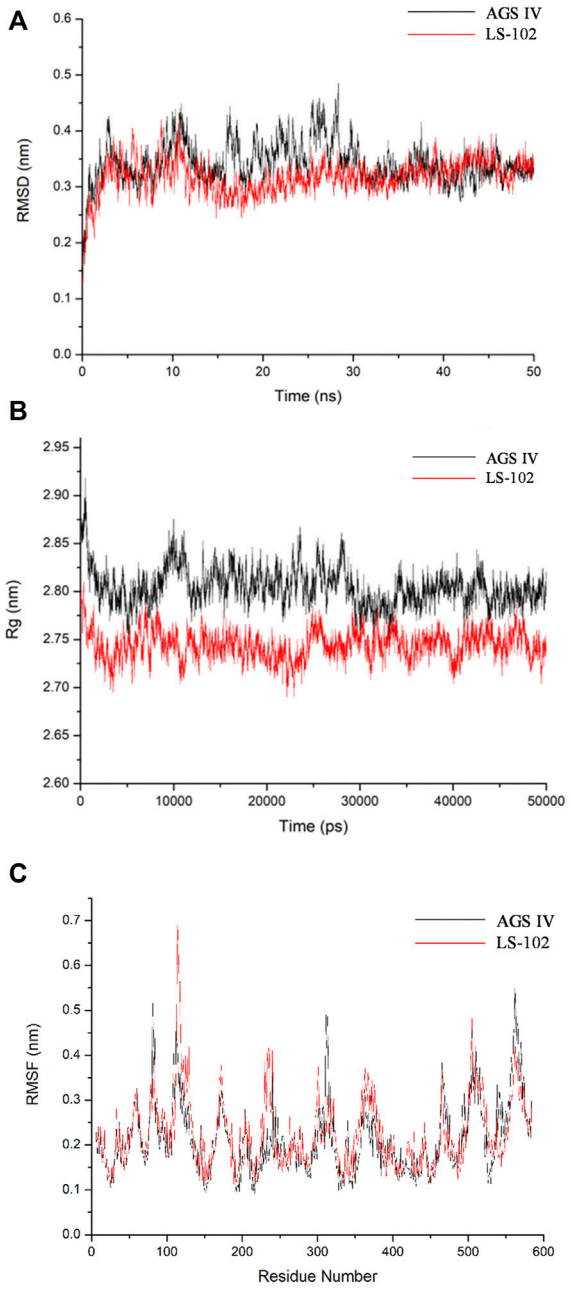

FIGURE 3
Molecular dynamics simulation of HSA–ligand complex for 50 ns time scale **(A)** Root-mean-square deviation (RMSD) of Cα-atoms for HSA-AGS IV/LS102 complex. **(B)** Radius of gyration values for HSA present in systems. **(C)** RMSF values of HSA/AGS IV and HSA/LS-102 complex were plotted against residue numbers.

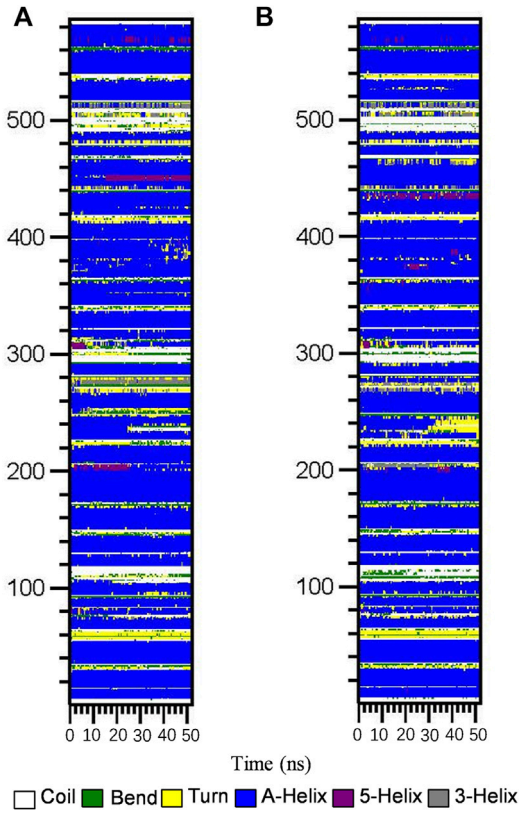

FIGURE 4
Structural changes of HSA-AGS IV **(A)** and the HSA-LS102 **(B)** complex during simulation

AGS IV and LS-102 binding sites on HSA. By monitoring the changes in the AGS IV/LS-102 HSA binding rate in the absence and presence of probes and then calculating the percentage of probe displacement, the drug binding site can be predicted.

The competitive binding experimental results are shown in Table 2. Concentration-dependent binding was not observed over the selected concentration range. Following the addition of different levels of warfarin into the HSA–LS-102 solution, the binding rates were significantly reduced compared to those without warfarin ($p < 0.01$). This indicates that the addition of warfarin significantly affected the binding of LS-102 to HSA, thereby increasing the free concentration of LS-102 and enhancing its effect, which suggests that LS-102 and warfarin share the same binding site (site I). The binding site of LS-102 is thought to be subdomain IIA of HSA (He et al., 2008). In contrast, in the presence of ibuprofen, the binding rate of the HSA–LS-102 system increased slightly at doses of 0.3 and 1.2 mg/ml, which indicates that the introduction of ibuprofen into HSA–LS-102 cannot compete with LS-102 but conversely promotes LS-102 and HSA. This is similar to previous studies that have shown that ibuprofen binding to HSA provokes the enhanced binding of (*S*)-lorazepam acetate (Fitos et al., 1999). Moreover, in the AGS IV binding system, the combination of warfarin affects the HSA–AGS IV interaction and consistently reduces the binding rates. Interestingly, the binding rates changed when ibuprofen was administered, with a slight

TABLE 3 Calculated values that contributed to binding-free energy from Poisson Boltzmann surface area (MM/PBSA).

Analytes	Van der waal energy	Electrostatic energy	Polar solvation energy	SASA energy	Binding energy
AGS IV	−340.247±16.998	−72.705±22.211	313.271±42.201	−36.313±1.665	−135.994±26.807
LS-102	−321.458±20.459	−116.843±26.138	391.229±52.868	−35.977±1.570	−83.049±31.142

All values, standard deviations and averages, are expressed in kcal mol^{-1}

TABLE 4 Quantitative results of LS-102 and AGS IV on heart rate in zebrafish after astemizole induction (n = 10).

Inducer concentration (μM)	Groups	Concentrations (μg/ml)	Heart rate (beats/min) (Mean±SE)		
			2 h	6 h	24 h
4	Control	–	173 ± 2	169 ± 2	194 ± 2
	Model	–	145 ± 2***	146 ± 2***	86 ± 24***
	AGS IV	250	148 ± 1**	146 ± 2*	75 ± 25**
	LS-102	27.8	156 ± 1	158 ± 1	45 ± 23**
		83.3	157 ± 2	153 ± 1*	128 ± 21*
		250	160 ± 1	167 ± 1	162 ± 7*

*$p < 0.05$.
**$p < 0.01$.
***$p < 0.001$, vs. Control group.

decrease in the binding rates at concentrations of 0.06 and 0.3 mg/ml and an increase at 1.2 mg/ml, suggesting that AGS IV mainly attaches to both sites I and II of HSA.

Sites I and II are similar in size and shape, possessing elongated hydrophobic pockets with cationic amino acid residues near their entrances. Generally, site I preferentially integrates with bulky heterocyclic ligands, and site II preferentially recognizes aromatic compounds. However, these structural features are not strict prerequisites for site binding since many drugs bind to both binding sites, albeit with different binding energies (Petitpas et al., 2003). Based on site marker experiments, we found that AGS IV and LS-102 are likely to attach to both sites I and II of HSA, but that site I may be the primary binding site, especially the binding rates of HSA–LS-102, which showed significant displacement by warfarin, whereas ibuprofen did not.

4.4 Molecular docking study

Next, molecular docking was applied to simulate AGS IV/LS-102 and HSA to obtain more information about the binding interaction between ligands on HSA at the atomic level and validate the experimental results (Trott and Olson, 2010). The structure of HSA has three homologous domains, and domain I is composed of residues 1–195, II (196–383), and III (384–585). Each domain is further divided into two subdomains (named A and B) to comprise six subdomains, IA, IB, IIA, IIB, IIIA, and IIIB. The two subdomains in each domain constitute a hydrophobic cavity. HSA contains two principal drug binding sites, sites I and II, which are located in the specialized cavities of subdomains IIA and IIIA, respectively. The sole tryptophan residue (Trp 214) of HSA is in subdomain IIA, which contains a large hydrophobic cavity that many drugs can bind to (Xiang et al., 2016).

Figure 2 shows the best docking models of AGS IV and LS-102 for HSA. The AGS IV and LS-102 molecules superimposed well and were located at the interface of subdomains IIA and IIIA in the center of the serum albumin molecule, with the structures primarily buried in the subdomain IIA hydrophobic cavity. We also found that subdomain IIIA is an open pocket in which part of the hydroxyl group on the five-membered ring of ligands can fit into (Figures 2A,B). Hydrophobic and hydrogen were shown to be the most significant interactions of the binding mode, with approximately 23 residues located within a 4 Å distance from the ligands (Figure 2B). The cycloastragenol fused ring of these tetracyclic triterpenoids was inserted into the hydrophobic cavity of the site pocket formed by Lys-199, Trp-214, Val-344, Glu-450, Leu-198, Asp-451, Lys-195 and Ala-291, while the xylopyranosyloxy and glucopyranoside were situated in a larger hydrophobic cavity formed by Cys-245, Cys-253, His-288, Glu-292, Ser-192 and Gln-196 (Chen et al., 2014). Additionally, several hydroxy groups of AGS IV generate a hydrogen bond network with the polar residues present in the

TABLE 5 Quantitative results of LS-102 and AGS IV on SV-BA spacing after astemizole induction in zebrafish (n = 10).

Inducer concentrations (μM)	Groups	Concentrations (μg/ml)	SV-BA spacing (μm) (Mean±SE)		
			2 h	6 h	24 h
4	Control	–	150 ± 4	149 ± 5	164 ± 3
	Model	–	206 ± 5***	236 ± 5***	251 ± 6***
	AGS IV	250	210 ± 4***	242 ± 7**	241 ± 4**
	LS-102	27.8	179 ± 7*	204 ± 6	250 ± 6**
		83.3	157 ± 3	168 ± 4**	228 ± 7*
		250	151 ± 3	158 ± 6**	174 ± 9

*$p < 0.05$.
**$p < 0.01$.
***$p < 0.001$, vs. Control group.

site pocket, including Lys-195, Arg-257 and Glu-292, with bond distances of 3.3 Å, 3.1 Å and 2.8 Å, respectively. Furthermore, a carboxyl and hydroxyl group of LS-102 formed H-bonds with two residues present at the inner site I pocket, including Lys-195 and Arg-257, with bond distances of 3.3 Å and 3.2 Å, respectively.

Therefore, the moderate interaction of hydrophobic and hydrogen bonds in the active site pockets is considered essential for the stable conformation of the HSA-ligand complex, while the binding sites of subdomains IIA and IIIA are preferentially involved. This is in agreement with the result of a previous study showing that hydrophobicity and hydrogen bonds are significant factors that control triterpenoid-albumin binding (Maciazek-Jurczyk et al., 2018). Overall, the above analysis fits extremely well with the site experimental results. Thus, our study offers a rational molecular explanation for the site competitive binding experiment in which increasing warfarin and ibuprofen concentrations in the drug group-HSA system influenced the binding rates.

The ASA values of residues were calculated for HSA, HSA-AGS IV, and HSA-LS-102 and are presented in Supplementary Table S3. It was found that the average values of ΔASA for the residues near the binding sites were approximately 42.02 $Å^2$ and 42.17 $Å^2$ for AGS IV and LS-102 in the binding interaction, respectively, both of which are much greater than 10 $Å^2$, indicating that AGS IV and LS-10 effectively and tightly bind to the active sites of HSA (Wang et al., 2011). The residues Lys-195, Arg-257 and Glu-292 of HSA suffer a considerable change (90.48%, 64.83%, and 47.02%, respectively) in ASA due to the hydrogen bonding interactions with LS-102 as might be expected. The loss of ASA by hydrophobic residues is 14.05%, 43.27%, 43.31%, 62.26%, 76.71%, 90.82%, 91.57%, and 95.24% for Glu-450, Gln-196, His-288, Ser-192, Ala-291, Trp-214, Asp-451, Lys-199 and Leu-198, respectively. Therefore, ASA calculations may prove that hydrogen bonds and hydrophobic interactions play essential roles in the binding of AGS IV/LS-102 to HSA, which is in agreement with the results of the docking study.

Notably, there is a significant difference between AGS IV and LS-102 when binding with HSA according to the plasma protein binding experiments, while the docking results here show that AGS IV and LS-102 overlap very well and are located in the same pocket of HSA. We suspect that the carboxyl group of LS-102 improves the metabolic stability and through allosteric modulation arise among the binding sites.

4.5 Analysis of the dynamic trajectories

Molecular docking is a static mode of ligand binding; hence, coupling docking with MD simulation can further elucidate the dynamic behavior and possible geometric changes in the AGS IV/LS-102 HSA complex under simulated physiological conditions. Through the analysis of the output trajectories, dynamic structural properties such as the RMSD, Rg and secondary structure were obtained to evaluate the stability and conformational changes of the HSA-ligand complex (Lakshmi et al., 2017). The RMSD was calculated to understand the protein stability by superimposing C-alpha atoms in the active site pocket along the 50 ns MD trajectories (Figure 3A). For all systems, the RMSD values varied between 2.5–5 Å, and both reached stability in the first 12 ns time scale. The fluctuations were relatively small during the remainder of the simulation process, with a slight fluctuation between 15 and 30 ns in the HSA–AGS IV complex. The results demonstrate that the conformation of HSA in the AGS IV/LS-102 complex was slightly changed, and that the simulation time is sufficient for the refinement in the period used. Additionally, the Rg value for the complex against time scale was determined and is shown in Figure 3B. Generally, Rg represents the HSA compactness, and a higher Rg value indicates a looser structure in a specific region of the protein. During the simulation, the Rg plot showed no significant change in either system, but the average Rg values of HSA in AGS IV (approximately 2.80 nm) were slightly higher than those in LS-102 (approximately 2.75 nm), revealing that the

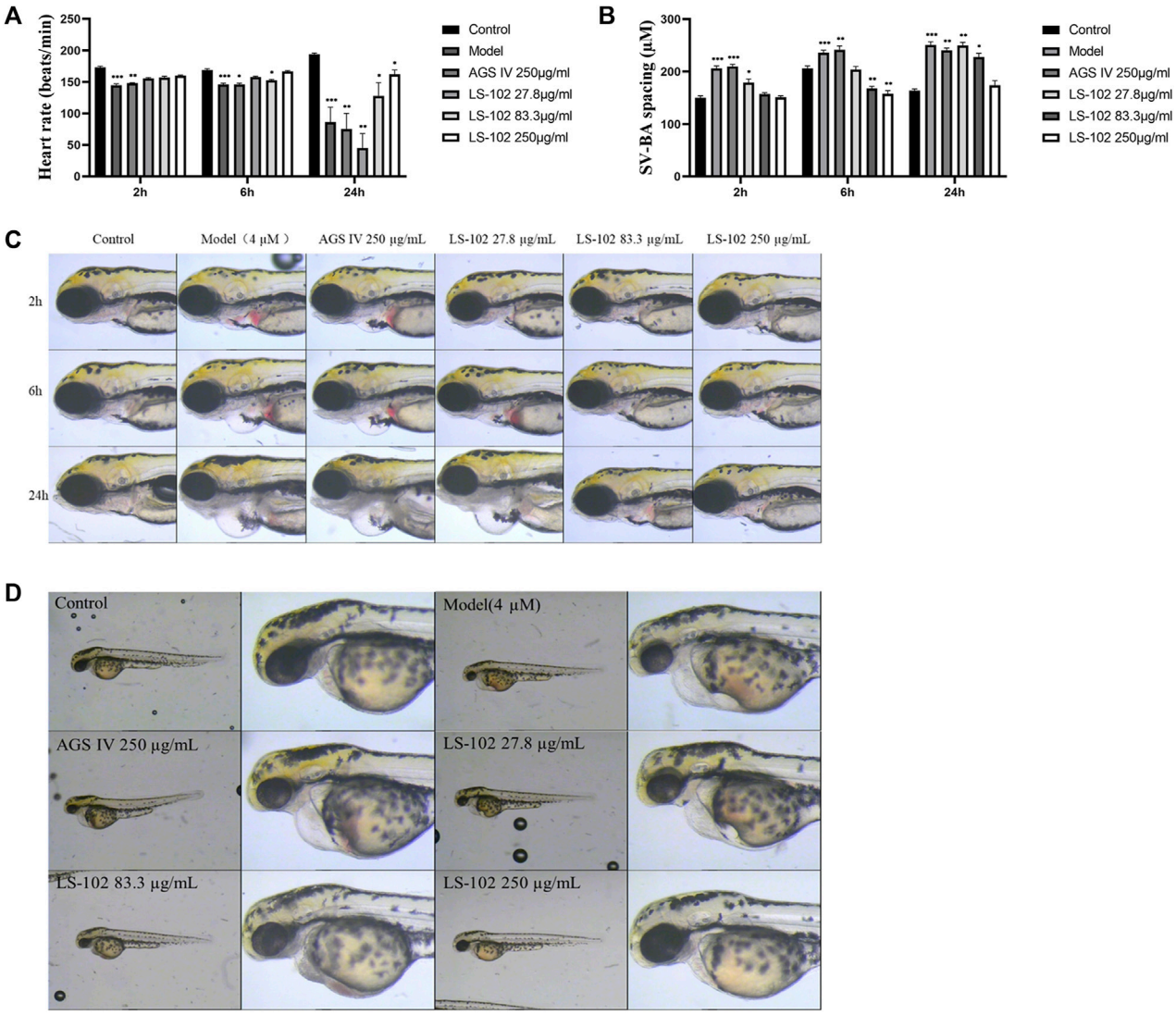

FIGURE 5
(A) Changes in heart rate of zebrafish after induction of 4 μM astemizole by LS-102 and AGS IV, respectively. **(B)** Zebrafish SV-SA spacing after cotreatment of LS-102 and AGS IV with 4 μM astemizole. **(C)** Typical picture of SV-BA spacing after cotreatment with AGS IV and LS-102 and 4 μM astemizole. **(D)** Typical picture of zebrafish heart after cotreatment of AGS IV and LS-102 with 4 μM astemizole. *$p < 0.05$, **$p < 0.01$, ***$p < 0.001$, vs. Control group.

combination of LS-102 and HSA made HSA more compact than in AGS IV. The RMSF plots indicate the fluctuation of residue relative to the average position of the protein to a certain extent, and the result can be used as the data index to study the dynamic movement of the protein–ligand complex (Gan et al., 2018). RMSF analyses were performed based on the 50 ns trajectory and plotted against all residues for the HSA-AGS IV and HSA-LS-102 systems (Figure 3C). As shown, residues within the loop regions of HSA-AGS IV and HSA-LS-102 display higher flexibility, and a similar pattern of flexibility is observed for these complexes. The binding affinity of HSA molecules can be influenced by amino acid residues (Senthilkumar et al., 2016). The RMSF values for binding site I remained low, indicating that these residues are rigid compared with other residues, and this suggests that the binding affinity of site I can be affected by AGS IV/LS-102 binding.

Subsequently, the DSSP method was used to investigate the changes in the secondary structure of proteins (Moradi et al., 2018). Figure 4 shows the structural changes of the HSA–ligand complex during simulation. Structural displacements are observed in some regions, while some of the α-helix contents changes to a 5-helix. The percentages of different structure types are listed in Supplementary Table S4 and are mainly composed of A-helix, of which AGS IV is 0.69 and LS-102 is 0.70, along with

TABLE 6 Quantitative results of the effect of LS-102 and AGS IV on the prevention of thrombosis in zebrafish (n = 10).

Groups	Concentrations (μg/ml)	Staining intensity of cardiac red blood cells (pixels) (mean ± se)	Antithrombotic effect (%)
Control	–	2305 ± 32	–
Model	–	1397 ± 45	–
Aspirin	25	2036 ± 92***	70***
AGS IV	100	1446 ± 54	5
LS-102	6.25	1280 ± 119	−13
	12.5	1521 ± 72	14
	25	1597 ± 65	22
	50	1796 ± 54***	44***
	100	1950 ± 33***	61***

***p < 0.001, vs. Model group.

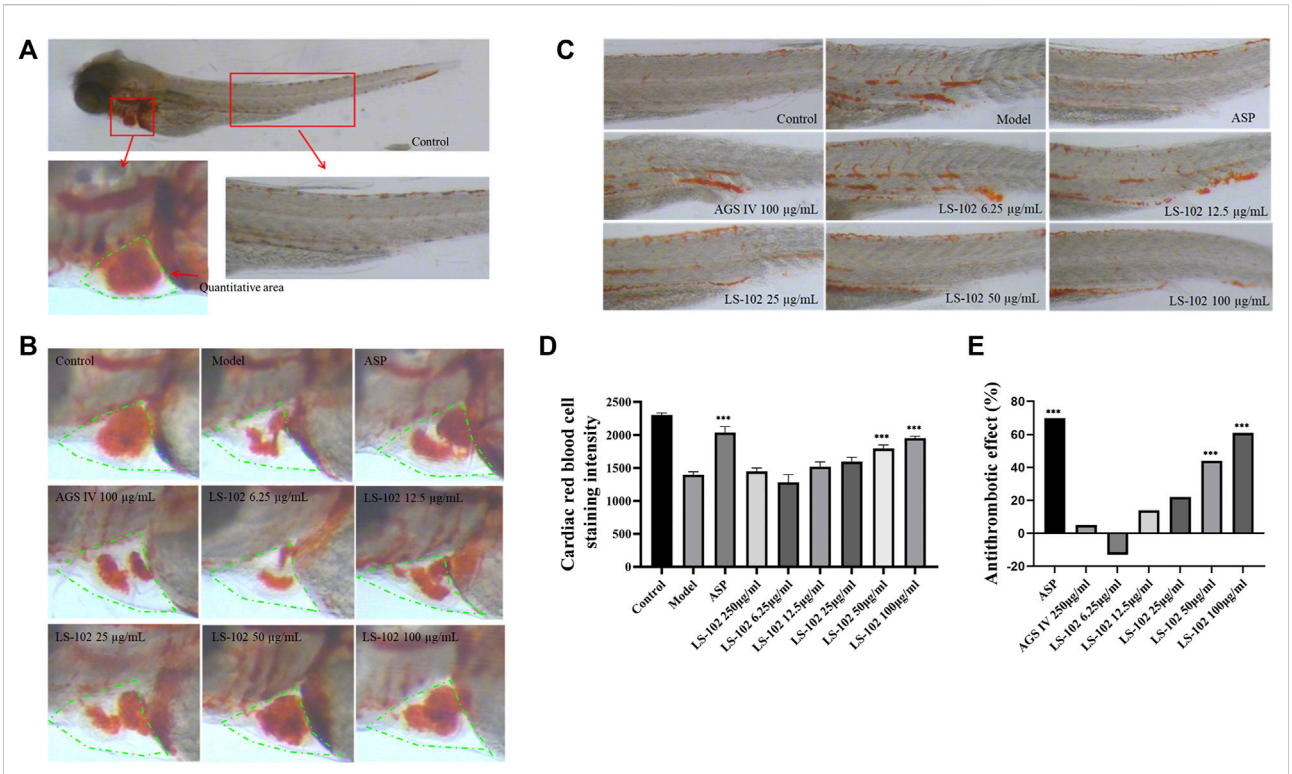

FIGURE 6
(A) 3 dpf Albino strain zebrafish stained with *o-Dianisidine* (green area is the quantitative red blood cell area). **(B)** Typical staining of zebrafish heart red blood cells after AGS IV and LS-102 treatment. **(C)** Typical graph for qualitative evaluation of zebrafish thrombosis after AGS IV and LS-102 treatment. **(D)** Erythrocyte staining intensity (pixels) in zebrafish hearts treated with LS-102 and AGS IV. **(E)** Thrombosis prevention in zebrafish treated with LS-102 and AGS IV. ***p < 0.001, vs. Model group.

some Bend, Turn, 3-Helix and 5-Helix. This observation showed that the differences between HSA binding to AGS IV and LS-102 are negligible, which indicates that there is no substantial change in the secondary structure of the protein upon interacting with the two ligands. Moreover, although the whole secondary structure of HSA-LS-102 increased by approximately 0.01, the

bend content decreased within the same range. These observations strongly emphasize the existence of a safe interaction between AGS IV and LS-102 in the HSA complex, whereas LS-102 has no adverse effect on protein structures and conformation.

Next, MM/PBSA analysis was performed to calculate the main driving force for physical adsorption of the complex (Yu et al., 2016), the results of which are listed in Table 3. Obviously, van der Waals, electrostatic, polar solvation and solvent accessible surface area (SASA) energy make the greatest contributions to the total binding-free energy. The results showed that the HSA/AGS IV complex provides more negative van der Waals energies (−340.247 kcal/mol) than the LS-102 complexes (−321.458 kcal/mol), which may be due to the stronger hydrophobic interactions. Therefore, we conclude that van der Waals forces are the driving force for binding. Although electrostatic energy (−72.705 and −116.843 kJ/mol for AGS IV and LS-102, respectively) is also favorable forbinding in a vacuum, it is offset by the polar solvation energy (313.271 and 391.229 kJ/mol) when considering the solvation effect. A positive polar solvation energy shows an unfavorable electrostatic effect on solvation; this may be the result of the hydrophobic interactions of the ligand in HSA, which also resulted in negative SASA energy (−36.313 and −35.977 kcal/mol for AGS IV and LS-102, respectively). Finally, the binding conformations of AGS IV exhibited lower binding energies (−135.994 kcal/mol) compared to LS-102 (−83.049 kcal/mol), indicating that AGS IV had a stronger binding ability of HSA than LS-102, which is in balance with the results of the plasma protein binding studies.

4.6 Maximum-tolerated concentration (MTC) of LS-102 and AGS IV in zebrafish

Zebrafish have become widely used as biological models in drug toxicity tests (Bournele and Beis, 2016). As shown in Supplementary Table S5, the MTC assay showed no mortality in zebrafish at concentrations of LS-102 ranging from 1 to 100 μg/ml, and 13.3% and 100% mortality at concentrations of 250 and 500 μg/ml, respectively. Therefore, the MTC of LS-102 used in the experiment was determined to be 100 μg/ml.

4.7 Comparison of LS-102 and AGS IV on astemizole-induced cardiotoxicity in zebrafish embryos

Zebrafish have become immensely powerful model organisms for uncovering mechanisms of cardiac development and function (Liu and Stainier, 2012). In the current study, we used astemizole to induce cardiotoxicity in zebrafish embryos to detect the corresponding cardiac performance alterations. After treatment of LS-102 and AGS IV with 4 μM of astemizole, the heart rate and SV-BA spacing of zebrafish in the model group were compared with those of the normal group, $p < 0.001$, indicating successful modeling. After treatment of LS-102 and AGS IV with 4 μM of astemizole for 2 h and 6 h, respectively, LS-102 improved the slowed heart rate and increased the SV-BA spacing in zebrafish at 27.8, 83.3, and 250 μg/ml concentrations. After 24 h, LS-102 improved the slowed heart rate at 250 μg/ml and the increase in SV-BA spacing at 83.3 and 250 μg/ml, while the AGS IV group showed no significant changes.

After treatment of zebrafish with LS-102 and AGS IV and 4 μM astemizole for 48 h, 100% of zebrafish in the model group developed cardiac vesicle edema and blood flow deficiency. In the 27.8 μg/ml LS-102 concentration group, 100% of zebrafish showed cardiac vesicle edema and loss of blood flow. In the 83.3 μg/ml concentration group, 83.3% showed pericardial edema and venous sinus stasis, 26.7% showed a loss of blood flow, and 56.7% showed slow blood flow. In the 250 μg/ml concentration group, the zebrafish mortality was 30%, but the zebrafish showed no significant toxicity. This indicated that 83.3 and 250 μg/ml of LS-102 had an ameliorating effect on the developmental toxicity of zebrafish hearts induced by 4 μM astemizole. The results are shown in Tables 4, 5; Supplementary Table S6 and Figure 5.

4.8 Comparison of LS-102 and AGS IV on arachidonic acid-induced thrombosis in zebrafish

Zebrafish is a useful model for thrombosis studies because their platelet function shares many similar features to that in humans, including the function of arachidonic acid metabolism enzymes (Lang et al., 2010). The staining intensity of zebrafish heart erythrocytes in the model group (1397 pixels) compared to the control group (2305 pixels; $p < 0.001$), indicated successful modeling. The intensity of erythrocyte staining in zebrafish hearts of the positive control drug 25 μg/ml of the aspirin group (2036 pixels) compared to the model group ($p < 0.001$), and the preventive effect of the aspirin group on thrombosis in zebrafish was 70%, indicating the preventive effect of aspirin on thrombosis. The preventive effect of AGS IV on thrombosis was insignificant at 5% compared to the model group ($p > 0.05$). Notably, the intensity of erythrocyte staining at concentrations of 6.25, 12. 5, 25, 50, and 100 μg/ml of LS-102 was 1280, 1521, 1597, 1796 and 1950 pixels, respectively, and the preventive effect on thrombosis was −13%, 14%, 22%, 44%, and 61%, compared to the model group. ($p > 0.05$ for the 6.25, 12.5 and 25 μg/ml concentration groups and $p < 0.001$ for the 50 and 100 μg/ml concentration groups). These results indicate that LS-102 at concentrations of 50 and 100 μg/mL has a preventive effect on arachidonic acid-induced thrombosis in zebrafish. The results are shown in Table 6 and Figure 6. In summary, LS-102 was shown to ameliorate the heart rate slowing and SV-BA interval increase

and prevent thrombosis in zebrafish, which may indicate its cardioprotective activity (Lu et al., 2021). As the drug-HSA binding rate is an important factor in evaluating efficacy and safety, LS-102, with moderate binding affinity to HSA may increase its tissue distribution and thus improve bioavailability, which may help explain the improved biological activity, although more research is needed to prove this inference.

5 Conclusion

The results of interaction studies show that LS-102 displays moderate binding of HSA by experimental and *in silico* methods, and there are no clear conformation changes, meaning that this newly synthesized drug can be considered to have no side effects. The substitution of the carboxyl group in LS-102 may be a factor that exhibited allosteric regulation on binding properties. As LS-102 showed protective effects on the heart and appropriate pharmacokinetic properties, our results are important for understanding its overall distribution, metabolism and efficacy in the human body at the molecular level. Moreover, our results highlight its safety and promising drug treatment efficacy, thus providing crucial information for clinical medicine. Ultimately, this simple and validated method provides enhanced support for drug discovery and development, while having the advantages of being less costly and time-consuming. In zebrafish experiments, LS-102 was shown to ameliorate astemizole-induced heart rate slowing and SV-BA interval increase in zebrafish and prevent arachidonic acid-induced thrombosis in zebrafish. These findings lay the foundation for further research on the mechanism of action and targets of LS-102 and provide a valuable experimental basis for future clinical applications. Moreover, our results suggest that computational simulation is consistent with experimental findings, thereby confirming the establishment of a validated and convenient method to study the molecular interaction between HSA and its ligands.

Data availability statement

The raw data supporting the conclusion of this article will be made available by the authors, without undue reservation.

Ethics statement

The studies involving human participants were reviewed and approved by Clinical Research Ethics Committee of Macau University of Science and Technology. Written informed consent for participation was not required for this study in accordance with the national legislation and the institutional requirements. The animal study was reviewed and approved by Animal Ethics Committee of the State Key Laboratories for Quality Research in Chinese Medicines, Macau University of Science and Technology.

Author contributions

The project was conceptually designed by L-SQ and PL. The majority of the experiments were performed by Y-JW, Z-HL, and J-YL. Data analysis and interpretation were carried out by J-YL, YZ, R-YW, and X-YC. The manuscript was prepared by Y-JW, Z-HL, J-YL, L-SQ, and PL. All authors discussed the results and implications and commented on the manuscript.

Funding

This research was financially supported by the National Key Research and Development Program of China (No. 2018YFC1602403), Sichuan Science and Technology Program (No. 2022YFH0117), Macao Science and Technology Development Fund (0157/2019/A3) and Biological Resources Program, CAS (KFJ-BRP-008-007).

Conflict of interest

The authors declare that the research was conducted in the absence of any commercial or financial relationships that could be construed as a potential conflict of interest.

Publisher's note

All claims expressed in this article are solely those of the authors and do not necessarily represent those of their affiliated organizations, or those of the publisher, the editors and the reviewers. Any product that may be evaluated in this article, or claim that may be made by its manufacturer, is not guaranteed or endorsed by the publisher.

Supplementary material

The Supplementary Material for this article can be found online at: https://www.frontiersin.org/articles/10.3389/fphar.2022.987882/full#supplementary-material

References

Abboud, R., Charcosset, C., and Greige-Gerges, H. (2017). Interaction of triterpenoids with human serum albumin: A review. *Chem. Phys. Lipids* 207, 260–270. doi:10.1016/j.chemphyslip.2017.05.011

Benet, L. Z., and Hoener, B. A. (2002). Changes in plasma protein binding have little clinical relevance. *Clin. Pharmacol. Ther.* 71, 115–121. doi:10.1067/mcp.2002.121829

Bournele, D., and Beis, D. (2016). Zebrafish models of cardiovascular disease. *Heart fail. Rev.* 21, 803–813. doi:10.1007/s10741-016-9579-y

Chen, L., Du, J., Dai, Q., Zhang, H., Pang, W., and Hu, J. (2014). Prediction of anti-tumor chemical probes of a traditional Chinese medicine formula by HPLC fingerprinting combined with molecular docking. *Eur. J. Med. Chem.* 83, 294–306. doi:10.1016/j.ejmech.2014.06.037

Chen, Y. C., Wang, H. M., Niu, Q. X., Ye, D. Y., and Liang, G. W. (2016). Binding between saikosaponin C and human serum albumin by fluorescence spectroscopy and molecular docking. *Molecules* 21, 153. doi:10.3390/molecules21020153

Chen, L., Chen, X. Y., Wang, Q. L., Yang, S. J., Zhou, H., Ding, L. S., et al. (2020). Astragaloside IV derivative (LS-102) alleviated myocardial ischemia reperfusion injury by inhibiting Drp1^{Ser616} phosphorylation-ediated mitochondrial fission. *Front. Pharmacol.* 11, 1083. doi:10.3389/fphar.2020.01083

Ermakova, E. A., Danilova, A. G., and Khairutdinov, B. I. (2020). Interaction of ceftriaxone and rutin with human serum albumin. WaterLOGSY-NMR and molecular docking study. *J. Mol. Struct.* 1203, 127444. doi:10.1016/j.molstruc.2019.127444

Fitos, V. J., Simonyi, M., and Hermansson, J. (1999). Stereoselective allosteric binding interaction on human serum albumin between ibuprofen and lorazepam acetate. *Chirality* 11 (2), 115–120. doi:10.1002/(SICI)1520-636X(1999)11:2<115::AID-CHIR6>3.0.CO;2-R

Gan, R., Zhao, L., Sun, Q., Tang, P., Zhang, S., Yang, H., et al. (2018). Binding behavior of trelagliptin and human serum albumin: Molecular docking, dynamical simulation, and multi-spectroscopy. *Spectrochim. Acta. A Mol. Biomol. Spectrosc.* 202, 187–195. doi:10.1016/j.saa.2018.05.049

Ghuman, J., Zunszain, P. A., Petitpas, I., Bhattacharya, A. A., Otagiri, M., and Curry, S. (2005). Structural basis of the drug-binding specificity of human serum albumin. *J. Mol. Biol.* 353, 38–52. doi:10.1016/j.jmb.2005.07.075

He, Y., Wang, Y., Tang, L., Liu, H., Chen, W., Zheng, Z., et al. (2008). Binding of puerarin to human serum albumin: a spectroscopic analysis and molecular docking. *J. Fluoresc.* 18, 433–442. doi:10.1007/s10895-007-0283-0

Huang, C. R., Wang, G. J., Wu, X. L., Li, H., Xie, H. T., Lv, H., et al. (2006). Absorption enhancement study of astragaloside IV based on its transport mechanism in caco-2 cells. *Eur. J. Drug Metab. Pharmacokinet.* 31 (1), 5–10. doi:10.1007/BF03190635

Ibrahim, N., Haney, I., Kim, S., Nallet, J. P., and Nepveu, F. (2010). Interactions between antimalarial indolone-N-oxide derivatives and human serum albumin. *Biomacromolecules* 11, 3341–3351. doi:10.1021/bm100814n

Jiao, Q., Wang, R., Jiang, Y., and Liu, B. (2018). Study on the interaction between active components from traditional Chinese medicine and plasma proteins. *Chem. Cent. J.* 12, 48. doi:10.1186/s13065-018-0417-2

Kabiri, M., Amiri-Tehranizadeh, Z., Baratian, A., Saberi, M. R., and Chamani, J. (2012). Use of spectroscopic, zeta potential and molecular dynamic techniques to study the interaction between human holo-transferrin and two antagonist drugs: Comparison of binary and ternary systems. *Molecules* 17, 3114–3147. doi:10.3390/molecules17033114

Kim, O. T., Le, M. D., Trinh, H. X., and Nong, H. V. (2016). *In silico* studies for the interaction of tumor necrosis factor-alpha (TNF-alpha) with different saponins from Vietnamese ginseng (Panax vietnamesis). *Biophys. Physicobiol.* 13, 173–180. doi:10.2142/biophysico.13.0_173

Lakhani, N. (2005). Evaluation of the Pharmacokinetic-Pharmacodynamic relationship, Metabolism and Plasma Protein Binding of the novel antitumor agent, 2-Methoxyestradiol (2ME2). following oral administration in patients with solid tumors. *Medice. Biol.*

Lakshmi, P., Mondal, M., Ramadas, K., and Natarajan, S. (2017). Molecular interaction of 2, 4-diacetylphloroglucinol (DAPG) with human serum albumin (HSA): The spectroscopic, calorimetric and computational investigation. *Spectrochimica Acta Part A Mol. Biomol. Spectrosc.* 183, 90–102. doi:10.1016/j.saa.2017.04.012

Lang, M. R., Gihr, G., Gawaz, M. P., and Müller, I. (2010). Hemostasis in *Danio rerio*: is the zebrafish a useful model for platelet research? *J. Thromb. Haemost.* 8, 1159–1169. doi:10.1111/j.1538-7836.2010.03815.x

Liang, Y., Zhou, Y.-Y., Liu, Y.-N., Guan, T.-Y., Zheng, X., Dai, C., et al. (2013). Study on the plasma protein binding rate of Schisandra lignans based on the LC-IT-TOF/MS technique with relative quantitative analysis. *Chin. J. Nat. Med.* 11, 442–448. doi:10.1016/S1875-5364(13)60066-7

Liu, J., and Stainier, D. Y. (2012). Zebrafish in the study of early cardiac development. *Circ. Res.* 110, 870–874. doi:10.1161/CIRCRESAHA.111.246504

Liu, Z. S.-J., Xu, W-R., Shen, X-P., Shang, Q., and Tang, L-D. (2013). The study on plasma protein binging of glucoside compounds. *Tianjin J. Traditional Chin. Med.* 30 (10), 621–628.

Lombardo, O. R. S., Shalaeva, M. Y., and Gao, F. (2002). Prediction of volume of distribution values in humans for neutral and basic drugs using physicochemical measurements and plasma protein binding data. *J. Med. Chem.* 45 (13), 2867–2876. doi:10.1021/jm0200409

Lu, Y.-Y., Chen, J.-F., Song, J.-Y., Du, Z.-Y., Wang, J.-L., Qian, Y., et al. (2019). Pharmacokinetics study of 16 representative components from Baoyuan Decoction in rat plasma by LC–MS/MS with a large-volume direct injection method. *Phytomedicine* 57, 148–157. doi:10.1016/j.phymed.2018.09.002

Lu, X., Lu, L., Gao, L., Wang, Y., and Wang, W. (2021). Calycosin attenuates doxorubicin-induced cardiotoxicity via autophagy regulation in zebrafish models. *Biomed. Pharmacother.* 137, 111375. doi:10.1016/j.biopha.2021.111375

Maciazek-Jurczyk, M., Szkudlarek, A., Chudzik, M., Pozycka, J., and Sulkowska, A. (2018). Alteration of human serum albumin binding properties induced by modifications: A review. *Spectrochim. Acta. A Mol. Biomol. Spectrosc.* 188, 675–683. doi:10.1016/j.saa.2017.05.023

Metsu, D., Lanot, T., Fraissinet, F., Concordet, D., Gayrard, V., Averseng, M., et al. (2020). Comparing ultrafiltration and equilibrium dialysis to measure unbound plasma dolutegravir concentrations based on a design of experiment approach. *Sci. Rep.* 10, 12265. doi:10.1038/s41598-020-69102-y

Moradi, S., Taran, M., and Shahlaei, M. (2018). Investigation on human serum albumin and Gum Tragacanth interactions using experimental and computational methods. *Int. J. Biol. Macromol.* 107, 2525–2533. doi:10.1016/j.ijbiomac.2017.10.129

Morris, G. M., Goodsell, D. S., Halliday, R. S., Huey, R., Hart, W. E., Belew, R. K., et al. (1998). Automated docking using a Lamarckian genetic algorithm and an empirical binding free energy function. *J. Comput. Chem.* 19, 1639–1662. doi:10.1002/(sici)1096-987x(19981115)19:14<1639::aid-jcc10>3.0.co;2-b

Nevidalova, H., Michalcova, L., and Glatz, Z. (2018). In-depth insight into the methods of plasma protein-drug interaction studies: Comparison of capillary electrophoresis-frontal analysis, isothermal titration calorimetry, circular dichroism and equilibrium dialysis. *Electrophoresis* 39, 581–589. doi:10.1002/elps.201700325

Petitpas, I., Bhattacharya, A. A., Twine, S., East, M., and Curry, S. (2001). Crystal structure analysis of warfarin binding to human serum albumin: anatomy of drug site I. *J. Biol. Chem.* 276, 22804–22809. doi:10.1074/jbc.M100575200

Petitpas, P. C. E., Ha, C. E., Bhattacharya, A. A., Zunszain, P. A., Ghuman, J., Curry, S., et al. (2003). Structural basis of albumin–thyroxine interactions and familial dysalbuminemic hyperthyroxinemia. *Proc. Natl. Acad. Sci. U. S. A.* 100 (11), 6440–6445. doi:10.1073/pnas.1137188100

Qing, L. S., Peng, S. L., Liang, J., and Ding, L. S. (2017). Astragalosidic acid: A new water-soluble derivative of astragaloside IV prepared using remarkably simple TEMPO-mediated oxidation. *Molecules* 22, E1275. doi:10.3390/molecules22081275

Qing, L. S., Chen, T. B., Sun, W. X., Chen, L., Luo, P., Zhang, Z. F., et al. (2019). Pharmacokinetics Comparison, intestinal absorption and acute toxicity assessment of a novel water-soluble astragaloside IV derivative (astragalosidic acid, LS-102). *Eur. J. Drug Metab. Pharmacokinet.* 44, 251–259. doi:10.1007/s13318-018-0515-5

Raftery, T. D., Jayasundara, N., and Di Giulio, R. T. (2017). A bioenergetics assay for studying the effects of environmental stressors on mitochondrial function *in vivo* in zebrafish larvae. *Comp. Biochem. Physiol. C. Toxicol. Pharmacol.* 192, 23–32. doi:10.1016/j.cbpc.2016.12.001

Ren, S., Zhang, H., Mu, Y., Sun, M., and Liu, P. (2013). Pharmacological effects of astragaloside IV: a literature review. *J. Tradit. Chin. Med.* 33, 413–416. doi:10.1016/s0254-6272(13)60189-2

Ruiter, A. F., Teeninga, N., Nauta, J., Endert, E., and Ackermans, M. T. (2012). Determination of unbound prednisolone, prednisone and cortisol in human serum and saliva by on-line solid-phase extraction liquid chromatography tandem mass spectrometry and potential implications for drug monitoring of prednisolone and prednisone in saliva. *Biomed. Chromatogr.* 26, 789–796. doi:10.1002/bmc.1730

Senthilkumar, R., Marimuthu, P., Paul, P., Manojkumar, Y., Arunachalam, S., Eriksson, J. E., et al. (2016). Plasma protein binding of anisomelic acid: Spectroscopy and molecular dynamic simulations. *J. Chem. Inf. Model.* 56, 2401–2412. doi:10.1021/acs.jcim.6b00445

Sun, W. X., Zhang, Z. F., Xie, J., He, Y., Cheng, Y., Ding, L. S., et al. (2019). Determination of a astragaloside IV derivative LS-102 in plasma by ultra-performance liquid chromatography-tandem mass spectrometry in dog plasma and its application in a pharmacokinetic study. *Phytomedicine* 53, 243–251. doi:10.1016/j.phymed.2018.09.019

Talbert, A. M., Tranter, G. E., Holmes, E., and Francis, P. L. (2002). Determination of drug– plasma protein binding kinetics and equilibria by chromatographic profiling: Exemplification of the method using l-tryptophan and albumin. *Anal. Chem.* 74, 446–452. doi:10.1021/ac010643c

Tang, J., Luan, F., and Chen, X. (2006). Binding analysis of glycyrrhetinic acid to human serum albumin: fluorescence spectroscopy, FTIR, and molecular modeling. *Bioorg. Med. Chem.* 14, 3210–3217. doi:10.1016/j.bmc.2005.12.034

Tesseromatis, A. A., and Alevizou, A. (2008). The role of the protein-binding on the mode of drug action as well the interactions with other drugs. *Eur. J. Drug Metab. Pharmacokinet.* 33 (4), 225–230. doi:10.1007/BF03190876

Trott, O., and Olson, A. J. (2010). AutoDock Vina: improving the speed and accuracy of docking with a new scoring function, efficient optimization, and multithreading. *J. Comput. Chem.* 31, 455–461. doi:10.1002/jcc.21334

Vallner, J. J. (1977). Binding of drugs by albumin and plasma protein. *J. Pharm. Sci.* 66 (4), 447–465. doi:10.1002/jps.2600660402

Van Der Spoel, D., Lindahl, E., Hess, B., Groenhof, G., Mark, A. E., and Berendsen, H. J. C. (2005). GROMACS: Fast, flexible, and free. *J. Comput. Chem.* 26, 1701–1718. doi:10.1002/jcc.20291

Wang, G., Wang, D., Li, X., and Lu, Y. (2011). Exploring the binding mechanism of dihydropyrimidinones to human serum albumin: spectroscopic and molecular modeling techniques. *Colloids Surf. B Biointerfaces* 84, 272–279. doi:10.1016/j.colsurfb.2011.01.016

Wang, Q.-L., Xie, J., Li, X.-D., Ding, L.-S., Liang, J., Luo, P., et al. (2017). Development of a nano-SiO_2 based enzyme-linked ligand binding assay for the determination of ibuprofen in human urine. *Talanta* 167, 617–622. doi:10.1016/j.talanta.2017.03.011

Warsi, M. S., Habib, S., Talha, M., Mir, A. R., Alam, K., Ali, A., et al. (2021). Characterization of human serum albumin modified by hair dye component, 4-chloro-1, 2-phenylenediamine: Role in protein aggregation, redox biology and cytotoxicity. *J. Mol. Liq.* 331, 115731. doi:10.1016/j.molliq.2021.115731

Xiang, Y. H., Duan, L. L., Ma, Q., Lv, Z. Z., Zhu, R. H., and Zhang, Z. Y. (2016). Fluorescence spectroscopy and molecular simulation on the interaction of caffeic acid with human serum albumin. *Luminescence* 31, 1496–1502. doi:10.1002/bio.3135

Xu, L. M., Yang, B., Yin, Q-Y., and Lu, Y. (2016). Determination of protein-binding rate of adenosine and astragaloside Ⅳ in Anchuanshu pills in human plasma by LC-MS/MS. *Cent. South Pharm.* 14 (03), 282–285.

Xu, L., Hu, Y. X., Li, Y. C., Liu, Y. F., Zhang, L., Ai, H. X., et al. (2017). Study on the interaction of paeoniflorin with human serum albumin (HSA) by spectroscopic and molecular docking techniques. *Chem. Cent. J.* 11, 116. doi:10.1186/s13065-017-0348-3

Yang, F., Zhang, Y., and Liang, H. (2014). Interactive association of drugs binding to human serum albumin. *Int. J. Mol. Sci.* 15, 3580–3595. doi:10.3390/ijms15033580

Yu, H., Li, D., Xu, F., Pan, Q., Chai, P., Liu, B., et al. (2016). The binding affinity of human serum albumin and paclitaxel through MMPBSA based on docked complex. *Mol. Simul.* 42, 1460–1467. doi:10.1080/08927022.2016.1198479

Yue, Y., Liu, J., Fan, J., and Yao, X. (2011). Binding studies of phloridzin with human serum albumin and its effect on the conformation of protein. *J. Pharm. Biomed. Anal.* 56, 336–342. doi:10.1016/j.jpba.2011.05.018

Zhang, F., Xue, J., Shao, J., and Jia, L. (2012). Compilation of 222 drugs' plasma protein binding data and guidance for study designs. *Drug Discov. Today* 17, 475–485. doi:10.1016/j.drudis.2011.12.018

Zsila, F., Bikadi, Z., Malik, D., Hari, P., Pechan, I., Berces, A., et al. (2011). Evaluation of drug-human serum albumin binding interactions with support vector machine aided online automated docking. *Bioinformatics* 27, 1806–1813. doi:10.1093/bioinformatics/btr284

frontiers | Frontiers in Pharmacology

TYPE Original Research
PUBLISHED 23 September 2022
DOI 10.3389/fphar.2022.1007310

Check for updates

OPEN ACCESS

EDITED BY
Arshad Mahmood,
Al Ain University, United Arab Emirates

REVIEWED BY
Syed Shams Ul Hassan,
Shanghai Jiao Tong University, China
Hammad Ahmad,
COMSATS University Islamabad, Pakistan

*CORRESPONDENCE
Muhammad Haseeb Ur Rehman,
haseeb114@hotmail.com
Uzma Saleem,
uzma95@gmail.com

SPECIALTY SECTION
This article was submitted to Predictive Toxicology, a section of the journal Frontiers in Pharmacology

RECEIVED 30 July 2022
ACCEPTED 24 August 2022
PUBLISHED 23 September 2022

CITATION
Rehman MH, Saleem U, Ahmad B and Rashid M (2022), Phytochemical and toxicological evaluation of Zephyranthes citrina. *Front. Pharmacol.* 13:1007310. doi: 10.3389/fphar.2022.1007310

COPYRIGHT
© 2022 Rehman, Saleem, Ahmad and Rashid. This is an open-access article distributed under the terms of the Creative Commons Attribution License (CC BY). The use, distribution or reproduction in other forums is permitted, provided the original author(s) and the copyright owner(s) are credited and that the original publication in this journal is cited, in accordance with accepted academic practice. No use, distribution or reproduction is permitted which does not comply with these terms.

Phytochemical and toxicological evaluation of Zephyranthes citrina

Muhammad Haseeb Ur Rehman*[,1], Uzma Saleem*[,1], Bashir Ahmad[2] and Memoona Rashid[3]

[1]Department of Pharmacology, Faculty of Pharmaceutical Sciences, Government College University, Faisalabad, Pakistan, [2]Department of Pharmacology, Hamza College of Pharmaceutical and Allied Health Sciences, Lahore, Pakistan, [3]Akhtar Saeed College of Pharmacy, Canal Campus Lahore, Lahore, Pakistan

Drugs obtained from medicinal plants have always played a pivotal role in the field of medicine and to identify novel compounds. Safety profiling of plant extracts is of utmost importance during the discovery of new biologically active compounds and the determination of their efficacy. It is imperative to conduct toxicity studies before exploring the pharmacological properties and perspectives of any plant. The present work aims to provide a detailed insight into the phytochemical and toxicological profiling of methanolic extract of *Zephyranthes citrina* (MEZ). Guidelines to perform subacute toxicity study (407) and acute toxicity study (425) provided by the organization of economic cooperation and development (OECD) were followed. A single orally administered dose of 2000 mg/kg to albino mice was used for acute oral toxicity testing. In the subacute toxicity study, MEZ in doses of 100, 200, and 400 mg/kg was administered orally, consecutive for 28 days. Results of each parameter were compared to the control group. In both studies, the weight of animals and their selected organs showed consistency with that of the control group. No major toxicity or organ damage was recorded except for some minor alterations in a few parameters such as in the acute study, leukocyte count was increased and decreased platelet count, while in the subacute study platelet count increased in all doses. In the acute toxicity profile liver enzymes Alanine aminotransferase (ALT), as well as, aspartate aminotransferase (AST) were found to be slightly raised while alkaline phosphatase (ALP) was decreased. In subacute toxicity profiling, AST and ALT were not affected by any dose while ALP was decreased only at doses of 200 and 400 mg/kg. Uric acid was raised at a dose of 100 mg/kg. In acute toxicity, at 2000 mg/kg, creatinine and uric acid increased while urea levels decreased. Therefore, it is concluded that the LD_{50} of MEZ is more than 2000 mg/kg and the toxicity profile of MEZ was generally found to be safe.

KEYWORDS

***Zephyranthes citrina*, UHPLC/MS, phytochemical analysis, toxicological study, LD_{50}**

1 Introduction

Plants have historically been utilized as a fundamental source of new drugs. Herbal drugs have vast acceptability in the general population because of social beliefs regarding their excellent healing capacity, and the ability to improvise emotional well-being, thereby, augmenting the quality of life since ancient times (Aslam and Ahmad, 2016; Jamshidi et al., 2018). According to a report by the World Health Organization (WHO), nearly 80% population of low to middle-income countries (LMICs) is dependent on plant-based drugs to alleviate their primary health-related issues (Al-Nahain et al., 2014; Hoyler et al., 2018). Due to their myriad benefits, there is even a greater turnaround towards herbal remedies. These benefits include comparatively fewer adverse drug reactions whereas delivering promising outcomes (Muhammad I. et al., 2021). Moreover, certain reports state that herbal treatments trim down the pill burden (Rahimi et al., 2009). Plant-based drugs are used to treat various acute and chronic medical conditions such as parasitic infestation (Li Z et al., 2022), malaria, cancer (Majid M. et al., 2022), neurological disorders, age related degenerative disorders (Jin K. et al., 2022) chronic inflammation (Muhammad I. et al., 2022), cardiovascular and liver diseases, fungal (Chen H. et al., 2021) and bacterial infections (Yang L. et al., 2022), sleep disturbances such as insomnia, diabetes mellitus, and many others (Chandrasekaran & Venkatesalu, 2004; AlMamun, 2020). Medicinal plants provide cost-effectiveness and ease of use. Owing to their easy accessibility, inexpensive thrifty nature, and safety profile, the acceptability of herbal medicines has risen considerably, in recent times (Sandhya et al., 2006). Phytochemicals isolated from plant extracts have remained the mainstay of drug discovery (Muhammad I., and ul Hassan S.S., et al., 2021). Even in the present era of modern medicine, chemical compounds isolated from the plants are of particular interest because these compounds serve as a potential lead for newer drugs. Crude extracts of plants, as well as isolated phytochemicals, are screened for various *in vivo*, *in vitro*, and *in silico* pharmacological activities (Kundu P., et al., 2002). Plant extracts may possess both pharmacological and toxicological properties due to the presence of bioactive molecules (Yang J. et al., 2020). Extracts of various plants in different formulations, as well as isolated constituents, have widely been used as household remedies during the modern medicine era for the treatment of many diseases (Farnsworth, N. R. 1966).

Medicinal plants may contain toxic and pharmacologically active constituents. Some medicinal plants may intrinsically be toxic in terms of their phytochemicals which may be associated with adverse effects if used inadequately and improperly. Therefore, in the discovery of biologically active compounds (Zhuo, Z. et al., 2020), toxicity evaluation is the primary and mandatory parameter that needs to be assessed prior to its pharmacological screening and clinical application (Pour et al., 2011). Toxicity studies not only provide a correlation between the animal and human response by depicting the efficacy and safety profile but also help in ascertaining the dose of extracts for further screening (Anwar et al., 2021a). Thereby, toxicity studies safeguard the exposed population from the possible harms of the test compounds. Furthermore, these also help in appropriate dose assessment to be employed in end users (Mensah et al., 2019). Benefits of toxicological evaluation of plant extracts in animal models also include a controlled exposure time, examination of different tissues for possible harms, and determining the effect on different biomarkers (Arome and Chinedu, 2013). Conclusively, the toxicity study beneficially demarcates between toxic dose and therapeutic dose (Anwar et al., 2021b). Animal models are recommended for executing toxicological evaluations which comply with the organization of economic cooperation and development (OECD) guidelines.

Amaryllidaceae is a large family of plants that consists of 75 genera and 1,600 species (Christenhusz M.J.M. et al., 2016). Amaryllidaceae is famous for its alkaloids that have diverse biological activities. Numerous plants of Amaryllidaceae have traditionally been used as folklore medicine for the treatment of several ailments throughout the world (Biswas & Paul, 2022). *Zephyranthes citrina* (*Z. citrina*) is a naturally occurring perennial bulbous plant that belongs to Amaryllidaceae. Z. citrina has bright yellow flowers, green leaves, and bulbous stems. It is commonly known as Rain Lily because the flowering tops bloom in the rainy season (Jin and Yao, 2019). *Z. citrina* has been a relatively less explored plant for its pharmacological activities. A few pharmacological activities such as antimicrobial (Singh et al., 2010), antiprotozoal (Kaya et al., 2011), antimalarial (Herrera et al., 2001), anti-inflammatory (Aslam et al., 2016), and *in vitro* anticholinesterase activity which indicates its potential use in Alzheimer's disease (Kohelová et al., 2021) have been reported so far.

Therefore, the present work aims at investigating the phytochemical and toxicity profiles of different doses of methanolic extracts of *Zephyranthes citrina* (MEZ) in order to report and identify the expected hazards in different doses using different protocols. The study has evaluated acute oral and subacute toxicity in mice models to ensure the safety and suitability of MEZ for further for its applicability in pharmacological screening.

2 Materials and methods

2.1 Chemicals

Methanol (I0962907) was purchased from Merck KGaA Germany. Pyrogallol solution was purchased from Oxford

Labs (India). Other chemicals such as Carboxymethyl cellulose, sulfanilamide, Ethylenediamine tetraacetic acid (EDTA), Griess reagent, N-1- naphthylethyleneamine dihydrochloride, thiobarbituric acid, anhydrous aluminium chloride, copper sulfate, sodium phosphate dibasic heptahydrate and sodium phosphate monobasic monohydrate, phosphoric acid, picric acid, sodium carbonate, sodium hydroxide, sodium-potassium tartrate, gallic acid, Folin-Ciocalteu reagent, and quercetin were purchased from Sigma Aldrich United States.

2.2 Experimental validation

2.2.1 Collection and authentication of plant material

The whole plant of *Z. citrina* was collected from the botanical garden of Government College University, Lahore (GCUL) Lahore during the flowering season from July to September. Plants have rush-like leaves and bulbous roots. Leaves bear yellow flowers that are Specific to *Z. citrina* within the entire family Amaryllidaceae. Authentication and validation of the plant were done by Prof. Dr. Zaheer Ud Din, botanist and taxonomist, at GCUL. The specimen of the plant was deposited in the Herbarium of the department of Botany GCUL vide voucher number (GC. Herb. Bot. 3553).

2.2.2 Plant material preparation

Whole plants of *Z. citrina* were washed with tap water to remove debris (Saleem u et al., 2019). Leaves and flowers were separated from the bulbous part and air dried. Each bulb was cut into three slices and then dried in a hot air oven at 40°C until constant weight (López, S. et al., 2002). Once fully dried all parts of the plants were mixed together and ground by mechanical milling until a fine powder was obtained.

2.2.3 Preparation of methanolic extract of *Z. citrina*

Powdered tissue of plant material (2 kg) was subjected to cold maceration, in the ratio of 1:2 with methanol (4 L), and was stirred every 8 h periodically, for 14 days. After the completion of the extraction period, initial filtration of the macerate was done through a filtration cloth to obtain the supernatant, separated from the macerated powder. This supernatant was subjected to subsequent filtration by passing it through a Buchner funnel assembly and Whatman filter paper number 1 under reduced pressure. This secondary filtration removed solid particulate matter suspended in the filtrate. Finally, a rotary evaporator was used for the evaporation of methanol from pure filtrate at 40°C under reduced pressure which yielded a dark brown gummy mass. The MEZ was kept in an airtight container between 2–8°C.

2.3 Estimation of total phenolic and flavonoid content

The Standard Folin-Ciocalteu reagent method was used for the determination of the total phenolic content (TPC) of MEZ (Terfassi, S, et al., 2021). Gallic acid was used as a standard for the determination of TPC. Briefly described, 1 ml of MEZ (final concentration 1 mg/ml) was mixed in 1 ml of Folin-Ciocalteu's phenolic reagent. The solution was kept for 5 min and then 7% of Sodium carbonate (10 ml) was added and mixed. Then 13 ml of deionized distilled water was added to the previously made solution and thoroughly mixed for uniformity. This solution was incubated for one and a half hours in the dark at room temperature. After the incubation period, the absorbance was taken at 750 nm. Gallic acid solution was prepared and a calibration curve was constructed and extrapolated for the determination of the TPC of MEZ. The procedure was carried out in triplicate. Results were expressed as Gallic acid equivalents in milligram per Gram (GAE/g) of the dried sample (Saeed, N. et al., 2012).

For the determination of total flavonoid content (TFC) spectrophotometric method using anhydrous aluminium chloride ($AlCl_3$ $6H_2O$) was used. Quercetin was employed as a standard.

Method followed is, 0.3 ml MEZ extract was mixed with 3.4 ml of 30% methanol, 0.15 ml of $NaNO_2$ (0.5 M) and 0.15 ml of $AlCl_3.6H_2O$ (0.3 M). The solution was kept for 5 min and then 1 ml of sodium hydroxide was added to this solution. The whole solution was gently but thoroughly mixed and absorbance was measured at 506 nm. A standard curve was constructed using quercetin standard solution prepared by the above-mentioned procedure. The result for TFC was calculated and shown as milligram of quercetin equivalent per Gram of dried extract (mg QE/g) (Saeed, N. et al., 2012).

2.4 Antioxidant assay

In vitro, free radical scavenging activity was measured by a 2, 20 - diphenyl-1-picrylhydrazyl (DPPH) assay. The reaction of the DPPH assay depends on the capability of the plant extract samples to scavenge free radicals. The reaction is visually noticeable because the color changes from purple to yellow because of its ability to donate hydrogen. 24 mg DPPH was dissolved in 100 ml methanol to prepare the stock solution. This solution was stored at 20°C. The working solution was made by diluting DPPH with methanol until the final concert. Of DPPH becomes 0.267 mM in 0.004% methanol having an absorbance of almost 0.98 ± 0.02 at 517 nm by using the spectrophotometer. Then an aliquot of 1.5 ml was mixed in 50 µl of plant extract sample at varying concentrations between 10–500 µg/ml. This mixture was mixed thoroughly and incubated for 30 min in the dark at room temperature (Mishra, K. et al., 2012). The

absorbance was recorded at 517 nm. The control solution was prepared by the same method mentioned above without any plant extract sample. Percentage DPPH scavenging activity was calculated by using Eq. 1 (Saeed, N. et al., 2012).

$$\text{Free Radical Scavenging Activity (\%)} = \frac{\text{Absorbance of control} - \text{Absorbance of sample}}{\text{Absorbance of control}} \times 100. \quad (1)$$

2.5 UHPLC–MS analysis for secondary metabolite profiling

Profiling of Secondary metabolites was carried out by reversed-phase ultra-high performance liquid chromatography-mass spectrometry (RP-UHPLC-MS) analytical technique. Agilent 1,290 Infinity ultra-high performance liquid chromatography system that has been attached to Agilent 6,520 Accurate–Mass Q-TOF mass spectrometer having dual electrospray ionization (ESI) source was used. Details and specifications of the column that was used are; Agilent Zorbax Eclipse XDB-C18 has a narrow bore size of 2.1 × 150 mm, 3.5 μm (P/N 930990-902). The temperature of 4°C for the auto-sampler and 25°C for the column was maintained. Two different mobile phase solutions were used A) 0.1% formic acid in water and B) 0.1% formic acid in acetonitrile. The mobile phase flow rate was kept at 0.5 ml/min 1.0 μl methanolic extract solution of the plant prepared in HPLC grade methanol was injected for 25 min And post-run time was 5 min. A complete scan of MS analysis using ESI negative ionization mode spanned over a complete range of *m/z* 100–1,000. Nitrogen was supplied both as nebulizing (flowrate 25 L/h) and drying gas (flowrate 600 L/h). The drying gas temperature was kept constant at 350°C. The capillary voltage was 3,500 V meanwhile fragmentation voltage had been optimized at 125 V. Data processing was done with Agilent mass hunter Qualitative Analysis B. 05.00, the Method used was Metabolomics −2017–0000.4 m (H. Saleem et al., 2019). Compound identification was done from the database: METLIN _AM_PCDL-N-170502. cdb with parameters as Match tolerance: 5 ppm. Positive Ions: +H, +Na, + NH_4, negative Ions: H.

2.6 Experimental animals

Healthy adult Swiss albino mice were used as the experimental animals which were kept in the animal house of Government College University, Faisalabad, Pakistan. Standard controlled conditions were provided to the animals regarding temperature (22 ± 2°C) and humidity (45%–50%), 12 h light, and 12 h dark cycles having access to water and food, freely. Prior approval to conduct all the animal studies, including acute oral toxicity and subacute toxicity, was taken from Institutional Review Board, GC University Faisalabad vide letter number GCU/ERC/2141. Animals were treated ethically according to guidelines, rules, and regulations provided by the National Institute of Health (NIH, United States).

TABLE 1 Groups and doses of subacute toxicity study.

Group	Dose
1	Control (5–10 ml/kg Normal Saline)
2	MEZ[a] 100 mg/kg of body weight
3	MEZ 200 mg/kg of body weight
4	MEZ 400 mg/kg of body weight

[a]MEZ: Methanolic Extract of *Z. citrina*.

2.7 Toxicity studies protocols

2.7.1 Acute oral toxicity

The OECD (Organization for Economic Corporation and Development) 425 guidelines (2001), were followed to conduct an acute oral toxicity study. Five healthy adult albino mice were used for acute oral toxicity tests. Animals were kept on fasting overnight with access to water *ad libitum*. Initially, only one animal, out of five, was administered 2,000 mg/kg body weight, as a single dose, of MEZ via an oral route through gastric lavage, and was subjected to observation for 24 h. If no mortality occurred to that animal, a single dose of 2,000 mg/kg of MEZ was administered, via the same route, to the remaining four animals. All the animals were observed for any signs of physical and behavioral alterations for 14 days

2.7.2 Subacute toxicity

The OECD 407 guidelines (2008), with slight modification, were followed to conduct the subacute toxicity study. 40 healthy albino mice were used in the study. Animals were divided into four groups. Each group consisted of five females and five male animals. All animals, except the control, were administered different doses of extract (Table 1) for 28 days via an oral route through gastric lavage once daily. Physical conditions and behavioral aspects of animals were noted at the beginning of the experiment. Animals were observed daily for any change in weight and any sign of physical anomalies.

2.7.3 Weights of animals and their selected organs

During acute oral toxicity body weights of all the animals in all the groups were recorded at day zero, which was marked just before the start of the study, and then subsequently at days 1, 2, and 14. During the subacute study, body weights were measured on days 1, 7, 21, and 28. At the conclusion of the study, excision

of the animals was carried out selected organs were separated and weighed.

2.8 Hematological parameter and biochemical markers measured in acute and subacute toxicity studies

After the completion of each study, animals were anesthetized by administering 5% isoflurane mixed with oxygen. A cardiac puncture was done for the collection of blood samples. Then these blood samples were subjected to hematological and biochemical analysis. Mindray BC3000 Plus hematology analyzer was used for hematologic analysis while for biochemical analysis Mindray BA88A was used. In regards to hematology following parameters were analyzed: Various aspects of platelet count, red blood cell (RBC) count, hematocrit, hemoglobin, mean corpuscular hemoglobin (MCH), mean corpuscular hemoglobin concentration (MCHC), total leukocyte count (TLC), and differential leukocyte count including both granulocytes and agranulocytes.

For the analysis of various biochemical markers, plasma and serum were prepared, separately. For the preparation of serum, a whole blood sample was coagulated at room temperature in a vacutainer and then it was centrifuged at a speed of 2,000 × g for 10 min. While plasma was prepared by collecting whole blood in an anticoagulant-containing vacutainer and then centrifuged at 2,000 × g for 10 min. Biochemical markers evaluated include liver function tests (LFTs), renal function tests (RFTs), and lipid profile (Liu C.et al., 2022). LFTs included AST, ALT, ALP, and protein. RFTs included urea, uric acid, creatinine, and bilirubin. The lipid profile included triglycerides (TGs), cholesterol, high-density cholesterol (HDL), and low-density cholesterol (LDL).

2.9 Histopathological studies

Selected organs such as the brain, heart, kidney, and liver were processed and preserved in a 4% formaldehyde solution. The organ specimens were embedded and fixed in paraffin wax and sections were made. Sliced sections were subsequently subjected to a fixation on slides and stained with hematoxylin and eosin (H & E) stain and histologically examined (Rajeh, M.A.B., 2012).

2.10 Observation of animal behavior and physical changes

All the animals were observed during acute for clinical signs of behavioral and physical alteration such as itching, eye, and nasal discharge, skin lesion, respiratory distress, abnormal movements and urination, and food and water intake. Any change in these parameters was recorded (Saleem H. et al., 2019).

TABLE 2 Total content of bioactive compounds and antioxidant activity of MEZ.

Assay	Parameter	Results
Percent extract yield		19.7%
Content of bioactive compounds	Total flavonoid content	37.92 ± 0.26
	Total phenolic content	25.93 ± 0.19
Free radical scavenging activity	DPPH (%)	88.23 ± 2.95

2.11 Statistical analysis

GraphPad Prism 9.0 was used to interpret the data and expressed as standard deviation (±SD).

3 Results

3.1 Phytochemical composition and antioxidant activity

The methanolic extract of *Z. citrina* contains an abundant amount of phenolic and flavonoid compounds and was measured with reference to their standards and Gallic acid and Quercetin, respectively. Free radical scavenging activity by the DPPH method showed excellent antioxidant activity. Results for TPC, TFC, and antioxidant activity are mentioned in Table 2.

3.1.1 Secondary metabolite profiling (UHPLC–MS analysis)

UHPLC - MS Analysis of methanolic extract of *Z. citrina* was performed to determine the possible secondary metabolites and phytochemical components. The analysis showed that it contains 44 phytochemical compounds that belong to alkaloids, amino acids, carboxylic acids, flavonoids, phenolics, and a few other chemical classes. The phytochemical composition, retention time, base peak (*m/z*), chemical class, molecular mass, and formula are described in Table 3. The total ion chromatogram is shown in Figure 1.

3.2 Weights of animals and their selected organs in acute and subacute toxicity

During both the studies body weights were monitored and recorded are described in Table 4 and Figure 2. The average body weights with a standard deviation of all treated and control animals during the subacute toxicity study of both male and female groups were observed from the day 1 to day 28th (Figures 2A,B respectively). MEZ did not show any considerable difference in body weights of animals from day 1–28 in comparison to control. The average body weights with SD of

TABLE 3 UHPLC-MS analysis of methanolic extract of Z. citrina.

S. No.	RT[a] (Min.)	Base peak (m/z)	Molecular Mass	Proposed compound	Compound class	Molecular formula
1	2.294	272.9595	273.9647	Ribose-1-arsenate	Carbohydrate	C5 H11 As O8
2	2.474	241.0926	242.0998	D-erythro-D-galacto-octitol	Alditol	C8 H18 O S
3	2.485	173.1052	174.1125	L-Arginine	Amino Acid	C6 H14 N4 O S
4	2.501	224.0787	225.086	Acyclovir	Purine Analog	C8 H11 N5 O3
5	2.508	340.1261	341.1332	His Ala Asp	Amino Acid	C13 H19
6	2.522	335.1586	336.1648	N2-Fructopyra-nosylarginine	Phenolic	C12 H24 N4 O7
7	2.601	266.083	267.0902	PD 98059	Flavonoid	C16 H13 N O3
8	2.623	264.0987	265.1059	Agaritinal	Amino Acid derivative	C12 H15 N3 O4
9	2.649	219.0403	220.0479	Quinazoline acetic acid (3(2H)-Quinazolineacetic acid, 1,4-dihydro-2,4-dioxo-	Alkaloid	C10 H8 N2 O4
10	2.683	195.0519	196.0592	L-Gulonate	Carbohydrate	C6 H12 O7
11	2.686	165.0415	166.0488	1-Methylxanthine	Alkaloid	C6 H6 N4 O2
12	2.706	179.0573	180.0647	Theobromine	Alkaloid	C7 H8 N4 O2
13	2.747	683.2275	342.1186	Nigerose (Sakebiose)	Carbohydrate	C12 H22 O11
14	2.752	387.1165	388.1237	Fructoselysine 6-phosphate	Glycated protein	C12 H25 N2 O10 P
15	2.836	701.1932	666.2244	Maltotetraose	Carbohydrate	C24 H42 O21
16	2.843	539.1408	504.1714	Panose	Carbohydrate	C18 H32 O16
17	2.891	827.2702	828.2771	Maltopentaose	Carbohydrate	C30 H52 O26
18	2.921	989.3229	990.3299	Maltohexaose	Carbohydrate	C36 H62 O31
19	2.926	369.1042	370.1118	2′,3′,5′-triacetyl-5-Azacytidine	Pyrimidine nucleoside analogue	C14 H18 N4 O8
20	2.95	1,151.374	1,152.381s	Celloheptaose	Sugar	C42 H72 O36
21	2.966	149.0459	150.0532	L-Lyxose	Aldehyde	C5 H10 O5
22	2.973	339.0972	304.1293	2′-Deoxymugineic acid	Carboxylic acid	C12 H20 N2 O7
23	2.978	366.1165	367.124	Met Ser Met	Protein	C13 H25 N3 O5 S2
24	3.093	133.015	134.0225	3,3-Dimethyl-1,2-dithiolane	Dithiolanes	C5 H10 S2
25	3.259	290.0886	291.0959	Sarmentosin epoxide	Glycoside	C11 H17 N O8
26	3.939	191.0202	192.0275	Citric acid	Carboxylic acid	C6 H8 O7
27	4.026	128.0359	129.0431	N-Acryloylglycine	Amino acid	C5 H7 N O3
28	4.164	243.0624	244.0698	Uridine	Pyrimidine Nucleoside	C9 H12 N2 O6
29	4.403	130.0873	131.0945	L-Leucine	Amino acid	C6 H13 N O2
30	4.534	180.0666	181.0738	3-Amino-3-(4-hydroxyphenyl) propanoate	Amino acid	C9 H11 N O3
31	4.58	292.1404	293.1476	N-(1-Deoxy-1-fructosyl) leucine	Leucine & derivative	C12 H23 N O7
32	4.729	288.1242	289.1314	Norcocaine	Alkaloid	C16 H19 N O4
33	4.828	103.0403	104.0475	D (-)-β-hydroxy butyric acid	Carboxylic acid	C4 H8 O3
34	10.042	255.0519	256.0591	Piscidic Acid	Phenolic	C11 H12 O7
35	10.536	153.0197	154.0269	3,4-Dihydroxybenzoic acid	Phenolic	C7 H6 O4
36	10.887	385.0568	386.0645	Shoyuflavone A	Flavanoids	C19 H14 O9
37	11.228	175.0613	176.0685	3-propylmalic acid	Carboxylic acid	C7 H12 O5
38	11.325	239.0563	240.0636	(1R,6R)-6-Hydroxy-2-succinylcyclohexa-2,4-diene-1-carboxylate	Gamma keto acid	C11 H12 O6
39	11.382	215.0827	216.09	Desethyletomidate	Ethylester	C12 H12 N2 O2
40	11.573	183.03	184.0373	4-O-Methyl-gallate	Phenolic	C8 H8 O5
41	11.948	306.0619	307.0692	Narciclasine	Alkaloid	C14 H13 N O7
42	11.949	352.067	353.0745	2,5-Diamino-6-hydroxy-4-(5′-phosphoribosylamino)-pyrimidine	N-glycosyl	C9 H16 N5 O8 P
43	13.461	187.0977	188.105	Nonic Acid	Pyruvic Acid	C9 H16 O4
44	17.614	293.1765	294.1838	Gingerol	Phenolic	C17 H26 O4

[a]RT: retention time.

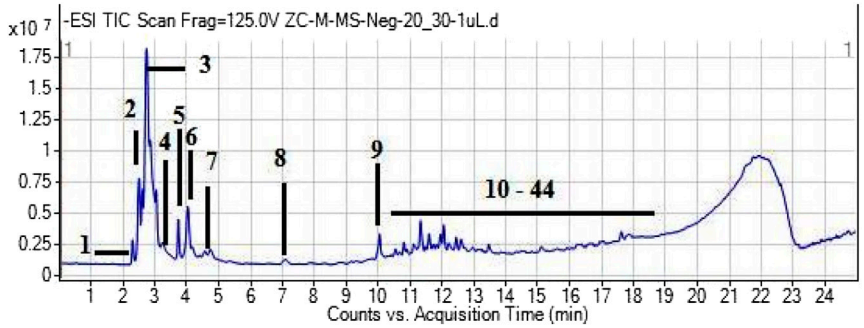

FIGURE 1
UHPLC - MS chromatogram of MEZ showing phytochemical profiling of extract.

TABLE 4 Selected organ weights with standard deviation of treated and control group animals during acute and subacute toxicity Study.

	Dose (mg/kg)	Liver	Kidney	Pancreases	Lungs	Heart	Stomach	Brain
Acute Toxicity	**2000**	1.56 ± 0.09	0.43 ± 0.06	0.12 ± 0.018	0.26 ± 0.0 4	0.14 ± 0.02	0.25 ± 0.02	0.39 ± 0.017
	Control	1.53 ± 0.05	0.41 ± 0.03	0.14 ± 0.03	0.24 ± 0.04	0.12 ± 0.01	0.24 ± 0.014	0.40 ± 0.02
Subacute Toxicity (Male)	**100**	1.30 ± 0.03	0.44 ± 0.03	0.12 ± 0.01	0.27 ± 0.01	0.13 ± 0.003	0.23 ± 0.01	0.42 ± 0.02
	200	1.15 ± 0.08	0.35 ± 0.03	0.11 ± 0.18	0.21 ± 0.01	0.13 ± 0.003	0.22 ± 0.02	0.40 ± 0.01
	400	1.58 ± 0.06	0.42 ± 0.04	0.15 ± 0.02	0.29 ± 0.02	0.14 ± 0.01	0.24 ± 0.01	0.37 ± 0.03
	Control	1.57 ± 0.03	0.42 ± 0.03	0.14 ± 0.01	0.22 ± 0.01	0.12 ± 0.01	0.23 ± 0.012	0.39 ± 0.015
Subacute Toxicity (Female)	**100**	1.46 ± 0.04	0.42 ± 0.03	0.13 ± 0.01	0.26 ± 0.01	0.13 ± 0.04	0.22 ± 0.01	0.4 ± 0.02
	200	1.47 ± 0.08	0.37 ± 0.03	0.10 ± 0.018	0.22 ± 0.01	0.137 ± 0.008	0.23 ± 0.02	0.4 ± 0.017
	400	1.68 ± 0.09	0.42 ± 0.02	0.15 ± 0.01	0.28 ± 0.02	0.13 ± 0.01	0.24 ± 0.02	0.39 ± 0.03
	Control	1.46 ± 0.08	0.34 ± 0.04	0.13 ± 0.02	0.25 ± 0.03	0.12 ± 0.009	0.24 ± 0.03	0.38 ± 0.03

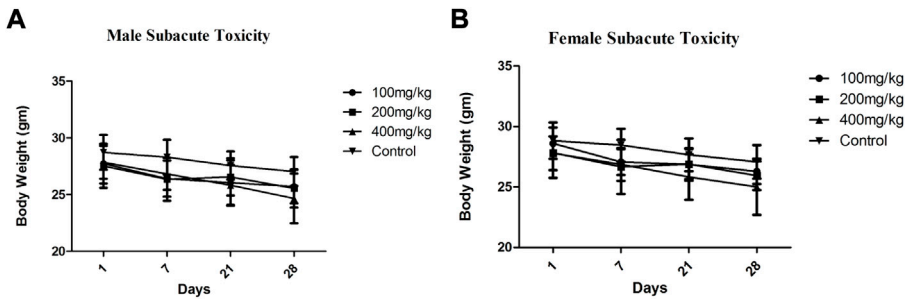

FIGURE 2
Average body weights ±SD of Male **(A)** and female **(B)** animals treated at different doses along with control during subacute toxicity study.

animals treated at 2,000 mg/kg and control group animals during the acute toxicity study were observed and mentioned in Figure 3. The acute toxicity study which was carried out on days 0, 1, 2, and 14 showed no major change in body weights of the treated group in comparison to control group (Figure 3).

Organ weights, measured at the completion of subacute and acute oral toxicity studies, are described in Table 4. Organ weights of MEZ-treated animals in both studies were comparable to the control groups which depicts that MEZ is not involved in organ damage.

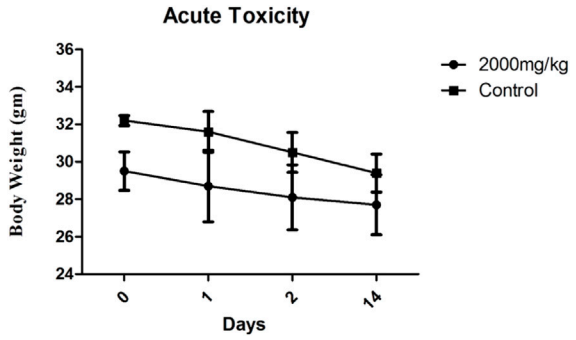

FIGURE 3
Average body weights ±SD of treated animals at 2,000 mg/kg dose along with control group during acute toxicity study.

3.3 Hematological analysis in subacute and acute oral toxicity studies

Blood samples were collected at the end of both studies through cardiac puncture and were subjected to CBC analysis. During the acute oral toxicity study, WBCs were raised significantly at the dose of 2,000 mg/kg in comparison to control group animals. Upon detailed analysis, granulocyte count was also found to be raised. Erythrocyte count was normal in the treatment group while the platelet count was decreased in comparison to the control group. Results of hematological parameters of acute oral toxicity study are shown in Table 5.

During the subacute study of both male and female animals, CBC analysis showed no major change in any WBC and RBC count in all treatment groups of both genders. Platelet count was relatively higher in both male and female mice of the treatment groups than in the control group. Results of both male and female animals are shown in Table 6.

3.4 Biochemical markers in acute and subacute studies

Figure 4 and Table 7 describe the results of subacute and acute studies respectively of various biochemical markers such as LFTs (AST, ALT, ALP, and protein), RFTs (Uric acid, urea, creatinine, and bilirubin), and total lipid profile (cholesterol, triglycerides, HDL, and LDL). During the subacute study, there was no change in levels of AST, and ALT in all treated groups while the level of ALP was decreased at doses of 200 and 400 mg/kg in treated groups. The level of ALP in animals treated at a dose of 100 mg/kg remained comparable to the control group. During the acute toxicity study in the treatment group levels of AST and ALT were raised while that of ALP was decreased in comparison to control. Results of LFTs for both male and female animals' subacute study are shown in Figures 4A,B, respectively.

RFT (Uric acid, urea, creatinine, and bilirubin) analysis at the end of the subacute study of treated animals at all doses showed comparable results for bilirubin and creatinine in both genders in comparison to the control group. The levels of uric acid were higher in the treatment groups at doses of 100 mg/kg in comparison to other treatment and control groups. The level of urea was less in all treatment groups other than the control group. The RFT profile showed similar results regardless of gender (Figures 4C,D). During the acute toxicity study levels of creatinine and uric acid were higher, while the levels of urea were less in the treatment group as compared to the control group. The level of bilirubin and total protein was comparable in the control and treatment groups (Table 7).

Total lipid profile analysis showed no significant difference in any treatment group at any dose during the subacute and acute toxicity study. Figures 4E,F describe the total lipid profile in male and female animals respectively of all treated and control groups. Results of the lipid profile of the acute toxicity study are shown in Table 7.

3.5 Histopathology analysis

Histopathologic examination of slides revealed no major toxicity concern in the morphology of selected organs. Brain, kidney, liver, and heart tissue showed normal morphological features in all treatment groups in acute and subacute toxicity studies. No signs of necrosis were observed in any tissue in any treatment group. However, the liver showed slight cytoplasmic ballooning and fatty tissue deposit at various doses in the subacute toxicity studies.

3.6 Animal behavior and physical changes

During the acute oral toxicity study, all animals that were treated with 2,000 mg/kg of MEZ remained healthy and showed no clinical signs of any abnormality in observed parameters. Results are shown in Table 8.

4 Discussion

Drugs obtained from natural sources play an imperative role in the field of medicine and in the development of novel agents, as well. The ethnobotanical knowledge could be helpful in serving mankind by conducting new research and exploring novel drug products. In parallel to the discovery of new biologically active compounds and determination of their efficacy, safety profiling of these compounds and plant extracts is of utmost importance. Many regulations are in place for prior pre-clinical studies

TABLE 5 Complete blood count of treated and control group animals during acute oral toxicity study.

Dose	Complete blood count (CBC)														
	WBC	**LYM**	**MID**	**GRA**	**LYM**	**MID**	**GRA**	**RBC**	**HGB**	**MCV**	**HCT**	**MCH**	**MCHC**	**RDWsd**	**RDWcv**
	103/μL	**103/μL**	**103/μL**	**103/μL**	**%**	**%**	**%**	**106/μL**	**g/dL**	**fL**	**%**	**pg**	**g/dL**	**fL**	**%**
2000 mg/kg	26.50 ± 2.27	4.58 ± 0.07	1.53 ± 0.26	0.74 ± 0.1	80.6 ± 0.20	18.9 ± 0.20	12.61 ± 0.24	8.59 ± 0.25	14.5 ± 0.5	52 ± 0.35	45.76 ± 0.29	17.83 ± 0.29	31.93 ± 0.51	27.20 ± 0.36	17.16 ± 0.31
CONTROL	7.19 ± 0.20	6.92 ± 0.09	0.66 ± 0.04	0.23 ± 0.07	90.21 ± 0.16	52.3 ± 0.18	2.32 ± 0.1	8.28 ± 0.49	13.37 ± 0.34	48.9 ± 0.75	41.08 ± 0.25	16.08 ± 0.66	32.80 ± 0.61	28.07 ± 0.21	18.97 ± 0.42
	PLT			MPV		PCT		PDWsd		PDWcv		PLC-R		PLC-C	
	103/μL		fL		%		fL		%		%		103/μL		
2000 mg/kg	375.67 ± 6.51		7.13 ± 0.15		0.68 ± 0.03		31.31 ± 0.14		44.0 ± 0.75		22.3 3 ± 0.58		215 ± 4.58		
CONTROL	594.00 ± 3.61		7.26 ± 0.10		0.41 ± 0.02		8.41 ± 0.31		47.93 ± 0.31		23.90 ± 0.38		140.23 ± 0.21		

10.3389/fphar.2022.1007310

TABLE 6 Complete blood count of treated and control group animals during subacute toxicity study.

Dose (mg/kg)	Male							Female						
WBC's	WBC	LYM	MID	GRA	LYM	MID	GRA	WBC	LYM	MID	GRA	LYM	MID	GRA
	103/µL	103/µL	103/µL	103/µL	%	%	%	103/µL	103/µL	103/µL	103/µL	%	%	%
100	5.43 ± 0.15	3.9 ± 0.01	1.07 ± 0.12	0.623 ± 0.08	72.3 ± 0.20	17.3 ± 0.40	10.33 ± 0.15	5.40 ±	3.90 ±	1.00 ±	0.60 ±	72.10 ±	17.70 ±	10.20 ±
200	5.503 ± 0.06	4.78 ± 0.02	0.58 ± 0.04	0.21 ± 0.1	85.46 ± 0.4	10.8 ± 0.46	3.343 ± 0.06	5.50 ±	4.80 ±	0.60 ±	0.20 ±	85.90 ±	10.70 ±	3.40 ±
400	5.63 ± 0.32	2.55 ± 0.06	2.77 ± 0.08	0.31 ± 0.04	43.36 ± 1.30	50.5 ± 0.50	5.58 ± 0.080	5.90 ±	2.61 ±	2.70 ±	0.31 ±	43.80 ±	50.50 ±	5.65 ±
CONTROL	6.18 ± 0.13	5.34 ± 0.06	0.6 ± 0.02	0.11 ± 0.02	88.16 ± 0.25	48.3 ± 0.1	2.09 ± 0.04	6.33 ±	5.35 ±	0.58 ±	0.11 ±	87.90 ±	9.46 ±	2.13 ±

RBC	RBC	HGB	MCV	HCT	MCH	MCHC	RDWsd	RDWcv	RBC	HGB	MCV	HCT	MCH	MCHC	RDWsd	RDWcv
	106/µL	g/dL	fL	%	pg	g/dL	fL	%	106/µL	g/dL	fL	%	pg	g/dL	fL	%
100	8.74 ± 0.25	14.80 ± 0.52	52.20 ± 0.34	45.60 ± 0.29	17.00 ± 0.28	32.50 ± 0.51	27.50 ± 0.36	17.50 ± 0.31	8.31 ± 0.27	13.90 ± 0.48	51.60 ± 0.30	46.10 ± 0.29	16.50 ± 0.26	31.50 ± 0.48	26.80 ± 0.33	16.90 ± 0.29
200	9.31 ± 0.33	14.10 ± 0.31	47.53 ± 0.27	44.37 ± 0.31	16.07 ± 0.29	32.23 ± 0.47	31.60 ± 0.35	22.23 ± 0.26	9.32 ± 0.23	13.90 ± 0.51	46.90 ± 0.28	44.30 ± 0.27	15.90 ± 0.21	32.90 ± 0.43	31.90 ± 0.29	21.90 ± 0.28
400	6.12 ± 0.29	10.70 ± 0.26	46.40 ± 0.30	33.10 ± 0.28	15.90 ± 0.27	33.90 ± 0.36	31.10 ± 0.33	22.10 ± 0.27	6.86 ± 0.26	11.20 ± 0.47	47.20 ± 0.29	32.40 ± 0.31	16.40 ± 0.29	34.70 ± 0.41	30.40 ± 0.31	21.40 ± 0.26
CONTROL	8.28 ± 0.26	13.37 ± 0.25	48.92 ± 0.21	41.08 ± 0.27	16.08 ± 0.30	32.80 ± 0.34	28.07 ± 0.35	18.97 ± 0.28	8.53 ± 0.26	13.70 ± 0.51	49.00 ± 0.31	41.80 ± 0.26	16.10 ± 0.15	32.90 ± 0.37	28.20 ± 0.28	19.20 ± 0.28

Platelets	PLT	MPV	PCT	PDWsd	PDWcv	PLC-R	PLC-C	PLT	MPV	PCT	PDWsd	PDWcv	PLC-R	PLC-C
	103/µL	fL	%	fL	%	%	103/µL	103/µL	fL	%	fL	%	%	103/µL
100	976.00 ± 165.50	7.00 ± 0.13	0.68 ± 0.31	7.90 ± 1.62	44.80 ± 7.82	22.00 ± 3.32	211.00 ± 20.34	982.00 ± 170.64	7.30 ± 0.42	0.72 ± 0.37	8.20 ± 1.20	43.30 ± 6.39	23.00 ± 2.29	214.00 ± 38.36
200	>1,000 ± 132.76	7.90 ± 0.34	0.80 ± 0.24	9.50 ± 0.96	48.20 ± 8.92	32.00 ± 4.51	324.00 ± 31.24	1,002.00 ± 210.21	7.40 ± 0.69	0.84 ± 0.64	9.32 ± 0.92	47.50 ± 7.23	31.00 ± 3.79	319.00 ± 41.36
400	815.00 ± 210.20	9.10 ± 0.45	0.83 ± 0.34	12.20 ± 0.94	51.20 ± 10.2	35.80 ± 3.98	376.00 ± 52.61	792.00 ± 118.85	9.90 ± 1.20	0.80 ± 0.72	12.50 ± 1.04	50.20 ± 8.02	46.00 ± 8.41	372.00 ± 36.41
CONTROL	597.00 ± 314.24	7.33 ± 0.52	0.43 ± 0.31	8.19 ± 1.26	48.00 ± 7.92	24.00 ± 3.26	340.00 ± 34.2	595.00 ± 206.39	7.15 ± 0.83	0.40 ± 0.36	8.25 ± 1.14	48.20 ± 7.05	23.48 ± 3.92	348.10 ± 45.92

10.3389/fphar.2022.1007310

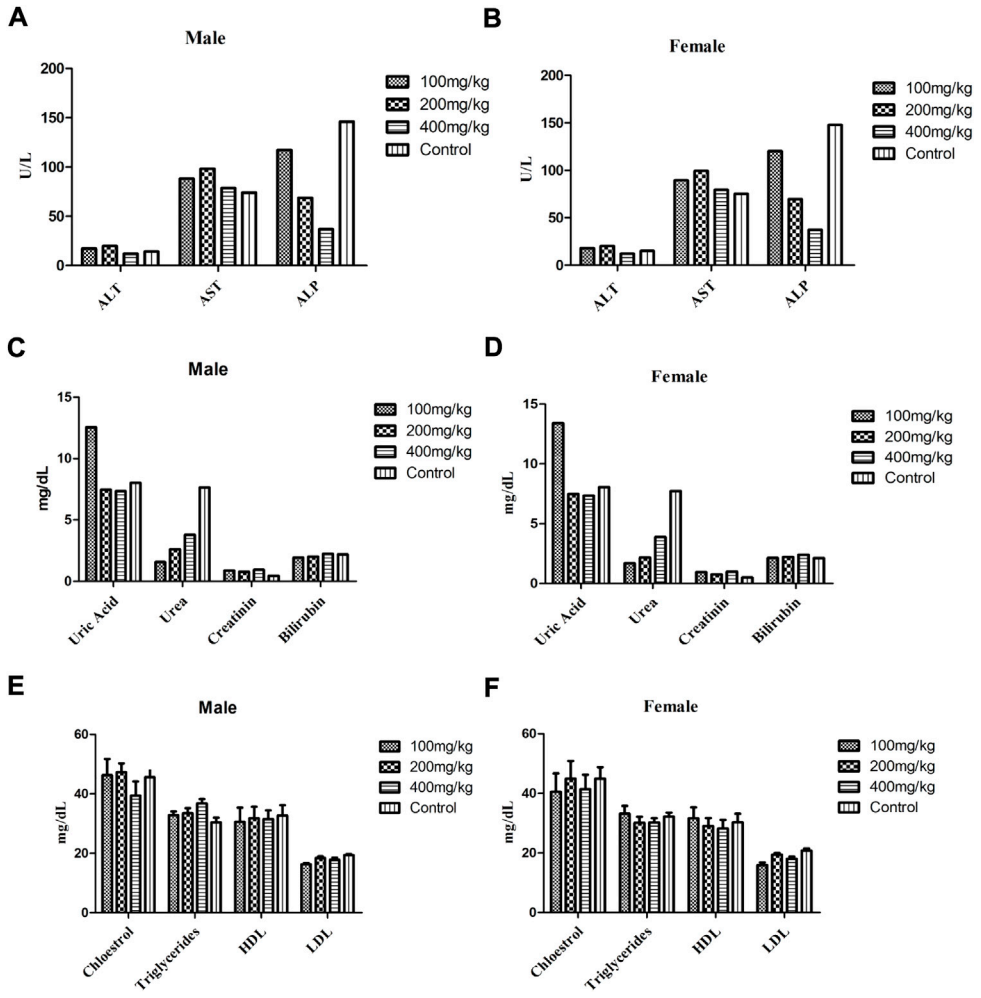

FIGURE 4
Biochemical markers with ±SD in both male and female animals of treatment and control group during subacute study, LFTs **(A,B)**, RFTs **(C,D)** and total lipid profile **(E,F)**, respectively.

regarding the safety of new compounds (Aslam and Ahmed, 2016). To ensure the safety of humans from the lethal effects of the test compounds, a toxicological evaluation of the test compound is carried out which follows standard protocols set forth by regulatory bodies (Anwar et al., 2021b). The protocols strictly emphasize the safety of the human population which regulates the laws regarding the toxicological evaluation of all test compounds prior to their approval. It further comprises the administration of single and repeated doses and requires different evaluations on both genders of animals. This serves as the basis of various guidelines for acute oral and subacute toxicological evaluation in animal models. Oral acute toxicity is conducted with the single maximum dose of 2000 mg/kg in order to explicit any deleterious effects from the test compound while subacute toxicity is carried out by the repeated doses of the test compound for 28 days to study their impact or effect on any abnormality in various predefined parameters (Klaassen and Amdur, 2013; Abubakar et al., 2019).

An acute oral toxicity study is also crucial in determining the LD_{50} of unknown extracts and phytochemicals. This dose determination at the preclinical stage is helpful in determining the safety margin of the test compound. It also provides information about at what doses further pharmacological screening could be carried out (Mohs and Greig, 2017). Therefore, to assess the phytochemical composition, MEZ was subjected to UHPLC–MS analysis. The LC/MS analysis determined the presence of a diverse array of chemicals in MEZ which include alkaloids, phenols and flavonoids, and carbohydrates. Although most of the constituents can be found in the scientific literature many of these have not been reported previously in Z. citrina described in Table 4 (Kohelová et al., 2021; Biswas and Paul, 2022). MEZ showed excellent free

TABLE 7 Biochemical marker analysis after treatment of 2000 mg/kg and control group during acute toxicity study.

Biochemical marker	Unit	2000 mg/kg	Control
ALT	U/L	28.9 ± 2.15	14 ± 1.43
AST	U/L	100.5 ± 3.62	74 ± 2.7
ALP	U/L	119.5 ± 10.57	145 ± 6.69
Uric Acid	mg/dL	12.43 ± 0.19	8.13 ± 0.08
Urea	mg/dL	1.6 ± 0.36	7.7 ± 0.22
Creatinine	mg/dL	0.82 ± 0.05	0.46 ± 0.1
Protein	g/dL	15.4 ± 0.38	13.13 ± 0.20
Bilirubin	mg/dL	1.91 ± 0.22	2.24 ± 0.15
Cholesterol	mg/dL	44.73 ± 4.68	48.23 ± 3.42
Triglycerides	mg/dL	37.92 ± 1.73	35.36 ± 1.56
HDL	mg/dL	27.32 ± 3.72	30.22 ± 2.58
LDL	mg/dL	12.34 ± 0.78	15.94 ± 0.64

TABLE 8 Effect of test doses of MEZ on clinical signs of behavioral and physical parameters in the acute oral toxicity study.

Clinical parameter	Control	2,000 mg/kg
Itching	-	-
Eye discharge	-	-
Nasal discharge	-	+
Skin lesion	-	-
Respiratory distress	-	-
Abnormal movement	-	-
Urination	Normal	Normal
Food intake	Normal	Normal
Water Intake	Normal	Normal

No clinical sign (-), mild clinical sign present (+), Moderate to Severe sign present (++).

radical scavenging and antioxidant activity by the DPPH method (88%). The antioxidant activity of MEZ is possibly due to the presence of diverse antioxidant phytochemicals such as flavonoids, and phenolic compounds. The possible phytochemicals that may be responsible for antioxidant activity present in MEZ are methyl gallate and gingerol. Enzymes that are involved in antioxidant activities are upregulated by methyl gallate. Therefore, methyl gallate protects different tissues, for example, the heart, neurons, adipose tissue, hepatocytes, RBCs, and renal cells against the deleterious effects of toxic compounds. Methyl gallate also possesses anti-HIV properties as well (Ng, T. B. et al., 2018). Gingerol has free radical scavenging activity and therefore inhibits lipid peroxidation and acts as an antioxidant (Masuda, Y. et al., 2004).

Due to the presence of multiple arrays of phytochemicals in MEZ, its acute oral and subacute toxicity study was also conducted to assess implications on various hematological, biochemical and behavioral parameters because any variation in body and organ weights, hematological parameters, and biochemical markers can provide a piece of substantial evidence for the toxicological profiling of plant extracts (Variya et al., 2019). MEZ was subjected to toxicity testing through oral acute toxicity and subacute toxicity in Swiss albino mice. OECD guidelines for both studies were used. With the assumption of the test compound is nontoxic, the limit test was performed (Prabu et al., 2013). This means the test compound has been evaluated at the highest dose of 2000 mg/kg which also identifies a lethal dose (Bhattacharya et al., 2011). Outcomes revealed that no cases of mortality and morbidity were found upon MEZ administration at 2,000 mg/kg dose which declares it nontoxic at 2,000 mg/kg. The subacute toxicity of MEZ was assessed for 28 days at different doses of 100, 200, and 400 mg/kg of body weight. These variations may be induced by the test compound or its metabolites. As the results indicated (Table 4) no noticeable alterations in body weight or organ weights (liver, kidney, pancreas, lungs, heart, stomach, and brain) and no lethal effects were found throughout both the studies. No alterations in the behavioral parameters of animals were found (Table 8). Likewise, neither mortality nor morbidity was seen throughout the test period which was depicted by all animals in both studies did not show signs of weight loss. During toxicity studies, a considerable change in the total body weight of animal or organ weight is attributed to unfavorable physiological (food intake, stress, and diurnal changes) or pathological events (immunomodulation) (Dybing et al., 2002) which show that MEZ is non-toxic. Therefore, the MEZ is found to be safe at tested doses and the oral LD_{50} was considered to be greater than 2000 mg/kg in mice.

Blood dyscrasias or alterations of hematological parameters could also indicate toxicity of the plant extracts. All the blood corpuscles originate from uncommitted pluripotent hematopoietic stem cells within the bone marrow. These stem cells upon appropriate signals are converted into committed pluripotent hematopoietic stem cells. These committed cells then produce colony-forming units (CFUs) and individual blood cells are formed (Broxmeyer, H. E., 1988). Regarding hematological parameters, MEZ at 2,000 mg/kg dose elevated the level of granulocyte count while there was a slight decrease in platelet count. The slight increase in granular leukocytes may be attributed to immunomodulation (Anwar, F. et al., 2021). No considerable change was observed in the subacute study at different doses in WBCs and RBCs. Only the platelet count was found a bit higher at all doses than the control value in both male and female mice. This might be attributed to the immuno-stimulatory behavior, on bone marrow, expressed by MEZ and different phytochemicals such as phenols and flavonoids may be responsible for this (Onuh, S. N., 2012). All other parameters were either normal or with slight variations but well within the normal limits.

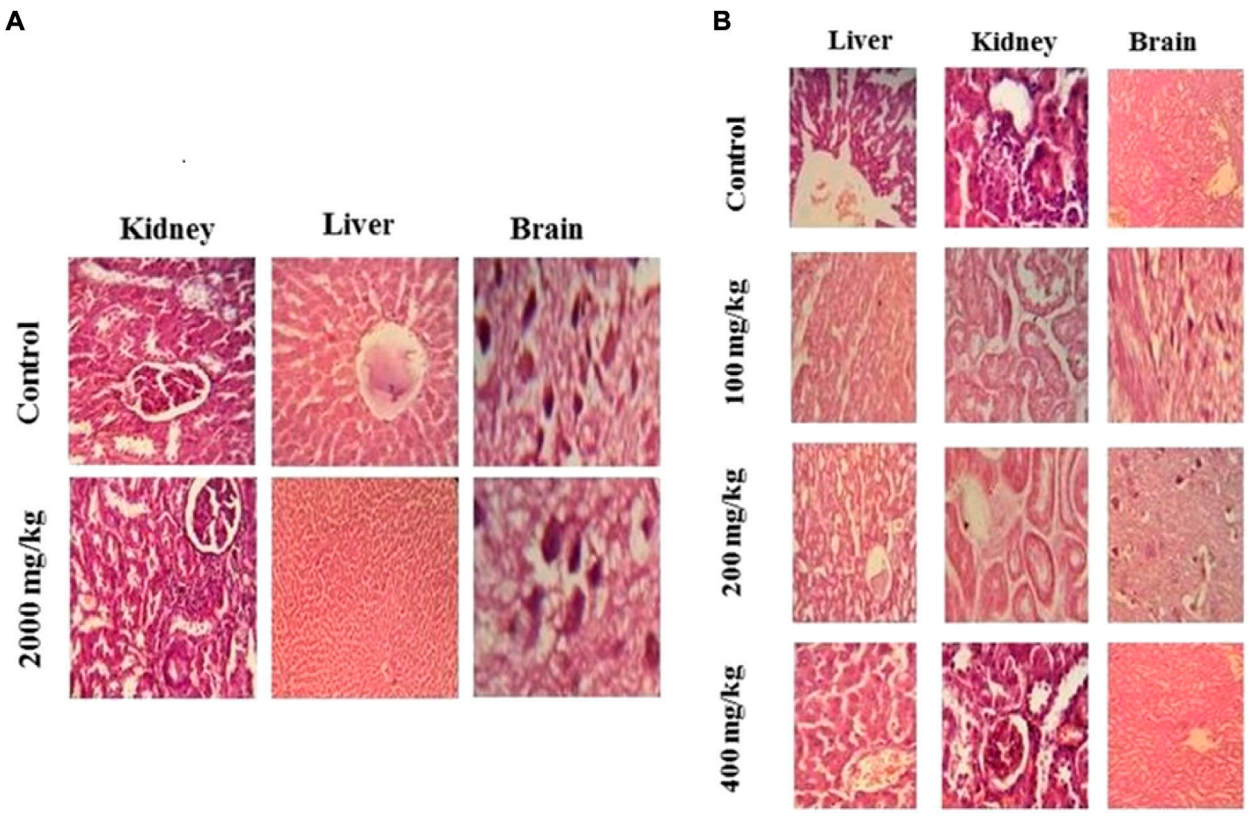

FIGURE 5
H & E stained histopathological analysis of selected organs. Acute oral toxicity study **(A)** and subacute toxicity study **(B)**.

Assessment of liver and kidney functions is considered vital for the toxicity profiling of plant extracts. Therefore, liver function tests (LFTs) and renal function tests (RFTs) may greatly indicate the signs of toxicity induced by plant extracts. The liver is majorly connected with the metabolism while the kidneys are related to the excretion of elimination of drug substances. Findings of acute toxicity studies revealed the elevation in ALT and AST levels at the dose of 2,000 mg/kg with the decline in ALP level. An increase in ALT level indicates hypertrophy, as it is the sole sensitive biomarker for liver functioning while a high AST level is associated with hepatic damage at the cellular level and ALP, symbolizes biliary function (Ozer et al., 2008; Anwar et al., 2021a). Histologic evaluation of liver tissue showed mild ballooning of cytoplasm and mild fatty tissue deposition which correlates to an increase in AST level. The study did not report any unusual change in RFT except a slight increase in uric acid which may be due to interference with uric acid metabolism or decreased urate excretion (Asiwe, J. N., 2022). Histologic evaluation showed normal morphological features of the kidney which excludes any kidney damage. The lipid profile was measured by cholesterol, triglyceride, HDL, and LDL levels. No considerable variation was observed on the lipid profile of MEZ over treated mice with a meager elevation on triglycerides only which shows good tolerability of MEZ over a wide range of doses and depicts its safety. Safety profile of MEZ is well enough to create any harm at the cellular or molecular level. Thus the MEZ emerged safe to be used in the medicinal field for its pharmacological activities.

5 Conclusion

Conclusively the hematological, and biochemical markers, histological study, and other physical observations confirm the safety and tolerability of MEZ with minor and insignificant alterations in a few parameters. A mild increase in uric acid shows interference with uric acid metabolism or excretion. Histologic evaluation liver showed slight oxidative stress on liver tissue which was confirmed by an increased level of AST in mice treated at doses of 2,000 mg/kg in the acute toxicity study. The LD_{50} of MEZ is greater than 2,000 mg/kg. MEZ is safe at tested doses and can be explored for any future pharmacological evaluation in the mice model. Yan et al., 2020.

Data availability statement

The raw data supporting the conclusions of this article will be made available by the authors, without undue reservation.

Ethics statement

Prior approval to conduct all the animal studies, including acute oral toxicity and subacute toxicity, was taken from Institutional Review Board, GC University Faisalabad vide letter number GCU/ERC/2141. Animals were treated ethically according to guidelines, rules, and regulations provided by the National Institute of Health (NIH, United States). Written informed consent was obtained from the owners for the participation of their animals in this study.

Author contributions

Experimental work and data collection: MHR; research supervisors: US and BA; statistical analysis: MR.

Conflict of interest

The authors declare that the research was conducted in the absence of any commercial or financial relationships that could be construed as a potential conflict of interest.

Publisher's note

All claims expressed in this article are solely those of the authors and do not necessarily represent those of their affiliated organizations, or those of the publisher, the editors and the reviewers. Any product that may be evaluated in this article, or claim that may be made by its manufacturer, is not guaranteed or endorsed by the publisher.

Supplementary material

The Supplementary Material for this article can be found online at: https://www.frontiersin.org/articles/10.3389/fphar.2022.1007310/full#supplementary-material

References

Abubakar, A., Nazifi, A., Hassan, F., Duke, K., and Edoh, T. (2019). Safety assessment of chlorophytum alismifolium tuber extract (liliaceae): Acute and sub-acute toxicity studies in wistar rats. *J. Acute Dis.* 8 (1), 21. doi:10.4103/2221-6189.250374

Al Mamun, A. (2022). Amaryllidaceae alkaloids of genus Narcissus and their biological activity. In *Pharmacognosy and nutraceuticals, faculty of pharmacy in hradec králové. Date of defense*, 22–042022.

Al-Nahain, A., Jahan, R., and Rahmatullahofficinale, M. Zingiber (2014). *A potential plant against rheumatoid arthritis*. London: Hindawi.

Anwar, F., Saleem, U., Ahmad, B., Ismail, T., Mirza, M. U., Ahmad, S., et al. (2021a). Acute oral, subacute, and developmental toxicity profiling of naphthalene 2-yl, 2-chloro, 5-nitrobenzoate: Assessment based on stress response, toxicity, and adverse outcome pathways. *Front. Pharmacol.* 12, 810704. doi:10.3389/fphar.2021.810704

Anwar, F., Saleem, U., Rehman, A. U., Ahmad, B., Froeyen, M., Mirza, M. U., et al. (2021b). Toxicity evaluation of the naphthalen-2-yl 3, 5-dinitrobenzoate: A drug candidate for alzheimer disease. *Front. Pharmacol.* 12, 607026. doi:10.3389/fphar.2021.607026

Arome, D., and Chinedu, E. (2013). The importance of toxicity testing. *J. Pharm. Biosci.* 4, 146–148.

Asiwe, J. N., Kolawole, T. A., Anachuna, K. K., Ebuwa, E. I., Nwogueze, B. C., Eruotor, H., et al. (2022). Cabbage juice protect against Lead-induced liver and kidney damage in male Wistar rat. *Biomarkers.* 27 (2), 151–158. doi:10.1080/1354750X.2021.2022210

Aslam, M. S., and Ahmad, M. S. (2016). Worldwide importance of medicinal plants: Current and historical perspectives. *Recent Adv. Med.* 2, 909.

Bhattacharya, S., Zhang, Q., Carmichael, P. L., Boekelheide, K., and Andersen, M. E. (2011). Toxicity testing in the 21 century: Defining new risk assessment approaches based on perturbation of intracellular toxicity pathways. *PloS One* 6 (6), e20887. doi:10.1371/journal.pone.0020887

Biswas, I., and Paul, D. (2022). *Phytochemical and biological aspects of Zephyranthes citrina baker: A mini-review*.

Broxmeyer, H. E., Williams, D. E., and Gentile, P. S. (1988). The production of myeloid blood cells and their regulation during health and disease. *Crit. Rev. Oncol. Hematol.* 8 (3), 173–226. doi:10.1016/s1040-8428(88)80016-7

Chandrasekaran, M., and Venkatesalu, V. (2004). Antibacterial and antifungal activity of Syzygium jambolanum seeds. *J. Ethnopharmacol.* 91 (1), 105–108. doi:10.1016/j.jep.2003.12.012

Chen, H., and Wang, Q. (2021). Regulatory mechanisms of lipid biosynthesis in microalgae. *Biol. Rev. Camb. Philos. Soc.* 96 (5), 2373–2391. doi:10.1111/brv.12759

Christenhusz, M. J. M., and Byng, J. W. (2016). *number known plants species world its Annu. increase. Phytotaxa* 261 (201), 10–11646.

Dybing, E., Doe, J., Groten, J., Kleiner, J., O'Brien, J., Renwick, A. G., et al. (2002). Hazard characterisation of chemicals in food and diet. Dose response, mechanisms and extrapolation issues. *Food Chem. Toxicol.* 40 (2-3), 237–282. doi:10.1016/s0278-6915(01)00115-6

Farnsworth, N. R. (1966). Biological and phytochemical screening of plants. *J. Pharm. Sci.* 55 (3), 225–276. doi:10.1002/jps.2600550302

Hoyler, E., Martinez, R., Mehta, K., Nisonoff, H., and Boyd, D. (2018). Beyond medical pluralism: Characterising health-care delivery of biomedicine and traditional medicine in rural Guatemala. *Glob. Public Health* 13 (4), 503–517. doi:10.1080/17441692.2016.1207197

Jamshidi-Kia, F., Lorigooini, Z., and Amini-Khoei, H. (2018). Medicinal plants: Past history and future perspective. *J. Herbmed Pharmacol.* 7 (1), doi:10.15171/jhp.2018.01

Jin, K., Yan, Y., Chen, M., Wang, J., Pan, X., Liu, X., et al. (2022). Multimodal deep learning with feature level fusion for identification of choroidal neovascularization activity in age-related macular degeneration. *Acta Ophthalmol.* 100 (2), e512-e520. doi:10.1111/aos.14928

Jin, Z., and Yao, G. (2019). Amaryllidaceae and sceletium alkaloids. *Nat. Prod. Rep.* 36(10), 1462–1488. doi:10.1039/c8np00055g

Klaassen, C. D., and Amdur, M. O. (2013). *Casarett and doull's toxicology: The basic science of poisons*. New York, NY: McGraw-Hill.

Kohelová, E., Maříková, J., Korábečný, J., Hulcová, D., Kučera, T., Jun, D., et al. (2021). Alkaloids of Zephyranthes citrina (Amaryllidaceae) and their implication to Alzheimer's disease: Isolation, structural elucidation and biological activity. *Bioorg. Chem.* 107, 104567, doi:10.1016/j.bioorg.2020.104567

Kundu, P., Debnath, S. L., and Sadhu, S. K. (2022). Exploration of pharmacological and toxicological properties of aerial parts of blumea lacera, a common weed in Bangladesh. *Clin. Complementary Med. Pharmacol.* 2 (3), 100038, doi:10.1016/j.ccmp.2022.100038

Li, Z., Teng, M., Jiang, Y., Zhang, L., Luo, X., Liao, Y., et al. (2022). YTHDF1 negatively regulates Treponema pallidum-induced inflammation in THP-1 macrophages by promoting SOCS3 translation in an m6A-dependent manner. *Front. Immunol.* 13, doi:10.3389/fimmu.2022.857727

Liu, C., Wang, Y., Li, L., He, D., Chi, J., Li, Q., et al. (2022). Engineered extracellular vesicles and their mimetics for cancer immunotherapy. *J. Control. Release* 349, 679–698. doi:10.1016/j.jconrel.2022.05.062

López, S., Bastida, J., Viladomat, F., and Codina, C. (2002). Acetylcholinesterase inhibitory activity of some Amaryllidaceae alkaloids and Narcissus extracts. *Life Sci.* 71 (21), 2521–2529. doi:10.1016/s0024-3205(02)02034-9

Majid, M., Farhan, A., Asad, M. I., Khan, M. R., Hassan, S. S. U., Haq, I. U., et al. (2022). An extensive pharmacological evaluation of new anti-cancer triterpenoid (nummularic acid) from Ipomoea batatas through *in vitro*, in silico, and *in vivo* studies. *Molecules* 27 (8), 2474. doi:10.3390/molecules27082474

Masuda, Y., Kikuzaki, H., Hisamoto, M., and Nakatani, N. (2004). Antioxidant properties of gingerol related compounds from ginger. *Biofactors* 21 (1-4), 293–296. doi:10.1002/biof.552210157

Mensah, M. L., Komlaga, G., Forkuo, A. D., Firempong, C., Anning, A. K., and Dickson, R. A. (2019). Toxicity and safety implications of herbal medicines used in Africa. *Herb. Med.* 63, 1992–0849.

Mishra, K., Ojha, H., and Chaudhury, N. K. (2012). Estimation of antiradical properties of antioxidants using DPPH assay: A critical review and results. *Food Chem.* 130 (4), 1036–1043. doi:10.1016/j.foodchem.2011.07.127

Mohs, R. C., and Greig, N. H. (2017). Drug discovery and development: Role of basic biological research. *Alzheimers Dement.* 3 (4), 651–657. doi:10.1016/j.trci.2017.10.005

Muhammad, I., Luo, W., Shoaib, R. M., Li, G. L., ul Hassan, S. S., Yang, Z. H., et al. (2021a). Guaiane-type sesquiterpenoids from Cinnamomum migao HW Li: And their anti-inflammatory activities. *Phytochemistry* 190, 112850. doi:10.1016/j.phytochem.2021.112850

Muhammad, I., ul Hassan, S. S., Cheung, S., Li, X., Wang, R., Zhang, W. D., et al. (2021b). Phytochemical study of Ligularia subspicata and valuation of its anti-inflammatory activity. *Fitoterapia* 148, 104800. doi:10.1016/j.fitote.2020.104800

Ng, T. B., Wong, J. H., Tam, C., Liu, F., Cheung, C. F., Ng, C. C., et al. (2018). "Methyl gallate as an antioxidant and anti-HIV agent," in *HIV/AIDS* (Academic Press), 161–168.

Onuh, S. N., Ukaejiofo, E. O., Achukwu, P. U., Ufelle, S. A., Okwuosa, C. N., and Chukwuka, C. J. (2012). Haemopoietic activity and effect of crude fruit extract of Phoenix dactylifera on peripheral blood parameters. *Int. J. Biol. Med. Res.* 3 (2), 1720–1723.

Ozer, J., Ratner, M., Shaw, M., Bailey, W., and Schomaker, S. (2008). The current state of serum biomarkers of hepatotoxicity. *Toxicology* 245 (3), 194–205. doi:10.1016/j.tox.2007.11.021

Pour, B. M., Latha, L. Y., and Sasidharan, S. (2011). Cytotoxicity and oral acute toxicity studies of Lantana camara leaf extract. *Molecules* 16 (5), 3663–3674. doi:10.3390/molecules16053663

Prabu, P. C., Panchapakesan, S., and Raj, C. D. (2013). Acute and sub-acute oral toxicity assessment of the hydroalcoholic extract of withania somnifera roots in wistar rats. *Phytother. Res.* 27 (8), 1169–1178. doi:10.1002/ptr.4854

Rahimi, R., Mozaffari, S., and Abdollahi, M. (2009). On the use of herbal medicines in management of inflammatory bowel diseases: A systematic review of animal and human studies. *Dig. Dis. Sci.* 54 (3), 471–480. doi:10.1007/s10620-008-0368-x

Rajeh, M. A. B., Kwan, Y. P., Zakaria, Z., Latha, L. Y., Jothy, S. L., and Sasidharan, S. (2012). Acute toxicity impacts of Euphorbia hirta L extract on behavior, organs body weight index and histopathology of organs of the mice and *Artemia salina*. *Pharmacogn. Res.* 4 (3), 170–177. doi:10.4103/0974-8490.99085

Saeed, N., Khan, M. R., and Shabbir, M. (2012). Antioxidant activity, total phenolic and total flavonoid contents of whole plant extracts Torilis leptophylla L. *BMC Complement. Altern. Med.* 12 (1), 221. doi:10.1186/1472-6882-12-221

Saleem, H., Htar, T. T., Naidu, R., Nawawi, N. S., Ahmad, I., Ashraf, M., et al. (2019a). Biological, chemical and toxicological perspectives on aerial and roots of *Filago germanica* (L.) huds: Functional approaches for novel phyto-pharmaceuticals. *Food Chem. Toxicol.* 123, 363–373. doi:10.1016/j.fct.2018.11.016

Saleem, H., Zengin, G., Locatelli, M., Ahmad, I., Khaliq, S., Mahomoodally, M. F., et al. (2019b). Pharmacological, phytochemical and *in-vivo* toxicological perspectives of a xero-halophyte medicinal plant: Zaleya pentandra (L.) Jeffrey. *Food Chem. Toxicol.* 131, 110535. doi:10.1016/j.fct.2019.05.043

Saleem, U., Raza, Z., Anwar, F., Chaudary, Z., and Ahmad, B. Systems pharmacology based approach to investigate the *in-vivo* therapeutic efficacy of Albizia lebbeck (L.) in experimental model of Parkinson's disease. *BMC Complement. Altern. Med.* 2019c Dec 5;19(1):352. doi:10.1186/s12906-019-2772-5

Sandhya, B., Thomas, S., Isabel, W., and Shenbagarathai, R. (2006). Ethnomedicinal plants used by the Valaiyan community of Piranmalai hills (reserved forest), Tamilnadu, India.-a pilot study. *Afr. J. Tradit. Complement. Altern. Med.* 3 (1), 101–114. doi:10.4314/ajtcam.v3i1.31145

Terfassi, S., Dauvergne, X., Cérantola, S., Lemoine, C., Bensouici, C., Fadila, B., et al. (2021). First report on phytochemical investigation, antioxidant and antidiabetic activities of Helianthemum getulum. *Nat. Prod. Res.*, 36, 2806–2813. doi:10.1080/14786419.2021.1928664

Variya, B. C., Bakrania, A. K., Madan, P., and Patel, S. S. (2019). Acute and 28-days repeated dose sub-acute toxicity study of gallic acid in albino mice. *Regul. Toxicol. Pharmacol.* 101, 71–78. doi:10.1016/j.yrtph.2018.11.010

Yan, J., Yao, Y., Yan, S., Gao, R., Lu, W., and He, W. (2020). Chiral protein supraparticles for tumor suppression and synergistic immunotherapy: An enabling strategy for bioactive supramolecular chirality construction. *Nano Lett.* 20 (8), 5844–5852. doi:10.1021/acs.nanolett.0c01757

Yang, L., Wu, X., Luo, M., Shi, T., Gong, F., Yan, L., et al. (2022). Na^+/Ca^{2+} induced the migration of soy hull polysaccharides in the mucus layer *in vitro*. *Int. J. Biol. Macromol.* 199, 331–340. doi:10.1016/j.ijbiomac.2022.01.016

Zhuo, Z., Wan, Y., Guan, D., Ni, S., Wang, L., Zhang, Z., et al. (2020). A loop-based and AGO-Incorporated virtual screening model targeting AGO-Mediated miRNA–mRNA interactions for drug discovery to rescue bone phenotype in genetically modified Mice. *Adv. Sci.* 7 (13), 1903451. doi:10.1002/advs.201903451

frontiers | Frontiers in Pharmacology

TYPE Original Research
PUBLISHED 26 September 2022
DOI 10.3389/fphar.2022.981996

Check for updates

OPEN ACCESS

EDITED BY
Fawad Ali Shah,
Riphah International University, Pakistan

REVIEWED BY
Muhammad Abbas,
Riphah International University, Pakistan
Jing Zhou,
Nanjing University of Chinese Medicine, China

*CORRESPONDENCE
Wenzhou Zhang,
zlyyzhangwenzhou0551@zzu.edu.cn,
hnzzzwzx@sina.com
Ziqiao Yuan,
figaroyzq@163.com,
figaroyzq@zzu.edu.cn

†These authors have contributed equally to this work

SPECIALTY SECTION
This article was submitted to Predictive Toxicology, a section of the journal Frontiers in Pharmacology

RECEIVED 30 June 2022
ACCEPTED 23 August 2022
PUBLISHED 26 September 2022

CITATION
Qin T, Hasnat M, Zhou Y, Yuan Z and Zhang W (2022), Macrophage malfunction in Triptolide-induced indirect hepatotoxicity. *Front. Pharmacol.* 13:981996. doi: 10.3389/fphar.2022.981996

COPYRIGHT
© 2022 Qin, Hasnat, Zhou, Yuan and Zhang. This is an open-access article distributed under the terms of the Creative Commons Attribution License (CC BY). The use, distribution or reproduction in other forums is permitted, provided the original author(s) and the copyright owner(s) are credited and that the original publication in this journal is cited, in accordance with accepted academic practice. No use, distribution or reproduction is permitted which does not comply with these terms.

Macrophage malfunction in Triptolide-induced indirect hepatotoxicity

Tingting Qin[1,2,3,4†], Muhammad Hasnat[5†], Yang Zhou[6†], Ziqiao Yuan[1,2*] and Wenzhou Zhang[1,3,4*]

[1]Department of Pharmacy, The Affiliated Cancer Hospital of Zhengzhou University and Henan Cancer Hospital, School of Pharmaceutical Sciences, Zhengzhou University, Zhengzhou, China, [2]Key Laboratory of Advanced Drug Preparation Technologies, Ministry of Education, School of Pharmaceutical Sciences, Zhengzhou University, Zhengzhou, China, [3]Henan Engineering Research Center for Tumor Precision Medicine and Comprehensive Evaluation, The Affiliated Cancer Hospital of Zhengzhou University and Henan Cancer Hospital, Zhengzhou University, Zhengzhou, China, [4]Henan Provincial Key Laboratory of Anticancer Drug Research, The Affiliated Cancer Hospital of Zhengzhou University and Henan Cancer Hospital, Zhengzhou University, Zhengzhou, China, [5]Institute of Pharmaceutical Sciences, University of Veterinary and Animal Sciences, Lahore, Pakistan, [6]Children's Hospital Affiliated to Zhengzhou University, Henan Children's Hospital, Zhengzhou Children's Hospital, Zhengzhou University, Zhengzhou, China

Background and Objective: Indirect hepatotoxicity is a new type of drug-induced hepatotoxicity in which the character of a drug that may induce its occurrence and the underlying mechanism remains elusive. Previously, we proved that Triptolide (TP) induced indirect hepatotoxicity upon LPS stimulation resulting from the deficiency of cytoprotective protein of hepatocyte. However, whether immune cells participated in TP-induced indirect hepatotoxicity and the way immune cells change the liver hypersensitivity to LPS still need to be deeply investigated. In this study, we tried to explore whether and how macrophages are involved in TP-induced indirect hepatotoxicity.

Method: Firstly, TP (500 μg/kg) and LPS (0.1 mg/kg) were administrated into female C57BL/6 mice as previously reported. Serum biochemical indicators, morphological changes, hepatic macrophage markers, as well as macrophage M1/M2 markers were detected. Secondly, macrophage scavenger clodronate liposomes were injected to prove whether macrophages participated in TP-induced indirect hepatotoxicity. Also, the ability of macrophages to secrete inflammatory factors and macrophage phagocytosis were detected. Lastly, reverse docking was used to find the target of TP on macrophage and the possible target was verified *in vivo* and in RAW264.7 cells.

Results: TP pretreatment increased the liver hypersensitization to LPS accompanied by the recruitment of macrophages to the liver and promoted the transformation of macrophages to M1 type. Depletion of hepatic macrophages almost completely alleviated the liver injury induced by TP/LPS. TP pretreatment increased the secretion of pro-inflammatory factors and weakened the phagocytic function of macrophages upon LPS exposure. Reverse docking results revealed that MerTK might be the real target of TP.

Conclusion: TP disrupts inflammatory cytokines profile and phagocytic function of hepatic macrophages, resulting in the production of massive inflammatory factors and the accumulation of endotoxin in the liver,

ultimately leading to the indirect hepatotoxicity of TP. MerTK might be the target of TP on the macrophage, while the binding of TP to MerTK should be investigated *in vivo* and *in vitro*.

KEYWORDS

Triptolide, LPS, MERTK, hepatic macrophage, hypersensitization

Introduction

Typically, drug-induced liver injury was classified into direct or idiosyncratic. Direct hepatotoxicity is caused by the intrinsic toxicity of the agents (Acetaminophen, Aspirin, and Chemotherapy agents) (Chen et al., 2019). The agents (Amoxicillin–clavulanate, Isoniazid, Polygonum multiflorum) that may cause idiosyncratic hepatotoxicity usually have low cytotoxicity to liver cells, and the occurrence of idiosyncratic hepatotoxicity results from patients themselves, such as HLA mutation (Hoofnagle and Bjornsson, 2019). Recently, a new type of drug-induced liver injury, indirect hepatotoxicity, was proposed (Hoofnagle and Bjornsson, 2019). In contrast to direct and idiosyncratic hepatotoxicity, indirect hepatotoxicity was caused by the action of agents on the liver or immune system and is tightly related to the pharmacological effects of the agents. Indirect toxicity is gradually recognized by researchers while its mechanisms have not been elucidated.

Triptolide (TP), the main compound derived from the traditional Chinese medicine *Tripterygium wilfordii Hook F.*, possesses strong bioactivities for the treatment of tumor and autoimmune diseases, especially rheumatoid arthritis, systemic lupus erythematosus, and nephrotic syndrome (Li et al., 2014). As the major active and toxic compound of Tripterygium wilfordii multiglycoside in clinical practice, most of the published research articles focused on the direct hepatotoxicity induced by the high dose of TP (Wang et al., 2014; Hasnat et al., 2019a; Yuan et al., 2019a; Hasnat et al., 2019b). Previously, we proposed a new perspective of TP-associated hepatotoxicity, liver hypersensitization upon Lipopolysaccharide (LPS) treatment (Yuan et al., 2019b). Additionally, we proved that TP pretreatment increased the sensitivity of hepatocytes to TNF-α stimulation, which was mainly released by macrophages upon LPS treatment. A mechanistic study uncovered that the inhibition of c-FLIP (cellular FLICE-like inhibitory protein) by TP resulted in hepatocytes' hypersensitization upon TNF-α stimulation (Yuan et al., 2020). These results implied the crosstalk between immune cells, especially macrophages which are the main source of TNF-α, and hepatocytes in TP/LPS-induced liver injury. Thus, identification of the functional changes in immune cells and exploring the key mechanisms will be of great significance to elucidate the pathogenesis of TP-induced indirect hepatotoxicity.

LPS, a component of the outer cell wall of gram-negative bacteria, is the ligand of TLR4 on the surface of macrophages. The binding of LPS on TLR4 activates TRIF and Myd88 pathway, ultimately leading to the production of pro-inflammatory factors, such as IL-1, IL-6, TNF-α, IL-8, and others (Skirecki and Cavaillon, 2019). Liver macrophages, which function as scavenging bacteria and microbial products along with initiating or suppressing the immune response, can be classified into two populations and play different roles in liver immune homeostasis (Krenkel and Tacke, 2017). $CD11b^{+}$ macrophages derived from infiltrating monocytes of blood functioned as the production of massive inflammatory factors. While liver-resident macrophages expressed low $CD11b^{low}$ (also known as Kupffer cells), maintaining homeostasis of the liver via phagocytosis, cleaning of cellular debris, regulation of cholesterol homeostasis, and mediation of anti-microbial defense (Ju and Tacke, 2016; Wen et al., 2021). Macrophage malfunction has been proved to participate in NAFLD, liver fibrosis, hepatocellular carcinoma, and acetaminophen-induced acute hepatotoxicity. Also, modulation of macrophage polarization/reprogramming, inhibition of Kupffer cell activation, and dampening of monocyte recruitment serve as the principal patterns for treating macrophage-related liver disease (Tacke, 2017; van der Heide et al., 2019). Targeting macrophage ASK1 (ASK1 inhibitor Selonsertib), CCR5 (CCR5 antagonist Maraviroc), CCR2 (CCR2/5 due-inhibitor Cenicriviroc), and CSF1 (CSF1R antibody and inhibitor) have been proved to have a good therapeutic effect on acute liver failure. NASH, liver fibrosis, HIV, and liver cancer (Marra and Tacke, 2014; Stutchfield et al., 2015; Lefebvre et al., 2016; Tacke, 2017; Challa et al., 2019). Recently, a new macrophage efferocytosis receptor c-mer tyrosine kinase (MerTK) was proposed to be an ideal target for liver disease treatment. The activation of TLR receptors could initial the activation of TRAF3 and TRAF6, which in turn activate NF-κB and IRF3, leading to the production of inflammatory factors and type I interferons. Also, interferon signaling further stimulates the production of interferon via STAT1 and upregulates the TAM receptors (Tyro3/Axl/MerTK) (O'Neill, 2007). It has been proved that macrophage MerTK activated HSCs and induced liver fibrosis via ERK-TGFβ1 pathway (Cai et al., 2020). Macrophage MerTK also relieved liver inflammation in acute liver failure (Cai et al., 2016; Cai et al., 2018). Additionally, MerTK inhibitor augmented the anti-PD-1 therapy in cancer cells (Holtzhausen et al., 2019; Kasikara et al., 2019). Mechanistic studies revealed

that the bio-activities of MerTK depended on its effect on the secretion of inflammatory factors and phagocytic functions of macrophages (Rothlin et al., 2007; Graham et al., 2014; Vago et al., 2021).

Considering the crucial role of TNF-α in TP-induced indirect hepatotoxicity and inflammatory secretions by hepatic macrophages, we proposed that the function of hepatic macrophages might be disrupted by TP, leading to the massive production of TNF-α and abnormal accumulation of LPS in the liver. The abundant TNF-α coordination along with the deficiency of the pro-survival signal induced by TP as reported in our previous research led to liver injury accompanied by hepatocyte apoptosis and necrosis (Yuan et al., 2020). In this study, the abundance of hepatic macrophages, phagocytosis, and inflammatory secretions by hepatic macrophages were detected to testify the functional changes in macrophages after TP/LPS treatment. Moreover, the clodronate liposomes were injected to deplete hepatic macrophages and to prove whether hepatic macrophages participated in TP-induced indirect hepatotoxicity. Additionally, reverse docking was used to predict the possible target of TP in macrophages and MerTK expression was verified *in vivo* and *in vitro*.

Materials and methods

Material

TP (CAS number 38748-32-2, purity >98%) was purchased from MedChemExpress (Shanghai, China). LPS (L2755) was purchased from Sigma-Aldrich (St. Louis, MO, United States). Trizol reagent used for RNA isolation, Reverse Transcription Kit used for reverse transcription of RNA to cDNA, and SYBR Green Master Mix used for qPCR, were obtained from Vazyme Biotech Co., Ltd. (Nanjing, Jiangsu, China). Mouse recombinant Growth arrest-specific protein 6 (GAS6, 8310-GS) was purchased from R&D Systems, Inc. (Minneapolis, MN, United States).

Primary antibodies against p-MerTK (ab14921) and cleaved caspase-3 (9661) were purchased from Abcam (Cambridge, United Kingdom) and Cell Signaling Technology (Boston, MA, United States) respectively. Antibodies against GAPDH (10494-1-AP), Myeloperoxidase (MPO, 22225-1-AP), CD11b (21851-1-AP), and F4/80 (28463-1-AP) were purchased from Proteintech (Chicago, IL, United States). HRP Conjugated AffiniPure Goat Anti-rabbit (BA1054) and HRP Conjugated AffiniPure Goat Anti-mouse antibodies were purchased from Boster Biological Technology Co.Ltd. (Wuhan, Hubei, China). ELISA kits of IL-1β (KE10003), TNF-α (KE10002), and IL-6 (KE10007) were purchased from Proteintech. The endotoxin detection kit (EC80545S) was purchased from Bioendo Technology Co., Ltd. (Xiamen, Fujian, China). Clodronate liposomes and its negative control were purchased from Yeasen Biotechnology Co., Ltd. (Shanghai, China).

Animal and pharmacological treatments

Animal treatment was described in our previous research (Yuan et al., 2019b; Yuan et al., 2020; Zhang et al., 2022). C57BL/6 mice used in this experiment were purchased from SPF (Beijing) Biotechnology Co., Ltd. Briefly, TP (500 μg/kg, i.g.) was administered daily through gavage for 7 days followed by a single dose of LPS (0.1 mg/kg, i.p.) 2 h after the last dose of TP into female C56BL/6 mice (6–8 weeks old). The phagocytic function and level of hepatic macrophages were determined 6 h after LPS injection. Serum inflammatory factors were detected 1 h, 3 h, and 6 h after LPS injection, respectively.

To prove the involvement of hepatic macrophages in TP/LPS induced hepatotoxicity, Clodronate liposomes (200 μL/mouse, i.p.) and its negative control were injected 48 h before LPS administration to deplete macrophages (Zeng et al., 2020). Mice were sacrificed 6 h after LPS treatment and blood, as well as liver samples, were collected for further examination. All experimental procedures involving mice were complied with the ARRIVE guidelines and were permitted by the Animal Ethics Committee, Zhengzhou University.

Blood biochemistry analysis

After collection, blood samples were stored at room temperature for 1 h and then centrifuge for 10 min at 3500 rpm/min. Serum was collected for blood biochemistry analysis. Serum alanine aminotransferase (ALT), aspartate aminotransferase (AST), albumin (ALB), alkaline phosphatase (ALP), and total protein were detected using kits from Weiteman Biotech (Nanjing, Jiangsu, China). Serum total bile acid (TBA) was determined using the kit from Jiancheng Bioengineering Institute (Nanjing, Jiangsu, China). All kits were used according to the manufacturer's instructions.

Histopathological examination

Liver sections were collected and fixed with 10% formaldehyde for 24 h. After embedding in paraffin and slicing with a tissue sectioner, liver sections were used for hematoxylin and eosin (H&E) staining to examine the morphology. Additionally, immunohistochemistry (IHC) staining of MPO, F4/80, CD11b, and cleaved caspase-3 were used to determine inflammatory infiltration, macrophage number, and apoptosis rate of hepatocytes respectively. All the slices were observed with ANNORAMIC MIDI II (3DHISTECH Ltd., Budapest, Hungary).

TABLE 1 The primer sequences used for qPCR assay in mice.

Gene	Forward primer (5′-3′)	Reverse primer (5′-3′)
Gapdh	CATCACTGCCACCCAGAAGACTG	ATGCCAGTGAGCTTCCCGTTCAG
Adgre1	CGTGTTGTTGGTGGCACTGTGA	CCACATCAGTGTTCCAGGAGAC
Itgam	TACTTCGGGCAGTCTCTGAGTG	ATGGTTGCCTCCAGTCTCAGCA
Cd68	GGCGGTGGAATACAATGTGTCC	AGCAGGTCAAGGTGAACAGCTG
Il12b	TTGAACTGGCGTTGGAAGCACG	CCACCTGTGAGTTCTTCAAAGGC
Nox2	GAGACAGGGAAGTCTGAAGCAC	CCAGCAGTAGTTGCTCCTCTTC
Il1b	TGGACCTTCCAGGATGAGGACA	GTTCATCTCGGAGCCTGTAGTG
Mrc1	GTTCACCTGGAGTGATGGTTCTC	AGGACATGCCAGGGTCACCTTT
Arginase1	CATTGGCTTGCGAGACGTAGAC	GCTGAAGGTCTCTTCCATCACC
Retnla	CAAGGAACTTCTTGCCAATCCAG	CCAAGATCCACAGGCAAAGCCA
SOCS1	AGTCGCCAACGGAACTGCTTCT	GTAGTGCTCCAGCAGCTCGAAA
SOCS3	GGACCAAGAACCTACGCATCCA	CACCAGCTTGAGTACACAGTCG

Cell culture

The mouse monocyte/macrophage cell line RAW264.7 was purchased from China Cell Culture Center (Shanghai, China). The cell was cultured in DMEM with 10% FBS at 37°C in a humidified 5% CO_2 atmosphere. Cells were seeded into the 6-well plate to determine the effect of TP (20 nmol/L) and LPS (50 ng/ml) on p-MerTK expression. When the cells reached 40%–50% confluence, TP was added to the medium. Twenty-4 hours after TP treatment, the cell pellet was collected for further detection. To investigate the effect of TP on *SOCS1* (Suppressor Of Cytokine Signaling 1) and *SOCS3* (Suppressor Of Cytokine Signaling 3) expression after Gas6, cells were seeded into the 6-well plate. When the cells reached 80%–90% confluence, TP (20 nmol/L) was added 1 h before Gas6 (50 nmol/L). 30 min, 60 min, 90 min, and 120 min after Gas6 exposure, cells were collected for further detection.

RNA extraction and qPCR

A total of 50 mg liver tissue was separated from liver samples stored at −80°C and RNA was extracted with TRIzol reagent. After the quantification with Nanodrop 3000 (Thermo Fisher Scientific, Waltham, MA, United States), 1 μg of total RNA of each sample was reverse transcribed to cDNA with Reverse Transcription Kit. The relative mRNA expression of macrophage markers and inflammatory factors were determined by QuantStudio six Flex (Thermo Fisher Scientific) with SYBR Green Master Mix and normalized with *Gapdh*. The primers used in this paper were listed in Table 1.

Western blot analysis

A total of 100 mg liver protein was used for the protein extraction with RIPA Lysis Buffer (Solarbio Science & Technology Co., Ltd., Beijing, China). After quantification with BCA kit (Solarbio Science & Technology Co.,Ltd.), the protein was mixed with a 4×loading buffer containing protease and phosphatase inhibitor cocktail (P1049, Beyotime Biotechnology, Shanghai China). The same amount of protein was added to each well for SDS-PAGE with gels ranging from 10% to 12%. The protein was then transferred onto nitrocellulose filter membrane (Pall Corporation, NY, United States). The membranes were then incubated with secondary antibodies for 1 h and visualized at Tanon-5200 Chemiluminescent Imaging System (Tanno, Shanghai, China) using an ECL detection kit (Millipore, Danvers, MA, United States). The relative protein expression was normalized with GAPDH and analyzed with ImageJ 1.52a (Bethesda, MD, United States).

Molecular docking

Autodock Vina 1.1.2 (The Scripps Research Institute, La Jolla, CA United States) was used to analyze the binding of TP to MerTK. Briefly, TP was docked into the crystal structure of human TAK1 ligand-binding domains (RCSB code: 7VAX) under default parameters. TP-MerTK interaction was calculated with Autodock Tools 1.5.6 and visualized with PyMOL 2.5.0. The details of our steps are present in the previous research (Zhao et al., 2019).

10.3389/fphar.2022.981996

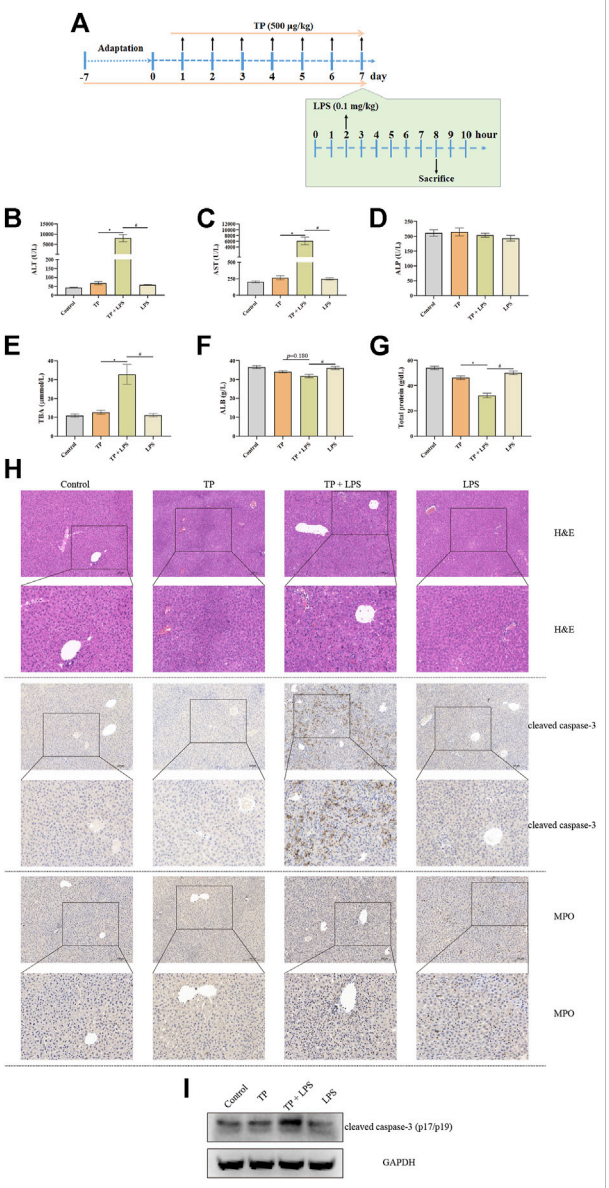

FIGURE 1
TP treatment increased the sensitivity of the liver to LPS administration. **(A)** Schematic presentation of the experimental procedure to prove the hypersensitivity of TP (500 μg/kg) in pretreated mice to LPS (0.1 mg/kg). **(B–G)** Levels of serum ALT, AST, ALP, TBA, ALB, and total protein in mice treated with TP and LPS (n = 8). **(H)** Pictures of liver tissue sections stained by H&E (top panels), analyzed by IHC for MPO (middle panels), or analyzed by cleaved caspase-3 (bottom panels) (×200). **(I)** Representative protein bands of cleaved caspase-3 after TP/LPS treatment, with GAPDH as the loading control. Results were expressed as means ± SEM. Statistical analysis was performed using One-way ANOVA followed by Tukey's Multiple Comparison Test. $p < 0.05$ was considered to be statistically different.

Statistical analysis

Data of this research were analyzed by GraphPad Prism 8.0.1. (GraphPad Software, San Diego, CA, United States). All the data are presented in Mean ± SEM. One-way ANOVA followed by Tukey's Multiple Comparison Test was performed to analyze the differences between groups. p-values < 0.05 were considered to be statistically significant.

Result

TP-treatment increased the sensitivity of the liver to LPS administration

Although TP, as well as Tripterygium wilfordii multiglycoside, the fat-soluble mixture refined from *Tripterygium wilfordii Hook F.* commonly used for the treatment of rheumatoid arthritis (RA) and immune diseases in clinical practice, might induce severe liver injury as observed in clinical report, our previous research proved that the direct hepatotoxicity of TP might not be the main reason for TP-induced hepatotoxicity (Li et al., 2014). Additionally, we proposed that the indirect toxicity of TP might be the main reason for TP-induced hepatotoxicity. In this study, TP (500 μg/kg) was administrated continuously for 7 days followed by a single dose of LPS (0.1 mg/kg) (Figure 1A). Six hours after LPS stimulation, serum and liver samples were collected for further detection. We found that TP and LPS co-treatment significantly increased serum ALT and AST, the two transaminases reflecting the degree of the liver damage, while TP and LPS alone had little effect on ALT and AST (Figures 1B,C). Moreover, TP/LPS co-treatment increased the serum TBA levels while did not affect serum ALP, reflecting that TP/LPS co-treatment might not attract bile duct cells (Figures 1D,E). Serum ALB and Total protein were also decreased by TP/LPS co-treatment, implying TP/LPS might disrupt liver protein synthesis (Figures 1F,G). Liver H&E staining revealed that TP/LPS co-treatment promoted hepatic cell apoptosis and necrosis, which was further proved by IHC staining and western blot of cleaved caspase-3 (Figures 1H,I). Moreover, TP/LPS co-treatment promoted the recruitment of inflammatory cells, as reflected by the IHC staining of MPO (Figure 1H). Overall, our results proved that TP pretreatment increased the sensitivity of the liver to LPS, accompanied by inflammatory cell infiltration. However, the actual role of immune cells in TP/LPS-induced indirect hepatotoxicity still needs to be investigated.

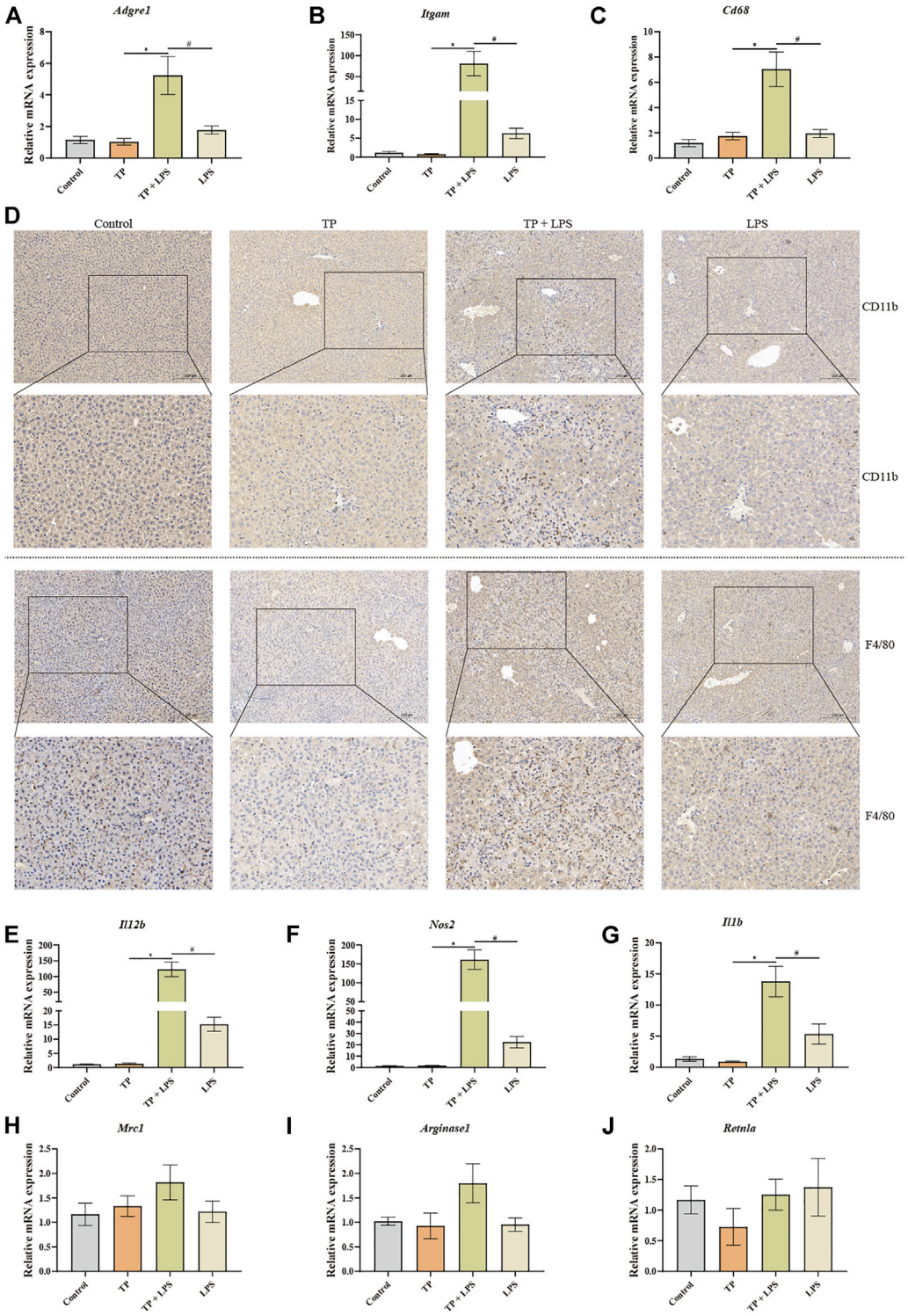

FIGURE 2
TP-induced indirect hepatotoxicity accompanied by macrophage recruitment and fostered the polarization of macrophages to M1 type. **(A–C)** The relative mRNA levels of hepatic macrophage markers *Adgre1*, *Itgam*, and *Cd68* were detected by qPCR with *Gapdh* as the internal control ($n = 8$). **(D)** Pictures of liver tissue sections analyzed by IHC for CD11b (top panels) and F4/80 (bottom panels) (×200). **(E–J)** The relative mRNA levels of M1 macrophage markers (*IL12b*, *Nos2*, and *Il1b*) and M2 macrophage markers (*Mrc1*, *Arginase1*, and *Retnla*) after TP/LPS treatment, with *Gapdh* as the internal control ($n = 8$). Results were expressed as means ± SEM. Statistical analysis was performed using One-way ANOVA followed by Tukey's Multiple Comparison Test. $p < 0.05$ was considered to be statistically different.

TP-induced indirect hepatotoxicity accompanied by macrophage recruitment and fostered the polarization of macrophages to M1 type

Liver macrophages, the key cellular component of liver non-parenchymal cells, are essential to maintain liver homeostasis and promote or regress liver injury (Krenkel and Tacke, 2017). We speculated that liver macrophages might promote liver injury after TP/LPS co-treatment. To prove this, we detected the number of macrophages with IHC staining and qPCR. The results of qPCR revealed that macrophage markers *Adgre1* (encoding F4/80), *Itgam* (encoding CD11b), and *Cd68* were substantially increased in TP/LPS co-treatment group (especially *Itgam*), while TP and LPS alone had little effect on the expressions of *Adgre1* and *Cd68*. Additionally, LPS slightly increased the expression of *Itgam* (Figure 2A–C). The IHC staining of F4/80 and CD11b also firmly confirmed the qPCR results (Figure 2D). Hepatic macrophages can be divided into two parts, liver resident macrophages (also known as Kupffer cells) originating from erythromyeloid progenitors of the yolk sac expressing CD68 and blood-derived originating from hematopoietic stem macrophages expressing CD11b. The dramatic increase in CD11b implied that TP/LPS co-treatment mainly recruited blood-derived monocytes to the liver and significantly increased hepatic macrophages. Additionally, macrophages can also be divided into two different and opposing functional phenotypes, traditionally named M1-type (pro-inflammatory type) and M2-type (anti-inflammatory type). The alteration in macrophage polarization determines the outcome of several liver diseases (Kazankov et al., 2019). Our result revealed that TP alone had no obvious effect on M1 macrophages (*IL-12b*, *Nos2*, and *IL1b*) as well as M2 macrophage markers (*Mrc1*, *Arginase1*, and *Retnla*). LPS treatment partly increased the M1 macrophage markers while having little effect on M2 macrophage markers, which was consistent with the published results (Wang et al., 2018). Unexpectedly, TP/LPS co-treatment boosted the expression of M1 macrophage markers while did not affect M2 macrophage markers (Figures 2E–J). Overall, our result implied that TP/LPS co-treatment increased hepatic macrophage numbers mainly from blood-derived monocytes. Moreover, macrophages might aggravate the liver injury via skewing macrophages to M1 pro-inflammatory type.

Depletion of macrophages alleviated TP-induced indirect hepatotoxicity

To investigate the effect of hepatic macrophages in TP-induced indirect hepatotoxicity, we depleted macrophages via clodronate liposomes, which can be phagocytized by macrophages and ultimately result in macrophage death. We injected the clodronate liposomes and its negative control (200 μl/mouse) on day 5 after TP administration, finding that depletion of macrophages apparently tempered the liver injury induced by TP/LPS co-treatment, as reflected by decreasing serum ALT, AST, and TBA levels (Figure 3B–C). Furthermore, H&E staining revealed that clodronate liposomes pretreatment alleviated the morphological changes after TP/LPS administration. Western blot and IHC staining of cleaved caspase-3 and MPO implied that clodronate liposomes weakened the apoptosis rate and the recruitment of inflammatory cells (Figures 3E,F). We additionally confirmed that clodronate liposomes pretreatment reduced the recruitment of macrophages to the liver, reflected by the decrease in CD11b and F4/80 positive cells (Figure 4). Thus, depletion of hepatic macrophages observably diminished the hepatotoxicity of TP/LPS accompanied by relieving hepatic apoptosis, necrosis, and inflammatory reactions.

Malfunctioning of macrophages in TP-induced indirect hepatotoxicity

Although hepatic macrophages had been proved to involve in TP/LPS-induced hepatotoxicity, the way through which macrophages participated in the indirect hepatotoxicity of TP remained unclear. Hepatic macrophages functioned for phagocytosis, recognition of danger signals, the release of inflammatory factors, antigen presentation, and orchestrating immune response (Guillot and Tacke, 2019). Among them, phagocytosis and inflammatory reactions are two main functions of hepatic macrophages. When hepatocytes are undergoing necrosis, they may release death-associated molecular-pattern molecules, such as IL-1α, HMGB1, mtDNA, and HSPs, which further recruit neutrophils, dendritic cells, NK cells, and others for promoting inflammatory reactions (Gong et al., 2020). Thus, it is irrational to detect the effect of TP on the inflammatory function of macrophages 6 h after LPS administration. In our previous experiment, we found that TP/LPS co-treatment could not induce liver damage 1 h and 3 h after LPS treatment. Additionally, LPS promoted the releasing of inflammation factors in a time-dependent manner in previous reports (Shaw et al., 2007; Lu et al., 2012; Filliol et al., 2017). Thus, we detected IL-1β, IL-6, and TNF-α 1 h, 3 h, and 6 h after LPS application (Figure 5A). Our results proved that LPS increased serum IL-1β, TNF-α, and IL-6, 1 h after LPS application while these pro-inflammatory factors returned to normal subsequently. To our surprise, TP pretreatment increased the production of pro-inflammatory factors upon LPS exposure, compared with the LPS treated group (Figures 5C–E). These results proved that TP pretreatment changed the ability of macrophages to secrete inflammatory factors. Moreover, we detected the serum endotoxin levels, discovering that serum endotoxin content was higher in TP/LPS co-treatment group

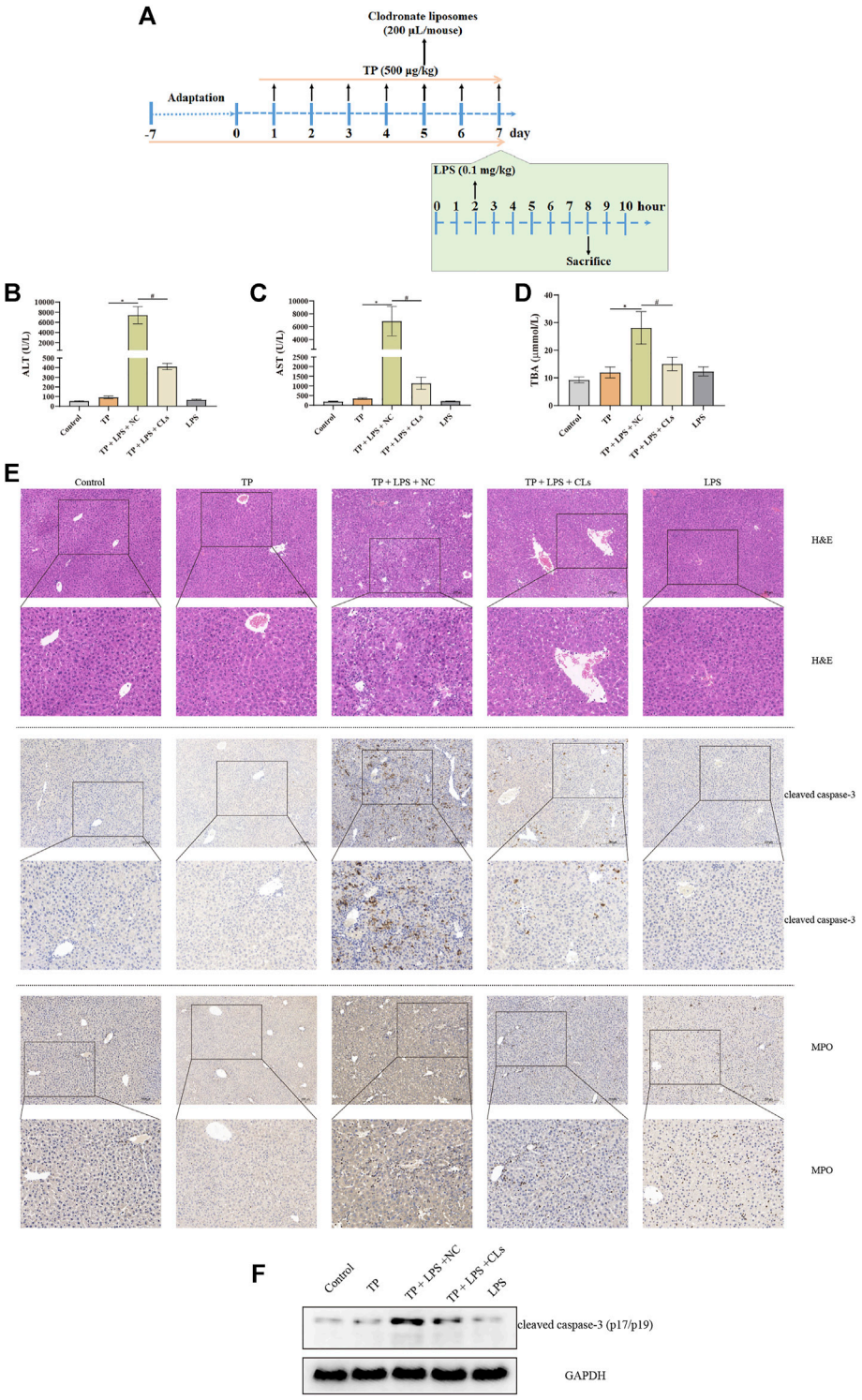

FIGURE 3
Depletion of macrophages alleviated TP-induced indirect hepatotoxicity, accompanied by relieving inflammatory reaction and hepatocyte apoptosis. **(A)** Schematic presentation of the experimental procedure to investigate the effect of depletion of macrophages in TP/LPS-induced hepatotoxicity. **(B–D)** Levels of serum ALT, AST, and TBA in mice having liver macrophages and then treatment with TP and LPS (n = 8). **(E)** Pictures of liver tissue sections stained by H&E (top panels), analyzed by IHC for apoptosis marker cleaved caspase-3 (middle panels) or analyzed by inflammatory marker MPO (bottom panels) (×200). **(F)** Representative protein bands of cleaved caspase-3 after the depletion of macrophages, with GAPDH as the loading control. Results were expressed as means ± SEM. Statistical analysis was performed using One-way ANOVA followed by Tukey's Multiple Comparison Test. $p < 0.05$ was considered to be statistically different.

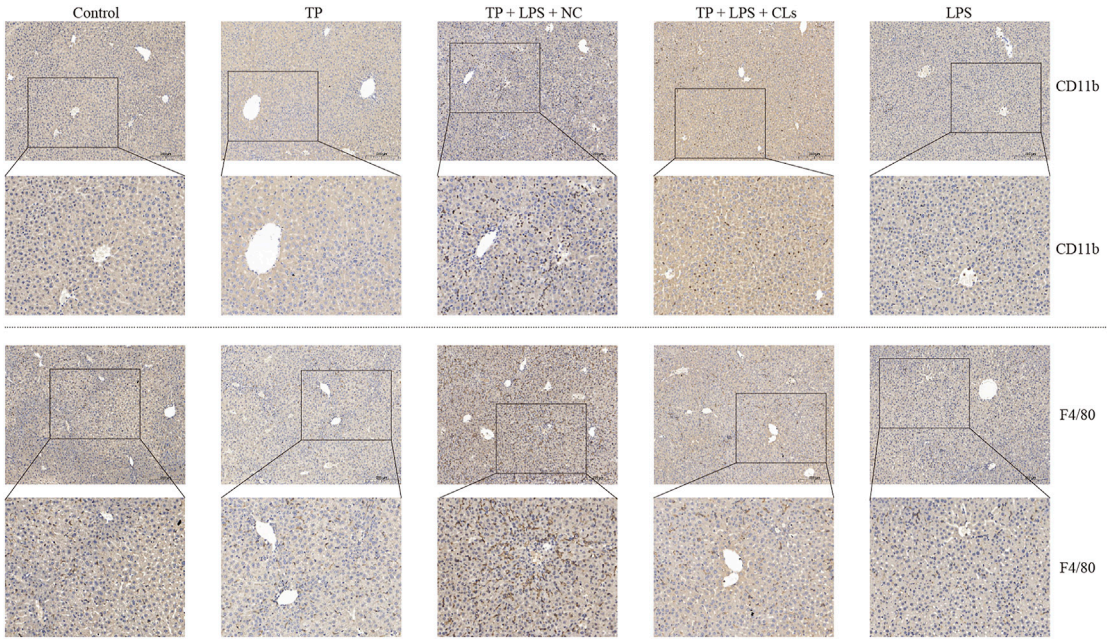

FIGURE 4
Clodronate liposomes administration constrained the recruitment of macrophages to the liver. Pictures of liver tissue sections were analyzed by IHC for macrophage markers CD11b (top panels) and F4/80 (bottom panels) (×200).

compared with LPS treated alone, which might also be one reason for the boost increase in pro-inflammatory factors (Figure 5B). Physiologically, endotoxin can be phagocytized in macrophages. The accumulation of endotoxin in serum in the TP/LPS co-treatment group implied TP pretreatment weakened the phagocytic capacity of hepatic macrophages. Overall, the results in this part proved that TP pretreatment affected the inflammatory secretion and phagocytic capacity of hepatic macrophages, which might be the main reason for TP/LPS-induced hepatotoxicity.

Macrophage MerTK might severed as the new target for TP-induced indirect hepatotoxicity

To further investigate the target of TP on the macrophage, we used reversed docking technology. TP was used as the ligand to bind to the protein structure in RCSB Protein Data Bank (https://www.pdbus.org/). We selected the top 100 proteins and tried to illustrate their bioactivity with macrophages. Among them, we found MerTK, a receptor tyrosine kinase that could regulate macrophage inflammatory secretion, phagocytosis, and polarization. MerTK restricted inflammatory secretion, promoted macrophage phagocytosis, and also skewed macrophages polarization to M2 type (Cai et al., 2016; Grabiec et al., 2018; Triantafyllou et al., 2018; Zhou et al., 2020; Vago et al., 2021; Wu et al., 2021). The binding of LPS to TLR4 led to the production of inflammatory factors, which in turn up-regulated MerTK. MerTK upregulation could selectively induce the production of SOCS1 and SOCS3, ultimately blocking the inflammatory response (O'Neill, 2007; Rothlin et al., 2007). The molecule docking results implied that TP might bind to MerTK (Asp741), which is the key amino acid residue for MerTK activation (Figure 6A). *In vivo* and *in vitro* western blot analysis proved that LPS evaluated the expression of p-MerTK, while TP inhibited MerTK phosphorylation, suggesting that TP could inhibit the bioactivity of MerTK (Figure 6B). Moreover, we selected the widely accepted MerTK ligand, Growth arrest-specific gene 6 (Gas6), to investigate the effect of TP on Gas6-induced MerTK activation according to the published research. We found that Gas6 time-dependent increase in *SOCS1* and *SOCS3* transcription happened within 120 min, while TP pretreatment restrained this process (Figures 6C,D). Thus, we proved that TP inhibited the activation of MerTK upon LPS and Gas6 stimulation, the binding of TP to MerTK (Asp741) might be responsible for these processes.

Discussion

Indirect hepatotoxicity, mainly generated from the use of drugs clinically, is a type of toxicity secondary to the pharmacological effects of drugs, providing a new direction

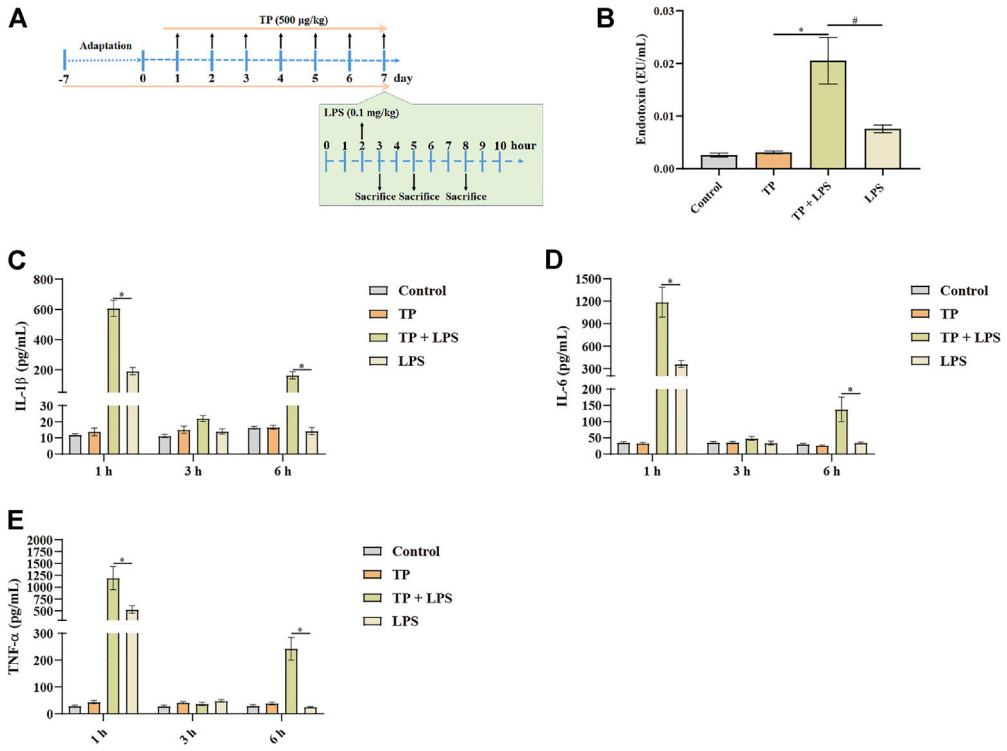

FIGURE 5
Malfunctioning of macrophages in TP-induced indirect hepatotoxicity. **(A)** Schematic presentation of the experimental procedure to investigate the time-dependent release of inflammatory factors in mice treated with TP (500 μg/kg) and LPS (0.1 mg/kg). **(B)** Serum endotoxin content in mice treated with TP and LPS (n = 8) 6 h after LPS injection. **(C–E)** Changes in serum TNF-α, IL-6, and IL-1β in mice after the treatment of TP and LPS (n = 8). Results were expressed as means ± SEM. Statistical analysis was performed using One-way ANOVA and Two-way ANOVA followed by Tukey's Multiple Comparison Test. $p < 0.05$ was considered to be statistically different.

for rational interpretation of clinically relevant drug-induced liver injury. For example, Risperidone and Haloperidol may increase body weight and the incidence of fatty liver disease (Kumra et al., 1997). The application of anticancer chemotherapeutic agents may reactivate hepatitis B (Di Bisceglie et al., 2015). Moreover, antineoplastic checkpoint inhibitors and TNF-α antagonists may induce immune-mediated liver injury due to their immune regulatory effects. Although indirect hepatotoxicity is gradually accepted by researchers, the underlying mechanisms and the animal models to investigate drug-induced indirect liver injury are still elusive. Previously, we proposed that the inhibition of c-FLIP by TP is responsible for TP-induced indirect hepatotoxicity. Additionally, the deficiency of c-FLIP increased the hepatocyte hypersensitivity to TNF-α. Thus, it is rational to explore the interaction between TNF-α secreting immune cells and hepatocytes.

We speculated that hepatic macrophages, which are the main source of TNF-α in LPS stimulation, might participate in TP-induced indirect liver injury. To prove our hypothesis, we detected the F4/80, the marker of macrophages, finding that TP/LPS co-treatment increased the number of macrophages in the liver. Additionally, CD11b, the marker of monocyte-derived macrophages also dramatically increased, revealing that TP/LPS co-treatment recruited blood-derived monocytes to the liver to participate in inflammatory responses. Macrophage polarization has been proved to hold a central position in a variety of liver diseases, including acetaminophen-induced liver injury, liver fibrosis, as well as non-alcoholic fatty liver disease (Luo et al., 2017; Zhang et al., 2019; Li et al., 2020; Shu et al., 2021). The ambivalent function of macrophages in different models of liver diseases reflects that there exist different subsets of macrophages that show opposing bio-activities. Generally, macrophages can be divided into proinflammatory M1 and immunoregulatory M2 subtypes. M1 macrophages function to release the pro-inflammatory factors, and clearance of bacteria, and viruses. In contrast, M2 macrophages could accelerate wound healing and exert anti-inflammatory activity. In this study, we found that LPS alone promoted macrophage polarization towards M1. However, TP/LPS significantly increased M1 macrophage markers, suggesting that M1 macrophages might recruit massive immune cells which were responsible for liver injury

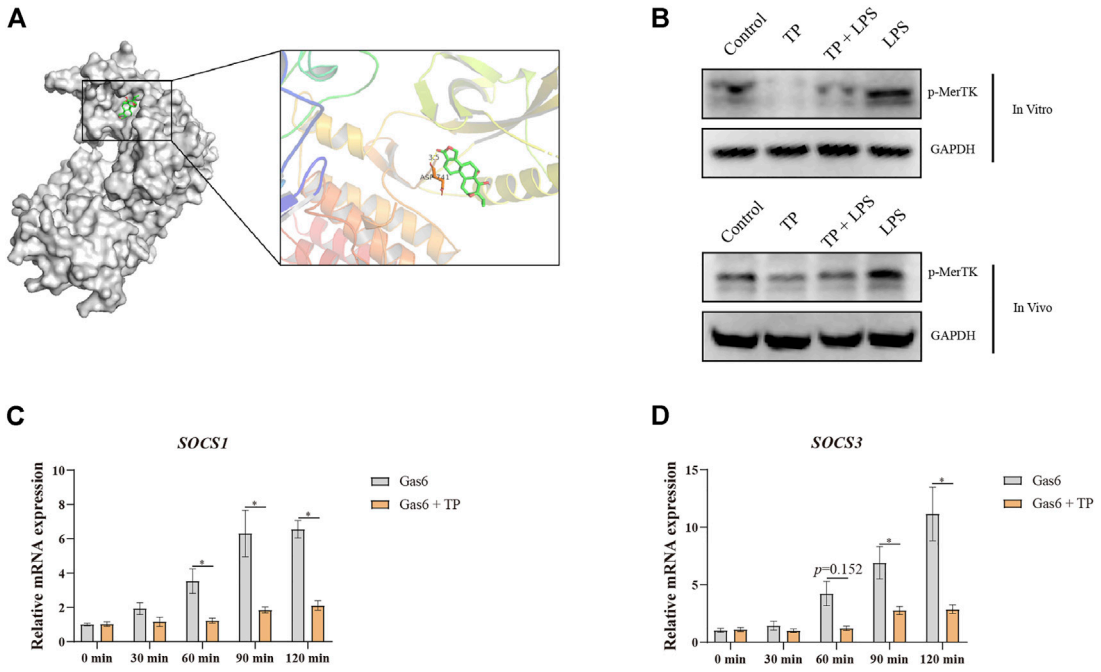

FIGURE 6
Macrophage MerTK might be the new target for TP. **(A)** Molecular docking of TP and MerTK (RCSB code: 7VAX) visualized with PyMOL. **(B)** Representative protein bands of p-MerTK in RAW264.7 cells (top panels) and mice (bottom panels) after TP and LPS treatment, with GAPDH as the loading control. The procedure of *in vivo* experiment was illustrated in Figure 1. In the *in vitro* experiment, TP (20 nmol/L) was preincubated 2 h before LPS (50 ng/ml). Twenty-4 hours after LPS, cells were collected for western blot analysis. **(C,D)** RAW264.7 cells were preincubated with TP (20 nmol/L) for 2 h and then stimulated with Gas6 (50 nmol/L). Cells were harvested at the indicated time points. The relative mRNA levels of *SOCS1* and *SOCS3* were detected by qPCR with *Gapdh* as the internal control ($n = 4$). Results were expressed as means ± SEM. Statistical analysis was performed using Two-way ANOVA followed by Tukey's Multiple Comparison Test. $p < 0.05$ was considered to be statistically different.

induced by TP/LPS co-treatment. To prove this, we depleted liver macrophages with clodronate liposomes. Clodronate liposomes could be phagocytized by macrophages, ultimately promoting macrophage death when injected *in vivo*. As expected, pre-treatment with clodronate liposomes almost completely alleviated the liver injury induced by TP/LPS. We supposed that cutting off the production of TNF-α was the main reason for this phenomenon (Yuan et al., 2020).

Next, we tried to investigate whether TP-treatment could disrupt the normal function of hepatic macrophages. Macrophage phagocytosis has been recognized as an important function in relieving inflammatory reactions (Underhill and Goodridge, 2012; Kourtzelis et al., 2020). Moreover, liver macrophages recognize liver injury and subsequently trigger their activation, ultimately promoting the release of inflammatory chemokines and cytokines, and also the recruitment of inflammatory cells. In this study, we detected inflammatory cytokine secretion and phagocytosis of LPS by macrophages (Figures 5B–E). To our surprise, a time-dependent *in vivo* experiment found that TP/LPS significantly promoted the release of IL-1β, IL-6, and TNF-α at the early time treatments after LPS exposure, in comparison with LPS treatment alone. Under physiological conditions, a low dose of LPS was taken by hepatic macrophages. The structure of lipid A in LPS was hydrolyzed by acyloxyacyl hydrolase in the macrophages, finally inactivating LPS (Shao et al., 2007). In our experiment, we detected plasma endotoxin concentration and found that TP pre-treatment repressed the degradation of LPS. These results firmly implied the macrophage malfunction in TP-induced indirect hepatotoxicity.

Then, we used reverse docking to find the target of TP in macrophages. The molecular docking results proved that TP might bind to MerTK, a newly found TAM receptor that is responsible for the maintenance of liver immune tolerance via inhibiting the production of inflammatory factors upon LPS stimulation and promoting macrophage efferocytic capacity. Existing studies proved that loss of MerTK amplified the inflammatory response of LPS and macrophage MerTK promoted the dissolution of inflammation in acute liver failure (O'Neill, 2007; Cai et al., 2016; Triantafyllou et al., 2018; Bernsmeier et al., 2015). Moreover, MerTK is the key receptor to maintain macrophage efferocytic capacity and its deficiency impairs the clearance of dead cells by macrophages (Caberoy et al., 2010; Grabiec et al., 2018; Gerlach et al., 2021).

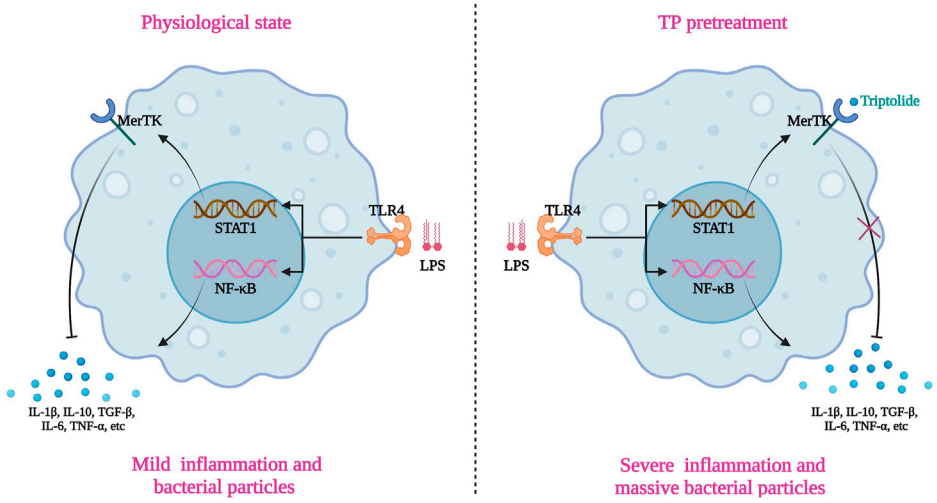

FIGURE 7
Schematic presentation indicated the suggested mechanisms by which macrophages malfunction in TP/LPS-induced indirect hepatotoxicity. The graphic was created with BioRender.com (aggrement number: XI24A5DAOR).

MerTK has also been reported to increase the M1 to M2 ratio in tumor-associated macrophages and microglial cells (Oliva et al., 2021; Wu et al., 2021). Also, MerTK deficiency in macrophages increases the sensitivity of the liver to LPS (Triantafyllou et al., 2018). These researches firmly implied that MerTK might be the true target of TP in macrophages. Our results revealed that TP inhibited the up-regulation of p-MerTK upon LPS *in vivo* and *in vitro*, which was in accordance with the molecular docking results. On binding to MerTK, Gas6 has been proved to activate the SOCS1/SOCS3 pathway. Our results also found that TP pre-treatment hindered the activation of SOCS1/SOCS3 when treated with Gas6, implying that TP inhibited the activation of MerTK. However, the binding site of TP with MerTK still needs to be proved. Also, the efferocytic capacity of MerTK relies on cGAS/STING/TBK1/IFN-β pathway, and the inflammation regulatory function of MerTK is dependent on the STAT1/SOCS1/SOCS3 pathway (O'Neill, 2007). Whether the disruption of these two pathways actually participates in TP-induced indirect hepatotoxicity needs to be further investigated. Additionally, whether the inhibition of MerTK increases the risk of indirect hepatotoxicity needs more experimental results.

Conclusion

TP broke the immune tolerance state of hepatic macrophage via binding and inactivate MerTK, which limited the uptake of bacterial particles (including LPS) and intense the production of pro-inflammatory factors upon LPS stimulation (Figure 7). The malfunction of macrophages together with cytoprotective protein c-FLIP deficiency in hepatocyte proved in our previous research, ultimately resulting in TP-induced indirect hepatotoxicity (Yuan et al., 2020). Targeting hepatic macrophages might be the alternative option for the treatment of indirect hepatotoxicity of TP.

Data availability statement

The raw data supporting the conclusions of this article will be made available by the authors, without undue reservation.

Ethics statement

The animal study was reviewed and approved by All experimental procedures involving mice were complied with the ARRIVE guidelines and were permitted by the Animal Ethics Committee, Zhengzhou University.

Author contributions

TQ, ZY, and WZ participated in the research design. TQ, YZ, MH, and WZ carried out the experiments. TQ and YZ performed the data analysis. MH, TQ and ZY wrote the manuscript.

Funding

This study was supported by the National Natural Science Foundation of China (82104551 for TQ) and the Science and

Technology Research Project of Henan Province (222102310077 for ZY).

Conflict of interest

The authors declare that the research was conducted in the absence of any commercial or financial relationships that could be construed as a potential conflict of interest.

Publisher's note

All claims expressed in this article are solely those of the authors and do not necessarily represent those of their affiliated organizations, or those of the publisher, the editors and the reviewers. Any product that may be evaluated in this article, or claim that may be made by its manufacturer, is not guaranteed or endorsed by the publisher.

Supplementary material

The Supplementary Material for this article can be found online at: https://www.frontiersin.org/articles/10.3389/fphar.2022.981996/full#supplementary-material

SUPPLEMENTARY FIGURE S1
Graph depicting percentage of liver with cleaved caspase-3 (A), MPO (B), CD11b (C), and F4/80 (D) positive cells in mice treated with TP (500 μg/kg), LPS (0.1 mg/kg) or both. Results were expressed as means ± SEM. Statistical analysis was performed using One-way ANOVA followed by Tukey's Multiple Comparison Test. $p < 0.05$ was considered to be statistically different.

SUPPLEMENTARY FIGURE S2
Graph depicting percentage of liver with cleaved caspase-3 (A), MPO (B), CD11b (C), and F4/80 (D) positive cells in mice treated with TP (500 μg/kg), LPS (0.1 mg/kg), Clodronate liposomes (200 μL/mouse) or its negative control. Results were expressed as means ± SEM. Statistical analysis was performed using One-way ANOVA followed by Tukey's Multiple Comparison Test. $p < 0.05$ was considered to be statistically different.

References

Bernsmeier, C., Pop, O. T., Singanayagam, A., Triantafyllou, E., Patel, V. C., Weston, C. J., et al. (2015). Patients with acute-on-chronic liver failure have increased numbers of regulatory immune cells expressing the receptor tyrosine kinase MERTK. *Gastroenterology* 148, 603–615. doi:10.1053/j.gastro.2014.11.045

Caberoy, N. B., Zhou, Y., and Li, W. (2010). Tubby and tubby-like protein 1 are new MerTK ligands for phagocytosis. *Embo J.* 29, 3898–3910. doi:10.1038/emboj.2010.265

Cai, B., Dongiovanni, P., Corey, K. E., Wang, X., Shmarakov, I. O., Zheng, Z., et al. (2020). Macrophage MerTK promotes liver fibrosis in nonalcoholic steatohepatitis. *Cell Metab.* 31, 406–421. doi:10.1016/j.cmet.2019.11.013

Cai, B., Kasikara, C., Doran, A. C., Ramakrishnan, R., Birge, R. B., and Tabas, I. (2018). MerTK signaling in macrophages promotes the synthesis of inflammation resolution mediators by suppressing CaMKII activity. *Sci. Signal.* 11, eaar3721. doi:10.1126/scisignal.aar3721

Cai, B., Thorp, E. B., Doran, A. C., Subramanian, M., Sansbury, B. E., Lin, C. S., et al. (2016). MerTK cleavage limits proresolving mediator biosynthesis and exacerbates tissue inflammation. *Proc. Natl. Acad. Sci. U. S. A.* 113, 6526–6531. doi:10.1073/pnas.1524292113

Challa, T. D., Wueest, S., Lucchini, F. C., Dedual, M., Modica, S., Borsigova, M., et al. (2019). Liver ASK1 protects from non-alcoholic fatty liver disease and fibrosis. *EMBO Mol. Med.* 11, e10124. doi:10.15252/emmm.201810124

Chen, D., Ni, H. M., Wang, L., Ma, X., Yu, J., Ding, W. X., et al. (2019). p53 up-regulated modulator of apoptosis induction mediates acetaminophen-induced necrosis and liver injury in mice. *Hepatology* 69, 2164–2179. doi:10.1002/hep.30422

Di Bisceglie, A. M., Lok, A. S., Martin, P., Terrault, N., Perrillo, R. P., and Hoofnagle, J. H. (2015). Recent US food and drug administration warnings on Hepatitis B reactivation with immune-suppressing and anticancer drugs: Just the tip of the iceberg? *Hepatology* 61, 703–711. doi:10.1002/hep.27609

Filliol, A., Piquet-Pellorce, C., Raguenes-Nicol, C., Dion, S., Farooq, M., Lucas-Clerc, C., et al. (2017). RIPK1 protects hepatocytes from Kupffer cells-mediated TNF-induced apoptosis in mouse models of PAMP-induced hepatitis. *J. Hepatol.* 66, 1205–1213. doi:10.1016/j.jhep.2017.01.005

Gerlach, B. D., Ampomah, P. B., Yurdagul, A., Jr., Liu, C., Lauring, M. C., Wang, X., et al. (2021). Efferocytosis induces macrophage proliferation to help resolve tissue injury. *Cell Metab.* 33, 2445–2463.e8. doi:10.1016/j.cmet.2021.10.015

Gong, T., Liu, L., Jiang, W., and Zhou, R. (2020). DAMP-sensing receptors in sterile inflammation and inflammatory diseases. *Nat. Rev. Immunol.* 20, 95–112. doi:10.1038/s41577-019-0215-7

Grabiec, A. M., Goenka, A., Fife, M. E., Fujimori, T., and Hussell, T. (2018). Axl and MerTK receptor tyrosine kinases maintain human macrophage efferocytic capacity in the presence of viral triggers. *Eur. J. Immunol.* 48, 855–860. doi:10.1002/eji.201747283

Graham, D. K., DeRyckere, D., Davies, K. D., and Earp, H. S. (2014). The TAM family: Phosphatidylserine sensing receptor tyrosine kinases gone awry in cancer. *Nat. Rev. Cancer* 14, 769–785. doi:10.1038/nrc3847

Guillot, A., and Tacke, F. (2019). Liver macrophages: Old dogmas and new insights. *Hepatol. Commun.* 3, 730–743. doi:10.1002/hep4.1356

Hasnat, M., Yuan, Z., Naveed, M., Khan, A., Raza, F., Xu, D., et al. (2019). Drp1-associated mitochondrial dysfunction and mitochondrial autophagy: A novel mechanism in triptolide-induced hepatotoxicity. *Cell Biol. Toxicol.* 35, 267–280. doi:10.1007/s10565-018-9447-8

Hasnat, M., Yuan, Z., Ullah, A., Naveed, M., Raza, F., Baig, M. M. F. A., et al. (2019). Mitochondria-dependent apoptosis in triptolide-induced hepatotoxicity is associated with the Drp1 activation. *Toxicol. Mech. Methods* 30, 124–133. doi:10.1080/15376516.2019.1669247

Holtzhausen, A., Harris, W., Ubil, E., Hunter, D. M., Zhao, J., Zhang, Y., et al. (2019). TAM family receptor kinase inhibition reverses MDSC-mediated suppression and augments anti-PD-1 therapy in melanoma. *Cancer Immunol. Res.* 7, 1672–1686. doi:10.1158/2326-6066.CIR-19-0008

Hoofnagle, J. H., and Bjornsson, E. S. (2019). Drug-induced liver injury - types and phenotypes. *N. Engl. J. Med.* 381, 264–273. doi:10.1056/NEJMra1816149

Ju, C., and Tacke, F. (2016). Hepatic macrophages in homeostasis and liver diseases: From pathogenesis to novel therapeutic strategies. *Cell. Mol. Immunol.* 13, 316–327. doi:10.1038/cmi.2015.104

Kasikara, C., Davra, V., Calianese, D., Geng, K., Spires, T. E., Quigley, M., et al. (2019). Pan-TAM tyrosine kinase inhibitor BMS-777607 enhances anti–PD-1 mAb efficacy in a murine model of triple-negative breast cancer. *Cancer Res.* 79, 2669–2683. doi:10.1158/0008-5472.CAN-18-2614

Kazankov, K., Jørgensen, S. M. D., Thomsen, K. L., Møller, H. J., Vilstrup, H., George, J., et al. (2019). The role of macrophages in nonalcoholic fatty liver disease and nonalcoholic steatohepatitis. *Nat. Rev. Gastroenterol. Hepatol.* 16, 145–159. doi:10.1038/s41575-018-0082-x

Kourtzelis, I., Hajishengallis, G., and Chavakis, T. (2020). Phagocytosis of apoptotic cells in resolution of inflammation. *Front. Immunol.* 11, 553. doi:10.3389/fimmu.2020.00553

Krenkel, O., and Tacke, F. (2017). Liver macrophages in tissue homeostasis and disease. *Nat. Rev. Immunol.* 17, 306–321. doi:10.1038/nri.2017.11

Kumra, S., Herion, D., Jacobsen, L. K., Briguglia, C., and Grothe, D. (1997). Case study: Risperidone-induced hepatotoxicity in pediatric patients. *J. Am. Acad. Child. Adolesc. Psychiatry* 36, 701–705. doi:10.1097/00004583-199705000-00022

Lefebvre, E., Moyle, G., Reshef, R., Richman, L. P., Thompson, M., Hong, F., et al. (2016). Antifibrotic effects of the dual CCR2/CCR5 antagonist Cenicriviroc in animal models of liver and kidney fibrosis. *PLoS One* 11, e0158156. doi:10.1371/journal.pone.0158156

Li, M., Sun, X., Zhao, J., Xia, L., Li, J., Xu, M., et al. (2020). CCL5 deficiency promotes liver repair by improving inflammation resolution and liver regeneration through M2 macrophage polarization. *Cell. Mol. Immunol.* 17, 753–764. doi:10.1038/s41423-019-0279-0

Li, X. J., Jiang, Z. Z., and Zhang, L. Y. (2014). Triptolide: Progress on research in pharmacodynamics and toxicology. *J. Ethnopharmacol.* 155, 67–79. doi:10.1016/j.jep.2014.06.006

Lu, J., Jones, A. D., Harkema, J. R., Roth, R. A., and Ganey, P. E. (2012). Amiodarone exposure during modest inflammation induces idiosyncrasy-like liver injury in rats: Role of tumor necrosis factor-alpha. *Toxicol. Sci.* 125, 126–133. doi:10.1093/toxsci/kfr266

Luo, W., Xu, Q., Wang, Q., Wu, H., and Hua, J. (2017). Effect of modulation of PPAR-γ activity on Kupffer cells M1/M2 polarization in the development of non-alcoholic fatty liver disease. *Sci. Rep.* 7, 44612. doi:10.1038/srep44612

Marra, F., and Tacke, F. (2014). Roles for chemokines in liver disease. *Gastroenterology* 147, 577–594. doi:10.1053/j.gastro.2014.06.043

O'Neill, L. A. (2007). TAMpering with toll-like receptor signaling. *Cell* 131, 1039–1041. doi:10.1016/j.cell.2007.11.032

Oliva, M., Chepeha, D., Araujo, D. V., Diaz-Mejia, J. J., Olson, P., Prawira, A., et al. (2021). Antitumor immune effects of preoperative sitravatinib and nivolumab in oral cavity cancer: SNOW window-of-opportunity study. *J. Immunother. Cancer* 9, e003476. doi:10.1136/jitc-2021-003476

Rothlin, C. V., Ghosh, S., Zuniga, E. I., Oldstone, M. B., and Lemke, G. (2007). TAM receptors are pleiotropic inhibitors of the innate immune response. *Cell* 131, 1124–1136. doi:10.1016/j.cell.2007.10.034

Shao, B., Lu, M., Katz, S. C., Varley, A. W., Hardwick, J., Rogers, T. E., et al. (2007). A host lipase detoxifies bacterial lipopolysaccharides in the liver and spleen. *J. Biol. Chem.* 282, 13726–13735. doi:10.1074/jbc.M609462200

Shaw, P. J., Hopfensperger, M. J., Ganey, P. E., and Roth, R. A. (2007). Lipopolysaccharide and trovafloxacin coexposure in mice causes idiosyncrasy-like liver injury dependent on tumor necrosis factor-alpha. *Toxicol. Sci.* 100, 259–266. doi:10.1093/toxsci/kfm218

Shu, B., Zhou, Y. X., Li, H., Zhang, R. Z., He, C., and Yang, X. (2021). The METTL3/MALAT1/PTBP1/USP8/TAK1 axis promotes pyroptosis and M1 polarization of macrophages and contributes to liver fibrosis. *Cell Death Discov.* 7, 368. doi:10.1038/s41420-021-00756-x

Skirecki, T., and Cavaillon, J. M. (2019). Inner sensors of endotoxin - implications for sepsis research and therapy. *FEMS Microbiol. Rev.* 43, 239–256. doi:10.1093/femsre/fuz004

Stutchfield, B. M., Antoine, D. J., Mackinnon, A. C., Gow, D. J., Bain, C. C., Hawley, C. A., et al. (2015). CSF1 restores innate immunity after liver injury in mice and serum levels indicate outcomes of patients with acute liver failure. *Gastroenterology* 149, 1896–1909. doi:10.1053/j.gastro.2015.08.053

Tacke, F. (2017). Targeting hepatic macrophages to treat liver diseases. *J. Hepatol.* 66, 1300–1312. doi:10.1016/j.jhep.2017.02.026

Triantafyllou, E., Pop, O. T., Possamai, L. A., Wilhelm, A., Liaskou, E., Singanayagam, A., et al. (2018). MerTK expressing hepatic macrophages promote the resolution of inflammation in acute liver failure. *Gut* 67, 333–347. doi:10.1136/gutjnl-2016-313615

Underhill, D. M., and Goodridge, H. S. (2012). Information processing during phagocytosis. *Nat. Rev. Immunol.* 12, 492–502. doi:10.1038/nri3244

Vago, J. P., Amaral, F. A., and van de Loo, F. A. J. (2021). Resolving inflammation by TAM receptor activation. *Pharmacol. Ther.* 227, 107893. doi:10.1016/j.pharmthera.2021.107893

van der Heide, D., Weiskirchen, R., and Bansal, R. (2019). Therapeutic targeting of hepatic macrophages for the treatment of liver diseases. *Front. Immunol.* 10, 2852. doi:10.3389/fimmu.2019.02852

Wang, L., Xu, D., Li, L., Xing, X., Liu, L., Ismail Abdelmotalab, M., et al. (2018). Possible role of hepatic macrophage recruitment and activation in triptolide-induced hepatotoxicity. *Toxicol. Lett.* 299, 32–39. doi:10.1016/j.toxlet.2018.08.017

Wang, X., Jiang, Z., Xing, M., Fu, J., Su, Y., Sun, L., et al. (2014). Interleukin-17 mediates triptolide-induced liver injury in mice. *Food Chem. Toxicol.* 71, 33–41. doi:10.1016/j.fct.2014.06.004

Wen, Y., Lambrecht, J., Ju, C., and Tacke, F. (2021). Hepatic macrophages in liver homeostasis and diseases-diversity, plasticity and therapeutic opportunities. *Cell. Mol. Immunol.* 18, 45–56. doi:10.1038/s41423-020-00558-8

Wu, H., Zheng, J., Xu, S., Fang, Y., Wu, Y., Zeng, J., et al. (2021). Mer regulates microglial/macrophage M1/M2 polarization and alleviates neuroinflammation following traumatic brain injury. *J. Neuroinflammation* 18, 2. doi:10.1186/s12974-020-02041-7

Yuan, Z., Hasnat, M., Liang, P., Yuan, Z., Zhang, H., Sun, L., et al. (2019). The role of inflammasome activation in Triptolide-induced acute liver toxicity. *Int. Immunopharmacol.* 75, 105754. doi:10.1016/j.intimp.2019.105754

Yuan, Z., Yuan, Z., Hasnat, M., Zhang, H., Liang, P., Sun, L., et al. (2020). A new perspective of triptolide-associated hepatotoxicity: The relevance of NF- kappa B and NF- kappa B-mediated cellular FLICE-inhibitory protein. *Acta Pharm. Sin. B* 10, 861–877. doi:10.1016/j.apsb.2020.02.009

Yuan, Z., Zhang, H., Hasnat, M., Ding, J., Chen, X., Liang, P., et al. (2019). A new perspective of triptolide-associated hepatotoxicity: Liver hypersensitivity upon LPS stimulation. *Toxicology* 414, 45–56. doi:10.1016/j.tox.2019.01.005

Zeng, X., Liu, G., Peng, W., He, J., Cai, C., Xiong, W., et al. (2020). Combined deficiency of SLAMF8 and SLAMF9 prevents endotoxin-induced liver inflammation by downregulating TLR4 expression on macrophages. *Cell. Mol. Immunol.* 17, 153–162. doi:10.1038/s41423-018-0191-z

Zhang, H., Yuan, Z., Zhu, Y., Yuan, Z., Wang, J., Nong, C., et al. (2022). Th17/Treg imbalance mediates hepatic intolerance to exogenous lipopolysaccharide and exacerbates liver injury in triptolide induced excessive immune response. *J. Ethnopharmacol.* 295, 115422. doi:10.1016/j.jep.2022.115422

Zhang, X., Fan, L., Wu, J., Xu, H., Leung, W. Y., Fu, K., et al. (2019). Macrophage p38α promotes nutritional steatohepatitis through M1 polarization. *J. Hepatol.* 71, 163–174. doi:10.1016/j.jhep.2019.03.014

Zhao, G., Elhafiz, M., Jiang, J., Das, D., Li, Z., Zhou, W., et al. (2019). Adaptive homeostasis of the vitamin D-vitamin D nuclear receptor axis in 8-methoxypsoralen-induced hepatotoxicity. *Toxicol. Appl. Pharmacol.* 362, 150–158. doi:10.1016/j.taap.2018.11.002

Zhou, Y., Fei, M., Zhang, G., Liang, W. C., Lin, W., Wu, Y., et al. (2020). Blockade of the phagocytic receptor MerTK on tumor-associated macrophages enhances P2x7r-dependent STING activation by tumor-derived cGAMP. *Immunity* 52, 357–373. doi:10.1016/j.immuni.2020.01.014

frontiers | Frontiers in Pharmacology

TYPE Original Research
PUBLISHED 26 September 2022
DOI 10.3389/fphar.2022.999078

Check for updates

OPEN ACCESS

EDITED BY
Fareeha Anwar,
Riphah International University (Lahore), Pakistan

REVIEWED BY
Sakina Mussarat,
Kohat University of Science and Technology, Pakistan
Xuewei Ye,
Zhejiang University, China

*CORRESPONDENCE
Syed Shams ul Hassan,
Shams1327@yahoo.com
Simona Bungau,
Simonabungau@gmail.com
Ihsan-ul Haq,
ihsn99@yahoo.com,
ihaq@qau.edu.pk

SPECIALTY SECTION
This article was submitted to Predictive Toxicology, a section of the journal Frontiers in Pharmacology

RECEIVED 20 July 2022
ACCEPTED 18 August 2022
PUBLISHED 26 September 2022

CITATION
Baig MW, Majid M, Nasir B, Hassan SSu, Bungau S and Haq I-u (2022), Toxicity evaluation induced by single and 28-days repeated exposure of withametelin and daturaolone in Sprague Dawley rats. *Front. Pharmacol.* 13:999078. doi: 10.3389/fphar.2022.999078

COPYRIGHT
© 2022 Baig, Majid, Nasir, Hassan, Bungau and Haq. This is an open-access article distributed under the terms of the Creative Commons Attribution License (CC BY). The use, distribution or reproduction in other forums is permitted, provided the original author(s) and the copyright owner(s) are credited and that the original publication in this journal is cited, in accordance with accepted academic practice. No use, distribution or reproduction is permitted which does not comply with these terms.

Toxicity evaluation induced by single and 28-days repeated exposure of withametelin and daturaolone in Sprague Dawley rats

Muhammad Waleed Baig[1], Muhammad Majid[2], Bakht Nasir[1,3], Syed Shams ul Hassan[4,5]*, Simona Bungau[6]* and Ihsan-ul Haq[1]*

[1]Department of Pharmacy, Quaid-i-Azam University, Islamabad, Pakistan, [2]Faculty of Pharmacy, Capital University of Science and Technology, Islamabad, Pakistan, [3]Charles Institute of Dermatology, School of Medicine, University College Dublin, Dublin, Ireland, [4]Shanghai Key Laboratory for Molecular Engineering of Chiral Drugs, School of Pharmacy, Shanghai Jiao Tong University, Shanghai, China, [5]Department of Natural Product Chemistry, School of Pharmacy, Shanghai Jiao Tong University, Shanghai, China, [6]Department of Pharmacy, Faculty of Medicine and Pharmacy, University of Oradea, Oradea, Romania

Safe preclinical dose determination is predictive of human toxicity and can have a profound impact on the overall progress of the compound in early drug discovery process. In this respect, current study sought to investigate for the first time the acute and subacute oral toxicity of two pharmacologically active natural compounds i.e., withametelin and daturaolone in Sprague Dawley rats following OECD guideline 420 and 407, respectively. As per acute toxicity studies, withametelin and daturaolone were characterized as Globally Harmonized System (GHS) category 4 and 5 compounds, respectively. Sub-acute daily dose of withametelin was 5, 2.5, and 1.25 mg/kg but, for daturaolone, it was 10, 5, and 2.5 mg/kg. High dose (5 and 2.5 mg/kg) withametelin groups showed dose dependent changes in the general, hematological, biochemical and histopathological parameters in both sexes, the most prominent being hyperthyroidism while no toxicity was observed at lower doses (1.25 and 0.75 mg/kg), No Observable Adverse Effect Level (NOAEL) being 1.25 mg/kg. Daturaolone was comparatively safer and showed dose dependent significant changes in hepatic enzyme (Alanine Transaminase), bilirubin, creatinine, and glucose levels while histological changes in testes were also observed. Lower doses (5, 2.5, and 1.25 mg/kg) of daturaolone showed no significant toxic effects and 5 mg/kg was declared as its NOAEL. Depending upon our findings, starting effective oral dose levels of 1.25 mg/kg/day for withametelin and 5 mg/kg/day for daturaolone are proposed for repeated dose (up to 28 days) preclinical pharmacological evaluation models. Long term studies with more behavioral, biochemical, histopathological and hormonal parameters are proposed to strengthen the findings.

KEYWORDS

withametelin, daturaolone, toxicity, *in vivo*, Datura

1 Introduction

Natural products continue to contribute significantly to human health and longevity. They are promising pools for discovering high-strength structural diversity and different bioactive scaffolds have tendency to be developed directly or used as a starting point for optimizing new drugs (Khan et al., 2019; Hassan et al., 2021; Majid et al., 2022). One of the main criteria that applies to new drugs for research is to evaluate the safe dose and potential toxicity risk before human studies are carried out (Hassan et al., 2022; Shams ul Hassan et al., 2022). In this regard, pre-clinical studies estimate the initial dose of any drug candidate for advance testing (Shams ul Hassan et al., 2021). Withametelin (Baig et al., 2020) and daturaolone (Baig et al., 2021) were isolated in our previous studies. Withametelins is a subclass of withanolides mainly found in Datura genus (Chen et al., 2011; Muhammad et al., 2021). Withametelin possess antifungal (Singh et al., 2001) cytotoxicity against lung (Rao et al., 2016), liver, prostate and mammary cell lines (Baig et al., 2020). Its antileukemia effects are attributed to the inhibition of the spread of acute myeloid leukemia by targeting the signalling pathways of oncogenic kinase, which regulate the progression and survival of the cell cycle, thus resulting in an induction of apoptosis (Akhtar et al., 2020). It relieves vincristine-induced neuropathic pain by analyzing results from behavior, biochemistry, histopathology and computational data, the molecular mechanism being associated with the suppression of TRPV1/TRPM8/P2Y nociception and MAPK signalling in mice (Khan et al., 2021b). It also shows neuroprotective properties by modulating the oxidative stress by Nrf2/Keap1/HO-1 in the CNS and the neuroinflammatory stress by TLR4/IκB-α/NF-κB/AP-1 in the CNS (Khan et al., 2021a). Moreover, daturaolone is an amyrin type triterpenoid affective in fever, muscle relaxation and gastrointestinal problems (Bawazeer et al., 2020a). It significantly inhibits inflammation and cancer markers (NF-κB and NO, as shown in silico and *in vitro* models. In addition, powerful *in vivo* anti-inflammatory, anti-nociceptive and antidepressants had also been observed (Baig et al., 2021). Daturaolone also significantly inhibits α-glucosidase and β-secretase and can be used as an excellent template compound for new drugs used in diabetes and Alzheimer's disease (Bawazeer et al., 2020b). Both natural compounds were proposed for their detailed mechanistic, toxicity profile, and clinical studies. Early detection of preclinical doses that predict human toxicity can have a significant impact on the development of compounds.

Financial investment increases exponentially as new chemicals move through discovery and development stages. Modern toxicologists can significantly influence expenditure by predicting safe doses and potential toxicological/side effects in advance (Lai, 2020; Obireddy and Lai, 2021a). Early detection of preclinical doses that are predictive of human toxicity can have a profound impact on the overall progression of the compound, its development costs, and clinical trials (Lai et al., 2021; Chen et al., 2022). Identifying preclinical and predictable safety liability at the beginning of the process might lead to better candidates being designed and selected (Anjum et al., 2017). Many efforts in toxicity research focus on the application of new technologies. Nevertheless, when separated from traditional (*in vivo*) toxicological principles, compounds cannot be developed. National and international regulators assess toxicological data to understand intrinsic toxicology of chemicals (Ji et al., 2020; Obireddy and Lai, 2021b). Effects of different doses in animal model systems is extrapolated to human exposure to understand potential risks. The main decisive factor is the determination of adverse reactions required to protect exposed people and the exposure levels at which these effects occur (Parasuraman, 2011).

In line with this, our study aimed to generate information on toxicity testing needed for the risk assessment of withametelin and daturaolone which has been identified in a study of oral toxicity in rodents by single dose and repeated dose for 28 days. A systematic toxicity assessment was carried out to generate data supporting the identification of appropriate starting doses and possible adverse reactions.

2 Material and methods

2.1 Animals

Sprague Dawley rats of either sex were procured from National Institute of Health (NIH). The overall wellbeing of rats was guaranteed. In the current study, one hundred forty two (142) rats aged seven to 8 weeks weighing in range of ~190–220 g were used. Animals were placed in their respective aluminium cages with soft wood splinters on floor. Surroundings were maintained with temperature 23–25°C and air humidity of 50 ± 10% with a 12 h light/dark cycle. The bedding was regularly replaced with new wood splinters to avoid health risks and infections in research animals. Animals were housed in the Primate facility of Faculty of Biological Sciences, Quaid-i-Azam University Islamabad, Pakistan in compliance with the National Institute of Health, United States guidelines for the care and use of laboratory animals. They were provided with standard rodent food and water *ad libitum*. Study was conducted after ethical approval from the Institutional Animal Ethics Committee (letter number # BEC-FBS-QAU2019-135) and adhered with strict cautions to diminish animal distress.

2.2 Acute oral toxicity testing

Acute toxicity tests with only observational study were carried out for the selected doses of withametelin and daturaolone following the Organization for Economic

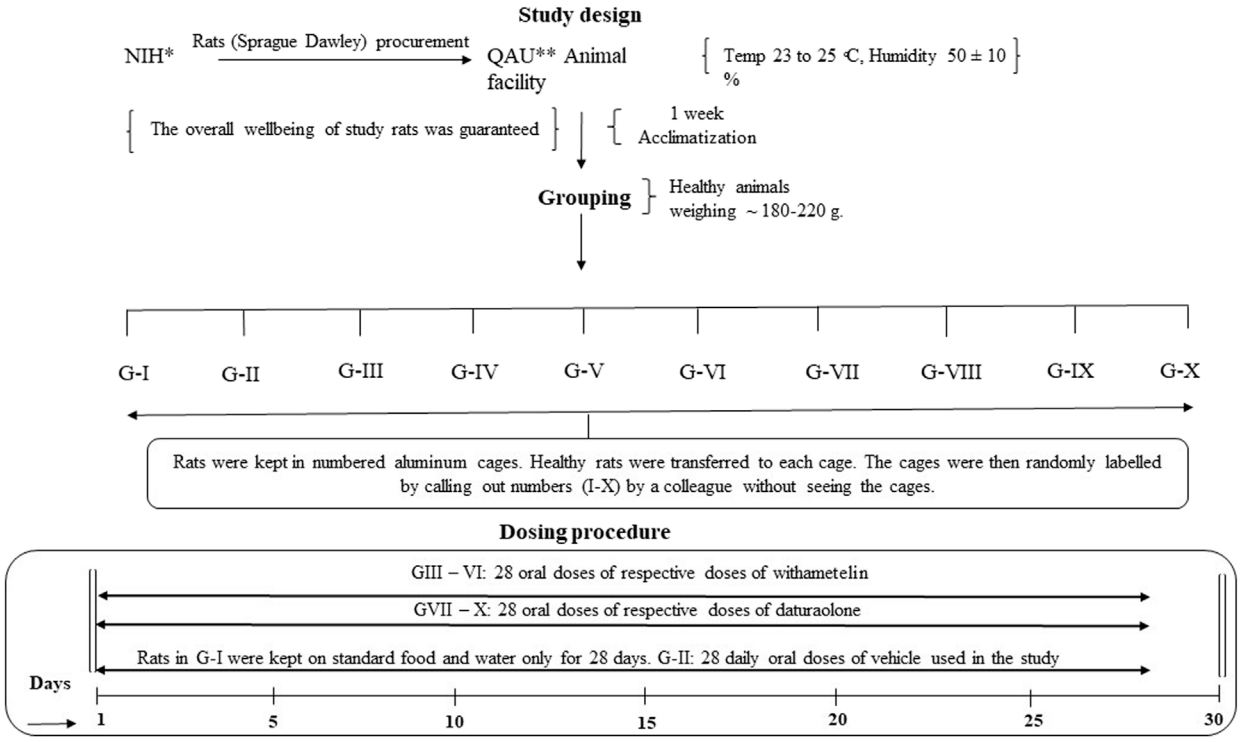

Rats in GIII–X were given respective doses in the morning. Doses were orally administered through sterilized disposable oral gavage.
* National Institute of Health, Islamabad, Pakistan. **Quaid-i-Azam University Islamabad, Pakistan.

FIGURE 1
The experimental design of 28-days *in vivo* toxicity evaluation performed in Sprague Dawley rats.

Cooperation and Development (OECD) guideline 420, fixed-dose procedure with slight changes according to system suitability (Liu et al., 2016; Xiao et al., 2020). Principle is to use only moderately toxic doses and potentially fatal dose planning should be avoided. In addition, doses known to cause serious pain and suffering due to corrosion or serious irritation do not need to be administered. The initial doses chosen for observation studies were 5, 50, and 300 mg/kg. After a week of acclimatization, the animals were randomly divided into seven groups (3 males and three females). Group-I (vehicle control) was administered 10% DMSO in CMC. Group-II-IV were given different doses of withametelin while group-V-VII were administered selected doses of daturaolone. The rats were fasted overnight before dose and 2 h after treatment. The test material was administered by gavage in a single dose. The dose volume was calculated in advance based on the last body weight recorded for each animal. Toxicity signs such as change in body weight, ptosis, abnormal posture, abnormal respiration, diarrhoea and diuresis, lethargy, ataxia, abnormal gait, tremors, convulsion, prostrate, coma, lacrimation and exopthalmus were observed. The beginning and duration of observed toxic symptoms were systematically recorded. After dosing, the animal was monitored for 48 h to observe its survival and if any signs of toxicity occured. The first group of rats had no signs of toxicity and survived for 48 h. Therefore, rats in the second group received higher doses and were observed as before. The 300 mg/kg compound study took place because the second group of animals also survived more than 48 h. Three rats were administered with 300 mg/kg dose of withametelin and daturaolone and the survival time and toxic signs were observed. Animals surviving from highest dose were observed at least once for 14-days observational period. During this study, the body weight of the rats were measured and recorded on day 1, 7, and 14.

2.3 Repeated dose 28-day oral toxicity study

2.3.1 Study design

A repeat dose toxicity study was conducted in rodents for selected doses of withametelin and daturaolone following the OECD guideline 407, Repeated Dose 28-Day Oral Toxicity

procedure with slight modifications as per system suitability (Wu et al., 2015; Yimam et al., 2018) (Figure 1). After a week of acclimatization, rats were randomly divided into 10 groups, each group consisted of ten rats (5 males (M) and 5 females (F)). Rats were given oral gavage doses of withametelin (5, 2.5, 1.25, 0.75 mg/kg/day) and daturaolone (10, 5, 2.5, 1.25 mg/kg/day) at 7–8 weeks of age for at least 28 days. Doses were selected on the basis of our acute toxicity test and previously published *in vitro* and *in vivo* data. Negative control group was given only saline while vehicle control group was given only 10% DMSO in CMC. The daily dose volume was calculated in advance based on the most recent weight of each animal. The endpoints included clinical observations, body weight, water and feed consumption values, hematology, serum chemistry levels, thyroid levels and histopathological findings. Study design is as follows:

Group I: Normal control (Untreated, standard food only)
Group II: Vehicle control (10% DMSO in CMC)
Group III: Withametelin (5 mg/kg)
Group IV: Withametelin (2.5 mg/kg)
Group V: Withametelin (1.25 mg/kg)
Group VI: Withametelin (0.75 mg/kg)
Group VII: Daturaolone (10 mg/kg)
Group VIII: Daturaolone (5 mg/kg)
Group IX: Daturaolone (2.5 mg/kg)
Group X: Daturaolone (1.25 mg/kg)

2.3.2 General observations

Clinical observations were made in all animals outside the house cage once before first administration of dose, thereafter, once every week and before necropsy. Signs sought included changes in skin, fur, eyes or mucous membranes, occurrence of secretions and excretions, lacrimation, piloerection, pupil size, respiratory pattern, changes in gait, posture, response to handling, excessive grooming and circling or bizarre behavior (self-mutilation, walking backwards).

2.3.3 Body weight, food and water consumption

The weight of each rat was recorded once a week and immediately before the necropsy. Similarly, food and water consumption was measured weekly and results were expressed as mean ± SD.

2.3.4 Collection of blood samples and serum separation

At the end of the experiment, rats were left without food for 24 h, breathed with isofluorane anesthesia, and were euthanized *via* cervical displacement. Blood samples were obtained from the heart of animals by intracardiac injection. Serum was separated from the collected blood samples by centrifugation at 4°C (6,000 rpm) for 15 min. The serum was stored at −20°C until biochemical testing was carried out.

2.3.5 Estimation of hematological parameters

Blood samples were collected into sterile tubes with anticoagulant (EDTA-K_2) for hematological tests. Hematological measurements include: red blood cells (RBC), hemoglobin (Hb), hematocrit (HCT), mean corpuscle volume (MCV), mean corpuscle hematocrit (MCHT), erythrocyte sedimentation rate (ESR), platelets, white blood cells (WBC), lymphocyte, monocyte, neutrophil, eosinophil using automatic hematology analyzer (Díez-Quijada et al., 2021).

2.3.6 Assessment of biochemical parameters

Blood samples were collected into sterile tubes without anticoagulant for biochemical tests (serum). Alanine transaminase (ALT), aspartate aminotransferase (AST), alkaline phosphatase (ALP), bilirubin, creatinine, albumin, total serum protein (protein), urea, cholesterol and triglycerides using automatic chemistry analyzer (Roche Diagnostics, IN, United States) (Nasir et al., 2020; Díez-Quijada et al., 2021).

2.3.7 Hormonal analysis

Triiodothyronine (T3), thyroxine (T4), and thyroid-stimulating hormone (TSH) were measured at the end of the test period. T3 and T4 were determined using the automatic immunoassay system (IMX, Abbott Laboratories, Abbott Park, Ill., United States), and TSH was measured with a microplate reader (UVmax, Molecular Devices, Sunnyvale, Calif., United States) (Díez-Quijada et al., 2021).

2.3.8 Organ weights

The following organs were weighed at necropsy: brain, kidney, heart, liver, lungs, spleen, testis, ovary and uterus.

2.3.9 Histological investigation (hematoxylin-eosin staining)

The following organs were fixed in 10% neutral buffered formalin and examined: heart, liver, kidney, testes and intestine. Evaluation of any change in histology was carried out using paraffin-associated staining protocols. After the dissection, the tissues were fixed for 12 h at room temperature with a buffer solution of 10% formalin (pH 7.4). The removal of the infiltrating wax and water traces was guaranteed via numerous ethanol (50, 70, 90, and 100%) washings of the fixed tissue. Small pieces of the incorporated tissue (3–5 m thick) were divided to prepare slides and latter stained with Eosin and Hematoxylin (H and E) (Majid et al., 2019).

2.4 Statistical analysis

The data were analyzed using one-way variation analysis (ANOVA) and then subsequently appropriate post-hoc tests. The results are represented as the mean ± SD of the respective parameters and $p < 0.05$ was considered statistically significant.

TABLE 1 Acute toxicity assessment of withametelin and daturaolone at different doses.

Parameters	Days (1-14)						
	Withametelin				Daturaolone		
	Vehicle control	5 mg/kg	50 mg/kg	300 mg/kg	5 mg/kg	50 mg/kg	300 mg/kg
Δ Body weight	✗	✗	✗	✓	✗	✗	✗
Ptosis	✗	✗	✗	✗	✗	✗	✗
Abnormal Posture	✗	✗	✗	✓	✗	✗	✗
Abnormal respiration	✗	✗	✗	✗	✗	✗	✗
Diarrhoea and diuresis	✗	✗	✗	✓	✗	✗	✗
Lethargy	✗	✗	✗	✓	✗	✗	✗
Ataxia	✗	✗	✗	✗	✗	✗	✗
Abnormal gait	✗	✗	✗	✓	✗	✗	✗
Tremors	✗	✗	✗	✗	✗	✗	✗
Convulsion	✗	✗	✗	✗	✗	✗	✗
Prostrate Coma	✗	✗	✗	✗	✗	✗	✗
Lacrimation	✗	✗	✗	✗	✗	✗	✗
Exopthalmus	✗	✗	✗	✗	✗	✗	✗

N = 4. ✗ = absent, ✓ = present.

TABLE 2 Body weight, morbidity, and mortality after acute toxicity studies of withametelin and daturaolone at selected doses.

	Withametelin (mg/kg)				Daturaolone (mg/kg)		
	0	5	50	300	5	50	300
Body weight (g)							
Day 1	210.8 ± 4.24	215.36 ± 4.32	214.21 ± 3.23	215.63 ± 3.96	218.29 ± 2.34	215.67 ± 5.61	217.89 ± 5.58
Day 7	232.4 ± 3.76	236.38 ± 5.48	239.21 ± 3.76	225 ± 4.32	239.23 ± 4.45	235.14 ± 3.39	237.85 ± 5.11
Day 14	256.4 ± 3.76	261.31 ± 5.48	252.40 ± 5.31	238 ± 5.17	264.46 ± 3.90	261.29 ± 4.22	258.39 ± 6.16
Morbidity							
Day 1	0/3	0/3	0/3	0/3	0/3	0/3	0/3
Day 7	0/3	0/3	0/3	2/3	0/3	0/3	0/3
Day 14	0/3	0/3	0/3	0/3	0/3	0/3	0/3
Mortality							
Day 1	0/3	0/3	0/3	0/3	0/3	0/3	0/3
Day 7	0/3	0/3	0/3	0/3	0/3	0/3	0/3
Day 14	0/3	0/3	0/3	0/3	0/3	0/3	0/3

3 Results

3.1 Acute toxicity assessment

No changes in clinical symptoms, such as external appearance, behaviour, mental state and daily activities, were observed due to treatment except at 300 mg/kg withametelin group (Table 1). Morbidity was observed in 2/3 animals up to day 5 but no animal died even at a dose of 300 mg/kg (Table 2). Change in weight, abnormal posture, abnormal gait and diarrhoea were observed in 300 mg/kg group. Changes in weight clearly showed some damage caused by test material. Withametelin was characterized as GHS (globally harmonized classification system in mg/kg body weight) category 4 compound with evident toxicity at 300 mg/kg in acute toxicity assessment. Observable parameters and weight changes in different dose groups are mentioned in Table 1. In Daturaolone, no changes related to treatment have been observed (Table 1). A soft fecal consistency was observed in all rats in the treatment

10.3389/fphar.2022.999078

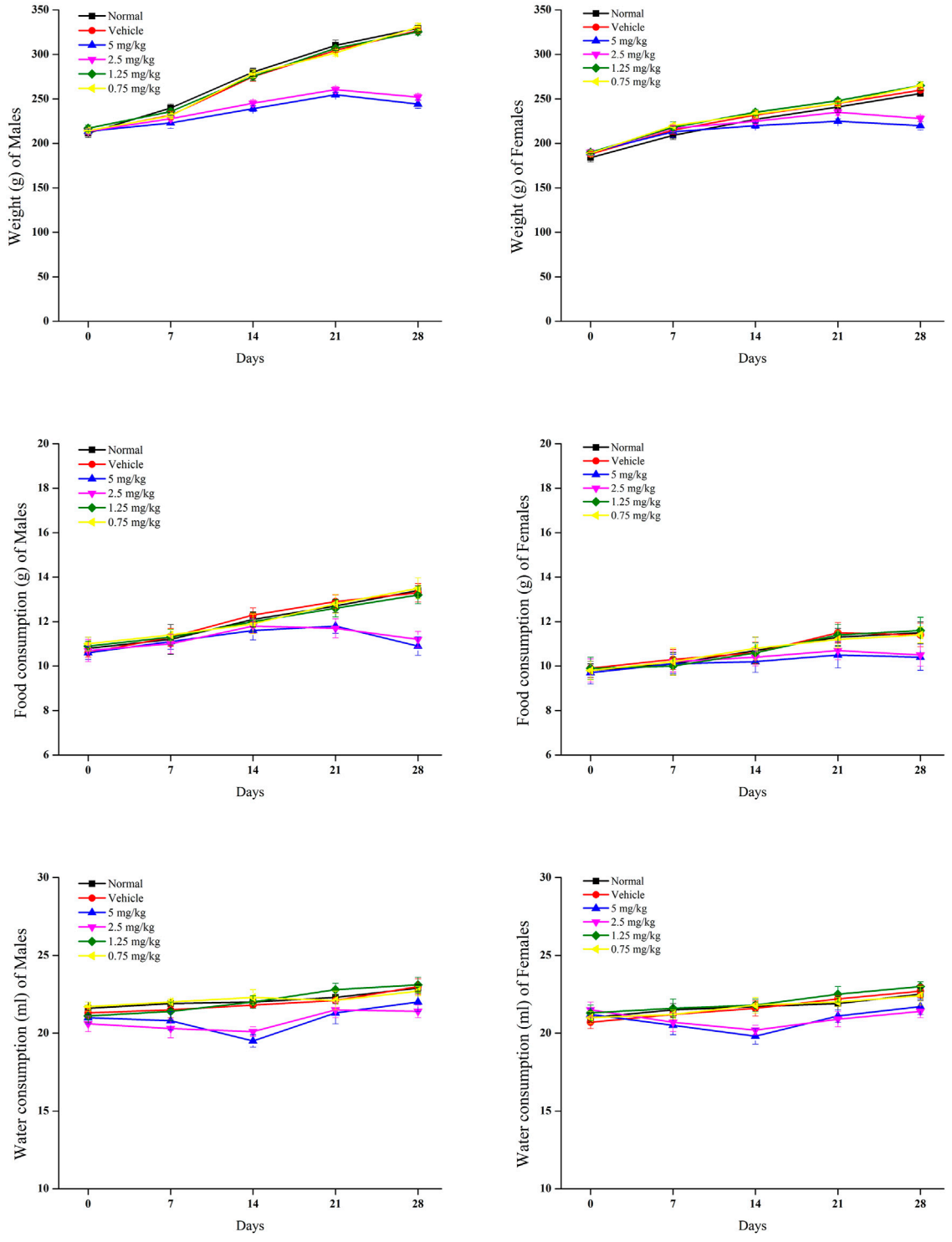

FIGURE 2
Mean food intake, water consumption, and weekly weight gain of rats in 28 days feeding study of withametelin.

groups; however, this symptom was not observed on 2nd day after administration. No changes were observed after gross necroscopy of both compounds (data not shown). As per observations, it was assumed that daturaolone was GHS category 5 or unclassified compound which might show toxicity at 2000 mg/kg. Experiment was not performed at 2000 mg/kg due to insufficient quantity of compound and requirement to observe the effects of multiple daily dosing of daturaolone on rats.

3.2 Repeated dose sub-acute toxicity *in vivo*

3.2.1 General observations

No death was seen in all males and females of withametelin and daturaolone groups. The increased incidence of post-dosing salivation was observed in all treatment groups of withametelin. The softness in fecal consistency was observed on fifth day in all groups (withametelin) which gradually eased over 2 weeks. The control group had neither diarrhea nor melena. Abnormal gait (2/5 males) in last week was also seen with piloerection. In case of daturaolone, no general observational symptom was observed at all doses.

3.2.2 Body weight, food, and water consumption

In relation to the control group, rat body weights were significantly reduced in groups of 5 and 2.5 mg/kg withametelin (Figure 2). A significant weight reduction was observed in males between 2 and 4 weeks, respectively while a significant reduction in body weight was observed in the female group during the 3rd to 4th week, respectively. In the 1.25 mg/kg and 0.75 mg/kg withametelin groups, the weight difference was not significant compared to the control group. (Figure 2A). At 5 and 2.5 mg/kg withametelin groups, and at 3 and 4 weeks, the consumption of the food of male and female rats was significantly reduced. Compared to control rats, there was no significant decrease in food efficiency between female and male rats who were fed 1.25 mg/kg and 0.75 mg/kg withametelin (Figure 2B). Water consumption decreased considerably when noted on 14th day, but then it became normal in the third and fourth week (Figure 2). Significant weight reduction observed in high-dosed male rats was due to the administration of 5 mg and 2.5 mg/kg of withametelin. Since water consumption changes were temporary and had low magnitude, they were not considered to be associated with the treatment. In the case of daturaolone, male and female rats groups of all doses showed no significant changes in weight and nutrition parameters (Figure 3).

3.2.3 Hematological paramaeters

Hematological analysis results are presented in Table 3. We observed significant changes in RBC associated parameters, while a significant increase of platelets and neutrophils in withametelin (5 mg/kg) and daturaolone (10 mg/kg) treated rats. The level of platelets remained high at 2.5 mg/kg withametelin, but lower than the 5 mg/kg-withametelin group. The hematology indices values in high-dose groups with withametelin and daturaolone that do not correspond to the normal control have dose dependent clinical significance or toxicity. There was no significant difference between WBCs and its associated response variables or red cell indices between treated and non-treated rats at lower doses of both compounds, respectively.

3.2.4 Biochemical parameters

Biochemical analysis result values are presented in Table 4. In withametelin dosed 5 and 2.5 mg/kg groups, significant increase of ALT and AST were observed while plasma glucose levels were significantly low in comparison to control. In thyroid profile, low TSH and high T3 and T4 was observed. Cholesterol and triglyceride levels were also lowered in 5 mg/kg withametelin groups. All other tested biochemical parameters were normal. In daturaolone dosed 10 mg/kg male and female groups, significant difference was noted regarding ALT, bilirubin, creatinine and glucose indices between treated and untreated rats. Insignificant changes in thyroid profile i.e., low TSH and high T3 and T4 were observed Biochemical parameter values in high dose withametelin and daturaolone groups that are not within the normal range have shown dose dependent clinical significance or toxicity.

3.2.5 Relative organ weight and histopathological investigation

No significant changes were detected in organ weight parameters were observed when comparing control groups and high or low dose groups of both compounds (Table 5). The H&E histological analysis of the withametelin group confirmed the treatment-related changes in liver, kidney and testicle (male) of rats at 5 mg/kg and 2.5 mg/kg when compared to the control group (Figure 4). The toxic effects on the liver and kidneys of males were more profound. In the kidneys, a mild infiltration of mononuclear inflammatory cells around tubules and the degeneration of epithelial cells was observed in 4/5 of males and 2/5 of females. All rats observed renal glomerular capsule space distention. Interstitial swelling and congestion at 5 mg/kg withametelin were also seen. Pink proteinacious material in the lumens of the proximal convoluted tubules were also observed in 3/5 males and 2/5 females. Testes in control groups showed standard morphology of seminiferous tubes with active sperm generation. The treatment group with withametelin (5 mg/kg) showed an increase in the interstitial space between the seminiferous tubes, an increase in the lumen size and spermatogenesis stages showed mild sloughing. Low doses (1.25 mg/kg and 0.75 mg/kg) showed normal seminiferous tubes, the germ epithelium with proliferating germ cells at different stages such as spermatids,

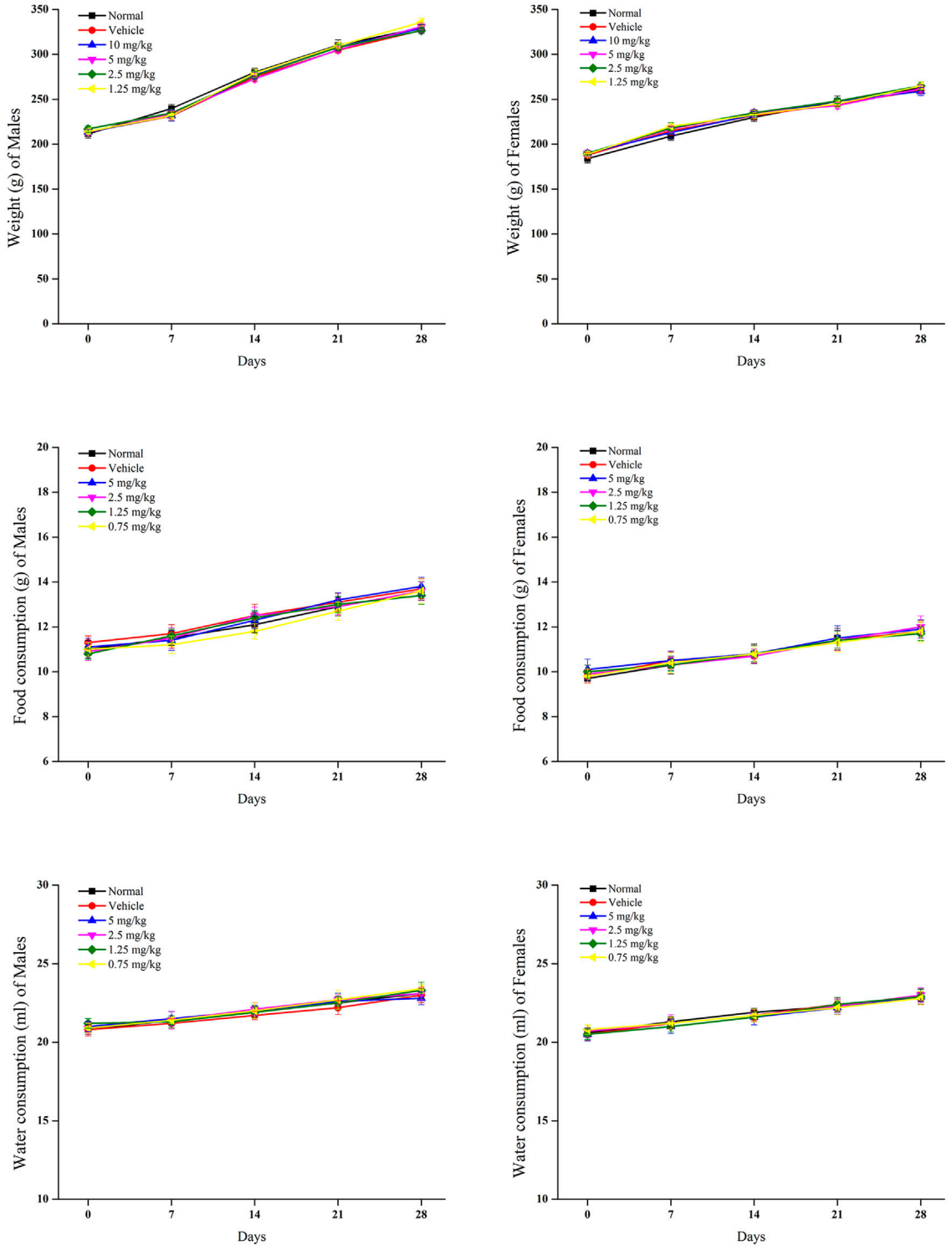

FIGURE 3
Mean food intake, water consumption, and weekly weight gain of rats in 28 days feeding study of daturaolone.

spermatocytes, spermatogonia were observed. In the liver, there was an increase in the sinusoidal space, a slight infiltration of inflammatory cells, swelling, and sinusoidal congestion in 5 and 2.5 mg/kg groups in comparison to control was observed. No significant adverse toxicity was observed in other male or female systems of rats.

TABLE 3 Hematology results after 28 days respectively.

Parameter	Sex	Hematological data									
		Withametelin						Daturaolone			
		Normal	Vehicle	5	2.5	1.25	0.75	10	5	2.5	1.25
RBC ($\times 10^6$)/μL	M	6.91 ± 0.98	6.74 ± 0.96	6.14 ± 0.91*	6.87 ± 0.57	7.56 ± 0.76	6.98 ± 0.78	6.21 ± 0.56	6.83 ± 0.78	6.98 ± 0.75	6.65 ± 0.82
	F	7.73 ± 1.21	7.35 ± 1.67	6.26 ± 1.21*	7.03 ± 1.45	7.78 ± 2.49	7.64 ± 1.69	7.19 ± 1.65	7.60 ± 1.63	7.77 ± 2.64	7.68 ± 1.64
Hb (g/dl)	M	14.5 ± 1.23	14.77 ± 2.14	11.53 ± 1.23*	13.93 ± 1.38	14.83 ± 1.63	13.89 ± 1.64	12.33 ± 1.34*	13.96 ± 2.14	14.32 ± 1.63	13.81 ± 1.78
	F	16.1 ± 1.25	16.86 ± 2.13	16.7 ± 1.27*	15.8 ± 1.44	15.94 ± 1.35	16.78 ± 1.65	14.90 ± 1.45*	16.92 ± 2.45	16.71 ± 1.66	16.74 ± 1.56
HCT (%)	M	48.8 ± 2.32	49.82 ± 4.33	42.3 ± 2.47*	46.4 ± 2.43	50.76 ± 3.76	49.09 ± 2.79	40.10 ± 2.78*	50.23 ± 4.76	50.74 ± 3.78	49.02 ± 2.36
	F	52.0 ± 3.08	53.08 ± 3.45	45.5 ± 2.76*	51.6 ± 3.00	53.02 ± 4.73	52.04 ± 8.72	45.39 ± 3.98*	57.52 ± 3.23	53.12 ± 4.72	52.05 ± 8.74
MCV (fL)	M	69.9 ± 3.32	71.85 ± 3.37	60.32 ± 4.12*	68.40 ± 5.37	71.95 ± 4.78	68.98 ± 2.88	72.67 ± 3.26	72.20 ± 3.54	71.45 ± 4.79	68.91 ± 2.63
	F	66.73 ± 2.98	68.53 ± 3.98	57.35 ± 2.76*	63.77 ± 3.65	66.73 ± 2.98	68.98 ± 2.18	70.20 ± 2.97	68.94 ± 3.26	66.54 ± 2.91	68.99 ± 2.26
MCHC (%)	M	30.04 ± 1.20	29.67 ± 2.22	32.32 ± 1.45	30.5 ± 2.76	31.39 ± 2.68	31.34 ± 4.76	26.45 ± 1.15	28.39 ± 2.15	31.24 ± 2.64	31.35 ± 4.64
	F	31.43 ± 2.23	32.12 ± 1.93	28.43 ± 2.65*	30.34 ± 3.19	33.73 ± 2.45	34.09 ± 1.76	27.87 ± 2.46	32.65 ± 1.35	33.43 ± 2.49	34.01 ± 1.57
ESR (mm/hr)	M	3.98 ± 0.08	3.76 ± 0.05	4.19 ± 0.09	3.80 ± 0.07	3.96 ± 0.03	3.87 ± 0.04	3.78 ± 0.08	3.82 ± 0.03	3.92 ± 0.01	3.82 ± 0.03
	F	4.23 ± 0.06	4.10 ± 0.09	4.33 ± 0.07	4.25 ± 0.05	4.09 ± 0.05	3.95 ± 0.03	3.74 ± 0.05	3.98 ± 0.06	3.78 ± 0.04	3.93 ± 0.02
Platelets ($\times 10^3$)/μL	M	1358 ± 176	1420 ± 189	1892 ± 151*	1677 ± 223*	1315 ± 279	1402 ± 254	**1665 ± 157***	1410 ± 163	1480 ± 270	1434 ± 246
	F	1262 ± 152	1356 ± 174	**1774 ± 170***	**1554 ± 235***	1369 ± 234	1323 ± 245	**1590 ± 162***	1309 ± 153	1354 ± 232	1325 ± 227
WBC ($\times 10^3$)/μL	M	9.42 ± 1.34	10.32 ± 1.51	**12.09 ± 1.51***	**11.49 ± 2.76***	9.54 ± 1.74	9.74 ± 1.87	**12.97 ± 1.54***	9.89 ± 1.47	9.51 ± 1.78	9.79 ± 1.74
	F	7.23 ± 0.87	8.56 ± 1.85	10.29 ± 0.70*	9.94 ± 0.87*	7.49 ± 0.90	7.41 ± 0.67	9.36 ± 0.86*	8.19 ± 1.68	7.47 ± 0.98	7.49 ± 0.63
Lymphocyte %	M	80.25 ± 4.21	83.25 ± 3.29	85.63 ± 5.36	82.44 ± 3.76	82.24 ± 4.29	80.29 ± 3.10	80.44 ± 4.26	81.47 ± 3.11	82.28 ± 4.21	80.23 ± 3.15
	F	82.16 ± 3.43	85.14 ± 4.67	88.82 ± 5.49	83.12 ± 3.56	84.15 ± 3.76	82.17 ± 3.44	81.98 ± 3.87	83.39 ± 4.78	84.35 ± 3.73	82.15 ± 3.56
Monocyte	M	0.20 ± 0.02	0.22 ± 0.06	0.21 ± 0.02	0.19 ± 0.03	0.18 ± 0.01	0.20 ± 0.01	0.23 ± 0.02	0.22 ± 0.08	0.19 ± 0.02	0.21 ± 0.02
	F	0.18 ± 0.01	0.19 ± 0.03	0.18 ± 0.01	0.16 ± 0.04	0.15 ± 0.07	0.18 ± 0.06	0.20 ± 0.01	0.20 ± 0.04	0.18 ± 0.05	0.17 ± 0.04
Neutrophil %	M	11.3 ± 1.43	10.5 ± 1.65	19.6 ± 2.87*	15.21 ± 1.56*	10.9 ± 2.22	11.4 ± 2.98	14.78 ± 1.67*	10.78 ± 1.58	9.59 ± 2.28	11.24 ± 2.78
	F	8.29 ± 2.30	7.97 ± 1.69	17.2 ± 1.36*	12.96 ± 3.44*	8.46 ± 1.35	8.04 ± 1.43	11.19 ± 2.55*	8.54 ± 2.55	7.88 ± 1.31	7.88 ± 1.31
	F	1.27 ± 0.05	1.64 ± 0.09	1.44 ± 0.06	1.25 ± 0.08	1.16 ± 0.02	1.26 ± 0.03	1.32 ± 0.02	1.47 ± 0.07	1.16 ± 0.01	1.21 ± 0.04
Eosinophil %	M	2.21 ± 0.21	2.34 ± 0.29	2.03 ± 0.34	2.34 ± 0.34	2.34 ± 0.26	2.29 ± 0.54	2.27 ± 0.17	2.30 ± 0.21	2.29 ± 0.29	2.27 ± 0.49
	F	1.98 ± 0.68	2.10 ± 0.77	1.76 ± 0.54	1.99 ± 0.67	1.99 ± 0.62	1.84 ± 0.59	2.07 ± 0.49	1.88 ± 0.63	1.97 ± 0.54	1.80 ± 0.43

Results are expressed as mean ± SD.

*$p < 0.05$ was considered significantly different as compared with the controls.

10.3389/fphar.2022.999078

TABLE 4 Serum clinical chemistry of rats sacrificed after 28-days repeated oral dose toxicity evaluation.

Parameter	Sex	Biochemical Data									
		Withametelin						Daturaolone			
		Normal	Vehicle	5	2.5	1.25	0.75	10	5	2.5	1.25
ALT U/L	M	29.31 ± 3.42	28.72 ± 2.91	39.91 ± 3.41*	35.14 ± 3.4*	30.36 ± 3.21	31.26 ± 2.56	34.89 ± 3.45*	30.14 ± 2.94	30.43 ± 3.23	29.30 ± 2.59
	F	22.52 ± 3.93	21.23 ± 2.18	32.26 ± 2.54*	29.87 ± 3.9*	31.51 ± 4.56	28.20 ± 4.21	27.97 ± 5.23*	25.67 ± 3.36	31.53 ± 4.65	28.65 ± 4.22
AST U/L	M	123.43 ± 3.98	133.52 ± 5.23	143.07 ± 4.21*	147.92 ± 7.24*	120.20 ± 4.67	125.87 ± 4.87	132.13 ± 5.67	125.87 ± 5.21	120.53 ± 4.83	125.54 ± 4.85
	F	110.97 ± 5.21	121.43 ± 6.42	135.45 ± 3.22*	139.53 ± 6.35*	107.57 ± 6.21	114.65 ± 4.86	120.78 ± 8.96	127.72 ± 5.55	107.63 ± 6.81	114.23 ± 4.82
ALP U/L	M	226.08 ± 10.23	237.98 ± 15.23	201.57 ± 15.68*	190.86 ± 13.74*	220.10 ± 12.46	222.71 ± 12.30	238.76 ± 13.38	240.92 ± 10.30	220.67 ± 12.93	222.62 ± 12.35
	F	150.97 ± 15.21	166.82 ± 8.77	133.93 ± 19.41*	141.83 ± 10.83*	155.71 ± 16.82	154.87 ± 16.71	170.87 ± 14.30	151.87 ± 6.21	155.87 ± 16.57	154.12 ± 16.76
Bilirubin mg/mL	M	3.82 ± 0.76	3.23 ± 1.23	3.56 ± 0.81	3.54 ± 0.79	3.15 ± 0.53	3.17 ± 0.62	4.80 ± 0.53*	3.68 ± 0.43	3.27 ± 0.47	3.45 ± 0.60
	F	2.43 ± 0.58	2.74 ± 0.93	2.63 ± 1.12	2.78 ± 0.91	2.56 ± 0.71	2.64 ± 0.54	3.58 ± 0.43*	2.73 ± 0.26	2.59 ± 0.54	2.34 ± 0.51
Albumin mg/dL	M	3.96 ± 0.94	3.87 ± 0.76	3.90 ± 0.78	3.99 ± 0.53	3.78 ± 0.48	3.99 ± 0.70	3.88 ± 0.62	3.68 ± 0.76	3.82 ± 0.51	3.67 ± 0.72
	F	4.17 ± 0.68	4.23 ± 0.54	3.61 ± 0.51	3.92 ± 0.78	3.80 ± 0.62	4.23 ± 0.39	4.37 ± 0.63	4.14 ± 0.52	3.78 ± 0.59	4.74 ± 0.33
Urea mg/dL	M	29.23 ± 1.78	31.70 ± 2.79	28.46 ± 1.48	39.87 ± 2.30	28.44 ± 3.34	30.44 ± 3.22	30.65 ± 3.67	29.89 ± 2.87	28.48 ± 3.40	30.83 ± 3.25
	F	30.26 ± 2.84	29.74 ± 4.32	30.78 ± 5.75	28.03 ± 3.34	29.30 ± 4.43	29.73 ± 3.21	32.11 ± 1.47	32.76 ± 3.62	29.28 ± 4.36	29.82 ± 3.22
BUN mg/dL	M	14.44 ± 1.19	15.23 ± 2.39	14.22 ± 2.19	15.25 ± 2.49	14.11 ± 1.18	15.23 ± 2.14	15.87 ± 2.30	16.12 ± 1.53	14.17 ± 1.21	15.54 ± 2.15
	F	15.17 ± 1.20	14.28 ± 2.30	13.47 ± 2.34	14.92 ± 1.37	14.25 ± 2.34	15.45 ± 3.33	16.24 ± 2.94	14.78 ± 1.67	14.32 ± 2.41	15.25 ± 3.32
Creatinine mg/dL	M	0.83 ± 0.13	0.89 ± 0.16	0.61 ± 0.57*	0.87 ± 0.19	0.82 ± 0.10	0.80 ± 0.14	1.93 ± 0.21*	0.90 ± 0.31	0.85 ± 0.09	0.57 ± 0.16
	F	0.81 ± 0.24	0.86 ± 0.27	0.57 ± 0.34*	0.86 ± 0.27	0.80 ± 0.16	0.79 ± 0.14	1.75 ± 0.30*	0.88 ± 0.07	0.82 ± 0.15	0.28 ± 0.17
Protein mg/dL	M	6.97 ± 0.51	6.74 ± 0.54	6.99 ± 0.76	6.12 ± 0.64	7.19 ± 0.76	6.95 ± 0.75	6.72 ± 0.87	6.75 ± 0.32	7.24 ± 0.71	6.34 ± 0.71
	F	6.73 ± 0.52	6.64 ± 0.49	6.34 ± 0.54	6.42 ± 0.46	6.89 ± 0.43	6.72 ± 0.86	6.79 ± 0.25	6.82 ± 0.24	6.94 ± 0.45	6.83 ± 0.83
Glucose mg/dL	M	82.78 ± 10.25	85.34 ± 9.54	68.49 ± 8.27*	73.29 ± 5.49*	86.19 ± 8.36	84.29 ± 11.49	65.93 ± 6.92*	81.78 ± 9.63	86.54 ± 8.46	84.25 ± 11.42
	F	94.56 ± 12.68	99.46 ± 10.89	75.24 ± 8.47*	83.72 ± 6.37*	91.24 ± 11.24	96.58 ± 9.34	78.48 ± 9.65*	92.54 ± 9.42	91.38 ± 11.12	96.63 ± 9.36
Cholesterol mMol/L	M	74.90 ± 4.91	77.64 ± 2.49	68.47 ± 2.31*	71.88 ± 3.43*	73.79 ± 6.24	75.55 ± 4.17	76.81 ± 4.86	80.32 ± 3.49	73.82 ± 6.66	75.28 ± 4.13
	F	55.81 ± 3.67	59.76 ± 4.59	49.18 ± 2.72*	51.37 ± 2.99*	57.86 ± 3.08	58.79 ± 3.52	63.44 ± 3.84	61.78 ± 4.38	57.89 ± 3.11	58.72 ± 3.55
Triglycerides mMol/L	M	90.29 ± 4.29	92.36 ± 5.19	83.46 ± 5.16*	81.79 ± 3.47*	89.24 ± 3.57	91.81 ± 6.76	96.19 ± 4.98	92.41 ± 3.81	89.62 ± 3.63	91.61 ± 6.71
	F	72.39 ± 5.18	77.31 ± 4.48	65.48 ± 7.64*	68.59 ± 6.64*	75.91 ± 6.49	74.22 ± 4.39	77.90 ± 5.92	74.21 ± 5.84	75.84 ± 6.50	74.48 ± 4.38
TSH ng/mL	M	4.82 ± 0.24	4.79 ± 0.29	3.14 ± 0.11*	3.88 ± 0.71*	4.70 ± 0.51	4.84 ± 0.43	4.58 ± 0.46	4.93 ± 0.25	4.69 ± 0.52	4.37 ± 0.41
	F	4.61 ± 0.34	4.66 ± 0.75	3.39 ± 0.26*	4.09 ± 0.64*	4.58 ± 0.25	4.65 ± 0.53	4.42 ± 0.37	4.54 ± 0.34	4.63 ± 0.26	4.52 ± 0.56
T3 ng/mL	M	1.75 ± 0.09	1.79 ± 0.24	1.88 ± 0.43*	1.80 ± 0.72*	1.73 ± 0.41	1.76 ± 0.53	1.73 ± 0.04	1.55 ± 0.28	1.69 ± 0.45	1.68 ± 0.51
	F	1.69 ± 0.10	1.74 ± 0.35	1.79 ± 0.58*	1.77 ± 0.57*	1.70 ± 0.23	1.61 ± 0.47	1.80 ± 0.16	1.59 ± 0.30	1.60 ± 0.26	1.63 ± 0.48
T4 ng/mL	M	60.47 ± 3.47	61.30 ± 4.76	81.24 ± 4.39*	75.73 ± 6.97*	64.19 ± 2.16	62.29 ± 4.13	65.53 ± 2.88	57.40 ± 3.76	57.38 ± 2.14	62.31 ± 4.12
	F	58.76 ± 2.64	63.67 ± 4.87	78.61 ± 5.37*	73.49 ± 6.84*	65.29 ± 3.42	60.94 ± 4.62	67.87 ± 3.52	54.63 ± 6.23	60.73 ± 3.49	60.48 ± 4.67

Results are expressed as mean ± SD.

*$p < 0.05$ was considered significantly different as compared with the controls.

10.3389/fphar.2022.999078

Treatment-related changes in rats liver and kidney and some more pronounced positive effects on testis (male) were also observed by H & E histology analyses in the group of daturaolone treated (10 mg/kg) as compared to the control group. No gender differential toxic affect was seen. In the kidney, the glomerular space of the kidney was distended and the epithelial cells around the tube were degenerated. In rats with high dose (10 mg/kg), the kidneys showed mild tubular kidney nephrosis characterized by increased cell proliferation, degenerated epithelial cells with the adsorption of pink proteinaceous material in the lumen of compressed proximal tubules (Figure 5). In addition, we found a mild tubular renal necrosis, vacuolar cytoplasm and pyknotic nuclei separated from the tubular lumen base membrane. The treated group of daturaolone (10 mg/kg) testes showed very few interstitial spaces between the seminiferous tubules and a decrease in the size of the lumen. At lower doses (1.25 and 0.75 mg/kg), a slight increase compared to normal seminiferous tubes with germ epithelium that containing germ cells were found proliferating at different stages at higher pace were observed which might signify its aphrodisiac character. In the liver, increase in sinusoidal space, mild inflammatory cell infiltration, edema and sinusoidal congestion were observed in 10 mg/kg groups in comparison to control. There were no significant adverse toxic effects observed at high dose on any other systemic organs of rats either male or female. Despite its lipophilic nature, no toxic effects were seen on the brain and tissues with normal neurocytes having well-defined nuclei in brain cortex were observed when compared to control.

4 Discussion

It is desirable to determine toxic end points at the beginning of the development of new molecules. Although secondary metabolites are mainly used for their biological benefits, their toxicity may limit their usage. Acute toxicity assessment fixed dose procedure (OECD guideline 420) at 5, 50, and 300 mg/kg with only the sighting study was performed. After years of controversy and discussion, the LD_{50} test was finally abolished at the end of 2002. Three substitute animal tests, the Fixed Dose Procedure, the Acute Toxic Class Method and the Up and Down procedures have been set up to significantly improve the welfare of animals (Botham, 2004). The method of fixed doses used in our study originates from a method proposed by the British Society of Toxicology (1984). As a final point, a reduction in the number of animals used for acute toxic testing and, if possible, avoiding fatalities are the final objective. Instead of using lethality, it is based on a clear toxic signal observed at a certain fixed dose level that is valid at the termination point in the European Economic Community (EEC) acute toxicity classification system (Lipnick et al., 1995).

In acute studies, no treatment related changes by daturaolone at all doses were observed while weight loss, abnormal posture, abnormal gait, diarrhoea and lethargy were observed in 300 mg/kg withametelin group as compared to control group. Changes in weight clearly showed some damage caused by test material (Liu et al., 2016). This weight decline might be due to the reduction in the use of food which was also observed in 28 days repeated dose study, indicating that withametelin might have adverse effects on the reduction of appetite. This was also due to mild diarrhea observed in first few days of a single dose, which was accompanied by lethargy. Withametelin was characterized as GHS category 4 drug with evident toxicity at 300 mg/kg while daturaolone as GHS category 5 or unclassified compound which might show toxicity at 2000 mg/kg in acute toxicity assessment. Weight differences are influenced by several factors such as growth hormone and somatostatin changes in hormone status as seen in sexual steroid secretion which influence maturation patterns and subsequential changes in neurotransmitters affecting food consumption. Furthermore, the rat environment and type of treatment can also be stressful for rat, resulting in weight changes (Zainul Azlan et al., 2020). Changes in weight are considered to be indicators of adverse reactions caused by chemical components. In the subacute toxicity, body weight gain, food and water consumption were normal in the daturaolone groups but significantly reduced in high dose (5 mg/kg withametelin) males and females. Meanwhile, during the treatment period, food consumption in both genders was significantly reduced during the treatment period. Insufficient nutrition may contribute to weight loss. However, a significant reduction in weight in high doses may be partly due to a reduction in food consumption (Li et al., 2022). In repeated dose-toxicity studies, dose-dependent transient salivation was also observed in groups treated with withametelin. The salivation affects two different dopamine receptors i.e., dopamine receptor (D1) and an invertebrate-specific D1-like dopamine receptor (D1L) (Li et al., 2018). D1 receptors act on the epithelial cells of the salivary glands acini for inward fluid transport. D1L modulates each acinus to excrete saliva from acini to the saliva ducts. It is likely that this is due to the action of myoepithelial cells and valves to pump/gate. Withametelin has the ability to dock with dopamine receptors (Baig et al., 2020) but checking the specific interaction with D1 receptors is proposed. Abnormal gait in last week was also seen with piloerection in rats given withametelin (5 and 2.5 mg/kg). Studies on withametelin has been associated with brain in our previous work ameliorating oxidative stress in brain and spinal cord (Khan et al., 2021b; 2021a). High doses of isolated compounds can be toxic due to their potential to react causing prooxidative effects or damaging beneficial ROS concentrations that normally exist under physiological conditions and are necessary for optimal cell function (Bouayed and Bohn, 2010). Aggressive antioxidative stress undermines the angiogenesis of endothelial cells in the brain and the functions of blood brain barrier (Mentor and Fisher, 2017). The automatic gait process is mediated by the brain stem to the spinal cord (Takakusaki, 2017). Daily dosing of 5 mg/kg might have cause detrimental effect on cerebral cortex causing abnormal gait but histopathological analysis suggested otherwise.

The hematopoietic system is one of the most vulnerable organs to the effects of hazardous substances and plays a significant role in

TABLE 5 Relative organ weight values of different organs of withametelin and daturaolone after necropsy.

Parameter	Sex	Relative organ weight per 100 g body weight									
		Withametelin (mg/kg)						Daturaolone (mg/kg)			
		Normal	Vehicle	5	2.5	1.25	0.75	10	5	2.5	1.25
Brain	M	0.45 ± 0.03	0.46 ± 0.02	0.45 ± 0.03	0.47 ± 0.05	0.46 ± 0.02	0.48 ± 0.03	0.46 ± 0.04	0.48 ± 0.04	0.47 ± 0.03	0.47 ± 0.04
	F	0.67 ± 0.04	0.69 ± 0.03	0.66 ± 0.07	0.69 ± 0.07	0.68 ± 0.04	0.69 ± 0.05	0.67 ± 0.06	0.68 ± 0.04	0.67 ± 0.03	0.68 ± 0.03
Kidney	M	0.68 ± 0.02	0.69 ± 0.03	0.68 ± 0.02	0.65 ± 0.02	0.67 ± 0.03	0.70 ± 0.08	0.68 ± 0.04	0.67 ± 0.03	0.68 ± 0.04	0.70 ± 0.07
	F	0.66 ± 0.03	0.66 ± 0.03	0.65 ± 0.03	0.68 ± 0.04	0.67 ± 0.03	0.66 ± 0.04	0.68 ± 0.03	0.66 ± 0.05	0.66 ± 0.05	0.68 ± 0.02
Heart	M	0.27 ± 0.02	0.28 ± 0.04	0.26 ± 0.02	0.29 ± 0.05	0.29 ± 0.04	0.30 ± 0.04	0.27 ± 0.02	0.28 ± 0.02	0.28 ± 0.02	0.29 ± 0.01
	F	0.28 ± 0.02	0.30 ± 0.03	0.27 ± 0.02	0.31 ± 0.08	0.31 ± 0.03	0.30 ± 0.03	0.28 ± 0.01	0.32 ± 0.03	0.32 ± 0.04	0.31 ± 0.02
Liver	M	2.97 ± 0.41	3.23 ± 0.02	3.31 ± 0.41	3.27 ± 0.46	3.33 ± 0.02	3.24 ± 0.02	3.30 ± 0.43	3.20 ± 0.42	3.27 ± 0.05	3.19 ± 0.03
	F	2.73 ± 0.22	3.15 ± 0.06	3.09 ± 0.25	3.23 ± 0.32	3.25 ± 0.08	3.18 ± 0.05	3.12 ± 0.22	3.26 ± 0.31	3.15 ± 0.04	3.23 ± 0.02
Lungs	M	0.33 ± 0.09	0.31 ± 0.05	0.34 ± 0.09	0.32 ± 0.03	0.32 ± 0.07	0.33 ± 0.05	0.35 ± 0.07	0.34 ± 0.02	0.33 ± 0.03	0.35 ± 0.04
	F	0.41 ± 0.02	0.39 ± 0.05	0.42 ± 0.03	0.44 ± 0.05	0.40 ± 0.05	0.38 ± 0.08	0.41 ± 0.04	0.43 ± 0.04	0.41 ± 0.06	0.42 ± 0.07
Spleen	M	0.16 ± 0.01	0.18 ± 0.02	0.16 ± 0.05	0.18 ± 0.05	0.17 ± 0.02	0.16 ± 0.02	0.17 ± 0.06	0.19 ± 0.03	0.18 ± 0.03	0.17 ± 0.03
	F	0.17 ± 0.01	0.17 ± 0.03	0.18 ± 0.04	0.19 ± 0.03	0.17 ± 0.06	0.17 ± 0.04	0.19 ± 0.07	0.18 ± 0.02	0.18 ± 0.05	0.18 ± 0.02
Testis	M	0.98 ± 0.04	0.96 ± 0.02	0.96 ± 0.05	0.99 ± 0.05	0.98 ± 0.04	0.98 ± 0.02	0.96 ± 0.04	0.98 ± 0.06	0.99 ± 0.02	0.95 ± 0.03
Ovary	F	0.83 ± 0.05	0.84 ± 0.04	0.86 ± 0.06	0.84 ± 0.03	0.83 ± 0.06	0.84 ± 0.07	0.85 ± 0.03	0.86 ± 0.04	0.85 ± 0.05	0.85 ± 0.05
Uterus	F	0.26 ± 0.03	0.25 ± 0.05	0.27 ± 0.04	0.28 ± 0.04	0.26 ± 0.06	0.25 ± 0.04	0.28 ± 0.02	0.27 ± 0.05	0.26 ± 0.05	0.27 ± 0.03

Results are expressed as mean ± SD.
*$p < 0.05$ was considered significantly different as compared with the controls.

both pathological and normal situations. The blood profile gives important details on how the body responds to stress and injury. As a result, a considerable amount of harmful substances are first exposed to blood cells. When findings from animal research are extrapolated (Shakya et al., 2020), changes in the hemotopoietic system have a better prognostic value for human toxicity. Unlike water or vehicle-treated rats, hematopoietic parameters were modified with withametelin and daturaolone treatment, which could prove their dangerous effect on the hematopoietic system. We observed significant decrease in daturaolone (10 mg/kg) and withametelin (5 and 2.5 mg/kg) treated RBC parameters suggesting possible indication of normocytic and microcytic anemia, respectively. A significant increase in platelets in the high dosed groups of withametelin only is contrary to previous findings where withametelin increased coagulation time via single oral administration (Baig et al., 2020). Thus, secondary thrombocytosis is the cause of this rise in platelet count. Both substances caused neutrophilic leukocytosis, as evidenced by an increase in haematological markers and a neutrophil infiltration of the liver by histology neutrophils. There are not many neutrophils that live in the liver, although they frequently patrol the sinusoids of the liver. They are the primary phagocyte types in charge of pathogen clearance and are capable of being quickly recruited into the liver after acute liver damage. However, overly active neutrophils may harm the liver. Neutrophils are therefore seen as a double-edged sword in acute liver inflammation (Tang et al., 2021).

ALT and AST were disturbed significantly by high dose withametelin while only ALT levels were changed by daturaolone which might have resulted in altered permeability of the hepatocellular membrane causing a release of these soluble cytosolic enzymes. Enzymes escape out from the hepatocytes causing elevation in the blood. ALP is considered to be a cholestasis inducer enzyme of hepatobiliary origin used widely to detect abnormal bile flow and has minimal activity in normal liver tissues. The ALP value in rats is reduced by food consumption and body weight reduction or frequent exposure to toxicological doses which might have lead to a decline in value (Ramaiah, 2007). Therefore, it is inconclusive to predict whether lowered ALP levels by withametelin were due to decreased food consumption or cholestasis has occurred. Low hemoglobin levels in daturaolone (10 mg/kg) might be due to abnormally high bilirubin. Bilirubin is generated from the stepwise catalytic degradation of hemoglobin by heme oxygenase and biliverdin reductase (Chung et al., 2019). This strengthens our previous hypothesis of anemia by withametelin. Withametelin and daturaolone also lowered glucose levels. Daturaolone is known to inhibit α-glucosidase (Bawazeer et al., 2020b) while withametelin inhibits both α-amylase and α-glucosidase enzymes (unpublished data). Natural components promote antioxidant defense and suppress the production of proinflammatory cytokines, producing

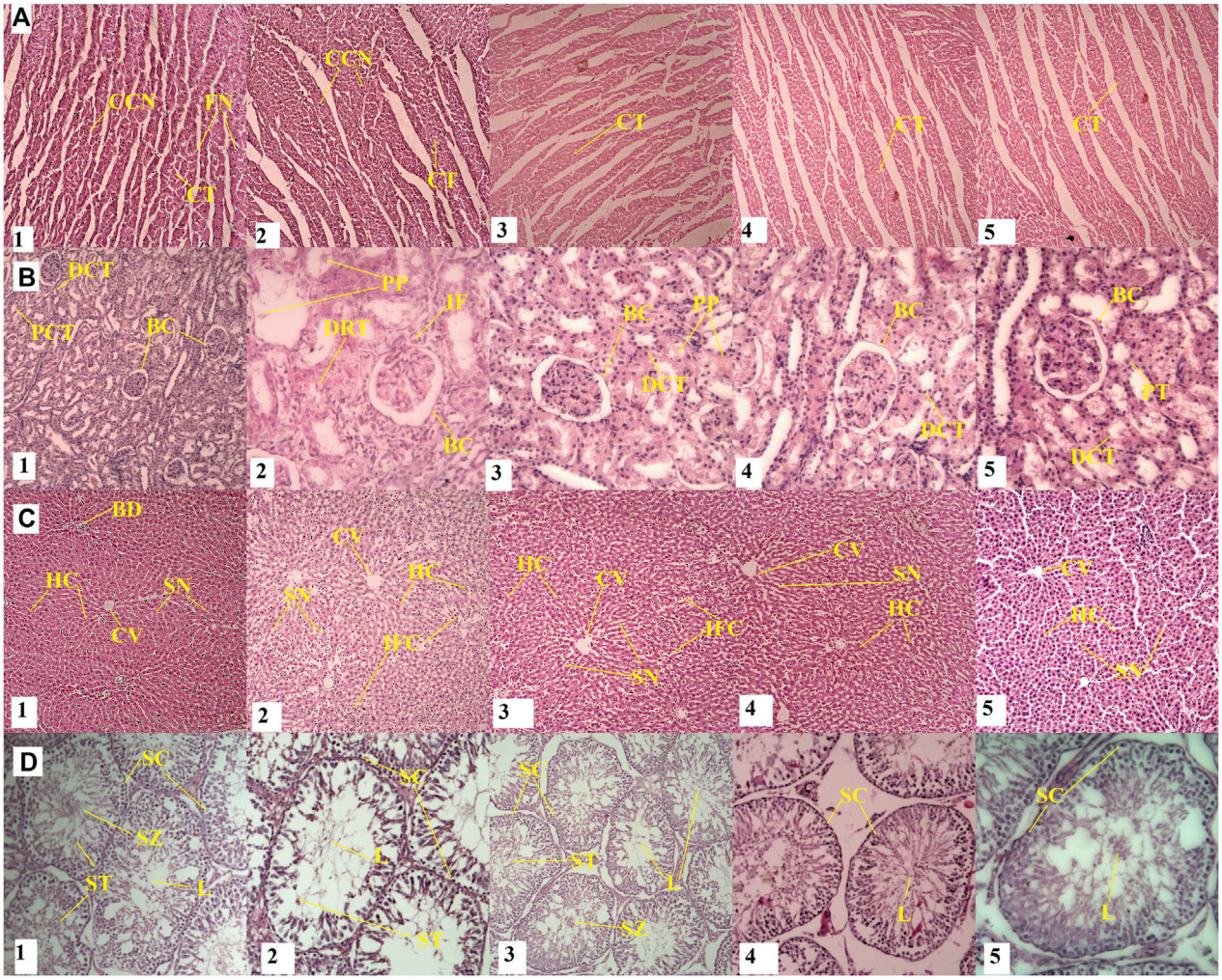

FIGURE 4
Effect of withametelin on the histology of organs. In the kidneys (B2 and B3), a mild infiltration of mononuclear inflammatory cells around tubules and the degeneration of epithelial cells, renal glomerular capsule space distention, interstitial swelling and congestion, and Pink proteinacious material at 5 mg/kg withametelin (B3) were seen. Tested in the treatment group with withametelin (5 mg/kg) (D2) showed an increase in the interstitial space between the seminiferous tubes, an increase in the lumen size and spermatogenesis stages showed mild sloughing. In the liver, there was an increase in the sinusoidal space, a slight infiltration of inflammatory cells, swelling, and sinusoidal congestion in 5 (C2) and 2.5 (C3) mg/kg groups in comparison to control was observed. No histological changes were seen in heart. A-D represents, heart kidney, liver and testes respectively. 1-5 represents different dose groups i.e., normal or vehicle, 5, 2.5, 1.25, and 0.75 mg/kg. CCN; Cardiac cell nucleus, CT, Cardiac tissue; FN, Fibroblast nucleus; BC, Bowman's Capsule; DCT, Distal convoluted tubules; PCT, Proximal convoluted tubules; PP, Pink proteinaceous material; DRT, Damaged renal tubule; BD, Biliary duct; HC, Hepatocytes; SN, Sinusoids; CV, Central vein; IFC, Inflammatory cells; SC, Spermatocytes; SZ, Spermatozoa; ST, Spermatids; L, Lumen.

biological activity by improving antioxidant defence mechanisms. Low-cellular stressor dosages of chemicals lead to an adaptive response that increases the antioxidant capacity of cells (Rong et al., 2020).

Hyperthyroidism noted in withametelin (5 and 2.5 mg/kg) groups might be associated with reduction in serum creatinine caused by reduction in overall muscle mass (Iglesias et al., 2017). The decrease in cholesterol and triglycerides observed could be due to increased LDL receptor expression in hepatocytes, increased activity of liver enzymes that reduce lipids, resulting in a reduction in low-density lipoprotein levels by hyperthyroidism. Thyroid hormones also increase expression of A1 apolipoprotein, the main component of high density lipoprotein (Malik and Hodgson, 2002). Histopathological changes in the testicles may also be caused by hyperthyroidism, which delays the development of the Leydig cells and has a negative impact on sperm formation. Other effects secondary to thyrotoxicity such as decrease in total body water and exchangeable potassium, increase in cardiac output and increase in systolic blood pressure needs detailed investigation and validation.

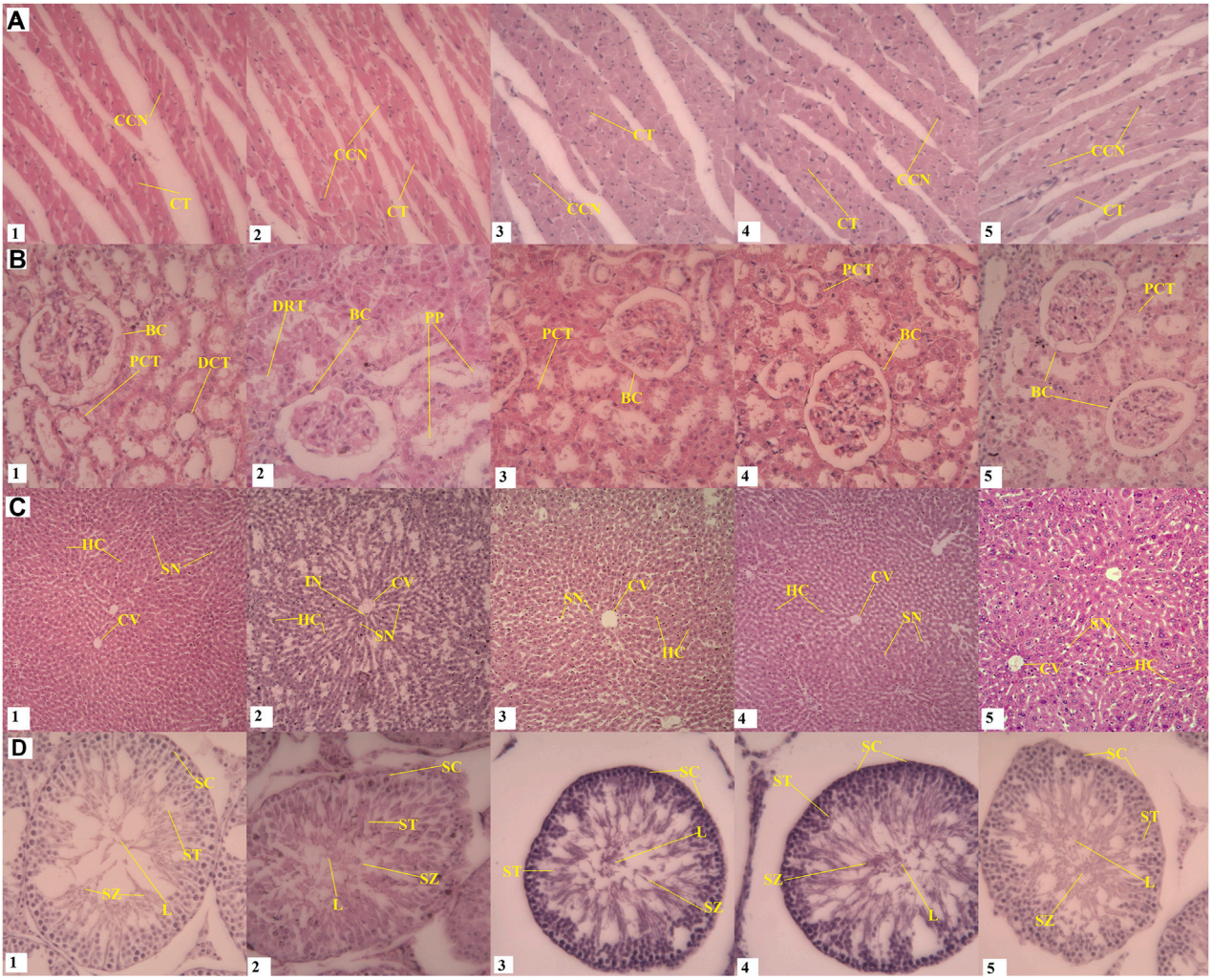

FIGURE 5
Effect of daturaolone on the histology of organs. Kidney histopathology (B2) showed mild tubular kidney nephrosis, cell proliferation, degenerated epithelial cells, adsorption of pink proteinaceous material in the lumen of compressed proximal tubules. Mild tubular renal necrosis and vacuolar cytoplasm from the tubular lumen base membrane. Testes (D2) showed very few interstitial spaces between the seminiferous tubules and a decrease in the size of the lumen. In D3 and D4, a slight increase compared to normal seminiferous tubes with germ epithelium that contain germ cells were found proliferating at different stages at higher pace were observed which might signify aphrodisiac character. In the liver (C2), increase in sinusoidal space, mild inflammatory cell infiltration, edema and sinusoidal congestion were observed in comparison to control (C1) No histological changes were seen in heart. A-D represents heart, kidney, liver and testes respectively. 1-5 represents different dose groups i.e., normal or vehicle, 10, 5, 2.5 and 1.25 mg/kg. CCN; Cardiac cell nucleus, CT, Cardiac tissue; FN, Fibroblast nucleus; BC, Bowman's Capsule; DCT, Distal convoluted tubules; PCT, Proximal convoluted tubules; PP, Pink proteinaceous material; DRT, Damaged renal tubule; BD, Biliary duct; HC, Hepatocytes; SN, Sinusoids; CV, Central vein; IFC, Inflammatory cells; SC, Spermatocytes; SZ, Spermatozoa; ST, Spermatids; L, Lumen.

5 Conclusion

In summary, GHS classification model characterize withametelin as category 4 and daturaolone as category 5 compound in acute toxicity studies. After the 28-days repeated oral dose subacute toxicity study, NOAEL of withametelin is 1.25 mg/kg and of daturaolone is 5 mg/kg. Weight loss, hyperthyroidism, high platelets, neutrophils, ALT and AST in high dose (5 and 2.5 mg/kg) withametelin groups was prominently observed. Abnormal biochemical changes mainly in ALT levels and glucose indices were seen in high dose (10 mg/kg) daturaolone groups. Sex specific testicular histological changes were also observed by both compounds. Long term studies with more behavioral, biochemical, histopathological and hormonal parameters are proposed to strengthen the findings.

Data availability statement

The raw data supporting the conclusions of this article will be made available by the authors, without undue reservation.

Ethics statement

The animal study was reviewed and approved by Institutional Animal Ethics Committee of Department of Pharmacy, Quaid e Azam University (letter number # BEC-FBS-QAU2019-135).

Author contributions

MWB: Methodology, Software, Validation, Investigation, Writing original draft, Funding acquisition, Review, Revision and Editing I-UH Supervision, Resources, Project administration, Writing Review and Editing, SSUH and SB Resources, Project administration, Writing Review and Editing MM: Methodology, Validation, Review, Revision and Editing BN: Methodology, Software, Review, Revision and Editing.

Acknowledgments

HEC Pakistan is acknowledged for the funding through Indigenous PhD fellowship program for Muhammad Waleed Baig to execute the study. The authors wish to thank to University of Oradea, Oradea, Romania for financial support in publishing this paper.

Conflict of interest

The authors declare that the research was conducted in the absence of any commercial or financial relationships that could be construed as a potential conflict of interest.

Publisher's note

All claims expressed in this article are solely those of the authors and do not necessarily represent those of their affiliated organizations, or those of the publisher, the editors and the reviewers. Any product that may be evaluated in this article, or claim that may be made by its manufacturer, is not guaranteed or endorsed by the publisher.

References

Akhtar, N., Baig, M. W., Haq, I.-U., Rajeeve, V., and Cutillas, P. R. (2020). Withanolide metabolites inhibit PI3K/AKT and MAPK pro-survival pathways and induce apoptosis in acute myeloid leukemia cells. *Biomedicines* 8, E333. doi:10.3390/biomedicines8090333

Anjum, K., Abbas, S. Q., Akhter, N., Shagufta, B. I., Shah, S. A. A., and Hassan, S. S. ul (2017). Emerging biopharmaceuticals from bioactive peptides derived from marine organisms. *Chem. Biol. Drug Des.* 90, 12–30. doi:10.1111/cbdd.12925

Baig, M. W., Fatima, H., Akhtar, N., Hussain, H., Okla, M. K., et al. (2021). Anti-inflammatory potential of daturaolone from Datura innoxia mill.: *In silico*, *in vitro* and *in vivo* studies. *Pharm. (Basel, Switz.* 14, 1248. doi:10.3390/ph14121248

Baig, M. W., Nasir, B., Waseem, D., Majid, M., Khan, M. Z. I., et al. (2020). Withametelin: A biologically active withanolide in cancer, inflammation, pain and depression. *Saudi Pharm. J.* 28, 1526–1537. doi:10.1016/j.jsps.2020.09.021

Bawazeer, S., Rauf, A., and Bawazeer, S. (2020a). Gastrointestinal motility, muscle relaxation, antipyretic and acute toxicity screening of amyrin type triterpenoid (daturaolone) isolated from Datura metel linnaeus (Angel's Trumpet) Fruits. *Front. Pharmacol.* 11, 544794. doi:10.3389/fphar.2020.544794

Bawazeer, S., Rauf, A., and Bawazeer, S. (2020b). Potent *in vitro* α-Glucosidase and β-Secretase Inhibition of Amyrin-Type Triterpenoid Isolated from Datura metel Linnaeus (Angel's Trumpet) Fruits. *Biomed. Res. Int.* 2020, 8530165. doi:10.1155/2020/8530165

Botham, P. A. (2004). Acute systemic toxicity--prospects for tiered testing strategies. *Toxicol. Vitro* 18, 227–230. doi:10.1016/s0887-2333(03)00143-7

Bouayed, J., and Bohn, T. (2010). Exogenous antioxidants--Double-edged swords in cellular redox state: Health beneficial effects at physiologic doses versus deleterious effects at high doses. *Oxid. Med. Cell. Longev.* 3, 228–237. doi:10.4161/oxim.3.4.12858

Chen, J., Zou, Q., and Li, J. (2022). DeepM6ASeq-EL: Prediction of Human N6-Methyladenosine (M6A) Sites with LSTM and Ensemble Learning. *Front. Comput. Sci.* 16, 162302. doi:10.1007/s11704-020-0180-0

Chen, L.-X., He, H., and Qiu, F. (2011). Natural withanolides: an overview. *Nat. Prod. Rep.* 28, 705–740. doi:10.1039/c0np00045k

Chung, J. O., Park, S.-Y., Chung, D. J., and Chung, M. Y. (2019). Relationship between anemia, serum bilirubin concentrations, and diabetic retinopathy in individuals with type 2 diabetes. *Medicine* 98, e17693. doi:10.1097/MD.0000000000017693

Díez-Quijada, L., Moyano, R., Molina-Hernández, V., Cameán, A. M., and Jos, Á. (2021). Evaluation of toxic effects induced by repeated exposure to Cylindrospermopsin in rats using a 28-day feeding study. *Food Chem. Toxicol.* 151, 112108. doi:10.1016/j.fct.2021.112108

Hassan, S. S. U., Muhammad, I., Abbas, S. Q., Hassan, M., Majid, M., Jin, H. Z., et al. (2021). Stress driven discovery of natural products from actinobacteria with anti-oxidant and cytotoxic activities including docking and admet properties. *Int. J. Mol. Sci.* 22, 11432. doi:10.3390/ijms222111432

Hassan, S. S. U., Zhang, W.-D., Jin, H.-Z., Basha, S. H., and Priya, S. V. S. S. (2022). *In-silico* anti-inflammatory potential of guaiane dimers from Xylopia vielana targeting COX-2. *J. Biomol. Struct. Dyn.* 40, 484–498. doi:10.1080/07391102.2020.1815579

Iglesias, P., Bajo, M. A., Selgas, R., and Díez, J. J. (2017). Thyroid dysfunction and kidney disease: An update. *Rev. Endocr. Metab. Disord.* 18, 131–144. doi:10.1007/s11154-016-9395-7

Ji, X., Hou, C., Gao, Y., Xue, Y., Yan, Y., and Guo, X. (2020). Metagenomic analysis of gut microbiota modulatory effects of jujube (Ziziphus jujuba Mill.) polysaccharides in a colorectal cancer mouse model. *Food Funct.* 11, 163–173. doi:10.1039/c9fo02171j

Khan, A., Shal, B., Khan, A. U., Bibi, T., Islam, S. U., Baig, M. W., et al. (2021a). Withametelin, a novel phytosterol, alleviates neurological symptoms in EAE mouse model of multiple sclerosis via modulation of Nrf2/HO-1 and TLR4/NF-κB signaling. *Neurochem. Int.* 151, 105211. doi:10.1016/j.neuint.2021.105211

Khan, A., Shal, B., Khan, A. U., Ullah, R., Baig, M. W., Ul Haq, I., et al. (2021b). Suppression of TRPV1/TRPM8/P2Y Nociceptors by Withametelin via Downregulating MAPK Signaling in Mouse Model of Vincristine-Induced Neuropathic Pain. *Int. J. Mol. Sci.* 22, 6084. doi:10.3390/ijms22116084

Khan, I., Abbas, T., Anjum, K., Abbas, S. Q., Shagufta, B. I., Shah, S. A. A., et al. (2019). Antimicrobial potential of aqueous extract of Camellia sinensis against representative microbes. *Pak. J. Pharm. Sci.* 32, 631–636.

Li, X., Liao, X., Yan, X., Yuan, Y., Yuan, Z., Liu, R., et al. (2022). Acute and subacute oral toxicity of artemisinin-hydroxychloroquine sulfate tablets in rats. *Regul. Toxicol. Pharmacol.* 129, 105114. doi:10.1016/j.yrtph.2022.105114

Lai, W.-F., Gui, D., Wong, M., Döring, A., Rogach, A. L., He, T., et al. (2021). A self-indicating cellulose-based gel with tunable performance for bioactive agent delivery. *J. Drug Deliv. Sci. Technol.* 63, 102428. doi:10.1016/j.jddst.2021.102428

Lai, W.-F. (2020). Non-conjugated polymers with intrinsic luminescence for drug delivery. *J. Drug Deliv. Sci. Technol.* 59, 101916. doi:10.1016/j.jddst.2020.101916

Li, C., Jiang, W., Gao, Y., Lin, F., Zhu, H., Wang, H., et al. (2018). Acute, subchronic oral toxicity, and genotoxicity evaluations of LPM570065, a new potent triple reuptake inhibitor. *Regul. Toxicol. Pharmacol.* 98, 129–139. doi:10.1016/j.yrtph.2018.07.011

Lipnick, R. L., Cotruvo, J. A., Hill, R. N., Bruce, R. D., Stitzel, K. A., Walker, A. P., et al. (1995). Comparison of the up-and-down, conventional LD50, and fixed-dose acute toxicity procedures. *Food Chem. Toxicol.* 33, 223–231. doi:10.1016/0278-6915(94)00136-c

Liu, X., Zheng, L., Zhang, R., Liu, G., Xiao, S., Qiao, X., et al. (2016). Toxicological evaluation of advanced glycation end product Nε-(carboxymethyl)lysine: Acute and subacute oral toxicity studies. *Regul. Toxicol. Pharmacol.* 77, 65–74. doi:10.1016/j.yrtph.2016.02.013

Majid, M., Farhan, A., Asad, M. I., Khan, M. R., Hassan, S. S. U., Haq, I.-U., et al. (2022). An Extensive Pharmacological Evaluation of New Anti-Cancer Triterpenoid (Nummularic Acid) from Ipomoea batatas through *in vitro*, *in silico*, and *in vivo* Studies. *Molecules.* 27, 2474. doi:10.3390/molecules27082474

Majid, M., Ijaz, F., Baig, M. W., Nasir, B., Khan, M. R., and Haq, I.-U. (2019). Scientific Validation of Ethnomedicinal Use of Ipomoea batatas L. Lam. as Aphrodisiac and Gonadoprotective Agent against Bisphenol A Induced Testicular Toxicity in Male Sprague Dawley Rats. *Biomed. Res. Int.*, 8939854. doi:10.1155/2019/8939854

Malik, R., and Hodgson, H. (2002). The relationship between the thyroid gland and the liver. *QJM Mon. J. Assoc. Physicians* 95, 559–569. doi:10.1093/qjmed/95.9.559

Mentor, S., and Fisher, D. (2017). Aggressive Antioxidant Reductive Stress Impairs Brain Endothelial Cell Angiogenesis and Blood Brain Barrier Function. *Curr. Neurovasc. Res.* 14, 71–81. doi:10.2174/1567202613666161129113950

Muhammad, I., Shams ul Hassan, S., Cheung, S., Li, X., Wang, R., Zhang, W. D., et al. (2021). Phytochemical study of Ligularia subspicata and valuation of its anti-inflammatory activity. *Fitoterapia* 148, 104800. doi:10.1016/j.fitote.2020.104800

Nasir, B., Baig, M. W., Majid, M., Ali, S. M., Khan, M. Z. I., Kazmi, S. T. B., et al. (2020). Preclinical anticancer studies on the ethyl acetate leaf extracts of Datura stramonium and Datura inoxia. *BMC Complement. Med. Ther.* 20, 188. doi:10.1186/s12906-020-02975-8

Obireddy, S. R., and Lai, W.-F. (2021a). Multi-Component Hydrogel Beads Incorporated with Reduced Graphene Oxide for pH-Responsive and Controlled Co-Delivery of Multiple Agents. *Pharmaceutics* 13, 313. doi:10.3390/pharmaceutics13030313

Obireddy, S. R., and Lai, W.-F. (2021b). Preparation and characterization of 2-hydroxyethyl starch microparticles for co-delivery of multiple bioactive agents. *Drug Deliv.* 28, 1562–1568. doi:10.1080/10717544.2021.1955043

Parasuraman, S. (2011). Toxicological screening. *J. Pharmacol. Pharmacother.* 2, 74–79. doi:10.4103/0976-500X.81895

Ramaiah, S. K. (2007). A toxicologist guide to the diagnostic interpretation of hepatic biochemical parameters. *Food Chem. Toxicol.* 45, 1551–1557. doi:10.1016/j.fct.2007.06.007

Rao, P. C., Begum, S., Jahromi, M. A. F., Jahromi, Z. H., Sriram, S., and Sahai, M. (2016). Cytotoxicity of withasteroids: withametelin induces cell cycle arrest at G2/M phase and mitochondria-mediated apoptosis in non-small cell lung cancer A549 cells. *Tumour Biol.* 37, 12579–12587. doi:10.1007/s13277-016-5128-5

Rong, X., Jiang, L., Qu, M., Hassan, S. S. U., and Liu, Z. (2020). Enhancing Therapeutic Efficacy of Donepezil by Combined Therapy: A Comprehensive Review. *Curr. Pharm. Des.* 27, 332–344. doi:10.2174/1381612826666201023144836

Shakya, A., Chaudhary, S. K., Bhat, H. R., and Ghosh, S. K. (2020). Acute and sub-chronic toxicity studies of Benincasa hispida (Thunb.) cogniaux fruit extract in rodents. *Regul. Toxicol. Pharmacol.* 118, 104785. doi:10.1016/j.yrtph.2020.104785

Shams ul Hassan, S., Abbas, S. Q., Hassan, M., and Jin, H.-Z. (2021). Computational Exploration of Anti-Cancer Potential of Guaiane Dimers from Xylopia vielana by Targeting B-Raf Kinase Using Chemo-Informatics, Molecular Docking and MD Simulation Studies. *Anticancer. Agents Med. Chem.* 21, 731–746. doi:10.2174/1871520621666211013115500

Shams ul Hassan, S., Qamar Abbas, S., Ali, F., Ishaq, M., Bano, I., Hassan, M., et al. (2022). A Comprehensive *in silico* Exploration of Pharmacological Properties, Bioactivities, Molecular Docking, and Anticancer Potential of Vieloplain F from Xylopia vielana Targeting B-Raf Kinase. *Molecules* 27, 917. doi:10.3390/molecules27030917

Singh, U. P., Prakash, O., and Ray, A. B. (2001). Antifungal Activity of Withametelin, a Withanolide Isolated from Datura metel. *Mycobiology* 29, 96–99. doi:10.1080/12298093.2001.12015768

Takakusaki, K. (2017). Functional Neuroanatomy for Posture and Gait Control. *J. Mov. Disord.* 10, 1–17. doi:10.14802/jmd.16062

Tang, J., Yan, Z., Feng, Q., Yu, L., and Wang, H. (2021). The Roles of Neutrophils in the Pathogenesis of Liver Diseases. *Front. Immunol.* 12, 625472. doi:10.3389/fimmu.2021.625472

Wu, X., Wan, D., Xie, C., Li, T., Huang, R., Shu, X., et al. (2015). Acute and sub-acute oral toxicological evaluations and mutagenicity of N-carbamylglutamate (NCG). *Regul. Toxicol. Pharmacol.* 73, 296–302. doi:10.1016/j.yrtph.2015.07.009

Xiao, Y., Zhu, S., Wu, G., ul Hassan, S. S., Xie, Y., Ishaq, M., et al. (2020). Chemical Constituents of Vernonia parishii. *Chem. Nat. Compd.* 56, 134–136. doi:10.1007/s10600-020-02963-x

Yimam, M., Jiao, P., Hong, M., Brownell, L., Kim, H.-J., Lee, Y.-C., et al. (2018). Repeated dose 28-day oral toxicity study of a botanical composition composed of Morus alba and Acacia catechu in rats. *Regul. Toxicol. Pharmacol.* 94, 115–123. doi:10.1016/j.yrtph.2018.01.024

Zainul Azlan, N., Abd Ghafar, N., Mohd Yusof, Y. A., and Makpol, S. (2020). Toxicity study of Chlorella vulgaris water extract on female Sprague Dawley rats by using the Organization for Economic Cooperation and Development (OECD) Guideline 420. *J. Appl. Phycol.* 32, 3063–3075. doi:10.1007/s10811-020-02195-0

frontiers | Frontiers in Pharmacology

TYPE Original Research
PUBLISHED 28 September 2022
DOI 10.3389/fphar.2022.987800

Check for updates

OPEN ACCESS

EDITED BY
Fareeha Anwar,
Riphah International University (Lahore), Pakistan

REVIEWED BY
Qurat Ul Ain,
Riphah International University (Lahore), Pakistan
Uzma Saleem,
Government College University, Pakistan

*CORRESPONDENCE
Zi-hui Yang,
yangzihui_2021@hunau.edu.cn
Jian-guo Zeng,
zengjianguo@hunau.edu.cn

SPECIALTY SECTION
This article was submitted to Predictive Toxicology, a section of the journal Frontiers in Pharmacology

RECEIVED 06 July 2022
ACCEPTED 06 September 2022
PUBLISHED 28 September 2022

CITATION
Dong Z, Tang S-s, Ma X-l, Tan B, Tang Z-s, Li C-h, Yang Z-h and Zeng J-g (2022), Acute, chronic, and genotoxic studies on the protopine total alkaloids of the Macleaya cordata (willd.) R. Br. in rodents.
Front. Pharmacol. 13:987800.
doi: 10.3389/fphar.2022.987800

COPYRIGHT
© 2022 Dong, Tang, Ma, Tan, Tang, Li, Yang and Zeng. This is an open-access article distributed under the terms of the Creative Commons Attribution License (CC BY). The use, distribution or reproduction in other forums is permitted, provided the original author(s) and the copyright owner(s) are credited and that the original publication in this journal is cited, in accordance with accepted academic practice. No use, distribution or reproduction is permitted which does not comply with these terms.

Acute, chronic, and genotoxic studies on the protopine total alkaloids of the *Macleaya cordata* (willd.) R. Br. in rodents

Zhen Dong[1,2], Shu-sheng Tang[3], Xiao-lan Ma[4], Bin Tan[1,2], Zhao-shan Tang[5], Chang-hong Li[5], Zi-hui Yang[1,2]* and Jian-guo Zeng[1,2]*

[1]College of Veterinary Medicine, Hunan Agricultural University, Changsha, China, [2]Key Laboratory of Chinese Veterinary Medicine in Hunan Province, Hunan Agricultural University, Changsha, China, [3]College of Veterinary Medicine, China Agricultural University, Beijing, China, [4]College of Veterinary Medicine, Shanxi Agricultural University, Jinzhong, China, [5]Hunan MICOLTA Biological Resources Co.,Ltd, Changsha, China

The protopine alkaloids are widely distributed within the opium poppy family and have a wide range of pharmacological effects. MPTA is a product of the protopine total alkaloids extracted from the *Macleaya cordata* (Willd.) R. Br. Previously, we reported good anti-inflammatory activity of MPTA as well as oral acute and sub-chronic toxicity studies in rats. In order to perform a systematic toxicological safety assessment of MPTA, oral acute toxicity, genotoxicity (bone marrow cell chromosome aberration test, sperm abnormality test, bone marrow cell micronucleus test, and rat teratogenicity test), and chronic toxicity in mice were performed in this study. In the oral acute toxicity test, the LD_{50} in ICR mice was 481.99 mg/kg, with 95% confidence limits ranging from 404.27 to 574.70 mg/kg. All three mutagenicity tests tested negative in the range of 60.25–241.00 mg/kg. The results of the teratogenicity test in rats showed no reproductive or embryonic developmental toxicity at only 7.53 mg/kg, which can be considered as a no observed effect level (NOEL) for the teratogenicity test. Therefore, MPTA is safe for use at the doses tested, but attention should be paid to the potential risk to pregnant animals and the safety evaluation and toxicity mechanisms in target animals should be further investigated.

KEYWORDS

Macleaya cordata (willd.) R. Br., protopine alkaloids, acute toxicity, chronic toxicity, mutagenicity, teratogenicity, reproductive toxicity, embryonic developmental toxicity

Introduction

Protopine alkaloids (PAs), represented by protopine (PRO) and allocryptopine (ALL), are a class of berberine ring-opening compounds containing carbonyl groups, which are widely distributed within the poppy family, such as *Macleaya cordata* (Willd.) R. Br., *Hypecoum erectum* L., *Eomecon chionantha* Hance, and *Corydalisyanhusuo* W.T. Wang,

which is often used in traditional Chinese medicine (Cai et al., 2020; Lu et al., 2020; Xu et al., 2021; Yuan et al., 2021). There is abundant evidence that PRO is one of the material bases for the traditional effects of *Corydalisyanhusuo* W.T. Wang, namely promoting the flow of qi and blood and relieving pain. PRO and ALL were also considered to be quality markers for Yuanhu Zhitong tablets, an herbal formula containing *Corydalisyanhusuo* W.T. Wang (Li et al., 2018). Modern pharmacological studies have shown that PRO has anti-platelet agglutination and antithrombotic effects, and inhibits both phospholipase and thromboxane synthase (Shiomoto et al., 1990, 1991; Saeed et al., 1997); PRO can exert analgesic effects by modulating dopamine receptor D2 (DRD2) mRNA expression and inhibiting voltage-gated sodium channels (Xu et al., 2021; Zhang et al., 2021); PRO and ALL have also been reported to have potential anti-inflammatory, anti-cancer, antioxidant and anti-arrhythmic activities (Fu et al., 2016; Alam et al., 2019; Nigdelioglu Dolanbay et al., 2021; Yuan et al., 2021). Previously, we reported that protopine total alkaloids (MPTA), isolated from the acidic waste stream used for the extraction of the benzophenanthridine alkaloids in *Macleaya cordata* (*M. cordata*), showed good inhibitory effects on carrageenan and xylene-induced inflammatory edema in rats (Dong et al., 2022b). We have also experimented with the use of MPTA in laying hens to improve intestinal health and egg quality (Liu et al., 2022).

Although PAs exhibit good pharmacological activity, little information on their toxicology has been reported. To date, only one study has reported oral acute toxicity results in mice for PRO isolated from *M. cordata* (Hu et al., 2021). In that study, PRO was considered to be the most toxic compound in *M. cordata*, with an oral LD_{50} of 313.10 mg/kg in mice. Our laboratory previously conducted oral acute toxicity and 90-days subchronic toxicity studies of MPTA in SD rats. The oral LD_{50} of MPTA for rats was 481.99 mg/kg, and at the dose tested, MPTA showed no significant subchronic toxicity, with a no observed effect level (NOEL) considered to be 96.40 mg/kg/day (Dong et al., 2022a). Other than that, other toxicological information is still unclear. Therefore, in order to systematically understand the safety of MPTA and to describe the potential systemic and genotoxic risks of MPTA under long-term exposure, this study conducted oral acute toxicity tests in mice, chronic toxicity tests in rats and standardized genotoxicological studies on MPTA with reference to the Chinese Regulations for the Registration of Veterinary Drugs and the Compendium of Technical Guidelines for Veterinary Drug Research to provide support and guidance for further clinical studies on MPTA.

Materials and methods

Reagents and test drugs

MPTA (PRO ≥35%, and ALL ≥15%) was supplied by Hunan MICOLTA Biological Resources Co. Cyclophosphamide (CTX) was purchased from Tianjin Chemical Reagent Company (Tianjin, China). Other reagents were purchased from Aladdin (Shanghai, China) and Sinopharm Chemical Reagent Co., Ltd (Shanghai, China).

Animals

Sprague Dawley (SD) rats and Institute of Cancer Research (ICR) mice were purchased from Beijing Vital River Laboratory Animal Technology Co., Ltd (Beijing, China). The animals were housed in a standard GLP-compliant environment (room temperature: 22–24°C; relative humidity: 55 ± 10%, 12-h artificial light/dark cycle) and given a standard maintenance diet and clean drinking water. All test animals were examined for general physical condition and environmental acclimatization for 7 days. Mice were fasted for 8 h prior to gavage administration of MPTA, but were allowed to drink freely. All animal experiments were approved by the Animal Ethics Committee of China Agricultural University (WTPJ20120022) and strictly followed American Veterinary Medical Association. During the test, test animals with obvious toxicity symptoms or near death were euthanized promptly.

Experimental design and methods

Oral acute toxicity test in mice

This part of the test was conducted according to the guidelines for acute toxicity (LD_{50} determination) of

TABLE 1 Oral acute toxicity of MPTA to mice (n = 10).

Dose group (mg/kg)	Number of animals	Number of deaths	Mortality rate (%)	Survival rate (%)
1000.00	10	10	100	0
666.67	10	8	80	20
444.44	10	4	40	60
296.30	10	1	10	90
197.53	10	0	0	100

TABLE 2 Effect of MPTA on sperm malformation in mice (n = 5).

Groups	Sperm test count	Abnormal sperm count	Sperm abnormality rate	Percentage of each type of abnormal sperm (%)						
				No hook	Banana-shaped	Amorphous	Fathead	Tail-folded	Double-headed	Double-tailed
241.00 mg/kg	5 × 1000	134	2.76 ± 0.84	12.69 ± 0.82	14.93 ± 0.15**	33.58 ± 0.47	14.18 ± 0.27*	14.93 ± 0.73	3.73 ± 0.65	5.97 ± 0.14**
120.50 mg/kg	5 × 1000	141	2.91 ± 0.82	14.89 ± 0.94*	14.18 ± 0.59**	34.04 ± 0.88	13.48 ± 0.69	12.77 ± 0.79	2.84 ± 0.41	7.80 ± 0.51*
60.25 mg/kg	5 × 1000	118	2.42 ± 0.63	10.17 ± 0.50	11.86 ± 0.66**	36.44 ± 1.23	13.56 ± 0.52	11.02 ± 0.67	5.93 ± 0.49*	11.02 ± 0.75
Negative control	5 × 1000	135	2.78 ± 0.91	11.85 ± 0.70	21.48 ± 1.19	29.63 ± 1.12	10.37 ± 0.73	13.33 ± 0.79	2.96 ± 0.41	10.37 ± 0.73
Positive control	5 × 1000	418	9.12 ± 1.44**	9.57 ± 0.97	7.66 ± 1.05**	51.20 ± 2.13**	11.00 ± 1.49	10.77 ± 1.41	3.83 ± 0.70	5.98 ± 1.07**

Note: Data are compared with negative controls, * indicates significant differences ($p < 0.05$), ** indicates significant differences ($p < 0.01$).

veterinary drugs issued by the Ministry of Agriculture and Rural Affairs of the People's Republic of China (MARA, PRC) (Ministry of Agriculture and Rural Affairs of PRC, 2009d). Based on the results of the pre-experiments, the doses were determined as 1000.00, 666.67, 444.44, 296.30 and 197.53 mg/kg. Fifty ICR mice, weighing 18–22 g, were randomly divided into five groups of 10 mice each, with five males and five females in each group. Mice were gavaged with 0.2 ml of suspension per 10 g body weight (i.g). General status observations, signs of intoxication and mortality were monitored and recorded at 30 min, 1, 2, 4 and 8 h after drug administration. The animals were observed twice a day for 7 days. All animals that died during the observation period were subjected to necropsy.

Sperm abnormality test in mice

The sperm aberration test refers to the guidelines for sperm abnormality tests in mice of veterinary drugs of MARA, PRC (Ministry of Agriculture and Rural Affairs of PRC, 2009c). Fifty male ICR mice (25–35 g) were randomly divided into five groups of 10 mice each. The assigned mice were administered MPTA at 60.25 mg/kg, 120.50 mg/kg, and 241.00 mg/kg for five consecutive days, respectively. Distilled water and CTX (40 mg/kg) were administered to the negative control and positive control groups, respectively. On day 35 after the first dose, five mice were randomly selected and executed in each test group. Selected mice were removed twice from the epididymis and smears of sperm specimens were made in a standard procedure that could be used for observation (Wang et al., 2015). Sperm morphology was examined under a microscope, and normal and various types of abnormal sperms under the same field of view were counted and recorded (Anwar et al., 2022).

Mouse bone marrow cell micronucleus test

The micronucleus test was designed using the guidelines for bone marrow cell micronucleus test in mice of veterinary drugs of MARA, PRC (Ministry of Agriculture and Rural Affairs of PRC, 2009a). One hundred ICR mice (25–30 g) were randomly divided into five groups of 20 mice each, with 10 males and 10 females in each group. The doses administered to each group of mice were 60.25 mg/kg, 120.50 mg/kg and 241.00 mg/kg, respectively, and two doses were administered, with the second dose administered 24 h after the first dose. Mice in the negative control group were administrated the same volume of distilled water, and the positive control group was administrated 40 mg/kg CTX. The mice were executed 6 h after the second gavage, and the femur was removed from both sides of each mouse, the muscle was shaved off, the surface blood was wiped off with filter paper, and

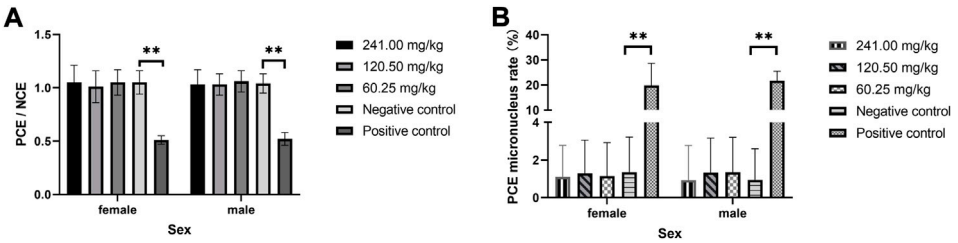

FIGURE 1
Effect of MPTA on bone marrow micronucleus test in mice (n = 20, females = 10, males = 10) **(A)** Effect of MPTA on PCE/NCE values; **(B)** Effect of MPTA on PCE micronucleus rate. Data are compared with negative controls, and * indicates significant differences ($p < 0.05$).

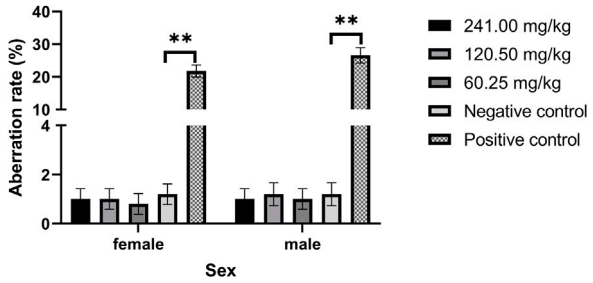

FIGURE 2
Effect of MPTA on the rate of chromosomal aberrations in mouse bone marrow cells (n = 16, females = 8, males = 8). Data are compared with negative controls, and * indicates significant differences ($p < 0.05$).

both ends of the femur were cut off. The bone marrow cavity was then flushed several times with about 0.5 ml of fetal bovine serum using a 1 ml syringe equipped with a No. Six needle, and the bone marrow flush solution was mixed to make smears. Smears were fixed in methanol for 15 min, and stained with Giemsa dye for 15 min and observed under oil microscope for normochromatic erythrocyte (NCE) and polychromatic erythrocytes (PCE). Count the number of PCEs containing micronuclei in 1000 PCEs and count the ratio of PCE to NCE in 200 cells.

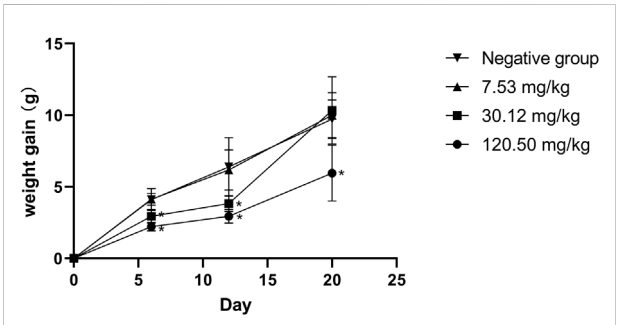

FIGURE 3
Effect of MPTA on body weight gain in pregnant rats.

Mouse bone marrow cell chromosome aberration test

The chromosome aberration test was conducted in accordance with the guidelines for bone marrow cell chromosome aberration test in mice of veterinary drugs of MARA, PRC (Ministry of Agriculture and Rural Affairs of PRC, 2009e). Eighty ICR mice (25–30 g) were randomly divided into five groups of 16 mice each, half being females and the other half being males. Three dose groups (60.25 mg/kg, 120.50 mg/kg and 241.00 mg/kg) were set up and administered three times at 24 h intervals. CTX (40 mg/kg) was used as a positive control and distilled water as a negative control. Twenty-4 hours after the last dose, five mice from each group were randomly selected for humane execution. 4 h before execution, the animals were injected intraperitoneally with 0.04% colchicine (4 mg/kg). Using 5 ml of 2.2% sodium citrate solution, bone marrow from the femur was washed into a 10 ml centrifuge tube. The bone marrow was suspended by pipetting, then centrifuged at 1000 r/min for 10 min, and the supernatant was discarded to collect the precipitated bone marrow cells. Bone marrow cells were fixed using methanol: acetic acid (3:1), and stained with Giemsa solution for 15 min 100 metaphase cells were observed in each animal, and cells with abnormal chromosome structure and number were observed and recorded.

Traditional teratogenicity test in rats

The teratogenicity test followed the guidelines for classical teratogenicity tests in rats of veterinary drugs of MARA, PRC (Ministry of Agriculture and Rural Affairs of PRC, 2009b). Eighty uncrossed young females (220–250 g) and 40 sexually mature males (250–300 g) of SD rats were used for teratogenicity tests. Based on the acute toxicity results, three dose groups of

TABLE 3 Effect of MPTA on reproductive function in rats (n = 12).

Groups	Ovary weight (g)	Uterus weight (g)	Number of corpus luteum	Average number of nidation	Average number of live fetuses
120.50 mg/kg	0.13 ± 0.02	5.77 ± 0.59	13.92 ± 2.35	14.00 ± 1.21	3.67 ± 2.99
30.12 mg/kg	0.14 ± 0.02	5.46 ± 0.68	13.67 ± 1.30	13.17 ± 1.27	11.08 ± 2.19
7.53 mg/kg	0.14 ± 0.02	6.13 ± 0.85	14.92 ± 1.44	13.67 ± 1.56	13.42 ± 1.68
Negative control	0.14 ± 0.02	5.57 ± 0.35	14.00 ± 1.41	13.25 ± 1.86	13.58 ± 1.62

Note: Data are compared with negative controls, and * indicates significant differences ($p < 0.05$).

TABLE 4 Effect of MPTA on the survival rate of rat embryos (n = 12).

Groups	Number of nidation	Number of live fetuses (♀/♂)	Embryo absorption rate (%)	Fetal death rate (%)	Fetal survival rate (%)
120.50 mg/kg	168	21/23	73.81* (124/168)	0 (0/168)	26.19* (44/168)
30.12 mg/kg	158	72/61	15.82* (25/158)	0 (0/158)	84.18* (133/158)
7.53 mg/kg	161	75/82	1.83 (3/164)	0 (3/164)	98.17 (161/164)
Negative control	163	84/75	2.52 (4/159)	0 (0/159)	97.55 (159/163)

Note: Data are compared with negative controls, and * indicates significant differences ($p < 0.05$).

TABLE 5 Effect of MPTA on the development of rat embryos (n = 12).

Groups	Placenta weight (g)	Fetal rat weight (g)	Fetal rat body length (cm)	Fetal rat tail length (cm)
120.50 mg/kg	0.39 ± 0.13*	2.81 ± 0.89*	2.81 ± 0.89*	1.05 ± 0.33
30.12 mg/kg	0.50 ± 0.01	3.51 ± 0.07*	3.29 ± 0.13*	1.21 ± 0.04
7.53 mg/kg	0.52 ± 0.01	3.60 ± 0.05	3.52 ± 0.06	1.21 ± 0.02
Negative control	0.50 ± 0.03	3.64 ± 0.13	3.57 ± 0.09	1.22 ± 0.01

Note: Data are compared with negative controls, and * indicates significant differences ($p < 0.05$).

7.53 mg/kg, 30.12 mg/kg and 120.50 mg/kg, and a negative control group (distilled water) were set up with 20 female and 10 male rats in each group. Two female and one male rats were assigned to each cage for mating. Mating success was determined by checking whether sperm could be observed in the vaginal smear of female rats, and the day was taken as day 0 of pregnancy, and continued until 12 pregnant rats were reached in each group. Mated female rats were housed individually in transparent polycarbonate cages and were allowed to feed and drink freely. All pregnant rats were administered by gavage once daily from day 7 to day 16 of gestation. Pregnant rats were weighed on days 0, 7, 12, 16 and 20 of conception, and observed daily for general behavior, intoxication and death, and in case of death, post-mortem examinations were performed. All pregnant rats were executed at day 20 of gestation, ovaries and uterus were removed and examined for the number of corpus luteum, number of absorbed fetuses, number of stillbirths, number of live fetuses, male to female ratio in live fetuses, position of the live fetuses in the uterus and weight of ovaries, uterus and uterus attached to the fetus (including amniotic fluid). Afterwards, the weight, body length and tail length of the live fetuses were measured and the live fetuses were examined for cosmetic deformities.

Half of the live fetuses from each litter were fixed by ethanol for 2–3 weeks. The fixed specimens were rinsed in running water and put into potassium hydroxide solution transparently for 72 h, and then put into alizarin red S staining solution (2%, pH = 4.2) for staining for 48 h, and shaken lightly 1–2 times a day. After the skull was stained red, the fetal mouse specimens were removed and placed in two different concentrations of glycerol-potassium hydroxide solution transparently, and removed after all the skeletal specimens were stained red and the soft tissue was discolored. The fetal specimens were observed under a transmission light source using a stereomicroscope, and the number of sternums, incomplete ossification, rib and limb bone abnormalities,

10.3389/fphar.2022.987800

TABLE 6 Teratogenic effects of MPTA in rats (n = 12).

Groups	Appearance malformations			Skeletal malformations			Visceral malformations		
	Number of fetal mice examined	Teratogenesis rate (%)	Maternal malformation rate (%)	Number of fetal mice examined	Teratogenesis rate (%)	Maternal malformation rate (%)	Number of fetal mice examined	Teratogenesis rate (%)	Maternal malformation rate (%)
120.50 mg/kg	44	0	0	20	80.00* (16/20)	66.67* (8/12)	24	0	0
30.12 mg/kg	133	0	0	55	10.91 (6/55)	33.33 (4/12)	78	0	0
7.53 mg/kg	161	0	0	69	4.35 (3/69)	16.67 (2/12)	92	0	0
Negative control	159	0	0	68	5.88 (4/68)	16.67 (2/12)	91	0	0

Note: Teratogenesis rate (%) = (number of teratology/number of fetal rats examined) × 100%; maternal malformation rate (%) = (number of pregnant rats with teratology/number of pregnant rats examined) × 100%. Data are compared with negative controls, and * indicates significant differences ($p < 0.05$).

and spinal development (fusion or longitudinal cleft) were examined and recorded in each test group. The other half of the live fetus was placed in Bouin's fixative solution and the fetal viscera were examined after 2 weeks of fixation, and the size, shape and relative position of the organs in different sections of the fetal rat were observed and recorded for abnormalities (Anwar et al., 2021a; 2021b).

Chronic toxicity test in rats

Two hundred SD rats (70–90 g) were randomly divided into four groups including three dose groups (48.20 mg/kg, 9.64 mg/kg and 1.93 mg/kg) and one negative control group (no addition). MPTA was added to the diets at each dose [daily dietary intake of rats was calculated as 8% (1–90 days) and 6% (91–180 days) of body weight, respectively)] and given to the test rats via *ad libitum* feeding. During the feeding test, the behavior, mental status, food and water intake, toxicity and death of the rats were observed and recorded daily. The body weight, food intake and water intake of all rats were measured every 5 days.

On days 45, 90, 135 and 180 of the experiment, 10 rats in each group (five males and five females) were randomly selected and anesthetized by intraperitoneal injection of urethane (ethyl carbamate). Blood samples were obtained by cardiac puncture for further hematological examinations such as red blood cell count (RBC), white blood cell count (WBC), platelet count (PLT) and hemoglobin (HGB), as well as alanine aminotransferase (ALT), aspartate aminotransferase (AST), total protein (TP), albumin (ALB), creatinine (CR), blood urea nitrogen (BUN), glucose (GLU) and total cholesterol (TCH). The rats were dissected for suspicious histological lesions, and the major organs (heart, liver, spleen, lungs, kidneys, gastrointestines, testes and ovaries) were weighed and the corresponding organ coefficients were calculated. Organ coefficient = organ weight/body weight. At the end of the test, histopathological examinations were performed on the major organs of rats in the 48.20 mg/kg and control groups, as well as on suspicious lesions observed during gross autopsy, and on rats in the lower dose group if toxicity-related lesions were found.

Statistical analysis

Appropriate statistical analysis of the data was performed using SPSS 26.0 (International Business Machines Corporation, Armonk, USA) with *t*-test and one-way ANOVA for body weight, feed intake, water intake, hematology, and clinical chemistry results; Percentages were tested using two tests. Image production was

performed by GraphPad Prism 9.0.0 (GraphPad Software, San Diego, USA). *p*-values less than 0.05 were considered statistically different.

Results

Acute toxicity in mice

In acute toxicity tests, death in ICR mice occurred 8–24 h after administration (Table 1), and clinical signs of toxicity were slowed movement and sedentary. Gross autopsy of the dead mice did not reveal any significant pathological changes in the major organs. The oral acute toxicity LD_{50} of MPTA in mice was calculated to be 481.99 mg/kg (95% confidence interval 404.24–574.70 mg/kg) based on the modified Kärber's method (Mantel, 1967).

Sperm abnormality test in mice

In the sperm aberration test, the positive drug, CTX, significantly increased the number of aberrations and the aberration rate of mouse sperm ($p < 0.01$), in which the proportion of amorphous sperm increased and the proportion of banana-shaped, double-tailed sperm decreased. Compared with the negative control group, MPTA at 120.50 mg/kg increased the number of no-hook sperm; all three dose groups of MPTA and CTX decreased the number of banana-shaped sperm; except for CTX which significantly increased the number of amorphous sperm, none of the MPTA treatment groups were significantly different; 241.00 mg/kg, 120.50 mg/kg MPTA and CTX also reduced the number of double-tailed sperm; except for that, only 60.25 mg/kg MPTA increased the number of double-headed sperm. MPTA in the tested range (60.25–241.00 mg/kg) did not cause significant differences ($p > 0.05$) in the total sperm abnormality rate in mice

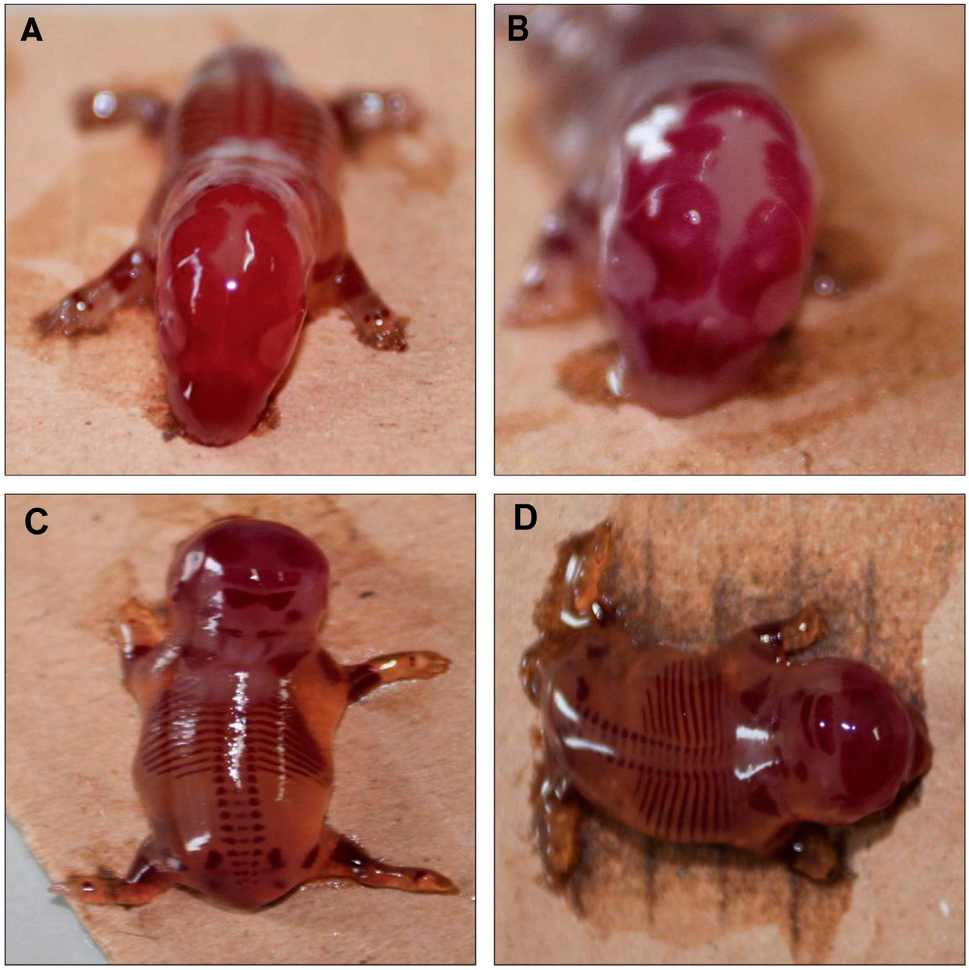

FIGURE 4
Effect of MPTA on skeletal deformities in fetal rats **(A)** Normal skull; **(B)** delayed skull ossification; **(C)** normal occipital bone; **(D)** delayed occipital ossification.

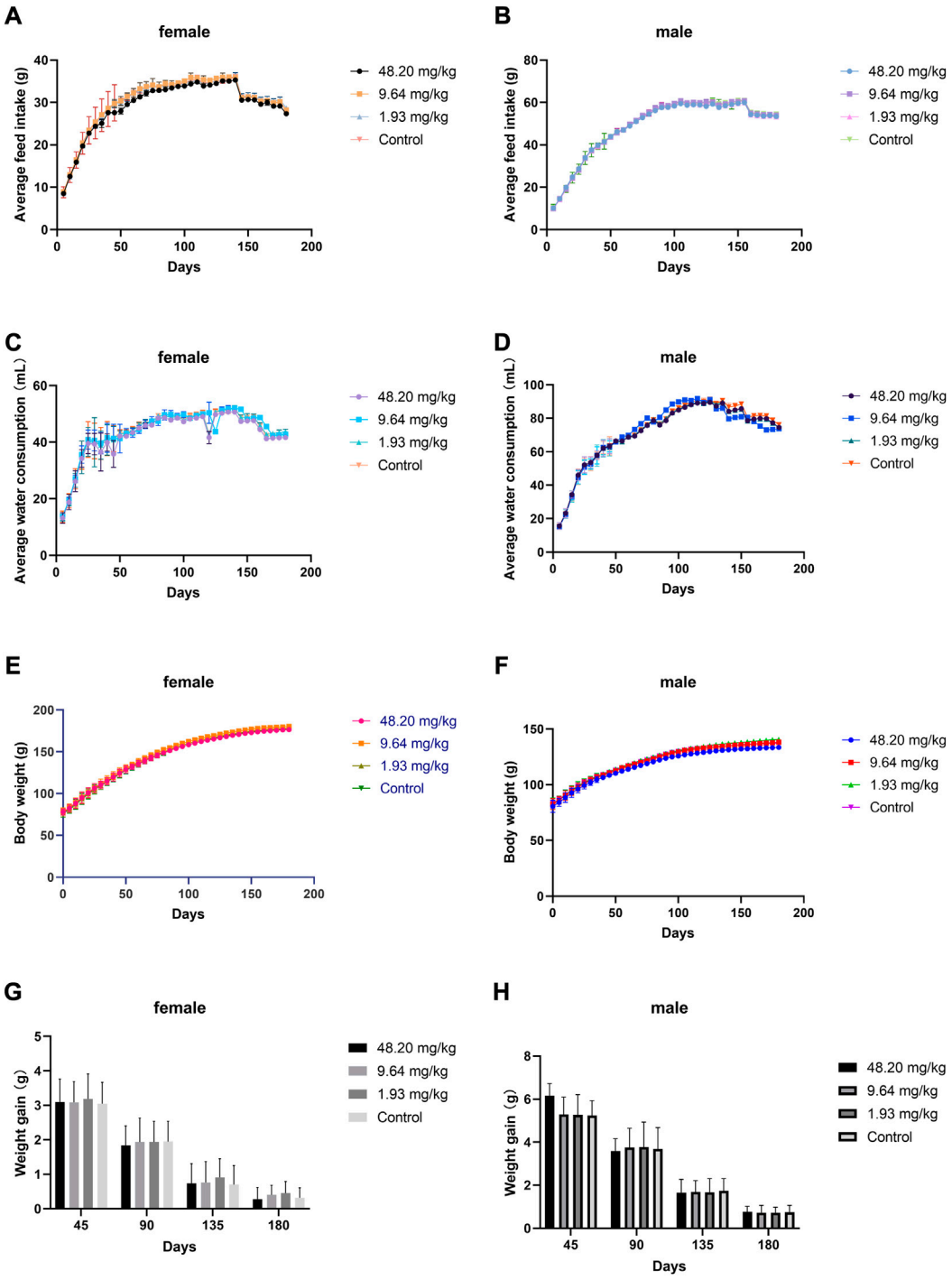

FIGURE 5
Effects of feeding MPTA for 180 days on feeding, drinking, body weight and weight gain of rats **(A)** Effect of MPTA on feed intake of female rats; **(B)** Effect of MPTA on feed intake of male rats; **(C)** Effect of MPTA on water intake of female rats; **(D)** Effect of MPTA on water intake of male rats; **(E)** Effect of MPTA on body weight of female rats; **(F)** Effect of MPTA on body weight of male rats; **(G)** Effect of MPTA on weight gain of female rats; **(H)** Effect of MPTA on weight gain of female rats.

TABLE 7 Effect of MPTA on hematological parameters.

Groups	Hematology parameters							
	HGB (g/L)		RBC (M/mm^3)		WBC (th/mm^3)		PLT (th/mm^3)	
	F	M	F	M	F	M	F	M
45 days								
48.20 mg/kg	152.03 ± 7.56	155.80 ± 7.90	7.18 ± 0.58	7.77 ± 0.34	8.11 ± 0.54	11.88 ± 1.32	472.80 ± 65.66	464.00 ± 84.32
9.64 mg/kg	157.80 ± 8.11	154.11 ± 11.01	7.85 ± 0.51	7.41 ± 0.38	8.41 ± 0.62	12.02 ± 1.90	444.00 ± 60.98	435.00 ± 44.89
1.93 mg/kg	164.34 ± 13.48	153.00 ± 5.69	7.56 ± 0.61	7.57 ± 0.35	7.89 ± 0.28	12.97 ± 1.79	435.60 ± 70.52	452.60 ± 54.55
Control	156.40 ± 9.79	150.12 ± 8.52	7.29 ± 0.47	7.23 ± 0.49	8.32 ± 0.61	12.85 ± 0.86	468.50 ± 68.72	454.60 ± 60.88
90 days								
48.20 mg/kg	149.80 ± 7.73	150.20 ± 12.45	7.18 ± 0.58	7.92 ± 0.32	8.11 ± 0.56	9.50 ± 0.64	473.20 ± 65.96	403.40 ± 53.81
9.64 mg/kg	149.90 ± 9.42	151.42 ± 11.70	7.45 ± 0.47	7.86 ± 0.38	7.58 ± 0.85	9.76 ± 1.16	377.20 ± 59.87	379.80 ± 69.00
1.93 mg/kg	154.20 ± 8.45	150.60 ± 8.62	7.45 ± 0.49	7.89 ± 0.37	7.56 ± 0.52	10.22 ± 0.82	400.00 ± 52.51	376.00 ± 56.98
Control	147.40 ± 10.09	153.42 ± 10.18	7.31 ± 0.52	7.66 ± 0.52	7.10 ± 0.47	9.84 ± 0.58	373.00 ± 66.02	361.80 ± 60.45
135 days								
48.20 mg/kg	149.60 ± 7.76	157.35 ± 6.24	7.24 ± 0.57	7.77 ± 0.32	8.15 ± 0.57	8.36 ± 0.85	472.00 ± 66.21	461.60 ± 85.46
9.64 mg/kg	155.40 ± 7.61	156.31 ± 21.75	7.47 ± 0.61	7.43 ± 0.43	8.47 ± 0.67	8.04 ± 0.79	448.20 ± 61.47	439.60 ± 42.19
1.93 mg/kg	156.98 ± 12.58	156.80 ± 6.94	7.63 ± 0.59	7.53 ± 0.47	7.97 ± 0.28	8.59 ± 0.43	440.60 ± 71.21	456.40 ± 54.80
Control	154.20 ± 10.09	154.72 ± 7.77	7.25 ± 0.49	7.19 ± 0.49	8.28 ± 0.62	7.97 ± 0.86	469.40 ± 69.51	459.60 ± 58.08
180 days								
48.20 mg/kg	149.60 ± 7.76	149.80 ± 7.57	7.24 ± 0.57	8.31 ± 0.75	8.15 ± 0.57	7.97 ± 0.45	472.00 ± 66.21	403.00 ± 54.86
9.64 mg/kg	149.70 ± 8.47	153.22 ± 11.86	7.48 ± 0.48	7.79 ± 0.37	7.76 ± 0.50	7.94 ± 1.14	377.00 ± 58.89	381.60 ± 68.05
1.93 mg/kg	154.00 ± 9.40	150.80 ± 9.24	7.51 ± 0.51	7.81 ± 0.37	7.60 ± 0.54	8.23 ± 0.82	399.80 ± 53.80	376.20 ± 57.30
Control	147.60 ± 9.31	153.62 ± 11.24	7.24 ± 0.49	7.58 ± 0.50	7.42 ± 0.51	7.94 ± 0.58	373.20 ± 64.11	362.00 ± 59.96

Note: F is female, M is male.

compared to the negative control group, although the different treatment groups had different effects on the type of sperm abnormalities. The results showed that MPTA at doses ranging from 60.25–241.00 mg/kg did not cause sperm malformations in mice (Table 2).

Mouse bone marrow cell micronucleus test

The results of the micronucleus test of MPTA in mouse bone marrow cells are shown in Figure 1. The rate of PCE micronucleus in bone marrow cells of female and male mice in the positive control group was significantly higher than that of the corresponding sex in the negative control group ($p < 0.01$). In contrast, the PCE micronucleus rate in both sexes in each dose group of MPTA was not significantly different from that of the negative control group ($p > 0.05$). And the PCE/NCE values also showed the same trend. The results showed that there was no effect on the micronucleus rate of bone marrow cells in the dose range of 60.25–241.00 mg/kg in both males and females.

Mouse bone marrow cell chromosome aberration test

As shown in Figure 2, the chromosomal aberration rates of female and male mice cells in each dose group of MPTA (60.25–241.00 mg/kg) were not significant ($p > 0.05$) and significantly lower ($p < 0.01$) than those of the positive control group. The results showed that chromosomal aberrations were not significantly induced in the dose range of 60.25–241.00 mg/kg.

Traditional teratogenicity test in rats

During the test period, the pregnant rats in the three MPTA dose groups (7.53 mg/kg, 30.12 mg/kg and 120.50 mg/kg) and

TABLE 8 Effect of MPTA on clinical chemistry indices in rats.

Groups	Clinical chemistry parameters															
	ALB (mmol/L)		ALT (U/L)		AST (U/L)		BUN (mmol/L)		TCH (mmol/L)		CR (μmol/L)		GLU (mmol/L)		TP (G/L)	
	F	M	F	M	F	M	F	M	F	M	F	M	F	M	F	M
45 days																
48.20 mg/kg	27.44 ± 5.37	32.56 ± 5.28	37.75 ± 4.38	32.60 ± 5.15	192.77 ± 18.76	178.92 ± 17.68	7.83 ± 1.00	9.01 ± 0.31	1.40 ± 0.39	1.61 ± 0.37	83.54 ± 11.14	87.77 ± 15.20	8.07 ± 0.70	8.67 ± 0.79	65.71 ± 8.10	75.93 ± 4.58
9.64 mg/kg	28.51 ± 6.51	33.51 ± 6.52	29.84 ± 8.03	31.84 ± 8.84	192.72 ± 19.94	178.80 ± 20.33	8.76 ± 0.72	9.88 ± 0.95	1.21 ± 0.47	1.59 ± 0.43	76.59 ± 6.00	81.64 ± 4.65	8.03 ± 0.96	8.56 ± 0.83	61.67 ± 4.09	75.27 ± 4.27
1.93 mg/kg	30.64 ± 2.23	34.05 ± 5.24	29.99 ± 4.06	31.66 ± 7.81	191.23 ± 20.52	181.28 ± 15.48	8.34 ± 0.95	9.57 ± 0.69	1.39 ± 0.34	1.68 ± 0.30	75.87 ± 6.44	80.88 ± 5.87	8.43 ± 0.42	8.57 ± 1.06	62.55 ± 4.41	76.18 ± 3.74
Control	30.96 ± 2.39	33.52 ± 6.38	28.55 ± 3.39	31.88 ± 6.04	193.88 ± 19.13	183.61 ± 20.95	8.22 ± 0.66	8.74 ± 0.82	1.48 ± 0.48	1.71 ± 0.37	75.95 ± 5.88	79.79 ± 1.94	8.27 ± 1.07	8.65 ± 0.68	62.68 ± 3.18	76.03 ± 4.52
90 days																
48.20 mg/kg	30.07 ± 3.82	36.92 ± 2.41	34.77 ± 3.16	46.42 ± 11.09	177.05 ± 25.49	180.96 ± 25.46	6.63 ± 1.10	7.23 ± 0.79	1.11 ± 0.39	1.19 ± 0.62	74.17 ± 4.55	84.32 ± 4.12	8.15 ± 0.76	8.29 ± 0.57	68.00 ± 5.33	72.80 ± 6.27
9.64 mg/kg	31.30 ± 5.08	40.98 ± 5.11	32.90 ± 5.09	37.93 ± 4.97	177.22 ± 25.55	181.17 ± 25.30	6.15 ± 0.90	7.06 ± 0.62	1.43 ± 0.45	1.47 ± 0.38	72.63 ± 5.19	82.71 ± 5.74	8.22 ± 0.76	8.62 ± 0.73	68.64 ± 6.26	73.64 ± 5.03
1.93 mg/kg	31.33 ± 5.06	40.05 ± 4.23	32.73 ± 5.10	38.53 ± 3.87	177.03 ± 25.26	185.27 ± 21.58	6.22 ± 0.57	6.98 ± 0.85	1.46 ± 0.38	1.70 ± 0.49	73.28 ± 6.40	80.93 ± 3.87	8.20 ± 0.96	8.56 ± 0.67	68.08 ± 4.79	75.66 ± 4.45
Control	31.38 ± 5.03	40.93 ± 5.13	32.03 ± 2.75	37.70 ± 5.62	168.19 ± 25.32	181.08 ± 25.38	7.71 ± 0.75	7.33 ± 0.68	1.43 ± 0.42	1.52 ± 0.38	92.13 ± 6.09	83.23 ± 5.34	6.53 ± 1.10	8.55 ± 0.83	68.08 ± 4.79	73.04 ± 5.09
135 days																
48.20 mg/kg	36.42 ± 6.43	39.68 ± 6.31	35.79 ± 8.67	42.03 ± 8.29	153.13 ± 19.70	171.38 ± 19.66	6.74 ± 0.48	6.85 ± 0.96	1.28 ± 0.57	2.45 ± 0.19	85.63 ± 6.58	93.58 ± 5.11	7.31 ± 0.82	8.36 ± 0.62	70.05 ± 3.49	83.07 ± 4.45
9.64 mg/kg	36.51 ± 6.63	39.62 ± 6.44	35.89 ± 8.61	41.96 ± 8.59	153.32 ± 15.47	171.33 ± 19.44	6.85 ± 0.86	6.85 ± 0.86	1.35 ± 0.44	2.43 ± 0.30	84.93 ± 5.79	93.68 ± 5.47	7.30 ± 0.72	8.48 ± 0.57	70.30 ± 2.72	83.11 ± 4.23
1.93 mg/kg	36.64 ± 6.63	41.63 ± 2.20	35.93 ± 9.01	42.49 ± 8.18	153.27 ± 19.70	179.26 ± 15.06	6.94 ± 0.52	6.94 ± 0.52	1.34 ± 0.55	2.36 ± 0.40	85.08 ± 7.21	93.83 ± 5.11	7.27 ± 0.49	8.01 ± 0.75	70.67 ± 4.74	80.87 ± 6.26
Control	36.39 ± 4.04	39.55 ± 6.31	32.03 ± 2.75	43.12 ± 9.15	157.39 ± 14.87	171.28 ± 19.58	7.03 ± 0.75	7.03 ± 0.75	1.42 ± 0.57	2.25 ± 0.17	83.36 ± 4.55	94.23 ± 4.63	7.30 ± 0.75	8.32 ± 0.79	70.95 ± 3.95	82.55 ± 4.20
180 days																
48.20 mg/kg	40.90 ± 5.15	34.42 ± 5.05	38.00 ± 5.21	33.80 ± 5.23	168.20 ± 25.54	186.85 ± 25.55	7.34 ± 0.69	7.48 ± 0.66	1.93 ± 0.49	1.85 ± 0.51	90.68 ± 5.17	80.93 ± 5.44	6.70 ± 0.83	7.27 ± 0.71	77.68 ± 5.35	71.50 ± 5.44
9.64 mg/kg	40.90 ± 5.05	33.05 ± 4.41	37.90 ± 5.16	35.63 ± 3.47	168.30 ± 25.76	188.46 ± 29.22	7.42 ± 0.93	7.29 ± 0.92	1.90 ± 0.71	1.78 ± 0.63	90.66 ± 4.51	82.00 ± 6.17	6.59 ± 1.13	7.43 ± 1.10	77.68 ± 5.53	69.71 ± 2.64
1.93 mg/kg	39.68 ± 3.90	30.89 ± 3.08	33.08 ± 4.97	35.84 ± 3.1	166.95 ± 23.38	175.95 ± 9.99	7.33 ± 0.55	7.00 ± 0.39	1.74 ± 0.62	1.82 ± 0.51	88.83 ± 1.59	79.43 ± 4.06	6.76 ± 0.73	7.45 ± 0.39	75.56 ± 3.79	70.16 ± 5.51
Control	40.75 ± 4.98	34.45 ± 5.01	37.10 ± 5.14	33.93 ± 4.87	168.19 ± 25.10	160.55 ± 20.69	7.71 ± 0.75	7.43 ± 0.71	1.71 ± 0.44	1.78 ± 0.42	92.13 ± 6.09	34.56 ± 5.10	6.53 ± 1.10	7.22 ± 0.80	76.24 ± 3.69	71.66 ± 5.44

Note: F is female, M is male.

10.3389/fphar.2022.987800

TABLE 9 Effect of MPTA on organ coefficients in rats.

Groups	Organ coefficient (%)													
	Liver		Kidney		Spleen		Stomach and intestines		Lung		Heart		Testicles	Ovaries
	F	M	F	M	F	M	F	M	F	M	F	M		
48.20 mg/kg	3.52 ± 0.25	2.58 ± 0.15	0.69 ± 0.05	0.60 ± 0.03	0.20 ± 0.02	0.16 ± 0.00	9.38 ± 0.99	7.28 ± 0.33	0.54 ± 0.05	0.47 ± 0.04	0.38 ± 0.01	0.32 ± 0.02	0.59 ± 0.03	0.04 ± 0.01
9.64 mg/kg	3.79 ± 0.18	2.47 ± 0.12	0.74 ± 0.04	0.57 ± 0.03	0.20 ± 0.01	0.15 ± 0.01	9.36 ± 0.67	6.94 ± 0.31	0.53 ± 0.05	0.44 ± 0.04	0.35 ± 0.02	0.32 ± 0.01	0.55 ± 0.04	0.04 ± 0.00
1.93 mg/kg	3.80 ± 0.23	2.51 ± 0.17	0.74 ± 0.05	0.58 ± 0.05	0.20 ± 0.01	0.16 ± 0.01	9.36 ± 0.58	7.05 ± 0.63	0.54 ± 0.07	0.46 ± 0.02	0.39 ± 0.03	0.33 ± 0.02	0.57 ± 0.02	0.04 ± 0.00
Control	3.50 ± 0.36	2.45 ± 0.14	0.68 ± 0.06	0.56 ± 0.04	0.19 ± 0.02	0.15 ± 0.01	8.85 ± 0.48	6.90 ± 0.48	0.50 ± 0.03	0.43 ± 0.04	0.37 ± 0.02	0.32 ± 0.02	0.56 ± 0.04	0.04 ± 0.00

Note: F is female, M is male. Organ coefficient = (organ weight/body weight) × 100%.

FIGURE 6
Histopathological effects of MPTA on major organs of rats. Magnification of heart, liver, spleen, kidney in 48.20 mg/kg dose group and heart, spleen, lung, duodenum in control group were ×400; magnification of lung, duodenum in 48.20 mg/kg dose group and liver, kidney in control group were ×200.

the negative control group did not show any poisoning or death, nor did they show any significant abnormalities in diet, water intake and clinical performance. Compared with the control group, the rats in the 120.50 mg/kg and 30.12 mg/kg groups

10.3389/fphar.2022.987800

showed significantly delayed weight gain ($p < 0.05$), while the 7.53 mg/kg group showed no significant difference ($p > 0.05$) (Figure 3). The results showed a lack of maternal toxicity in pregnant rats only at 7.53 mg/kg. After execution of the pregnant rats on day 20 of gestation, the indicators related to reproductive function such as ovarian weight, uterine weight, number of corpus luteum, mean fertility rate and mean fetal survival rate in the abdomen of pregnant rats in each test group are shown in Table 3. Further examination of embryos revealed that no stillbirths occurred in any of the four groups, but the embryo absorption rate was significantly higher in the 120.50 mg/kg and 30.12 mg/kg groups compared to the negative control group ($p < 0.05$), and the fetal survival rate was significantly lower ($p < 0.05$) (Table 4). In addition, the placental weight, fetal rat weight and fetal rat body length in the abdomen of pregnant rats were significantly lower ($p < 0.05$) in both 120.50 mg/kg and 30.12 mg/kg groups compared to the negative control group (Table 5), which showed that there were some effects of MPTA on rat fetal development at doses of 120.50 mg/kg-30.12 mg/kg.

Table 6 shows the statistical results of MPTA on fetal malformations in appearance, skeletal malformations and visceral malformations in rats. No external and internal malformations were observed in the MPTA dose groups and the negative control group. Retarded ossification (mainly in the skull and occipital bones) was observed in all four groups (Figure 4), with the percentage of fetal rats with retarded ossification in the negative control group within the normal historical control range of the laboratory. By statistical analysis, MPTA induced a higher rate of malformed fetuses and maternal malformations at a dose of 120.50 mg/kg ($p < 0.05$). There was no significant effect of 7.53–30.12 mg/kg on the occurrence of teratogenicity and maternal malformation rate. Therefore, MPTA at doses of 7.53–30.12 mg/kg had no teratogenic effect on the appearance, bones and viscera of fetal rats. In conclusion, MPTA did not affect the feeding, drinking and weight gain of pregnant SD rats at a dose of 7.53 mg/kg, and had no significant effects on the reproductive function, embryonic survival and growth, and the appearance, skeletal and visceral malformations of the fetuses of pregnant rats. Therefore, the NOEL of the MPTA teratogenic test can be considered as 7.53 mg/kg.

Chronic toxicity test in rats

During the test period (180 days), animals in the three dose groups (48.20 mg/kg, 9.64 mg/kg and 1.93 mg/kg) and the negative control group of MPTA did not show any abnormal behavior. The feed intake, water consumption, body weight and weight gain of the animals in each test group are shown in Figures 5A–H. There were no significant differences in feed intake, water consumption, body weight and weight gain between the three dose groups of MPTA and the negative control group during the test period ($p > 0.05$). The hematological results of HGB, WBC, RBC, and PLT for each test group at days 45, 90, 135, and 180 of the trial are shown in Table 7. The results of clinical chemistry such as ALT, AST, BUN, CR, GLU, TP, ALB and TCH are shown in Table 8. The hematological and clinical chemistry of the rats in each dose group were not significantly affected from the negative control group ($p > 0.05$). Throughout the test period, no animals showed poisoning and death, and gross autopsy of surviving animals showed no abnormal lesions, and the organ coefficients of rats in each test group were not significantly different from those of the negative control group (Table 9). Further histopathological examination of the rats in the 48.20 mg/kg group and the negative control group showed no significant pathological changes in the major organs of the heart, liver, kidney, spleen, lung, kidney, etc. in both groups as seen in Figure 6. In conclusion, MPTA had no significant effects on feeding, drinking and weight gain of rats in the dose range of 1.93–48.20 mg/kg, and no significant effects on hematological, clinical chemistry and histopathological examinations, and did not show chronic toxicity. Therefore, the NOEL of 180-days chronic toxicity test in rats can be considered as 48.20 mg/kg.

Discussion

PAs have been widely used due to their good pharmacological activity (Xiao et al., 2007; Bae et al., 2012; Sreenivasmurthy et al., 2022), but scientific evaluation studies on their toxicity and side effects are lacking. A complete and systematic safety evaluation is essential for the safety of clinical drug use. Except for the previous oral acute toxicity and 90-days repeated dosing toxicity studies of MPTA in rats (Dong et al., 2022a), no further risk assessment of MPTA has been reported. In this study, oral acute toxicity test in mice, *in vivo* genotoxicity test, teratogenicity test in rats and chronic toxicity test were conducted to further evaluate the possible toxicity risk of MPTA during use and to provide data support for subsequent residue evaluation.

The oral LD_{50} of MPTA was 481.99 mg/kg in rats (Dong et al., 2022a), and since the dose selection for the *in vivo* genotoxicity test carried out in this study was based on mice, the oral acute toxicity of MPTA to ICR mice was carried out, and coincidentally, the LD_{50} in mice was also 481.99 mg/kg, and according to the chemical toxicity classification criteria, MPTA is According to the chemical toxicity classification, MPTA is of moderate toxicity (51–500 mg/kg). The previously reported effective dose of 5.08 mg/kg for MPTA to exert anti-inflammatory effects is considered to have a manageable safety distance, although no clear safety range has been obtained.

MPTA has good properties for use as a potential anti-inflammatory agent, but a large number of toxicities and adverse effects have been reported for nonsteroidal anti-inflammatory drugs (NSAIDs) in clinical practice, such as irritation of the gastrointestinal mucosa (Melarange et al., 1994), biochemical abnormalities due to mild liver damage (Portmann et al., 1975; Ali et al., 2011), hematopoietic dysfunction (Canada and Burka, 1968; Wiesen et al., 2009), interstitial nephritis due to prolonged oral administration (Lucas et al., 2019; Klomjit and Ungprasert, 2022), bleeding in delivery (aspirin) (Hastie et al., 2021) and fetal malformations (indomethacin) (Klein et al., 1981; Sangem et al., 2008). Therefore, this study focused on the long-term toxicity, genotoxicity and toxicity to reproductive development of MPTA. Hematological tests are often used to assess the physiological and pathological status of the body. Parameters such as WBC, RBC, HGB and PLT can reflect the inflammatory status of the body and the effect of drugs on the hematopoietic system. In chronic toxicity tests, MPTA at the doses tested (48.20–1.93 mg/kg) did not produce significant effects on hematological parameters in rats. The effects on liver and kidney are often reflected by clinical chemistry, as liver injury due to the drug often causes concomitant increases in ALT and AST, while kidney injury also causes increases in serum parameters such as BUN and CR. In this test, MPTA did not have a significant effect on clinical chemistry parameters in the rats at the doses tested. The organ coefficients can be used to initially locate the toxic target organs of the drug, and there were no significant differences between the dose groups of MPTA and the control group in this study. Histopathological examination is considered the "gold standard" for disease/toxic injury diagnosis (Karadag Soylu, 2020), and in further histopathological examination, the highest dose of 48.20 mg/kg MPTA did not cause significant toxic lesions in major organs susceptible to NSAIDs, such as liver, kidney, and intestine. Therefore, it can be concluded that MPTA lacks the risk of chronic toxicity.

Genotoxicity studies are an important part of drug entry into clinical trials and marketing, and are closely related to other studies, especially carcinogenicity and reproductive toxicity (Ellinger-Ziegelbauer et al., 2009). In the three *in vivo* genetic mutation tests (sperm abnormality test, micronucleus test and chromosomal aberration test) conducted in this study, all test results were negative at the doses tested (60.25–241.00 mg/kg) and therefore MPTA was not considered genotoxic. In the next teratogenic test in rats, we found that body weight gain was inhibited in females at the tested doses of 30.12 mg/kg and 120.50 mg/kg and that embryonic uptake and fetal malformation rates were increased compared to the negative control group. In another *in vitro* study, California poppy extracts containing PRO showed no inhibitory effect in placental cells (BeWo b30) and the comet assay did not show genotoxic potential. However, as data on the pharmacokinetic profile of PRO are lacking, it cannot be demonstrated that the concentrations tested *in vitro* can achieve sufficient *in vivo* effects (Spiess et al., 2022b). In addition, it has been shown that an increase in 5-Hydroxytryptamine leads to an inhibition of weight gain in pregnant mice and reduces maternal estrogen and progesterone levels leading to early fetal developmental disorders (Han et al., 2022). It is possible that the potential embryonic developmental toxicity of MPTA also affects the levels of estrogen in rats. The results of another study also showed that PRO can be transferred from the mother to the fetal circuit and reach homeostasis through the placental barrier (Spiess et al., 2022a). This also provides a partial explanation for the potential embryotoxicity risk of PRO, but the cause of embryotoxicity due to MPTA and its safety for target animals should still be further investigated.

It is worth noting that MPTA is a mixture and its toxicity results can only be representative of the test substance itself, as the toxic effects of the mixture depend on the composition of the substances in the mixture, the proportions, and the interactions between the compounds (independent, synergistic, additive, or antagonistic) (Bart et al., 2022). Therefore, the main active substance in MPTA should be further tested when used alone.

Conclusion

The oral LD_{50} of MPTA was 480 mg/kg. In a test of long-term repeated dosing, no signs of potential toxicity were shown at different doses. It lacks mutagenicity, but there may be reproductive toxicity or embryonic developmental toxicity at dosage levels above 7.53 mg/kg. This study suggests that MPTA could be used for further drug development studies. Detailed in-depth studies will continue afterwards to address the teratogenicity results.

Data availability statement

The original contributions presented in the study are included in the article/supplementary material, further inquiries can be directed to the corresponding authors.

Ethics statement

The animal study was reviewed and approved by the Animal Ethics Committee of China Agricultural University.

Author contributions

Conceptualization, ZD and J-GZ; methodology, ZD and S-ST; software, ZD; validation, ZD, and Z-HY; formal analysis, ZD and X-LM; resources, C-HL and J-GZ; data curation, X-LM and BT; writing—original draft preparation, ZD; writing—review and editing, ZD and S-ST; visualization, ZD; supervision, C-HL and Z-ST; project administration, Z-HY; All authors have read and agreed to the published version of the manuscript.

Acknowledgments

We thank the China Agricultural University for their support on the experiments.

Conflict of interest

Authors Z-ST and C-HL were employed by Hunan MICOLTA Biological Resources Co., Ltd.

The remaining authors declare that the research was conducted in the absence of any commercial or financial relationships that could be construed as a potential conflict of interest.

Publisher's note

All claims expressed in this article are solely those of the authors and do not necessarily represent those of their affiliated organizations, or those of the publisher, the editors and the reviewers. Any product that may be evaluated in this article, or claim that may be made by its manufacturer, is not guaranteed or endorsed by the publisher.

References

Alam, M. B., Ju, M.-K., Kwon, Y.-G., and Lee, S. H. (2019). Protopine attenuates inflammation stimulated by carrageenan and LPS via the MAPK/NF-κB pathway. *Food Chem. Toxicol.* 131, 110583. doi:10.1016/j.fct.2019.110583

Ali, S., Pimentel, J. D., and Ma, C. (2011). Naproxen-induced liver injury. *Hepatobiliary Pancreat. Dis. Int.* 10, 552–556. doi:10.1016/s1499-3872(11)60093-3

Anwar, F., Saleem, U., Rehman, A.-U., Ahmad, B., Froeyen, M., Mirza, M. U., et al. (2021a). Toxicity evaluation of the naphthalen-2-yl 3, 5-dinitrobenzoate: A drug candidate for alzheimer disease. *Front. Pharmacol.* 12, 607026. doi:10.3389/fphar.2021.607026

Anwar, F., Saleem, U., Rehman, A.-U., Ahmad, B., Ismail, T., Mirza, M. U., et al. (2021b). Toxicological screening of 4-phenyl-3, 4-dihydrobenzo[h]quinolin-2(1H)-one: A new potential candidate for alzheimer's treatment. *ACS Omega* 6, 10897–10909. doi:10.1021/acsomega.1c00654

Anwar, F., Saleem, U., Rehman, A., Ahmad, B., Ismail, T., Mirza, M. U., et al. (2022). Acute oral, subacute, and developmental toxicity profiling of naphthalene 2-yl, 2-chloro, 5-nitrobenzoate: Assessment based on stress response, toxicity, and adverse outcome pathways. *Front. Pharmacol.* 12, 810704. doi:10.3389/fphar.2021.810704

Bae, D. S., Kim, Y. H., Pan, C.-H., Nho, C. W., Samdan, J., Yansan, J., et al. (2012). Protopine reduces the inflammatory activity of lipopolysaccharide-stimulated murine macrophages. *BMB Rep.* 45, 108–113. doi:10.5483/BMBRep.2012.45.2.108

Bart, S., Short, S., Jager, T., Eagles, E. J., Robinson, A., Badder, C., et al. (2022). How to analyse and account for interactions in mixture toxicity with toxicokinetic-toxicodynamic models. *Sci. Total Environ.* 843, 157048. doi:10.1016/j.scitotenv.2022.157048

Cai, Q., Meng, J., Ge, Y., Gao, Y., Zeng, Y., Li, H., et al. (2020). Fishing antitumor ingredients by G-quadruplex affinity from herbal extract on a three-phase-laminar-flow microfluidic chip. *Talanta* 220, 121368. doi:10.1016/j.talanta.2020.121368

Canada, A. T., and Burka, E. R. (1968). Aplastic anemia after indomethacin. *N. Engl. J. Med.* 278, 743–744. doi:10.1056/nejm196803282781329

Dong, Z., Tang, S., Li, C., Tang, Z., Yang, Z., and Zeng, J. (2022a). Safety assessment of MPTA: An oral acute and 90-day sub-chronic toxicity study in Sprague-Dawley rats. *Regul. Toxicol. Pharmacol.* 133, 105188. doi:10.1016/j.yrtph.2022.105188

Dong, Z., Wang, Y., Tang, Z., Li, C., Jiang, T., Yang, Z., et al. (2022b). Exploring the anti-inflammatory effects of protopine total alkaloids of Macleaya cordata (willd.) R. Br. *Front. Vet. Sci.* 9, 935201. doi:10.3389/fvets.2022.935201

Ellinger-Ziegelbauer, H., Aubrecht, J., Kleinjans, J. C., and Ahr, H.-J. (2009). Application of toxicogenomics to study mechanisms of genotoxicity and carcinogenicity. *Toxicol. Lett.* 186, 36–44. doi:10.1016/j.toxlet.2008.08.017

Fu, Y.-C., Zhang, Y., Tian, L.-Y., Li, N., Chen, X., Cai, Z.-Q., et al. (2016). Effects of allocryptopine on outward potassium current and slow delayed rectifier potassium current in rabbit myocardium. *J. Geriatr. Cardiol.* 13, 316–325. doi:10.11909/j.issn.1671-5411.2016.04.008

Han, Y., Zhang, M., Duan, J., Li, L., Du, J., Cheng, H., et al. (2022). Maternal prepregnancy 5-hydroxytryptamine exposure affects the early development of the fetus. *Front. Physiol.* 13, 761357. doi:10.3389/fphys.2022.761357

Hastie, R., Tong, S., Wikström, A.-K., Sandström, A., Hesselman, S., and Bergman, L. (2021). Aspirin use during pregnancy and the risk of bleeding complications: A Swedish population-based cohort study. *Am. J. Obstet. Gynecol.* 224, 95.e1–95.e12. doi:10.1016/j.ajog.2020.07.023

Hu, W., Yang, F., Liu, W., Guo, L., Ai, L., Zhang, X., et al. (2021). Potential toxicity evaluation of protopine in Macleaya cordata (willd.) R. Br.-A bioactivity guided approach. *Front. Vet. Sci.* 8, 752767. doi:10.3389/fvets.2021.752767

Karadag Soylu, N. (2020). Update on hepatocellular carcinoma: A brief review from pathologist standpoint. *J. Gastrointest. Cancer* 51, 1176–1186. doi:10.1007/s12029-020-00499-5

Klein, K. L., Scott, W. J., Clark, K. E., and Wilson, J. G. (1981). Indomethacin-placental transfer, cytotoxicity, and teratology in the rat. *Am. J. Obstet. Gynecol.* 141, 448–452. doi:10.1016/0002-9378(81)90610-4

Klomjit, N., and Ungprasert, P. (2022). Acute kidney injury associated with non-steroidal anti-inflammatory drugs. *Eur. J. Intern. Med.* 101, 21–28. doi:10.1016/j.ejim.2022.05.003

Li, K., Li, J., Su, J., Xiao, X., Peng, X., Liu, F., et al. (2018). Identification of quality markers of Yuanhu Zhitong tablets based on integrative pharmacology and data mining. *Phytomedicine* 44, 212–219. doi:10.1016/j.phymed.2018.03.002

Liu, H., Lin, Q., Liu, X., Huang, P., Yang, Z., Cao, M., et al. (2022). Effects of dietary bopu powder supplementation on serum antioxidant capacity, egg quality, and intestinal microbiota of laying hens. *Front. Physiol.* 13, 902784. doi:10.3389/fphys.2022.902784

Lu, M., Li, K., He, H., Cheng, Y., and Yang, P. (2020). Systematic characterization of alkaloids in Eomecon chionantha Hance using ultrahigh-performance liquid chromatography-tandem quadrupole Exactive Orbitrap mass spectrometry with a four-step screening strategy. *Rapid Commun. Mass Spectrom.* 34, e8880. doi:10.1002/rcm.8880

Lucas, G. N. C., Leitão, A. C. C., Alencar, R. L., Xavier, R. M. F., Daher, E. D. F., da Silva Junior, G. B., et al. (2019). Pathophysiological aspects of nephropathy caused by non-steroidal anti-inflammatory drugs. *J. Bras. Nefrol.* 41, 124–130. doi:10.1590/2175-8239-JBN-2018-0107

Mantel, N. (1967). Adaptation of Kärber's method for estimating the exponential parameter from quantal data, and its relationship to birth, death, and branching processes. *Biometrics* 23, 739–746. doi:10.2307/2528425

Melarange, R., Blower, P., and Spangler, R. (1994). Comparison of the anti-inflammatory activity and gastrointestinal irritancy of nabumetone, ibuprofen, and diclofenac in rats following chronic administration. *Eur. J. Rheumatol. Inflamm.* 14, 23–27.

Ministry of Agriculture and Rural Affairs of PRC (2009a). *Guidelines for bone marrow cell micronucleus test in mice of veterinary drugs*. Beijing: Notice No. 442 of the Ministry of Agriculture of the people's Republic of China, 1–7.

Ministry of Agriculture and Rural Affairs of PRC (2009b). *Guidelines for classical teratogenicity tests in rats of veterinary drugs*. Beijing: Notice No. 442 of the Ministry of Agriculture of the people's Republic of China, 1–9.

Ministry of Agriculture and Rural Affairs of PRC (2009c). *Guidelines for sperm abnormality tests in veterinary mice*. Beijing: Notice No. 442 of the Ministry of Agriculture of the people's Republic of China, 1–4.

Ministry of Agriculture and Rural Affairs of PRC (2009d). *Guidelines for the acute toxicity (LD50 determination) of veterinary drugs*. Beijing: Notice No. 442 of the Ministry of Agriculture of the people's Republic of China, 1–18.

Ministry of Agriculture and Rural Affairs of PRC (2009e). *Guildelines for bone marrow cell chromosome aberration test in mice of veterinary drugs*. Beijing: Notice No. 442 of the Ministry of Agriculture of the people's Republic of China, 1–7.

Nigdelioglu Dolanbay, S., Kocanci, F. G., and Aslim, B. (2021). Neuroprotective effects of allocryptopine-rich alkaloid extracts against oxidative stress-induced neuronal damage. *Biomed. Pharmacother.* 140, 111690. doi:10.1016/j.biopha.2021.111690

Portmann, B., Talbot, I. C., Day, D. W., Davidson, A. R., Murray-Lyon, I. M., and Williams, R. (1975). Histopathological changes in the liver following a paracetamol overdose: Correlation with clinical and biochemical parameters. *J. Pathol.* 117, 169–181. doi:10.1002/path.1711170307

Saeed, S. A., Gilani, A. H., Majoo, R. U., and Shah, B. H. (1997). Anti-thrombotic and anti-inflammatory activities of protopine. *Pharmacol. Res.* 36, 1–7. doi:10.1006/phrs.1997.0195

Sangem, M., Asthana, S., and Amin, S. (2008). Multiple courses of indomethacin and neonatal outcomes in premature infants. *Pediatr. Cardiol.* 29, 878–884. doi:10.1007/s00246-007-9166-z

Shiomoto, H., Matsuda, H., and Kubo, M. (1990). Effects of protopine on blood platelet aggregation. II. Effect on metabolic system of adenosine 3', 5'-cyclic monophosphate in platelets. *Chem. Pharm. Bull.* 38, 2320–2322. doi:10.1248/cpb.38.2320

Shiomoto, H., Matsuda, H., and Kubo, M. (1991). Effects of protopine on blood platelet aggregation. III. Effect of protopine on the metabolic system of arachidonic acid in platelets. *Chem. Pharm. Bull.* 39, 474–477. doi:10.1248/cpb.39.474

Spiess, D., Abegg, V. F., Chaveau, A., Treyer, A., Oufir, M., Reinehr, M., et al. (2022a). Placental passage of protopine in an *ex vivo* human perfusion system. *Planta Med.* doi:10.1055/a-1829-9546

Spiess, D., Winker, M., Dolder Behna, A., Gründemann, C., and Simões-Wüst, A. P. (2022b). Advanced *in vitro* safety assessment of herbal medicines for the treatment of non-psychotic mental disorders in pregnancy. *Front. Pharmacol.* 13, 882997. doi:10.3389/fphar.2022.882997

Sreenivasmurthy, S. G., Iyaswamy, A., Krishnamoorthi, S., Senapati, S., Malampati, S., Zhu, Z., et al. (2022). Protopine promotes the proteasomal degradation of pathological tau in Alzheimer's disease models via HDAC6 inhibition. *Phytomedicine.* 96, 153887. doi:10.1016/j.phymed.2021.153887

Wang, J., Sun, F., Tang, S., Zhang, S., and Cao, X. (2015). Acute, mutagenicity, teratogenicity and subchronic oral toxicity studies of diaveridine in rodents. *Environ. Toxicol. Pharmacol.* 40, 660–670. doi:10.1016/j.etap.2015.08.022

Wiesen, A., Wiesen, J., Limaye, S., and Kaushik, N. (2009). Mesalazine-induced aplastic anemia. *Am. J. Gastroenterol.* 104, 1063. doi:10.1038/ajg.2008.164

Xiao, X., Liu, J., Hu, J., Li, T., and Zhang, Y. (2007). Protective effect of protopine on the focal cerebral ischaemic injury in rats. *Basic Clin. Pharmacol. Toxicol.* 101, 85–89. doi:10.1111/j.1742-7843.2007.00075.x

Xu, Y., Sun, J., Li, W., Zhang, S., Yang, L., Teng, Y., et al. (2021). Analgesic effect of the main components of Corydalis yanhusuo (yanhusuo in Chinese) is caused by inhibition of voltage gated sodium channels. *J. Ethnopharmacol.* 280, 114457. doi:10.1016/j.jep.2021.114457

Yuan, H.-L., Zhao, Y.-L., Qin, X.-J., Liu, Y.-P., Yang, X.-W., and Luo, X.-D. (2021). Diverse isoquinolines with anti-inflammatory and analgesic bioactivities from Hypecoum erectum. *J. Ethnopharmacol.* 270, 113811. doi:10.1016/j.jep.2021.113811

Zhang, X., Wang, Y., Zhang, K., Sheng, H., Wu, Y., Wu, H., et al. (2021). Discovery of tetrahydropalmatine and protopine regulate the expression of dopamine receptor D2 to alleviate migraine from Yuanhu Zhitong formula. *Phytomedicine.* 91, 153702. doi:10.1016/j.phymed.2021.153702

frontiers | Frontiers in Pharmacology

TYPE Original Research
PUBLISHED 24 October 2022
DOI 10.3389/fphar.2022.1002037

Check for updates

OPEN ACCESS

EDITED BY
Arshad Mahmood,
Al Ain University, United Arab Emirates

REVIEWED BY
Fawad Ali,
Kohat University of Science and Technology, Pakistan
Izhar Ullah,
University of Poonch Rawalakot, Pakistan

*CORRESPONDENCE
Uzma Saleem,
Uzma95@gmail.com

SPECIALTY SECTION
This article was submitted to Predictive Toxicology, a section of the journal Frontiers in Pharmacology

RECEIVED 24 July 2022
ACCEPTED 08 September 2022
PUBLISHED 24 October 2022

CITATION
Manan M, Saleem U, Ahmad B, Aslam N, Anwar A and Zafar A (2022), Anti-arthritic and toxicological evaluation of ethanolic extract of Alternanthera bettzickiana in rats.
Front. Pharmacol. 13:1002037.
doi: 10.3389/fphar.2022.1002037

COPYRIGHT
© 2022 Manan, Saleem, Ahmad, Aslam, Anwar and Zafar. This is an open-access article distributed under the terms of the Creative Commons Attribution License (CC BY). The use, distribution or reproduction in other forums is permitted, provided the original author(s) and the copyright owner(s) are credited and that the original publication in this journal is cited, in accordance with accepted academic practice. No use, distribution or reproduction is permitted which does not comply with these terms.

Anti-arthritic and toxicological evaluation of ethanolic extract of *Alternanthera bettzickiana* in rats

Maria Manan[1], Uzma Saleem [1]*, Bashir Ahmad[2], Nosheen Aslam[3], Asifa Anwar[4] and Aimen Zafar[5]

[1]Department of Pharmacology, Faculty of Pharmaceutical Sciences, Government College University Faisalabad, Faisalabad, Pakistan, [2]Hamza College of Pharmaceutical and Allied Health Scieces, Lahore, Pakistan, [3]Deparment of Biochemistry, Government College University Faisalabad, Faisalabad, Pakistan, [4]Department of Pharmacy, Lahore Medical and Dental College, Lahore, Pakistan, [5]University Institute of Food Science and Technology, University of Lahore, Lahore, Pakistan

In many developing countries, medicinal plants have long been used for therapeutic purposes due to their low cost and toxicity. This study evaluated the safety and anti-arthritic potential of *Alternanthera bettzickiana* ethanolic extract (ABEE). Acute oral toxicity (OECD 425) was tested in the safety evaluation. A limit test was used to identify the LD_{50} value. For an acute oral toxicity study a dose of 2000 mg/kg of ABEE was given orally to the treatment group, and the control group received distilled water at a rate of 10 ml/kg. Biochemical, hematological, and histopathological analyses were performed after 14 days. A formaldehyde 2% w/v solution was injected *via* i.p. to rats of all groups to prepare the arthritic model. Five groups were divided into control ($D.H_2O$), standard (Diclofenac), and three groups receiving the plant extract at dose levels of 125 mg/kg, 250 mg/kg, and 500 mg/kg respectively. Treatment was continued for 10 days. Paw diameter and hematological and biochemical variables were quantified. ELISA was performed for the estimation of inflammatory cytokines. In the acute oral toxicity study, no mortality or morbidity were observed, so the LD_{50} of this plant was greater than 2000 mg/kg. ABEE decreased the paw diameter with the restoration of hematological and biochemical changes. SOD and CAT levels were increased while decreasing the MDA, NO, TNF-α, and IL-6 levels in arthritic rats. It is concluded that the use of *A. bettzickiana* has low toxicity, and it can be used for the treatment of arthritis.

KEYWORDS

rheumatoid arthritis, *Alternanthera bettzickiana*, acute oral toxicity, ELISA, C-reactive protein

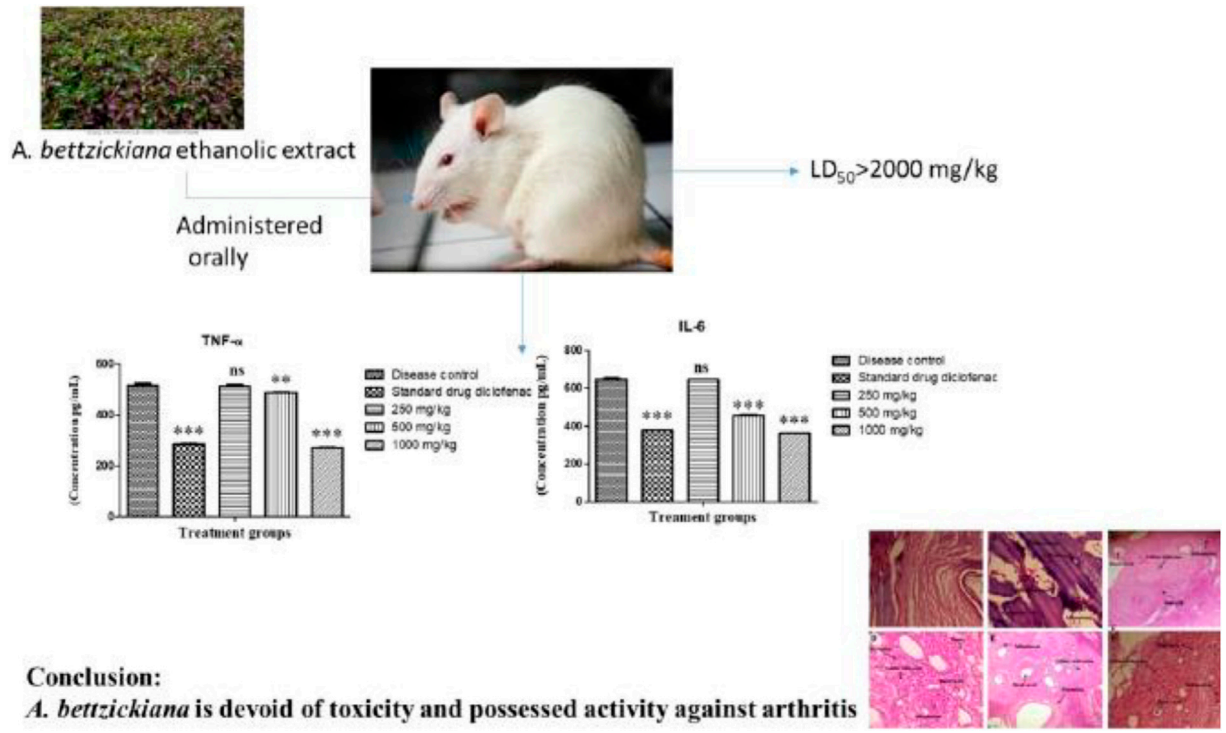

GRAPHICAL ABSTRACT

1 Introduction

The traditional use of herbal medicines was common before the evolution of synthetic and semisynthetic medicines and remains common (Giaid et al., 1993; Rahman and Gulshana, 2014; Jain et al., 2021). Many populations in developing countries depend upon herbal remedies because they are accessible and highly trusted therapy. Their use is increasing due to their availability, efficacy, and patient acceptability (Patil and Gaikwad, 2010; Benzie and Wachtel-Galor, 2011). These therapies possess natural potentials that help in competing disorders, such as arthritis, renal and hepatic disorders, and obesity (Kunle et al., 2012). Herbal preparations are taken by approximately 12% of the population in the United States in 1993 (Eisenberg et al., 1993; Eisenberg et al., 1998). It is generally thought that herbal therapies do not show side effects, in contrast to synthetic medications (Latha et al., 2010; Li and Wang, 2021).

The efficacies of herbal plants are rarely tested, despite of their significant use (Calixto, 2000; Unuofin et al., 2018). The safety of herbal remedies has become a prime focus of researchers examining herbal remedies (Chen et al., 2006). It is important to standardize the herbal preparations utilized in the treatment of various disorders (Hunter, 2008; Unuofin et al., 2018). Plants possessing biological activity should show less toxicity due to long-term use. However, many traditional remedies used in traditional medicines have shown toxic effects (Ertekin et al., 2005; Koduru et al., 2006). Paracelsus, the father of toxicology, said that all substances are poisons, but it is the dose that differentiates between treatment and poison (Hunter, 2008). Many medicines are produced from herbal remedies. Many of these preparations depend upon the use of agents in folkloric medicines. Rheumatoid arthritis is a systemic inflammatory autoimmune disease with no cure. It is marked by the consistent swelling of the synovial joints, which gives rise to bone and cartilage erosion. The objective of therapy is to alleviate joint damage, conserve function, and avert disability. RA can cause irreversible joint destruction in untreated patients within 2 years (Lee et al., 2021). Moreover, initial joint destruction in patients with recent onset could be associated with later disability (Maillefert et al., 2004). Ultimately, several organs may be affected. The main targets of disease are joints but it can affect other systems of body. *Alternanthera bettzickiana* belongs to the Amaranthaceae family. Amaranthaceae includes nearly 65 genera and more than 900 species. The family is widely distributed across tropical regions. Plants in this family are used for ornamental purposes, like *A. salixifolius*, *Celosia cristata*, *Iresine herbtsii*, etc., and some are edible and used as vegetables, such as *A. hybridus*, *A. spinosus*, *A. tricolor*, *A. viridis*, etc. (Rahman and Gulshana, 2014). *A. bettzickiana* has been cultivated in many places across the world and is native to South America. It is also called the border plant, the red calico, and the Baptist plant. Locally in Pakistan, it is also called *nanthra*.

It is frequently utilized as a bordering plant, with a food and ornamental use. Its leaves can be green, red, or both. Its leaves are used as vegetable and spinach. Its leaves are also cooked with vegetables and served with rice (Pamila and Karpagam, 2017a). It possesses wound healing, soft laxative, blood purifying, galactagogue, and fever-reducing properties. Traditionally, it is used for reducing gastrointestinal discomfort and the prophylaxis of dementia and in the treatment of arthritis in Thailand (Álvarez, 2009; Maneenoon et al., 2015). It also possess anti-Alzheimer's, antimicrobial, diuretic, hemolytic, cytotoxic, anti-inflammatory, and mutagenic activities (Barksby et al., 2007; Phusricom et al., 2013; Vidhya et al., 2015; Akhtar et al., 2017; Pamila and Karpagam, 2017a). This study was carried out to assess the acute toxicity and anti-arthritic activity of *A. bettzickiana* using a formaldehyde-induced arthritis model.

2 Materials and methods

2.1 Collection

The aerial parts of the plant were collected from Punjab in March 2019. Plant identification and authentication was performed by Dr. Mansoor, Department of Botany, University of Agriculture Faisalabad (UAF), and voucher no. 520-1-13 was issued for a crude sample of UAF herbarium.

2.2 Preparation of extract

Microwave extraction technology was used for the preparation of the extract. The extraction procedure involves three cycles after setting the microwave to 9,000 W. In the first cycle, 750 ml ethanol is used, while in the other two cycles, 500 ml ethanol was added to 100 g powder in three beakers. Beakers were placed into the microwave oven and cooked for 2 min. The microwave oven door remained open for a period of 30 s. This procedure was repeated five times. The same process was repeated for other cycles. The extract was filtered by muslin cloth and then by whatman filter paper to obtain filtrate. The filtrate from every cycle was collected, and the solvent was evaporated at 40°C. The extract was kept in amber colored bottles (Shah et al., 2017).

2.3 Animal husbandry

Following the OECD guideline 425, nonpregnant female Wistar rats weighing 130 ± 30 g and aged 9–10 weeks were randomly taken. Rats were housed under standard conditions for 5 days to acclimatize them. The animal house was kept at 22 ± 3°C with 30–70% relative humidity. The light and dark cycle was 12 h long. The rats were given a standard laboratory diet with tap water.

2.4 Approval from animal's ethics committee

The study was carried out after taking permission from animal's ethics committee, Govt. College University Faisalabad with Ref. No. GCUF/ERC/2143.

2.5 Acute oral toxicity study (OECD 425)

The rats were housed under standard conditions in the animal house of Govt. College University Faisalabad (GCUF) for 5 days to acclimatize them with new environment. The limit test dose of 2000 mg/kg dose was given. Rats were fasted 3–4 h before dosing but provided with water. Dosing was given to single rats on the basis of weight. Rats were strictly monitored for initial 30 min and then for 4 hours. Food was given 1–2 h after dosing. Four rats were given the same dose orally after survival of first rat. The same procedure was adopted for control group of five rats. The control group was administered distilled water. Both groups were observed for the toxic effects for first 6 h and then for a duration of 14 days. The surviving rats were noticed for any toxic reaction. The weight of animals was recorded as well. After 14 days rats were again weighed and blood was accumulated *via* cardiac puncture under chloroform anesthesia. The serum was isolated for carrying out biochemical and hematological analysis. Vital organs (liver, heart, and kidney) were removed from slaughtered rats after cervical dislocation. The weight of these organs was recorded. The organs were preserved in 10% formaldehyde solution and were implanted in paraffin wax (Saleem et al., 2017).

2.5.1 Hematological and biochemical analysis

Blood from both treated and vehicle control rats was collected in EDTA-containing tubes for hematological analysis. Hemoglobin (Hb), total RBC, white blood cells (WBC) count, platelets, mean corpuscular volume (MCV), packed cell volume (PVC), monocytes (M), neutrophils (N), mean corpuscular hemoglobin (MCH), eosinophils (E), mean corpuscular hemoglobin concentration (MCHC), and lymphocytes (L) were determined using Mythic CBC analyzer. Serum was separated for biochemical analysis. Cholesterol, triglycerides, low density lipoprotein (LDL), high density lipoprotein (HDL), very low density lipoprotein (VLDL), bilirubin, alanine aminotransferase (ALT), aspartate aminotransferase (AST), alkaline phosphatase, urea, blood urea nitrogen, creatinine, uric acid, proteins, albumin, globulin, A/G ratio, rheumatoid factor (RF), and C-reactive

TABLE 1 Effect of ABEE (at limit dose 2000 mg/kg p.o.) and vehicle treatment on body weight of rats in acute toxicity study.

Groups	Body weight on 1st day (g)	Body weight on 14th day (g)
Control group (Distilled water)	141.94 ± 2.24	145 ± 3.80^{ns}
Treatment group (ABEE 2000 mg/kg)	132 ± 6.27	138 ± 2.91^{ns}

Values are presented as means ± SEMs (n = 5) and analyzed with two-way ANOVA followed by a Bonferroni posttest. ns, nonsignificant as compared to disease control. ABEE, *Alternanthera bettzickiana* ethanolic extract.

protein (CRP) were measured using Tecno 786 bio chemistry analyzer (Anwar et al., 2021b).

2.5.2 Histopathological analysis

Vital organs separated from slaughtered rats were fixed in formalin (10%) and then implanted in paraffin wax. Sections were slashed at 5 mm and stained with hematoxylin and eosin. Histopathological modifications were studied under a photomicroscope (Anwar et al., 2021a).

2.6 *In vivo* assessment of anti-arthritic potential by formaldehyde-induced arthritis

Wistar albino rats weighing 150–180 g were used. Rats were divided into five groups of five rats each. Group 1 (disease control group): rats were injected with formaldehyde solution on the first and third day of experiment. Group 2 (Diclofenac sodium treated): rats were injected with formaldehyde solution, as in group 1, and administered diclofenac sodium daily at a dose of 10 mg/kg for 10 days. Groups 3–5 (ABEE treated) rats received formaldehyde solution as in group 1 and were administered ABEE at a dose of 250, 500, 1,000 mg/kg, respectively, for 10 days. All treatments were dissolved in distilled water and given orally; 30 min after drug administration, arthritis was developed by a sub-plantar injection of 0.1 ml of 2% w/v formaldehyde solution on days 1 and 3 of the experiment (Uttra et al., 2019). Arthritis was assessed by measuring mean increase in paw diameter by Vernier caliper for 10 days. The percentage inhibition of edema was calculated utilizing the following formula:

$$\%\,\text{inhibition} = \frac{Vc - Vt}{Vt} * 100 \quad (1)$$

where Vc is the paw diameter of disease control and Vt is the paw diameter of treated.

2.6.1 Arthritis evaluation by hematological and biochemical parameters

The rats were slaughtered under chloroform anesthesia after 10 days of study, and blood was collected *via* cardiac puncture. The hematological factors (red blood cells, hemoglobin, white blood cells, erythrocyte sedimentation rate, and platelet count) were measured by Mythic CBC analyzer while biochemical variables (alanine aminotransferase, alkaline phosphatase, aspartate aminotransferase, creatinine, rheumatoid factor, C-reactive protein, and urea) were determined with Tecno 786 bio chemistry analyzer. Next, animals were sacrificed by painless procedure by cervical dislocation under anesthesia (Saleem et al., 2020a).

2.6.2 Enzyme linked immunosorbent assay

ELISA was performed to determine the concentrations of tumor necrosis factor and interleukin 6 in serum using kit protocols (Elabscience, Catalog Number E-EL-R0019 and E-EL-R0015) (Cheng et al., 2015).

2.6.3 Determination of oxidative stress biomarkers

The serum concentration of nitric oxide was measured using Nitric Oxide ELISA kit (Elabscience, Catalog number E-BC-K036). Microplate ELISA Reader (BI, United States, 800TS-UV) was used to measure the absorbance. Serum levels of superoxide dismutase (Elabscience, Catalog number E-BC-K020), catalase (Elabscience, Catalog number E-BC-K106), and malondialdehyde (Elabscience, Catalog number E-EL-0060) were determined after the study ended (Saleem et al., 2020b).

2.7 Statistical analysis

The results were presented as means ± SEMs (n = 5), and the statistical significance was analyzed by two-way ANOVA, followed by Bonferroni's posttest, and applied by Graph Pad Prism 5 software. $p \leq 0.05$ was considered to indicate statistical significance.

3 Results

3.1 Acute oral toxicity study

3.1.1 Body weight and behavioral changes

The administration of ABEE showed no mortality throughout the study. Experimental animals were

TABLE 2 Behavioral pattern of rats treated with ABEE (2000 mg/kg p.o.) during acute toxicity study.

Parameters	Observations of vehicle control and ABEE-treated group											
	30 min		4 h		24 h		48 h		7 days		14 days	
	VCG	ABTG	VCG	ABTG	VCG	ABTG	VCG	ABTG	VCG	ABTG	VCG	ABTG
Eyes	N	N	N	N	N	N	N	N	N	N	N	N
Respiration	N	↑	N	N	N	N	N	N	N	N	N	N
Itching	P	P	P	P	P	P	P	P	P	P	NF	NF
Sleep	N	N	N	N	N	N	N	N	N	N	N	N
Fur	N	E	N	N	N	N	N	N	N	N	N	N
Urination	N	N	N	N	N	N	N	N	N	N	N	N
Gait	N	SI	N	SI	N	SI	N	SI	N	N	N	N
Convulsion/tremor	NF	P	NF	P	NF	P	NF	P	NF	NF	NF	NF
Somatomotor activity	N	MD	N	MD	N	MD	N	MD	N	MD	N	N
Salivation	N	N	N	N	N	N	N	N	N	N	N	N
Coma	NF	NF	NF	NF	NF	NF	NF	NF	NF	NF	NF	NF
Feces consistency	N	N	N	N	N	N	N	N	N	N	N	N
Mucous membrane	N	N	N	N	N	N	N	N	N	N	N	N
Mortality	NF	NF	NF	NF	NF	NF	NF	NF	NF	NF	NF	NF

CG, control group; ABTG, *Alternanthera bettzickiana* treated group; N, normal; E, elevated; P, present; SI, slightly elevated; ↑, increased; MD, moderately decreased; NF, not found.

TABLE 3 Effect of ABEE (at limit dose 2000 mg/kg p.o.) and vehicle treatment on weight of organs and organ-to-body weight indices in acute toxicity study.

Groups	Heart	Kidney	Liver
Weight of organs (g)			
Control group (distilled water)	0.67 ± 0.01	0.51 ± 0.03	4.16 ± 0.02
Treatment group (ABEE 2000 mg/kg)	0.58 ± 0.01^{ns}	0.49 ± 0.01^{ns}	4.20 ± 0.13^{ns}
Organ-to-body weight indices			
Control group (distilled water)	0.462 ± 0.027	0.351 ± 0.017	2.868 ± 0.029
Treatment group (ABEE 2000 mg/kg)	0.420 ± 0.025 ^{ns}	0.355 ± 0.010 ^{ns}	3.043 ± 0.010 ^{ns}

Values are presented as means ± SEMs ($n = 5$) and analyzed by two-way ANOVA followed by a Bonferroni posttest. ns, nonsignificant as compared to disease control. ABEE, *Alternanthera bettzickiana* ethanolic extract; organ-to-body weight index = (organ weight ×100)/body weight.

observed for 14 days with special consideration. The body weights of vehicle control and ABEE-treated rats were increased, as shown in Table 1. Slight behavioral changes were recorded in treated rats, such as convulsions, and tremor was recorded in ABEE treated rats after during initial 3 h. Any effect on the fur of the treated animals were elevated for 2 h after dosing. Somatomotor activity was decreased during experimental period. The respiratory rate was also increased in extract treated rats for one and half hour after dosing then it became normal. Itching was observed during first week of study in both groups. Other behavioral features were normal compared with vehicle control rats (Table 2).

3.1.2 Organ-to-body weight index

Organ-to-body weight index was determined and is presented in Table 3; it showed no remarkable changes among the groups. No lesions were observed on isolated organs, such as the liver, heart, or kidney, of the treated animals.

3.1.3 Effect of ABEE on hematological and biochemical variables in acute oral toxicity study

The hematological and biochemical profiles of rats treated with ABEE are shown in Tables 4 and 5. No significant change was observed for hemoglobin, RBCS, ESR and TLC, neutrophils, eosinophils, lymphocytes, or monocytes, in contrast to vehicle control group. It should also be noted that there were no

TABLE 4 Effect of ABEE (at limit dose 2000 mg/kg p.o.) on hematologic variables in acute toxicity study.

Parameters	Units	Control group	Treatment group (2000 mg/kg)
Hemoglobin	g/dL	15.2 ± 1.14	16.8 ± 0.86^{ns}
TLC	*10^9/L	6.3 ± 0.76	7.3 ± 0.57^{ns}
ESR	mm/1st h	6 ± 1.1.4	7.4 ± 0.71^{ns}
RBC	*10^{12}/L	6.57 ± 0.67	7.14 ± 0.93^{ns}
HCT (PCV)	%	37.2 ± 1.33	36.6 ± 0.94^{ns}
MCV	Fl	62.8 ± 0.64	58.3 ± 2.91^{ns}
MCH	Pg	25.4 ± 2.70	26.4 ± 0.49^{ns}
MCHC	%	53.2 ± 2.28	48.2 ± 0.60^{ns}
Platelets	*10^9/L	937 ± 11.7	1,437 ± 8.95***
Neutrophils	%	4 ± 0.35	5 ± 0.35^{ns}
Lymphocytes	%	90 ± 9.06	93 ± 5.59^{ns}
Monocytes	%	5 ± 0.35	2 ± 0.48^{ns}
Eosinophils	%	1 ± 0.22	2 ± 0.48^{ns}
RF	IU/mL	23.6 ± 1.34	19.62 ± 0.97^{ns}
CRP	mg/L	3.70 ± 0.65	2.80 ± 0.58^{ns}

Values are presented as means ± SEMs ($n = 5$) and analyzed by two-way ANOVA followed by a Bonferroni posttest. ns, nonsignificant, ***$p < 0.001$ as compared to disease control. ABEE, *Alternanthera bettzickiana* ethanolic extract.

TABLE 5 Effect of ABEE (at limit dose 2000 mg/kg p.o.) on biochemical variables in an acute toxicity study.

Parameters	Units	Control group	Treatment group (2000 mg/kg)
Lipid profile			
Cholesterol	mg/dL	81 ± 1.70	74 ± 3.25^{ns}
Triglycerides	mg/dL	97 ± 4.49	86 ± 5.40^{ns}
High density lipoprotein	mg/dL	24 ± 4.52	23 ± 2.12^{ns}
Low density lipoprotein	mg/dL	73 ± 6.21	66 ± 4.95^{ns}
Very low density lipoprotein	mg/dL	19 ± 2.28	17 ± 2.02^{ns}
Liver function test			
Bilirubin	mg/dL	0.37 ± 0.01	0.34 ± 0.01^{ns}
AST	U/L	63 ± 6.51	57 ± 6.51^{ns}
ALT	U/L	52 ± 6.96	48 ± 3.42^{ns}
Alkaline phosphatase	U/L	216 ± 8.34	143 ± 6.58***
Albumin	g/L	3.30 ± 0.02	2.90 ± 0.03^{ns}
Globulin	g/L	2.9 ± 0.02	2.4 ± 0.02^{ns}
Proteins	g/L	6.20 ± 0.53	5.30 ± 0.60***
A/G ratio	g/L	1.1 ± 0.007	1.20 ± 0.01^{ns}
Renal function test			
Urea	mg/dL	18 ± 2.02	16 ± 2.02^{ns}
BUN	mg/dL	10 ± 1.14	9 ± 0.70^{ns}
Creatinine	mg/dL	0.56 ± 0.02	0.41 ± 0.01^{ns}
Uric acid	mg/dL	3.20 ± 0.44	2.90 ± 0.03^{ns}

Values are presented as means ± SEMs ($n = 5$) and analyzed by two-way ANOVA followed by a Bonferroni posttest. ns, nonsignificant, ***$p < 0.001$, as compared to disease control. ABEE, *Alternanthera bettzickiana* ethanolic extract.

significant alterations in HCT, MCHC, MCH, or MCV in comparison to vehicle control rats. The platelet count was raised significantly in the treatment group ($p < 0.001$) when compared with the vehicle control group. It was noted that rats showed no significant changes in LDL, VLDL, cholesterol, HDL, or triglycerides values of the treatment group relative to the

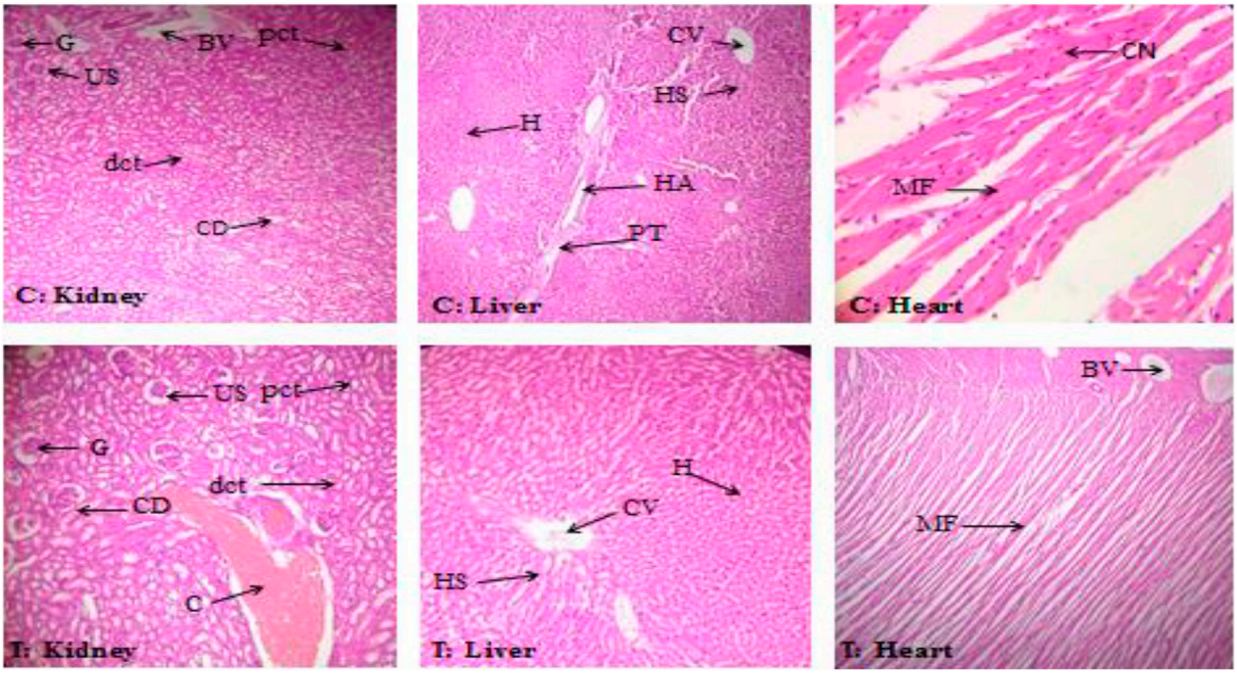

FIGURE 1
Histopathological assessment of kidney, liver, and heart of the control group (C) and the treatment group (T) at 40 × and 10 × magnification. G: glomerulus; US: urinary space; BV: blood vessel; pct: proximal convoluted tubules; dct: distal convoluted tubules; CD: collecting duct; C: congestion; H: hepatocytes; CV: central vein; HS: hepatic sinusoid; HA: hepatic artery; PT: portal triad; CN: central nuclei; MF: myocardial fibrils.

TABLE 6 Effects of ABEE on paw diameter of formaldehyde-induced arthritic rats.

Treatment groups	Paw diameter					
	Day 0	Day 2	Day 4	Day 6	Day 8	Day 10
Disease control	3.83 ± 0.32	5.84 ± 0.55	7.86 ± 0.539	9.97 ± 0.316	10.51 ± 0.628	12.98 ± 0.412
Standard drug diclofenac (10 mg/kg)	3.44 ± 0.184^{ns}	4.95 ± 0.270^{ns} (15.23%)	5.91 ± 0.283** (24.80%)	5.42 ± 0.212*** (45.63%)	4.34 ± 0.298*** (58.70%)	3.79 ± 0.201*** (70.80%)
ABEE 250 m/kg	3.74 ± 0.292^{ns}	5.54 ± 0.595^{ns} (5.13%)	6.83 ± 0.430^{ns} (13.10%)	6.41 ± 0.607*** (35.70%)	5.72 ± 0.354*** (45.57%)	5.63 ± 0.336*** (56.62%)
ABEE 500 mg/kg	3.69 ± 0.116^{ns}	5.19 ± 0.20^{ns} (11.13%)	6.26 ± 0.519* (20.35%)	5.93 ± 0.604*** (40.52%)	4.94 ± 0.185*** (52.99%)	4.51 ± 0.212*** (65.25%)
ABEE 1000 mg/kg	3.69 ± 0.311^{ns}	4.58 ± 0.58^{ns} (21.57%)	5.47 ± 0.342*** (30.40%)	4.64 ± 0.381*** (53.46%)	3.85 ± 0.430*** (63.36%)	3.62 ± 0.130*** (72.11%)

Results are presented as means ± SEMs ($n = 5$) and analyzed by two-way ANOVA followed by a Bonferroni posttest. ns, nonsignificant, ***$p < 0.001$, as compared to disease control. ABEE, *Alternanthera bettzickiana* ethanolic extract.

vehicle control group values (Table 5). The levels of aspartate aminotransferase (AST), alanine aminotransferase (ALT), proteins, globulin, albumin, A/G ratio were altered nonsignificantly in the treatment group in contrast to vehicle control rats. Nonsignificant variation was recorded in the urea, blood urea nitrogen, creatinine, uric acid, and total bilirubin levels of treatment rats when compared with vehicle control rats (Table 5). Alkaline phosphatase and protein levels were decreased significantly in the treatment group relative to the vehicle control group.

3.1.4 Histopathological assessment in acute oral toxicity study

Histopathological assessment showed no structural changes in the kidney, liver, or heart tissue of ABEE-treated rats. Histopathological assessment showed that ABEE did not lead to

TABLE 7 Effects Of ABEE on hematological and biochemical variables of formaldehyde-induced arthritic rats.

Parameters	Disease control	Standard (10 mg/kg)	ABEE (250 mg/kg)	ABEE (500 m/kg)	ABEE (1,000 mg/kg)
Hb	4.59 ± 0.43	15.23 ± 1.03***	10.51 ± 1.84*	12.31 ± 1.41**	16.10 ± 1.07***
ESR	17 ± 1.07	8.00 ± 1.41**	14 ± 2.12^{ns}	11 ± 1.41*	7 ± 1.17***
RBCs	4.58 ± 0.48	10.91 ± 0.55***	5.99 ± 0.58^{ns}	9.88 ± 1.14**	11.78 ± 1.30***
WBCs	19.63 ± 1.68	10.38 ± 1.04***	18.6 ± 0.88^{ns}	13.59 ± 1.41**	7.57 ± 0.34***
Platelets	1958 ± 19.14	972.80 ± 8.06***	1,343 ± 17.82***	1,153 ± 11.60***	851 ± 5.00***
AST	78.75 ± 3.68	47.90 ± 3.70***	75.90 ± 4.56^{ns}	59.78 ± 0.44**	31.60 ± 2.30***
ALP	254 ± 8.78	105.23 ± 3.80***	253.65 ± 6.51^{ns}	200.56 ± 17.40**	98.38 ± 4.11***
ALT	48 ± 5.59	25 ± 1.58***	37 ± 1.14^{ns}	30 ± 1.61**	17 ± 1.84***
Urea	42.80 ± 1.51	17 ± 1.41***	32 ± 1.41***	21 ± 0.74***	15 ± 1.84***
Creatinine	4.3 ± 0.277	2.40 ± 0.44**	3.60 ± 0.114^{ns}	2.50 ± 0.412**	1.8 ± 0.326***
CRP	21.3 ± 2.70	12.78 ± 1.30*	16.51 ± 1.58^{ns}	10.53 ± 1.84**	7.54 ± 1.84***
RF	22 ± 1.19	10 ± 1.70***	15.04 ± 1.01**	13 ± 0.65***	9 ± 2.00***

Results are presented as means ± SEMs (n = 5) and analyzed by one-way ANOVA followed by a Bonferroni posttest. ns, nonsignificant; ***p < 0.001; **p < 0.01; *p < 0.05 as compared to disease control. Hb, hemoglobin; ESR, erythrocyte sedimentation rate; RBCs, red blood cells; WBCs, white blood cells; AST, aspartate aminotransferase; ALP, alkaline phosphatase; ALT, alanine aminotransferase; CRP, C-reactive protein; RF, rheumatoid factor; BUN, blood urea nitrogen; HDL, high-density lipoprotein; LDL, low-density lipoprotein; ABEE, *Alternanthera bettzickiana* ethanolic extract.

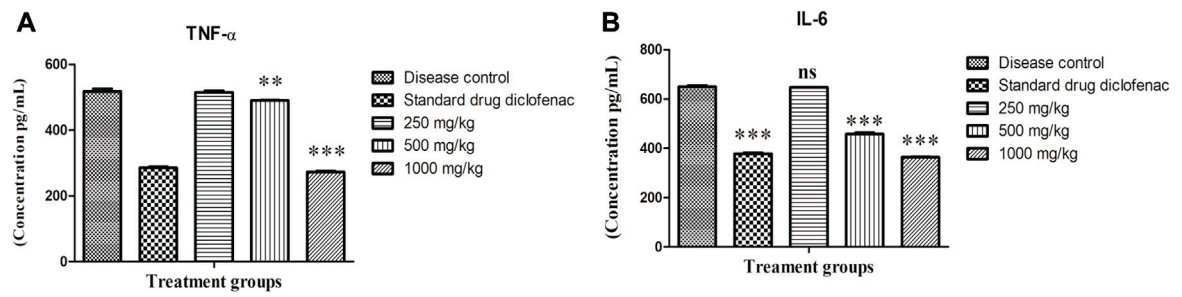

FIGURE 2
Effect of *Alternanthera bettzickiana* ethanolic extract on inflammatory mediators **(A)** TNF-α and **(B)** IL-6 in formaldehyde-induced arthritis. Results are presented as means ± SEMs (n = 5) and analyzed by one-way ANOVA followed by a Bonferroni posttest. ns, nonsignificant; ***p < 0.001; **p < 0.01 as compared to disease control. ABEE, *Alternanthera bettzickiana* ethanolic extract.

any side effects on physiological features, and the architecture of the vehicle control and acute toxicity groups was found to be similar, with only slight congestion being recorded in the kidney tissues of treatment rats (Figure 1). The overall histopathological assessment of kidney liver and heart sections of ABEE-treated rats showed no remarkable variation in contrast to vehicle control group, which means that the plant was safe at a 2000 mg/kg dose.

3.2 Effect of *Alternanthera bettzickiana* ethanolic extract in formaldehyde-induced arthritis in Wistar rats

3.2.1 Effect on paw diameter

Table 6 sums up the effects of ABEE (250, 500, 1,000 mg/kg) and diclofenac sodium (10 mg/kg) in formaldehyde-induced arthritis. Formaldehyde injection showed a swelling of left hind paw of all rats on the first and third days. The increase in paw inflammation was recorded for 4 days, and then it was found attenuating in treated rats in a concentration dependent manner. ABEE at a 1,000 mg/kg dose exhibited maximum inhibitory effect (72.11%) on paw diameter, while 500 and 250 mg/kg extract revealed a 65.25% and 56.62% reduction in paw diameter respectively. Diclofenac sodium (10 mg/kg) rats showed 70.80% decrease (p < 0.001) in paw diameter at day 10. These results indicated that ABEE at 1,000 mg/k exhibited a peak effect, and the outcomes were prominent relative to the standard drug diclofenac sodium.

3.2.2 Effect on hematological and biochemical variables

The blood and serum parameters of animals administered with ABEE and diclofenac sodium are shown in Table 7.

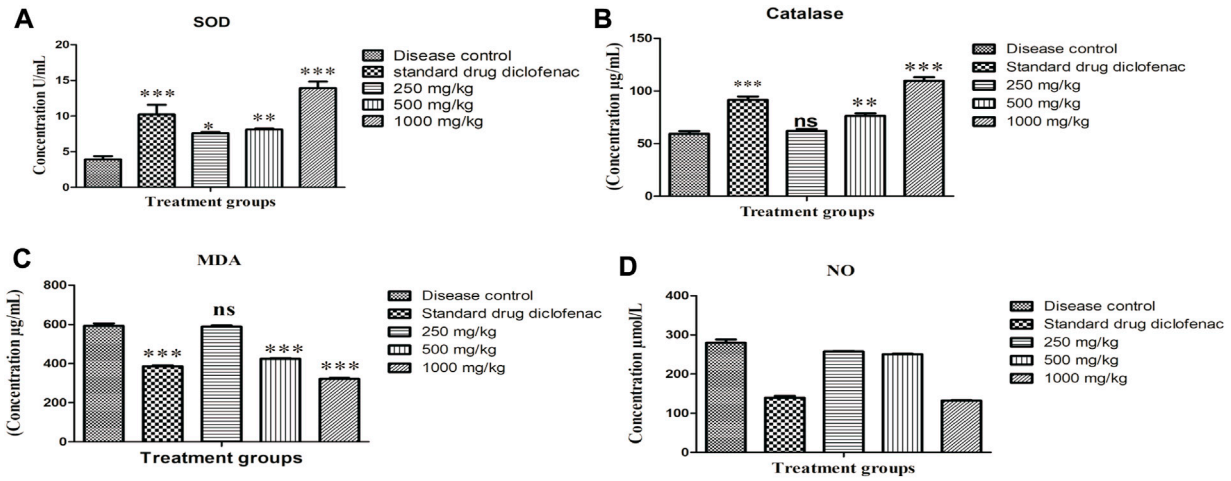

FIGURE 3
Effect of *Alternanthera bettzickiana* ethanolic extract on oxidative stress biomarkers **(A)** SOD, superoxide dismutase, **(B)** catalase, **(C)** MDA, malondialdehyde, and **(D)** NO, nitric oxide in formaldehyde induced arthritis. Results are presented as mean ± SEM ($n = 5$) and analyzed with one-way ANOVA followed by a Bonferroni posttest. ***$p < 0.001$; **$p < 0.01$; * $p < 0.05$; ns, nonsignificant as compared to disease control. ABEE, *Alternanthera bettzickiana* ethanolic extract.

Changes in these parameters were evaluated after 10 days of formaldehyde induction in rats of various groups. Hematological and biochemical variables, such as elevation in ALP, AST, ALT, platelets, WBCs count, creatinine, CRP, urea, and RF, in addition to reduction in RBCs and hemoglobin, were observed in disease control group. Similarly, administration with ABEE and standard drug diclofenac sodium significantly ($p < 0.001$) averted abnormal modifications of hematological variables in treatment groups altered by the formaldehyde injection. Furthermore, ALP, ALT, and AST levels noticeably increased in disease control rats and significantly decreased in animals treated with 500 and 1,000 mg/kg ABEE, while 250 mg/kg dose of extract exhibited nonsignificant decrease in ALP, ALT, and AST levels in treatment group relative to the disease control group. Similarly, the standard drug diclofenac sodium also significantly decreased ALP, ALT, and AST levels in treated group, by contrast to disease control group. Moreover, the noticeably increased creatinine and urea concentrations in disease control animals were significantly decreased with ABEE and standard drugs in treatment rats. Additionally increased serum values of CRP and RF were observed in disease control animals, while administration with ABEE and standard drug diclofenac sodium significantly decreased CRP and RF levels in treatment groups. These results indicated that ABEE at 1,000 mg/k exhibited peak effects, and outcomes were prominent as compared to standard drug diclofenac sodium.

3.2.3 Effect on serum levels of TNF-α and IL-6: ELISA study

An elevated level of TNF-α ($p < 0.001$) was noticed in disease control rats (517.59 ± 8.355 pg/ml), although the elevation was significantly decreased by administration of ABEE at 1,000 mg/kg (273.45 ± 2.30 pg/ml), 500 mg/kg (490.00 ± 1.70 pg/ml) and diclofenac sodium (285.79 ± 2.91 pg/ml) when compared with disease control rats (Figure 2A). An abnormally increased level of IL-6 was noted in the serum of the disease control group (649.91 ± 4.52 pg/ml). This elevated level was significantly ($p < 0.001$) decreased by ABEE at 1,000 mg/kg (363.50 ± 2.31 pg/ml), 500 mg/kg (457.53 ± 5.70 pg/ml), and diclofenac sodium (377.91 ± 2.98 pg/ml) (Figure 2B). The most effective dose of plant extract, which, exhibited the highest decrease in serum concentration of TNF-α and IL-6, was 1,000 mg/kg.

3.2.4 Effect on oxidative stress biomarkers

The outcomes of oxidative stress exhibited that SOD (3.93 ± 0.447 U/mL) and CAT concentrations in serum (59.31 ± 2.47 U/L) were significantly reduced ($p < 0.001$) in disease control animals. However diclofenac sodium (10 mg/kg), 500 and 1,000 mg/kg concentration of plant extract increased ($p < 0.001$) the serum concentrations of SOD and CAT in adjuvant-injected groups, as shown in Figure 3A,B respectively. MDA (592.53 ± 12.26 ng/ml) and NO concentrations in serum (279.81 ± 8.518 µmol/L) were also remarkably elevated ($p < 0.001$) in disease control animals. MDA and NO concentrations were significantly reduced by

diclofenac sodium and plant extract in adjuvant-injected groups as shown in Figure 3C,D respectively.

4 Discussion

Plants have been utilized for the treatment of various disorders for a very long time (Ridtitid et al., 2008). Therapy with medicinal plants is acquiring popularity because WHO supports their proper ethno-medicinal use and calls for the safety assessment of herbal therapy (Daswani et al., 2006; Ogbonnia et al., 2010; Vaghasiya et al., 2011). Who highlights the validation of safe usage of herbal medicines by conducting different toxicity studies? No mortality was found, although some alterations in behavior, such as a decrease in somatomotor activity, elevated respiratory rate, tremor, and itching were noted in acute toxicity group (Table 1). It was noted that water and food intake were normal during the study period, and body weight changes were found to be nonsignificant, which indicates normal protein, lipid, and carbohydrate metabolism inside the body (Zhang et al., 2022). These nutrients are important for performing various physiological functions in human body (Stevens and Mylecraine, 1994; Saleem et al., 2017).

The liver, lungs, kidney, spleen, and heart are major human organs and are important targets sites of any metabolic toxin agent. The metabolic reactions initiated by toxic substances mostly target the heart, kidney, and liver (Vaghasiya et al., 2011). When rats were slaughtered after 14 days, no lesions were observed on macroscopic assessment of liver, heart, and kidney in contrast to vehicle control group. Statistically, no significant alterations were observed in organ-to-body weight index in rats of acute toxicity group in comparison to control group. Substances are classified into five groups on the basis of LD50 values following globally harmonized classification system (Saleem et al., 2017). ABEE can be placed in group 5 because it falls in a lower-toxicity category (LD50 > 2000 mg/kg).

Animal health is assessed by various variables, such as serum biomarker assessment. Liver damage induced by any toxic substance could cause increased total proteins and increased AST and ALT levels (Ozer et al., 2008; Ramaiah, 2011). Statistically nonsignificant increases in globulin, total proteins, and ALT levels were noticed in acute toxicity study. Hepatocellular injury enhances membrane permeability and causes a discharge of aminotransferases in blood (Ali et al., 2008; Ogunlana et al., 2013). ALP is a marker of biliary tract blockage (Manjunatha et al., 2005). In this study, ALP value was significantly reduced (Table 3), which shows hepatoprotective activity of plant (Saleem et al., 2016). Hyperlipidemias are due to other factors like therapies, diet, and disorders, such as tumors, diabetes, hypothyroidism, or nephrosis (Hou et al., 2022). Decreased values of triglycerides, cholesterol, high density lipoprotein, low density lipoprotein, and very low density lipoprotein (Table 3) were observed in acute toxicity group (Saleem et al., 2017; Zhang et al., 2022).

Histopathological assessment is a benchmark for assessing pathological signs exhibited in simultaneous study in which the architecture of organs of treated rats was normal, toxicological signs were not present, and matches with vehicle rats architecture, showing harmless findings of ABEE with LD50 value more than 2000 mg/kg. Toxic substances are metabolically changed into harmless substances in the liver, which is the principal area for metabolism (Harizal et al., 2010; Li et al., 2022). At initial phase signs in hepatocytes are not understandable because of suitability of liver to revive the injurious tissues (Salawu et al., 2009). Histopathological assessment of vital organs did not show any inflammation and degeneration, and only slight congestion was observed in kidney tissues of acute toxicity group. The absence of lesions in liver, kidney, and heart indicate the safety level of plants in experimental animals. The results exhibit that overall no noxious signs were observed during the study period and LD50 was greater than 2000 mg/kg (Saleem et al., 2017).

Formaldehyde-induced arthritis is an appropriate method of assessing the anti-proliferative potential and evaluate anti-arthritic agents. Formaldehyde induces arthritis by breaking down proteins at the site of injection, which produces an immune response against the degraded substances (Nair et al., 2012). Arthritic action of formaldehyde consists of two phases. In the initial phase, substance P is released, while in the late phase bradykinin, histamine, serotonin, and prostaglandin are released, which results in marked permeability and vasodilation (Bischoff, 2008). These mediators are responsible for hyperalgesia by stimulating nerve terminals and pain receptors. Hence, hypersensitivity is evoked at the injection site (Desai Nilesh et al., 2012). It has been revealed that CNS acting drugs hinder both phases uniformly, but peripherally acting drugs hamper the late phase (Uttra and Hasan, 2017).

In the present study, the inhibition of paw edema is due to the potential of *A. bettzickiana* to prevent protein denaturation. It may be due to a decrease in the release of inflammatory mediators. The impediment of both phases of inflammation shows that *A. bettzickiana* acts on CNS. Formaldehyde induces an arthritic model that resembles human arthritis, thus allowing for the evaluation of the anti-arthritic activity of test substance. Formaldehyde injection develops localized inflammation.

TNF-α and IL-6 promote joint damage, bone erosion, and cell death in the inflamed joints (Zheng et al., 2014). The increased formation of TNF-α leads to increase in the expression of IL-6 and IL-1β, which in turn produce the degrading enzymes responsible for osteoclast differentiation, thus stimulating the development of arthritic erosion and vasodilation in the edematous area (Cheng, 2015; Sano, 2011). IL-6 causes bone resorptions and autoantibody production (Alvarez, 2009). Any substance that blocks the production of

IL-6 and TNF-α causes a significant revolution in the management of rheumatoid arthritis (Nair et al., 2012).

Reactive oxygen species (ROS) are formed as a consequence of metabolism and different environmental factors, such as cigarette smoke or air pollutants. ROS are produced at low concentrations in all tissues. In general, different antioxidant systems regulate this formation. High concentration or insufficient removal of ROS leads to oxidative stress (Gambhir et al., 1997). ROS are active and can harm cell structures, such as proteins, nucleic acids, lipids, and carbohydrates. They can change their functions. The disturbance in balance between oxidants and antioxidants is called oxidative stress. The control of redox state is important for cell proliferation and cell viability. The antioxidant system is of two types. This includes enzymatic and nonenzymatic antioxidants that are effective in neutralizing damaging effects of ROS (Birben, 2012), although in disease conditions, the antioxidant system can be overcome. Oxidative stress comes up with many disease conditions, such as cancer atherosclerosis, diabetes, asthma, and hypertension. The main enzymatic antioxidants are GSH-px, catalase, and SOD. SOD plays crucial role in free radical defense (Kumar et al., 2016). Glutathione peroxidase and catalase inhibit the accumulation of H_2O_2 by changing it into water and oxygen.

Decomposition of lipids produces many products including malondialdehyde (Halliwell, 1991; Baskol et al., 2005). Lipid peroxidation is a well-accepted mechanism of cell damage and it indicates oxidative stress in tissues and is an indicator of lipid peroxidation. Increased levels of MDA are reported in the plasma of rheumatoid arthritis patients (Karatas et al., 2003; Taysi et al., 2002). Nitric oxide is an endogenously formed molecule that possesses important functions in cell signaling and participates in different physiological processes. Radical species that cause oxidative activity in an inflamed joint include reactive oxygen and nitrogen species. These mediate cartilage damage (Ali et al., 2008). NO performs different functions in inflamed areas, such as apoptosis, signal transduction, and mitochondrial function (Phillips et al., 2010). Elevated concentrations of NO in synovial fluid and serum have been reported in rheumatoid arthritis (Ersoy ET., 2010). The current study explains the promising effect of ABEE in formaldehyde-induced arthritis. The results of current study showed that ABEE at dose of 1,000 mg/kg deceased edematous reactions suggesting that constituents of *A. bettzickiana* target biphasic reactions (Table 6).

The outcomes of a previous study showed that ABEE decreased oxidative stress and mRNA expression of pro-inflammatory biomarkers (NF-kB, IL-6, TNF-α, IL-1β, and COX-2), although it increased mRNA expression of immunoregulatory cytokines (IL-4, I-kB, and IL-10). These mechanisms could be accountable for the anti-inflammatory and the anti-arthritic potential of plants. The anti-inflammatory potential of ABEE may be due to the existence of many phytochemicals, such as n-hexadecanoic acid, linoleic acid, phytol, vitamin E, Ar-turmerone, squalene, and farnesol, which possess anti-inflammatory activity (Pamila and Karpagam, 2017b; Manan et al., 2020).

5 Conclusion

This study concluded that *Alternanthera bettzickiana* ethanolic extract has low toxicity, as even a 2 g/kg dose did not showed any mortality or morbidity, and no difference was observed in biochemical and hematological parameters in comparison to the control group. Outcomes also proposed that the oral administration of ABEE in arthritic animals remarkably decreased paw thickness and inhibited abnormal changes in hematological and biochemical variables. *Alternanthera bettzickiana* may be used as an optimal therapy for the treatment of rheumatoid arthritis.

Data availability statement

The raw data supporting the conclusion of this article will be made available by the authors, without undue reservation.

Ethics statement

The study was reviewed and approved by the Animal Ethics Committee, Government College University Faisalabad (Ref. No. GCUF/ERC/2143).

Author contributions

US supervised the project, US and BA drafted the manuscript, MM and NA did the experimental work. AA and AZ helped in dta analyses.

Conflict of interest

The authors declare that the research was conducted in the absence of any commercial or financial relationships that could be construed as a potential conflict of interest.

Publisher's note

All claims expressed in this article are solely those of the authors and do not necessarily represent those of their affiliated organizations, or those of the publisher, the editors, and the reviewers. Any product that may be evaluated in this article, or claim that may be made by its manufacturer, is not guaranteed or endorsed by the publisher.

References

Akhtar, M., Sharif, A., Saleem, M., Saleem, A., Akhtar, B., Raza, M., et al. (2017). Genotoxic and cytotoxic potential of Alternanthera Bettzickiana, an important ethno-medicinal plant. *Cell. Mol. Biol.* 63 (8), 109–114. doi:10.14715/cmb/2017.63.8.23

Ali, T., Bhalli, J. A., Rana, S. M., and Khan, Q. M. (2008). Cytogenetic damage in female Pakistani agricultural workers exposed to pesticides. *Environ. Mol. Mutagen.* 49 (5), 374–380. doi:10.1002/em.20395

Álvarez, J. L. P. (2009). Interleukin 6 in the physiopathology of rheumatoid arthritis. *Reumatol. Clin.* 5 (1), 34–39. doi:10.1016/S1699-258X(09)70203-7

Anwar, F., Saleem, U., Ahmad, B., Ismail, T., Mirza, M. U., Ahmad, S., et al. (2021a). Acute oral, subacute, and developmental toxicity profiling of naphthalene 2-yl, 2-chloro, 5-nitrobenzoate: Assessment based on stress response, toxicity, and adverse outcome pathways. *Front. Pharmacol.* 12, 810704. doi:10.3389/fphar.2021.810704

Anwar, F., Saleem, U., Rehman, A.-U., Ahmad, B., Froeyen, M., Mirza, M. U., et al. (2021b). Toxicity evaluation of the naphthalen-2-yl 3, 5-dinitrobenzoate: A drug candidate for alzheimer disease. *Front. Pharmacol.* 12, 607026. doi:10.3389/fphar.2021.607026

Barksby, H., Lea, S., Preshaw, P., and Taylor, J. (2007). The expanding family of interleukin-1 cytokines and their role in destructive inflammatory disorders. *Clin. Exp. Immunol.* 149 (2), 217–225. doi:10.1111/j.1365-2249.2007.03441.x

Benzie, I. F., and Wachtel-Galor, S. (2011). *Herbal medicine: Biomolecular and clinical aspects*. Boca Raton, Florida, United States: CRC Press.

Bischoff, S. C. (2008). Quercetin: Potentials in the prevention and therapy of disease. *Curr. Opin. Clin. Nutr. Metab. Care* 11 (6), 733–740. doi:10.1097/MCO.0b013e32831394b8

Calixto, J. (2000). Efficacy, safety, quality control, marketing and regulatory guidelines for herbal medicines (phytotherapeutic agents). *Braz. J. Med. Biol. Res.* 33, 179–189. doi:10.1590/s0100-879x2000000200004

Chen, X., Zhou, H., Liu, Y., Wang, J., Li, H., Ung, C., et al. (2006). Database of traditional Chinese medicine and its application to studies of mechanism and to prescription validation. *Br. J. Pharmacol.* 149 (8), 1092–1103. doi:10.1038/sj.bjp.0706945

Cheng, X.-L., Xin-Guang, L., Qi, W., Ling, Z., Lian-Wen, Q., Ping, L., et al. (2015). Anti-inflammatory and anti-arthritic effects of guge fengtong formula: *In vitro* and *in vivo* studies. *Chin. J. Nat. Med.* 13 (11), 842–853. doi:10.1016/S1875-5364(15)30088-1

Daswani, G., Brijesh, S., and Birdi, J. (2006). "Preclinical testing of medicinal plants: Advantages and approaches," in Paper presented at the Workshop Proceedings on Approaches towards Evaluation of Medicinal Plants Prior to Clinical Trial, Pune, India, November 8, 2006.

Desai Nilesh, V., Patkar Atul, A., Shinde Shilpa, S., and Arwade Aboli, S. (2012). Protective effect of aqueous extract of Aegle marmelos against formaldehyde induced arthritis in rats. *Int. Res. J. Pharm. App Sci.* 2 (4), 66–72.

Eisenberg, D. M., Davis, R. B., Ettner, S. L., Appel, S., Wilkey, S., Van Rompay, M., et al. (1998). Trends in alternative medicine use in the United States, 1990-1997: Results of a follow-up national survey. *Jama* 280 (18), 1569–1575. doi:10.1001/jama.280.18.1569

Eisenberg, D. M., Kessler, R. C., Foster, C., Norlock, F. E., Calkins, D. R., and Delbanco, T. L. (1993). Unconventional medicine in the United States prevalence, costs, and patterns of use. *N. Engl. J. Med.* 328 (4), 246–252. doi:10.1056/NEJM199301283280406

Ertekin, V., Selimoğlu, M. A., and Altinkaynak, S. (2005). A combination of unusual presentations of Datura stramonium intoxication in a child: Rhabdomyolysis and fulminant hepatitius. *J. Emerg. Med.* 28 (2), 227–228. doi:10.1016/j.jemermed.2004.11.006

Giaid, A., Yanagisawa, M., Langleben, D., Michel, R. P., Levy, R., Shennib, H., et al. (1993). Expression of endothelin-1 in the lungs of patients with pulmonary hypertension. *N. Engl. J. Med.* 328 (24), 1732–1739. doi:10.1056/NEJM199306173282402

Harizal, S., Mansor, S., Hasnan, J., Tharakan, J., and Abdullah, J. (2010). Acute toxicity study of the standardized methanolic extract of Mitragyna speciosa Korth in rodent. *J. Ethnopharmacol.* 131 (2), 404–409. doi:10.1016/j.jep.2010.07.013

Hou, Q., Huang, J., Xiong, X., Guo, Y., and Zhang, B. (2022). Role of nutrient-sensing receptor GPRC6A in regulating colonic group 3 innate lymphoid cells and inflamed mucosal healing. *J. Crohn's. Colitis* 20, 1293–1305. doi:10.1093/ecco-jcc/jjac020

Hunter, P. (2008). A toxic brew we cannot live without. Micronutrients give insights into the interplay between geochemistry and evolutionary biology. *EMBO Rep.* 9 (1), 15–18. doi:10.1038/sj.embor.7401148

Jain, S., Vaidya, A., Gupta, P. K., Rosenholm, J. M., and Bansal, K. K. (2021). Antiarthritic activities of herbal isolates: A comprehensive review. *Coatings* 11 (11), 1329. doi:10.3390/coatings11111329

Koduru, S., Grierson, D., and Afolayan, A. (2006). Antimicrobial activity of solanum aculeastrum. *Pharm. Biol.* 44 (4), 283–286. doi:10.1080/13880200600714145

Kunle, O. F., Egharevba, H. O., and Ahmadu, P. O. (2012). Standardization of herbal medicines-A review. *Int. J. Biodivers. Conserv.* 4 (3), 101–112. doi:10.5897/ijbc11.163

Latha, B. P., Reddy, R. M., Ismail, S. M., and Vijaya, T. (2010). Medicinal plants and their derivatives as potential source in treatment of obesity. *Asian J. Exp. Biol. Sci.* 1 (4), 719–727.

Lee, H.-J., Lee, W.-J., Hwang, S.-C., Choe, Y., Kim, S., Bok, E., et al. (2021). Chronic inflammation-induced senescence impairs immunomodulatory properties of synovial fluid mesenchymal stem cells in rheumatoid arthritis. *Stem Cell Res. Ther.* 12 (1), 502–516. doi:10.1186/s13287-021-02453-z

Li, H., and Wang, F. (2021). Core-shell chitosan microsphere with antimicrobial and vascularized functions for promoting skin wound healing. *Mater. Des.* 204, 109683. doi:10.1016/j.matdes.2021.109683

Li, Z., Teng, M., Jiang, Y., Zhang, L., Luo, X., Liao, Y., et al. (2022). YTHDF1 negatively regulates Treponema pallidum-induced inflammation in THP-1 macrophages by promoting SOCS3 translation in an m6A-dependent manner. *Front. Immunol.* 13, 857727. doi:10.3389/fimmu.2022.857727

Maillefert, J. F., Combe, B., Goupille, P., Cantagrel, A., and Dougados, M. (2004). The 5-yr HAQ-disability is related to the first year's changes in the narrowing, rather than erosion score in patients with recent-onset rheumatoid arthritis. *Rheumatology* 43 (1), 79–84. doi:10.1093/rheumatology/keg465

Manan, M., Saleem, U., Akash, M. S. H., Qasim, M., Hayat, M., Raza, Z., et al. (2020). Antiarthritic potential of comprehensively standardized extract of Alternanthera bettzickiana: *In vitro* and *in vivo* studies. *ACS omega* 5 (31), 19478–19496. doi:10.1021/acsomega.0c01670

Maneenoon, K., Khuniad, C., Teanuan, Y., Saedan, N., Prom-in, S., Rukleng, N., et al. (2015). Ethnomedicinal plants used by traditional healers in Phatthalung Province, Peninsular Thailand. *J. Ethnobiol. Ethnomed.* 11 (1), 43. doi:10.1186/s13002-015-0031-5

Manjunatha, B., Vidya, S., Dhiman, P., Pallavi, R., and Mankani, K. (2005). Hepatoprotective activity of Leucas hirta against CCl 4 induced hepatic damage in rats. *Indian J. Exp. Biol.* 43, 722.

Nair, V., Singh, S., and Gupta, Y. (2012). Evaluation of disease modifying activity of Coriandrum sativum in experimental models. *Indian J. Med. Res.* 135 (2), 240–245.

Ogbonnia, S., Mbaka, G., Anyika, E., Osegbo, O., and Igbokwe, N. (2010). Evaluation of acute toxicity in mice and subchronic toxicity of hydroethanolic extract of Chromolaena odorata (L.) King and Robinson (Fam. Asteraceae) in rats. *Agric. Biol. J. N. Am.* 1 (5), 859–865. doi:10.5251/abjna.2010.1.5.859.865

Ogunlana, O. O., Ogunlana, O. E., Adeneye, A. A., Udo-Chijioke, O., Dare-Olipede, T., Olagunju, J. A., et al. (2013). Evaluation of the toxicological profile of the leaves and young twigs of Caesalpinia bonduc (Linn) roxb. *Afr. J. Tradit. Complement. Altern. Med.* 10 (6), 504–512. doi:10.4314/ajtcam.v10i6.20

Ozer, J., Ratner, M., Shaw, M., Bailey, W., and Schomaker, S. (2008). The current state of serum biomarkers of hepatotoxicity. *Toxicology* 245 (3), 194–205. doi:10.1016/j.tox.2007.11.021

Pamila, U. A., and Karpagam, S. (2017a). Antimicrobial activity of alternanthera bettzickiana (regel) g. Nicholson and its phytochemical contents. *Int. J. Pharm. Sci. Res.* 8 (6), 2594–2599. doi:10.13040/IJPSR.0975-8232.8(6).2594-99

Pamila, U. A., and Karpagam, S. (2017b). GC-MS analysis of ethanolic extract of Alternanthera philoxeroides and Alternanthera bettzickiana from India. *World Res. J. Biol. Biol. Sci.* 4, 002–004.

Patil, U. H., and Gaikwad, D. (2010). Phytochemical profile and antibacterial activity of stem bark of Anogeissus latifolia. *Pharmacogn. J.* 2 (17), 70–73. doi:10.1016/s0975-3575(10)80014-8

Phusricom, S., Chatuphonprasert, W., Monthakantirat, O., Pearaksa, P., and Jarukamjorn, K. (2013). Alternanthera sessilis and Alternanthera bettzickiana improved superoxide dismutase and catalase activities in the livers of ovariectomized mice. *J. Appl. Biopharm. Pharmacokinet.* 1 (2), 64–71. doi:10.14205/2309-4435.2013.01.02.2

Rahman, A., and Gulshana, M. I. A. (2014). Taxonomy and medicinal uses on amaranthaceae family of Rajshahi, Bangladesh. *Appl. Ecol. Environ. Sci.* 2 (2), 54–59. doi:10.12691/aees-2-2-3

Ramaiah, S. K. (2011). Preclinical safety assessment: Current gaps, challenges, and approaches in identifying translatable biomarkers of drug-induced liver injury. *Clin. Lab. Med.* 31 (1), 161–172. doi:10.1016/j.cll.2010.10.004

Ridtitid, W., Sae-Wong, C., Reanmongkol, W., and Wongnawa, M. (2008). Antinociceptive activity of the methanolic extract of Kaempferia galanga Linn. in experimental animals. *J. Ethnopharmacol.* 118 (2), 225–230. doi:10.1016/j.jep.2008.04.002

Salawu, O., Chindo, B., Tijani, A., Obidike, I., Salawu, T., and Akingbasote, A. J. (2009). Acute and sub-acute toxicological evaluation of the methanolic stem bark extract of Crossopteryx febrifuga in rats. *Afr. J. Pharm. Pharmacol* 3 (12), 621–626.

Saleem, A., Saleem, M., and Akhtar, M. F. (2020a). Antioxidant, anti-inflammatory and antiarthritic potential of Moringa oleifera Lam: An ethnomedicinal plant of Moringaceae family. *South Afr. J. Bot.* 128, 246–256. doi:10.1016/j.sajb.2019.11.023

Saleem, A., Saleem, M., Akhtar, M. F., Shahzad, M., and Jahan, S. (2020b). Polystichum braunii extracts inhibit Complete Freund's adjuvant-induced arthritis via upregulation of I-κB, IL-4, and IL-10, downregulation of COX-2, PGE2, IL-1β, IL-6, NF-κB, and TNF-α, and subsiding oxidative stress. *Inflammopharmacology* 28 (6), 1633–1648. doi:10.1007/s10787-020-00688-5

Saleem, U., Ahmad, B., Ahmad, M., Erum, A., Hussain, K., and Irfan Bukhari, N. (2016). Is folklore use of Euphorbia helioscopia devoid of toxic effects? *Drug Chem. Toxicol.* 39 (2), 233–237. doi:10.3109/01480545.2015.1092040

Saleem, U., Amin, S., Ahmad, B., Azeem, H., Anwar, F., and Mary, S. (2017). Acute oral toxicity evaluation of aqueous ethanolic extract of Saccharum munja Roxb. roots in albino mice as per OECD 425 TG. *Toxicol. Rep.* 4, 580–585. doi:10.1016/j.toxrep.2017.10.005

Stevens, K., and Mylecraine, L. (1994). "Issues in chronic toxicology," in *Principles and methods of toxicology* (Boca Raton, Florida, United States: CRC Press), 673.

Unuofin, J. O., Otunola, G. A., and Afolayan, A. J. (2018). Evaluation of acute and subacute toxicity of whole-plant aqueous extract of Vernonia mespilifolia Less. in Wistar rats. *J. Integr. Med.* 16 (5), 335–341. doi:10.1016/j.joim.2018.07.003

Uttra, A. M., and Hasan, U. H. (2017). Anti-arthritic activity of aqueous-methanolic extract and various fractions of Berberis orthobotrys Bien ex Aitch. *BMC Complement. Altern. Med.* 17 (1), 371. doi:10.1186/s12906-017-1879-9

Uttra, A. M., Shahzad, M., Shabbir, A., Jahan, S., Bukhari, I. A., Assiri, A. M., et al. (2019). Ribes orientale: A novel therapeutic approach targeting rheumatoid arthritis with reference to pro-inflammatory cytokines, inflammatory enzymes and anti-inflammatory cytokines. *J. Ethnopharmacol.* 237, 92–107. doi:10.1016/j.jep.2019.03.019

Vaghasiya, Y., Shukla, V., and Chanda, S. (2011). Acute oral toxicity study of Pluchea arguta boiss extract in mice. *J. Pharmacol. Toxicol.* 6 (2), 113–123. doi:10.3923/jpt.2011.113.123

Vidhya, T., Suji, T., Dhatchayani, R., Priya, C., and Bhaskara Rao, K. (2015). Evaluation of *in-vitro* antioxidant, antimicrobial activities and GC-MS analysis of Alternanthera bettizicikiana linn. Leaf extracts. *Int. J. Pharmacogn. Phytochemical Res.* 7, 1072.

Zhang, Z., Cui, F., Cao, C., Wang, Q., and Zou, Q. (2022). Single-cell RNA analysis reveals the potential risk of organ-specific cell types vulnerable to SARS-CoV-2 infections. *Comput. Biol. Med.* 140, 105092. doi:10.1016/j.compbiomed.2021.105092

frontiers | Frontiers in Pharmacology

TYPE Original Research
PUBLISHED 16 November 2022
DOI 10.3389/fphar.2022.1005154

Check for updates

OPEN ACCESS

EDITED BY
Sarfraz Ahmad,
University of Malaya, Malaysia

REVIEWED BY
Uzma Saleem,
Government College University, Faisalabad, Pakistan
Muhamamd Haseeb Ur. Rehman,
Government College University Faisalabad, Pakistan
Irum Shahzadi,
COMSATS University Islamabad, Pakistan

*CORRESPONDENCE
Arif-ullah Khan,
arif.ullah@riphah.edu.pk
Syed Shams ul Hassan,
shams1327@yahoo.com
Simona Bungau,
simonabungau@gmail.com

SPECIALTY SECTION
This article was submitted to Predictive Toxicology, a section of the journal Frontiers in Pharmacology

RECEIVED 28 July 2022
ACCEPTED 24 October 2022
PUBLISHED 16 November 2022

CITATION
Aslam H, Khan A-u, Qazi NG, Ali F, Hassan SSu and Bungau S (2022), Pharmacological basis of bergapten in gastrointestinal diseases focusing on H^+/K^+ ATPase and voltage-gated calcium channel inhibition: A toxicological evaluation on vital organs. *Front. Pharmacol.* 13:1005154. doi: 10.3389/fphar.2022.1005154

COPYRIGHT
© 2022 Aslam, Khan, Qazi, Ali, Hassan and Bungau. This is an open-access article distributed under the terms of the Creative Commons Attribution License (CC BY). The use, distribution or reproduction in other forums is permitted, provided the original author(s) and the copyright owner(s) are credited and that the original publication in this journal is cited, in accordance with accepted academic practice. No use, distribution or reproduction is permitted which does not comply with these terms.

Pharmacological basis of bergapten in gastrointestinal diseases focusing on H^+/K^+ ATPase and voltage-gated calcium channel inhibition: A toxicological evaluation on vital organs

Huma Aslam[1], Arif-ullah Khan[1]*, Neelum Gul Qazi[1], Fawad Ali[2], Syed Shams ul Hassan[3,4]* and Simona Bungau[5]*

[1]Riphah Institute of Pharmaceutical Sciences, Riphah International University, Islamabad, Pakistan, [2]Department of Pharmacy, Kohat University of Science and Technology, Kohat, Pakistan, [3]Shanghai Key Laboratory for Molecular Engineering of Chiral Drugs, School of Pharmacy, Shanghai Jiao Tong University, Shanghai, China, [4]Department of Natural Product Chemistry, School of Pharmacy, Shanghai Jiao Tong University, Shanghai, China, [5]Department of Pharmacy, Faculty of Medicine and Pharmacy, University of Oradea, Oradea, Romania

Aim and objectives: This study aimed to establish a pharmacological basis for evaluating the effects of bergapten (5-methoxypsoralen) in gastrointestinal diseases and assessment of its toxicological profile.

Methods: The pharmacokinetic profile was evaluated using the SwissADME tool. AUTODOCK and PyRx were used for evaluating the binding affinities. The obtained results were further investigated for a post-dock analysis using Discovery Studio Visualizer 2016. The Desmond software package was used to conduct molecular dynamic simulations of best bound poses. Bergapten was further investigated for antidiarrheal, anti-secretory, charcoal meal transit time, anti-ulcer, anti-*H. pylori* activity.

Results: Bergapten at a dose of 50, 100, and 200 mg/kg was proved effective in reducing diarrheal secretions, intestinal secretions, and distance moved by charcoal meal. Bergapten at the aforementioned doses acts as a gastroprotective agent in the ethanol-induced ulcer model that can be attributed to its effectiveness against *H. pylori*. Bergapten shows concentration-dependent relaxation of both spontaneous and K^+ (80 mM)-induced contractions in the isolated rabbit jejunum model; the Ca^{2+} concentration–response curves (CRCs) were shifted to the right showing potentiating effect similar to papaverine. For molecular investigation, the H^+/K^+ ATPase inhibitory assay indicated inhibition of the pump comparable to omeprazole. Oxidative stress markers GST, GSH, and catalase showed increased expression, whereas the expression of LPO (lipid peroxidation) was reduced. Histopathological examination indicated marked improvement in cellular morphology. ELISA and western blot confirmed the reduction in

inflammatory mediator expression. RT-PCR reduced the mRNA expression level of H^+/K^+ ATPase, confirming inhibition of the pump. The toxicological profile of bergapten was evaluated by an acute toxicity assay and evaluated for behavioral analysis, and the vital organs were used to analyze biochemical, hematological, and histopathological examination.

Conclusion: Bergapten at the tested doses proved to be an antioxidant, anti-inflammatory, anti-ulcer, and antidiarrheal agent and relatively safe in acute toxicity assay.

KEYWORDS

bergapten, gastroprotective, anti-ulcer, H/K ATPase, calcium channel blocking, acute toxicity, molecular simulations

1 Introduction

More than 8 million people worldwide die from gastrointestinal conditions each year, which include gastrointestinal malignancies, gastroesophageal reflux disease, *Helicobacter pylori* infection, peptic ulcer disease, inflammatory bowel disease, celiac disease, and functional gastrointestinal dysfunction (Milivojevic and Milosavljevic, 2020). The prevalence of GI diseases has an increasing trend owing to the environmental factors including lifestyle, hygiene, and infection exposures (Ohama et al., 2007). Multiple GI disorders including inflammatory bowel disease, gastric ulcers, *Helicobacter pylori (H. pylori)* infections, colorectal cancers, diarrhea, constipation, and gastroesophageal reflux disease are most prevailing globally. According to surveys performed by the World Gastroenterology Organization, *H. pylori* infection is most common in the adult population and has shown median prevalence in about 50% of the world population. WHO data for recent global disease burden reports diarrheal diseases to be among the top 10 causes of death globally. Diarrheal diseases account for approximately 1.4 million deaths worldwide in 2016. Colorectal cancer is the fourth leading cause of cancer related death, accounting for over 4,900 deaths in 2014 (Jones et al., 2017). Although treatment options are available, the consequences and mortalities are still a problem because of poor treatment adherence of the patients usually due to multidrug dosing regimens.

The gastrointestinal tract shows contractile motions along with secretions throughout the tract; hence, any alteration in these may cause increased or decreased GI motility and contractions, which may further cause certain conditions such as diarrhea, constipation, abdominal cramping, and indigestion. Intestinal motility, on the other hand, may be affected by underlying disease conditions or certain medications (Hasler et al., 2010). While some ailments such as ulcers are associated with the imbalance in protective and aggravating factors in GIT, many bacterial infections also cause this imbalance and contribute toward breaching of the mucus lining. Therefore, strenuous antibiotic therapy is often recommended that causes patient non-compliance (Nyssen et al., 2021). Moreover psychological health, overall health condition, and dietary factors that influence intestinal content can also affect sensory signaling and, hence, motility in the gastrointestinal tract (Hasler et al., 2010). The imbalance in aggressive and protective aspects leads to increase in acid secretions from gastroparietal cells causing ulcers. Other aspects such as gastrin, histamine, muscarinic, and prostaglandin-E2 signaling may also affect H^+/K^+ ATPase, which is involved in the release of H^+ ions causing an acidic environment (Mishra, 2016). Therefore, H^+/K^+ ATPase is a promising target while treating ulcers. Calcium channel blockers, on the other hand, also proved therapeutically beneficial in ulcers and other GI motility ailments by increasing microcirculation, gastric function, and GI motility by affecting signaling pathways (Fomina, 2020; Khakimov, 2021). Medicinal science so far has not been able to produce any efficient remedial drug in contrast to gastrointestinal disorders which can completely eradicate the disease, and current treatment options provide temporary relief of symptoms (Irvine et al., 2006).

Secondary metabolites from nature, predominantly plants, are still a research hotspot because of their promising novel scaffolds against chronic diseases (Muhammad et al., 2021a; Memariani et al., 2021; Majid et al., 2022). Medicinal plants are used traditionally as a source of complementary and alternative medicine in gastrointestinal disorders (Bahmani et al., 2014). Medicinal plants and their isolated compounds account for approximately 30% of all pharmaceuticals, becoming globally important in recent years (Khan et al., 2019; Muhammad et al., 2021b; Ul Hassan et al., 2021). Additionally, herbal treatments have demonstrated good long-term economic potential to cure problems of the gastrointestinal system. Bergapten (5-methoxypsoralen) is a furanocoumarin that is commonly found in lemon, grapefruit, fig, Cnidii Fructus, and many medicinal plants (Liang et al., 2021). It acts as an antioxidant, anti-insect, analgesic, anti-inflammatory, anticoagulant, and anticancer agent (Yu et al., 2016). Plants from the Apiaceae and Rutaceae family contain furanocoumarins as major phytoconstituents and have proved their potential in several GI disorders. Medicinal plants from these families contain bergapten as one of main constituents, therefore leading to basis for selection of this compound to evaluate scientifically for

gastrointestinal disorders (Abbaskhan et al., 2011; Vera Saltos et al., 2013). Recent studies proved bergapten to have antidiabetic properties, and due to its ability to cross the blood–brain barrier, it is expected to be a useful therapeutic agent in certain brain ailments such as diabetes-associated Alzheimer's, epilepsy, and depression (Liang et al., 2021). Bergapten was also found to have good binding affinity and potential to act as protease inhibitor against SARS-CoV-2 during *in silico* analysis (Chidambaram et al., 2020). Through *in vivo* and *in silico* evaluation of bergapten, it could be formulated into a suitable dosage form. In this study, we have initially tested bergapten through *in silico* studies using a docking analysis and molecular dynamic simulation studies against selected favorable target proteins involved in GI ailments.

The aim of this study was to assess the potential capability of bergapten as a therapeutic agent in several GI diseases. Assuming that bergapten modulates the expression of proteins in the GI tract, it was evaluated for its effectiveness including anti-spasmodic, anti-motility, gastrointestinal transient time, anti-ulcer potential, calcium channel blocking, anti-*H. pylori,* H^+/K^+ ATPase activity, histopathological examination, immunohistochemistry, ELISA, western blotting assay, RT-PCR, and computational analysis including molecular simulation studies. Importantly, the gastroprotective role of bergapten in gastric ulcers and its regulation at the molecular and organ/tissue damage level is examined focusing on H^+/K^+ ATPase and calcium channel blocking activity. *In silico* and proteomic approaches aid in understanding the biochemical mechanism and, as a result, may untangle the complicated signaling network that affects cellular function such as apoptosis and inflammation.

2 Materials and methods

2.1 Chemicals

Castor oil was bought from a company in Pakistan called Karachi Chemical Industries. All the other ingredients came from Sigma Chemicals Co. in St. Louis, Missouri, United States; they were as follows: acetylcholine, activated charcoal, bergapten, ethanol, loperamide, verapamil, papaverine, atropine, and omeprazole.

2.2 Animals

The studies were conducted according to the "Principles of Laboratory Animal Care" and the rules of the Research and Ethics Committee of the Riphah Institute of Pharmaceutical Sciences (RIPS) (Ref. no. REC/RIPS/2019/021). Sprague Dawley rats (190–240 g) of either gender, rabbits (1.0–2.0 kg), and Balb/c mice were used in the study (20–25 g). At an animal house at RIPS, Islamabad, all the animals were kept in a controlled environment.

2.3 Computational studies

Reference pharmaceuticals' three-dimensional structures were created in 2016 using the Discovery Studio Visualizer by adding polar hydrogen atoms; then, they were turned into a PDB file. Papaverine, phenylephrine, pirenzepine, atropine, domperidone, calmidazolium, verapamil, and ranitidine were some of the most commonly used drugs for docking. The RCSB Protein Data Bank was used to choose and get targets related to gut physiology. Calmodulin, dopaminergic D2, adrenergic 1 receptor, histaminergic H2, muscarinic M1, mu-opioid, phosphodiesterase enzyme, and H^+/K^+ ATPase with their PDB IDs 1CTR, 6CM4, P35348, P25021, 5CXV, 6DDE, 6DDE, and 1T3S, respectively, were chosen. DSV was used to clean up the structures. PyRx was used to dock molecules (Faheem et al., 2021; Shams ul Hassan et al., 2021).

2.4 SwissADME

SwissADME is an online method to access the ADME (Absorption, Distribution, Metabolism, and Excretion), that is, the pharmacokinetic profile including drug likeliness, physicochemical, lipophilicity, solubility properties, and medicinal chemistry (Faheem et al., 2021; Shams ul Hassan et al., 2022).

2.5 Molecular dynamics simulation

The probable binding interactions of the target protein H^+/K^+ ATPase and voltage-dependent calcium channel (VDCC) were predicted using a docking analysis. Later, molecular docking simulation of H^+/K^+ ATPase–bergapten and VDCC–bergapten complexes were conducted using the Desmond software package of SCHRÖDINGER 2020-3 version. The aforementioned complexes were placed in a molecular simulation in an orthorhombic box that was automatically created and supplemented by 55,180 and 13,403 for the complexes H^+/K^+ ATPase-bergapten and VDCC-bergapten, respectively. Utilizing liquid simulations with optimized potential, the model is further enhanced (OPLS5). NaCl was added to make the solution isotonic and to neutralize the system's complexes (Na = 52.06 mM and Cl = 50.74 mM). Counter ions were injected to provide an electrically stable environment. Temperature and pressure were maintained at 300 K using a Nose–Hoover thermostat and 1.01325 bars using Martyna–Tobias–Klienbarostate, respectively. The MD simulation total time was 100 ns. The Eswald method was used for calculating electrostatic interactions. The simulation interaction diagram tool in the Desmond package was used to evaluate interaction behavior between the ligand and protein. Structural optimization of ligand was performed using the density functional theory method. The Desmond software gives results in the form of RMSD for the protein and

RMSF for the residue. These are then used to evaluate the results further (Ali et al., 2022; Hassan et al., 2022).

2.6 Castor oil-induced diarrhea

This protocol was conducted as previously described by Ansari et al. (2019). Balb/c mice were randomly allocated to five groups for bergapten and fasted for 24 h (08:00–08:00), before experimentation. Animals were kept in separate cages and distributed in equal groups lining the floor of cage with absorbent paper. After an hour, negative control mice were administered 10 ml/kg of castor oil orally (P.O.). Mice in the positive control group were given loperamide hydrochloride at a dose of 2 mg/kg of body weight. Following the administration of bergapten at dosages of 50 and 100 mg/kg, diarrhea was induced by administering castor oil (10 ml/kg) orally. Animals were placed in separate cages lined with white paper. Each animal was monitored for a whole period of 4 hours in order to ascertain the time of the commencement of diarrhea and the presence or absence of diarrheal droppings. The percentage of diarrheal protection was evaluated according to the Sisay et al. (2017).

2.7 Assessment of intestinal fluid accumulation

Intestinal fluid accumulation was determined using the method described by Ansari et al. (2019). An enteropooling assay was used to evaluate the accumulation of intestinal fluid. Mice fasting for 24 h (08:00–08:00) were removed and kept into six designated cages, each holding five mice. Group I and II were administered with normal saline (10 ml/kg) and castor oil (10 ml/kg, p.o.), respectively. In addition, 1 h prior to induction with castor oil (10 ml/kg, p.o.), bergapten at doses of 50, 100, and 200 mg/kg was given intraperitoneally to Group III, IV, and V, respectively. Standard drug atropine at dose 10 mg/kg was given to VI group. Mice were sacrificed after 30 min, intestine was removed and weighed. The results were articulated as (Pi/Pm) x 1000, where Pi is the weight (g) of the intestine and Pm is the weight of the animal.

2.8 Charcoal meal transit time

The inhibitory activity of the propulsion of a charcoal meal in rats was estimated utilizing bergapten. The rats were fasted for 24 h, but had a free access to water. The test groups received the doses of bergapten at 50, 100, and 200 mg/kg body weight doses; the positive control group received atropine sulfate (0.1 mg/kg, i.p.), while the negative control group received normal saline (10 ml/kg, p.o.). All groups were treated with a period marker 25 mg/kg (10% activated charcoal suspension in 5% gum acacia) 1 hour after pretreatment. After all treatments, animals were sacrificed. The small intestine was excised, and then the distance traveled by charcoal meal 1 ml of marker through the organ was expressed as a percentage of the length of the small intestine according to the following expression (Ansari et al., 2021):

$$\text{Peristaltic index (PI\%)} = (\text{Distance moved by charcoal meal} / \text{total length of intestine})\,(\text{cm}) \times 100.$$

For further evaluation of % inhibition, the peristaltic index is used.

% inhibition = (PIC-PIT)/PIC X 100,

where PIC = peristaltic index of control and PIT = peristaltic index of test group.

2.9 Effect of bergapten on the motility of isolated tissue preparations

Before experimentation, the rabbits were fasted for 24 h (08:00–08:00), although they were given free access to water. It was around 10–12 cm after cervical dislocation that the jejunum was separated and cleansed with Tyrode's solution. Before administering the medication, 2 cm of jejunum was suspended in Tyrode's solution. Later, 30 min of acclimatization in a controlled environment with 95% oxygen and 5% carbon dioxide (carbogen) supply enabled the jejunal section to adapt to the new environment. They were recorded by connecting the force displacement transducer (model FDT-33) through the bridge amplifier and power Lab 4/25 data recording equipment to a computer running the lab data acquisition and analysis application on the computer. Each preparation was stabilized with a concentration of ACh (0.3 M) (AD Instrument, Sydney Australia). The percent change in jejunal contractions was examined at various levels of bergapten concentration (Rehman et al., 2011; Rehman et al., 2012). High K^+(80 mM) depolarizes the preparations for smooth muscle contractions by opening voltage-dependent Ca^{2+} channels, which results in extracellular Ca^{2+} influx and has a contractile effect. Substances that inhibit the high K^+-induced contraction are thought to block Ca^{2+} influx through L-type Ca^{2+} channels. After the generated contraction had initially plateaued (often within 7–10 min), test dosages were increased cumulatively to produce concentration-dependent inhibitory responses. The tissue was allowed to stabilize in regular Tyrode's solution before being switched to Ca^{2+} free Tyrode's solution containing EDTA (0.1 mM) for 30 min. This was carried out to validate the test substance's Ca^{2+} antagonist effect. Additionally, tissue was put in a Tyrode's solution that contained K^+ but no Ca^{2+}. The control concentration–response curves (CRCs) of Ca^{2+} were

produced after a 30-min incubation period. The tissue was pretreated with test dose for 1 h after it was established that the control Ca^{2+} CRCs were super-imposable (often after two cycles). To detect the Ca^{2+} antagonist effect, the CRCs of Ca^{2+} were reconstructed in the presence of various concentrations of the test substance (Khan and Gilani, 2009).

2.10 Anti-*Helicobacter pylori* activity

The resistant strains of *H. pylori* clinical isolates were obtained from PINSTECH (Pakistan Institute of Nuclear Science and Technology, Islamabad, Pakistan). Identification assays including morphology, gram staining, urease test, and catalase tests were performed for checking microaerophilic growth (at 37°C) (Ullah et al., 2019). The disc diffusion method was used to analyze an antibacterial effect of bergapten, measuring the zone of inhibition in mm using 5 mg of bergapten per disc. The obtained *H. pylori* clinical isolate SJ 2013 10^8 cfu/ml was resistant to antibiotics such as amoxicillin, clarithromycin, and metronidazole. These isolates were inoculated on Columbia blood agar (CM 0331B, Oxoid, UK) enriched with 5% defibrinated sheep blood. Discs impregnated were applied and incubated at 37°C for 72 h under microaerophilic conditions using the Campylobacter gas generation kit (BR 0056A, Oxoid, United Kingdom). After completion of incubation of 72 h, the diameter around each disc was measured to access the zones of inhibition. The microdilution method with brain heart infusion (BHI) broth was used to access minimum inhibitory concentration (MIC) for bergapten. Serial dilution by two folds in BHI broth with serum was used, and final concentrations of extracts were 0.625–5.0 mg/ml. The concentration at which with no visual growth or turbidity was observed was considered as MIC.

2.11 Ethanol-induced ulcer assay

The rats of either sex that weighed between 250 and 280 g were randomly divided into groups and kept for a 24-h fast. As a negative control, Group 1 was given 10 ml/kg of normal saline and Group 2 received omeprazole 20 mg/kg as a standard drug. Groups 3, 4, and 5 were given 50, 100, and 200 mg/kg of bergapten, respectively. In order to induce stomach ulcers in all of the animals, 1 ml/100 g of absolute ethanol (100%) was administered intraperitoneally after an hour of treatment. Animals were sacrificed 1 hour after consuming ethanol. Stomachs were removed and washed with normal saline, and each lesion was calculated according to the protocol previous studied by Noor et al. (2017) and Li et al. (2022). For further proteomic analysis, the gastric tissues were reserved in a bio-freezer (−80°C).

Primers	Tm	Sequence (5′–3′)
Rat_BetaActin_Forward	60.5°C	CCCGCGAGTACAACCTTCT
Rat_BetaActin_Reverse	59.5°C	CGTCATCCATGGCGAACT
H^+/K^+ ATPase forward	52.3°C	TATGAATTGTACTCAGTGGA
H^+/K^+ ATPase reverse	53.9°C	TGGTCTGGTACTTCTGCT

2.12 H^+/K^+ ATPase inhibitory assay

The inhibitory effect of bergapten on rat gastric H^+/K^+ ATPase inhibitory effect was accessed using a commercially available colorimetric H^+/K^+ ATPase activity assay screening kit (catalog No. E-BC-K122-S, Elabscience USA). A bio-freezer (−80°C) was used to retain the treated stomach tissues before they were homogenised at 15,000 using the Silent Crusher M. (Heidolph). After centrifugation at 3500 rpm for 10 min, the homogenate was finally separated. We used a spectrophotometric assay (660 nm) to check for the release of inorganic phosphate from the collected supernatant after it had been collected (He et al., 2018). In addition, 1 μmol of inorganic phosphorus released by ATP hydrolysis by ATPase of 1 mg of tissue protein per hour is defined as 1 ATPase activity and expressed as μmol Pi/mg prot/hour.

2.13 Determination of oxidative stress markers

The supernatant collected after homogenization and centrifugation, respectively, of isolated rat gastric tissue at 1500 rpm for 30 min, the level of glutathione (GSH), glutathione-S-transferase (GST), catalase, and lipid peroxidation (LPO) was examined in the supernatant. The oxidation of GSH and DTNP (2,2′-Dithiobis (5-nitropyridine)) produces 2-nitro-5-thiobenzoic acid, which is a yellow end product. To access the levels of GSH after oxidizing GSH and DTNP, a microplate reader was used to measure absorbance at 412 nm and expressed as μmole/mg of protein. Formation of CDNB (2,4-dinitrochlorobenzene) conjugate is used to access GST levels. Conjugate formation is measured by absorbance at 340 nm using the extinction coefficient of the product formed and is expressed as μmoles of CDNB conjugate/min/mg of proteins. Catalase activity is measured in moles H2O2/min/mg of protein by measuring the degradation of H_2O_2 and using microplate reader to measure absorbance at 240 nm. LPO (lipid peroxidation) values are measured in TBARS (thiobarbituric acid reactive substances) nmoles/min/mg protein. The end product of LPO is malondialdehyde, which is measured using a microplate reader and absorbance at 532 nm (Qazi et al., 2022). For SOD (superoxide dismutase), an assay was performed according to Dengiz et al. (2007). Superoxide radicals generated by xanthine and xanthine oxidase and reaction with nitro blue tetrazolium produces formazan dye. Superoxide dismutase

activity was estimated by inhibition of the aforementioned reaction and inhibition determined at 560 nm and expressed as millimole per minute per milligram tissue (mmol/min/mg/tissue).

2.14 Morphology analysis, histopathology, and H&E staining

A total of five rats were used in each group for morphological examination. For fixation of the stomach tissues, 4% paraformaldehyde is used, and until further analysis, tissues are implanted and fixed in paraffin. The fixed tissues were then sectioned using a rotary microtome at 5 µm. These were stained with hematoxylin and eosin (H&E) and observed under an optical microscope, and photos were taken according to Ansari et al. (2021) and Liu et al. (2022a).

2.15 Proteomics of stomach tissues by using enzyme-linked immunosorbent assay

Tumor necrosis factor alpha (TNF-α), prostaglandin-E_2 (PGE_2), and interleukin-8 (IL-8) were detected according to the manufacturer's instructions. The stomach tissues (n = 3) stored in the bio-freezer (−80°C) were homogenize at 15 rpm × 1000 using Silent Crusher M (Heidolph) and later centrifuged (at 1350 × g for 1 h) for collection of supernatants. It was then analyzed for quantification of TNF-α (Catalog No: E-EL-R0019), PGE2 (Catalog No: E-EL-0034), and IL-8 (Catalog No: EKF57830) using an Elabscience Rat ELISA kit (Liu Z. et al., 2022b).

2.16 Western blot analysis

To determine the expression of inflammatory mediators involved in progression of ulcer, a western blot analysis was used. Sample proteins (n = 3) from each experimental group were prepared with the addition of laemmli buffer, vortexed, and incubated at a temperature of 96°C for 10 min. These were then placed in ice for 10 min after incubation and again vortexed. After preparation of gel protein samples were loaded in polyacrylamide gels separated by SDS/PAGE. The negative charge on SDS is used for protein denaturation, and polyacrylamide allows the movement of protein at altered speed based on their charge. After separation of proteins, they were shifted to polyvinylidene fluoride (PVDF) membrane for the trans blot process. A 5% skimmed milk solution was prepared in TBST (Tris-buffered saline with Tween) buffer and used for washing and blocking membranes for non-specific binding. Primary antibodies including phosphorylated nuclear factor kappa β (SC-271908 Santa Cruz Biotechnology, Dallas, TX, United States), tumor necrosis factor α (SC-52B83 Santa Cruz Biotechnology, Dallas, TX, United States), and COX-2 (SC-514489 Santa Cruz Biotechnology, Dallas, TX, United States) were applied on membranes and were incubated for 16 h at 4°C. Membranes were washed in TBST buffer for 10 min, and anti-mouse secondary antibody was applied for 3–4 h at room temperature. By interacting and binding with the primary antibody, the secondary antibody detects target protein. The PVDF membrane was then again washed in TBST, and proteins on the PVDF membrane were transferred to X-ray sheet. Band density was measured and standardized to β-actin (Noman et al., 2022).

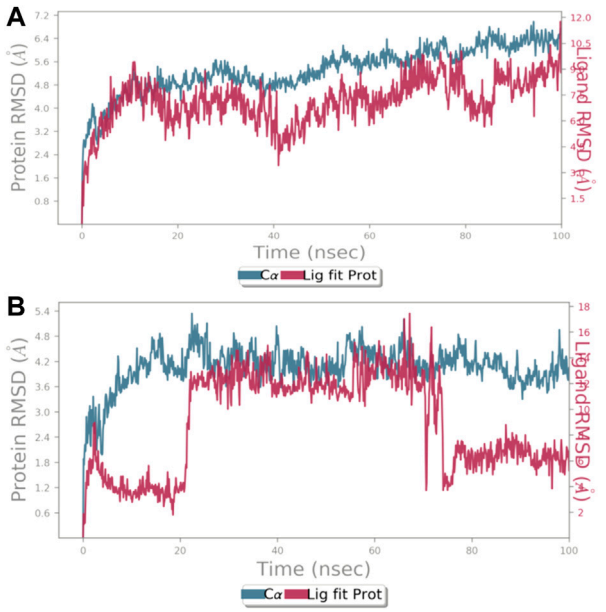

FIGURE 1
(A) represents root mean square deviation (RMSD) for protein 4UX2 shown in blue and RMSD of bergapten shown in red. **(B)** RMSD for protein 1T3S shown in blue and RMSD of bergapten shown in red using the Desmond software package.

2.17 Reverse transcription-polymerase chain reaction analysis

Following the manufacturer's instructions, the TRIzol technique was used to extract total ribonucleic acid (RNA) after homogenization of gastric tissues (n = 3), and cDNA was synthesized by reverse transcriptase enzyme using 1–2 µg of total RNA. cDNA was then amplified by real-time PCR using a thermocycler. Beta-actin expression levels were used to normalize mRNA expression. For real-time quantitative PCR, the relative gene expression was determined by using the $2^{-\Delta\Delta-CT}$ method (Ali et al., 2022). Primers sequences for β-actin and H^+/K^+ ATPase are as follows:

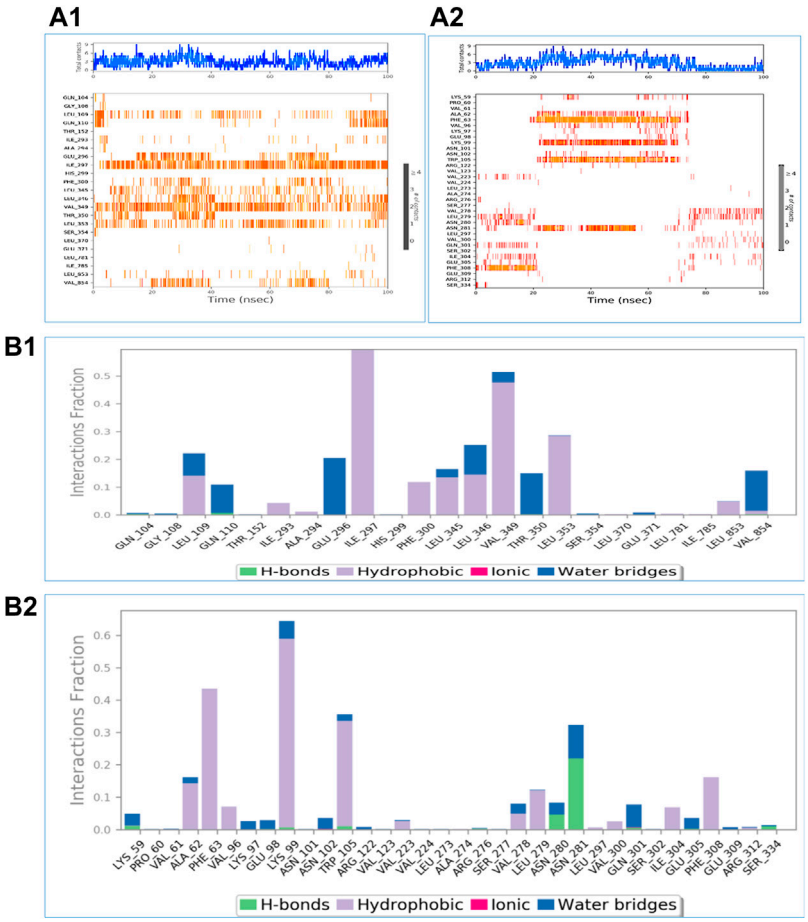

FIGURE 2
A time-based depiction of the multiple interactions and contacts including hydrogen, hydrophobic, ionic bonds, and water bridges between bergapten vs. 4UX2 and 1T3S are presented in **(A1,A2)**, respectively. The total number of specific interactions between the protein and the ligand is shown in the top panel. The interacting residues with the ligand are shown in the bottom panel. Some residues form more than one specific contact with the ligand, and these are indicated by deeper hue of Orange, according to the scale to the right of the plot. **(B1,B2)** exhibit protein interactions between 4UX2 and bergapten and 1T3S and bergapten, respectively. These interactions are categorized as hydrogen bonds, hydrophobic, ionic, and water bridges.

2.18 Toxicity studies

In total, two groups of female rats (n = 5) were obtained. One was control group and the other treatment group. In this study, we used non-pregnant, nulliparous female rats to test acute toxicity of bergapten. One animal at a time was fasted overnight and administered with 2000 mg/kg of bergapten in accordance with OECD standards 425 (Saleem et al., 2017; Song and Wu., 2022). The rat was observed for 24 h, and if it survived, the other rats in the therapy group were given the same treatment; writhing, salivation, twitching, convulsions, loss of fur, and stress were among the symptoms seen. These symptoms were observed for 48 h, followed by 14 days of daily monitoring. As soon as the animals had been anaesthetized and their essential organs removed, blood was drawn from their hearts by cardiac puncture. For example, these blood samples were used to determine the moist weight of their organs and to compile antioxidant profiles and tests to determine how well their livers and kidneys functioned.

2.18.1 Biochemical analysis of the toxicity study

Biochemical markers such as lipid profile (cholesterol, triglyceride, low-density lipoprotein (LDL), very-low-density lipoprotein (VLDL), and high-density lipoprotein (HDL)), renal function tests (urea, uric acid, and creatinine), liver function tests (alanine aminotransferase (ALT), bilirubin, aspartate aminotransferase (AST), and alkaline phosphate (ALP)), and total protein were estimated using a Randox kit.

TABLE 1 Effect of bergapten and loperamide against castor oil-induced diarrhea in mice.

Treatment (mg/kg)	No. of wet feces	Total no. of feces	Average weight of wet feces (gm)	Average weight of total feces (gm)	% inhibition of defecation	% WWFO	% WTFO
Saline (10 ml/kg) + castor oil (10 ml/kg)	8.0 ± 0.3	8.2 ± 0.02	0.46 ± 0.03	0.5 ± 0.01	0	0	0
Bergapten (50 mg/kg) + castor oil (10 ml/kg)	4.8 ± 0.3	6.7 ± 0.2	0.31 ± 0.05	0.42 ± 0.01	40.0***	67.39	81.7
Bergapten (100 mg/kg) + castor oil (10 ml/kg)	0 ± 0.0	1.6 ± 0.19	0 ± 0.0	0.25 ± 0.03	100***	0	19.51
Loperamide (2 mg/kg) + castor oil (10 ml/kg)	0 ± 0.0	2.2 ± 0.2	0 ± 0.0	0.11 ± 0.03	100***	0	22

Values are expressed as mean ± SEM $n = 5$. One-way analysis of variance (ANOVA) followed by *post hoc* Tukey's test, ***$p < 0.001$ vs. castor oil group.

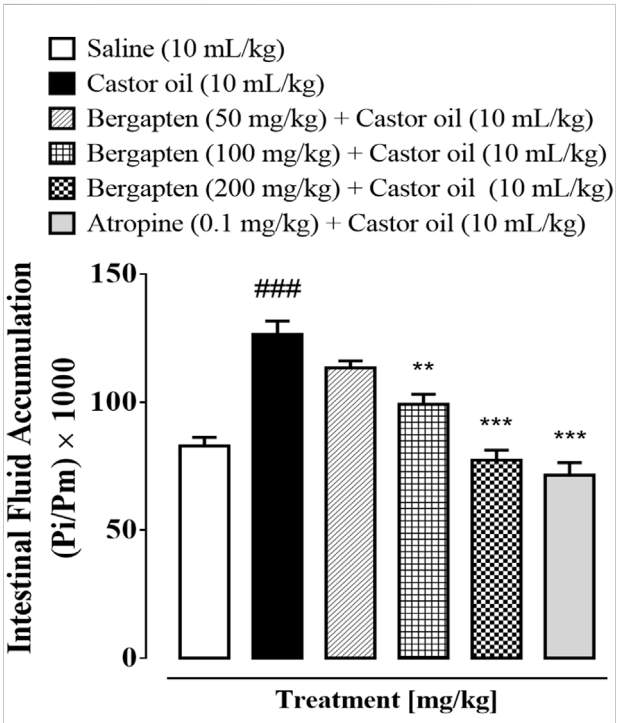

FIGURE 3
Inhibitory effect of bergapten and atropine on castor oil–induced fluid accumulation in mice. The anti-secretory effect is expressed as Pi/Pm x 1000 (g), where Pi is the weight of the small intestine and Pm is the weight of mouse. Results are expressed as mean ± SEM, $n = 5$. One-way analysis of variance with *post hoc* Tukey's test. ###$p < 0.001$ vs. saline group, **$p < 0.01$ vs. castor oil group, ***$p < 0.001$ vs. castor oil group.

2.18.2 Hematological analysis of the toxicity study

EDTA tubes were used to collect blood samples from control and treated animal. HumaLyzer was used to access the hematological parameters such as complete blood count (CBC), hemoglobin (Hb) levels, red blood cell count, white blood cell count, platelet count, packed cell volume (PCV), mean corpuscular volume (MCV), mean corpuscular hemoglobin (MCH), neutrophils, lymphocytes, monocytes, and eosinophils (Lei et al., 2022).

2.18.3 Histopathological analysis of the toxicity study

The animals subjected to toxicity study were sacrificed and fixed in 10% formalin and embedded in paraffin wax. H&E (hematoxylin and eosin) staining was used to stain on paraffin embedded organ sections and slides were prepared and observed under a light microscope for further investigation.

2.19 Statistical analysis

Data were expressed as mean ± SEM ($n = 5$) and median effective concentrations (EC_{50}) having 95% confidence intervals. A statistical analysis of the results was carried out using one-way ANOVA followed by *post hoc* Tukey's test. Non-linear regression using GraphPad program (GraphPad, SanDiego, CA, United States) was used to analyze the concentration–response curves.

3 Results

3.1 Docking study

Energy levels and H-bonds determine docking assessment. Bergapten's binding affinities to protein receptors vary. Supplementary Table S1 provides atomic energy values (kcal/mol) and residues implicated in H-bonding, pi-pi bonding, and other hydrophobic interactions of bergapten and reference. Supplementary Figures S1–S11 illustrate bergapten's 2D interactions with typical medicines.

TABLE 2 Effect of bergapten and atropine on charcoal meal transit time in rats.

Treatment	Mean length of intestine (cm)	Distance moved by charcoal (cm)	Peristaltic index (PI) %	% inhibition
Saline (10 ml/kg)	94	0	0	0
charcoal (25 mg/kg)	92.6	90	96.9###	0
Bergapten (50 mg/kg) + charcoal (25 mg/kg)	81.2	54.2	66.74	31.26*
Bergapten (100 mg/kg) + charcoal (25 mg/kg)	81.2	50.8	59.3	38.92***
Bergapten (200 mg/kg) + charcoal (25 mg/kg)	91.8	48.2	55.33	43.01***
Atropine (0.1 mg/kg, i.p.) + charcoal (25 mg/kg)	90.8	16.4	18.06	81.40***

Values are expressed as mean ± SEM (n = 5). One-way analysis of variance (ANOVA) followed by *post hoc* Tukey's test.###$p < 0.001$ vs. saline group, *$p < 0.05$, ***$p < 0.001$ vs. charcoal group.

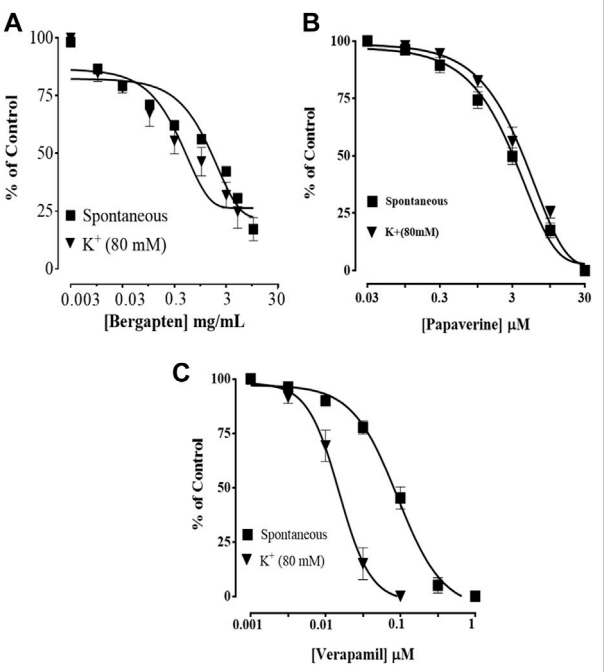

FIGURE 4
Concentration-dependent inhibitory effect on spontaneous and K^+ (80 mM)-induced contractions of **(A)** bergapten, **(B)** papaverine, and **(C)** verapamil in isolated tissue preparations. The result expressed as mean ± SEM, n = 3–5.

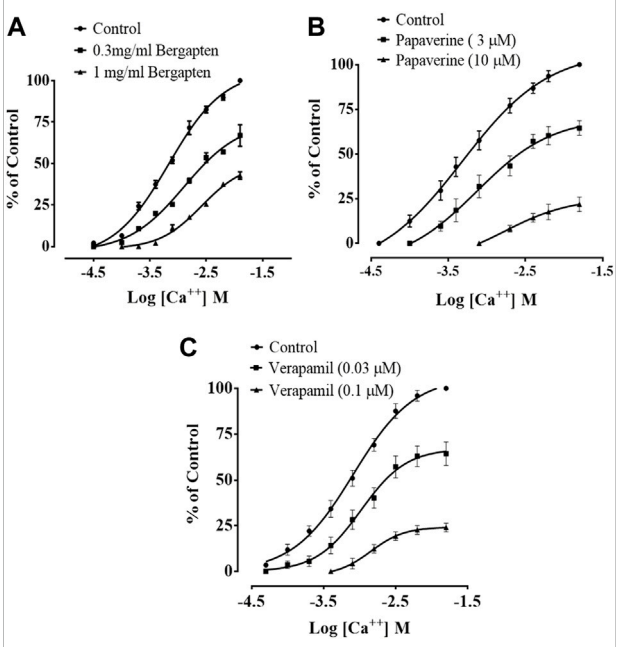

FIGURE 5
Effect of bergapten on concentration–response curves of Ca^{2+} in the absence and presence of increasing concentrations of **(A)** bergapten, **(B)** papaverine, and **(C)** verapamil in isolated rabbit jejunum preparations. The values shown are mean ± SEM, n = 3–4.

3.1.1 Targets information

The total residues, protein chains, number of atoms, charge, and heavy atoms on the protein target H^+/K^+ ATPase (4UX2) and voltage-gated L-type calcium channel (1T3S) assessed during simulation are presented in Supplementary Figures S12A, S13A. The RMSF in Å A° was 2.5 for 4UX2 and 5.5 for 1T3S indicated in Supplementary Figures S12B, S13B. In Supplementary Figures S12C, S13C, for 4UX2 and 1T3S, red represents alpha helices and blue beta strands.

3.1.2 Ligand information

In Supplementary Figure S14A, the root mean square deviation (RMSD), extendedness of the ligand as measured by the radius of gyration (rGyr), number of internal H-bonds within the ligand, molecular surface area (MolSA) calculation with 1.4 A° probe radius, solvent accessible surface area of the ligand (SASA), and polar surface area (PSA), which is contributed only by the oxygen and nitrogen atoms Supplementary Figure S14B shows Bergapten's structure, atom count, atomic mass, charge, molecular formula, fragments, and rotatable bonds.

TABLE 3 Protective effect of bergapten and omeprazole against ethanol-induced gastric ulcers in rats.

Treatment	Ulcer index	% inhibition
Saline 10 ml/kg	0 ± 0.0	–
Ethanol (1 ml/100 g)	10.0 ± 0.3$^{###}$	0
Bergapten (50 mg/kg) + ethanol (1 ml/100 g)	8.0 ± 0.13**	20
Bergapten (100 mg/kg) + ethanol (1 ml/100 g)	4.4 ± 0.21***	56
Bergapten (200 mg/kg) + ethanol (1 ml/100 g)	2.6 ± 0.3***	74
Omeprazole (20 mg/kg) + ethanol (1 ml/100 g)	1.4 ± 0.14***	86

Values are expressed as mean ± SEM $n = 5$. One-way analysis of variance ANOVA, followed by *post hoc* Tukey's test$^{###}p < 0.001$ vs. saline group, $^{**}p < 0.01$, $^{***}p < 0.001$ vs. ethanol group.

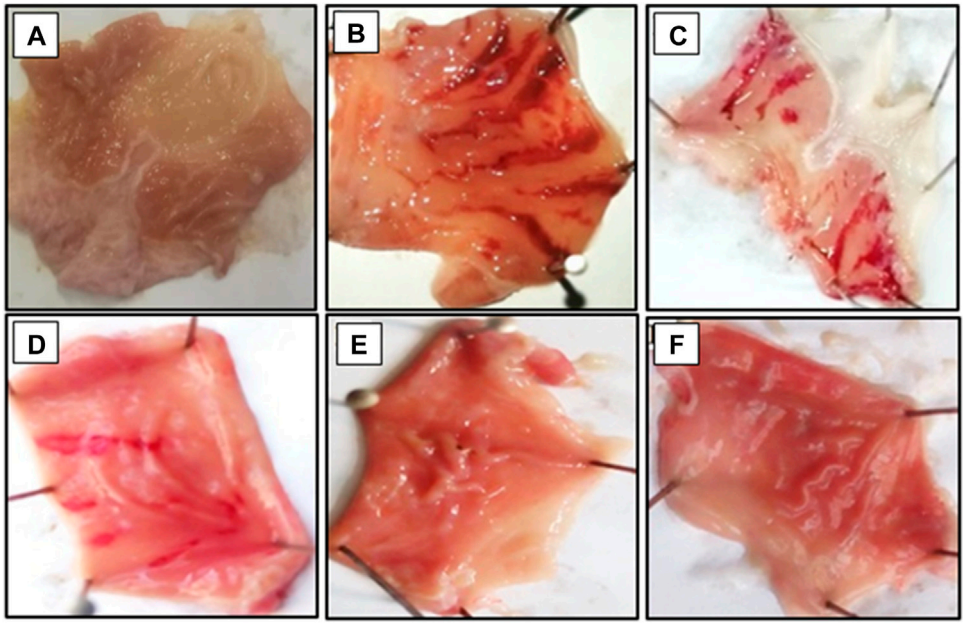

FIGURE 6
Gross-appearance of gastric mucosa in rat: **(A)** pre-treated with saline, 10 mL/kg, **(B)** Severe injuries are seen, as ethanol (1 mL/100 g) produced excessive hemorrhagic necrosis of gastric-mucosa **(C–E)** pretreated with bergapten at doses of 100, 150, and 200 mg/kg and **(F)** pretreated with omeprazole (20 mg/kg). The injuries reduce with increase of doses and omeprazole compare with ethanol treated group. At 200 mg/kg, bergapten showed most efficacious gastro- protective action.

3.2 SwissADME

Pharmacokinetic profile including drug likeliness, physicochemical, lipophilicity, and solubility properties are described in Supplementary Table S2.

3.3 Molecular dynamic simulations

Using the Desmond software package, molecular dynamic simulation was performed. The physiological environment was provided to the complexes and were run for 100 ns. RMSF of the atomic positions for bergapten on 4UX2 is shown in Supplementary Figures S15A and bergapten on IT3S is shown in Supplementary Figure S15B. Root mean square deviation (RMSD) of interaction between 4UX2 and IT3S with bergapten is shown in Figures 1A,B, respectively. Small deviation in RMSD shows stable binding. Interactions of bergapten with different amino acid residues on 4UX2 and 1T3S are displayed in Figures 2A1,A2, respectively. Some residues form more than one specific contact with the ligand, which is depicted as darker shade of orange. Other interactions including H-bonds, hydrophobic, ionic, and water bridges between bergapten vs. 4UX2 and 1T3S are represented in Figures 2B1,B2, respectively.

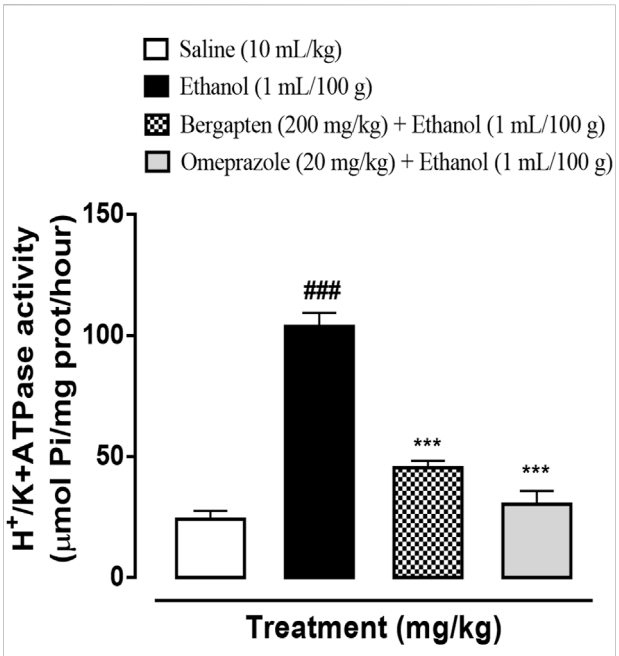

FIGURE 7
Effect of bergapten and omeprazole on decreasing rat gastric H^+/K^+ ATPase activity in the ethanol-induced gastric ulcer model. The data values are expressed as mean ± SEM (n = 3). One-way analysis of variance with *post hoc* Tukey's test. $^{###}p <$ 0.001 vs. saline group, $^{***}p < 0.001$ vs. ethanol group.

3.4 Effect of bergapten on castor oil-induced diarrhea

In contrast to the saline-treated negative control group, which showed no protection against castor oil-induced diarrhea, bergapten had a dose-dependent protective effect (50–100 mg/kg) in mice. To prevent diarrhea, bergapten offered 40% protection at 50 mg/kg, and 100% protection at 100 mg/kg ($p < 0.05$ vs. the saline group). Loperamide, a well-known antidiarrheal, prevented diarrhea in positive control shown in Table 1 ($p < 0.001$ vs. castor oil).

3.5 Effect of bergapten on intestinal fluid accumulation

When mice were given castor oil, which caused their intestines to fill up with fluid, 50–200 mg/kg of bergapten stopped the fluid from leaking out. Intestinal fluid buildup in the saline group was 86.5 1.2 (mean SEM, $n = 5$), but in the castor oil group, it was 124.16 1.96 ($^{###}p < 0.001$ vs. saline group). The amount of fluid buildup caused by castor oil was cut by bergapten at doses of 50, 100, and 200 mg/kg ($^{**}p < 0.01$ vs. castor oil group), 95.84 1.5 ($^{***}p < 0.001$ vs. castor oil group), and 75.98 0.91 ($^{***}p < 0.001$ vs. castor oil group). Figure 3 shows that 10 mg/kg of atropine decreased the amount of fluid in the gut to 72.71 1.2 ($^{***}p < 0.001$ vs. the castor oil group).

3.6 Effect on charcoal meal transit time

A dose-dependent delay in the passage of the charcoal meal through the small intestine is caused by bergapten. The saline group covered a distance of 94 cm. Bergapten at doses of 50, 100, and 200 mg/kg inhibited the transit of charcoal meal by 31.26%, 38.92%, and 43.01%, respectively ($^{***}p < 0.001$ vs. charcoal group). The inhibitory effect of atropine (0.1 mg/kg) is 81.40% ($^{***}p < 0.001$ vs. charcoal group) Table 2.

3.7 Effect of bergapten on spontaneous, K+-induced contractions and CCB effect

Figure 4 shows how bergapten, papaverine, and verapamil stop spontaneous and K^+ (80 mM)-induced contractions, with EC50 values of 0.0026 mg/ml (1.69–2.82, $n = 4$) and 0.0139 mg/ml (1.68–18.9, $n = 4$), respectively. Figure 4A shows that both natural contractions and contractions caused by K^+ (80 mM) were stopped by bergapten. Papaverine displayed non-specific inhibition in Figure 4B, with EC50 values of 0.4 µM (0.2–0.8, $n = 4$) for spontaneous contractions and 0.6 (0.3–1.3, $n = 4$) for high K^+ trigger contractions. Verapamil had an EC50 of 0.04 M (0.03–0.06, $n = 4$) against spontaneous contractions and 0.12 M (0.10–0.20, $n = 3$) against K^+-induced contractions (Figure 4C). Figure 5 demonstrates that when it was evaluated for calcium channel interaction, it shifted Ca^{2+} CRCs to the right, such as in papaverine and verapamil.

3.8 Effect on *H. pylori*

The zone of inhibition and MIC values were assessed against *H. pylori* isolate, which showed potent sensitivity by disc diffusion method for bergapten. It showed zone of inhibition of 30 ± 0.22 mm against isolate. The MIC value of 1.25 mg/ml was obtained (Supplementary Figure S16).

3.9 Effect on ethanol-induced ulcer

Bergapten, at doses ranging from 100 to 200 mg/kg, showed anti-ulcer activity in a dose-dependent manner. At dosages of 50, 100, and 200 mg/kg, bergapten induced inhibition that was, respectively, 20 percent, 56 percent, and 74 percent ($^{**}p <$ 0.01, $^{***}p < 0.001$ vs. the saline group). An inhibitory impact of 86 percent was achieved with 20 mg/kg of omeprazole

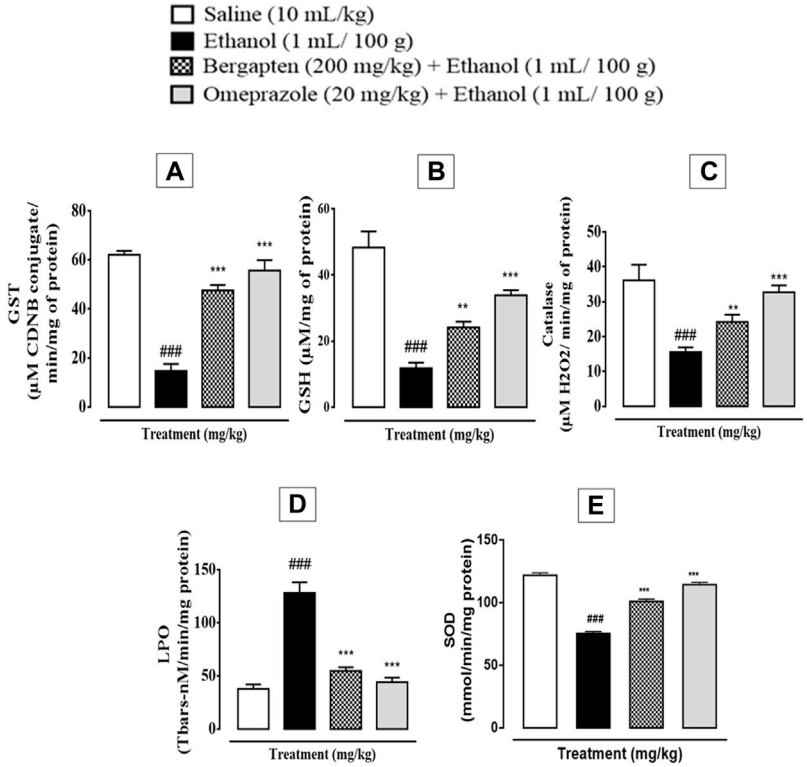

FIGURE 8
Effect of bergapten (200 mg/kg) and omeprazole groups against **(A)** glutathione-S-transferase (GST), **(B)** glutathione (GSH), **(C)** catalase, **(D)** lipid peroxidation (LPO), and **(E)** superoxide dismutase (SOD) in the ethanol-induced gastric ulcer model. The data are expressed as mean ± SEM (n = 3), and analyzed by one-way ANOVA with *post hoc* Tukey's test. $^{###}p < 0.001$ vs. saline group, $^{***}p < 0.001$, $^{**}p < 0.01$ vs. ethanol group.

(Table 3). The macroscopical examination revealed the presence of the rats' stomach mucosa (Figure 6).

3.10 Effect on H^+/K^+ ATPase activity

The ethanol-induced group demonstrated significant increase in H^+/K^+ ATPase activity proving the release of acids in the stomach ($^{###}p < 0.001$ *versus* saline group). The treatment groups including bergapten (200 mg/kg) and omeprazole (20 mg/kg) significantly reduced the pump activity ($^{***}p < 0.001$ *versus* ethanol group) shown in Figure 7.

3.11 Effect on oxidative stress markers

In ethanol-induced ulcer stomach tissues, the activity of GST, GSH, and catalase was dramatically decreased, while LPO was elevated ($^{###}p < 0.001$ in comparison to the saline group), which is a clear indication of oxidative stress. However, the levels of GST ($^{***}p < 0.001$ in comparison to the ethanol group), GSH ($^{**}p < 0.01$, $^{***}p < 0.001$ in comparison to the ethanol group), and catalase ($^{***}p < 0.001$ in comparison to the ethanol group) were significantly increased in the treatment groups that included bergapten (200 mg/kg) and omeprazole (20 mg/kg). Figure 8 shows that there was a substantial reduction in LPO levels across the treatment groups ($^{***}p < 0.001$ in comparison to the ethanol group). Superoxide dismutase activity indicated significant increase in SOD activity in the bergapten-treated group ($^{***}p < 0.001$ in comparison to the ethanol group) as compared to reduced activity in the ethanol group. This effect was similar to that produced by standard drug omeprazole ($^{***}p < 0.001$ in comparison to the ethanol group).

3.12 Histopathological analysis

Hematoxylin and eosin (H&E) staining was performed in order to distinguish among necrotic cells from intact one after administration of ethanol in stomach for further examination of gastroprotective effect of bergapten, as shown in Figure 9. In the stomach's most vulnerable regions, ethanol causes

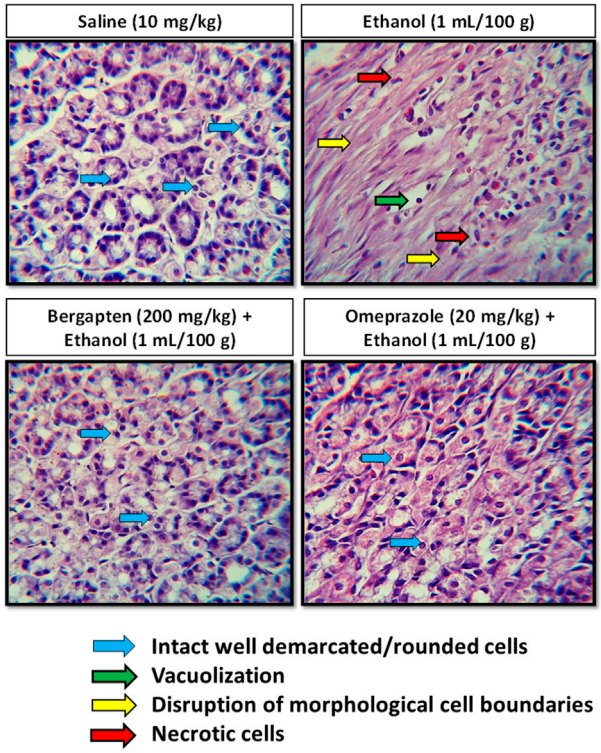

FIGURE 9
Histopathological slides of gastric tissues showing effect of pretreatment with **(A)** saline (10 ml/kg), **(B)** ethanol (1 ml/100 g), **(C)** bergapten (200 mg/kg), and **(D)** omeprazole (20 mg/kg) bergapten and omeprazole in the ethanol-induced ulcer model.

significant cellular alterations, whereas bergapten treatment lessens the damage. In comparison to the ethanol-treated group, a significant difference was seen in the control group. The injured region exhibits changed mucosal cell size and shape and aberrant color staining. Control animals' histology preparations indicated no alterations. Bergapten-treated groups had more viable cells than ethanol-treated ones.

3.13 Effect on TNF-α, PGE_2, and IL-8 expression

Figure 10 depicts the effect of bergapten on TNF-α, PGE2, and IL-8 in the stomach of an ethanol-induced ulcer model. Bergapten substantially reduced the expression of TNF-α, PGE_2, and IL-8 in both treatment groups as compared to the ethanol control group, according to a one-way ANOVA and *post hoc* Tukey's test. The results show a considerable difference between the treated group and the disease group. The degree of inflammatory mediator release from tissue in bergapten at doses of 100 and 200 mg/kg was considerably lower at higher doses. In contrast, bergapten has more pronounced effect with respect to omeprazole.

3.14 Western blot analysis

Western blot analysis (gastric tissues) confirmed that COX-2, TNF, and p-NFκB levels were increased in the ethanol-treated group ($^{###}p < 0.001$ versus saline group), but bergapten (200 mg/kg)- and omeprazole (20 mg/kg)-treated groups showed decreased expression levels as compared to the negative control group ($^{***}p < 0.001$ vs. ethanol group) Figures 11, 12.

3.15 Quantification of mRNA levels

RT-PCR determined the fold expression of H^+/K^+ ATPase in the ethanol-induced gastric ulcer model (Figure 13). The ethanol (1 ml/100)-administered group indicate increased expression of H^+/K^+ ATPase mRNA levels ($^{###}p < 0.001$ *versus* saline group). Bergapten (200 mg/kg) caused a significant decrease in expression levels ($^{***}p < 0.001$ vs. ethanol group). Omeprazole (20 mg/kg) also reduced the expression comparative to negative control group ($^{***}p < 0.001$ vs. ethanol group).

3.16 Toxicity studies

The OECD guidelines 425 were used to evaluate the safety profile of bergapten. After ingesting 2000 mg/kg of compound, the animal's fur and skin, feces consistency, urine's color, its breathing rhythm, and its sleeping patterns were all normal. There were no convulsions or signs of discomfort in any of the animals. Both groups' weights increased properly over the course of the 14-day treatment. The effect on behavioral parameters is given in Table 4, and the effect of 2000 mg/kg dose of bergapten on organ weight is given in Table 5. When comparing the weight of organs in drug-treated animals to the control group, no significant differences were identified.

3.16.1 Biochemical analysis

Effect on LFTs, RFTs, and oxidative stress markers are given in Figure 14. ALT and AST levels decreased in the bergapten group and ALP levels increased compared to the control group. RFTs indicated no renal toxicity signs based on RFTs outcome. Oxidative stress markers such as SOD, catalase, and GSH levels increased in the brain, kidney, and heart; however, GSH decreased in the liver indicating mild liver toxicity.

3.16.2 Hematological analysis

Effect on hematological parameters are given in Table 6. Bergapten showed a stable hematology profile. There was no evidence of hematological toxicity.

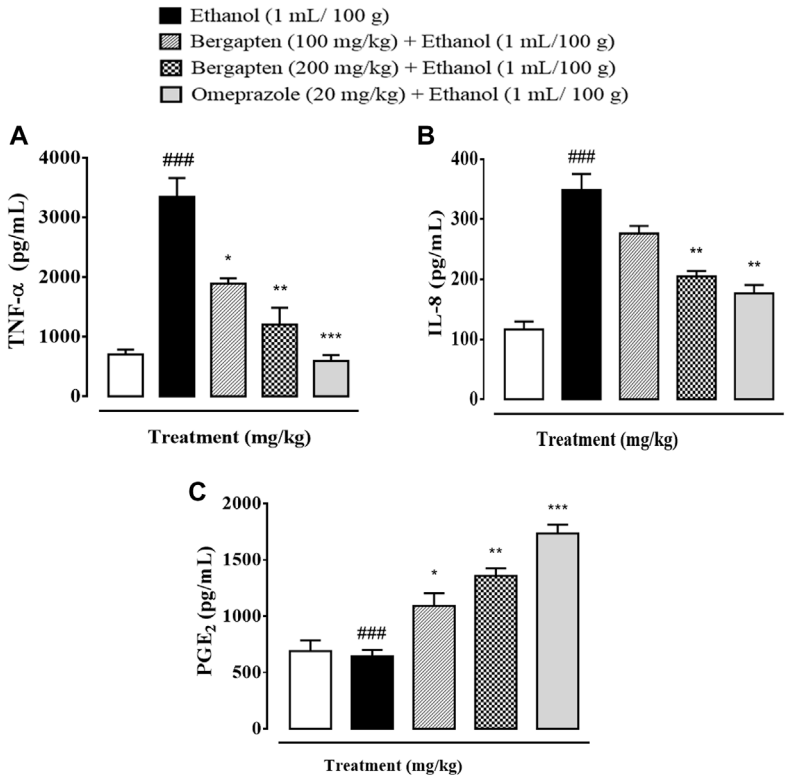

FIGURE 10
Effect of bergapten and omeprazole on **(A)** TNF-α (tumor necrosis factor alpha), **(B)** IL-8 (interleukin-8), and **(C)** PGE_2 (prostaglandin-E_2) expression in wound healing in the ethanol-induced gastric ulcer model examined by ELISA. The data are expressed as mean ± SEM ($n = 3$). One-way ANOVA with *post hoc* Tukey's test. $^{###}p < 0.001$ vs. saline group, $^{***}p < 0.001$, $^{**}p < 0.01$, $^{*}p < 0.05$ vs. ethanol group.

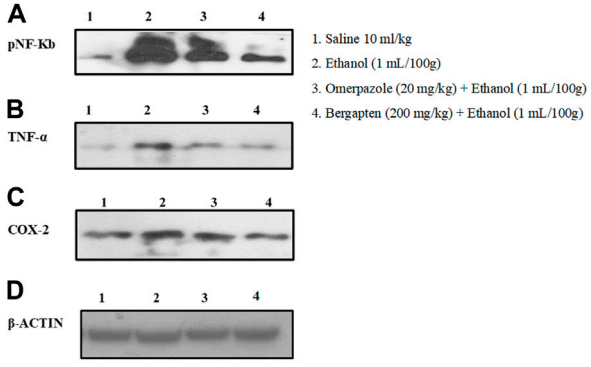

FIGURE 11
Pictorial representation showing inhibitory effect of bergapten and omeprazole groups against **(A)** phosphorylated nuclear factor kappa B (pNF-Kb), **(B)** tumor necrosis factor alpha (TNF-α), **(C)** cyclooxygenase 2 (COX-2), and **(D)** β-actin expression in ethanol-treated gastric tissues using western blot techniques, where 1 indicates saline group, 2 indicates the expression in ethanol groups, 3 indicates omeprazole group, and 5 indicates bergapten (200 mg/kg) group.

3.16.3 Histopathological analysis

There was no evidence of vacuolation, dystrophy, or atrophy in key organs such as the brain, liver, kidney, and heart according to histopathological investigation given in Figure 15.

4 Discussion

Based on a review of the literature on use of bergapten and plants with bergapten as the main phytoconstituent in gastric disorders like gastritis, constipation, and diarrhea, different tests were used to evaluate bergapten's anti-ulcer, anti-secretory, charcoal meal transit time, gastrointestinal motility, and anti-ulcer effects. An *in vitro*, *in silico*, *in vivo*, and proteomic approach was used for the explication of possible underlying mechanism(s) to rationalize aforementioned GIT ailments. Docking is a preliminary way of determining a ligand's affinity for a specific protein target (Zhang et al., 2021). Drug research and development heavily rely on molecular docking, which also determines target specificity and performs structure-based evaluation (Zhou et al., 2020; Faheem et al., 2021). For *in silico* studies initially bergapten was docked

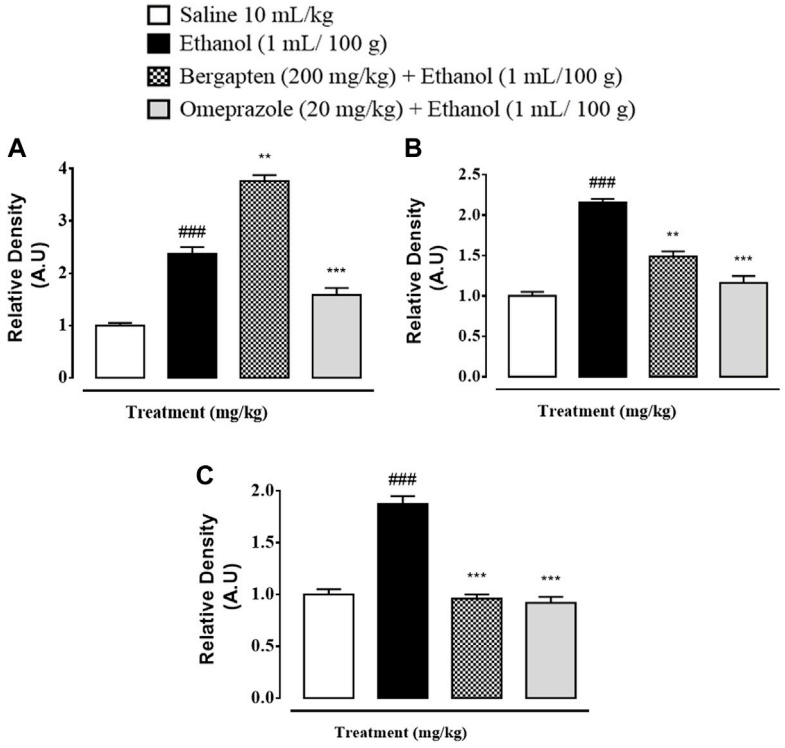

FIGURE 12
Graphical representation showing inhibitory effect of bergapten and omeprazole groups against **(A)** phosphorylated nuclear factor kappa B (pNF-Kb), **(B)** tumor necrosis factor alpha (TNF-α), and **(C)** cyclooxyegenase 2 (COX-2) in ethanol-treated gastric tissues using western blot techniques. The data are expressed as mean ± SEM (n = 3). One-way ANOVA with *post hoc* Tukey's test. $^{###}p < 0.001$ vs. saline group, $^{***}p < 0.001$, $^{**}p < 0.01$ vs. ethanol group.

against targets involved in GI ailments. Based on positive results, molecular docking simulation studies were conducted on the targets chosen for molecular studies, which included voltage-gated calcium channels (PDB ID: 1t3s) and H^+/K^+ ATPase (PDB ID:4ux2). This helped to strengthen the *in silico* results. Researchers have used PDB IDs from the Research Collaborator for Structural Bioinformatics Protein Database (RCSB PDB) to study the aforementioned target proteins in GI diseases (Pecsi et al., 2010). Docking analysis and molecular dynamic simulation studies were used to figure out the best positions. MD simulations let you see how molecules change shape, where their atoms are, and how they interact with their surroundings. The changes in these shapes helps access the structural interactions resulting best pose for ligand and protein complexes. This information is helpful to identify active pockets and poses that can be used to design ligands to best fit the target protein (Karplus and McCammon, 2002; Hernandez et al., 2016). Simulations were run for 100 ns in this study. The interactions were found to be stable, and the RMSF and RMSD values showed that targets proteins and bergapten worked well together. Less changes in RMSD show that interactions are strong (Faheem et al., 2021). This lead to the basis for further taking this research to animal testing by applying *in vivo* models.

To assess the effect of bergapten in gastrointestinal disorders such as castor oil-induced diarrhea, this study was design to measure the antidiarrheal effect of bergapten in rats similar to effect produced by loperamide, a standard drug while its possibly underlying mechanism were estimated through isolated tissue preparations also associated with reduction in gastric motility (Qazi et al., 2022). Castor oil is responsible for increasing intestinal fluid as well as diarrheal effect through its active metabolite, that is, ricinoleic acid. It changes the electrolyte and water transport and generates enormous contractions in the transverse and distal colon (Ansari et al., 2019). Bergapten acted as gut relaxant, observed antidiarrheal effects in the animal model. The calculated antidiarrheal effect of bergapten in rats, mediated possibly through the blockade of Ca^{2+} channels, evidence for its effectiveness in diarrhea, though additional mechanism(s) cannot be ruled out (Rehman et al., 2012). For charcoal meal transient time activity, bergapten in the small intestinal produced suppression of propulsion of charcoal marker in test doses just like standard drug atropine sulfate which has anticholinergic effect on GI transit leading to reduced motility (Ansari et al., 2019). The reduced motility causes sufficient reabsorption of water and contents through the intestine which can also be correlated to antidiarrheal findings of bergapten in this

10.3389/fphar.2022.1005154

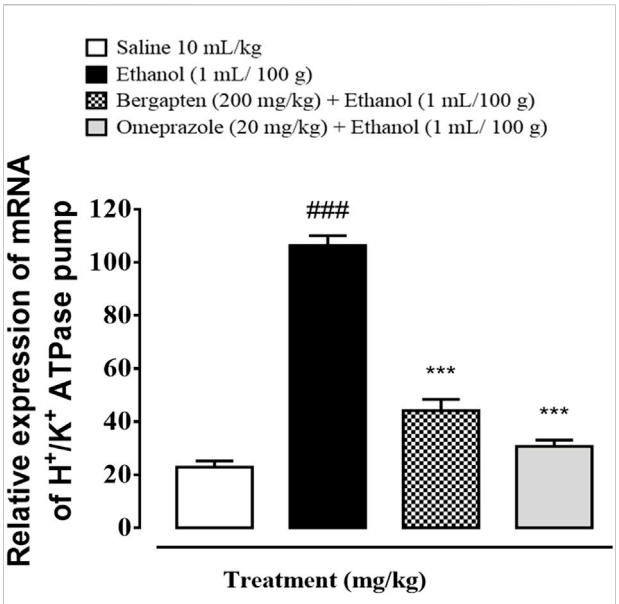

FIGURE 13
Graphical representation indicating effect of bergapten and omeprazole groups against mRNA expression of H^+/K^+ ATPase in ethanol-treated gastric tissues, using reverse transcriptase polymerase chain reaction (RT-PCR) technique. The data are expressed as mean ± SEM (n = 3). One-way ANOVA with *post hoc* Tukey's test. $^{###}p < 0.001$ vs. saline group, $^{***}p < 0.001$ vs. ethanol group.

TABLE 5 Effect of bergapten on the organ weight of treated and control rats (at limit dose 2000 mg/kg b.w. p.o).

Organs	Control	Bergapten (2000 mg/kg)
Heart	0.33 ± 0.3 g	0.38 ± 0.4 g
Kidney	1.0 ± 0.2 g	1.3 ± 0.2 g
Liver	6.4 ± 0.3 g	6.5 ± 0.5 g
Brain	1.39 ± 0.2 g	1.41 ± 0.1 g

study (Qazi et al., 2022). Other functional regulators involved in GI motility include acetylcholine, histamine, prostaglandins and ionic exchanges involving K^+ and Ca^{++} ions (Sadraei et al., 2022). Usually spasmolytic agents relax the GI tone and therefore are also found beneficial therapeutically in diarrhea. *In vitro* analysis was performed to find out what might be going on with the GIT inhibitory mechanism and the gastric mucosa. Bergapten produces its relaxant effect through the inhibition of Ca^{2+} channels. To figure out how it works, calcium channel blocking activity was carried out. Therefore, the spasmolytic effect of bergapten was studied through isolated rabbit jejunum assay, where bergapten proved to suppress both spontaneous and K^+ induced contractions. Bergapten pretreatment shifted the Ca^{2+} CRCs toward right similar to that of papaverine and verapamil that confirms the calcium channel blocking effect. Bergapten has the same Ca^{2+}-blocking effect as verapamil, but at a slightly higher concentration. Bergapten has a relaxing effect on smooth muscles, which may be caused by a combination of anticholinergic and Ca^{2+} antagonist mechanisms, which provides sound mechanistic background for its application in future for the hyperactive gut and airways disorders, such as abdominal colic, diarrhea and asthma that have prominent anticholinergic effect on intestinal transit (Rehman et al., 2011; Wen et al., 2022). A diminished gastric motility tone causes increase in stay of substances in intestine, which permits better water absorption. This finding proposes that bergapten has effect on the peristaltic movement of intestine which indicates its anti-motility activity results in anti-spasmodic

TABLE 4 Behavioral patterns of rats in bergapten-treated (2000 mg/kg p.o.) and control groups.

Parameters	30 min		4 h		24 h		48 h		7 days		14 days	
	CG	TG	CG	TG	CG	TG	CG	TG	CG	TG	CG	TG
Fur and skin	N	N	N	N	N	N	N	N	N	N	N	N
Itching	–	+	–	+	–	–	–	–	–	–	–	–
Eyes	N	N	N	N	N	N	N	N	N	N	N	N
Salivation	N	N	N	N	N	N	N	N	N	N	N	N
Mucous membrane	N	N	N	N	N	N	N	N	N	N	N	N
Respiration	N	↑	N	↑	N	N	N	N	N	N	N	N
Urination (color)	N	N	N	N	N	N	N	N	N	N	N	N
Faeces consistency	N	N	N	N	N	N	N	N	N	N	N	N
Convulsions and tremers	–	+	–	+	–	–	–	–	–	–	–	–
Sleep	N	N	N	N	N	N	N	N	N	N	N	N
Coma	–	–	–	–	–	–	–	–	–	–	–	–
Mortality	–	–	–	–	–	–	–	–	–	–	–	–

CG, control group; TG, bergapten-treated groups, N, normal; +, present; ↑, Increased; –, not found.

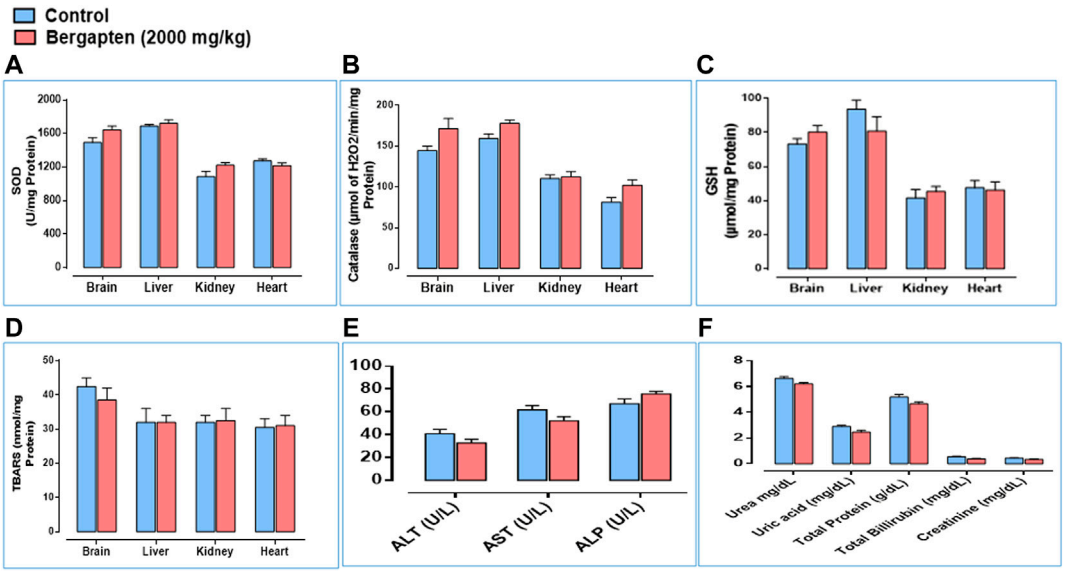

FIGURE 14
Toxicology assay findings showing **(A)** the expression level of SOD (superoxide dismutase), **(B)** expression level of catalase, **(C)** expression level of GSH (glutathione), **(D)** expression of TBARS (thiobarbituric acid reactive substances), **(E)** effect on liver function tests such as ALT (alanine transaminase), AST (aspartate aminotransferase), and ALP (alanine phosphatase). **(F)** Renal function test (RFTs) measuring urea, uric acid, total protein, total bilirubin, and creatinine levels in control and bergapten (2000 mg/kg)-treated rats.

TABLE 6 Effect of bergapten (at limit dose 2000 mg/kg b.w. p.o) on the complete blood count (CBC) and lipid profile of control group rats.

Parameters	Unit	Control	Bergapten (2000 mg/kg)
CBC			
Hb	g/dL	10.5 ± 0.1	10.9 ± 0.2
Total RBC	$*10^6$/uL	4.95 ± 0.4	5.2 ± 0.05
WBC count (TLC)	$*10^3$/uL	2.2 ± 0.11	3.5 ± 0.2
Platelets	$*10^5$/uL	256 ± 0.5	221 ± 1.9
HCT	%	31.3 ± 0.6	36.6 ± 0.2
MCV	Fl	50.9 ± 0.05	47.1 ± 0.9
MCHC	g/dL	34 ± 0.22	27.3 ± 0.6
Neutrophils	%	9.9 ± 0.8	10.2 ± 0.5
Lymphocytes	%	88 ± 1.4	95 ± 1.5
Monocytes	%	4 ± 0.12	3 ± 0.08
Eosinophils	%	2 ± 0.11	1 ± 0.04
MCH	Pg	15.7 ± 0.6	16 ± 0.018
Lipid profile			
Cholesterol	mg/dl	155 ± 1.5	170 ± 1.8
Triglycerides	mg/dl	130 ± 1	145 ± 1.2
H.D.L (cholesterol)	mg/dl	27 ± 0.68	31 ± 0.53
L.D.L (cholesterol)	mg/dl	107 ± 1.24	115 ± 0.78
V.L.D.L	mg/dl	30 ± 0.45	25 ± 1.2

properties. Similar effect to that of papaverine and verapamil standard calcium channel blocker. Ca^{2+} levels are increased in response to various stimuli released by the gut (such as histamine and prostaglandins), which stimulate the gut and eventually enhance its cytosolic concentration. In addition to non-targeted inhibitory action, the production of mediators that

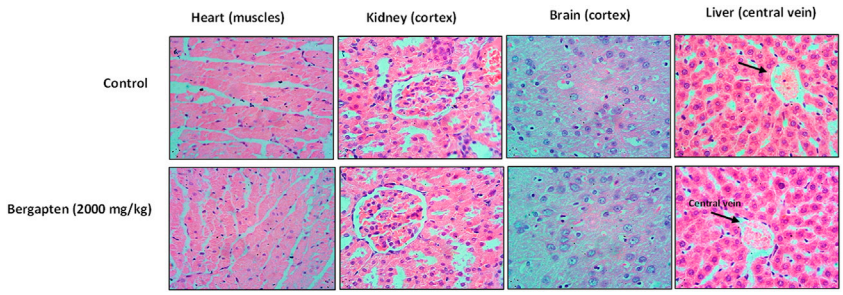

FIGURE 15
Hitopathological slides showing the effect of bergapten on vital organs of rats using hematoxylin and eosin staining histopathological method. Bar 50 μm, magnification × 40.

block the aforementioned channels is crucial (Mehmood et al., 2015).

Inflammation of the mucosal layer of the gastrointestinal (GI) tract is not only frequently associated with ulceration of those tissues, but it also plays a crucial role in both the formation and repair of the lesions (Raish et al., 2021). The mediators that orchestrate inflammatory responses can also affect the mucosa's resistance to injury caused by noxious chemicals, while others make the mucosa more vulnerable to injury. In the past 3 decades, there has been a change in perspective with regard to GI mucosal defence, moving away from a focus on the toxic secretions inside the lumen of the GI tract and toward a focus on the tissue responses that compose what is referred to as "mucosal defence." Nitric oxide, eicosanoids (prostaglandins, leukotrienes, and thromboxanes), neuropeptides, cytokines, and proteinases are among the essential GI mediators. These chemical mediators are possible targets for treatment (Mahmoud et al., 2019). In fact, targeting these mediators has recently shown to be successful in treating GI ulcerative/inflammatory disorders (Wallace and Chin, 1997). In gastrointestinal tract various aggressive and protective factors play important role in production and release of acid. Disturbance in these factors results in rupturing of mucosal protection which expose gastric lining to difference enzyme and acid production leading to the sores called ulcers (Tulassay and Herszényi, 2010). An ethanol-induced gastric model was used to explore the beneficial effect of bergapten through variety of mechanisms that stimulates ulcers including free radicals OH^{-}, NO production, mucus exhaustion, mucosal damage, release of superoxide anion, which ultimately prolonged the tissue oxidative stress and release of inflammatory mediators like TNF-α, PGE_2, and IL-8 (Wallace and Chin, 1997; Ansari et al., 2021). Bergapten showed marked inhibition on ethanol-induced gastric lesions in comparison to disease group. The potential of bergapten to produce anti-ulcer effect might be due to its CCB effect, as Ca^{2+} antagonist is well known to demonstrate such effects.

On the other hand, H^{+}/K^{+} ATPase is an enzyme located in the stomach's gastric membrane vesicles that catalyzes the exchange of intracellular H^{+} and external K^{+} as well as the hydrolysis of cytoplasmic ATP. Activation of the aforementioned pump causes release of protons causing acidic environment. This increase in acid production further damages the underlying mucosal membrane and its disruption may cause ulceration (Tulassay and Herszényi, 2010; He et al., 2018). Therefore, one of the therapeutic approaches is to reduce the acid production by inhibiting the H^{+}/K^{+} ATPase pump in the gastric membrane. For evaluating effect of bergapten in this regard *in vitro* inhibitory assay was conducted which revealed that bergapten inhibited the H^{+}/K^{+} ATPase pump effectively and comparable to the standard proton pump inhibitor available commercially, that is, Omeprazole. To further strengthen the results, RT-PCR study was conducted to reveal the expression levels of H^{+}/K^{+} ATPase. It was confirmed further through RT-PCR that expression level of H^{+}/K^{+} ATPase reduced significantly. By this we can confirm that underlying mechanism for gastroprotective anti-ulcer activity of bergapten is due to proton pump inhibition. In pathophysiology of gastric ulcers, oxidative stress plays a vital role. Antioxidant and nitric oxide free radical scavenging activity has been shown by bergapten, which may be responsible for its effectiveness as anti-ulcer agent and further validated by LPO, catalase, GST, GSH and SOD assay (Mehmood et al., 2015; Sisay et al., 2017; Liang et al., 2021). Increased oxidative stress provokes the release of pro-inflammatory mediators such as interleukin-8 (IL-8), TNF-α, COX-2 upregulation, and NF-ƙB activation that plays role in inflammatory cascade further aggaravating ulcer (Khan et al., 2011; Sisay et al., 2017). Furthermore, ELISA was done to quantify the protein expression of TNF-α, IL-8, and PGE-2. Bergapten has significantly attenuated necrosis in ulcerative tissue as compared to control achieved through proteomic analysis. Western blotting was also carried to evaluate the antiinflammtory response in ulcer. Bergapten protects the stomach of rats through inhibition of inflammatory markers such as TNF-α, p-NFκB, COX-2, and enhancing protective PGE2 response as illustrated in results of western blotting. The results were quite significant as compared to ethanol ($p < 0.001$ vs. normal saline). Histopathological examination also revealed the intact morphology of the bergapten pretreated

groups indicating effectiveness in preventing ethanol-induced mucosal injury. In pathophysiology of gastric ulcers one of the major contributors include H. *pylori* infections and H^+/K^+ ATPase pump. H. *pylori* infection is treated using combination of antibiotics termed as triple and quad therapy, as use of a single antibiotic shows significant relapse of the infection (He et al., 2018). Therefore, there is need of an agent that may concomitantly scavenge the bacterial infection as well as reduces acid secretions. Disc diffusion method utilized indicated efficacy of bergapten in scavenging the bacterial growth and showing a prominent zone of inhibition. To access the safety profile of bergapten, toxicological investigation is carried out. Bergapten has been reported to cause photosensitivity and apart from this aspect further toxicology evaluation has not been reported yet. In current study, OECD 425 guidelines were followed for conducting animal studies for acute toxicity accessment of bergapten. In acute toxicity analysis oral dosing helps to access the clinical safety in terms of dose ranges (Saleem et al., 2017). Bergapten is however classified with precautionary codes and hazard markers by GHS (globally harmonized system of classification) for chemicals due to its irritant nature to skin and to inhalation hazard.

5 Conclusion

The relevance of bergapten to the pharmaceutical industry is shown by the fact that researchers are actively investigating its potential as a result of the antidiarrheal, anti-secretory, anti-spasmodic, anti-motility, and anti-ulcer qualities that it has been shown to possess. Bergapten showed a strong affinity for the H^+/K^+ ATPase pump and voltage-gated L-type calcium channels. Further molecular simulations confirmed the favorable interactions with the aforementioned targets making it a favorable ligand for gastroprotection. Bergapten also increases the protective GST, GSH, and catalase and reduces the expression of LPO. It shows gastroprotective capability by reducing the prevalence of ulcer after ethanol ingestion. Furthermore, it has proved to be a safe natural compound in toxicity analysis which can be formulated into a new treatment option to cure multiple gastrointestinal ailments.

Data availability

The original contributions presented in the study are included in the article/Supplementary Material; further inquiries can be directed to the corresponding authors.

Ethics statement

The animal study was conducted according to the rules of the Research and Ethics Committee of the Riphah Institute of Pharmaceutical Sciences (Ref. no. REC/RIPS/2019/021), and the "Principles of Laboratory Animal Care" were followed when conducting the experiments.

Author contributions

Conceptualization: HA and A-uK; methodology: HA; experimentation, formal analysis, and investigation: HA and NQ; resources: A-uK; writing—original draft preparation: HA; MD simulations: HA and FA; anti-*H. pylori* activity: NQ; writing—review and editing: HA, SS, and SB; supervision: A-uK; and funding acquisition: SB. All authors have read and agreed to the published version of manuscript.

Acknowledgments

The authors are thankful to the Higher Education Commission for facilitating them in their research work. They wish to thank the University of Oradea, Oradea, Romania, for financial support in publishing this paper.

Conflict of interest

The authors declare that the research was conducted in the absence of any commercial or financial relationships that could be construed as a potential conflict of interest.

Publisher's note

All claims expressed in this article are solely those of the authors and do not necessarily represent those of their affiliated organizations, or those of the publisher, the editors, and the reviewers. Any product that may be evaluated in this article, or claim that may be made by its manufacturer, is not guaranteed or endorsed by the publisher.

Supplementary material

The Supplementary Material for this article can be found online at: https://www.frontiersin.org/articles/10.3389/fphar.2022.1005154/full#supplementary-material

SUPPLEMENTARY TABLE S1
Binding energy (kcal/mol) and post-dock analysis of the best conformational pose of bergapten with adrenergic α1 receptor, muscarinic M1, muscarinic M3, dopaminergic D2, calmodulin, voltage-gated L-type calcium channel, histaminergic H1, H+/K+ ATPase pump, histaminergic H2, mu-opioid, and phosphodiesterase enzyme.

SUPPLEMENTARY TABLE S2
Pharmacokinetic and drug likeliness profiling of bergapten using SwissADME tool.

References

Abbaskhan, A., Choudhary, M., Ghayur, M., Parween, Z., Shaheen, F., Gilani, A., et al. (2011). Biological activities of Indian celery, seseli diffusum (roxb. Ex Sm.) sant. & wagh. *Phytother. Res.* 26 (5), 783–786. doi:10.1002/ptr.3600

Ali, F., Khan, A., Muhammad, S., and Hassan, S. (2022). Quantitative real-time analysis of differentially expressed genes in peripheral blood samples of hypertension patients. *Genes.* 13 (2), 187. doi:10.3390/genes13020187

Ansari, S., Khan, A., Qazi, N., Shah, F., and Naeem, K. (2019). *In vivo*, proteomic, and in silico investigation of sapodilla for therapeutic potential in gastrointestinal disorders. *Biomed. Res. Int.* 2019, 1–19. doi:10.1155/2019/4921086

Ansari, S., Khan, A., Qazi, N., Shah, F., and Naeem, K. (2021). Proteomic analysis and *in vivo* studies reveal the potential gastroprotective effects of $CHCl_3$ and aqueous extracts of Ficus palmata. *Evid. Based. Complement. Altern. Med.* 2021, 1–11. doi:10.1155/2021/6613140

Bahmani, M., Zargaran, A., and Rafieian-Kopaei, M. (2014). Identification of medicinal plants of Urmia for treatment of gastrointestinal disorders. *Rev. Bras. De. Farmacogn.* 24 (4), 468–480. doi:10.1016/j.bjp.2014.08.001

Chidambaram, S., Ali, D., Alarifi, S., Radhakrishnan, S., and Akbar, I. (2020). *In silico* molecular docking: Evaluation of coumarin based derivatives against SARS-CoV-2. *J. Infect. Public Health* 13 (11), 1671–1677. doi:10.1016/j.jiph.2020.09.002

Dengiz, G. O., Odabasoglu, F., Halici, Z., Suleyman, H., Cadirci, E., and Bayir, Y. (2007). Gastroprotective and antioxidant effects of amiodarone on indomethacin-induced gastric ulcers in rats. *Arch. Pharm. Res.* 30 (11), 1426–1434. doi:10.1007/BF02977367

Faheem, M., Althobaiti, Y., Khan, A., Ullah, A., Ali, S., and Ilyas, U. (2021). Investigation of 1, 3, 4 oxadiazole derivative in PTZ-induced neurodegeneration: A simulation and molecular approach. *J. Inflamm. Res.* 14, 5659–5679. doi:10.2147/jir.s328609

Fomina, L. (2020). Calcium-phosphorus balance in comorbid peptic ulcer disease and arterial hypertension and its correction of calcium channel blockers. *Med. Alfavit.* 4 (38), 19–22. doi:10.33667/2078-5631-2019-4-38(413)-19-22

Hasler, W., Parkman, H., Wilson, L., Pasricha, P., Koch, K., Abell, T., et al. (2010). Psychological dysfunction is associated with symptom severity but not disease etiology or degree of gastric retention in patients with gastroparesis. *Am. J. Gastroenterol.* 105 (11), 2357–2367. doi:10.1038/ajg.2010.253

Hassan, S. S. U., Zhang, W.-D., Jin, H.-Z., Basha, S. H., and Priya, S. V. S. S. (2022). *In-silico* anti-inflammatory potential of guaiane dimers from Xylopia vielana targeting COX-2. *J. Biomol. Struct. Dyn.* 40, 484–498. doi:10.1080/07391102.2020.1815579

He, H., Li, X., Yu, H., Zhu, S., He, Y., Komatsu, K., et al. (2018). Gastroprotective effect of araloside A on ethanol- and aspirin-induced gastric ulcer in mice: Involvement of H+/K+-ATPase and mitochondrial-mediated signaling pathway. *J. Nat. Med.* 73 (2), 339–352. doi:10.1007/s11418-018-1256-0

Hernández-Rodríguez, M., C Rosales-Hernández, M., E Mendieta-Wejebe, J., Martínez-Archundia, M., and Correa Basurto, J. (2016). Current tools and methods in molecular dynamics (MD) simulations for drug design. *Curr. Med. Chem.* 23 (34), 3909–3924. doi:10.2174/0929867323666160530144742

Irvine, E., Whitehead, W., Chey, W., Matsueda, K., Shaw, M., Talley, N., et al. (2006). Design of treatment trials for functional gastrointestinal disorders. *Gastroenterology* 130 (5), 1538–1551. doi:10.1053/j.gastro.2005.11.058

Jones, N., Koletzko, S., Goodman, K., Bontems, P., Cadranel, S., Casswall, T., et al. (2017). Joint ESPGHAN/NASPGHAN guidelines for the management of *Helicobacter pylori* in children and adolescents (update 2016). *J. Pediatr. Gastroenterol. Nutr.* 64 (6), 991–1003. doi:10.1097/mpg.0000000000001594

Karplus, M., and McCammon, J. A. (2002). Molecular dynamics simulations of biomolecules. *Nat. Struct. Biol.* 9, 646–652. doi:10.1038/nsb0902-646

Khakimov, Z., Rakhmanov, A., and Bekova, N. (2021). study of the influence of calcium channel blockers on the state of rat stomach mucosa in indomethacin-induced gastropathy. *Am. J. Med. Med. Sci.* 11, 887–890. doi:10.5923/j.ajmms.20211112.09

Khan, A., and Gilani, A. (2009). Antidiarrheal, antisecretory, and bronchodilatory activities ofHypericum perforatum. *Pharm. Biol.* 47 (10), 962–967. doi:10.1080/13880200902960206

Khan, A., ur Rehman, N., AlKharfy, K. M., and Gilani, A. H. (2011). Antidiarrheal and antispasmodic activities of salvia officinalis are mediated through activation of K+ channels. *Bangladesh J. Pharmacol.* 6, 111–116. doi:10.3329/bjp.v6i2.9156

Khan, I., Abbas, T., Anjum, K., Abbas, S. Q., Shagufta, B. I., Shah, S. A. A., et al. (2019). Antimicrobial potential of aqueous extract of Camellia sinensis against representative microbes. *Pak. J. Pharm. Sci.* 32, 631–636.

Lei, J., Dong, Y., Hou, Q., He, Y., Lai, Y., Liao, C., et al. (2022). Intestinal microbiota regulate certain meat quality parameters in chicken. *Front. Nutr.* 9, 747705. doi:10.3389/fnut.2022.747705

Li, Z., Teng, M., Jiang, Y., Zhang, L., Luo, X., Liao, Y., et al. (2022). YTHDF1 negatively regulates Treponema pallidum-induced inflammation in THP-1 macrophages by promoting SOCS3 translation in an m6A-dependent manner. *Front. Immunol.* 13, 857727. doi:10.3389/fimmu.2022.857727

Liang, Y., Xie, L., Liu, K., Cao, Y., Dai, X., Wang, X., et al. (2021). Bergapten: A review of its pharmacology, pharmacokinetics, and toxicity. *Phytother. Res.* 35 (11), 6131–6147. doi:10.1002/ptr.7221

Liu, C., Wang, Y., Li, L., He, D., Chi, J., Li, Q., et al. (2022a). Engineered extracellular vesicles and their mimetics for cancer immunotherapy. *J. Control. Release* 349, 679–698. doi:10.1016/j.jconrel.2022.05.062

Liu, Z., Su, W., Ao, J., Wang, M., Jiang, Q., He, J., et al. (2022b). Instant diagnosis of gastroscopic biopsy via deep-learned single-shot femtosecond stimulated Raman histology. *Nat. Commun.* 13, 4050. doi:10.1038/s41467-022-31339-8

Mahmoud, Y. I., and Abd El-Ghaffar, E. A. (2019). Spirulina ameliorates aspirin-induced gastric ulcer in albino mice by alleviating oxidative stress and inflammation. *Biomed. Pharmacother.* 109, 314–321. doi:10.1016/j.biopha.2018.10.118

Majid, M., Farhan, A., Asad, M. I., Khan, M. R., Hassan, S. S. U., Haq, I.-U., et al. (2022). An extensive pharmacological evaluation of new anti-cancer triterpenoid (nummularic acid) from Ipomoea batatas through *in vitro*, in silico, and *in vivo* studies. *Molecules* 27, 2474. doi:10.3390/molecules27082474

Mehmood, M., Munir, S., Khalid, U., Asrar, M., and Gilani, A. (2015). Antidiarrhoeal, antisecretory and antispasmodic activities of Matricaria chamomilla are mediated predominantly through K+-channels activation. *BMC Complement. Altern. Med.* 15 (1), 75. doi:10.1186/s12906-015-0595-6

Memariani, Z., Abbas, S. Q., ul Hassan, S. S., Ahmadi, A., and Chabra, A. (2021). Naringin and naringenin as anticancer agents and adjuvants in cancer combination therapy: Efficacy and molecular mechanisms of action, a comprehensive narrative review. *Pharmacol. Res.* 171, 105264. doi:10.1016/j.phrs.2020.105264

Milivojevic, V., and Milosavljevic, T. (2020). Burden of gastroduodenal diseases from the global perspective. *Curr. Treat. Options Gastroenterol.* 18 (1), 148–157. doi:10.1007/s11938-020-00277-z

Mishra, V. (2016). Potent gastroprotective effect chrysophanol and emodin from rehum emodi via H+/K+atpase inhibition and increasing the PGE2 level in rats. *Nat. Products:An Indian J.* 12, 1–12.

Muhammad, I., Luo, W., Shoaib, R. M., Li, G., Hassan, U. S. S., Yang, Z., et al. (2021a). Guaiane-type sesquiterpenoids from Cinnamomum migao H. W. Li: And their anti-inflammatory activities. *Phytochemistry* 190, 112850. doi:10.1016/j.phytochem.2021.112850

Muhammad, I., Shams ul Hassan, S., Cheung, S., Li, X., Wang, R., Zhang, W. D., et al. (2021b). Phytochemical study of Ligularia subspicata and valuation of its anti-inflammatory activity. *Fitoterapia* 148, 104800. doi:10.1016/j.fitote.2020.104800

Noman, M., Qazi, N., Rehman, N., and Khan, A. (2022). Pharmacological investigation of brucine anti-ulcer potential. *Front. Pharmacol.* 13, 886433. doi:10.3389/fphar.2022.886433

Noor, A., Qazi, N., Nadeem, H., Khan, A., Paracha, R., Ali, F., et al. (2017). Synthesis, characterization, anti-ulcer action and molecular docking evaluation of novel benzimidazole-pyrazole hybrids. *Chem. Cent. J.* 11 (1), 85. doi:10.1186/s13065-017-0314-0

Nyssen, O., Vaira, D., Tepes, B., Kupcinskas, L., Bordin, D., Pérez-Aisa, Á., et al. (2021). Room for improvement in the treatment of *Helicobacter pylori* infection: Lessons from the European registry on *H. pylori* management (Hp-EuReg). *J. Clin. Gastroenterol.* 56 (2), e98–e108. doi:10.1097/mcg.0000000000001482

Ohama, T., Hori, M., and Ozaki, H. (2007). Mechanism of abnormal intestinal motility in inflammatory bowel disease: How smooth muscle contraction is reduced? *J. Smooth Muscle Res.* 43 (2), 43–54. doi:10.1540/jsmr.43.43

Pecsi, I., Leveles, I., Harmat, V., Vertessy, B., and Toth, J. (2010). Aromatic stacking between nucleobase and enzyme promotes phosphate ester hydrolysis in dUTPase. *Nucleic Acids Res.* 38 (20), 7179–7186. doi:10.1093/nar/gkq584

Qazi, N., Khan, A., Abbasi, S., Malik, I., and Naeem, K. (2022). Effect of rumex dentatus on gastrointestinal protection and toxicology in rodents via investigating H+/K+-ATPase, calcium channels, and PDE mediated signaling. *Front. Pharmacol.* 13, 936161. doi:10.3389/fphar.2022.936161

Raish, M., Shahid, M., Bin Jardan, Y. A., Ansari, M. A., Alkharfy, K. M., Ahad, A., et al. (2021). Gastroprotective effect of sinapic acid on ethanol-induced gastric ulcers in rats: Involvement of Nrf2/HO-1 and NF-κB signaling and antiapoptotic role. *Front. Pharmacol.* 12, 101. doi:10.3389/fphar.2021.622815

Rehman, N., Mehmood, M., Alkharfy, K., and Gilani, A. (2011). Studies on antidiarrheal and antispasmodic activities of lepidium sativum crude extract in rats. *Phytother. Res.* 26 (1), 136–141. doi:10.1002/ptr.3642

Rehman, N. U., Mehmood, M. H., Alkharfy, K. M., and Gilani, A. H. (2012). Studies on antidiarrheal and antispasmodic activities of lepidium sativum crude extract in rats. *Phytother. Res.* 26, 136–141. doi:10.1002/ptr.3642

Sadraei, H., Ghasemi, M., and Saranji, S. (2022). Evaluation of spasmolytic effects of naringenin on ileum contraction and intestinal charcoal meal transit: Involvement of ATP-sensitive K+ channels. *J. Herbmed Pharmacol.* 11 (2), 262–268. doi:10.34172/jhp.2022.31

Saleem, U., Amin, S., Ahmad, B., Azeem, H., Anwar, F., and Mary, S. (2017). Acute oral toxicity evaluation of aqueous ethanolic extract of Saccharum munja Roxb. roots in albino mice as per OECD 425 TG. *Toxicol. Rep.* 4, 580–585. doi:10.1016/j.toxrep.2017.10.005

Shams ul Hassan, S., Abbas, S. Q., Hassan, M., and Jin, H.-Z. (2021). Computational exploration of anti-cancer potential of guaiane dimers from xylopia vielana by targeting B-raf kinase using chemo-informatics, molecular docking and MD simulation studies. *Anticancer. Agents Med. Chem.* 21, 731–746. doi:10.2174/1871520621666211013115500

Shams ul Hassan, S., Qamar Abbas, S., Ali, F., Ishaq, M., Bano, I., Hassan, M., et al. (2022). A comprehensive in silico exploration of pharmacological properties, bioactivities, molecular docking, and anticancer potential of vieloplain F from xylopia vielana targeting B-raf kinase. *Molecules* 27, 917. doi:10.3390/molecules27030917

Sisay, M., Engidawork, E., and Shibeshi, W. (2017). Evaluation of the antidiarrheal activity of the leaf extracts of Myrtus communis Linn (Myrtaceae) in mice model. *BMC Complement. Altern. Med.* 17 (1), 103. doi:10.1186/s12906-017-1625-3

Song, K., and Wu, D. (2022). Shared decision-making in the management of patients with inflammatory bowel disease. *World J. Gastroenterol.* 28 (26), 3092–3100. doi:10.3748/wjg.v28.i26.3092

Tulassay, Z., and Herszényi, L. (2010). Retracted: Gastric mucosal defense and cytoprotection. *Best. Pract. Res. Clin. Gastroenterol.* 24 (2), 99–108. doi:10.1016/j.bpg.2010.02.006

Ul Hassan, S. S., Muhammad, I., Abbas, S. Q., Hassan, M., Majid, M., Jin, H. Z., et al. (2021). Stress driven discovery of natural products from actinobacteria with anti-oxidant and cytotoxic activities including docking and admet properties. *Int. J. Mol. Sci.* 22, 11432. doi:10.3390/ijms222111432

Ullah, I., Khan, M., Khan, A., Akhlaq, M., Mukhtiar, M., and Rasheed, F. (2019). Chemical identification, antibacterial effect and synergistic potential of mentha arvensis with 5-fluorouracil against HCT-116 colon cancer cell line. *Lat. Am. J. Pharm.* 38 (4), 762–770.

Vera Saltos, M., Naranjo Puente, B., Malafronte, N., and Braca, A. (2013). A new monoterpene glycoside fromSiparuna thecaphora. *Nat. Prod. Res.* 28 (1), 57–60. doi:10.1080/14786419.2013.843179

Wallace, J., and Chin, B. (1997). Inflammatory mediators in gastrointestinal defense and injury. *Proc. Soc. Exp. Biol. Med.* 214 (3), 192–203. doi:10.3181/00379727-214-44087

Wen, J., Zhang, J. W., Lyu, Y. X., Zhang, H., Deng, K. X., Chen, H. X., et al. (2022). Ethanol extract of Glycyrrhiza uralensis fisch: Antidiarrheal activity in mice and contraction effect in isolated rabbit jejunum. *Chin. J. Integr. Med.*, 1–8. doi:10.1007/s11655-022-3536-5

Yu, X., Azietaku, J., Li, J., An, M., He, J., Hao, J., et al. (2016). The pharmacokinetics, bioavailability and excretion of bergapten after oral and intravenous administration in rats using high performance liquid chromatography with fluorescence detection. *Chem. Cent. J.* 10 (1), 62. doi:10.1186/s13065-016-0212-x

Zhang, Z., Cui, F., Cao, C., Wang, Q., and Zou, Q. (2021). Single-cell RNA analysis reveals the potential risk of organ-specific cell types vulnerable to SARS-CoV-2 infections. *Comput. Biol. Med.* 140, 105092. doi:10.1016/j.compbiomed.2021.105092

Zhuo, Z., Wan, Y., Guan, D., Ni, S., Wang, L., Zhang, Z., et al. (2020). A loop-based and AGO-incorporated virtual screening model targeting AGO-mediated miRNA-mRNA interactions for drug discovery to rescue bone phenotype in genetically modified mice. *Adv. Sci.* 7, 1903451. doi:10.1002/advs.201903451

frontiers | Frontiers in Pharmacology

TYPE Original Research
PUBLISHED 23 November 2022
DOI 10.3389/fphar.2022.1053744

Check for updates

OPEN ACCESS

EDITED BY
Fareeha Anwar,
Riphah International University, Pakistan

REVIEWED BY
Naila Boby,
Kyungpook National University, South Korea
Samina Shabbir,
Guangdong Academy of Science (CAS), China
Farhath Sultana,
Icahn School of Medicine at Mount Sinai, United States

*CORRESPONDENCE
Muhammad Majid,
majidpharma808@gmail.com
Hui-Zi Jin,
kimhz@sjtu.edu.cn

SPECIALTY SECTION
This article was submitted to Predictive Toxicology,
a section of the journal
Frontiers in Pharmacology

RECEIVED 26 September 2022
ACCEPTED 31 October 2022
PUBLISHED 23 November 2022

CITATION
Hassan SSu, Abbas SQ, Muhammad I, Wu J-J, Yan S-K, Ali F, Majid M, Jin H-Z and Bungau S (2022), Metals-triggered compound CDPDP exhibits anti-arthritic behavior by downregulating the inflammatory cytokines, and modulating the oxidative storm in mice models with extensive ADMET, docking and simulation studies.
Front. Pharmacol. 13:1053744.
doi: 10.3389/fphar.2022.1053744

COPYRIGHT
© 2022 Hassan, Abbas, Muhammad, Wu, Yan, Ali, Majid, Jin and Bungau. This is an open-access article distributed under the terms of the Creative Commons Attribution License (CC BY). The use, distribution or reproduction in other forums is permitted, provided the original author(s) and the copyright owner(s) are credited and that the original publication in this journal is cited, in accordance with accepted academic practice. No use, distribution or reproduction is permitted which does not comply with these terms.

Metals-triggered compound CDPDP exhibits anti-arthritic behavior by downregulating the inflammatory cytokines, and modulating the oxidative storm in mice models with extensive ADMET, docking and simulation studies

Syed Shams ul Hassan[1,2], Syed Qamar Abbas[3], Ishaq Muhammad[1,2], Jia-Jia Wu[1,2], Shi-Kai Yan[1,2], Fawad Ali[4], Muhammad Majid[5]*, Hui-Zi Jin[1,2]* and Simona Bungau[6]

[1]Shanghai Key Laboratory for Molecular Engineering of Chiral Drugs, School of Pharmacy, Shanghai Jiao Tong University, Shanghai, China, [2]Department of Natural Product Chemistry, School of Pharmacy, Shanghai Jiao Tong University, Shanghai, China, [3]Department of Pharmacy, Sarhad University of Science and Technology, Peshawar, Pakistan, [4]Department of Pharmacy, Kohat University of Science and Technology, Kohat, Pakistan, [5]Faculty of Pharmacy, Hamdard University, Islamabad, Pakistan, [6]Department of Pharmacy, Faculty of Medicine and Pharmacy, University of Oradea, Oradea, Romania

Triggering through abiotic stress, including chemical triggers like heavy metals, is a new technique for drug discovery. In this research, the effect of heavy metal Nickel on actinobacteria *Streptomyces sp.* SH-1327 to obtain a stress-derived compound was firstly investigated. A new compound cyclo-(D)-Pro-(D)-Phe (CDPDP) was triggered from the actinobacteria strain SH-1327 with the addition of nickel ions 1 mM. The stress compound was further evaluated for its anti-oxidant, analgesic, and anti-inflammatory activity against rheumatoid arthritis through *in-vitro* and *in-vivo* assays in albino mice. A remarkable *in-vitro* anti-oxidant potential of CDPDP was recorded with the IC_{50} value of 30.06 ± 5.11 µg/ml in DPPH, IC_{50} of 18.98 ± 2.91 against NO free radicals, the IC_{50} value of 27.15 ± 3.12 against scavenging ability and IC_{50} value of 28.40 ± 3.14 µg/ml for iron chelation capacity. Downregulation of pro-inflammatory mediators (NO and MDA), suppressed levels of pro-inflammatory cytokines (TNF-α, IL-6, IL-Iβ) and upregulation of expressions of anti-oxidant enzymes (GSH, catalase, and GST) unveiled its anti-inflammatory potential. CDPDP was analyzed in human chondrocyte cell line CHON-001 and the results demonstrated that CDPDP significantly increased cell survival, and inhibited apoptosis of IL-1β treated chondrocytes and IL-1β induced matrix degrading markers. In addition, to evaluate the mitochondrial fitness of CHON-001 cells, CDPDP significantly upregulated pgc1-α, the master regulator of mitochondrial biogenesis, indicating that CDPDP provides protective effects in CHON-001

cells. The absorption, distribution, metabolism, excretion, and toxicity (ADMET) profile of the CDPDP showed that CDPDP is safe in cases of hepatotoxicity, cardiotoxicity, and cytochrome inhibition. Furthermore, docking results showed good binding of CDPDP with IL-6–17.4 kcal/mol, and the simulation studies proved the stability between ligand and protein. Therefore, the findings of the current study prospect CDPDP as a potent anti-oxidant and a plausible anti-arthritic agent with a strong pharmacokinetic and pharmacological profile.

KEYWORDS

actinobacteria, inflammation, arthritis, anti-oxidant, admet, molecular docking

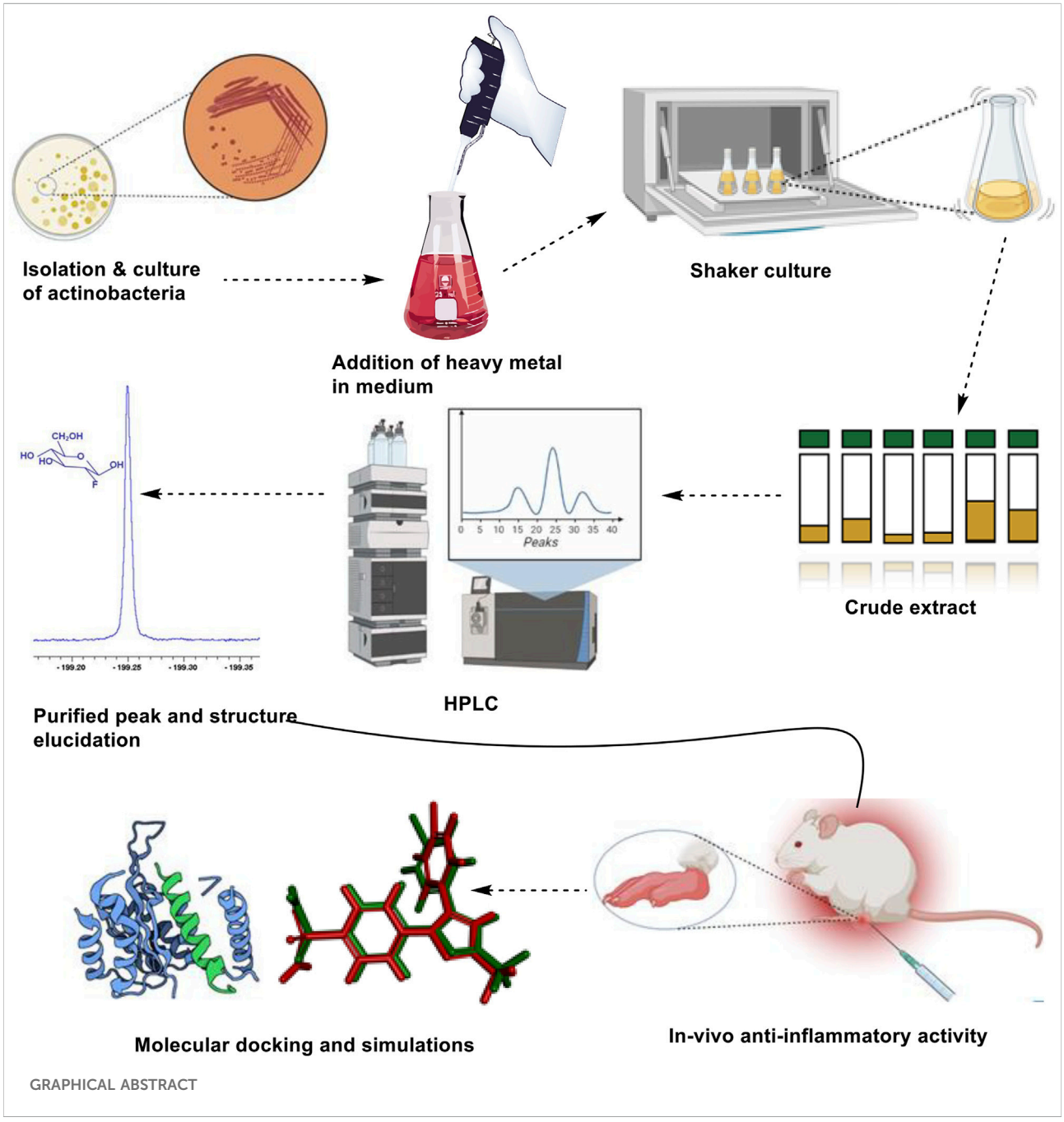

GRAPHICAL ABSTRACT

1 Introduction

Rheumatoid arthritis (RA) is a chronic inflammatory disease with a global frequency of around 5 per 1,000 persons, according to the World Health Organization. This condition affects women more often than men, and it is most commonly seen in the elderly. It is characterized by the inflammation of various joints and is accompanied by symptoms like periarticular osteopenia, osteitis, and synovitis (Majid et al., 2015; Majid et al., 2018). RA predominantly affects the covering of the synovial joints. It may cause increasing disability, early mortality, significant economic difficulties, and untimely death. The clinical signs of symmetric inflammation include redness, arthralgia, burning, and in severe cases, restriction in range of motion. The most often affected organs by RA are the knees, hands, wrists, and legs. The patients with RA reported feeling soreness and redness in their joints when examined. Most individuals with RA have impairment within 10 years of their diagnosis, making early detection even more critical to limit the inflammatory reaction and subsequent deterioration of joint cartilage and bones (Maryam et al., 2018; Dong et al., 2021).

Prognostic indicators that are associated with the prediction of RA may be divided into two categories: those that are associated with the estimation of signs or indications of RA and those that are associated with the monitoring of bone and cartilage deterioration. It has been shown that the activation of many pathogenic signaling systems occurs in RA, resulting in the progressive and permanent destruction of joint tissue. The growth and durability of fully established RA need the participation of a variety of cells, including dendritic cells, synovial cells, macrophages, and many other immune cells, such as rheumatoid arthritis synovial fibroblasts (RASF), compared to other forms of inflammatory disease (Khan et al., 2021). The various signaling mechanisms involved in the pathogenesis of RA, including Toll-like receptors (TLRs) of the innate immune system, apoptosis-encouraging effector molecules, intracellular kinases, signaling pathways, and proinflammatory cytokine facilitators such as interleukins (IL-6, IL-1β), tumor necrosis factor-alpha (TNF-α), and C-reactive proteins, are all important. Interactions between local cellular components result in the stimulation of cell growth and the degeneration of joints. RASF is not only triggered by primary response genes, proto-oncogenes, as well as intracellular motioning mechanisms that result in the creation and discharge of tissue-destructive chemicals, but proinflammatory cytokines often have a straight relationship with synovial inflammation. The cytokines IL-1β, IL-6, and TNF-α have been elaborated in the expansion of RA through activating the RASF. These cytokines are generated by stimulated macrophages which are richly found in the synovial membrane of the afflicted intersections and are thought to be responsible for the inflammation (Behl et al., 2022). Using nonsteroidal anti-inflammatory medicines (NSAIDs) is advised as first-line therapy to treat arthritis. NSAIDs exert their action by blocking the COX enzyme, which prevents the production of prostaglandins from occurring. Ibuprofen, diclofenac, piroxicam, ketoprofen, naproxen, and flurbiprofen are the most often prescribed NSAIDs to treat chronic pain (Vina et al., 2020). Ibuprofen is provided orally in doses of 200 and 400 mg, depending on the severity of the pain. Traditional synthetic disease-modifying-antirheumatic drugs (DMARDs), as well as biological DMARDs and other newly found treatments, such as targeted synthetic DMARDs, are used in the treatment of RA. During the acute phases, steroids are used to suppress active disease. With fast-developing treatment therapeutic options, a cure for RA has become an aim, with a decrease in pain, joint discomfort, and functional benefits. Despite this, a significant number of patients continue to suffer from serious health impairment, and they often discover that their "own treatment objectives, expectations, and ambitions, as well as those of their clinicians, are seldom satisfied," according to the American Journal of Medicine. Additional adverse effects of drugs, such as excess weight and insulin resistance, might increase the risk of cardiovascular disease and general morbidity, worsening the problem even more (Vina et al., 2020).

Stressed-out microorganisms have piqued the interest of researchers looking for novel sources of therapeutically useful chemicals (Ul Hassan et al., 2021). While conventional wisdom holds that metals hinder the creation of secondary metabolites, a new study illustrates that metals can excite or increase the activity of powerful medical and nutraceutical important metabolites. Abiotic variables, such as heavy metals, which have been shown to alter the attitude of secondary metabolism in molecular biology and chemical biology, may now transform the synthesis of natural chemicals. DNA sequencing and other innovative procedures have developed secondary metabolites. In pharmaceutical and nutraceutical development, natural ingredients have played a key role. Because of their superior safety and efficacy, natural medications have become more popular over synthetic pharmaceuticals in recent years. Several key challenges inhibit the biotransformation of chemicals into medications, even if microorganisms' capacity to generate fresh scaffolds looks limitless. Gene clusters and non-activated biosynthetic pathways might be a stumbling hurdle in the identification of secondary metabolites of these crucial medical medicines (Ding et al., 2016; Akhter et al., 2018). The term "sleeping gene clusters" refers to the current status of these gene clusters. This can be explicated through the stimulation of sleeping genes or the creation of compounds possessing stereochemical inclination which facilitates the metal complexation as well as transit in living structures. Metals-triggering plants and microbes are now being used to find

new natural products since they are a quick, speedy, and easy way to identify novel chemicals. Some studies are working on expanding the secondary metabolites outline, whereas others are unlocking the microbes intended for their innovative carbon frameworks. The current experiment employed a metal-stress technique to investigate the capacity of *Streptomyces* SH-1327 to yield the production of secondary metabolites with the help of metallic ions. The anti-arthritis activities of the metal-evoked generated molecule was assessed, along with ADMET, docking, and simulations, respectively.

2 Materials and methods

2.1 Soil sample collection

Marine soil sediment samples were obtained from Zhoushan island, Zhejiang, 100 m from sea shores. The sediments were collected in unpolluted areas near the sea shores on Zhoushan Island. The samples were then taken to the lab and kept at 4°C in the refrigerator.

2.2 Isolation and storage of SH1327

To obtain a 10^{-1} dilution, the fresh soil sample of about 1–2 g was immediately subjected to the pre-sterilized glass vials and diluted with simulated seawater. The mixture was sonicated for 1 min to liberate microorganisms tied to the soil particles, then shaken for 15 min at room temperature. The serial dilutions of up to 10^{-2}, 10^{-3}, and 10^{-4} were then prepared. To prevent fungal contamination, nystatin (0.05 g/L) was added to the pre-prepared isolation media (Gause's synthetic agar). Following the preparation of the dilutions, 100 µl aliquots of each dilution were inoculated on each media and disseminated with the pre-sterilized spreader. For 15–20 days, the plates were incubated at 28°C. Purified colonies of actinobacteria were collected and kept on agar media and stored at 4°C. The actinobacteria were identified by their morphology, most commonly their colors. Based on the ITS 16S segment, the SH-1312 strain was recognized as a *Streptomyces sp*.

2.3 Metal stress and normal cultivation

Metal stress as well as regular colonies of strain SH-1327 were tested in sequence using 500 ml Erlenmeyer flasks containing 200 ml Gause's media at 28°C in a rotatory shaker at 180 rpm for a total of 10 days in the shaker. In two flasks, a conventional batch growth of variant SH-1327 was performed as a control to ensure that the results were accurate. The stressed culture medium for SH-1327 was supplemented with different concentrations of $CuCl_2$, and $NiCl_2$ as 0.5 mM, 1 mM, 2 mM, and 4 mM/L, respectively. To remove the mycelium from the cultural medium, the EtOAc was also added twice having the same concentration.

2.4 HPLC technique and refinement of stress metabolite

The HPLC was performed by reversed-phase HPLC-UV (1,290 infinity II HDR-DAD Agilent technologies) using a C_{18} column in order to analyze the separated chemicals. HPLC was set up with 210 wavelengths with H_2O/MeOH gradients of 20%–100% for 0–30 min and 100% MeOH for 30–50 min, with a constant flow speed of 0.8 ml/min and a steady state frequency of 0.8 ml/min. Next, the stress-induced metabolite was isolated using HPLC at a constant flow rate of 9 ml/min with an 80% MeOH mobile phase.

2.5 Extraction and isolation

The 30 L of fermented broth were extracted using EtOAc (2 × 200 ml). Analytical HPLC was used to analyze the crude residue afterward the solvent was completely evaporated and the methanol was added to it and centrifuged for 10 min at 120,000 rpm. Initial screening was done by creating an H_2O/MeOH gradient of 20%–100% intended for 0–30 min after the HPLC. At 18.13 min, a new peak was discovered. On the Preparative HPLC, the chemical was purified by a steady dissolution medium of 80% MeOH, "MeOH: H_2O (80:20)." By studying literature, the structure of the strained stressed compound was oriented as a cyclo-(D)-Pro-(D)-Phe (CDPDP) (t_R = 14 min, 9.2 mg) (Brown and Teller, 1976).

2.6 Anti-oxidant assay

To evaluate the antioxidant potential of a stress compound, a multifaceted antioxidant evaluation of a stress compound was performed *via* a DPPH scavenging assay, $OH^{\bullet}$ radical scavenging assay, $NO^{\bullet}$ scavenging assay, and Iron chelating assay by following pre-described protocols (Majid et al., 2018).

2.7 *In vitro* anti-inflammatory activity

The anti-inflammatory efficacy was determined by employing the suppression of the albumin denaturation process, which was modified somewhat from the Leelaprakash and Mohan Dass (2011) methodology with minimal modifications. The test consists of reaction mixture of chemicals and a 1% aqueous phase of bovine albumin

fraction, with the pH of the reaction mixture adjusted to 7.4 before running the test. After incubation of the sample at 37°C for 20 min, heating to 51°C for 20 min was done. After cooling the samples, turbidity was measured at 660 nm. The experiment was repeated thrice and the % inhibition of protein denaturation was calculated as follows:

$$\text{Percentage inhibition} = \frac{(\text{Abs Control} - \text{Abs Sample})}{\text{Abs Controlo}} x\,100$$

2.8 Chondrocytes cell line and cell culture

CHON-001 cells were purchased from ATCC (Cat No. CRL-2846) and cultured according to instructions. Cells were grown in a complete DMEM medium enhanced with 1% P/S and 10% FBS and incubated in a 5% CO_2 incubator at 37°C. Cells were grown up to 80% confluence and each experiment was performed after three passages.

2.8.1 Trypan blue cell exclusion method

Cell viability was ensured with the dye exclusion method. Firstly, 1×10^5 cells from each group were seeded in 24 well cell culture plates and incubated in a 37°C incubator for 24 h and 48 h. Cells were harvested, washed with PBS, and dyed with 0.4% trypan blue for 10 min. Haemocytmeter was used to count the viable (non-stained) and dead (blue-stained) cells. The experiment was performed twice to get the accurate number of viable cells.

2.8.2 Quantitative- real-time PCR

1×10^5 CHON-001 cells/group were grown in 24 well plates until they become 80% confluent. Cells were trypsinized as well as washed with PBS after they were harvested. Further, they were collected and RNA was extracted by using the RNA extraction Trizol method (Invitrogen Trizol reagent cat # 15-596-018). Utilizing a reverse transcription kit, RNA was transformed into cDNA. Syber green PCR Kit (Maxima SYBR green flourescein qPCR master mix (2x) cat #k0243) was used for Q-PCR and results were analyzed using Graph Pad Prism version 7.0. The cycling temperature for PCR is mentioned in table S2. List of primers for quantitative real-time PCR.

2.8.2.1 Target genes cat. No (Qiagen)

The original primer sequence of qPCR is mention in Supplementary Table S1.

BCL2 QT00000721.
MMP-1 QT00014581.
MMP-3 QT00060025.
Col2a1 QT00049518.

2.9 *In vivo* studies

2.9.1 Animals

Adult male albino mice (4–5 weeks old; 24 ± 4 g) were bought from the National Institute of Health (NIH), Islamabad, Pakistan. The animals were kept with good care and with proper food supplements according to the ethical guidelines. All behavioral and biochemical tests were conducted following the guidelines of "The animal care guidelines of QAU" in a sterilized clean environment. The study was carried out after approval from the Bioethical Committee of QAU Islamabad with Ref. No: BCE- DOP-QAU. To avoid any experimental bias, the animals were chosen at random and the experiment was conducted using double blindness. Minimal mice were used for each group in this investigation, and the researchers took great care in minimizing the pain and distress of laboratory animals (Khan et al., 2021).

2.9.1.1 Experimental design

The experimental animals were separated into five groups, each with five mice, and maintained in aluminum cages under regulated conditions (12 h dark/light cycle, 25°C temperature). Prior to usage in experiments, all of the animals were fed a regular diet by following the standard protocols. The grouping was accordingly done as follows in all animal models.

Group-I: Normal (Control).
Group-II: Negative (Control).
Group-III: Positive (Control).
Group-IV: CDPDP (20 mg/kg).
Group-V: CDPDP (40 mg/kg).

2.9.2 Acute inflammatory models

2.9.2.1 Carrageenan-encouraged inflammation impediment in mice

The anti-inflammatory ability of CDPDP was assessed using a rat paw edema model caused by carrageenan (Ahsan et al., 2022). The medications were given 1 hour before being given 1 ml/kg of carrageenan suspension (0.9 percent w/v in saline) in each rat's left hind paw. Using a plethysmometer, the volume of the paws was measured over time (1, 3, 6, 12, 24 h). Results were calculated as:

$$\text{Edema volume} = PV_t - PV_c$$

Where PVt is paw volume (ml) at a certain time following carrageenan administration, before carrageenan administration, while PVc is paw volume (ml).

$$\text{Percent inhibition} = EV_c - EV_t / EV_c \times 100$$

Where EVc is the control group's edema volume. The edema volume of the treated group is denoted by EVt.

2.9.2.2 Croton oil-induced ear edema constraint

Minor modifications were done to induce edema in the methodology of Reanmongkol et al. (2009). Mice's right ears were infected with the irritating agent (5% croton oil) when 100 µl of an anesthetic solution was applied to the skin. Acetone was used as a delivery method for the medication. Croton oil was applied to the right ear 1 h before the application of CDPDP (5.0 mg/ear each). Anti-inflammatory medication ibuprofen (1 mg/ear) was used as a control. After the mice were sacrificed 4 h later, a plug (7 mm diameter) was taken from both the treated and untreated ears. The difference in weight in the two plugs was used to compute the percent inhibition of edema.

2.9.2.3 Croton oil-induced anus edema inhibition

Croton oil-induced edema of the anus was accomplished by adjusting Reanmongkol et al. (2009) approach. To induce anal necrosis, an anus-inducing agent was applied to the anus of mice for 10 s (0.2 ml of croton oil 6% in diethyl ether). Besides, CDPDD (40 and 20 mg/kg) and Ibuprofen (10 mg/kg) were administered orally OD for 3 days after directing croton oil. On the fourth day, the diameter within each heavily sedated mice anus (in millimeters) was measured with a vernier caliper, and the results were recorded.

2.9.3 Chronic anti-inflammatory model

2.9.3.1 CFA-induced inflammatory pain model

To investigate the properties of extracted CDPDP in the chronic inflammatory model. According to the study design, the experimental mice were randomly selected into five groups and the CFA-induced chronic pain model was employed in mice, as described above. A complete Freund's adjuvant (CFA) provoked arthritic model (Negative control) was created by injecting 25 µl of CFA into the mouse paw intraplantarly (i.pl). When arthritis had fully developed, the CDPDP's anti-inflammatory activity was evaluated using a therapeutic scoring rate and an observational study. Ibuprofen was given to the positive control group, whereas CDPDP (20 mg/kg and 40 mg/kg) was given to the treatment groups. The effects of CDPDP on the chronic model were examined for 22 days, with the clinical score being tracked from 14 to 22 days by measuring the swelling of the paws before edema induction on day one and subsequently (Khan et al., 2022).

2.9.3.2 Paw edema parameter in mice

The chronic (CFA-induced inflammation) model was used for the assessment of the pharmacological effects of a CDPDP (20 mg/kg) and CDPDP (40 mg/kg) compared to ibuprofen. The Edema parameter was measured using a dial thickness gauge after inflammation was induced in the mouse paw (Mitutoyo Corporation, Japan).

2.9.3.3 Thermal hyperalgesia

On a heat plate, a CDPDP (20 mg/kg) with different doses was evaluated for thermal hyperalgesia. Mice were placed on a heat plate with a temperature of 37 ± 0.5°C to explore thermal hyperalgesia. Responses were obtained at 0,7,14, 16, 18, and 20 days after treatment in the CFA -induced inflammatory model. However, the tickling, grimacing, and sucking of the paw over the heat plate were all positive responses for thermal hyperalgesia, and the total time the paw lasted on the heating plate was also measured. The investigational group animals were divided into five groups, as previously mentioned. A CDPDP and a commercially available Ibuprofen were used to compare the effects against chronic thermal hyperalgesia (Eo et al., 2014).

2.9.3.4 Mechanical allodynia

Mechanical allodynia was tested in the experimental animals using the Von Frey Filament technique to assess pain sensibility. All the experimental animals were placed in a plastic box with a small mesh floor to check the dorsal surface of the right hind paw for mechanical allodynia. The Von Frey Filament method was used to explore mechanical allodynia in a double-blinded study. The mice were separated into five groups, and the protocol was followed just as before. Mice withdrawal reflex was observed (three times out of five) through the filament to investigate the pain of the right hind paw as a positive reaction. The suppressive impact of the CDPDP (20 mg/kg) was further tested against CFA-induced paw edema in mice (Yu et al., 2012).

2.9.3.5 Collection of blood and organ sampling

Anesthetic agents (ketamine and xylazine at 16 mg and 60 mg, respectively, intraperitoneally) were used to anesthetize all of the experimental animals before the samples were taken after the activity. Immediately after the heart puncture, a blood sample was obtained and centrifuged for 5 min at 4050 RCF at 4°C. To perform several biochemical tests, the clear serum obtained from the blood sample was employed. A formalin solution of 10% was added to the Eppendorf tubes that contained the tissues and organs for histological and radiological examination (Ullah et al., 2018).

2.9.3.6 Hematology

The blood studies including the count of red blood cells (RBCs), white blood cells (WBCs), as well as platelets, were done using a Neubauer hemocytometer (Feinoptik, Germany). The amount of hemoglobin (Hb) in the blood was determined with the help of Sahli's hemoglobin meter. The modified Westergren method was used to determine the rate of erythrocyte sedimentation (ESR) (Nair et al., 2012).

2.10 Biochemical assays

2.10.1.Nitric oxide determination in plasma

Nitric oxide (NO), which is recognized as a basic characteristic of inflammation, is used to determine the degree of inflammation. It is a key sign of the ongoing inflammatory process and can be linked to the severity of the inflammation (Kim et al., 2002). NO levels in mice plasma were examined in this investigation to see if CDPDP had an impact on NO generation. All the experimental procedures were identical to those described in the preceding sections. To achieve a homogenous mixture, plasma (25 µl), an equal volume of normal saline, and Griess reagent were combined. The mixture was refrigerated for 1 h before the NO concentration was determined using a 450 nm microplate reader (Batool et al., 2017).

2.10.2 Effect of CDPDP on the antioxidant system

The liver is the most sensitive region to oxidative stress, and it expresses a variety of antioxidant systems to combat it, including glutathione (GSH), glutathione S transferase (GST), and catalase (Hitchon and El-Gabalawy, 2004). The effect of CDPDP on antioxidant enzymes such as catalase, GST, and GSH was studied. The effect of commercially available ibuprofen and a specially extracted compound on these pathways was investigated.

2.10.2.1 Reduced GSH assay

GSH levels were determined using paw tissue homogenates. Paw tissues were put in 2–3 ml of phosphate buffer and homogenized for 10–15 min at 13,500 rpm. The homogenate was centrifuged upto10 min at 9,080 rcf, the sediment was discarded and the supernatant was collected and preserved for further analysis. Following that, the Ellman reagent was used to calculate GSH (Khan et al., 2021). The results were represented as a percentage of the total GSH released.

2.10.2.2 GST assay

The purpose of this test was to see if the GST enzyme could conjugate GSH with 1-chloro-2-4-dinitrobenzene. Their activity was measured using a microplate reader at 340 nm. An assay combination without supernatant was used as a blank to check for nonspecific binding (Batool et al., 2017).

2.10.2.3 Catalase assay

The ability of catalase to degrade hydrogen peroxide was measured using a progressive decrease in absorbance at 240 nm. The percentage of catalase produced per gram of tissue was calculated (Batool et al., 2017).

2.10.2.4 Lipid peroxidation assay

Malonaldehyde (MDA) is an important element to study in lipid peroxidation (LPO) assays, however, the NSAIDs and CDPDP are thought to impact fat accumulation and enhance the effect on reactive oxygen species (ROS). The LPO was also tested using a CDPDP-based extract and commercially available ibuprofen. The percentage of MDA generated per gram of tissue was calculated (Kim et al., 2002).

2.10.2.5 LFT's and RFT's

With standard AMP diagnostic kits, the serum and urine of experimental mice were tested for several markers including Urea, Creatinine, AST, ALT, ALP, bilirubin, and albumin using a variety of different tests (Stattogger Strasse 31b 8,045 Graz, Austria). The Bradford method was used to screen the protein concentration (Nair et al., 2012).

2.10.3 Measurement of cytokines

Assays were performed using an ELISA kit (BD Bioscience Inc. San Diego, CA ELISA kit) to measure cytokine concentrations. Tissue samples were taken from all experimental groups under the instructions (Cui et al., 2020). The right hind paw was amputated on the last day of activity, and tissue proteins were isolated with a Phosphate buffer solution consisting of 0.005% tween 80, 0.4 M sodium chloride, and a protease inhibitor at a concentration of 100 mg/ml of solution. The samples were homogenized uniformly before being centrifuged for 5 min at 5,000 rpm to collect the supernatant, which was then kept at −80°C for further analysis.

2.11 ADMET analysis

ADMET (Absorption, distribution, metabolism, excretion, and Toxicity) are the essential measurement tools for any compound before being elected as a drug candidate. The online web tool swiss ADME (http://www.swissadme.ch/index.php) was used to obtain ADMET properties of the stress compound (Daina et al., 2017), and the Online web tool pkCSM (http://biosig.unimelb.edu.au/pkcsm/prediction) was used to predict the pharmacokinetic scores (Zhuo et al., 2020).

2.11.1 Prediction of cardiac toxicity

Blockage of the hERG K^+ channels has been linked to fatal cardiac arrhythmias. To predict cardiac toxicity, a free accessible online service pred-hERG 4.2 (http://predherg.labmol.com.br) was used for its early detection of potential hERG blockers and non-blockers (Braga et al., 2015).

2.11.2 Skin sensitization

Skin sensitization is a crucial phase in allergic contact dermatitis, a complex immune-mediated inflammatory skin reaction. Till now there are no *In-vitro* techniques to evaluate

the capacity of any compound for its skin sensitisation So, we have conducted the skin sensitization evaluation of a CDPDP through an *in-silico* technique from online web portal http://predskin.labmol.com.br/(Braga et al., 2017).

2.12 Molecular docking

2.12.1 Protein preparations

The 3 D crystal structure of Interleukin-6 protein (PDB ID: 1il6) and Tumor Necrosis Factor-alpha (PDB ID: 1tnf) was retrieved from the RCSB Protein data bank (https://www.rcsb.org/). The resulting structure was refined by utilizing the Protonate3D program (Dallakyan and Olson, 2015) to add partial charges and energy minimization by using the Molecular Operating Environment to pick the MMFF94x force-field (MOE, Version 2018.01). The MOE software's site finder function was used to locate the active cavity in the target protein.

2.12.2 Ligand preparation

CDPDP was selected to screen their potential inhibitory effect against Interleukin-6 protein (PDB ID: 1il6) and Tumor Necrosis Factor-alpha (PDB ID: 1tnf) protein using *in silico* tools. The ligands were optimized *via* Protonate3D and energy was minimized before the addition of the MOE ligand database. The 2 D chemical structure of the selected ligands was drawn using ChemDraw. The standard ibuprofen was used as a reference to compare the inhibitory effect of the selected plant-based compounds.

2.12.3 Docking analysis

CDPDP was docked with interacting residues of PDB ID: 1il6 and Tumor Necrosis Factor-alpha (PDB ID: 1tnf) protein by using the docking algorithm of MOE software. The MOE program used the "Triangular Matcher" technique to build a minimum energy structure, which was then used as the default ligand insertion strategy. Rescoring of simulated poses was done using the London dG scoring tool. Based on their root mean square deviation (RMSD) and S-score binding affinity values, CDPDP with the best and top conformation was identified after docking. The MOE LigX tool was used to examine the 2D plots of ligand-receptor interactions, and the best-docked complexes were displayed. MOE was used to generate 3D images of protein inhibitor complexes.

2.13 Molecular docking simulations

The MDS analysis was used to determine the ligand-protein stability interaction. The structure of the macromolecules transitions to the functional importance of the complex was also studied through MD simulations. To estimate the binding of the ligand in the cellular environment, simulations gather

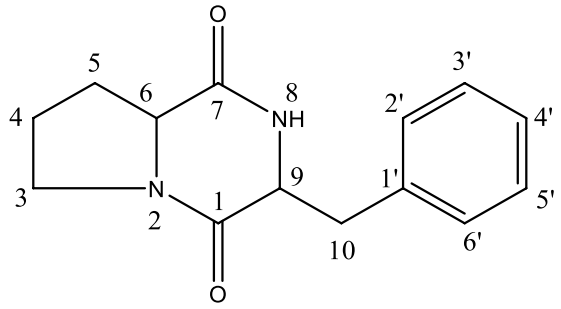

FIGURE 1
Chemical structure of CDPDP.

valuable atom movement concerning time using Newton's standard motion equation. The MD simulations of the CDPDP-IL-6 and Ibuprofen-IL-6 were performed for 100 ns using the Schrodinger suite's Desmond v:3.6 New York, United States module (Shams ul Hassan et al., 2022). The preliminary structure of MD simulations was followed by an established procedure where protein atoms were 10 Å away from the box, and the interaction of the complex derived from MD was the initial structure of respective MD simulations. Wizard of Maestro was used to minimize and optimize the ligand-receptor complex. Using the System Builder tool, a solvent standard TIP3P with an orthorhombic box was chosen for the systems. For simulation analysis, the OPLS 2005 was employed. The model's physiological circumstances were modified by the addition of 0.15 M NaCl (Ferreira et al., 2015). Finally, for all MDSs, simulations were run at a constant temperature of 300 K and pressure of 1 atm with an NPT ensemble. Furthermore, every 100 ps interval, the MDS trajectories were recorded. To measure the stabilities of protein-ligand interactions in simulations, the values of root mean square deviation (RMSD), RMSF, the radius of gyration, and SASA were determined for both protein and ligand. MDSs were run three times for each complex, with the same parameters each time.

2.13.1 MMGBSA calculations

The prime tool in maestro was used to reduce the ligand-receptor complexes. After minimization, the binding free energies (ΔG) of complexes were calculated using molecular mechanics generalized Born surface area (MMGBSA) before (0 ns) and after (100 ns) simulation. An OPLS_2005 force field was used throughout the computation of binding free energy.

2.14 Statistical analysis

The values for each test were expressed as the mean +standard deviation. Using Statistix 8.1 and Tukey's multiple

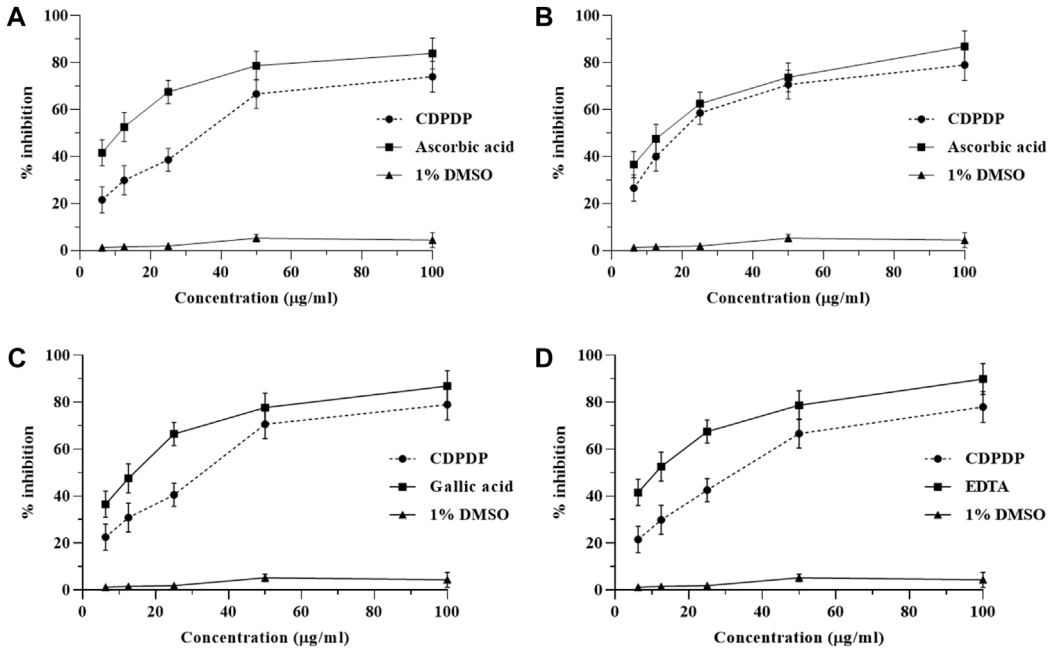

FIGURE 2
Representation of CDPDP antioxidant activity *in vitro*. Note: **(A)** DPPH radical scavenging properties, **(B)** $NO^{\bullet}$ scavenging activity, **(C)** $OH^{\bullet}$ scavenging activity, and **(D)** iron-chelating % inhibition. All values are represented as Mean ± SD (n = 3).

TABLE 1 *In vitro* anti-inflammatory assessment of CDPDP.

Samples	400 µg/ml	200 µg/ml	100 µg/ml
Control	–	–	–
Ibuprofen	71.35 ± 3.89^{a}	63.66 ± 3.12^{c}	61.53 ± 4.84^{cd}
CDPDP	68.54 ± 2.97^{b}	57.72 ± 3.54^{d}	54.19 ± 2.32^{e}

The data values displayed are the mean standard deviation ± (n = 3). The means in the column with distinct superscript (a-e) letters are substantially different ((p < 0.05).

comparison tests based on parametric examination of variance, the magnitudes of altered treatments to mice *in vivo* were evaluated. $p \leq 0.05$ was used to determine statistical significance for activity.

3 Results

3.1 HPLC profile of SH1327 with metal treated and untreated extracts

It was observed that an actinobacteria-stressed metabolite could be extracted using an HPLC configuration that took into account elution modes, mobile phase, monitoring wavelength, and column temperature. Earlier studies show that metals such as Nickel (Ni^{2+}), zinc (Zn^{2+}), Copper (Cu^{2+}), and mixed metals (Co^{2+}+Zn^{2+}) may induce the production of secondary metabolites in microorganisms. Two distinct types of metals nickel and copper were selected as initial elicitors. At 28°C, the culture experiment with strain SH1327 was conducted in Gause's medium containing ions of nickel and copper with four different starting concentrations. The experiment was carried out at 180 rpm in a rotatory shaker over 18 days. The metal $CuCl_2$ did not stimulate any compound in any concretion, however, two novel peaks were triggered in $NiCl_2$. Using a blank medium, one medium without strain, one medium without metal, and four sets of medium with different ionic concentrations. We confirmed the changes in the metabolic parameters that occurred when metals were exposed (0.5 mM–4 mM). An EtOAc extraction was performed on the culture broth (2 × 200 ml) by using a gauze filter to separate the mycelium from the culture broth. The chromatogram from HPLC revealed that *Streptomyces* actinobacteria have a unique stress-induced metabolite cyclo-(D)-Pro-(D)-Phe (CDPDP) was identified in metal-treated cultures, while it was not discovered in untreated cultures. In non-metal cultures, it was practically invisible. It was discovered that the blank variant SH-1327 did not create any metabolites when grown under standard conditions.

TABLE 2 Effect of CDPDP on carrageenan-induced paw edema in mice.

Groups	Percent edema inhibition				
	1st h	3rd h	6th h	12th h	24th h
Control (Saline)	–	–	–	–	–
Carrageenan control	–	–	–	–	–
Ibuprofen	39.92 ± 2.99[a]	58.87 ± 4.49[a]	81.27 ± 6.89[a]	77.86 ± 6.24[a]	73.36 ± 5.99[a]
CDPDP (20 mg/kg)	18.87 ± 1.69[c]	34.98 ± 2.92[c]	67.31 ± 5.11%[c]	65.78 ± 5.86[c]	58.89 ± 3.68[c]
CDPDP (40 mg/kg)	28.98 ± 2.96[b]	42.82 ± 3.68[b]	78.37 ± 4.92[b]	74.72 ± 6.02[b]	70.29 ± 4.57[b]

The data values displayed are the mean standard deviation ± (n = 6). The means in the column with distinct superscript (a-c) letters are substantially different ($p < 0.05$).

TABLE 3 Effect of *CDPDP* on croton oil-induced ear edema in mice.

Groups	Weight of left ear (mg)	Weight of right ear (mg)	Edema (Δ mg)	% Reduction of inflammation
a)				
Control (Saline)	80.04 ± 1.4	80.0 ± 2.02	–	–
Croton oil	91.4 ± 1.10	97.50 ± 2.1	6.10 ± 0.74	–
Ibuprofen	86.7 ± 1.67	87.86 ± 2.01	1.16 ± 0.10	80.47 ± 4.98[a]
CDPDP (20 mg/kg)	90.44 ± 1.7	92.73 ± 1.5	2.29 ± 0.20	61.99 ± 4.07[c]
CDPDP (40 mg/kg)	84.34 ± 2.1	86.07 ± 1.8	1.73 ± 0.15	71.98 ± 7.78[b]
b) Effect of CDPDP on croton oil-induced anal edema in mice				
Groups		Anus size (mm)	Edema (mm)	% reduction of inflammation
Control (Saline)		33.82 ± 0.89	–	–
Croton oil		45.92 ± 1.19	12.46 ± 0.7	–
Ibuprofen		35.95 ± 1.02	2.09 ± 0.11	81.99 ± 6.19[a]
CDPDP (20 mg/kg)		39.02 ± 1.59	4.48 ± 0.20	62.74 ± 4.06[c]
CDPDP (40 mg/kg)		38.12 ± 1.38	3.49 ± 0.27	69.78 ± 4.88[b]

The data values displayed are the mean standard deviation ± (n = 6). The means in the column with distinct superscript (a-c) letters are substantially different ($p < 0.05$).

3.2 Identification of metal-elicited metabolite

After the HPLC chromatogram at 18.13 min, a new peak was discovered (Supplementary Figure S1). On the Preparative HPLC, the chemical was purified by a steady dissolution medium of 80% MeOH, "MeOH: H_2O (80:20)." By studying literature, the structure of the strained stressed compound was oriented as a cyclo-(D)-Pro-(D)-Phe (CDPDP) (t_R = 14 min, 9.2 mg) (González-Menéndez et al., 2016) (Figure 1). As of this writing, this is the first case in which metal-elicitation-induced CDPDP was seen.

3.3 Antioxidant assay

In order to evaluate the potential of CDPDP as an antioxidant agent, multimode antioxidant tests were performed. In the DPPH test, CDPDP displayed promising outcomes, inhibiting the free radicals with 73.99% ± 5.12% at 100 μg/ml ratio, compared to the conventional ascorbic acid (83.81% ± 4.9%). The IC_{50} for CDPDP in DPPH was documented as 30.06 ± 5.11 μg/ml, even though IC_{50} for ascorbic acid was 10.08 ± 3.77 μg/ml. CDPDP inhibited NO free radicals by 76.79% ± 3.98%, compared to 86.89% ± 3.69% for ascorbic acid, with an IC_{50} of 18.98 ± 2.91 for CDPDP and 13.21 ± 3.41 μg/ml for ascorbic acid. Similarly, CDPDP demonstrated significant scavenging activity against $OH^{\bullet}$ radicals, suppressing 78.69% ± 4.93% radicals at a concentration of 100 μg/ml, compared to gallic acid (86.15% ±

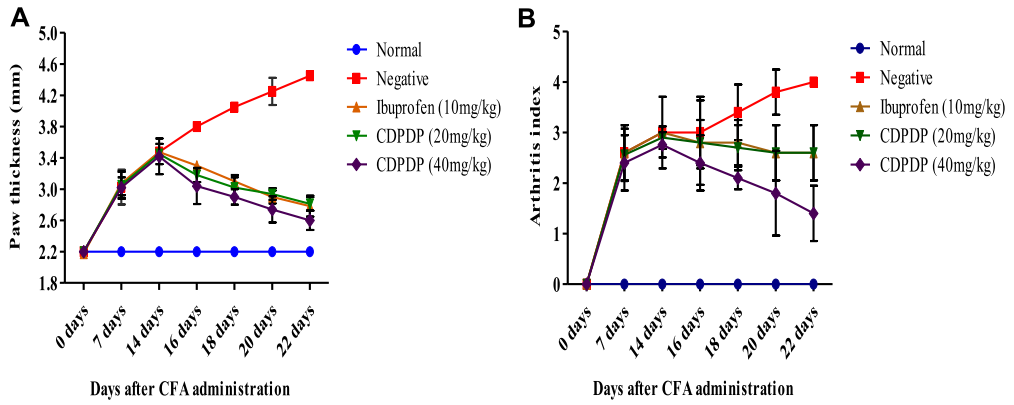

FIGURE 3
(A) Effect of chronic pre-treatment with CPPDP (20 and 40 mg/kg) on paw edema. After CFA injection, paw thickness was measured for a period of 0 up to 22 days. **(B)** Arthritic index where arthritic control (Negative) group has higher arthritic score compared to normal and test groups. Between days 14 and 22, the arthritic index of the animals treated with ibuprofen as well as CDPDP (20–40 mg/kg) exhibited a statistically significant decrease in the treated animals. Data sets are displayed as mean ± SD (n = 5) with significance difference at $p < 0.05$.

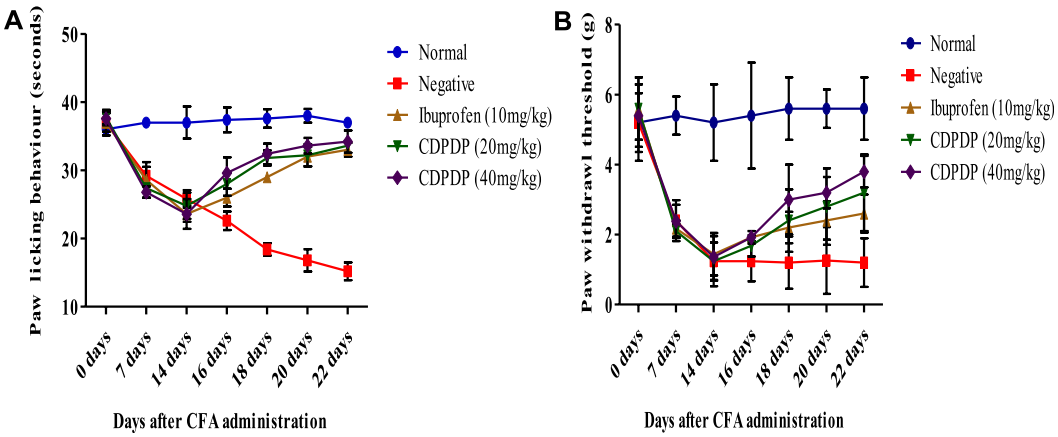

FIGURE 4
(A) Effect of chronic CDPDP pre-treatment on thermal hyperalgesia. The paw licking response was measured post-CFA injection from 0 to 22 days. **(B)** Effect of chronic CDPDP pre-treatment on cold allodynia. The paw withdrawal effect was measured on days 1 To 22 days after CFA administration. The data are expressed as the mean ± SD at $p < 0.05$ and $p < 0.01$.

3.67%) as a control. CDPDP and gallic acid have been verified to have IC_{50} values of 27.15 ± 3.12 and 12.42 ± 2.72 μg/ml, respectively. The iron chelation ability of CDPDP and standard were examined to assess the chelation strategy of compounds to hunt free radicals. CDPDP seemed to chelate 74.96% ± 5.79% of iron radicals (IC_{50} 28.40 ± 3.14 μg/ml), compared to EDTA with 88.52% ± 4.67% chelation capability and IC_{50} of 10.20 ± 3.16 μg/ml. Figure 2 depicts the entire set of results.

3.4 *In vitro* anti-inflammatory potential of CDPDP

The suppression of heat-induced albumin denaturation test was used to assess CDPDP's anti-inflammatory efficacy *in vitro*. At a concentration of 400 μg/ml, CDPDP inhibited protein denaturation by 68.54% ± 2.97% compared to the standard, ibuprofen (71.48% ± 4.71%). Table 1 presents a summary of the findings.

TABLE 4 The hematological examination of normal control besides arthritic rats.

Groups	RBCs ($\times10^6$)/μl	WBCs ($\times10^3$)/μl	Platelets ($\times10^3$)/μl	Hb (g/dl)	ESR (mm/h)
Control	6.72 ± 0.067^a	3.49 ± 0.039^a	589.79 ± 4.56^a	10.29 ± 0.8^a	4.32 ± 0.041^a
Negative Control	4.09 ± 0.026^e	6.99 ± 0.030^d	351.06 ± 2.49^d	6.29 ± 0.11^d	9.38 ± 0.058^c
Ibuprofen	5.46 ± 0.028^d	6.28 ± 0.019^c	489.4 ± 02.30^c	7.77 ± 0.68^c	4.99 ± 0.016^b
CDPDP (20 mg/kg)	5.76 ± 0.018^c	3.76 ± 0.008^b	550 ± 02.801^b	8.10 ± 0.46^b	4.89 ± 0.048^b
CDPDP (40 mg/kg)	5.99 ± 0.011^b	3.68 ± 0.012^{ab}	568 ± 02.703^{ab}	8.18 ± 0.66^b	4.81 ± 0.068^b

The data values displayed are the mean standard deviation ± (n = 6). The means in the column with distinct superscript (a-e) letters are substantially different ($p < 0.05$).

TABLE 5 Effect of CDPDP on liver function tests (LFT's).

Groups	ALT (U/L)	AST (U/L)	ALP (U/L)	Bilirubin (mg/ml)	Albumin (mg/dl)
a)					
Control	38.93 ± 0.48^a	25.9 ± 0.34^a	114.8 ± 1.9^a	6.79 ± 0.21^a	6.37 ± 0.24^a
Negative Control	97.29 ± 3.41^d	106.1 ± 2.1^d	346.09 ± 7.3^d	11.4 ± 0.19^d	2.69 ± 0.12^c
Ibuprofen	43.21 ± 2.43^b	34.0 ± 2.1^b	121.2 ± 3.7^b	7.12 ± 0.66^b	5.97 ± 0.21^{ab}
CDPDP (20 mg/kg)	46.74 ± 3.83^c	37.1 ± 2.4^c	137.3 ± 4.2^c	7.59 ± 0.06^c	5.68 ± 0.13^b
CDPDP (40 mg/kg)	43.6 ± 0.46^b	30.9 ± 0.7^b	120.8 ± 2.7^b	7.11 ± 0.29^b	5.99 ± 0.39^{ab}
b) Effect of CDPDP on renal function tests (RFT's)					
Groups	Urea (mg/dl)	BUN (mg/dl)	Creatinine (mg/dl)	GFR (ml/min)	Protein (mg/dl)
Control	51.4 ± 1.87^a	20.5 ± 0.33^a	1.48 ± 0.09^a	0.43 ± 0.03^a	5.12 ± 0.13^a
Negative Control	76.1 ± 2.41^d	50.8 ± 1.9^d	3.01 ± 0.16^d	0.07 ± 0.02^e	1.29 ± 0.11^b
Ibuprofen	54.9 ± 2.8^b	26.1 ± 2.4^b	1.63 ± 0.11^b	0.36 ± 0.04^{ab}	5.09 ± 0.07^a
CDPDP (20 mg/kg)	57.8 ± 3.5^c	26.9 ± 2.4^c	1.65 ± 0.10^c	0.34 ± 0.03^b	4.96 ± 0.06^{ab}
CDPDP (40 mg/kg)	55.9 ± 0.43^b	24.6 ± 0.5^b	1.63 ± 0.10^b	0.37 ± 0.03^{ab}	5.10 ± 0.32^a

Note: ALT, Alanine Aminotransferase/transaminase, AST, aspartate transaminase; ALP, alkaline phosphatase; BUN, blood urea nitrogen; GFR, Glomerular filteration rate. Data values represent Mean ± SD (n = 5). Means with different superscript (a-d) letters in the column are significantly ($p < 0.05$) different from one another.

3.5 Effect on carrageenan induced inflammation in mice

The anti-inflammatory capacity of the CDPDP was investigated through the Carrageenan-induced paw edema model (inflammatory model). The results declared that CDPDP has more significant anti-inflammatory activity than the control model. CDPDP (40 mg/kg) displayed determined inhibition of inflammation (78.37% ± 4.92%) at sixth h while CDPDP (20 mg/kg) displayed inhibition with a value of (67.31% ± 5.11%) compared to Ibuprofen (81.27% ± 6.89%). Table 2 presents a summary of the findings.

3.6 Croton oil-induced inflammation inhibition

The anti-inflammatory efficacy of the CDPDP was investigated further using a croton oil-induced ear edema and anal edema model (inflammatory model). The results showed that CDPDP (40 mg/kg) has significant anti-inflammatory actions linked to the control model. CDPDP (40 mg/kg) exhibited determined inhibition of the ear inflammation (71.98% ± 7.78%) while the CDPDP (20 mg/kg) shows inhibition with the score of (61.99% ± 4.07%), compared to Ibuprofen (80.47% ± 4.98%) (Table 3). Moreover, the CDPDP (40 mg/kg) showed maximal inhibition of anal inflammation (69.78% ± 4.88%), while the CDPDP (20 mg/kg) shows inhibition with a score of (62.74% ± 4.06%), compared to Ibuprofen (81.99% ± 6.19%) (Table 3).

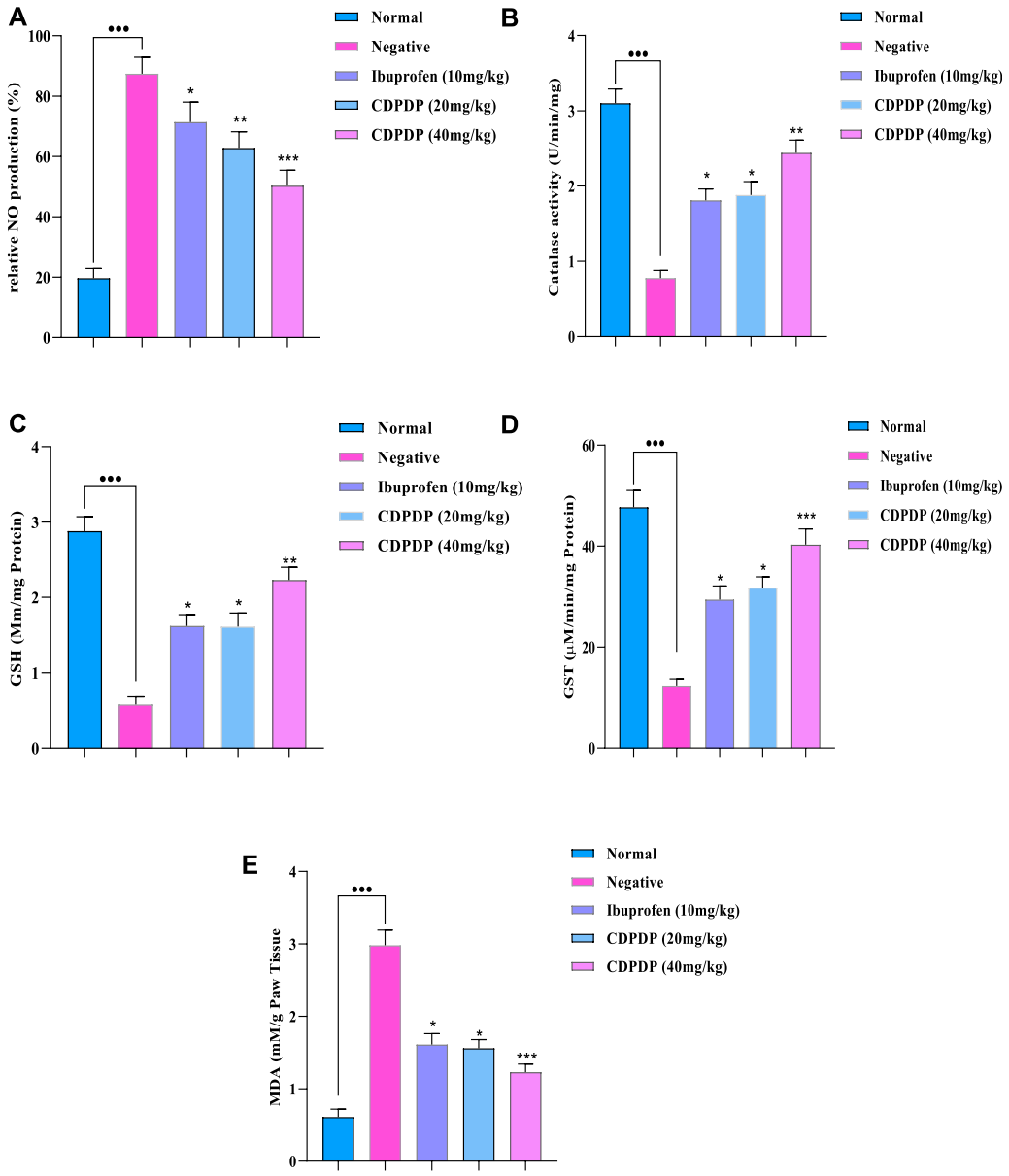

FIGURE 5
The pharmacological effect of CDPDP on the levels of nitrites and antioxidants in mice paw tissues is depicted in this graphic. The stressed compound CDPDP improved the antioxidant enzymes such as **(B)** catalase, **(C)** GSH, and **(D)** GST, while CDPDP treated RA mice model markedly attenuated the oxidative stress marker such as **(A)** NO and **(E)** MDA in comparison to other groups. NO: Nitric oxide, GSH: Glutathione, GST: Glutathione S transferase, MDA: Malonaldehyde. The data sets are expressed as the mean ± SD at $p < 0.05$ and $p < 0.01$.

3.7 Effect of CDPDP on paw edema in CFA-induced chronic arthritis model in mice

CFA sub planter injection in the right hind paw of mice resulted in a considerable chronic inflammation that lasted for 22 days. CDPDP (20 and 40 mg/kg) significantly reduced paw edema between days 14 and 22 (Figure 3A). Ibuprofen, a positive control, inhibited paw thickness significantly throughout the arthritis experiment. Arthritic scoring (Figure 3B) is indicating significant anti-arthritic activity of the compound at low and high doses.

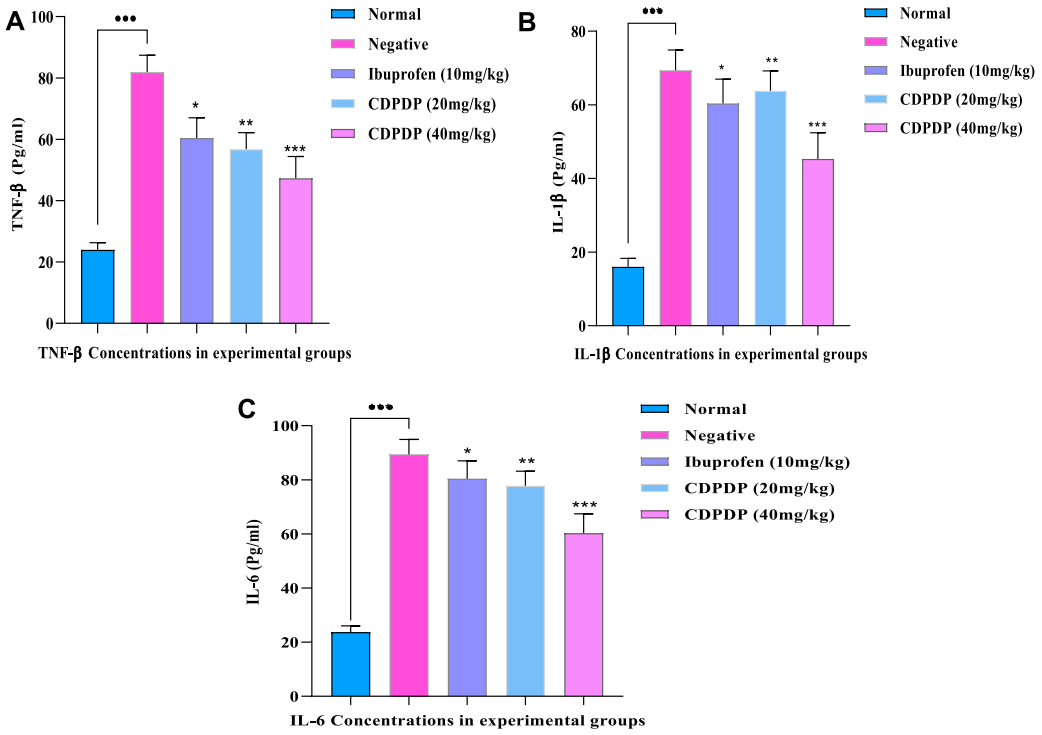

FIGURE 6
(A) TNF-α concentration in experimental groups **(B)** IL-Iβ concentration in experimental groups **(C)** IL-6 concentration in experimental groups. The data is expressed as the mean ± SD at $p < 0.05$ and $p < 0.01$.

3.8 Effect of CDPDP pre-treatment on mechanical hyperalgesia and mechanical allodynia

CDPDP (20 and 40 mg/kg) considerably reduced the mechanical hyperalgesia ($p < 0.0001$) at days 14–22 (Figure 4A). Mechanical nociception was likewise significantly reduced in the CFA-induced group on day 1 and then gradually reduced until day 21 (Figure 4A). Similarly, from day 14–22 of CFA injection, i.pl. treatment of CDPDP (20 and 40 mg/kg) dramatically reduced mechanical allodynia in mice, as seen in Figure 4B. Ibuprofen (10 mg/kg) also reduced CFA-induced mechanical allodynia. At days 14–21, CDPDP (40 mg/kg) revealed the most substantial increase in paw withdrawal threshold when compared to the negative control (Figure 4B).

3.9 Effect on arthritis-induced hematological variations

Table 4 shows the outcomes of the arthritis-related hematological changes. The findings revealed that as arthritis progresses, hematological values like hemoglobin (Hb), RBCs, and platelets decrease, while ESR and WBC levels increase in arthritic animals. As indicated in Table 5, CDPDP administration dramatically improved these hematological parameters.

3.10 Effect on biochemical levels

Many biochemical assays, such as the release of pro-inflammatory chemicals by NO, were examined. Pro-inflammatory chemicals are enhanced during inflammation, according to several studies. Chronic autoimmune disease pathophysiology is mostly influenced by an excess of NO, which can lead to tissue destruction and some other inflammatory responses. As a result, the NO assay was initiated to determine the impact of the stress chemical (CDPDP) on NO generation. Figure 5A shows that when the stress chemical (CDPDP) was used in comparison to the control groups, NO generation was significantly reduced ($p < 0.001$). Additionally, the assays for antioxidant enzymes and oxidative stress markers were carried out to evaluate the potential of the CDPDP-treated group, which significantly increased the catalase (Figure 5B), GSH (Figure 5C), GST (Figure 5D), and

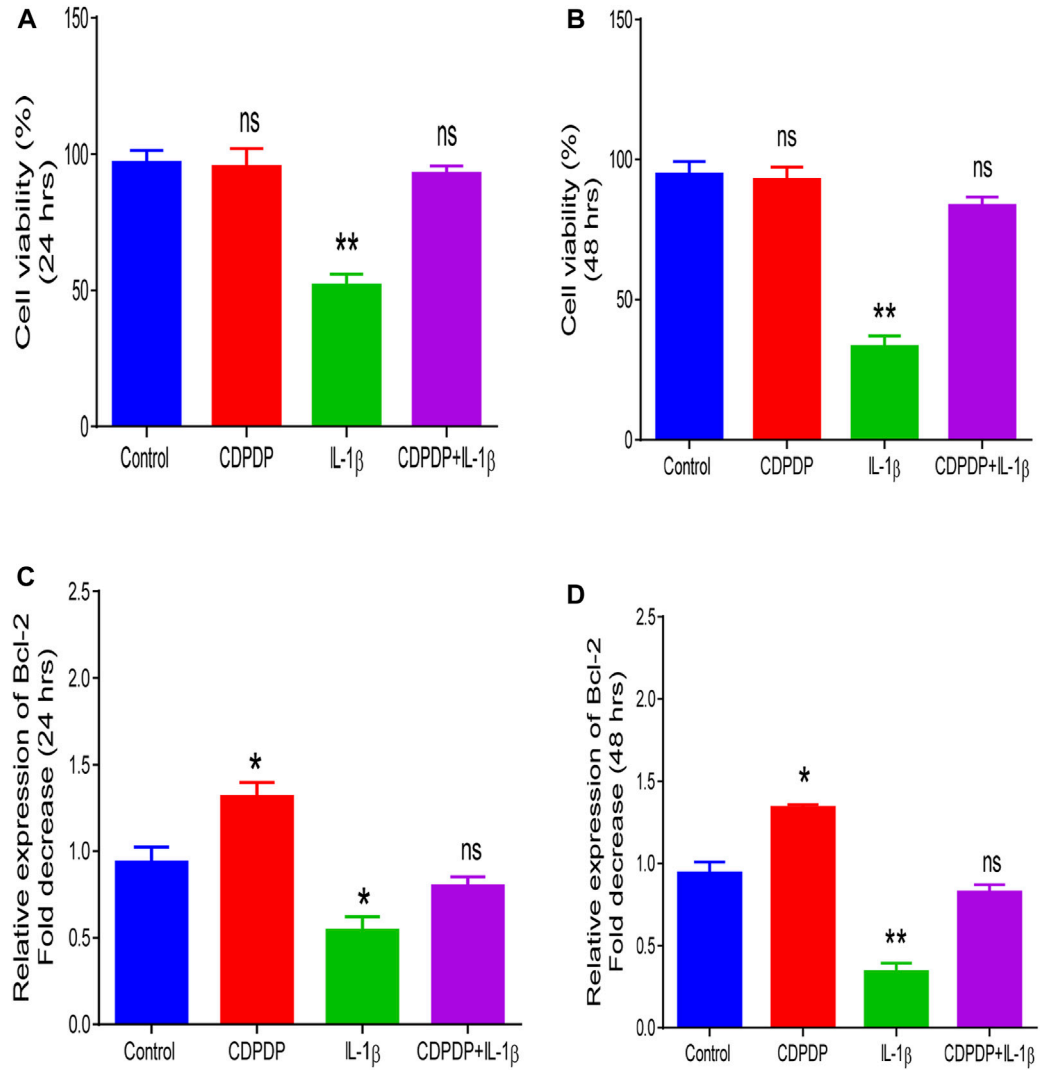

FIGURE 7
Chondrocytes were stained with trypan blue dye and trypan blue exclusion method was used to analyze CHON-001 cell viability at 24 h **(A)** and 48 h **(B)** Quantitative PCR was performed to measure **(C)** Relative Bcl-2 expression at 24 h and at **(D)** 48 h. Data is shown as mean ± SD (n = 3). Means with different superscripts in the columns are significantly ($p < 0.05$) different from one another.

MDA levels, which is an end product of lipid peroxidation, and decreased the MDA level (Figure 5E). As a result, when comparing the CDPDP (40 mg/kg) treatment to the other control groups, it was discovered to be the most effective.

3.10.1 Pro-inflammatory cytokines assay

Expression of TNF-α, IL-1β, and IL-6 in RA-affected tissues was significantly increased (p 0.001) by the CFA, which is a critical component of the amplification and progression of the disease. The effect of CDPDP on cytokine mediators such as TNF-α (Cat No: 560478), IL-1β (CAT No:557966), and IL-6 (CAT No:550950) in the paw tissue was investigated using ELISA assay kits. The findings of the assay showed the reduced expression of IL-6, IL-Iβ, and TNF-α levels in the CDPDP (40 mg/kg) group as compared to the negative and positive treated groups. CDPDP (40 mg/kg) was found to have better efficacy than the marketed drug, possibly due to its greater penetration and to its ability to be released from its target inflammatory site more quickly than from other locations (Figure 6).

3.11 Effect of CDPDP on liver and kidney

The results showed that CDPDP (20 and 40 mg/kg) was capable of restoring the stress-induced amended enzyme levels and biochemical parameters in the liver and kidney, such as ALT, AST, ALP, Urea, Creatinine, Albumin, and Bilirubin in arthritic

10.3389/fphar.2022.1053744

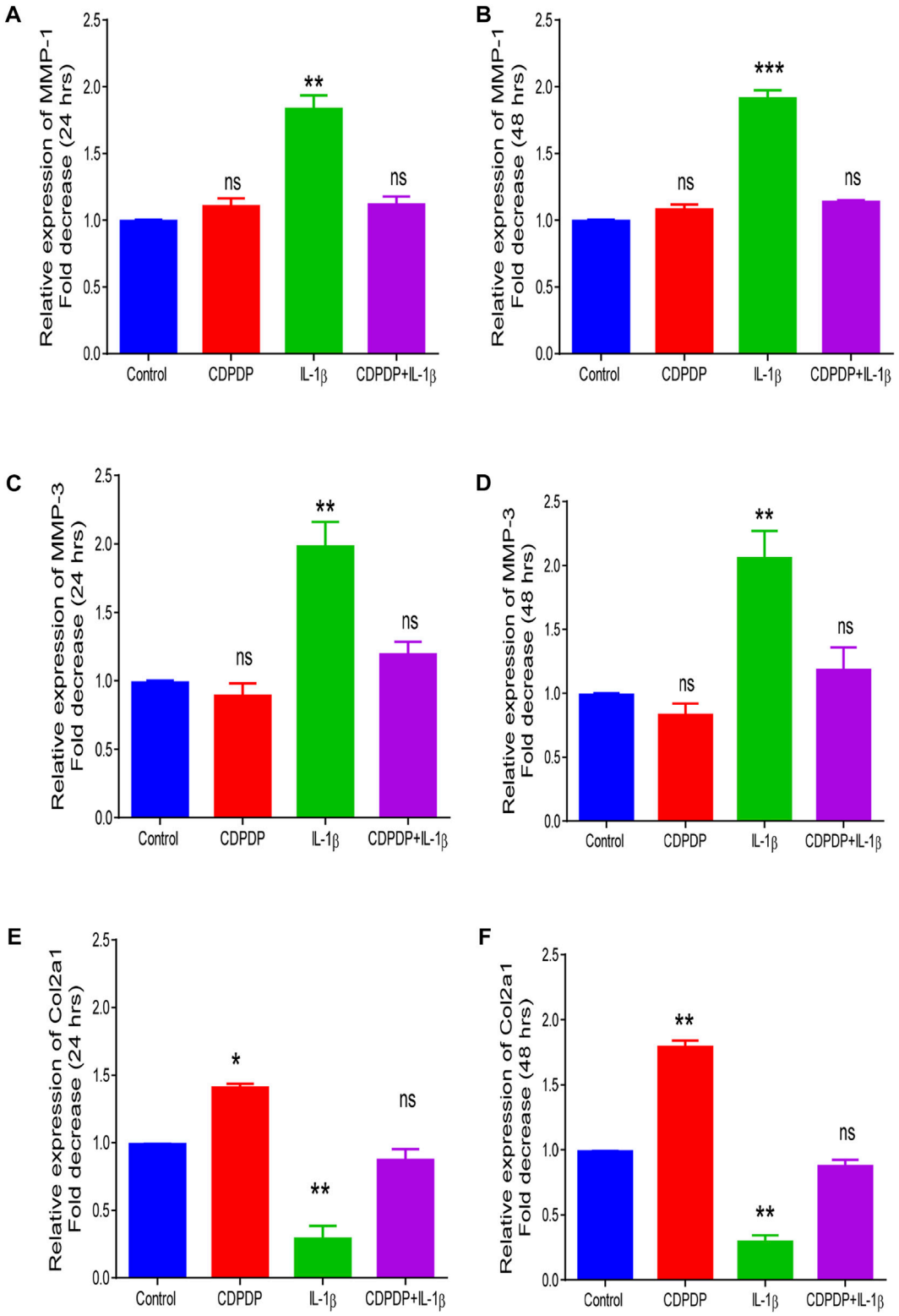

FIGURE 8
Quantitative PCR analysis chromatogram. **(A)** MMP-1 after 24 h **(B)** MMP-1 after 48 h **(C)** MMP-3 after 24 h **(D)** MMP-3 after 48 h **(E)** Col2a1 after 24 h **(F)** Col2a1 after 24 h. Data is shown as mean ± SD (n = 3). Means with different superscripts in the columns are significantly ($p < 0.05$) different from one another.

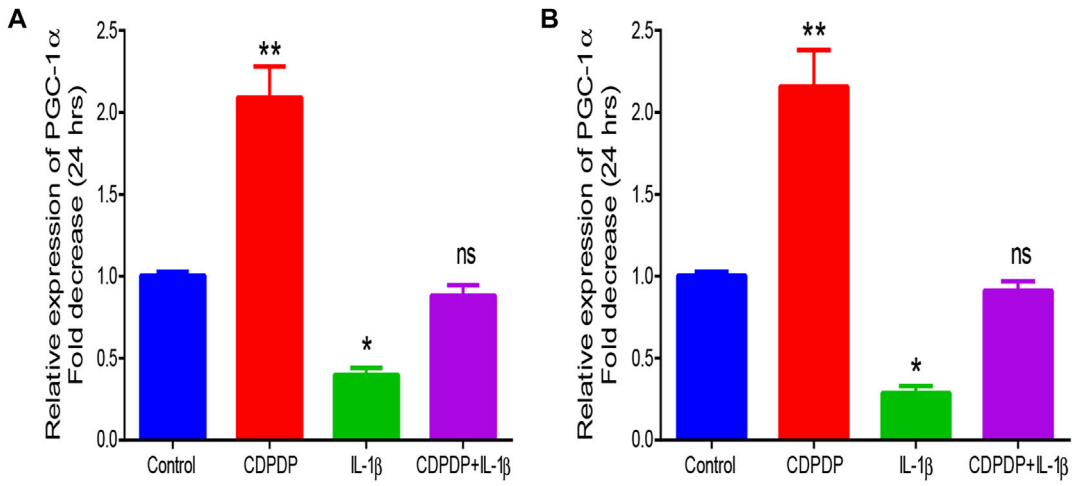

FIGURE 9
Quantitative PCR analysis chromatogram of **(A)** PGC-1α after 24 h **(B)** PGC-1α after 48 h. The data is expressed as the mean ± SD (n = 3) at $p < 0.05$ and $p < 0.01$.

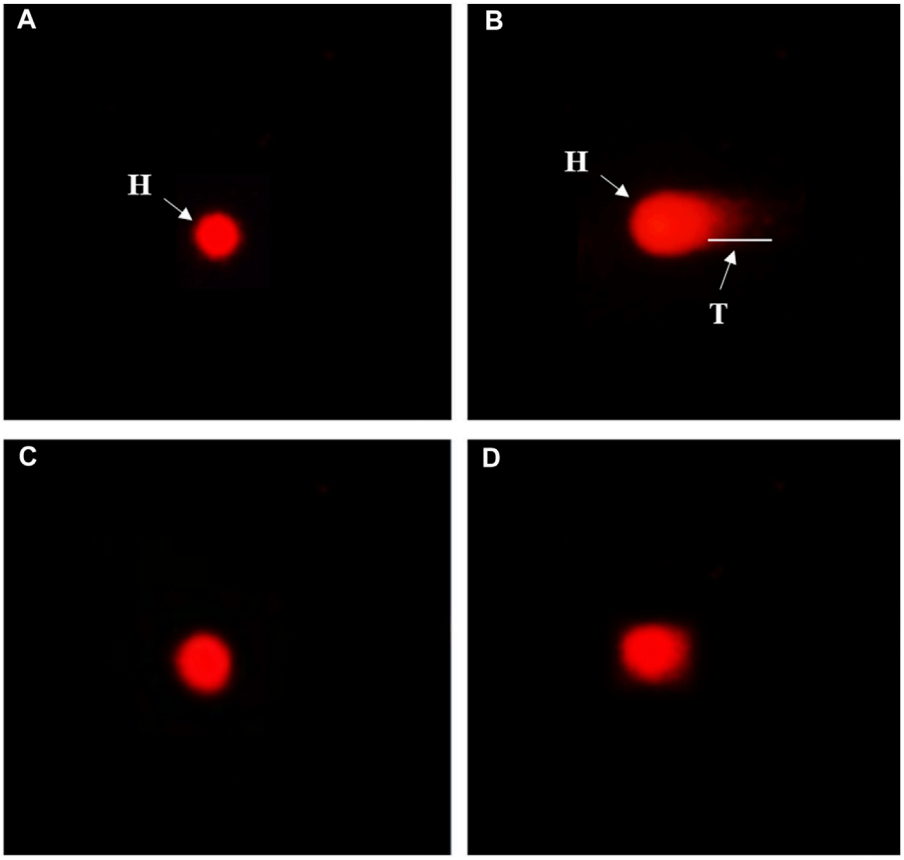

FIGURE 10
Genotoxicity evaluation of CDPDP on blood lymphocytes. Note: (**A**) The vehicle control (1% DMSO) (**B**) Ethyl methane sulfonate (20 μg/ml) (**C**) CDPDP (10 μg/ml) (**D**) CDPDP (20 μg/ml).

TABLE 6 Genotoxicity of CDPDP on blood lymphocytes was assessed using comet measurements.

Sample	Comet length (μm)	Head length (μm)	Tail length (μm)	% DNA in head	% DNA in tail	Tail moment (μm)
Control	42.6 ± 3.1	36.7 ± 2.5	5.9 ± 0.3	86.1 ± 2.8	13.9 ± 1.8$^{\beta}$	0.11 ± 0.03$^{\beta}$
EMS (20 μg/ml)	46.0 ± 3.6	31.0 ± 2.7	15.0 ± 3.4	67.39 ± 8.5	32.61 ± 5.8$^{¥}$	1.37 ± 0.11$^{¥}$
CDPDP (10 μg/ml)	40.4 ± 4.2	35.9 ± 1.8	4.5 ± 0.5	88.8 ± 2.1	11.2 ± 1.3$^{\beta}$	0.11 ± 0.04 $^{\beta}$
CDPDP (20 μg/ml)	40.1 ± 2.7	32.5 ± 1.4	7.6 ± 1.0	81.1 ± 2.4	18.9 ± 1.3$^{¥\beta}$	0.36 ± 0.04$^{¥\beta}$

Values are expressed as Mean ± SD (n = 3). Means with symbol "β" indicate non-significant difference from control; "¥" from EMS, treated group according to Kruskal–Wallis test at $p < 0.05$.

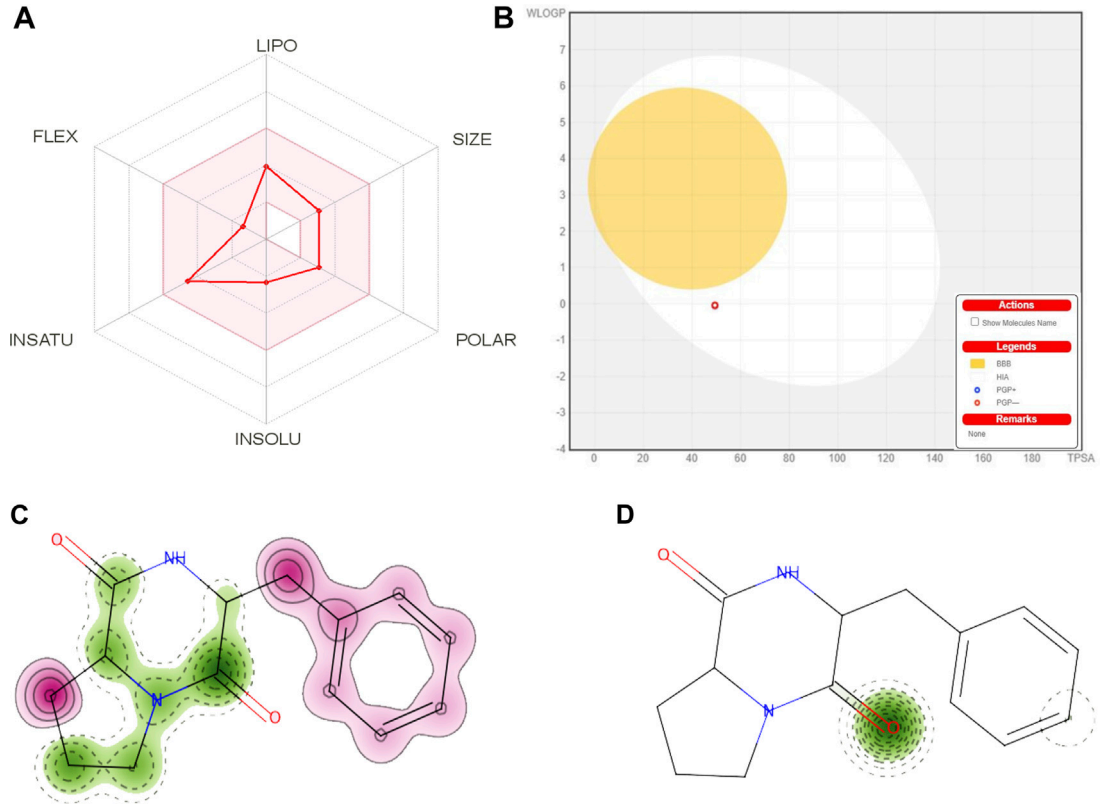

FIGURE 11
(A) A radar graphic showing CDPDP's bioavailability. The pink area indicates the physicochemical region for oral bioavailability, while the red stroke shows the parameters of oral bioavailability. **(B)** Swiss ADME online web tool for CDPDP predicted BOILED-Egg plot. Map of skin sensitization of CDPDP obtained from pred-skin. **(C)** h-CLAT **(D)** LLNA. The positive and negative contributions of individual atoms or pieces to the skin sensitization have been identified. The bright pink hue shows that an atom and fragment have made a detrimental impact on skin sensitization.

mice, and that it was also effective in reducing the stress-induced altered enzyme thresholds and biochemical parameters in the liver and kidney. Management of the CDPDP pointedly improved the biochemical as well as the enzymatic outline and detailed outcomes are accessible in Table 5.

3.12 Cell (chondrocytes) survival assessment

To assess the safer nature of isolated compounds CDPDP against human chondrocytes cell line (CHON-001), the MTT method was followed. Chondrocytes (CHON-001) were preserved with several levels of CDPDP for 24 h, 48 h, and

TABLE 7 Predicted pharmacokinetics parameters of CDPDP and Ibuprofen.

Properties	Parameters	CDPDP	Ibuprofen
Absorption	Water Solubility	−2.59	−3.36, S[a]
	GI[b]	81.53	94.01
	Log K_p (Skin permeation) cm/s	−6.80	−5.07
Distribution	BBB[a]	−0.075	0.302, Yes
	CNS permeation (Log PS)	−2.519	−1.695
	V_D[c] (human)	−0.168	−0.877
Metabolism	CYP1A2 inhibitor	No	No
	CYP2C9 inhibitor	No	No
	CYP2C19 inhibitor	No	No
	CYP3A4 inhibitor	No	No
	CYP2D6 inhibitor	No	No
Excretion	Total Clearance (log ml/min/kg)	0.282	0.263
	Renal OCT2 substrate	Yes	No

[a]Blood-brain barrier.
[b]Gastrointestinal.
[c]Volume of distribution.

72 h interval. Significant cell viability was observed on 24 h, 48 h, and 72 h exposure with CDPDP. CHON-001 cells showed significant time-dependent survival (>80%) when treated with CDPDP multiple concentrations (μg/ml). All results are displayed in Supplementary Figure S2.

3.12.1 Cell viability and apoptosis analysis of chondrocytes

During arthritic disease, there is a loss of cell survival signals, and enhanced apoptosis in chondrocytes, which according to research is the major factor causing arthritis (Goggs et al., 2003). IL-1β leads to activation of the inflammatory cascade in arthritis so chondrocytes treated with IL-1β are used as an *in-vitro* disease model (Chen et al., 2021). CDPDP did not negatively affect normal chondrocyte survival while IL-1β (10 ng/ml) significantly reduced the cell viability of CHON-001 cells as equated with the control (Figures 7A,B). Incubation of CHON-001 cells with CDPDP before IL-1β treatment led to an improvement in cell viability, and the non-significant difference was observed when compared with control at both time points (Figures 7A,B) Next, we analyzed relative Bcl-2 expression to get an idea of how does CDPDP affect cellular apoptosis in human chondrocyte cell lines. CDPDP-treated CHON-001 cells significantly upregulated relative Bcl-2 expression at both time points while IL-1β led to a decline in the anti-apoptosis marker. CDPDP reversed IL-1β induced decreased Bcl-2 expression, and a non-significant difference was observed between normal chondrocytes and IL-1β+CDPDP treated cells. There was a similar expression pattern at 24 h and 48 h time points (Figures 7C,D). Our results in Figure 7 signify that CDPDP can increase cell survival and inhibit apoptosis in chondrocytes during arthritic disease.

3.12.2 Cartilage turnover of chondrocytes

In arthritis, chondrocytes are responsible for the release of various matrix-degrading enzymes. IL-6 is mainly responsible for the release of these enzymes (Tseng et al., 2020; Xu et al., 2021). CDPDP did not alter gene expression profiles of MMP-1 and MMP3 when compared with control at 24 hs and 48 hs. On the other hand, IL-1β led to a rise in the level of these enzymes as evident from our qPCR data. Gene expression analysis of MMP-1 and MMP3 in chondrocytes incubated with CDPDP and IL-1β for 24 and 48 h also revealed no significant difference when compared with control suggesting the fact that CDPDP inhibits IL-1β induced rise in matrix-degrading enzymes concentrations. Col2a1 gene analysis revealed downregulation when treated with IL-1β but treatment with CDPDP + IL-1β significantly restored the downregulation due to IL-1β, and a non-significant difference between the control group and CDPDP + IL-1β group was observed. Our results in Figure 8 demonstrated that CDPDP can downregulate the genes involved in cartilage destruction and at the same time can upregulate protective genes like Col2a1.

3.12.3 Mitochondrial biogenesis of chondrocytes

PGC-1α gene is also called the master regulator of mitochondrial biogenesis. CDPDP upregulated the expression of PGC-1α when compared with control, while the opposite was observed when CHON-001 cells were preserved with IL-1β. CDPDP when used along IL-1β, it restored IL-1β-induced downregulation of PGC-1α Figure 9.

3.13 Comet assay

A comet test was performed on blood cells preserved by 10 and 20 μg/ml CDPDP sample, 20 μg/ml EMS (positive), and 1% DMSO in PBS (negative control). A CASP 1.2.3.b image processing of the photomicrographs from the fluorescence microscope was used to determine the degree of DNA damage. Tests were done on 50–100 lymphocytes per sample, measuring their length, head size, tail size, and moment of rotation. The amount of DNA found in the head and tail of lymphocytes was also evaluated. It was found that CDPDP (10 and 20 μg/ml) had no momentous effect on nuclear material, which is utilized as the standard control for genotoxicity studies. The tail length (15.0 ± 3.4 μm) of EMS-treated DNA is visibly representing the construction of nicks in nuclear content exhibiting the higher range of genotoxicity. Although no substantial toxicity to DNA was shown by any of the extracts, those with the lowest tail content were compared

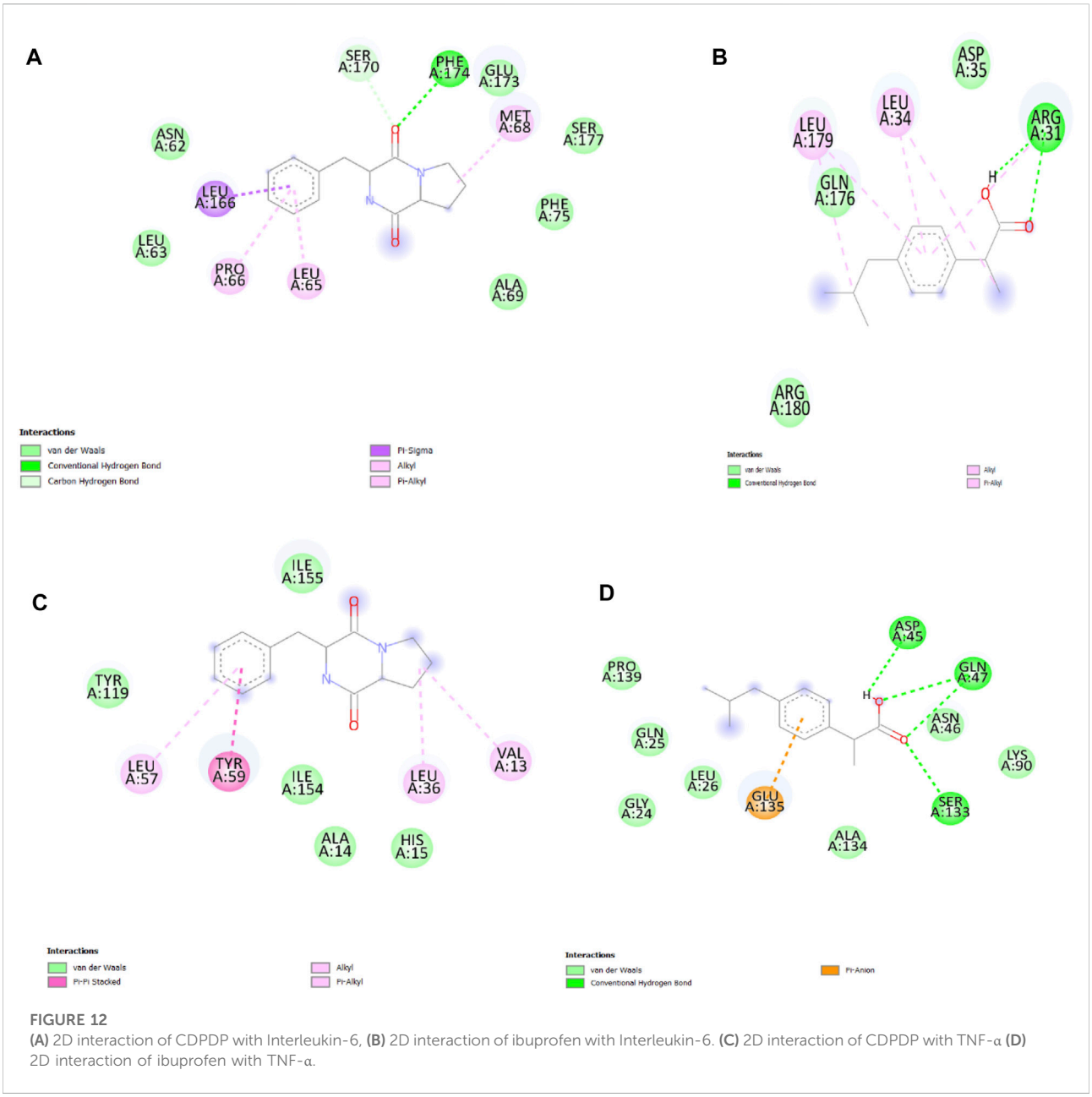

FIGURE 12
(A) 2D interaction of CDPDP with Interleukin-6, **(B)** 2D interaction of ibuprofen with Interleukin-6. **(C)** 2D interaction of CDPDP with TNF-α **(D)** 2D interaction of ibuprofen with TNF-α.

to the control. Figure 10; Table 6 show all of the florescent photomicrographs of the treated cells and their comet properties, respectively.

3.14 Pharmacokinetic and toxicological properties

Prediction studies for the stress compound CDPDP's absorption, distribution, metabolism, excretion, and toxicity (ADMET) were carried out.

3.14.1 Pharmacokinetic properties

The physicochemical properties of the CDPDP were looked at and separated into six major sets. Each group had a range that was good for oral bioavailability, comprising size (SIZE) 150 g/mol < MV < 500 g/mol, Insolubility (INSOLU) 0 < Log S (ESOL) < 6, Instauration (INSATU) 0.25 < Fraction Csp3 < 1, flexibility (FLEX) 0 < No. of rotatable ties <9, polarity (POLAR) 20Å2 < TPSA <130 $Å^2$, and lipophilicity (LIPO) 0.7 < (Log Po/w) XLOGP3 < +5.0, respectively. As measured by the Topological Polar Surface Area (TPSA) score, the CDPDP ranged in size from 20 $Å^2$ to 130 $Å^2$, showing CDPDP has strong transport characteristics *in vivo* (Figure 11A) (Supplementary

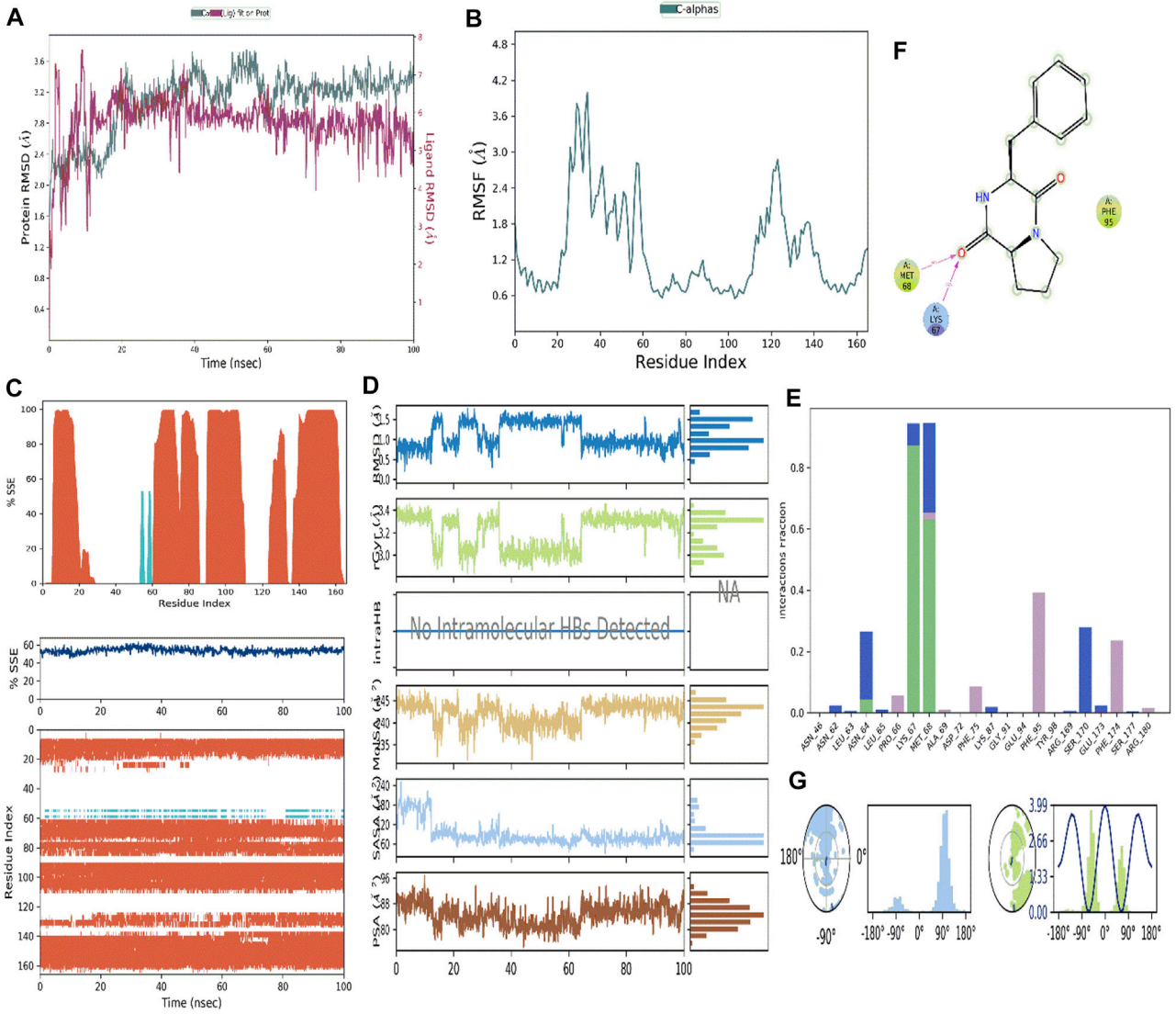

FIGURE 13
(A) RMSD analysis of CDPDP-IL-6 protein complex **(B)** Root Mean Square Fluctuation (RMSF) RMSF analysis of CDPDP-IL-6 protein complex **(C)** Protein Secondary Structure element distribution by residue index throughout the protein structures complexed with ligand CDPDP- IL-6 **(D)** Ligand properties with IL-6 protein **(E)** Protein-ligand contact histogram of CDPDP-IL-6 **(F)** Protein-ligand interaction of CDPDP-IL-6 **(G)** Ligand torsional plot of CDPDP.

Table S3). For pharmaceuticals or clinical trials, one of the most important factors is that a substance has a favorable physiochemical profile, which CDPDP has shown.

In order to prevent harmful effects on the central nervous system (CNS), the blood–brain barrier must be penetrated by chemicals that operate on the CNS. Inactive molecules in the CNS should not pass the blood-brain barrier. Before entering the pharmacological or clinical trials arena, every biomolecule must have its high gastrointestinal absorption (HIA) and CNS absorption properties verified. There was reduced BBB permeability in the stress compound CDPDP, which has a high HIA value. The white part (Figure 11B) is for GI (HIA) absorption, while the yellow region (yolk) is for BBB diffusion. In the grey zone, any chemical shows that it is neither absorbed nor BBB penetrant. For example, many cancerous cells use the P-gp efflux mechanism as a drug resistance mechanism (Qu et al., 2020). CDPDP is not a P-gp substratum, hence it is not sensitive to the outflow framework of P-gp. The less skin permeation Log Kp a molecule has, the less skin permeant it is. This is especially true for the CDPDP compound, which has shown less Log Kp. In addition, five main cytochromes (CYP) isoforms may be predicted using this method. Nearly 75% of commercially

available pharmaceuticals are metabolized by this enzyme isoform, which plays a critical role in excretion. When one of these isoforms is suppressed, significant drug-drug interactions occur. For example, the CDPDP did not affect the cytochrome isoform, and because it rapidly metabolizes, there are no interactions with these chosen cytochromes it might interfere with (Table 7). Dosing rates for steady-state concentrations are determined using the sum of renal and hepatic clearance. There was a problem with the CDPDP clearance value. Organic Cation Transporter 2 (OCT2) intermediates may have an influence on the unfavorable interactions that occur when OCT2 inhibitors and substrates are used together. CDPDP was found to be an OCT2 non-substrate in a recent study.

3.14.2 Toxicity assessment

Drugs must be evaluated for their toxicological profile when they first enter the clinical trials or production stages of the pharmaceutical industry. To determine the CDPDP's potential toxicity, it has been tested on several animals, including humans and oral mice, and in the environment) (Supplementary Table S4). This test is used to examine a compound's capacity to cause mutations in other organisms. Ames' hazardous classification was given to CDPDP, suggesting that they have been unlikely to be carcinogenic. Cardiovascular arrhythmias may be caused by the inhibition of potassium channels expressed by the human electroreceptor gene (hERG). According to the findings, CDPDP inhibits the expression, including both hERG I and hERG II. Aside from that, the molecule CDPDP was expected to be non-hepatotoxic, so it will not induce drug-induced liver damage. Besides considering environmental poisonousness, the online web browser GUSAR was utilized. The environmental toxicity was projected *via* an online web server using 96-h fathead minnow 50 percent fatal concentration, 48-h Daphnia Magna 50% lethal intensity, *Tetrahymena* pyriformis 50% inhibition zones concentration, and bio-concentration parameters, among other variables. With GUSAR's environmental toxicity prediction, CDPDP is within the application area of models in every instance. It is clear from the toxicity outline that the stress compound CDPDP has a strong protection outline, particularly in terms of hepatotoxicity.

3.14.3 Cardiac toxicity

The blocking of the hERG K+ channels is associated with deadly cardiac arrhythmias (Xue et al., 2022), and the FDA requires that every biomolecule that is considered as a therapeutic candidate be tested for hERG safety before being approved (Supplementary Figure S3). shows the prediction of CDPDP that was created after cardiac toxicity was predicted by pred-hERG and is based on this prediction. The positive and negative contributions of individual atoms or pieces to the hERG blockade have been identified. The bright pink hue shows that an atom and fragment have made a detrimental impact on the hERG blockade. The pred-hERG predictions projected that the stress compound CDPDP would not be cardiotoxic, with a 50 percent confidence level in this prediction. The findings have shown that CDPDP is less dangerous in terms of cardiac toxicity.

3.14.4 Skin sensitization

Chemo-induced skin sensitization is a complicated immunological condition that has a significant impact on both the sufferer's well-being and their capacity to function. Despite considerable advances in the development of innovative methods of evaluating the skin sensitization capability of chemical compounds, there seems to be no *in vitro* assay that corresponds well with human data. Computational QSAR models can be used to quickly screen chemicals for toxicity and provide valuable information. The stressed compound CDPDP was evaluated for its possible skin sensitization in the *in-vitro* human cell line activation test (h-CLAT) OECD442E and *in-vivo* local lymph node assay (LLNA) OECD429. The cellular response of CDPDP was evaluated against dendritic cells for the induction of inflammatory cytokines and the mobilization of dendritic cells. The h-CLAT- OECD442E results have shown that CDPDP was conducted as a non-sensitizer with a confidence score of 65.1% (Figure 11C). Furthermore, *in-vivo* (LLNA) evaluation of CDPDP was evaluated for tissue/organ response against the proliferation of antigen-specific T-cells (OECD429). The results have shown that CDPDP was conducted as a non-sensitizer with a confidence score of 98.5% (Figure 11D). From both cellular response and tissue/organ response, it also proved that the stressed compound CDPDP is a non-sensitizer for the histocompatibility complex represented by dendritic cells.

3.15 Docking analysis

The key residues of the selected active binding pocket of Interleukin-6 protein (PDB ID: 1il6) and Tumor Necrosis Factor-alpha (PDB ID: 1tnf) against CDPDP were found. Main ligand-protein interactions of CDPDP against Interleukin-6 protein include LEU166, PRO66 and MET68 in pi-stacking interactions, and PHE174 in hydrogen-bonding interaction (Figure 12A). In the case of Tumor Necrosis Factor-alpha TYR59, pi-stacking interactions were found (Figure 12C). To validate the docking protocol used in this study, the reference ligand, ibuprofen, was initially docked into the binding pocket of the Interleukin-6 protein (PDB ID: 1il6) and Tumor Necrosis Factor-alpha (PDB ID: 1tnf) protein domain. The result demonstrated a suitable binding pose of the reference ligand with a docking score of −17.2 kcal/mol. The interaction between ibuprofen and the binding sites of Interleukin-6 protein mainly involved the amino acids LEU179, and LEU34 in pi-stacking interactions, and ARG31 in hydrogen-bonding interactions (Figure 12B). The interaction between ibuprofen and the binding sites of Tumor Necrosis Factor-alpha protein mainly

involved the amino acids ASP45, GLN47, AND SER133 in hydrogen-bonding interaction (Figure 12D).

3.16 Molecular dynamics and simulation

MDS was performed for the CDPDP- Interleukin-6, CDPDP- Tumor Necrosis Factor-alpha, Ibuprofen-Interleukin-6, and Ibuprofen-Tumor Necrosis Factor-alpha structure complexes upto100 ns The parameters explored for analyses such as RMSD, RMSF, protein-ligand contact, RoG, and binding free energy.

3.16.1 RMSD analysis

The RMSD study was used to determine the stability of the simulation results. During the simulation, the protein's RMSD graph (left Y-axis) can provide insight into its structural conformation, while the ligand's RMSD graph (right Y-axis) indicates the stability of the ligand concerning a specific protein and its ligand-binding pocket (Figure 13A). CDPDP-Interleukin-6 protein-ligand complex remained stable and within acceptable RMSD limits throughout 100 ns simulation (Figure 13A).

3.16.2 RMSF assay

The RMSF is a measure of the macromolecule's particle deviation. It describes the pliability and stiffness of the protein structure. Since the N and C-terminal residues tend to fluctuate the most in MD trajectories, these residues have higher peaks (Figure 13B). Binding site residues with low RMSF values show that ligand-binding is highly stable. The percentages of helix and strand in CDPDP- IL-6 were discovered to be 52.5% and 1.28%, respectively, while the overall secondary structure elements (SSE) were found to be 53.77% (Figure 13C).

3.16.3 Simulation event analysis of ligand properties

The properties of the ligand which is complexed with the protein of IL-6 during simulation studies (Figure 13D) are as follows ligand RMSD was little fluctuating between 0.6 and 1.4 with an average of 0.8 A^0 which proves that compound is stable with the protein active site. Furthermore, the structural compactness of the protein was checked by the radius of gyration (Rg). The ligand showed very good stability from 0–40 and 60–100 ns but was little fluctuated from 40 to 60 ns. There was no intra-hydrogen bond found in this complex. Molecular surface area (MoLSA) was found to be maintained in the zone of 230–245, there were little fluctuations but later the ligand showed good stability. The solvent-accessible surface area (SASA) also showed some fluctuations in the start till 40ns but after that showed good stability till 100 ns The polar surface area was also maintained in the zone of 78–84.

3.16.4 Molecular interactions of protein-ligand

The interaction of the target protein with the ligand was monitored during the simulation. These interactions were categorized into four types: 1) Hydrogen Bonds, 2) Hydrophobic, 3) Ionic, and 4) Water bridges (Figures 13E,F).

According to the findings of this investigation, hydrogen bonds, water bridges, and hydrophobic interactions were the most important ligand-protein interactions observed. In CDPDP-IL-6, the complex showed hydrophobic interaction with PRO_66, PHE_95, and PHE_174 whereas LYS_67 and MET_68 were key in terms of hydrogen bonding (Figure 13E). While the hydrophobic interactions and positive charge on the structure of the ligand are shown in Figure 13F. Furthermore, the compound CDPDP torsions plot describes the no of rotatable bonds in the ligand from 0.00ns to 100 ns. Figure 13G depicts a 2 d depiction of the ligand in which rotatable bonds are color labeled according to their orientation. There were two rotatable bonds found in the structure consuming the energy at 3.99 kcal/mol.

3.17 MM-GBSA calculations

Total binding free energy was calculated for the CDPDP with IL-6 as shown in Supplementary Table S5. In IL-6, the binding free energy was calculated as −55.46 kcal/mol for the CDPDP.

4 Discussion

This research focused on isolating a metal-triggered anti-arthritic compound CDPDP from actinobacteria by abiotic stress. Furthermore, evaluating the *in vitro and in-vivo* pharmacological profile of CDPDP as an anti-inflammatory, anti-pyretic and anti-oxidant agent, including *In-silico* studies of ADMET, molecular docking and MD simulations strengthened its profile.

Metal-triggering technique is one of the new techniques which increases the chances for new secondary metabolite production. As proved by our previous findings, Metals-triggered compounds are generally absent in the normal culture method but after inducing abiotic stress (heavy metals) the new compound with its unique carbon skeletons appeared in stressed culture (Ul Hassan et al., 2021). The microorganisms sometimes show resistance towards the metals and therefore need to either increase the concentration of metals or use the combination of two or more metals to trigger the sleeping genes (Hassan et al., 2017; Shams ul Hassan et al., 2019; Ul Hassan et al., 2021). Our research shows that the actinobacteria strain initially did not respond to copper with different concentrations. However, after the addition of Nickel ions, the bacteria responded to

the metal ions in its environment and elicited a new peak as CDPDP.

Nowadays, many natural product researchers have driven their research toward untapping the secondary metabolites with promising anti-inflammatory and anti-oxidant properties (Mahmood et al., 2022; Qazi et al., 2022; Razzaq et al., 2022). When an allergic reaction occurs during croton-induced ear and anal inflammation, histamine is released, which results in vasodilation, edoema, increased vascular permeability, and the recruitment of eosinophils (Li et al., 2022). In response the rat's anal sphincter's smooth muscles acquire inflammation. It controls the function of leukocytes as well as their movement, together with the proliferation of T cells and B cells, and secretion of lysosomal enzymes in neutrophils (Majid et al., 2018). During the process of histamine-induced edoema, endothelial nitric oxide synthase, also known as eNOS, is extremely important. Because NO is directly responsible for the macromolecular surge generated by histamine inflammation, reducing NO levels may help to reduce inflammation (Song and Wu, 2022). This is because NO is immediately accounted for by the inflammatory process (Batool et al., 2017). Oral administration of CDPDP is used in this study to generate a systemic effect, with the goals of stabilizing the membrane of mast cells and reducing the production of NO and histamine. The adjuvant-induced inflammatory rat model has been used widely as a classical animal model. This model has several of the typical aspects as in human arthritic patients, including immunological and histological findings. Primary and secondary chronic arthritis can be induced by adjuvant-induction, which activates the cell-mediated immune response and promotes immunoglobulin synthesis in organisms. As a result of the high levels of pro-inflammatory cytokines released during adjuvant induced inflammation. Osteoclast differentiation, inflammation, and bone degradation are all influenced by pro-inflammatory cytokines and interleukins (Majid et al., 2018). The production of metallo-proteinases and the proliferation of synovial cells, both of which lead to cartilage deterioration, can be stopped by blocking TNF-, IL-1, IL-6, and NO. CDPDP with substantial inhibition capacity of these cytokines has significantly reduced CFA-induced inflammatory complications.

ADMET is a crucial stage for every kind of biomolecule before its biotransformation into a drug (Hassan et al., 2022). According to the ADMET profile of CDPDP, its absorption and distribution were moderate; CDPDP is safe in cases of hepatotoxicity, cardiotoxicity, and cytochrome inhibition. Furthermore, CDPDP has revealed that it is not a P-gp (P-glycoprotein) substrate; therefore, CDPDP is not susceptible to the efflux mechanism of P-gp, and many cancer cell lines utilize that as a drug resistance mechanism. CYP enzymes play a crucial role in drug excretion, and these isoforms are metabolizing almost 75% of market-available drugs. Inhibition of any of these isoforms results in causing some significant pharmacokinetics-based drug-drug interactions (Shams ul Hassan et al., 2021) CDPDP has not inhibited any CYP enzymes, which means MVL cannot create drug-drug interactions for those CYP enzyme-targeted drugs.

As evident from our study, CDPDP has shown encouraging results in terms of IL-6 and TNF-α inhibition in the sense of molecular docking. Therefore, in these ways, special attention should be placed on investigating this process's therapeutic importance. Further molecular docking simulations proved that CDPDP has good binding potential with IL-6 and binds within the active gorge.

Thus, the current study revealed the potential advantages of the metals-triggered compound CDPDP against arthritis and may be useful against different diseases. The research relied on *in vitro*, *in-vivo*, and computational tools that documented pharmacological properties and bioactivities predictions. Moreover, clinical studies are necessary to confirm the findings of the present work. Nonetheless, the results of this work will provide future guidance for the design and development of new lead compounds as anti-arthritic, anti-pyretic and anti-oxidant agents.

5 Conclusion

In the current research, the abiotic metal (Ni^{2+}) stress was employed to isolate a stressed molecule from actinobacteria, a natural substance called CDPDP. CDPDP's *in vivo* clinical profile as an anti-inflammatory medication against rheumatoid arthritis was further enhanced by ADMET investigations *in silico*, molecular docking, and simulation studies. The use of the metal-stress technique paves the way for the discovery of new secondary metabolites, as it enables researchers to focus on the most promising areas. Due to the prior discovery that stress-elicited compounds are often absent from standard cultures, this new chemical with its characteristic carbon skeletons appeared in the stressed culture method. As a result, they must either increase the concentration of metals or combine two or more different metals to activate the genes that have been dormant for a long time. Secondary metabolites with potential anti-inflammatory activities have become the focus of many natural product researchers in the last several years. As mentioned in Tables 1, 2 the CDPDP in its (40 mg/kg) dose has shown promising anti-inflammatory activity against R.A as compared to positive control Ibuprofen. A strong anti-inflammatory profile is demonstrated by these findings for CDPDP. Furthermore, for the biochemical assays and enzymatic studies as mentioned in Figures 7, 8. The compound CDPDP has shown promising results against TNFα, IL-6, GSH assay, GST assay, catalase, and NO production. In addition, the histopathological studies and X-ray reports have proved that CDPDP (40 mg/kg) remarkably finished the R.A and increased the fluid between

joints. The compound CDPDP also showed a safe profile for the kidney and liver after the dosage of the compound to mice evaluated after 6 h of administration. According to our findings, CDPDP has demonstrated promising outcomes in the context of molecular docking for the suppression of IL-6. As a result of these considerations, this process's therapeutic significance must be examined.

Data availability statement

The original contributions presented in the study are included in the article/Supplementary Material, further inquiries can be directed to the corresponding authors.

Ethics statement

The animal study was reviewed and approved by ethical committee of Capital University of Science and technology, Islamabad, Pakistan (Letter no. CU-PHM-019/2021 for the animal care and Letter no. CU-PHM-019/2021 for experimentation, dated 10/09/2021).

Author contributions

SH has written the original manuscript and performed experiments. SA analyzed the data. IM reevaluate the data for accuracy. FA performed molecular docking and simulations. JJ-W written the discussion. SB checking the data analyzing and funding acquisition. MM, S-KY, and H-ZJ supervision.

Funding

The work was supported by NSFCs (81973191), Shanghai Natural Science Fund (19ZR1428100), Shanghai Engineering Research Center for the Preparation of Bioactive Natural Products (16DZ2280200), the Scientific Foundation of Shanghai China (13401900103, 13401900101), the National Key Research and Development Program of China (2017YFC1700200).

Acknowledgments

The authors wish to thank University of Oradea, Oradea, Romania for financial support in publishing this paper.

Conflict of interest

The authors declare that the research was conducted in the absence of any commercial or financial relationships that could be construed as a potential conflict of interest.

Publisher's note

All claims expressed in this article are solely those of the authors and do not necessarily represent those of their affiliated organizations, or those of the publisher, the editors and the reviewers. Any product that may be evaluated in this article, or claim that may be made by its manufacturer, is not guaranteed or endorsed by the publisher.

Supplementary material

The Supplementary Material for this article can be found online at: https://www.frontiersin.org/articles/10.3389/fphar.2022.1053744/full#supplementary-material

References

Ahsan, H., Ayub, M., Irfan, H. M., Saleem, M., Anjum, I., Haider, I., et al. (2022). Tumor necrosis factor-alpha, prostaglandin-E2 and interleukin-1β targeted anti-arthritic potential of fluvoxamine: Drug repurposing. *Environ. Sci. Pollut. Res.* doi:10.1007/s11356-022-23142-1

Akhter, N., Liu, Y., Auckloo, B. N., Shi, Y., Wang, K., Chen, J., et al. (2018). Stress-driven discovery of new angucycline-type antibiotics from a marine streptomyces pratensis NA-ZhouS1. *Mar. Drugs* 16, 3311–E416. doi:10.3390/md16090331

Batool, R., Khan, M. R., and Majid, M. (2017). Euphorbia dracunculoides L. abrogates carbon tetrachloride induced liver and DNA damage in rats. *BMC Complement. Altern. Med.* 17, 223. doi:10.1186/s12906-017-1744-x

Behl, T., Chadha, S., Sehgal, A., Singh, S., Sharma, N., Kaur, R., et al. (2022). Exploring the role of cathepsin in rheumatoid arthritis. *Saudi J. Biol. Sci.* 29, 402–410. doi:10.1016/j.sjbs.2021.09.014

Braga, R. C., Alves, V. M., Muratov, E. N., Strickland, J., Kleinstreuer, N., Trospsha, A., et al. (2017). Pred-skin: A fast and reliable web application to assess skin sensitization effect of chemicals. *J. Chem. Inf. Model.* 57, 1013–1017. doi:10.1021/acs.jcim.7b00194

Braga, R. C., Alves, V. M., Silva, M. F. B., Muratov, E., Fourches, D., Lião, L. M., et al. (2015). Pred-hERG: A novel web-accessible computational tool for predicting cardiac toxicity. *Mol. Inf.* 34, 698–701. doi:10.1002/minf.201500040

Brown, J. N., and Teller, R. G. (1976). Crystal structure and molecular conformation of the hydrated cyclic hexapeptide cyclo(L-Ala-L-Pro-D-Phe)2. *J. Am. Chem. Soc.* 98, 7565–7569. doi:10.1021/ja00440a020

Chen, L., Huang, Y., Yu, X., Lu, J., Jia, W., Song, J., et al. (2021). Corynoxine protects dopaminergic neurons through inducing autophagy and diminishing neuroinflammation in rotenone-induced animal models of Parkinson's disease. *Front. Pharmacol.* 12, 642900. doi:10.3389/fphar.2021.642900

Cui, P., Qu, F., Sreeharsha, N., Sharma, S., Mishra, A., and Gubbiyappa, S. K. (2020). Antiarthritic effect of chitosan nanoparticle loaded with embelin against adjuvant-induced arthritis in Wistar rats. *IUBMB life* 72, 1054–1064. doi:10.1002/iub.2248

Daina, A., Michielin, O., and Zoete, V. (2017). SwissADME: A free web tool to evaluate pharmacokinetics, drug-likeness and medicinal chemistry friendliness of small molecules. *Sci. Rep.* 7, 42717–42813. doi:10.1038/srep42717

Dallakyan, S., and Olson, A. J. (2015). Small-molecule library screening by docking with PyRx. *Methods Mol. Biol.* 1263, 243–250. doi:10.1007/978-1-4939-2269-7_19

Ding, C., Wu, X., Auckloo, B. N., Chen, C. T. A., Ye, Y., Wang, K., et al. (2016). An unusual stress metabolite from a hydrothermal vent fungus aspergillus sp. Wu 243 induced by cobalt. *Molecules* 21, 105–111. doi:10.3390/molecules21010105

Dong, G., Xu, N., Wang, M., Zhao, Y., Jiang, F., Bu, H., et al. (2021). Anthocyanin extract from purple sweet potato exacerbate mitophagy to ameliorate pyroptosis in *Klebsiella pneumoniae* infection. *Int. J. Mol. Sci.* 22, 11422. doi:10.3390/ijms222111422

Eo, S., Cho, H., and Kim, S. (2014). Resveratrol regulates type II collagen and COX-2 expression via the ERK, p38 and Akt signaling pathways in rabbit articular chondrocytes. *Exp. Ther. Med.* 7, 640–648. doi:10.3892/etm.2014.1484

Ferreira, L. G., Dos Santos, R. N., Oliva, G., and Andricopulo, A. D. (2015). Molecular docking and structure-based drug design strategies. *Molecules* 20, 13384–13421. doi:10.3390/molecules200713384

Goggs, R., Carter, S. D., Schulze-Tanzil, G., Shakibaei, M., and Mobasheri, A. (2003). Apoptosis and the loss of chondrocyte survival signals contribute to articular cartilage degradation in osteoarthritis. *Vet. J.* 166, 140–158. doi:10.1016/S1090-0233(02)00331-3

González-Menéndez, V., Pérez-Bonilla, M., Pérez-Victoria, I., Martín, J., Muñoz, F., Reyes, F., et al. (2016). Multicomponent analysis of the differential induction of secondary metabolite profiles in fungal endophytes. *Molecules* 21, E234. doi:10.3390/molecules21020234

Hassan, S. S., Shah, S. A. A., Pan, C., Fu, L., Cao, X., Shi, Y., et al. (2017). Production of an antibiotic enterocin from a marine actinobacteria strain H1003 by metal-stress technique with enhanced enrichment using response surface methodology. *Pak. J. Pharm. Sci.* 30, 313–324.

Hassan, S. S. ul, Abdel-Daim, M. M., Behl, T., and Bungau, S. (2022). Natural products for chronic diseases: A ray of hope. *Molecules* 27, 5573. doi:10.3390/molecules27175573

Hitchon, C. A., and El-Gabalawy, H. S. (2004). Oxidation in rheumatoid arthritis. *Arthritis Res. Ther.* 6, 265–278. doi:10.1186/ar1447

Khan, D., Qindeel, M., Ahmed, N., Asad, M. I., Shah, K. U., and Rehman, A. R. (2021). Development of an intelligent, stimuli-responsive transdermal system for efficient delivery of Ibuprofen against rheumatoid arthritis. *Int. J. Pharm.* 610, 121242. doi:10.1016/j.ijpharm.2021.121242

Khan, F. A., Ali, G., Rahman, K., Khan, Y., Ayaz, M., Mosa, O. F., et al. (2022). Efficacy of 2-hydroxyflavanone in rodent models of pain and inflammation: Involvement of opioidergic and GABAergic anti-nociceptive mechanisms. *Molecules* 27, 5431. doi:10.3390/molecules27175431

Kim, S. J., Im, D. S., Kim, S. H., Ryu, J. H., Hwang, S. G., Seong, J. K., et al. (2002). Beta-catenin regulates expression of cyclooxygenase-2 in articular chondrocytes. *Biochem. Biophys. Res. Commun.* 296, 221–226. doi:10.1016/s0006-291x(02)00824-0

Leelaprakash, G., and Mohan Dass, S. (2011). Invitro anti-inflammatory activity of methanol extract of enicostemma axillare. *Int. J. Drug Dev. Res.* 3, 189–196.

Li, Z., Teng, M., Jiang, Y., Zhang, L., Luo, X., Liao, Y., et al. (2022). YTHDF1 negatively regulates Treponema pallidum-induced inflammation in THP-1 macrophages by promoting SOCS3 translation in an m6A-dependent manner. *Front. Immunol.* 13, 857727. doi:10.3389/fimmu.2022.857727

Mahmood, F., Khan, J. A., Mahnashi, M. H., Jan, M. S., Javed, M. A., Rashid, U., et al. (2022). Anti-inflammatory, analgesic and antioxidant potential of new (2S,3S)-2-(4-isopropylbenzyl)-2-methyl-4-nitro-3-phenylbutanals and their corresponding carboxylic acids through *in vitro*, in silico and *in vivo* studies. *Molecules* 27, 4068. doi:10.3390/molecules27134068

Majid, M., Khan, M. R., Shah, N. A., Ul Haq, I., Farooq, M. A., Ullah, S., et al. (2015). Studies on phytochemical, antioxidant, anti-inflammatory and analgesic activities of Euphorbia dracunculoides. *BMC Complement. Altern. Med.* 15, 349. doi:10.1186/s12906-015-0868-0

Majid, M., Nasir, B., Zahra, S. S., Khan, M. R., Mirza, B., and Haq, I.-U. (2018). Ipomoea batatas L. Lam. ameliorates acute and chronic inflammations by suppressing inflammatory mediators, a comprehensive exploration using *in vitro* and *in vivo* models. *BMC Complement. Altern. Med.* 18, 216. doi:10.1186/s12906-018-2279-5

Maryam, S., Khan, M. R., Shah, S. A., Zahra, Z., Majid, M., Sajid, M., et al. (2018). *In vitro* antioxidant efficacy and the therapeutic potential of Wendlandia heynei (Schult.) Santapau & Merchant against bisphenol A-induced hepatotoxicity in rats. *Toxicol. Res.* 7, 1173–1190. doi:10.1039/c7tx00322f

Nair, V., Kumar, R., Singh, S., and Gupta, Y. K. (2012). Investigation into the anti-inflammatory and antigranuloma activity of colchicum luteum baker in experimental models. *Inflammation* 35, 881–888. doi:10.1007/s10753-011-9389-2

Qazi, N. G., Khan, A., Abbasi, S. W., Shah, F. A., Rasheed, F., Ali, F., et al. (2022). Pharmacological basis of *Rumex hastatus* D. Don in gastrointestinal diseases with focusing effects on H^+/K^+-ATPase, calcium channels inhibition and PDE mediated signaling: Toxicological evaluation on vital organs. *Molecules* 27, 5919. doi:10.3390/molecules27185919

Qu, Y.-Y., Zhao, R., Zhang, H.-L., Zhou, Q., Xu, F.-J., Zhang, X., et al. (2020). Inactivation of the AMPK-GATA3-ECHS1 pathway induces fatty acid synthesis that promotes clear cell renal cell carcinoma growth. *Cancer Res.* 80, 319–333. doi:10.1158/0008-5472.CAN-19-1023

Razzaq, S., Minhas, A. M., Qazi, N. G., Nadeem, H., Khan, A., Ali, F., et al. (2022). Novel isoxazole derivative attenuates ethanol-induced gastric mucosal injury through inhibition of H +/K + -ATPase pump , oxidative stress and inflammatory pathways. *Molecules* 27, 5065. doi:10.3390/molecules27165065

Reanmongkol, W., Noppapan, T., and Subhadhirasakul, S. (2009). Antinociceptive, antipyretic, and anti-inflammatory activities of Putranjiva roxburghii Wall. leaf extract in experimental animals. *J. Nat. Med.* 63, 290–296. doi:10.1007/s11418-009-0336-6

Shams ul Hassan, S., Abbas, S. Q., Hassan, M., and Jin, H.-Z. (2021). Computational exploration of anti-cancer potential of guaiane dimers from xylopia vielana by targeting B-raf kinase using chemo-informatics, molecular docking and MD simulation studies. *Anticancer. Agents Med. Chem.* 21, 731–746. doi:10.2174/1871520621666211013115500

Shams ul Hassan, S., Jin, H. Z., Abu-Izneid, T., Rauf, A., Ishaq, M., and Suleria, H. A. R. (2019). Stress-driven discovery in the natural products: A gateway towards new drugs. *Biomed. Pharmacother.* 109, 459–467. doi:10.1016/j.biopha.2018.10.173

Shams ul Hassan, S., Qamar Abbas, S., Ali, F., Ishaq, M., Bano, I., Hassan, M., et al. (2022). A comprehensive in silico exploration of pharmacological properties, bioactivities, molecular docking, and anticancer potential of vieloplain F from xylopia vielana targeting B-raf kinase. *Molecules* 27, 917. doi:10.3390/molecules27030917

Song, K., and Wu, D. (2022). Shared decision-making in the management of patients with inflammatory bowel disease. *World J. Gastroenterol.* 28, 3092–3100. doi:10.3748/wjg.v28.i26.3092

Tseng, C.-C., Chen, Y.-J., Chang, W.-A., Tsai, W.-C., Ou, T.-T., Wu, C.-C., et al. (2020). Dual role of chondrocytes in rheumatoid arthritis: The chicken and the egg. *Int. J. Mol. Sci.* 21, 1071. doi:10.3390/ijms21031071

Ul Hassan, S. S., Muhammad, I., Abbas, S. Q., Hassan, M., Majid, M., Jin, H. Z., et al. (2021). Stress driven discovery of natural products from actinobacteria with anti-oxidant and cytotoxic activities including docking and admet properties. *Int. J. Mol. Sci.* 22, 11432. doi:10.3390/ijms222111432

Ullah, M. Z., Khan, A. U., Afridi, R., Rasheed, H., Khalid, S., Naveed, M., et al. (2018). Attenuation of inflammatory pain by puerarin in animal model of inflammation through inhibition of pro-inflammatory mediators. *Int. Immunopharmacol.* 61, 306–316. doi:10.1016/j.intimp.2018.05.034

Vina, E. R., Hannon, M. J., Masood, H. S., Hausmann, L. R. M., Ibrahim, S. A., Dagnino, J., et al. (2020). Nonsteroidal anti-inflammatory drug use in chronic arthritis pain: Variations by ethnicity. *Am. J. Med.* 133, 733–740. doi:10.1016/j.amjmed.2019.11.016

Xu, S., Tao, H., Cao, W., Cao, L., Lin, Y., Zhao, S.-M., et al. (2021). Ketogenic diets inhibit mitochondrial biogenesis and induce cardiac fibrosis. *Signal Transduct. Target. Ther.* 6, 54. doi:10.1038/s41392-020-00411-4

Xue, F., Cheng, J., Liu, Y., Cheng, C., Zhang, M., Sui, W., et al. (2022). Cardiomyocyte-specific knockout of ADAM17 ameliorates left ventricular remodeling and function in diabetic cardiomyopathy of mice. *Signal Transduct. Target. Ther.* 7, 259. doi:10.1038/s41392-022-01054-3

Yu, D. H., Yi, J. K., Yuh, H. S., Park, J. S, Kim, J. H, Bae, K. B., et al. (2012). Over-expression of extracellular superoxide dismutase in mouse synovial tissue attenuates the inflammatory arthritis. *Exp. Mol. Med.* 44, 529–535. doi:10.3858/emm.2012.44.9.060

Zhuo, Z., Wan, Y., Guan, D., Ni, S., Wang, L., Zhang, Z., et al. (2020). A loop-based and AGO-incorporated virtual screening model targeting AGO-mediated miRNA-mRNA interactions for drug discovery to rescue bone phenotype in genetically modified mice. *Adv. Sci.* 7, 1903451. doi:10.1002/advs.201903451

frontiers | Frontiers in Pharmacology

TYPE Original Research
PUBLISHED 30 November 2022
DOI 10.3389/fphar.2022.1051694

Check for updates

OPEN ACCESS

EDITED BY
Fareeha Anwar,
Riphah International University (Lahore), Pakistan

REVIEWED BY
Syed Mohammed Basheeruddin Asdaq, University of Almaarefa, Saudi Arabia
Salim Bouchentouf, University of Saida, Algeria

*CORRESPONDENCE
Xiuge Gao,
vetgao@njau.edu.cn

†These authors have contributed equally to this work and share first authorship

SPECIALTY SECTION
This article was submitted to Predictive Toxicology, a section of the journal Frontiers in Pharmacology

RECEIVED 23 September 2022
ACCEPTED 17 November 2022
PUBLISHED 30 November 2022

CITATION
Wang J, Jing X, Hua L, Zheng Y, Hu S, Xiao J, Guo D, Wu W, Ji H, Peng L, Jiang S and Gao X (2022), Hypertension related toxicity of chloroquine explains its failure against COVID-19: Based on rat model.
Front. Pharmacol. 13:1051694.
doi: 10.3389/fphar.2022.1051694

COPYRIGHT
© 2022 Wang, Jing, Hua, Zheng, Hu, Xiao, Guo, Wu, Ji, Peng, Jiang and Gao. This is an open-access article distributed under the terms of the Creative Commons Attribution License (CC BY). The use, distribution or reproduction in other forums is permitted, provided the original author(s) and the copyright owner(s) are credited and that the original publication in this journal is cited, in accordance with accepted academic practice. No use, distribution or reproduction is permitted which does not comply with these terms.

Hypertension related toxicity of chloroquine explains its failure against COVID-19: Based on rat model

Junqi Wang[1,2†], Xian Jing[1,2†], Lizhong Hua[3], Yuling Zheng[1,2], Shiheng Hu[1,2], Jing Xiao[1,2], Dawei Guo[1,2], Wenda Wu[1,2], Hui Ji[1,2], Lin Peng[1,2], Shanxiang Jiang[1,2] and Xiuge Gao[1,2]*

[1]MOE Joint International Research Laboratory of Animal Health and Food Safety, College of Veterinary Medicine, Nanjing Agricultural University, Nanjing, China, [2]Engineering Center of Innovative Veterinary Drugs, Center for Veterinary Drug Research and Evaluation, Nanjing Agricultural University, Nanjing, China, [3]School of Animal Husbandry and Veterinary Medicine, Jiangsu Vocational College of Agriculture and Forestry, Jurong, Jiangsu, China

Chloroquine was once thought to be a promising treatment for COVID-19 but it quickly failed due to its inefficiency and association with increased mortality. Further, comorbidities such as hypertension may have contributed this failure. The safety and toxicity of chloroquine at doses required for treating SARS-CoV-2 infection in hypertensive patients remain unknown. Herein, to investigate these effects, we performed a safety evaluation of chloroquine at the approved dose (63 mg/kg) and at a high dose (126 mg/kg) in hypertensive rats. We found that chloroquine increased the mortality of hypertensive rats to 18.2% and 100%, respectively, after 7 days. During the chloroquine exposure period, the bodyweight, feed, and water consumption of hypertensive rats were decreased significantly. In addition, we show that chloroquine induces prolongation of QTc interval, elevation of LDH and CK, and histopathological damage of the myocardium in hypertensive rats. Ocular toxicity was observed in hypertensive rats in the form of hemorrhage in the eyes and retinal damage. Furthermore, we also observed intestinal toxicity in hypertensive rats, which presented as thinning intestinal walls with hemorrhagic contents, and histopathological changes of the jejunum. Hepatotoxicity was also evidenced by elevated ALT, and vacuolization of hepatocytes was also observed. Nephrotoxicity was observed only in high dose chloroquine-treated hypertensive rats, presenting as alterations of urinalysis and renal function. Immune alterations were also found in high-dose chloroquine-treated hypertensive rats with elevation of serum IL-10, IL-1β and GRO, and moderate damage to the spleen. In summary, this study partially explains the reason for the failure of chloroquine as a COVID-19 therapy, and underlines the importance of safety evaluation and medical supervision of chloroquine to avoid patient harm, especially to those with hypertension.

KEYWORDS

COVID-19, safety evaluation, antiviral drug, toxicology, chloroquine, hypertension

Introduction

Chloroquine (CQ), a 4-aminoquinoline drug, has long been extensively used for controlling malaria and certain autoimmune diseases, including rheumatoid arthritis and systemic lupus erythematosus (Slater, 1993). Since the emergence of widespread resistance in *Plasmodium falciparum* and CQ-induced acute poisoning and death, the market value of CQ has declined, leading to its replacement with its analogue, hydroxychloroquine, which is safer and much more efficacious (Nirk et al., 2020). Recently, CQ has gained increased global attention due to its initial promise as a potential antiviral agent for combating SARS-CoV-2 in early preclinical studies (Huang et al., 2020; Multicenter collaboration group of Department of Science and Technology of Guangdong Province and Health Commission of Guangdong Province for chloroquine in the treatment of novel coronavirus pneumonia, 2020). Given the absence of specially approved drugs for use in COVID-19 cases and the impact of the ongoing COVID-19 pandemic, these exciting findings on the *in vitro* efficacy of CQ and hydroxychloroquine against SARS-CoV-2, along with preliminary clinical observations, prompted clinical trials and the emergency use of chloroquine worldwide (U.S. Food & Drug Administration, 2020; European Medicines Agency, 2020). Since then, numerous clinical trials of CQ and hydroxychloroquine, at various doses and regimens, were carried out during the fight against COVID-19 (Axfors et al., 2021). CQ and hydroxychloroquine were subsequently approved for emergency use in hospitalized COVID-19 patients by the Food and Drug Administration (FDA) and the European Medicines Agency (EMA) early on in the pandemic (U.S. Food & Drug Administration, 2020; European Medicines Agency, 2020). In China, CQ was officially recommended as a clinical trial drug for treating COVID-19 in the sixth edition of the Diagnosis and Treatment Program of COVID-19 (National Health Commission of the People's Republic of China, 2020). However, the promise of CQ and hydroxychloroquine faded quickly following disappointing outcomes from large randomized clinical trials, as confirmed by the World Health Organization (Consortium et al., 2021). The WHO declared that the failure of CQ/hydroxychloroquine against COVID-19 was due to invalid anti-SARS-CoV-2 effects, along with multiple side effects and increased mortality (Boulware et al., 2020; Axfors et al., 2021). Subsequently, all clinical trials and the emergency use of CQ for treating COVID-19 were completely halted in most countries based on these findings, which showed no benefits of CQ/hydroxychloroquine treatment and increased potential risks (Consortium et al., 2021). However, treatment of COVID-19 with CQ continued in some countries, including China (National Health Commission of the People's Republic of China, 2021) and India (Dinesh et al., 2021). Various publications have summarized and discussed the controversial journey of CQ/hydroxychloroquine (Das et al., 2021; Megarbane, 2021; Shah, 2021). However, the exact reasons underlying its failure against COVID-19 remain unclear; they may involve the narrow window between the CQ dosages related to toxicity and efficacy against SARS-CoV-2 strains.

On one hand, CQ has been demonstrated incompatible results against SARS-CoV-2 in different *in vitro* models (Hoffmann et al., 2020), suggesting its uncertain antiviral effects in further clinical trials. On the other hand, the dose and regimens of CQ and hydroxychloroquine were substantially higher than recommended in malaria or rheumatological conditions (Organization, 2015), leading to increased mortality and multiple side effects in hospitalized COVID-19 patients (Axfors et al., 2021). In addition, the physical health of some SARS-CoV-2-infected patients were very complicated because about 60–90% of hospitalized patients had comorbidities (Wiersinga, Rhodes, Cheng et al., 2020). This presented a challenge in terms of the safety evaluation of drugs used in clinical trials. Among these comorbidities, hypertension, one of the most common risk factors, has been linked to severe illness and mortality in COVID-19 (Zhou et al., 2020; Peng et al., 2021). A large-scale clinical trial including 5,700 individuals confirmed that COVID-19 patients hospitalized in the United States considered hypertension (56.6%) as the most common comorbidity (Rosenberg et al., 2020). Similar high rates of hypertension in hospitalized COVID-19 patients were found in clinical trials carried out in other countries, including, but not limited to China and Italy (Grasselli et al., 2020; Zhou et al., 2020). Importantly, hypertension alters metabolic status and SARS-CoV-2 infection damages multiple organs, especially the liver and lungs, thereby presenting a challenge for further safety evaluation of experimental anti-COVID-19 drugs in the clinic. Therefore, we hypothesized that hypertension may affect the determination of the safety and efficacy of CQ in clinical trials for treating COVID-19. In addition, CQ has been extensively used for suicide since the 1980s in France and Zimbabwe, among others (Riou et al. Baud, 1988; Clemessy et al., 1996; Ball et al. Nhachi, 2002). Unfortunately, CQ overdose has been the cause a large number of deaths. Ingestion of CQ in overdose induces hypotension, arrhythmias, acute dyspnea, coma, and fatal cardiac arrest, which are lethal risk factors during CQ self-poisoning. Taken together and considering that hypertension is one of the most common basic diseases in the elderly population, which is also the population that is most affected by severe COVID-19, this raising the question of whether CQ is safe to hypertensive individuals in clinical trials. Therefore, it is critically important to elucidate the potential toxic effects of CQ in models of hypertension. Moreover, such an investigation will also further accelerate the repurposing process of CQ for treatment of coronavirus related diseases.

In this study, to avoid the harmful effects induced by the irrational use of CQ in the general population, especially during the COVID-19 pandemic, and to further understand the potential toxic effects of CQ in hypertensive patients, we sought to investigate the toxicity of CQ by employing hypertensive rats due to animal disease model is one of the most efficient approaches to reveal potential toxicity and health

risk of chemicals, which will further help clinical pharmacists to recognize and avoid drug-induced risks especially the drugs on trial. Therefore, the present work focused on three aspects: 1) evaluating the safety of CQ in hypertensive rats using equivalent doses for anti-SARS-CoV-2 treatment; 2) understanding the toxic effects of CQ on hypertensive rats; 3) trying to elucidate the reason behind CQ toxicity and subsequent failure during the COVID-19 pandemic.

Materials and methods

Reagents and drugs

Nω-Nitro-L-arginine methyl ester hydrochloride (L-NAME, Sigma-Aldrich, N5751, St. Louis Missouri, United States), chloroquine phosphate (CQ, Aladdin, C129284, Shanghai, China), diethyl ether (Sinopharm Chemical Reagent, 10009318, analytical reagent, Shanghai, China), 4% paraformaldehyde (Biosharp, BL539A, Hefei, China), 0.9% (w/v) sodium chloride (Guojing Pharmaceutical Co., Ltd, Lishui, Zhejiang, China). Chloroquine phosphate was freshly prepared before use.

Animals

Male specific pathogen free (SPF) Wistar rats (N = 80, 5 weeks old, 200–250 g) were purchased from Charles River (Beijing Vital River Laboratory Animal Technology Co., Ltd., Beijing, China). All rats were reared in rooms of the experimental animal center of Nanjing Agricultural University. Three or four rats were kept per cage in the barrier system with constant-humidity (55% ± 5%), constant-temperature (24°C ± 1°C), and a natural 12 h/12 h light-dark cycle. Each rat was provided with sufficient diet obtained from Jiangsu Xietong, Inc. (Nanjing, China) and clean drinking water. The detailed composition of diet for all rats in this study is in accord with the formulation of AIN-93G (Reeves et al., 1993). The animal protocols carried out in this work were evaluated and approved by the Committee on Animal Welfare and Ethics of Nanjing Agricultural University (No.20210514069) in accordance with the Regulations on the Administration of Laboratory Animals in China.

Hypertensive rat model

A hypertensive rat model was established according to previous published protocols with minor alteration (Adaramoye et al., 2012; Lerman et al., 2019). Briefly, after a week of acclimatization, sixty 6-week-old rats (250 g ± 20 g) were randomly divided into two groups, namely, the normal control group (n = 10), and the model group (n = 50). Rats in the model group were treated by intraperitoneal (i.p.) injection of the non-specific NOS inhibitor, L-NAME, at a dose of 20 mg/kg twice daily for 6 weeks (Rees et al. Moncada, 1990; Bader, 2010). All rats in the control group received an equal volume of saline *via* i.p. injection. During the hypertension modeling period, rats were fed with the standard diet and clean tip water in the experimental environment. Rat tail artery pressure was measured by performing a non-invasive blood pressure measurement and analysis system (BP 2000, Softron, Beijing, China) at a fixed time every week. The systolic blood pressure (SBP) and the diastolic blood pressure (DBP) of rats in an awake and quiet state were recorded using a computerized data acquisition system (Softron, Beijing, China). SBP and DBP measurements were conducted three or four times to obtain average value. After administration of L-NAME for 6 weeks, rats with SBP (>160 mmHg) and DBP (100 mmHg) were used for subsequent studies. In addition, to avoid recovery of blood pressure, a low dose of L-NAME (10 mg/kg, once daily) was injected once daily in the morning 2 h before administration of CQ.

Dosage regimen of CQ in hypertensive rats

The hypertensive rats were randomly divided into three groups: 1) saline (n = 9, control group), 2) 63 mg/kg CQ (n = 11, equivalent to clinical dosage), 3) 126 mg/kg CQ (n = 12, high dose). These doses of CQ used in rats were equivalent to the human dose by calculation using the following formula: Animal equivalent dose (AED; mg/kg) = Human dose (HED; mg/kg) × Km ratio, where Km ratio = (Human Km / Animal Km), Km is estimated by dividing the average body weight (kg) of the species to its body surface area (m^2) (Xu et al., 2002). Nine healthy rats were used as negative controls in the following experiments. CQ solution and saline were administered to rats by gavage twice daily for seven consecutive days. During the administration period of CQ, all rats were given a standard diet and clean water *ad libitum*. A schematic diagram of animal experiments is shown in Figure 1.

Clinical observations

All rats were observed for any changes once daily during the acclimatization period and twice daily during the treatment period. Detailed clinical observations included behavior, reaction to treatment, or ill-health. Any abnormal conditions were recorded at the time in terms of nature and severity, date and time of onset, and duration. Observations for viability/mortality, food intake, and water consumption were recorded daily. Rats were weighed every 2 days. In addition, eye reactions of all rats were inspected visually twice daily after CQ administration.

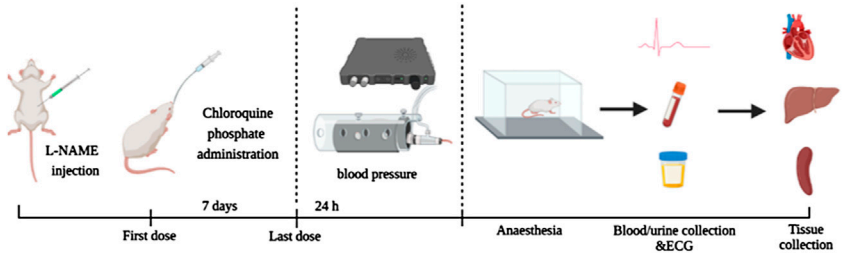

FIGURE 1
Schematic diagram of animal experiment.

Blood pressure (BP) determination

To understand the effects of CQ on SBP and DBP in rats, tail-cuffing was carried out every 3 days as previously described. Briefly, SBP and DBP of rats in an awake and quiet state were measured three or four times to obtain average values used for further analysis. All rats were monitored until they were too weak to support the BP assessment.

Electrocardiogram monitoring

In order to explore the effect of CQ on the heart rhythm of rats, we monitored the electrocardiogram on the eighth day. Five rats in each group were anesthetized with diethyl ether. After the rats were stabilized, ECG monitoring was carried out by performing BL-420N computerized bio-signal acquisition system (TaiMen, Chengdu, China) for at least 10 min according to previous report (Gao et al., 2022). After ECG of Rats in each group were collected, we analyzed the changes of rat cardiac cycle by statistical PR, QRS and QT intervals. The sudden deaths of rats received high-dose CQ on day 6 prevent us from performing ECG examinations at the pre-planned time. Unfortunately, rats in the approved and high dose of CQ group were extremely weak and could not support anaesthetization before ECG, making the urgent ECG monitoring on day 6.

Biological sample collection and pretreatment

At the end of the CQ administration period, all rats except those in the high-dose CQ treatment group were fasted for 12 h before the collection of rat plasma, serum, urine and organic tissues. Importantly, samples from rats in the high-dose CQ group were emergency collected on day 6 due to poor health and alarming mortality of most rats in this group. Three rats in the high-dose CQ group and five rats in each other group were selected to use metabolic cages for urine collection, and urine test within 1 h of sample collection. Next, we collected at least five copies of whole blood from rats in each group *via* the jugular vein. Here, 200 μl of blood was obtained from each rat and transferred to a EDTA tube for hematological examination. Subsequently, 800 μl of blood was collected from each rat in a non-anticoagulant tube, which was then centrifuged at 1,000 × g at 4°C for 10 min to obtain serum. After centrifugation, we obtained rat serum of each group at least in triplicate used for biochemical analysis and cytokine determination. The collected rat blood plasma was stored at 4°C and analyzed within 4 h while serum was stored at −20°C until further biochemical assessment and cytokine analysis. Furthermore, rats were kindly sacrificed under general anesthesia with anatomical examination, followed by collection of organs, including the heart, liver, spleen, lungs, kidneys, duodenum, jejunum, ileum, cecum, colon, rectum, skeletal muscle, pancreas, stomach, thymus, testicles, bladder, and eyeballs. The heart, liver, spleen, lungs, kidneys, and testicles were weighed to analyze organic index, whereby organ index = organ weight (g) * 100/body weight (g). The organ tissues were collected with minimum artificial damage in suitable sizes used for further histopathological examination. All obtained rat tissues, in triplicate, from each group were immediately immersed in 4% paraformaldehyde solution, and eyeballs were stored in Davidson's fixative solution for further histopathological examination as described below.

Hematological analysis

Hematological changes of hypertensive rats treated with different doses of CQ were detected using an automatic blood counter system (Mindray, Shenzhen, China). These hematological parameters included red blood cell (RBC), hematocrit (HCT), mean red blood cell volume (MCV), hemoglobin (HGB), mean corpuscular hemoglobin (MCH), mean corpuscular hemoglobin concentration (MCHC), RBC distribution width (RDW- SD), white blood cells (WBC), lymphocyte count (LYM), monocytes (MONO), neutrophils (NEUT), eosinophils (EO), basophils (BASO), platelets (PLT) and mean platelet volume (MPV). The obtained plasma samples were analyzed within 4 h of sampling.

Serum biochemical measurement

We detected serum biochemical changes, including glucose (GLU), total protein (TP), albumin (ALB), globulin (GLB), total bile acid (TBA), alanine aminotransferase (ALT), aspartame acid aminotransferase (AST), total bilirubin (T-BIL), alkaline phosphatase (ALP), lactate dehydrogenase (LDH), creatine kinase (CK), creatinine (Cr), uric acid (UA), total cholesterol (TC), triglycerides (TG), high-density lipoprotein cholesterol (HDL-C), low-density lipoprotein cholesterol (LDL-C), and amylase (AMY). Rat sera, at least in triplicate per group, were tested using an automatic biochemical analyzer (Beckman Coulter AU5800, Brea, CA, United States).

Urinary assay

Next, routine urine examination was carried out using a urine analyzer (Mindray, Shenzhen, China). The urine parameters include specific gravity, pH, WBC, nitrite, urobilinogen, protein, occult blood, ketone bodies, bilirubin, GLU, and vitamin C were tested and analyzed within 1 h of sample collection. Urine samples, at least in triplicate per group, were analyzed according to the manufacturer's instructions.

Serum cytokine assay

To further investigate the effect of CQ on cytokine levels in rat sera, multiple cytokines (TNF-α, IFN-γ, IL-1β, IL-4, IL-6, IL-2, IL-5, GRO/KC, IL-12p70 and IL-10) were analyzed using multiplex immunoassays on a Luminex xMAP (multi-analyte profiling) instrument (Luminex-200, Austin, America) with a commercial kit (LX-MultiDTR-10, LabEx, Shanghai, China) according to the manufacturer's instructions. In brief, the fluorescently labeled microspheres for different test substances were mixed, and the test substance or the amplified fragments were added to react with the labeled fluorescein. Driven by the flowing sheath fluid, the microspheres were passed through the red and green lasers in sequence in the Luminex-200 system (Luminex, Austin, United States). The obtained fluorescence values were translated to a concentration for the relevant cytokine based on previous established standard curves.

Histopathological examination

The obtained tissues, in triplicate per group, were used for histopathological analysis. Tissue slice preparation and staining procedures were carried out according to a previous study (Gao et al., 2022). Briefly, the fixed tissues were dehydrated, followed by transparency and embedding in paraffin for cutting into thin slices. The prepared tissue sections were subjected to hematoxylin and eosin (H&E) staining. Histopathological changes of each tissue slice were observed and photographed under a light microscope (Leica, Buffalo Grove, United States).

Statistical analysis

The data are presented as mean ± standard deviation (SD). Data were analyzed using SPSS (20.0 version, IBM, Chicago, United States) and tested by conducting two-way analysis of variance (ANOVA) along with the least-significant difference (LSD) test. A p value less than 0.05 was set as statistical differences in this study. In addition, log-rank (Mantel-Cox) test were performed to analyze the significance between different survival curves.

Results

CQ induces toxic effects and sudden death in hypertensive rats

During the dosing period, clinical signs such as depression, decreased activity, slow response to external stimuli were observed in rats in the 126 mg/kg CQ group on day 3, and the same symptoms were occurred in several rats in the 63 mg/kg CQ group on day 5. With increased CQ exposure, visible weight loss, ruffled fur, prostration, and weakened conditions were noted in most rats treated with both the approved dose and the high dose of CQ. In contrast, there were no abnormal signs in rats in the negative control group and hypertensive rats not receiving CQ. Subsequently, four rats in the high-dose CQ group were found dead on day 5, however, the mortality rate increased dramatically on day 6 after CQ treatment. At the end of CQ administration, compared with the 100% survival rate of hypertensive rats receiving saline, the survival rate of 63 mg/kg and 126 mg/kg CQ treated hypertensive rats decreased to 81.8% and 0% ($p < 0.0001$), respectively (Figure 2A). In addition, the feed intake and water consumption of hypertensive rats declined visibly after CQ treatment ($p < 0.0001$), while the water consumption of hypertensive rats received normal saline increased in comparison with healthy rats (Figures 2B,C). Moreover, the body weight of hypertensive rats decreased dramatically following CQ exposure, especially in the high-dose CQ group ($p < 0.0001$), compared to saline-treated animals (Figure 2D). Furthermore, during the entire administration period, the BP of hypertensive vehicle rats remained high. In contrast, at the last monitoring, the SBP and DBP of hypertensive rats receiving high-dose CQ were significantly decreased ($p < 0.01$), but BP returned to baseline (Figures 2E,F). Finally, as shown in Table 1, CQ increased several organ indexes of hypertensive rats compared to healthy rats and hypertensive rats that received

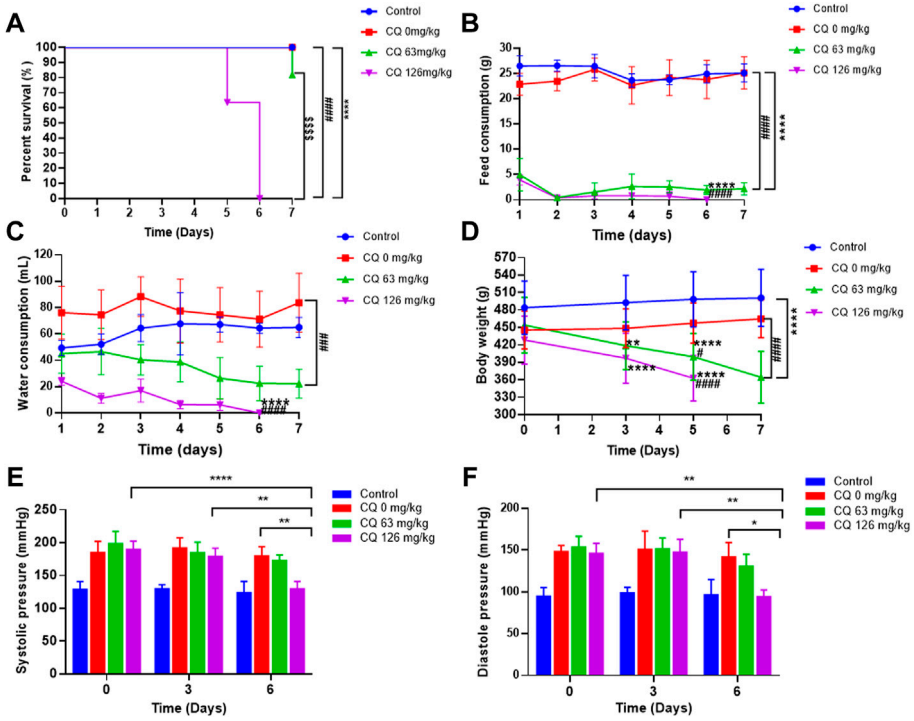

FIGURE 2
Effect of CQ on survival rate, feed and water consumption, body weight, and blood pressure of rats. Healthy and hypertensive rats orally administrated saline and CQ at two doses (63 mg/kg or 126 mg/kg) twice daily for seven consecutive days. **(A)** The survival rate of rats was recorded daily. ****, $p < 0.0001$, compared to healthy rats; ####, $p < 0.0001$, compared to hypertensive rats; $$$$, $p < 0.0001$, compared to CQ (63 mg/kg) group; Log-rank (Mantel-Cox) test were performed to analyze the significance between different survival curves. **(B, C)** The feed consumption and water consumption of rats were recorded daily. Data are shown as mean ± SD ($n = 3$); ****, $p < 0.0001$, and ####, $p < 0.0001$, compared to healthy and hypertensive rats, respectively;For water consumption, ###, $p < 0.001$, compared with healthy rats. **(D)** The body weight of rats was recorded on the day 0, 3, 5, and 7 of CQ administration. Data are shown as mean ± SD ($n = 9–12$); **, $p < 0.01$, and ****, $p < 0.0001$, compared to healthy rats; #, $p < 0.05$ and ####, $p < 0.0001$, compared to hypertensive rats. **(E, F)** The systolic pressure and diastolic blood pressure of all rats were monitored on 3 d and 6 d after CQ administration. Data are shown as mean ± SD ($n = 3–12$); *, $p < 0.05$; **, $p < 0.01$; ****, $p < 0.0001$.

TABLE 1 Organ indexes of hypertensive rats changed after CQ exposure.

Organ	Control	Hypertensive rats		
		CQ (0 mg/kg)	CQ (63 mg/kg)	CQ (126 mg/kg)
Heart	0.303 ± 0.039	0.339 ± 0.031	0.45 ± 0.037$^{****\#\#\#\#}$	0.427 ± 0.063$^{***\#}$
Liver	2.694 ± 0.203	2.585 ± 0.187	3.134 ± 0.397$^{\#}$	3.685 ± 1.052$^{**\#\#}$
Spleen	0.222 ± 0.025	0.196 ± 0.035	0.242 ± 0.074	0.16 ± 0.034
Lung	0.448 ± 0.069	0.461 ± 0.02	0.481 ± 0.068	0.567 ± 0.181
Kidney	0.585 ± 0.066	0.631 ± 0.063	0.787 ± 0.182*	0.846 ± 0.17*
Testis	0.762 ± 0.097	0.854 ± 0.109	0.914 ± 0.12	0.889 ± 0.119

Note: Data are shown as mean ± SD ($n = 3–9$).
*, $p < 0.05$, compared with control group; ***, $p < 0.001$, compared with control group; ****, $p < 0.0001$, compared with control group; #, $p < 0.05$, compared with CQ (0 mg/kg) group; ##, $p < 0.01$, compared with CQ (0 mg/kg) group; ###, $p < 0.001$, compared with CQ (0 mg/kg) group.

saline, these organs included the heart and liver. Similarly, CQ exposure elevated the kidney index of hypertensive rats ($p < 0.05$), compared to the control group, but not hypertensive rats that received saline. However, other organs such as the spleen, lungs, and testicles of hypertensive rats were not significant changed after CQ treatment.

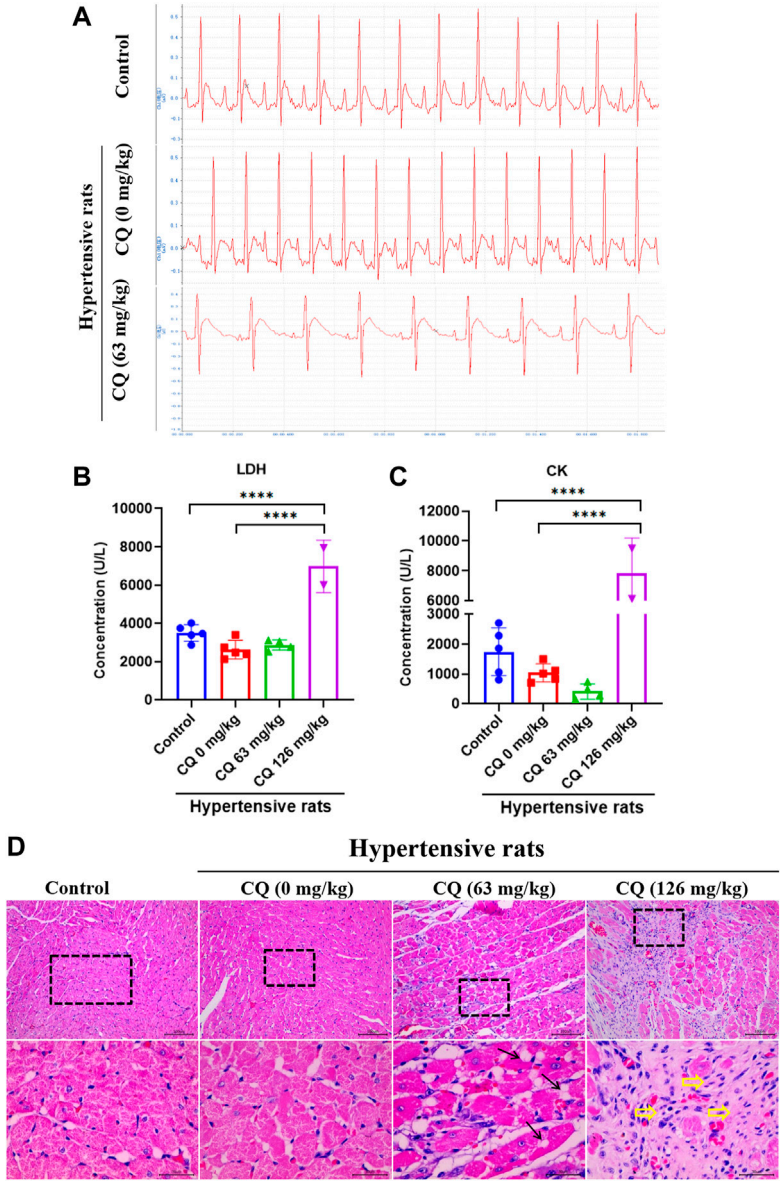

FIGURE 3
CQ damage to hearts in hypertensive rats. Healthy and hypertensive rats orally administrated saline and CQ at two doses (63 mg/kg or 126 mg/kg) twice daily for seven consecutive days. **(A)** ECG examination of CQ-treated hypertensive rats and rats in control group and negative group. **(B, C)** Effects of CQ on the levels of myocardial enzymes LDH and CK in rats at day 7. Data are shown as mean ± SD (n = 3–5); ****, $p < 0.0001$. **(D)** H&E staining of CQ-treated hearts in healthy rats and hypertensive rats at the end of drug administration period; Black arrows indicate vacuolar degeneration and yellow arrowheads present severe myocardial fibrosis and inflammatory cells infiltration; Bars = 30 μm or 100 μm.

CQ induces cardiotoxicity of hypertensive rats

Given the high mortality caused by CQ treatment, we next investigated the effect of CQ on the heart in hypertensive rats. Electrocardiogram (ECG) examinations showed that CQ (63 mg/kg) significantly prolonged the QT interval, but not the PR and QRS intervals in hypertensive rats, compared to healthy and hypertensive rats that had received saline (Figure 3A and Table 2). CQ (63 mg/kg) also decreased the heart rate (HR) of hypertensive rats significantly ($p < 0.05$) after the administration period (Table 2). Unfortunately, in this study, we failed to collect ECG parameters of high-dose CQ-treated hypertensive rats due to their poor health conditions and sudden death on day 6. In addition, to further understand the effect of CQ on cardiac functions of rats, we next determined myocardial

TABLE 2 Electrocardiogram changes of hypertensive rats induced by CQ.

Parameter	Control	Hypertensive rats	
		CQ (0 mg/kg)	CQ (63 mg/kg)
PR (ms)	52.17 ± 3.37	52.7 ± 3.75	59.81 ± 6.09
QRS (ms)	24.03 ± 2.77	23.52 ± 5.47	20.42 ± 2.01
QT (ms)	54.77 ± 6.74	66.13 ± 8.77	83.21 ± 12.44$^{**\#}$
HR (bpm)	392 ± 38.65	425.2 ± 25.4	330.8 ± 61.02$^{\#}$

Note: Data are shown as mean ± SD ($n = 5$); #, $p < 0.05$, compared with CQ (0 mg/kg) group; **, $p < 0.01$, compared with control group.

enzymes and histopathologic changes in CQ-treated hypertensive rats. As shown in Figures 3B,C, high-dose CQ significantly ($p < 0.0001$) elevated LDH and CK levels compared to healthy rats and hypertensive rats that had received saline. However, CQ (63 mg/kg) did not seem to induce any significant changes in LDH and CK in hypertensive rats (Figures 3B,C). Additionally, H&E staining results showed that CQ (63 mg/kg) caused obvious vacuolization degeneration in the hearts of hypertensive rats (black arrows in Figure 3D), and a large area of fibrotic tissue distribution and inflammatory cell infiltration were observed in hypertensive rats treated with CQ (126 mg/kg; yellow arrows in Figure 3D), while the heart slices of healthy rats and hypertensive rats that had received saline showed no marked changes (Figure 3D). In summary, CQ induced severe cardiotoxicity in hypertensive rats, especially at the high dose.

CQ induces ocular toxicity in hypertensive rats

Unfortunately, ocular toxicity was observed during CQ administration period, as shown in Figure 4A, blood secretions appeared in the corner of eyes from day 5 in hypertensive rats. In some severe conditions, blood was visible on the surface of eyeballs in hypertensive rats, especially in the high-dose CQ group on day 6. Subsequent histopathological examination showed that retina, crystalline lens and optic nerves in hypertensive rats were damaged to varying degrees (Figure 4B). Moreover, compared with healthy rats and hypertensive rats, high-dose CQ induced severe retina injuries as evidenced by bleeding in the nerve fiber layer in hypertensive rats treated with the approved dose of CQ, and vacuolar degeneration, as well as abnormal band formation in the inner and outer nuclear layers of high-dose CQ treated hypertensive rats. In addition, compared to animals in the approved CQ dose group, high-dose CQ induced irregular arrangement and slight swelling of the lens in hypertensive rats (Figure 4B). In addition, the optic nerves of hypertensive rats also displayed different degrees of vacuolar degeneration after two doses of CQ treatment. Other components in the eyes of hypertensive rats treated by CQ were not obviously changed (Supplementary Figure S1). In conclusion, CQ induces severe ocular toxicity in hypertensive rats.

CQ causes gastrointestinal toxicity in hypertensive rats

Considering that CQ caused a severe reduction in the feed and water consumption of hypertensive rats, we sought to further investigate whether intestinal toxicity was triggered by CQ. Anatomical examinations of rats revealed jejunums characterized by abnormal states, including thin jejunum walls, which were dark red in appearance with blood-containing intestinal contents (Figure 5A). In contrast, other intestinal segments of CQ-treated hypertensive rats were normal in appearance. In addition, intestinal changes in these rats were further analyzed by histopathological examination on jejunum samples. As shown in Figure 5B, compared to the control and hypertensive group, gastric hemorrhage and gastric villus disruption were observed in the approved- and high-dose CQ-treated hypertensive animals. The approved dose of CQ induced severe vacuolization of the bowel wall and intestinal villus disorder in the jejunums of hypertensive rats. However, high-dose CQ triggered more significant damage, including the shedding of intestinal villus and extreme vacuolization of the bowel wall in hypertensive rats (Figure 5B). Taken together, these data demonstrated that CQ induced varying degrees of gastrointestinal toxicity in hypertensive rats.

Chloroquine induces hepatotoxicity in hypertensive rats

Next, we evaluated the effect of CQ on the liver in hypertensive rats after the drug administration period. As shown in Figures 6A,B, compared with the negative control and hypertensive rats that had received saline, approved dose CQ significant increased ALT ($p < 0.01$) and AST ($p < 0.001$). Similarly, high-dose CQ also elevated ALT ($p < 0.0001$) and AST ($p < 0.0001$) in hypertensive rats significantly, compared to healthy rats and hypertensive rats that had received saline (Figure 6B). In addition, the levels of T-BIL, TBA and ALP in hypertensive rats were significant increased by high-dose CQ treatment ($p < 0.05$, $p < 0.01$, and $p < 0.001$, respectively), compared to healthy rats and hypertensive rats that had received saline (Figures 6C–E). In contrast, the levels of ALB in hypertensive rats were significant decreased in both CQ treatment groups compared to the negative control and hypertensive rats treated with saline (Figure 6F). However,

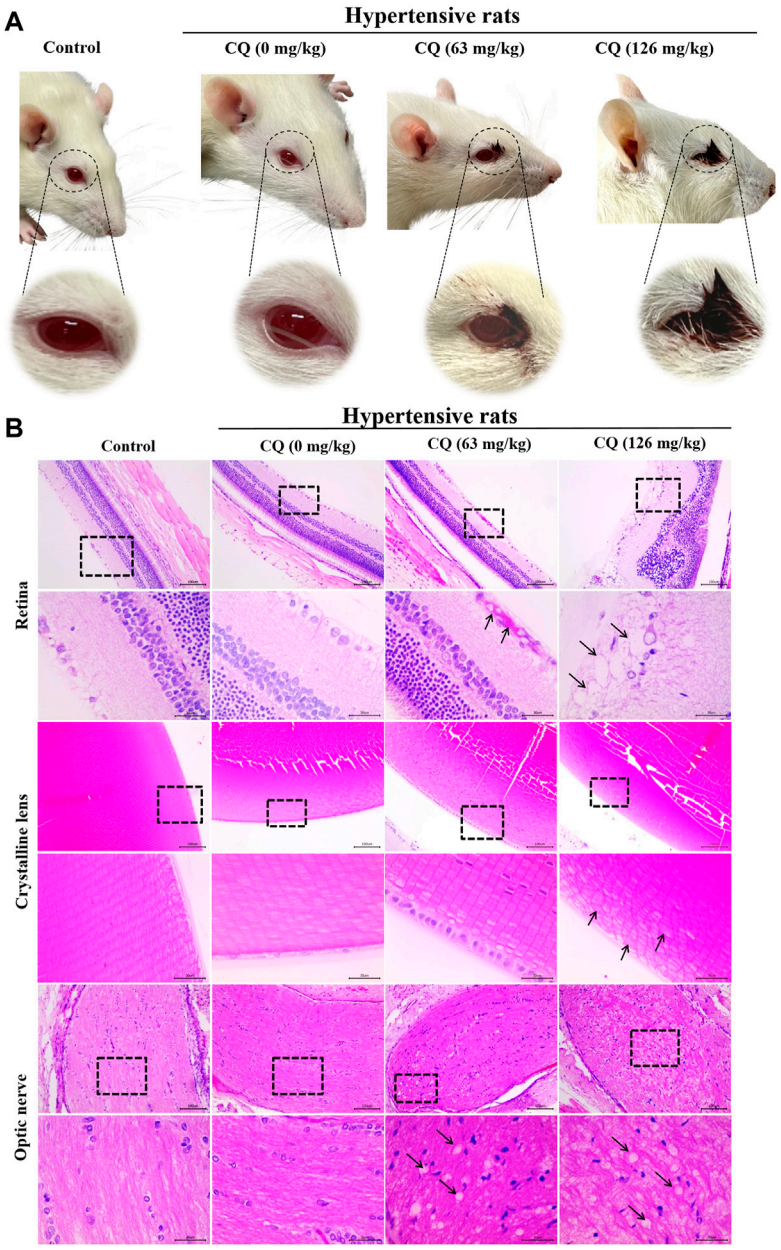

FIGURE 4
CQ induces ocular toxicity in hypertensive rats. Healthy and hypertensive rats orally administrated saline and CQ at two doses (63 mg/kg or 126 mg/kg) twice daily for seven consecutive days. **(A)** The ocular manifestation in CQ-treated hypertensive rats were observed during the CQ administration period. Blood secretions around eyes and visible hemorrhage on eyeballs were emerged in CQ-treated hypertensive rats. **(B)** Histopathological changes of the components of eyes in CQ-treated hypertensive rats. Rats received high-dose CQ showed obvious vacuolization of retinal nerve fiber layer, and hemorrhage was emerged in the nerve fiber layer of the approved dose CQ group. In high dose CQ group, crystalline lens was in disorder with slight swelling (black arrows). For optic nerve, two doses of CQ resulted in obvious vacuolar degeneration at different degrees in hypertensive rats (black arrows). Bars = 30 μm or 100 μm.

both doses of CQ did not change the levels of GLB and TP in hypertensive rats (Figures 6G,H). Furthermore, H&E staining showed that the approved dose of CQ induced a disorder of hepatic cords, vacuolar degeneration, which is consistent with hyperchromatic nuclei in liver cells (Figure 6I). The high-dose CQ resulted in more serious vacuolar degeneration of liver cells, along with the disorder of hepatic sinuses and hepatic lobules, and inflammatory infiltration around the central vein (Figure 6I). These above findings suggest that CQ induced dose-dependent liver damage and hepatotoxicity in hypertensive rats.

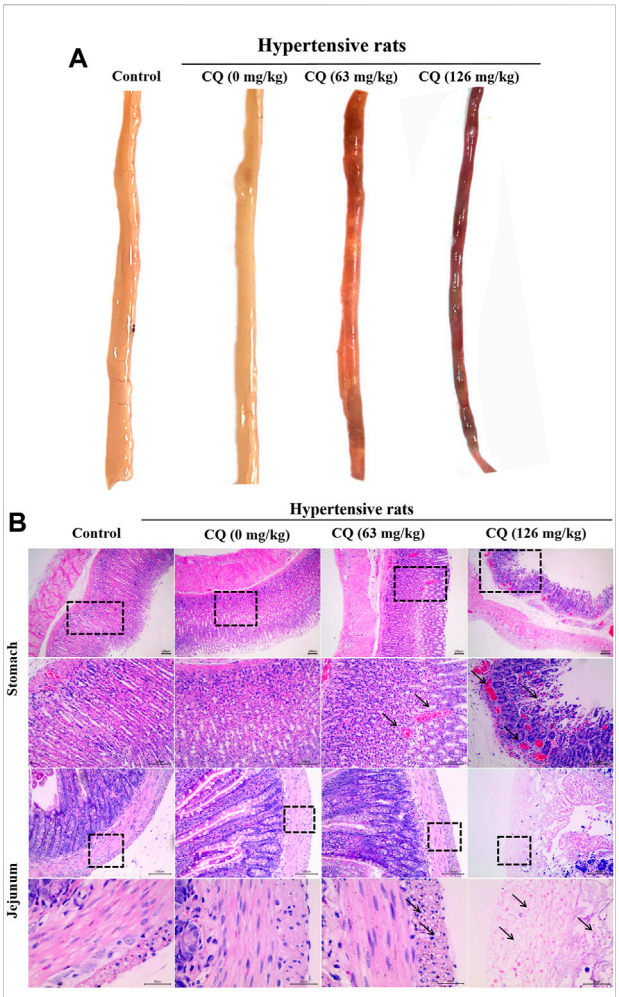

FIGURE 5
Effect of CQ on gastrointestinal tract of hypertensive rats. Healthy and hypertensive rats orally treated with saline and CQ at two doses (63 mg/kg or 126 mg/kg) twice daily for seven consecutive days. **(A)** Gross autopsy of jejunum in rats treated by CQ. Jejunum became thin and translucent, containing blood related intestinal contents, which was dark red in appearance. **(B)** Histopathological examination of stomach and jejunum in rats treated by CQ. Gastric hemorrhage and gastric villus disruption were found in CQ-treated hypertensive rats (black arrows). Severe vacuolization of intestinal wall and intestinal villus disruption/shedding were observed in CQ-treated hypertensive rats (black arrows). Representative images were obtained from at least triplicate experiments. Bars = 30 μm or 100 μm.

Chloroquine triggers nephrotoxicity in hypertensive rats

Given the CQ-induced changes in the kidney indices of hypertensive rats, we further investigated the effects of CQ on the kidneys. First, the effect of CQ on urine is shown in Table 3. Compared to healthy and hypertensive rats, leukocyte, protein and occult blood were positive in the urine of both CQ treatment groups. Nevertheless, other urinary parameters such as specific gravity, pH, nitrite, urobilinogen, ketone body, bilirubin, GLU, and vitamin C were not obviously changed after CQ treatment. Moreover, renal functions of hypertensive rats were evaluated by assessing the alterations of serum creatinine (Cr), uric acid (UA), and urea (Ur). As shown in Figures 7A–C, high-dose CQ but not the approved dose enhanced serum Cr, Ur and UA concentrations significantly ($p < 0.01$ or $p < 0.001$), compared to rats in the negative control and hypertensive groups. Finally, histopathological examination of kidneys was carried out and showed that renal tubular epithelial cells lose connection with slight staining following approved dose CQ exposure, and more serious injury of treated renal tubular epithelial cells was observed in high-dose CQ-treated hypertensive rats, showing extensive hyaline degeneration, dilation of kidney tubular lumen, and thinning of the renal tubular wall (Figure 7D). Collectively, these findings show that CQ causes dose-dependent kidney damage.

Chloroquine alters immune state of hypertensive rats

Furthermore, we investigated the effect of CQ on immunity in hypertensive rats at the end of the experimental period. First, blood immune cells were counted after CQ treatment (Table 4). Compared to the control and hypertensive groups, CQ significantly ($p < 0.0001$) decreased lymphocyte count in hypertensive rats. However, high-dose CQ treatment significantly increased the levels of monocytes ($p < 0.0001$) and eosinophils ($p < 0.05$ and $p < 0.0001$) in hypertensive rats (Table 4). The approved dose and high-dose CQ both enhanced the levels of neutrophils and basophils significantly, compared to those in the control ($p < 0.01$) and hypertensive groups ($p < 001$ and $p < 0.001$). There were no significant changes in WBCs after CQ treatment ($p > 0.05$). Second, analysis of serum inflammatory cytokines (Figures 8A–J) showed that high-dose CQ but not the approved dose CQ, elevated levels of IL-10 ($p < 0.001$ and $p < 0.0001$), IL-1β ($p < 0.01$) and GRO/KC ($p < 0.05$ and $p < 0.01$) compared to rats in the control and hypertensive groups. Nevertheless, the levels of serum IL-2, IL-4, IL-5, IL-6, IFN-γ, TNF-α, and IL-12p70 in hypertensive rats were not altered after two doses of CQ exposure (Figure 8). Lastly, histopathological changes in the spleens of CQ-treated rats were examined by H&E staining. CQ exposure caused slightly vacuolar degeneration (Figure 8K; black arrows) and slight stained nucleus. These findings suggest that CQ alters immune status and promotes inflammation in hypertensive rats.

Discussion

Following the repurposed use of CQ and its derivatives for treating COVID-19, numerous clinical studies and critical reviews have been carried out to evaluate the safety and

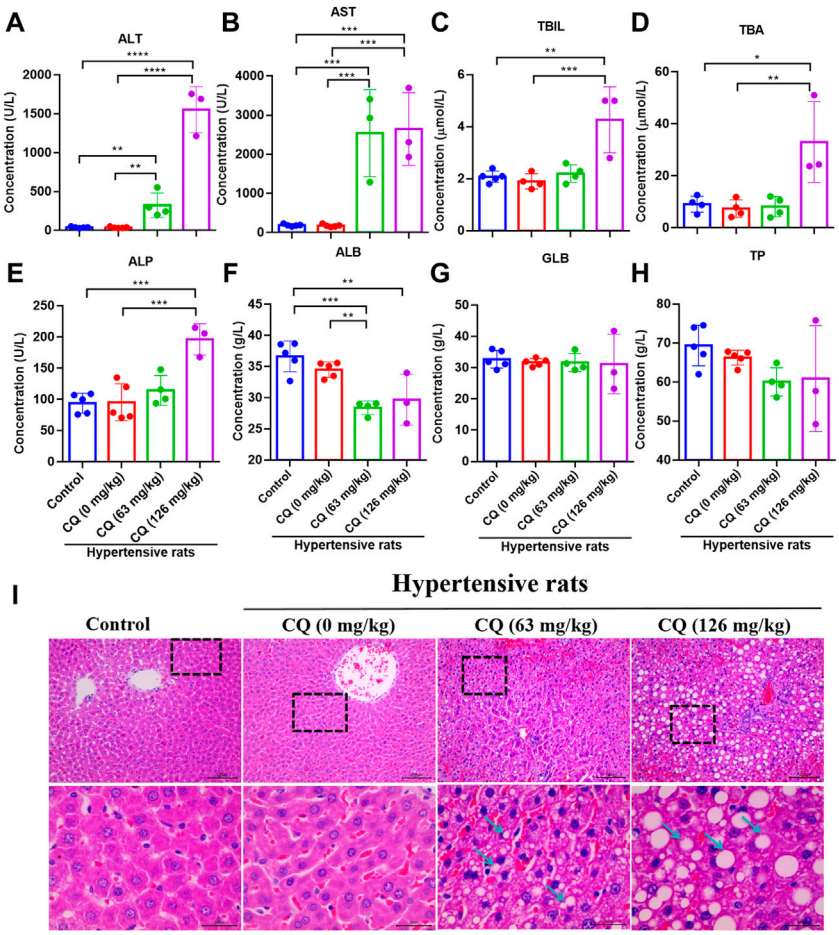

FIGURE 6
CQ alters hepatic enzymes and damages liver tissues. Healthy and hypertensive rats orally treated with saline and CQ at two doses (63 mg/kg or 126 mg/kg) twice daily for seven consecutive days. **(A-H)** The effects of CQ on hepatic enzymes in serum of hypertensive rats. Data are shown as mean ± SD (n = 3–5); ALB, albumin; GLB, globulin; TP, total protein; T-BIL, total bilirubin; AST, aspartate aminotransferase; ALT, alanine aminotransferase; TBA, total bile acid; ALP, alkaline phosphatase. *, $p < 0.05$; **, $p < 0.01$; ***, $p < 0.001$; ****, $p < 0.0001$. **(I)** Histopathological examination of liver in healthy rats and hypertensive rats after CQ treatment. The representative photographs of liver slices, vacuolar degeneration, disorder of hepatic cords and hepatic lobules are indicated by blue arrows. Scale bar was 30 μm or 100 μm.

efficacy of CQ/hydroxychloroquine (Axfors et al., 2021; Das et al., 2021; Junqueira and Rowe, 2021). Although CQ and hydroxychloroquine held some promise as potentially effective anti-SARS-CoV-2 agents during the early stages of the COVID-19 pandemic, they subsequently failed due to safety concerns and a lack of efficacy as shown in international large-scale randomized clinical trials (Consortium et al., 2021). The controversial journey of CQ/hydroxychloroquine prompted a series of scientific questions (Shah, 2021). For example, what is the safety range of CQ in patients with complications? Why did the use of CQ/hydroxychloroquine relate to higher mortality in COVID-19 patients following completion of clinical trials? What toxic events contribute to the failure of CQ in COVID-19 treatment regimens? We sought to answer some of these questions in this work.

Herein, we found that approved- and high-dose CQ induced significant death in hypertensive rats in a concentration-dependent manner. This was consistent with findings obtained from randomized clinical trials of CQ and hydroxychloroquine, showing that a high dosage of CQ (600 mg CQ twice daily for 10 days) caused more toxic effects and lethality in critically ill COVID-19 patients with heart disease (Borba et al., 2020). Unfortunately, our data also agrees with conclusions from the international collaborative meta-analysis in which hydroxychloroquine has been demonstrated to associate with high mortality in COVID-19 patients, while CQ presents no benefits against SARS-CoV-2 infection (Axfors et al., 2021). Although the enrolled patients tolerated low doses of CQ or hydroxychloroquine well in other clinical trials, adverse

TABLE 3 Effect of CQ on urine indexes in hypertensive rats.

Test items		Control	Hypertensive rats		
			CQ (0 mg/kg)	CQ (63 mg/kg)	CQ (126 mg/kg)
Quantitative measures					
Specific gravity		1.016 ± 0.005	1.023 ± 0.008	1.027 ± 0.004	1.027 ± 0.003
pH		6.5 ± 0	6.4 ± 0.548	6 ± 0.354	6 ± 0
Qualitative measures					
Leukocyte	Negative	5	3	1	0
	Trace	0	1	1	0
	1+	0	0	3	0
	2+	0	1	0	2
	3+	0	0	0	1
Nitrite	Negative	5	3	5	2
	1+	0	2	0	1
Urobilinogen	Negative	5	5	5	3
Protein	Negative	2	0	0	0
	Trace	2	0	0	0
	1+	1	0	0	0
	2+	0	3	2	0
	3+	0	2	3	3
Occult blood	Negative	5	5	2	1
	1+	0	0	3	0
	3+	0	0	0	2
Ketone body	Negative	5	2	4	2
	Trace	0	3	1	1
	1+	0	0	0	0
Bilirubin	Negative	5	5	4	3
	1+	0	0	1	0
	2+	0	0	0	0
Glucose	Negative	5	5	5	3
Vitamin C	Negative	5	5	5	3

events are often observed in COVID-19 patients (Self et al., 2020; Rea-Neto et al., 2021; Izcovich et al., 2022). Concerning the narrow safety range of CQ for treating viral diseases, the current approved doses and regimens may contribute to its mortality outcomes in the COVID-19 pandemic (Lacout et al. Perronne, 2021). In this regard, discussions on the dose selection of CQ and hydroxychloroquine were undertaken to provide optimized dose regimens for patients with varied conditions (Cui et al., 2020; Lacout et al., 2021). In addition to the dose regimens of CQ, the comorbid conditions of patients (e.g. heart disease and hypertension) may affect the outcomes of clinical evaluation (Gabor et al., 2021), unfortunately, persons with comorbidities were excluded in most trials, leading to a lack of available data for patients in these subgroups (Skipper et al., 2020; Tang et al., 2020). For hypertensive patients, CQ plays an antihypertension role as shown in one preclinical study (Wu et al., 2017), which is consistent with our data. However, the antihypertension function of CQ was of no benefit in terms of its efficacy in COVID-19 trials. Further studies are required to elucidate the mechanisms behind the antihypertensive effects of CQ.

In addition to the mortality induced by CQ in overdose, several toxic events were also recorded in hypertensive rats. Among these toxicities, cardiotoxicity may play a lethal role because of CQ induced QT interval prolongation related cardiac dysfunction. While CQ-induced cardiac disorder is rare in healthy individuals, this risk increases in patients at high-risk of drug-induced QT prolongation (Tleyjeh et al., 2021). Hypertension is a common complication in COVID-19 patients and may contribute to a high risk of cardiotoxicity, which has been demonstrated in several clinical trials and systematic reviews (Mercuro et al., 2020). Additionally, SARS-CoV-2 infection also induces

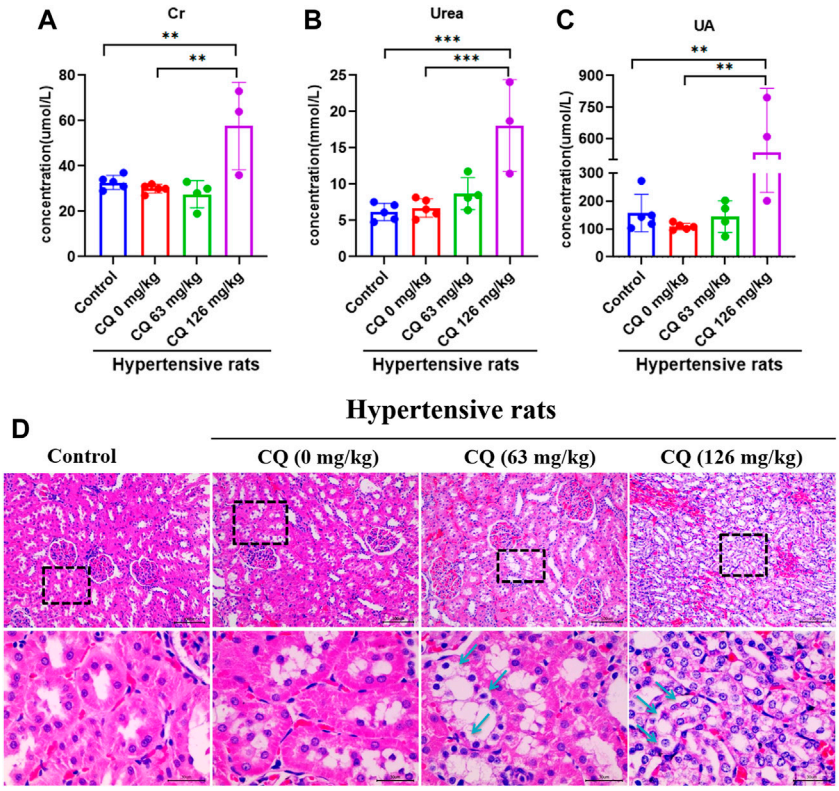

FIGURE 7
CQ induces nephrotoxicity of hypertensive rats. Healthy and hypertensive rats orally administrated saline and CQ at two doses (63 mg/kg or 126 mg/kg) twice daily for seven consecutive days. **(A–C)** The administration of high-dose CQ (126 mg/kg) elevated the hematological renal function indexes of hypertensive rats. Data are shown as mean ± SD (n = 3–5); Cr, creatinine; Ur, urea; UA, uric acid. **, $p < 0.01$; ***, $p < 0.001$. **(D)** CQ induced pathological damage of kidneys in hypertensive rats. Tubular epithelial cells loose connection with hyaline degeneration (black arrows) were observed in kidney slices of hypertensive rats treated with CQ (63 mg/kg), and extensive hyaline degeneration, dilation of kidney tubular lumen, and thinning of renal tubular wall (black arrows) were shown in kidney slices of hypertensive rats exposed to high dose CQ. Bars = 30 μm or 100 μm.

TABLE 4 Effect of CQ on blood immune cells in hypertensive rats.

Index	Control	Hypertensive rats		
		CQ (0 mg/kg)	CQ (63 mg/kg)	CQ (126 mg/kg)
WBC(10⁹/L)	8.59 ± 2.38	8.47 ± 2.07	8.41 ± 3.78	10.84 ± 1.04
LYM(10⁹/L)	5.74 ± 1.69	5.35 ± 1.8	1.04 ± 0.99$^{****,\#\#\#\#}$	0.76 ± 0.53$^{****,\#\#\#\#}$
MONO(10⁹/L)	0.27 ± 0.1	0.23 ± 0.1	0.54 ± 0.35	2.19 ± 0.9$^{****,\#\#\#\#,\$\$\$\$}$
NEUT(10⁹/L)	2.27 ± 0.61	2.35 ± 0.53	6.24 ± 2.81$^{**\#\#}$	5.94 ± 1.98$^{**\#\#}$
EO(10⁹/L)	0.16 ± 0.08	0.25 ± 0.08	0.05 ± 0.04$^{*\#\#\#\#}$	0.27 ± 0.07$^{*\$\$\$\$}$
BASO(10⁹/L)	0.15 ± 0.05	0.22 ± 0.08	0.73 ± 0.45$^{**\#\#}$	0.81 ± 0.23$^{***\#\#\#\#}$

Note: Data are shown as mean ± SD (n = 5–8); WBC, white blood cell; LYM, lymphocyte count; MONO, monocyte; NEUT, neutrophils; EO, eosinophils; BASO, basophils.
*$p < 0.05$, compared with control group; **, $p < 0.01$, compared with control group; ***, $p < 0.001$, compared with control group; ****$p < 0.0001$, compared with control group.
$^{\#\#}p$<0.01, compared with CQ (0 mg/kg) group.
$^{\#\#\#}p$<0.001, compared with CQ (0 mg/kg) group.
$^{\#\#\#\#}p$<0.0001, compared with CQ (0 mg/kg) group.
$^{\$\$\$\$}p$<0.0001, compared with CQ (63 mg/kg) group.

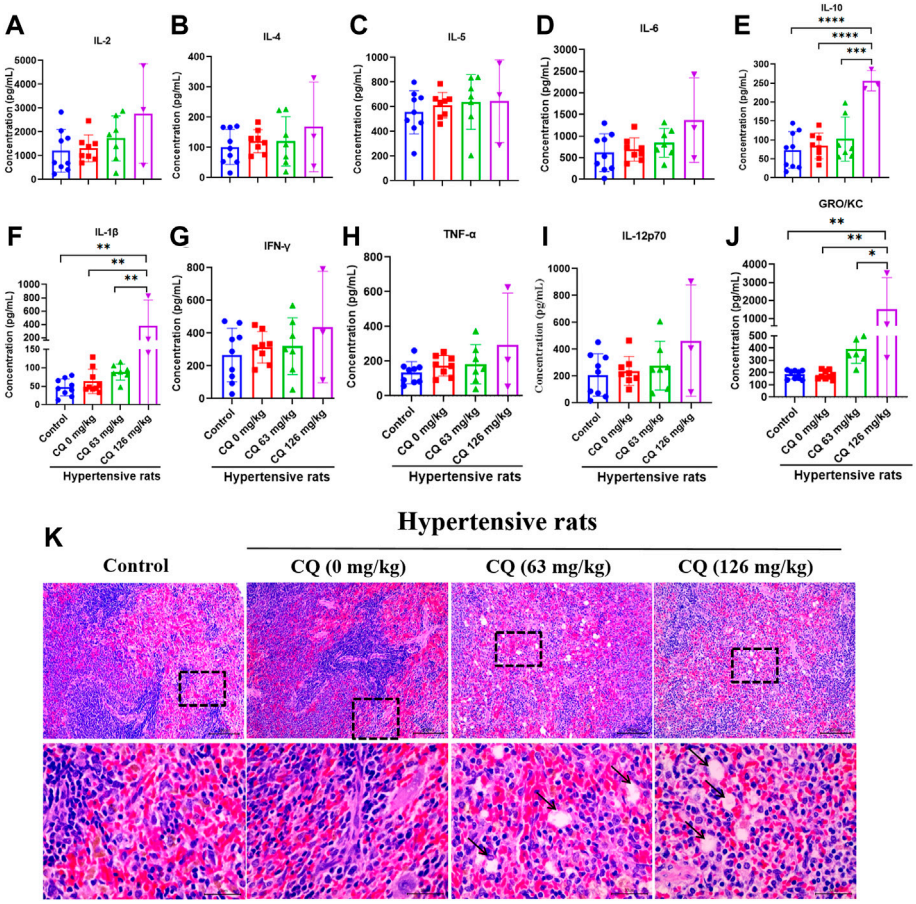

FIGURE 8
CQ alters immune responses in hypertensive rats. Healthy and hypertensive rats orally treated with saline and CQ at two doses (63 mg/kg or 126 mg/kg) twice daily for seven consecutive days. **(A–J)** After CQ treatment, serum of healthy and hypertensive rats was collected to analyze the levels of several inflammatory cytokines, including IL-2, IL-4, IL-5, IL-6, IL-10, IL-1β, IFN-γ, TNF-α, IL-12p70 and GRO/KC. Data are shown as mean ± SD ($n = 3–9$); *, $p < 0.05$; **, $p < 0.01$; ***, $p < 0.001$; ****, $p < 0.0001$. **(K)** CQ induced spleen pathological damage in hypertensive rats. Vacuolar degeneration was observed in hypertensive rats exposed to 63 mg/kg and 126 mg/kg CQ (black arrows). Bars = 30 μm or 100 μm.

acute and chronic damage to the cardiovascular system, resulting in a high risk of cardiac dysfunction with concurrent use of QT-prolonging drugs, such as CQ or azithromycin (Zheng et al. Xie, 2020). In this study, we observed sudden death of hypertensive rats following CQ exposure for 5–6 days, especially at high dose, which is closely associated to CQ-induced cardiotoxicity, including QT prolongation, myocardial damage and the release of myocardial enzymes. Taken together, cardiovascular risks must be considered when repurposing CQ and its derivatives for treating newly emerging diseases in persons with comorbidities, such as hypertension (Tleyjeh et al., 2021). In addition, severe ocular toxicity was observed in hypertensive rats treated by the two doses of CQ in this study. According to the recommendation by the American Academy of Ophthalmology, the maximum daily dose of CQ is ≤ 5 mg/kg for HCQ, and ≤2.3 mg/kg for CQ (Marmor et al., 2016). The recommended doses of CQ or HCQ in the guidelines for COVID-19 treatment are considerably higher than the maximum daily safe dose related to ocular toxicity, but this is unlikely to trigger retinal toxicity due to a relatively short exposure time. Considering that CQ is excreted in urine, renal dysfunction acts as a risk factor which increases systemic levels of CQ and the risk of ocular toxicity (Melles and Marmor, 2014). The observed ocular toxicity in hypertensive rats may be the result of CQ-induced renal damage, which we discuss below. Based on the possible ocular toxicity in repurposing CQ, it is our recommendation that risk factors related to retinopathy should be evaluated and excluded to avoid potential retinal toxicity prior to CQ or hydroxychloroquine prescription.

Furthermore, intestinal injury was another severe toxic effect in hypertensive rats caused by the approved dose and high dose of CQ. This adverse effect has been confirmed in clinical trials of

CQ in non-ICU hospitalized COVID-19 patients, thereby demonstrating increased gastrointestinal adverse events in CQ-treated patients other than hydroxychloroquine exposure (Verheijen et al., 2021). CQ-induced gastrointestinal toxicity can be detected during early stages of treatment based on the findings that the feed consumption and water intake of hypertensive rats decreased rapidly after 1 day of CQ exposure. During the first wave of the COVID-19 pandemic, reports of CQ- and hydroxychloroquine-associated adverse gastrointestinal events in the FDA Adverse Event Reporting System (FAERS) database increased (Perez et al., 2021), suggesting potential over use of CQ and hydroxychloroquine globally. Self-reported adverse symptoms such as nausea, diarrhea, and abdominal pain were also common effects in healthcare workers during hydroxychloroquine prophylaxis of COVID-19 (Nagaraja et al., 2020). These findings support the hypothesis that treatment with CQ is associated with an increased risk for gastrointestinal toxicities, thus suggesting discontinued use of high-dose CQ for treatment of emerging infectious diseases. However, CQ-induced intestinal toxicity is largely due to high dose treatment and has no relevance to hypertension. Given that the quick absorption of CQ in human body leads to an accumulation of CQ in solid organs such as the liver, heart, and kidneys (White and Watson, 2020), hepatotoxicity and nephrotoxicity are inevitable. In the current study, CQ-induced hepatotoxicity was observed in hypertensive rats including a significant increase of hepatic enzymes and histopathological damage. Hepatotoxicity was reported in a case characterized by a 10-fold increase in aminotransferase and alanine aminotransferase activities after two doses of hydroxychloroquine for treatment of COVID-19 (Falcao, Cavalcanti et al., 2020), but enzyme activities returned to normal after drug discontinuation. However, data related to CQ-induced hepatotoxicity is limited in COVID-19. Considering the use of other drugs such as azithromycin for anti-infection, the potential hepatotoxicity risk of CQ should not be ignored, rather liver function should be monitored during its use. In addition, severe renal injury was only observed in high-dose CQ rather than the approved-dose of CQ-treated hypertensive rats. Prevalence of CQ-induced nephrotoxicity seems to be rare since only a few case reports are available (Mahmoudi et al., 2021). Nevertheless, kidney dysfunction rate in SARS-CoV-2 infected patients is high in hospital (Cheng et al., 2020), which will further enhance the risk of CQ-induced nephrotoxicity. Additionally, direct CQ-mediated kidney damage remains due to its excretion and elimination (Wang et al., 2020), which further results in the accumulation of CQ in the body, leading to other side effects such as retinopathy. Nonetheless, hepatotoxicity and nephrotoxicity are closely related to high dose CQ treatment in the clinic, and are reversible upon drug withdrawal. Concerning the complexity of COVID-19 patient conditions especially in the elderly population with high risk of liver and kidney injury (Gabor et al., 2021), the alternative use of CQ should be approached with extreme caution and only in clinical trials.

In addition to the above discussed toxic effects, the immune-regulation function of CQ in hypertensive rats was observed in this study. We found that high-dose rather than the approved dose of CQ increased serum IL-10, IL-1β, and GRO. Since CQ and its derivatives are widely used for treating autoimmune diseases, the anti-inflammatory and immunomodulatory effects of CQ are beneficial for chronic inflammatory and autoimmune diseases over long term use (Rainsford et al., 2015). However, high-dose CQ significantly elevated some inflammatory cytokines, thereby presenting a potential risk of immune damage in hypertensive rats. Moreover, inflammatory markers such as IL-10 and GRO increased significantly in hospitalized COVID-19 patients (Savarraj et al., 2021), which will result in worse situations if these patients were treated with a high dose of CQ. This harmful effect of CQ on the immune system has been linked to endothelial cell injury, and may contribute to its failure in clinical trials during the COVID-19 pandemic (Gregorio et al., 2021). Therefore, the effects of CQ and its derivatives on the immune system especially in SARS-CoV-2 infected patients merit further investigation by analyzing data obtained from largely randomized clinical trials. The undesirable effects of CQ, particularly at high dose, have been demonstrated in hypertensive rats, and partly address its lack of clinical efficacy against COVID-19. Our study still has several limitations: 1) hypertensive rats were not infected by SARS-CoV-2 meaning we could not absolutely model COVID-19 patients complicated with hypertension; 2) the derivate of CQ with low toxicity, hydroxychloroquine, has not been evaluated in the current study; 3) the appropriate safe dose of CQ for hypertensive patients was not proposed based on the regimen used in this study. Despite these limitations, our findings aid our understanding of the failure reasons of CQ against COVID-19 due to its safety concerns, and emphasize that safety evaluation of CQ is a necessary step before its off-label use in the treatment of emerging infectious diseases.

Conclusion

In conclusion, the current dose and regimen of CQ used in trials for COVID-19 is not safe in hypertensive rats. The approved dose and high dose of CQ both increase the risk of mortality in hypertensive rats. CQ induces multiple toxic effects in hypertensive rats, among which, cardiotoxicity, ocular toxicity and intestinal toxicity are the most severe adverse effects. Furthermore, hepatotoxicity, nephrotoxicity and immune state alteration are related to overdose exposure of CQ in hypertensive rats. These findings collectively explain the failure reason of CQ in the battle against SARS-CoV-2, and underline the importance of safety evaluation and medical supervision of CQ to limit patient harm especially those with hypertension.

Data availability statement

The original contributions presented in the study are included in the article/Supplementary Material, further inquiries can be directed to the corresponding author.

Ethics statement

The animal study was reviewed and approved by Committee on Animal Welfare and Ethics of Nanjing Agricultural University (No.20210514069).

Author contributions

JW: Investigation, Writing-Original Draft, Validation. XJ: Methodology, Investigation, Writing-Original Draft. LH: Resources, Methodology. YZ: Methodology, Visualization. SH: Resources, Validation. JX: Visualization. DG: Writing-Review and Editing. WW: Writing-Review and Editing. HJ: Data Curation. LP: Software. SJ: Conceptualization, Supervision. XG: Conceptualization, Writing-Review and Editing, Funding acquisition.

Funding

This study was funded by China Postdoctoral Science Foundation funded project (2020T130057ZX) and a Project Funded by the Priority Academic Program Development of Jiangsu Higher Education Institutions (PAPD).

Acknowledgments

We would like to thank Dr. Yawei Qiu, Fang Chen, and Dr. Qian Gao for their help during rat feeding and sample collection. We thank Dr. Xiaohui Zhang for his assistance in reviewing histopathological sections.

Conflict of interest

The authors declare that the research was conducted in the absence of any commercial or financial relationships that could be construed as a potential conflict of interest.

Publisher's note

All claims expressed in this article are solely those of the authors and do not necessarily represent those of their affiliated organizations, or those of the publisher, the editors and the reviewers. Any product that may be evaluated in this article, or claim that may be made by its manufacturer, is not guaranteed or endorsed by the publisher.

Supplementary material

The Supplementary Material for this article can be found online at: https://www.frontiersin.org/articles/10.3389/fphar.2022.1051694/full#supplementary-material

References

Adaramoye, O. A., Nwosu, I. O., and Farombi, E. O. (2012). Sub-acute effect of N(G)-nitro-l-arginine methyl-ester (L-NAME) on biochemical indices in rats: Protective effects of Kolaviron and extract of Curcuma longa L. *Pharmacogn. Res.* 4 (3), 127–133. doi:10.4103/0974-8490.99071

Axfors, C., Schmitt, A. M., Janiaud, P., Van't Hooft, J., Abd-Elsalam, S., Abdo, E. F., et al. (2021). Mortality outcomes with hydroxychloroquine and chloroquine in COVID-19 from an international collaborative meta-analysis of randomized trials. *Nat. Commun.* 12 (1), 2349. doi:10.1038/s41467-021-22446-z

Bader, M. (2010). Rat models of cardiovascular diseases. *Methods Mol. Biol.* 597, 403–414. doi:10.1007/978-1-60327-389-3_27

Ball, D. E., Tagwireyi, D., and Nhachi, C. F. (2002). Chloroquine poisoning in Zimbabwe: A toxicoepidemiological study. *J. Appl. Toxicol.* 22 (5), 311–315. doi:10.1002/jat.864

Borba, M. G. S., Val, F. F. A., Sampaio, V. S., Alexandre, M. A. A., Melo, G. C., Brito, M., et al. (2020). Effect of high vs low doses of chloroquine diphosphate as adjunctive therapy for patients hospitalized with severe acute respiratory syndrome coronavirus 2 (SARS-CoV-2) infection: A randomized clinical trial. *JAMA Netw. Open* 3 (4), e208857. doi:10.1001/jamanetworkopen.2020.8857

Boulware, D. R., Pullen, M. F., Bangdiwala, A. S., Pastick, K. A., Lofgren, S. M., Okafor, E. C., et al. (2020). A randomized trial of hydroxychloroquine as postexposure prophylaxis for covid-19. *N. Engl. J. Med.* 383 (6), 517–525. doi:10.1056/NEJMoa2016638

Cheng, Y., Luo, R., Wang, K., Zhang, M., Wang, Z., Dong, L., et al. (2020). Kidney disease is associated with in-hospital death of patients with COVID-19. *Kidney Int.* 97 (5), 829–838. doi:10.1016/j.kint.2020.03.005

Clemessy, J. L., Taboulet, P., Hoffman, J. R., Hantson, P., Barriot, P., Bismuth, C., et al. (1996). Treatment of acute chloroquine poisoning: A 5-year experience. *Crit. Care Med.* 24 (7), 1189–1195. doi:10.1097/00003246-199607000-00021

Consortium, W. H. O. S. T., Pan, H., Peto, R., Henao-Restrepo, A. M., Preziosi, M. P., Sathiyamoorthy, V., et al. (2021). Repurposed antiviral drugs for covid-19 - interim WHO solidarity trial results. *N. Engl. J. Med.* 384 (6), 497–511. doi:10.1056/NEJMoa2023184

Cui, C., Zhang, M., Yao, X., Tu, S., Hou, Z., Jie En, V. S., et al. (2020). Dose selection of chloroquine phosphate for treatment of COVID-19 based on a physiologically based pharmacokinetic model. *Acta Pharm. Sin. B* 10 (7), 1216–1227. doi:10.1016/j.apsb.2020.04.007

Das, S., Ramachandran, A. K., Birangal, S. R., Akbar, S., Ahmed, B., and Joseph, A. (2021). The controversial therapeutic journey of chloroquine and hydroxychloroquine in the battle against SARS-CoV-2: A comprehensive review. *Med. Drug Discov.* 10, 100085. doi:10.1016/j.medidd.2021.100085

Dinesh, B., J, C. S., Kaur, C. P., Atiya, F., Yk, G., Avijit, H., et al. (2021). Hydroxychloroquine for sars CoV2 prophylaxis in healthcare workers - a multicentric cohort study assessing effectiveness and safety. *J. Assoc. Physicians India* 69 (6), 11–12. Available at: http://www.ncbi.nlm.nih.gov/pubmed/34472778.

European Medicines Agency (2020). COVID-19: Chloroquine and hydroxychloroquine only to Be used in clinical trials or emergency use programs. Available at: https://www.ema.europa.eu/en/documents/press-release/covid-19-chloroquinehydroxychloroquine-only-be-used-clinical-trials-emergency-use-programmes_en.pdf.

Falcao, M. B., Cavalcanti, L. P. D., Filgueiras, N. M., and de Brito, C. A. A. (2020). Case report: Hepatotoxicity associated with the use of hydroxychloroquine in a patient with COVID-19. *Am. J. Trop. Med. Hyg.* 102 (6), 1214–1216. doi:10.4269/ajtmh.20-0276

Gabor, J. J., Kreidenweiss, A., Weber, S., Salama, M., Sulyok, M., Sulyok, Z., et al. (2021). A call to caution when hydroxychloroquine is given to elderly patients with COVID-19. *Int. J. Infect. Dis.* 106, 265–268. doi:10.1016/j.ijid.2021.04.009

Gao, X., Jing, X., Wang, J., Zheng, Y., Qiu, Y., Ji, H., et al. (2022). Safety considerations of chloroquine in the treatment of patients with diabetes and COVID-19. *Chem. Biol. Interact.* 361, 109954. doi:10.1016/j.cbi.2022.109954

Grasselli, G., Greco, M., Zanella, A., Albano, G., Antonelli, M., Bellani, G., et al. (2020). Risk factors associated with mortality among patients with COVID-19 in intensive care units in lombardy, Italy. *JAMA Intern. Med.* 180 (10), 1345–1355. doi:10.1001/jamainternmed.2020.3539

Gregorio, P., da Cunha, R. S., Biagini, G., Bosquetti, B., Budag, J., Ortiz, A., et al. (2021). Chloroquine may induce endothelial injury through lysosomal dysfunction and oxidative stress. *Toxicol. Appl. Pharmacol.* 414, 115412. Artn 115412. doi:10.1016/j.taap.2021.115412

Hoffmann, M., Mosbauer, K., Hofmann-Winkler, H., Kaul, A., Kleine-Weber, H., Kruger, N., et al. (2020). Chloroquine does not inhibit infection of human lung cells with SARS-CoV-2. *Nature* 585 (7826), 588–590. doi:10.1038/s41586-020-2575-3

Huang, M., Li, M., Xiao, F., Pang, P., Liang, J., Tang, T., et al. (2020). Preliminary evidence from a multicenter prospective observational study of the safety and efficacy of chloroquine for the treatment of COVID-19. *Natl. Sci. Rev.* 7 (9), 1428–1436. doi:10.1093/nsr/nwaa113

Izcovich, A., Siemieniuk, R. A., Bartoszko, J. J., Ge, L., Zeraatkar, D., Kum, E., et al. (2022). Drug treatments for Covid-19: Living systematic review and network meta-analysis. *BMJ Open* 12 (3), m2980. doi:10.1136/bmj.m2980

Junqueira, D. R., and Rowe, B. H. (2021). Efficacy and safety outcomes of proposed randomized controlled trials investigating hydroxychloroquine and chloroquine during the early stages of the COVID-19 pandemic. *Br. J. Clin. Pharmacol.* 87 (4), 1758–1767. doi:10.1111/bcp.14598

Lacout, A., Lounnas, V., and Perronne, C. (2021). Timing and dosage may be the key in the realisation of hydroxychloroquine + azithromycin treatment benefit in Covid-19 elderly patients. *Int. J. Antimicrob. Agents* 57 (4), 106314. ARTN 106314. doi:10.1016/j.ijantimicag.2021.106314

Lerman, L. O., Kurtz, T. W., Touyz, R. M., Ellison, D. H., Chade, A. R., Crowley, S. D., et al. (2019). Animal models of hypertension: A scientific statement from the American heart association. *Hypertension* 73 (6), e87–e120. doi:10.1161/hyp.0000000000000090

Mahmoudi, J., Sadigh-Eteghad, S., Salehi-Pourmehr, H., Gharekhani, A., and Ziaee, M. (2021). Nephrotoxicity of chloroquine and hydroxychloroquine in COVID-19 patients. *Adv. Pharm. Bull.* 11 (1), 6–7. doi:10.34172/apb.2021.022

Marmor, M. F., Kellner, U., Lai, T. Y., Melles, R. B., Mieler, W. F., and American Academy of, O. (2016). Recommendations on screening for chloroquine and hydroxychloroquine retinopathy (2016 revision). *Ophthalmology* 123 (6), 1386–1394. doi:10.1016/j.ophtha.2016.01.058

Megarbane, B. (2021). Chloroquine and hydroxychloroquine to treat COVID-19: Between hope and caution. *Clin. Toxicol.* 59 (1), 70–71. doi:10.1080/15563650.2020.1748194

Melles, R. B., and Marmor, M. F. (2014). The risk of toxic retinopathy in patients on long-term hydroxychloroquine therapy. *JAMA Ophthalmol.* 132 (12), 1453–1460. doi:10.1001/jamaophthalmol.2014.3459

Mercuro, N. J., Yen, C. F., Shim, D. J., Maher, T. R., McCoy, C. M., Zimetbaum, P. J., et al. (2020). Risk of QT interval prolongation associated with use of hydroxychloroquine with or without concomitant azithromycin among hospitalized patients testing positive for coronavirus disease 2019 (COVID-19). *JAMA Cardiol.* 5 (9), 1036–1041. doi:10.1001/jamacardio.2020.1834

Multicenter collaboration group of Department of Science and Technology of Guangdong Province and Health Commission of Guangdong Province for chloroquine in the treatment of novel coronavirus pneumonia (2020). Expert consensus on chloroquine phosphate for the treatment of novel coronavirus pneumonia. *Zhonghua Jie He He Hu Xi Za Zhi* 43 (0), E019. doi:10.3760/cma.j.issn.1001-0939.2020.0019

Nagaraja, B. S., Ramesh, K. N., Dhar, D., Mondal, M. S., Dey, T., Saha, S., et al. (2020). HyPE study: Hydroxychloroquine prophylaxis-related adverse events' analysis among healthcare workers during COVID-19 pandemic: A rising public health concern. *J. Public Health* 42 (3), 493–503. doi:10.1093/pubmed/fdaa074

National Health Commission of the People's Republic of China (2020). Diagnosis and treatment of COVID-19 in China (the six edition for trial). Available at: http://www.nhc.gov.cn/yzygj/s7653p/202002/8334a8326dd94d329df351d7da8aefc2.shtml.

National Health Commission of the People's Republic of China (2021). Diagnosis and treatment Program of COVID-19 in China(the ninth edition for trial). Available at: http://www.nhc.gov.cn/xcs/zhengcwj/202003/46c9294a7dfe4cef80dc7f5912eb1989.shtml.

Nirk, E. L., Reggiori, F., and Mauthe, M. (2020). Hydroxychloroquine in rheumatic autoimmune disorders and beyond. *EMBO Mol. Med.* 12 (8), e12476. doi:10.15252/emmm.202012476

Organization, W. H. (2015). *Guidelines for the treatment of malaria*. 3rd edition. Geneva.

Peng, M., He, J., Xue, Y., Yang, X., Liu, S., and Gong, Z. (2021). Role of hypertension on the severity of COVID-19: A review. *J. Cardiovasc. Pharmacol.* 78 (5), e648–e655. doi:10.1097/FJC.0000000000001116

Perez, J., Roustit, M., Lepelley, M., Revol, B., Cracowski, J. L., and Khouri, C. (2021). Reported adverse drug reactions associated with the use of hydroxychloroquine and chloroquine during the COVID-19 pandemic. *Ann. Intern. Med.* 174 (6), 878–880. doi:10.7326/M20-7918

Rainsford, K. D., Parke, A. L., Clifford-Rashotte, M., and Kean, W. F. (2015). Therapy and pharmacological properties of hydroxychloroquine and chloroquine in treatment of systemic lupus erythematosus, rheumatoid arthritis and related diseases. *Inflammopharmacology* 23 (5), 231–269. doi:10.1007/s10787-015-0239-y

Rea-Neto, A., Bernardelli, R. S., Camara, B. M. D., Reese, F. B., Queiroga, M. V. O., and Oliveira, M. C. (2021). An open-label randomized controlled trial evaluating the efficacy of chloroquine/hydroxychloroquine in severe COVID-19 patients. *Sci. Rep.* 11 (1), 9023. doi:10.1038/s41598-021-88509-9

Rees, D. D., Palmer, R. M., Schulz, R., Hodson, H. F., and Moncada, S. (1990). Characterization of three inhibitors of endothelial nitric oxide synthase *in vitro* and *in vivo*. *Br. J. Pharmacol.* 101 (3), 746–752. doi:10.1111/j.1476-5381.1990.tb14151.x

Reeves, P. G., Nielsen, F. H., and Fahey, G. C. (1993). Ain-93 purified diets for laboratory rodents - final report of the American institute of nutrition ad hoc writing committee on the reformulation of the ain-76a rodent diet. *J. Nutr.* 123 (11), 1939–1951. doi:10.1093/jn/123.11.1939

Riou, B., Barriot, P., Rimailho, A., and Baud, F. J. (1988). Treatment of severe chloroquine poisoning. *N. Engl. J. Med.* 318 (1), 1–6. doi:10.1056/NEJM198801073180101

Rosenberg, E. S., Dufort, E. M., Udo, T., Wilberschied, L. A., Kumar, J., Tesoriero, J., et al. (2020). Association of treatment with hydroxychloroquine or azithromycin with in-hospital mortality in patients with COVID-19 in New York state. *JAMA* 323 (24), 2493–2502. doi:10.1001/jama.2020.8630

Savarraj, J., Park, E. S., Colpo, G. D., Hinds, S. N., Morales, D., Ahnstedt, H., et al. (2021). Brain injury, endothelial injury and inflammatory markers are elevated and express sex-specific alterations after COVID-19. *J. Neuroinflammation* 18 (1), 277. doi:10.1186/s12974-021-02323-8

Self, W. H., Semler, M. W., Leither, L. M., Casey, J. D., Angus, D. C., Brower, R. G., et al. (2020). Effect of hydroxychloroquine on clinical status at 14 Days in hospitalized patients with COVID-19: A randomized clinical trial. *JAMA* 324 (21), 2165–2176. doi:10.1001/jama.2020.22240

Shah, R. R. (2021). Chloroquine and hydroxychloroquine for COVID-19: Perspectives on their failure in repurposing. *J. Clin. Pharm. Ther.* 46 (1), 17–27. doi:10.1111/jcpt.13267

Skipper, C. P., Pastick, K. A., Engen, N. W., Bangdiwala, A. S., Abassi, M., Lofgren, S. M., et al. (2020). Hydroxychloroquine in nonhospitalized adults with early COVID-19 : A randomized trial. *Ann. Intern. Med.* 173 (8), 623–631. doi:10.7326/M20-4207

Slater, A. F. (1993). Chloroquine: Mechanism of drug action and resistance in Plasmodium falciparum. *Pharmacol. Ther.* 57 (2-3), 203–235. doi:10.1016/0163-7258(93)90056-j

Tang, W., Cao, Z. J., Han, M. F., Wang, Z. Y., Chen, J. W., Sun, W. J., et al. (2020). Hydroxychloroquine in patients with mainly mild to moderate coronavirus disease 2019: Open label, randomised controlled trial. *Bmj-British Med. J.* 369, m1849. Artn M1849. doi:10.1136/bmj.m1849

Tleyjeh, I. M., Kashour, Z., AlDosary, O., Riaz, M., Tlayjeh, H., Garbati, M. A., et al. (2021). Cardiac toxicity of chloroquine or hydroxychloroquine in patients with COVID-19: A systematic review and meta-regression analysis. *Mayo Clin. Proc. Innov. Qual. Outcomes* 5 (1), 137–150. doi:10.1016/j.mayocpiqo.2020.10.005

U.S. Food & Drug Administration (2020). Request for emergency use authorization for use of chloroquine phosphate or hydroxychloroquine sulfate supplied from the strategic national stockpile for treatment of 2019 coronavirus disease. Available at: https://www.fda.gov/media/136534.

Verheijen, S., van Luin, M., Bruggemann, R. J., de Mast, Q., Hassing, R. J., and Burger, D. M. (2021). More gastro-intestinal adverse events in non-ICU hospitalised COVID-19 patients treated with chloroquine versus hydroxychloroquine. *Int. J. Infect. Dis.* 103, 402–403. doi:10.1016/j.ijid.2020.12.010

Wang, B., Guo, H., Ling, L., Ji, J., Niu, J., and Gu, Y. (2020). The chronic adverse effect of chloroquine on kidney in rats through an autophagy dependent and independent pathways. *Nephron* 144 (2), 96–108. doi:10.1159/000503882

White, N. J., Watson, J. A., Hoglund, R. M., Chan, X. H. S., Cheah, P. Y., and Tarning, J. (2020). COVID-19 prevention and treatment: A critical analysis of chloroquine and hydroxychloroquine clinical pharmacology. *PLoS Med.* 17 (9), e1003252. doi:10.1371/journal.pmed.1003252

Wiersinga, W. J., Rhodes, A., Cheng, A. C., Peacock, S. J., and Prescott, H. C. (2020). Pathophysiology, transmission, Diagnosis, and treatment of coronavirus disease 2019 (COVID-19): A review. *JAMA* 324 (8), 782–793. doi:10.1001/jama.2020.12839

Wu, K., Zhang, Q., Wu, X. T., Lu, W. J., Tang, H. Y., Liang, Z. H., et al. (2017). Chloroquine is a potent pulmonary vasodilator that attenuates hypoxia-induced pulmonary hypertension. *Br. J. Pharmacol.* 174 (22), 4155–4172. doi:10.1111/bph.13990

Xu, S., Xu, S. S., Bian, R., Chen, X., Rulian, K., Xu, S. Y., et al. (2002). *Experimental methodology of Pharmacology*. Beijing: People's Health Publisher.

Zheng, Y. Y., Ma, Y. T., Zhang, J. Y., and Xie, X. (2020). COVID-19 and the cardiovascular system. *Nat. Rev. Cardiol.* 17 (5), 259–260. doi:10.1038/s41569-020-0360-5

Zhou, F., Yu, T., Du, R., Fan, G., Liu, Y., Liu, Z., et al. (2020). Clinical course and risk factors for mortality of adult inpatients with COVID-19 in wuhan, China: A retrospective cohort study. *Lancet* 395 (10229), 1054–1062. doi:10.1016/S0140-6736(20)30566-3

frontiers | Frontiers in Pharmacology

TYPE Original Research
PUBLISHED 23 January 2023
DOI 10.3389/fphar.2023.1107435

Check for updates

OPEN ACCESS

EDITED BY
Fareeha Anwar,
Riphah International University, Pakistan

REVIEWED BY
Atefeh Jafari,
Gilan University of Medical Sciences, Iran
Sasidharan Sreenivasan,
University of Science Malaysia (USM), Malaysia

*CORRESPONDENCE
Syed Mohammed Basheeruddin Asdaq,
sasdaq@gmail.com/sasdag@mcst.edu.sa
A. Muthukumar,
drmkpharmacologist@gmail.com

SPECIALTY SECTION
This article was submitted to Predictive Toxicology, a section of the journal Frontiers in Pharmacology

RECEIVED 24 November 2022
ACCEPTED 09 January 2023
PUBLISHED 23 January 2023

CITATION
Das K, Muthukumar A, Almuqbil M, Imran M, Rabaan AA, Halwani MA, Garout M, Alsaleh AA, Alissa M, Alwashmi ASS, Alshehri AA, Alsayyah A, Bhavani K, Mittal S, Gayathri R, Alomar NF, Rabbani SI and Basheeruddin Asdaq SM (2023), Nephroprotective potential of *Polyalthia longifolia* roots against vancomycin-induced renal toxicity in experimental animals.
Front. Pharmacol. 14:1107435.
doi: 10.3389/fphar.2023.1107435

COPYRIGHT
© 2023 Das, Muthukumar, Almuqbil, Imran, Rabaan, Halwani, Garout, Alsaleh, Alissa, Alwashmi, Alshehri, Alsayyah, Bhavani, Mittal, Gayathri, Alomar, Rabbani and Basheeruddin Asdaq. This is an open-access article distributed under the terms of the Creative Commons Attribution License (CC BY). The use, distribution or reproduction in other forums is permitted, provided the original author(s) and the copyright owner(s) are credited and that the original publication in this journal is cited, in accordance with accepted academic practice. No use, distribution or reproduction is permitted which does not comply with these terms.

Nephroprotective potential of *Polyalthia longifolia* roots against vancomycin-induced renal toxicity in experimental animals

Kuntal Das[1], A. Muthukumar[2]*, Mansour Almuqbil[3], Mohd. Imran[4], Ali A. Rabaan[5,6,7], Muhammad A. Halwani[8], Mohammed Garout[9], Abdulmonem A. Alsaleh[10], Mohammed Alissa[11], Ameen S. S. Alwashmi[12], Ahmad A. Alshehri[13], Ahmed Alsayyah[14], Keserla Bhavani[15], Swati Mittal[2], R. Gayathri[16], Nasser Fawzan Alomar[17], Syed Imam Rabbani[18] and Syed Mohammed Basheeruddin Asdaq[19]*

[1]Nitte College of Pharmaceutical Science, Yelahanka, Bangalore, India, [2]Central Animal House, Department of Pharmacology, Al-Ameen College of Pharmacy, Bangalore, India, [3]Department of Clinical Pharmacy, College of Pharmacy, King Saud University, Riyadh, Saudi Arabia, [4]Department of Pharmaceutical Chemistry, Faculty of Pharmacy, Northern Border University, Rafha, Saudi Arabia, [5]Molecular Diagnostic Laboratory, Johns Hopkins Aramco Healthcare, Dhahran, Saudi Arabia, [6]College of Medicine, Alfaisal University, Riyadh, Saudi Arabia, [7]Department of Public Health and Nutrition, The University of Haripur, Haripur, Pakistan, [8]Department of Medical Microbiology, Faculty of Medicine, Al Baha University, Al Baha, Saudi Arabia, [9]Department of Community Medicine and Healthcare for Pilgrims, Faculty of Medicine, Umm Al-Qura University, Makkah, Saudi Arabia, [10]Clinical Laboratory Science Department, Mohammed Al-Mana College for Medical Sciences, Dammam, Saudi Arabia, [11]Department of Medical Laboratory Sciences, College of Applied Medical Sciences, Prince Sattam bin Abdulaziz University, Al-Kharj, Saudi Arabia, [12]Department of Medical Laboratories, College of Applied Medical Sciences, Qassim University, Buraydah, Saudi Arabia, [13]Department of Clinical Laboratory Sciences, College of Applied Medical Sciences, Najran University, Najran, Saudi Arabia, [14]Department of Pathology, College of Medicine, Imam Abdulrahman Bin Faisal University, Dammam, Saudi Arabia, [15]Oxford College of Pharmacy, Bangalore, India, [16]Department of Pharmaceutics, KMCH College of Pharmacy, Coimbatore, India, [17]Equame Scientific and Research Center, Riyadh, Saudi Arabia, [18]Department of Pharmacology and Toxicology, College of Pharmacy, Qassim University, Buraydah, Saudi Arabia, [19]Department of Pharmacy Practice, College of Pharmacy, AlMaarefa University, Riyadh, Saudi Arabia

This study was done to investigate the possible nephroprotective effect of an ethanolic root extract of *Polyalthia Longifolia* (PL) on vancomycin-induced nephrotoxicity using curative and protective models. Vancomycin (150 mg/kg, intravenous) was given to healthy Wistar albino rats in the curative model before the start of treatment, whereas the protective group received vancomycin at the conclusion of the 10-day treatment procedure. Animals were divided into six groups for both models; group I served as the normal control, while groups II, III, IV, V, and VI were kept as toxic control, standard (selenium, 6 mg/kg), LDPL (low dose of PL 200 mg/kg), HDPL (high dose of PL 400 mg/kg), and HDPL + selenium (interactive) groups, respectively. Renal biomarkers [(uric acid, creatinine, blood urea nitrogen (BUN), serum proteins], and blood electrolyte levels were measured for all tested groups. When compared to the vancomycin group, the HDPL significantly ($p < 0.01$) showed greater effectiveness in lowering the BUN, potassium, and calcium levels. Additionally, in the curative model, there was a significant ($p < 0.05$) decrease in the blood levels of uric acid, creatinine, BUN, potassium, and calcium in the animals who received the combination of selenium and HDPL. Both LDPL and HDPL did not provide any distinguishable effect in the protective model, but groups that received HDPL with selenium did provide detectable protection by significantly lowering their levels of uric acid, BUN, serum potassium, and total serum protein in comparison to

the vancomycin control group. These findings indicate that, whether administered before or after renal damage is induced, the *Polyalthia longifolia* root extract provided only modest protection to nephrons, which require selenium support to prevent vancomycin-induced kidney damage.

KEYWORDS

antioxidants, antibiotics, biomarkers, vancomycin, kidney disease, treatment, Polyalthia longifolia, nephrotoxicity

Introduction

Drug-induced nephrotoxicity is a prominent cause of renal failure with potentially lethal effects, and it can impede pharmaceutical research and development (Elyasi et al., 2012; Kim and Moon, 2012). It underlines the importance of developing new approaches for early and more exact diagnosis to avoid drug-induced kidney injury (Radi, 2019). Vancomycin is one such antibiotic that is most frequently used in the treatment of infectious diseases but still can cause renal damage in patients. The drug is popular due to its bactericidal properties and relatively low cost. Vancomycin is reported to be a gold standard for the treatment of methicillin-resistant *Staphylococcus aureus* (MRSA) infection (Álvarez et al., 2016). The drug was found to have an anti-bacterial spectrum against *Streptococcus sp., Enterococcus sp., Actinomyces sp., Clostridium sp.,* and *Eubacterium sp*. The mechanism of action of vancomycin was identified to involve the inhibition of cross-linking of the peptidoglycan wall of the bacteria by binding to acyl-D-Ala-D-Ala terminal (Brown et al., 2019).

Vancomycin therapy failures in individuals with methicillin-resistant *Staphylococcus aureus* infections have resulted in larger vancomycin doses to meet the required trough concentrations of 10–20 g/ML (Stogios and Savchenko, 2020). Many concerns have been raised about the safety of such high vancomycin dosages, particularly their nephrotoxicity (Perazella, 2019). Vancomycin-induced renal damage has been documented in 10%–20% and 30%–40% of individuals, respectively. Its nephrotoxicity may be exacerbated by increased reactive oxygen species and oxidative stress (Filippone et al., 2017). High trough vancomycin levels (particularly >20 mg/L) or doses (>4 g/day), concomitant nephrotoxic agent treatment, prolonged therapy (even more than 7 days), ICU admission and underlying diseased states are all considered risk factors that might accelerate or worsen vancomycin-induced nephrotoxicity (Tantranont et al., 2021).

Since ancient times, natural resources such as plants played a vital role in human race sustainability on this Earth. Plants have provided oxygen, essential nutrients, and medicines to treat human diseases. Although, human race has achieved several technological advancements but still around 80% of the world population depends on plant resources for their primary healthcare needs (Ozaslan and Oguzkan, 2018). Polyalthia is derived from 'Greek' which means a cure for many diseases. *Polyalthia longifolia* (PL) belonging to the family *Annonaceae* is native to many countries in the Asian continent. PL is a tree that grows up to a height of 30 feet with weeping pendulous branches and long narrow lanceolate undulate margin leaves (Yao et al., 2019). The plant is reported to have several medicinal properties and the herbal preparation were used for duodenal ulcers, fever, skin diseases, diabetes, hypertension, helminthiasis, hepato-protective, antibacterial, anti-inflammatory, and anti-cancer (Chanda et al., 2011; Vijayarathna et al., 2017; Rai et al., 2021). The extracts of PL were reported to possess antiviral property (Yadav et al., 2020). Administration of PL was found to produce synergistic activity with antibiotics against methicillin-resistant *Staphylococcus aureus* (Kirubakari et al., 2020). Besides, two clerodane diterpenes isolated from PL were reported to exhibit anti-histaminic and anti-helicobacter pylori activities (Edmond et al., 2021). Furthermore, apoptosis-inducing properties essential for the eradication of tumors has been found in the extracts of PL (Afolabi et al., 2019). PL is reported to contain diterpenoids, alkaloids, tannins, and mucilage (Lee et al., 2009). Some of the important active ingredients identified were O-methyl bulbocapnin-N-oxide, N-methyl nandigerine-N-oxide, Oliver online-N-oxide, pendulamine A, 8-oxopolyalthiane and 13-halimadien-15-oic acid. These components have been linked to the reported pharmacological activities of the plant (Lee et al., 2009; Bhattacharya et al., 2015).

Therefore, this study was designed to investigate the protective and curative potential of *Polyalthia longifolia* against vancomycin-induced nephrotoxicity using biochemical markers (serum creatinine, BUN, serum uric acid, and total serum protein), and serum electrolytes (sodium, potassium, chloride, and calcium) measurements.

Materials and methods

Drugs, chemicals, and biomedical reagents

The chemicals and reagents used in the study were of analytical grade meant for research purposes. These were procured from the regular chemical supplier of the institution by placing an order in the central storehouse. Vancomycin was obtained from Cipla Limited, Bangalore, India, and diagnostic equipment from Oscar Medicare Private Limited, Bangalore, India.

Root extraction

In January 2021, matured and fresh roots were obtained from Lalbagh botanical garden in Bangalore, Karnataka, India. Dr. V. Rama Rao, Research Officer (S-2) Botany, and Dr. Sulochana Bhat, Assistant Director (S-4) In-charge, from the Central Ayurveda Research Institute, Bangalore, authenticated the plant roots, which were then deposited in the al-Ameen central herbarium. (Authentication/SMPU/CARI/BNG/2021-22/35). 3kg of adult *Polyalthia longifolia* leaves were collected, dried, and powdered. For 72 h, the powdered (1,200 g) roots were macerated in 80% ethanol. The final leaf extract was filtered through Whatman filter paper and lyophilized under reduced pressure. The yield percentage obtained was 31.12% w/w. The

ethanolic root extract was then subjected to additional pharmacological testing.

Selection of experimental animals

Six to 7 weeks old albino Wistar rats weighing 150–180 gm (equal number of male and female rats) was obtained from a central animal house at the Al-Ameen College of Pharmacy in Bangalore and kept in an animal room under standard environmental conditions (50% relative humidity, a light-dark cycle of up to 12 h, and a room temperature of 28°C). They were also fed a standard diet and given access to water at will. This investigation was confirmed by the institutional animal ethics committee (IAEC) and given their support. The normal rules and policies of CPCSEA were adhered while conducting experiments with testing animals and providing them with particular care (Reg. AACP/IAEC/JAN2020/10).

Protocol design

Method for the induction

The test drug as fine powder was suspended in 0.5% aqueous carboxyl methylcellulose (CMC) suspension. Every day, the test dose suspension was freshly prepared. A feeding cannula was used to administer the homogenized suspension, which had been thoroughly shaken for 1 min. The same method was used to make the daily new suspension. The animals were divided into six groups of six animals each at random. Vancomycin was given intravenously at a dose of 150 mg/kg body weight (Pais et al., 2020). The doses of *Polyalthia longifolia* for curative and protective models were selected based on the research reported in the literature (Oyeyemi et al., 2020).

Curative model protocol (Gao et al., 2020)

Group 1 (Normal control) animals were given a normal saline injection intraperitoneal on first day, and 0.3% CMC aqueous solution was given orally on the 6th day and continued for 10 days. Animals in Group 2 (Positive control) were given vancomycin 150 mg/kg i.v. on the first day, and 0.3% CMC aqueous solution was given orally on the 6th day for 10 days. Animals in Group 3 were given vancomycin 150 mg/kg i.v on the first day; however, starting on the 6th day, the standard drug, selenium, was also given in the dose of 6 mg/kg body weight once daily orally for the next 10 days. Animals in Groups 4 and 5 were given vancomycin 150 mg/kg i.v. on the first day; however, starting on the 6th day, lower (200 mg/kg) and higher (400 mg/kg) of PL, respectively (Oyeyemi et al., 2020), were also given orally once daily for the next 10 days. On the first day, Group 6 received vancomycin 150 mg/kg i.v; however, beginning on the 6th day a combination of selenium (6 mg/kg) with PL (400 mg/kg) was administered orally, daily for the next 10 days. Animals were fasted overnight with free access to drinking water and the sampling for biochemical estimation was done after 24 h of last dose of the treatment.

Protective model protocol (Liu et al., 2020)

Group 1 (Normal control): Animals were given 0.3% CMC aqueous solution orally for 10 days before receiving an i.v injection of normal saline on the 11th day. Group 2 (Positive control): Animals were given 0.3% CMC aqueous solution orally for 10 days, followed by 150 mg/kg i.v vancomycin on the 11th day. Animals in Group 3 received standard drug selenium at a dose of 6 mg/kg body weight orally once daily for 10 days, and vancomycin injection was given intravenously on the 11th day at a dose of 150 mg/kg bw. Animals in Group 4 received test drug PL at a dose of 200 mg/kg body weight (Oyeyemi et al., 2020) orally once daily for 10 days, and vancomycin injection was given intravenously on the 11th day at a dose of 150 mg/kg bw. Animals in Group 5 received test drug PL at a dose of 400 mg/kg body weight orally once daily for 10 days, and vancomycin injection was given intravenously on the 11th day at a dose of 150 mg/kg bw. Group-6 animals received standard drug selenium (6 mg/kg) and test drug PL (400 mg/kg, b.w) orally, once daily for 10 days, and vancomycin injection was given intravenously on the 11th day in the dose of 150 mg/kg bw. Animals were fasted overnight with free access to drinking water and the sampling for biochemical estimation was done after 24 h of vancomycin injection.

Biochemical assay

At the end of the experiment, the rats were anaesthetized for 50–60 s with isoflurane (EZ anaesthesia system), and 2–3 mL of blood was collected from the retro-orbital plexus for biochemical analysis. The biochemical parameters such as uric acid, creatinine, BUN, and total proteins were estimated using the diagnostic kits supplied by Oscar Medicare Pvt Ltd. In addition, blood electrolytes levels (sodium, potassium, chloride, and calcium) were also measured using the Oscar Medicare diagnostic kits. The procedure described in each user's manual of the kit was followed while estimating the biomarker parameters (URIC-ACID, 2020; Al-Doaiss et al., 2021). Samples were obtained from each animal of all groups (in multiple of six for each group) and coded for blinding.

Statistical investigation

For statistical purposes, GraphPad Prism Version 5.0 software ran a one-way analysis of variance (ANOVA) followed by Tukey's test on all the raw data collected during the study. Sample size of animals was calculated from the formula proposed in the literature. The degree of freedom, confidence interval (95%), repeat administration, and the number of groups in the study was considered while deciding the total number of rats needed (Arifin and Zahiruddin, 2017). Based on the calculation, 7-8 animals were included in each group and comprised of animals of both sexes. The values were given as mean SEM, and a *p-value* of 0.05 was statistically significant.

Results

Curative effect of PL and selenium against vancomycin-induced nephrotoxicity

Renal biomarkers

Comparison between the baseline values of uric acid, creatinine, BUN and total proteins with normal control indicated non-significant variation. Further, the observations indicated that administration of vancomcycin (150 mg/kg) non-significantly increased the uric acid

TABLE 1 Effect of curative administration of PL and selenium on the renal biomarkers in rats treated with vancomycin.

Renal biomarkers	Baseline values (NS, i,p)	Normal control (NS i.p + 0.3% CMC, p.o)	Positive control (150 mg/kg, i.v + 0.3% CMC, p.o)	Vanco (150 mg/kg i.v) +Standard selenium (6 mg/kg, p.o)	Vanco (150 mg/kg i.v) +PL (200 mg/kg, p.o)	Vanco (150 mg/kg i.v) +PL (400 mg/kg, p.o)	Vanco (150 mg/kg i.v) And selenium (6 mg/kg, p.o) + PL (400 mg/kg, p.o)
Uric acid (mg/dL)	1.81 ± 0.08	1.99 ± 0.10	2.66 ± 0.14	1.87 ± 0.05	1.93 ± 0.09	1.82 ± 0.03	1.72 ± 0.05*
Creatinine (mg/dL)	0.88 ± 0.04	0.82 ± 0.06	1.71 ± 0.08[a]	0.96 ± 0.08	1.28 ± 0.11	0.99 ± 0.09	0.76 ± 0.03**
BUN (mg/dL)	18.96 ± 1.06	17.62 ± 0.72	68.95 ± 1.33[a]	36.12 ± 1.07	50.57 ± 1.41	43.02 ± 1.44*	30.62 ± 1.00**
Total protein (g/dL)	5.96 ± 0.48	6.23 ± 0.17	6.87 ± 0.03	6.15 ± 0.03	6.39 ± 0.20	6.76 ± 0.14	6.69 ± 0.16

NS, Normal saline; CMC, Carboxy methylcellulose, Vanco—Vancomycin; PL, *Polyalthia longifolia*.
Values expressed as mean ± SEM; Statistics: One-way ANOVA.
[a]p< 0.05 compared with normal control; *$p < 0.05$, **$p < 0.01$, compared with positive control.

TABLE 2 Effect of curative administration of PL and selenium on blood electrolyte levels in rats treated with vancomycin.

Electrolyte levels (mmol/L)	Baseline values (NS, i,p)	Normal control (NS i.p + 0.3% CMC, p.o)	Positive control (150 mg/kg, i.v + 0.3% CMC, p.o)	Vanco (150 mg/kg i.v) +Standard selenium (6 mg/kg, p.o)	Vanco (150 mg/kg i.v) +PL (200 mg/kg, p.o)	Vanco (150 mg/kg i.v) +PL (400 mg/kg, p.o)	Vanco (150 mg/kg i.v) And selenium (6 mg/kg, p.o) + PL (400 mg/kg, p.o)
Sodium	153.21 ± 2.14	144.93 ± 0.84	155.25 ± 0.72	143.73 ± 0.48	149.12 ± 0.45	146.28 ± 0.45	142.33 ± 0.60
Potassium	6.23 ± 0.09	5.88 ± 0.23	6.30 ± 0.02	4.86 ± 0.05	5.91 ± 0.11*	5.53 ± 0.07**	4.37 ± 0.08***
Chloride	88.24 ± 0.72	94.95 ± 0.58	97.26 ± 0.39	93.04 ± 0.47	94.97 ± 0.32	92.95 ± 0.36	90.53 ± 0.39
Calcium	2.26 ± 0.39	2.64 ± 0.02	2.84 ± 0.05	2.74 ± 0.07	2.80 ± 0.05*	2.78 ± 0.11*	2.65 ± 0.02***

NS, Normal saline; CMC, Carboxy methylcellulose, Vanco—Vancomycin; PL, *Polyalthia longifolia*.
Values expressed as mean ± SEM, Statistics: One-way ANOVA; *$p < 0.05$, **$p < 0.01$, ***$p < 0.001$ compared with positive control.

levels compared to control group. Treatments such as selenium (6 mg/kg), low dose of PL (200 mg/kg) and high dose of PL (400 mg/kg) after vancomycin did no induced significant variation in uric acid levels. However, when selenium (6 mg/kg) and PL (400 mg/kg) was tested in combination, a significant ($p < 0.05$) reduction in uric acid level was observed compared to positive control group. On the other hand, administration of vancomycin (150 mg/kg) showed significant ($p < 0.05$) increase in creatinine levels compared to normal control group. Treatment of selenium (6 mg/kg), lower dose of PL (200 mg/kg) and higher dose of PL (400 mg/kg) did not produce any significant change in the creatinine level. Further, the combination of selenium (6 mg/kg) and PL (400 mg/kg) produced a significant ($p < 0.01$) reduction in creatinine level compared to positive control group. Similar observation was found for BUN, where vancomycin (150 mg/kg) significantly ($p < 0.05$) elevated its level and diminishing action was found only with combination of selenium and PL at high dose was tested. Moreover, none of the treatments significantly altered the total protein levels (Table 1).

Blood electrolytes

The observation of Table 2 suggests that administration of vancomycin (150 mg/kg) non-significantly increased the levels of sodium, potassium, chloride, and calcium. Treatment of selenium (6 mg/kg) did not produce significant alteration in the blood electrolyte levels. However, both lower dose (200 mg/kg) and higher dose (400 mg/kg) of PL showed significant reduction ($p < 0.05$) in the elevated potassium and calcium levels induced by vancomycin. These effects were found to become prominent ($p < 0.001$) when combination of selenium and PL (400 mg/kg) was tested in vancomycin. Moreover, no significant variation was observed when comparison was done between the baseline values and normal control values.

Protective effect of PL and selenium in vancomycin induced nephrotoxicity

Renal biomarkers

The observations from Table 3 suggest that vancomycin (150 mg/kg) treatment towards end of the study did not induce significant variation in uric acid level compared to normal control group. Similarly, selenium (6 mg/kg), PL (200 mg/kg) and PL (400 mg/kg) treatment also did not alter the uric acid level significantly. However, combination of selenium (6 mg/kg) and PL (400 mg/kg) produced a significant ($p < 0.01$) reduction in uric acid level compared to positive control group. The estimation of creatinine level indicated that vancomycin (150 mg/kg) significantly ($p < 0.05$)

TABLE 3 Effect of preventive administration of PL and selenium on renal biomarkers in vancomycin treated rats.

Renal biomarkers	Baseline values (NS, i,p)	Normal control (NS i.p + 0.3% CMC, p.o)	Positive control (150 mg/kg, i.v + 0.3% CMC, p.o)	Vanco (150 mg/kg i.v) +Standard selenium (6 mg/kg, p.o)	Vanco (150 mg/kg i.v) +PL (200 mg/kg, p.o)	Vanco (150 mg/kg i.v) +PL (400 mg/kg, p.o)	Vanco (150 mg/kg i.v) And selenium (6 mg/kg, p.o) + PL (400 mg/kg, p.o)
Uric acid (mg/dL)	1.78 ± 0.62	1.86 ± 0.04	2.66 ± 0.14	1.80 ± 0.06	1.93 ± 0.09	1.82 ± 0.03	1.69 ± 0.03**
Creatinine (mg/dL)	1.03 ± 0.11	1.15 ± 0.06	1.88 ± 0.07[a]	1.22 ± 0.08	1.60 ± 0.06	1.40 ± 0.13	1.01 ± 0.14
BUN (mg/dL)	15.82 ± 0.34	16.88 ± 0.61	28.98 ± 0.66[b]	21.24 ± 0.88	25.14 ± 0.33	22.03 ± 0.51	19.53 ± 0.48*
Total protein (g/dL)	6.79 ± 0.56	7.12 ± 0.02	6.87 ± 0.03	7.14 ± 0.01	7.21 ± 0.04	7.12 ± 0.01	7.39 ± 0.05*

NS, Normal saline; CMC, Carboxy methylcellulose, Vanco—Vancomycin; PL, *Polyalthia longifolia*.
Values expressed as mean ± SEM, Statistics: One-way ANOVA.
[a]p< 0.05.
[b]p< 0.01 compared with normal control; *$p < 0.05$, **$p < 0.01$ compared with positive control.

TABLE 4 Effect of preventive administration of PL and selenium on blood electrolyte levels in rats treated with vancomycin.

Electrolyte levels (mmol/L)	Baseline values (NS, i,p)	Normal control (NS i.p + 0.3% CMC, p.o)	Positive control (150 mg/kg, i.v + 0.3% CMC, p.o)	Vanco (150 mg/kg i.v) +Standard selenium (6 mg/kg, p.o)	Vanco (150 mg/kg i.v) +PL (200 mg/kg, p.o)	Vanco (150 mg/kg i.v) +PL (400 mg/kg, p.o)	Vanco (150 mg/kg i.v) And selenium (6 mg/kg, p.o) + PL (400 mg/kg, p.o)
Sodium	114.21 ± 1.85	125.20 ± 0.87	156.64 ± 0.65	133.37 ± 0.60	148.22 ± 0.79	138.74 ± 0.92	138.83 ± 0.73
Potassium	7.88 ± 0.46	7.01 ± 0.22	14.81 ± 0.61[a]	8.83 ± 0.16	11.71 ± 0.90	10.77 ± 0.37	9.75 ± 0.32*
Chloride	95.36 ± 1.09	105.71 ± 0.68	117.43 ± 0.39	91.25 ± 0.62	95.48 ± 0.73	92.95 ± 0.36	90.27 ± 0.63
Calcium	1.72 ± 0.55	1.64 ± 0.02	2.14 ± 0.10	1.74 ± 0.02	1.81 ± 0.01	1.73 ± 0.01	1.65 ± 0.02

NS, Normal saline; CMC, Carboxy methylcellulose, Vanco—Vancomycin; PL, *Polyalthia longifolia*.
Values expressed as mean ± SEM, Statistics: One-way ANOVA.
[a]$p < 0.05$ compared with normal control; *$p < 0.01$ compared with positive control.

increased it compared to normal control. Individual treatments of selenium (6 mg/kg), PL (200 mg/kg) and PL (400 mg/kg) did not affect the creatinine levels in vancomycin administered animals. However, combination of selenium (6 mg/kg) and PL (400 mg/kg) reduced significantly ($p < 0.05$) the blood creatinine levels compared to vancomycin group. Similar observations were recorded for BUN estimation, wherein vancomycin increased its level significantly ($p < 0.01$) compared to control group and none of the treated groups except combination of selenium (6 mg/kg) and PL (400 mg/kg) was found to be effective in reducing the BUN levels. The combined drug treatment reduced the BUN level significantly ($p < 0.05$) compared to vancomycin treated animals. The estimation of total protein levels indicated that the combination of selenium and PL significantly ($p < 0.05$) enhanced the level compared to positive control group, while other treatments did not induce any significant variation. No significant variation was observed when baseline values were compared with the normal control group.

Blood electrolytes

The influence of PL and selenium treatments on the blood electrolytes levels was recorded by estimating sodium, potassium, chloride, and calcium levels. Comparison of baseline data and normal control values revealed non-significant variation. Further, the observations indicated that none of the treatments significantly altered the blood sodium levels. Similarly, the findings of chloride and calcium estimations suggest that none of the treatments including vancomycin induced significant change in their serum levels. However, the blood potassium estimation suggests that vancomycin (150 mg/kg) significantly ($p < 0.05$) elevated its level compared to control. The combination of selenium (6 mg/kg) and PL (400 mg/kg) significantly ($p < 0.01$) reduced the elevated potassium level compared to vancomycin and none of the other treatments showed any significant variation (Table 4).

Discussion

The present study was conducted to evaluate the protective and curative potential of *Polyalthia longifolia* (PL) against vancomycin induced nephrotoxicity. Vancomycin is a complex tricyclic glycopeptide antibiotic obtained from the microorganism *Streptococcus orientalis*. The drug has erratic gastrointestinal

absorption characteristics and is thus mostly administered by parenteral route such as intravenous (Álvarez et al., 2016). Vancomycin is preferred for treating severe infections caused by different strains of microorganisms including some of the resistant ones. The drug is considered an effective alternative in patients hypersensitive to penicillins and/or cephalosporins as well admitted to intensive care units for the treatment of pneumonia, empyema, endocarditis, osteomyelitis, and soft tissue abscess (Brown et al., 2019). However, vancomycin treatment is reported to be associated with several adverse effects such as hypotension, tachycardia, phlebitis, nephrotoxicity, ototoxicity, exanthema, and hypersensitivity reactions (Filippone et al., 2017).

In this study, when vancomycin was administered on the first day (curative model), it significantly ($p < 0.05$) increased the creatinine and BUN levels (Table 1) without inducing marked variation in the blood electrolytes (Table 2). Similar observations were recorded in protective strategy when vancomycin was administered to animals on 11th day (Table 3). However, in this model, vancomycin was observed to increase the blood potassium level significantly ($p < 0.05$) compared to control group (Table 4).

The observation of this study suggested that vancomycin (150 mg/kg) has induced renal toxicity without altering the electrolyte levels, except the blood potassium levels. The findings contradict the earlier findings wherein vancomycin was reported to produce hypokalemia in patients receiving the drug. The study suggested that the infectious state of the patients could be an important factor related to vancomycin-induced hypokalemia (Karimzadeh et al., 2016). Further, the effect of vancomycin on renal parameters such as creatinine and BUN are in accordance with the previous research where vancomycin elevated these biomarkers in rats (Elaidy, 2013).

The experimental data available in the literature indicates that oxidative stress due to generation of reactive oxygen species as the major cause for nephrotoxicity. To support this, previous studies indicated that vancomycin lowered glutathione levels while increasing the lipid peroxidation in renal mitochondria (Xu et al., 2021). In kidney tissues, vancomycin was observed to inhibit antioxidant enzymes such as glutathione transferase, glutathione peroxidase and superoxide dismutase, causing cellular redox status to shift and toxic reactive oxygen species to rise (Guzel et al., 2020).

Several strategies have been attempted to improve the safety profile of vancomycin. One of the most logical approaches is to use a known antioxidant to reduce the oxidative stress-induced damages on the renal tissues (Kandemir et al., 2018). Some of the compounds derived from natural resources such as thymoquinone, curcumin and 1,5-Isoquinolinediol have been tested and were found to be efficacious in reducing the vancomycin-mediated nephrotoxicity (Dalaklioglu et al., 2010; Ahmida, 2012; Basarslan et al., 2012). Earlier studies have indicated that PL administration is well tolerated in different models of toxicity. The brine shrimp lethality assay revealed that PL possess very low level of general toxicity and the LC_{50} and LC_{90} values were observed to be 20 µg/ml and 70–80 µg/ml, respectively (Chanda et al., 2012). An *in-vivo* study conducted on Wistar rats indicated that the extract of PL did not produce any signs of toxicity when tested up to 3,240 mg/kg, b.w. The study suggested that administration of the extract for 14 days did not induce alteration in the body weight, food or water intake, organ weights, biochemical and hematology in both sexes of the animals (Jothy et al., 2013).

Administration of PL at lower dose (200 mg/kg) and higher dose (400 mg/kg) were tested for protective and curative action against vancomycin-induced renal damages. In the curative strategy, the monotherapy of PL (200 mg/kg) and selenium (6 mg/kg) to the vancomycin treated rats did not induce significant alteration in the levels of uric acid, creatinine, BUN and total proteins. Similarly, the higher dose of PL (400 mg/kg) also did not produced significant variation except for BUN, where it lowered the levels (37.6%) compared to positive control group. However, when combination of selenium (6 mg/kg) and PL (400 mg/kg) was tested in the vancomycin, a reduction was observed in the levels of uric acid (35.3%), creatinine (55.6%) and BUN (55.8%) compared to positive control group (Table 1). On the other hand, PL alone as well in combination with selenium showed a dose-dependent reduction on the levels of potassium and chloride in vancomycin-treated animals. The percentage reduction in potassium level was found to be 6.2% with PL—200 mg/kg, 12.2% with PL—400 mg/kg, 30.6% with combination, and chloride level was 1.4% with PL—200 mg/kg, 2.1% with PL—400 mg/kg, 6.6% with combination (Table 2)

The protocol to test the protective effect of test compounds indicated that the monotherapy of PL (200 and 400 mg/kg) as well as selenium (6 mg/kg) did not induced significant variation in the levels of uric acid, creatinine, BUN and total proteins compared to the positive control group. Further, when combination of higher dose of PL (400 mg/kg) and selenium (6 mg/kg) was tested in the vancomycin treated group, a reduction in the levels of uric acid (36.1%) and BUN (32.6%) and elevation of total proteins (7.4) was observed (Table 3). The monotherapy of PL and selenium did not produce significant alteration in the electrolyte levels but the combination of selenium (6 mg/kg) and PL (400 mg/kg) reduced (34.1%) the potassium level in vancomycin treated animals (Table 4).

The observations of the study indicated that PL in both the tested models did not induce significant reversal against vancomycin mediated renal changes (Table 1; Table 3). However, elevated potassium level was found to be significantly reduced in the curative strategy (Table 3). Selenium being a known antioxidant prevented the vancomycin-induced renal damages in an earlier study (Asefaw et al., 2020). However, in the present study it was used as standard and showed non-significant variation on the altered renal biomarker levels induced by vancomycin (Table 1; Table 3). The blood electrolyte levels were also found to be non-significantly influenced by selenium (Table 2; Table 4).

An important observation of the study is that when combination of selenium (6 mg/kg) and PL (400 mg/kg) was tested against vancomycin, a significant reversal of elevated uric acid, creatinine and BUN level was seen in both curative (Table 1) as well as protective models (Table 2). Uric acid is formed from metabolic breakdown of purine nucleotides, while creatinine is a waste product obtained from muscle and protein metabolism. During the urea cycle, liver produces urea as a waste substance from the protein digestion. These waste products are primarily removed by kidneys through glomerular filtration and the elevation of their levels in blood indicates the failure in the renal function (Sinha et al., 2016). Vancomycin in the earlier studies induced nephrotoxicity by affecting the glomerular filtration rate and the combination of the selenium with PL appears to have counteracted this action of vancomycin (Mehanna et al., 2022). Besides, the combination therapy was found to be effective in reducing the blood potassium levels in both curative and protective strategies (Table 2; Table 4). Earlier studies have

indicated that PL possesses antioxidant property (Chen et al., 2014).

Observations of this study suggest that combination of selenium and PL might have potentiated the antioxidant activity, and this might have effectively managed the oxidative stress generated by vancomycin in minimizing the nephrotoxicity, which was earlier not achieved with monotherapy. Further, PL has been reported to possess antimicrobial property [42] and this action could play a positive role in the therapeutic efficacy of vancomycin besides minimizing the toxicity reactions. Besides, the non-significant variation in the blood electrolyte levels indicated that none of the treatments tested in the study need additional therapeutic interventions such as diuretics to maintain the electrolyte homeostasis. However, more studies are required to precisely establish either the protective or curative role of PL in vancomycin induced systemic toxicity including testing the early nephrotoxicity biomarkers such as kidney injury molecule-1 (KIM-1) and neutrophil geletinase-associated lipocalin (NGAL).

Conclusion

It can be concluded that the nephroprotective effect of PL was correlated with its ability to improve renal function parameters. A possible mechanism of PL is increased glomerular filtration rate resulting in decreased serum creatinine while maintaining serum magnesium and potassium levels. PL's curative and protective effect against Vancomycin toxicity may also be due to its powerful antioxidant and detoxification properties and these might have prevented the inflammatory response to maintain the normal kidney function. The precise mechanism of action may be the subject of a separate, exhaustive study. Consequently, the present study classifies PL as a possible nephroprotective agent and supports the traditional natural claim regarding its activity and use in renal disorders.

Data availability statement

The original contributions presented in the study are included in the article/supplementary material, further inquiries can be directed to the corresponding author.

Ethics statement

The animal study was reviewed and approved by Institutional Animal Ethics Committee of Al-Ameen College of Pharmacy.

Author contributions

Under the supervision of KD, AM, KB, SM, and RG carried out the research methodology. MI, MA, AR, MH, MG, AA, MA, ASA, AAA, and SR were responsible for the formal hanalysis of the work while AA and NA participated in writing the original draft of the manuscript. KD administered the project and SB was instrumental in reviewing and editing of the manuscript.

Funding

The authors are also thankful to AlMaarefa University, Riyadh, Saudi Arabia for extending financial support to do this research.

Acknowledgments

The authors would like to acknowledge the financial support provided by the Researchers Supporting Project number (RSP2023R115), King Saud University, Riyadh, Saudi Arabia.

Conflict of interest

The authors declare that the research was conducted in the absence of any commercial or financial relationships that could be construed as a potential conflict of interest.

Publisher's note

All claims expressed in this article are solely those of the authors and do not necessarily represent those of their affiliated organizations, or those of the publisher, the editors and the reviewers. Any product that may be evaluated in this article, or claim that may be made by its manufacturer, is not guaranteed or endorsed by the publisher.

References

Afolabi, S. O., Olorundare, O. E., Babatunde, A., Albrecht, R. M., Koketsu, M., Syed, D. N., et al. (2019). Polyalthia longifolia extract triggers ER stress in prostate cancer cells concomitant with induction of apoptosis: Insights from *in vitro* and *in vivo* studies. *Oxid. Med. Cell Longev.* 2019, 6726312. doi:10.1155/2019/6726312

Ahmida, M. H. (2012). Protective role of curcumin in nephrotoxic oxidative damage induced by vancomycin in rats. *Exp. Toxicol. Pathol.* 64 (3), 149–153. doi:10.1016/j.etp.2010.07.010

Al-Doaiss, A., Jarrar, Y., Shati, A., Alfaifi, M., Al-Kahtani, M., and Jarrar, B. (2021). Renal alterations induced by chronic exposure to therapeutic doses of antihypercholestremic atorvastatin. *Endocr. Metab. Immune. Disord. Drug Targets.* 21 (11), 2043–2054. doi:10.2174/1871530321666210106105059

Álvarez, R., López Cortés, L. E., Molina, J., Cisneros, J. M., and Pachón, J. (2016). Optimizing the clinical use of vancomycin. *Antimicrob. Agents Chemother.* 60 (5), 2601–2609. doi:10.1128/AAC.03147-14

Arifin, W. N., and Zahiruddin, W. M. (2017). Sample size calculation in animal studies using resource equation approach. *Malays. J. Med. Sci.* 24 (5), 101–105. doi:10.21315/mjms2017.24.5.11

Asefaw, T., Wolde, M., Edao, A., Tsegaye, A., Teklu, G., Tesfay, F., et al. (2020). Assessment of liver and renal function tests among gasoline exposed gas station workers in Mekelle city, Tigray region, Northern Ethiopia. *PLoS One* 15 (10), e0239716. doi:10.1371/journal.pone.0239716

Basarslan, F., Yilmaz, N., Ates, S., Ozgur, T., Tutanc, M., Motor, V. K., et al. (2012). Protective effects of thymoquinone on vancomycin-induced nephrotoxicity in rats. *Hum. Exp. Toxicol.* 31 (7), 726–733. doi:10.1177/0960327111433185

Bhattacharya, A. K., Chand, H. R., John, J., and Deshpande, M. V. (2015). Clerodane type diterpene as a novel antifungal agent from Polyalthia longifolia var. pendula. *Eur. J. Med. Chem.* 94, 1–7. doi:10.1016/j.ejmech.2015.02.054

Brown, C. C., Manis, M. M., Bohm, N. M., and Curry, S. R. (2019). Oral vancomycin for secondary prophylaxis of *Clostridium difficile* infection. *Ann. Pharmacother.* 53 (4), 396–401. doi:10.1177/1060028018815170

Chanda, S., Baravalia, Y., and Kaneria, M. (2011). Protective effect of Polyalthia longifolia var. pendula leaves on ethanol and ethanol/HCl induced ulcer in rats and its antimicrobial potency. *Asian pac. J. Trop. Med.* 4 (9), 673–679. doi:10.1016/S1995-7645(11)60172-7

Chanda, S., Dave, R., Kaneria, M., and Shukla, V. (2012). Acute oral toxicity of Polyalthia longifolia var. pendula leaf extract in Wistar albino rats. *Pharm. Biol.* 50, 1408–1415. doi:10.3109/13880209.2012.682117

Chen, X. X., Liang, G., Chai, W. M., Feng, H. L., Zhou, H. T., Shi, Y., et al. (2014). Antioxidant and antityrosinase proanthocyanidins from Polyalthia longifolia leaves. *J. Biosci. Bioeng.* 118 (5), 583–587. doi:10.1016/j.jbiosc.2014.04.015

Dalaklioglu, S., Tekcan, M., Gungor, N. E., Celik-Ozenci, C., Aksoy, N. H., Baykal, A., et al. (2010). Role of the poly (ADP-ribose) polymerase activity in vancomycin-induced renal injury. *Toxicol. Lett.* 192 (2), 91–96. doi:10.1016/j.toxlet.2009.10.002

Edmond, M. P., Mostafa, N. M., El-Shazly, M., and Singab, A. N. B. (2021). Two clerodane diterpenes isolated from Polyalthia longifolia leaves: Comparative structural features, anti-histaminic and anti-Helicobacter pylori activities. *Nat. Prod. Res.* 35 (23), 5282–5286. doi:10.1080/14786419.2020.1753048

Elaidy, S. M. (2013). Protective effects of aminophylline on vancomycin-induced acute kidney injury in rats: Anti-oxidant and anti-inflammatory roles. *Suez Canal Univ. Med. J.* 16, 112–121. doi:10.21608/SCUMJ.2013.54222

Elyasi, S., Khalili, H., Dashti-Khavidaki, S., and Mohammadpour, A. (2012). Vancomycin-induced nephrotoxicity: Mechanism, incidence, risk factors and special populations. A literature review. *Eur. J. Clin. Pharmacol.* 68 (9), 1243–1255. doi:10.1007/s00228-012-1259-9

Filippone, E. J., Kraft, W. K., and Farber, J. L. (2017). The nephrotoxicity of vancomycin. *Clin. Pharmacol. Ther.* 102 (3), 459–469. doi:10.1002/cpt.726

Gao, L., Niu, X., Niu, T., Wang, X., Lu, X., Feng, Q., et al. (2020). Curative efficacy of extract from Ganjiangdazao recipe on functional dyspepsia in rats. *J. Tradit. Chin. Med.* 40 (4), 654–663. doi:10.19852/j.cnki.jtcm.2020.04.012

Guzel, S., Sahinogullari, Z. U., Canacankatan, N., Antmen, S. E., Kibar, D., and Coskun-Yilmaz, B. (2020). Potential renoprotective effects of silymarin against vancomycin-induced nephrotoxicity in rats. *Drug Chem. Toxicol.* 6, 630–636. doi:10.1080/01480545.2019.1584208

Jothy, S. L., Chen, Y., Kanwar, J. R., and Sasidharan, S. (2013). Evaluation of the genotoxic potential against H2O2-radical-mediated DNA damage and acute oral toxicity of standardized extract of Polyalthia longifolia leaf. *Evid. Based Compl. Altern. Med.* 2013, 925380. doi:10.1155/2013/925380

Kandemir, F. M., Yildirim, S., Kucukler, S., Caglayan, C., Mahamadu, A., and Dortbudak, M. B. (2018). Therapeutic efficacy of zingerone against vancomycin-induced oxidative stress, inflammation, apoptosis and aquaporin 1 permeability in rat kidney. *Biomed. Pharmacother.* 105, 981–991. doi:10.1016/j.biopha.2018.06.048

Karimzadeh, I., Haghighati, G., Ramzi, M., Sagheb, M. M., and Zomorodian, K. (2016). Electrolyte disorders during vancomycin treatment in hospitalized patients at hematology-oncology wards of Namazi hospital in Shiraz. *Trends Pharm. Sci.* 2 (3), 223–228.

Kim, S. Y., and Moon, A. (2012). Drug-induced nephrotoxicity, and its biomarkers. *Biomol. Ther.* 20 (3), 268–272. doi:10.4062/biomolther.2012.20.3.268

Kirubakari, B., Chen, Y., and Sasidharan, S. (2020). Synergistic effect of Polyalthia longifolia leaf and antibiotics against clinical isolates of methicillin-resistant *Staphylococcus aureus* (MRSA) by microscopic technique. *Antiinflamm. Antiallergy Agents Med. Chem.* 19 (3), 323–334. doi:10.2174/1871523018666190522112902

Lee, T. H., Wang, M. J., Chen, P. Y., Wu, T. Y., Wen, W. C., Tsai, F. Y., et al. (2009). Constituents of Polyalthia longifolia var. pendula. *J. Nat. Prod.* 72 (11), 1960–1963. doi:10.1021/np900207z

Liu, D., Wang, H., Zhang, Y., and Zhang, Z. (2020). Protective effects of chlorogenic acid on cerebral ischemia/reperfusion injury rats by regulating oxidative stress-related Nrf2 pathway. *Drug Des. devel. Ther.* 14, 51–60. doi:10.2147/DDDT.S228751

Mehanna, E. T., Khalaf, S. S., Mesbah, N. M., Abo-Elmatty, D. M., and Hafez, M. M. (2022). Anti-oxidant, anti-apoptotic, and mitochondrial regulatory effects of selenium nanoparticles against vancomycin induced nephrotoxicity in experimental rats. *Life Sci.* 288, 120098. doi:10.1016/j.lfs.2021.120098

Oyeyemi, A. O., Oseni, O. A., Babatunde, A. O., and Molehin, O. R. (2020). Modulatory effect of Polyalthia longifolia leaves against cadmium-induced oxidative stress and hepatotoxicity in rats. *J. Compl. Integr. Med.* 9. doi:10.1515/jcim-2019-0038

Ozaslan, M., and Oguzkan, S. B. (2018). Use of plant extracts in alternative medicine. *Pak. J. Biol. Sci.* 21 (1), 1–7. doi:10.3923/pjbs.2018.1.7

Pais, G. M., Liu, J., Avedissian, S. N., Hiner, D., Xanthos, T., Chalkias, A., et al. (2020). Lack of synergistic nephrotoxicity between vancomycin and piperacillin/tazobactam in a rat model and a confirmatory cellular model. *J. Antimicrob. Chemother.* 75 (5), 1228–1236. doi:10.1093/jac/dkz563

Perazella, M. A. (2019). Drug-induced acute kidney injury: Diverse mechanisms of tubular injury. *Curr. Opin. Crit. Care.* 25 (6), 550–557. doi:10.1097/MCC.0000000000000653

Radi, Z. A. (2019). Kidney pathophysiology, Toxicology, and drug-induced injury in drug development. *Int. J. Toxicol.* 38 (3), 215–227. doi:10.1177/1091581819831701

Rai, A. K., Singh, S. P., Pandey, A. R., Ansari, A., Ahmad, S., Sashidhara, K. V., et al. (2021). Flavonoids from Polyalthia longifolia prevents advanced glycation end products formation and protein oxidation aligned with fructose-induced protein glycation. *Nat. Prod. Res.* 35 (17), 2921–2925. doi:10.1080/14786419.2019.1672690

Sinha, R. A., Haikal, A., Hammoud, K. A., and Yu, A. S. (2016). Vancomycin and the risk of aki: A systematic review and meta-analysis. *Clin. J. Am. Soc. Nephrol.* 11, 2132–2140. doi:10.2215/CJN.05920616

Stogios, P. J., and Savchenko, A. (2020). Molecular mechanisms of vancomycin resistance. *Protein Sci.* 29 (3), 654–669. doi:10.1002/pro.3819

Tantranont, N., Hebert, S., and Truong, L. D. (2021). Vancomycin nephrotoxicity causing renal transplant acute kidney injury. *Transpl. Proc.* 53 (10), 2913–2917. doi:10.1016/j.transproceed.2021.09.033

URIC-ACID (2020). Principle and procedure for renal biomarkers estimation. Available from: https://oscarmedcare.com/URIC-ACID.php.

Vijayarathna, S., Oon, C. E., Chen, Y., Kanwar, J. R., and Sasidharan, S. (2017). Polyalthia longifolia Methanolic Leaf Extracts (PLME) induce apoptosis, cell cycle arrest and mitochondrial potential depolarization by possibly modulating the redox status in hela cells. *Biomed. Pharmacother.* 89, 499–514. doi:10.1016/j.biopha.2017.02.075

Xu, W., Mao, Z., Zhao, B., Ni, T., Deng, S., Yu, P., et al. (2021). Vitamin C attenuates vancomycin induced nephrotoxicity through the reduction of oxidative stress and inflammation in HK-2 cells. *Ann. Palliat. Med.* 10 (2), 1748–1754. doi:10.21037/apm-20-694

Yadav, P., Choudhury, S., Barua, S., Khandelwal, N., Kumar, N., Shukla, A., et al. (2020). Polyalthia longifolia leaves methanolic extract targets entry and budding of viruses-an *in vitro* experimental study against paramyxoviruses. *J. Ethnopharmacol.* 248, 112279. doi:10.1016/j.jep.2019.112279

Yao, L. J., Jalil, J., Attiq, A., Hui, C. C., and Zakaria, N. A. (2019). The medicinal uses, toxicities and anti-inflammatory activity of Polyalthia species (Annonaceae). *J. Ethnopharmacol.* 229, 303–325. doi:10.1016/j.jep.2018.10.001

frontiers | Frontiers in Pharmacology

TYPE Original Research
PUBLISHED 26 January 2023
DOI 10.3389/fphar.2023.1119360

Check for updates

OPEN ACCESS

EDITED BY
Tariq Ismail,
Abbottabad Campus, Pakistan

REVIEWED BY
Irum Shahzadi,
COMSATS University Islamabad, Pakistan
Izhar Ullah,
University of Poonch Rawalakot, Pakistan

*CORRESPONDENCE
Muhammad Naveed Mushtaq,
muhammad.mushtaq2@pharm.uol.edu.pk
Asifa Bashir,
aasifa.basheer@gmail.com

SPECIALTY SECTION
This article was submitted to Predictive Toxicology, a section of the journal Frontiers in Pharmacology

RECEIVED 08 December 2022
ACCEPTED 02 January 2023
PUBLISHED 26 January 2023

CITATION
Bashir A, Mushtaq MN, Younis W and Anjum I (2023), Fenchone, a monoterpene: Toxicity and diuretic profiling in rats. *Front. Pharmacol.* 14:1119360. doi: 10.3389/fphar.2023.1119360

COPYRIGHT
© 2023 Bashir, Mushtaq, Younis and Anjum. This is an open-access article distributed under the terms of the Creative Commons Attribution License (CC BY). The use, distribution or reproduction in other forums is permitted, provided the original author(s) and the copyright owner(s) are credited and that the original publication in this journal is cited, in accordance with accepted academic practice. No use, distribution or reproduction is permitted which does not comply with these terms.

Fenchone, a monoterpene: Toxicity and diuretic profiling in rats

Asifa Bashir*, Muhammad Naveed Mushtaq*, Waqas Younis and Irfan Anjum

Faculty of Pharmacy, The University of Lahore, Lahore, Pakistan

Fenchone is a monoterpene present in the essential oils of various plants, including *Foeniculum vulgare* and *Peumus boldus*. Previous studies confirmed the anti-inflammatory, antioxidant, wound-healing, antidiarrheal, antifungal, antinociceptive, and bronchodilator activities of fenchone. Owing to various pharmacological activities of Fenchone, the current research was designed to evaluate its diuretic activity along with toxicity profiling. For evaluating acute toxicity, OECD guideline 425 was followed in which a single dose of 2000 mg/kg was orally administered to rats. For evaluating the diuretic potential in rats, three doses of Fenchone (100, 200, and 400 mg/kg) were assayed in comparison to furosemide (15 mg/kg) as the standard drug, followed by measurements of urinary volume, urinary electrolytes, uric acid, and urinary creatinine in saline-loaded rats for 8 h. The acute toxicity study showed a significant increase in hemoglobin (Hb), red blood cells (RBCs), alkaline phosphatase (ALP), and alkaline transaminase (ALT) along with a significant decrease in serum triglycerides, cholesterol, and uric acid levels when compared with the control group. The oxidative stress parameter, superoxide dismutase (SOD), was increased in the heart and spleen. Nitrite (NO) and glutathione were significantly increased in the kidney. The acute diuretic effect of Fenchone (400 mg/kg) significantly increased the urinary output, electrolytes (Na^+, K^+, and Ca^{++}), urinary creatinine, and urinary uric acid in a dose-dependent manner. The Na^+/K^+ ratio was remarkably higher in the treatment group than that of the control group. The diuretic index, saluretic index, and Lipschitz value were also calculated from electrolyte concentration and urinary volume measurements, and the values were significantly increased in rats administered with fenchone at 400 mg/kg dose. The current study concluded that fenchone is safe and has remarkable diuretic action.

KEYWORDS

LD_{50}, oxidative stress, fenchone, sodium, potassium

Introduction

In order to develop and test newer molecules before clinical trials, toxicity studies of compounds are fundamental (Anwar et al., 2021). A very vital consideration for the toxicity studies is ensuring the safety of the animals exposed to the study compounds (Morton, 1998). International governing organizations for toxicity determines dose-related perils on human subjects by evaluating the effect of study compounds on animals (Lewis et al., 2002). Toxicity profiling allows easy assessment of tissues along with the approximation of several biochemical and pathophysiological parameters (Dandekar et al., 2010; Arome and Chinedu, 2013). An association can be established between toxic and therapeutic doses by conducting toxicity studies of newer agents, and these extensive studies allow the researchers to determine whether to further proceed with clinical trials or not (Aneela et al., 2011). These experiments not only

help in determining the safety of the newer agents in animal models but also foster the drug's suitability for its therapeutic use (Jothy et al., 2011).

Natural therapies from medicinal plants are vital for developing new treatment protocols. Most of the current therapies have been isolated from natural plant extracts and semi-synthesized or chemically synthesized using natural constituents (Wright, 2019). Due to recent technological advances, natural therapies serve as a preliminary source of developing newer and innovative therapeutic medications, encompassing a vast range of conditions (Shen, 2015). Modern research on drug discovery from medicinal plants includes complex methods linking phytochemical, biological, botanical, and molecular activities (Balunas and Kinghorn, 2005). Phytochemicals, as a part of plant constituents, express distinct bio-activities with better acceptability, lesser side effects, better safety profile, and more cost-effective approaches. Also, they are broadly inspected for their capacity to offer better health outcomes (Krum and Pellizzer, 1998).

Diuretics are the mainstay for treating hypertension, ascites, pulmonary edema, and congestive heart failure and are either used in combination with other agents or alone (Lahlou, Tahraoui, Israili, and Lyoussi, 2007). The irrational use of diuretics poses certain restrictions regarding their side effects, including metabolic imbalances, electrolyte disturbances, activation of the renin–angiotensin aldosterone system (RAAS), and sexual dysfunction, and these side effects lead to the quest for novel diuretic agents from plant sources (Schlickmann et al., 2018).

Fenchone exists as a bicyclic monoterpene and is present in the essential oil of various fragrant plants, including *Foeniculum vulgare* and *Peumus boldus* (Kim, Song, Cho, and Lee, 2020). Previous pharmacological research has confirmed the anti-inflammatory, antioxidant, wound-healing, antidiarrheal, antifungal, antinociceptive, and bronchodilator activities of fenchone (Him, Ozbek, Turel, and Oner, 2008; Slavchev et al., 2014; Keskin et al., 2017; de Souza Pessoa et al., 2020; Rehman, Ansari, Samad, and Ahmad, 2022). The therapeutic efficacy of the fruits of *Foeniculum vulgare* is generally accredited to its essential oils. Various research studies uncovered that the essential oils as well as the individual elements demonstrate unique therapeutic potentials (Rather, Dar, Sofi, Bhat, and Qurishi, 2016). Therefore, the modern medicine era necessitates designing and developing newer diuretic agents that not only enhance the cardiovascular potentials by reducing mortality but also overcome the harmful effects of the drugs (Younis et al., 2021). Fenchone being present in many aromatic plants has shown to be a promising diuretic for treating hypertension (Agarwal, Gupta, Agrawal, Srivastava, and Saxena, 2008). Therefore, based on the reported results of the plant, fenchone was selected as the study compound and its diuretic potential and acute toxicity in rat models were determined.

Materials and methods

Chemicals and drugs

The chemicals employed for the research included pyrogallol solution from Oxford Labs (India); trichloroacetic acid, Griess reagent, and Ellman's reagent (DNTB) from Omicron Sciences Limited (United Kingdom); and potassium phosphate buffer, carboxymethyl cellulose (CMC), thiobarbituric acid, furosemide, and fenchone (CAS No: 7,787-20-4) purchased from Sigma-Aldrich (United States).

Animals

Adult Wistar albino rats (weighing 150–250 gm) of age 4–8 weeks were housed in the animal house of The University of Lahore, Pakistan. All the animals were placed under normal conditions, provided with chow and water, and kept in a well-maintained atmosphere in a 12 h light/dark cycle at proper temperature (25°C ± 1°C). All animals were provided with housing environments in accordance with accepted principles for laboratory animal use and care (NIH publication number # 85-23, revised in 1985). All experimental procedures were approved (IREC-2022-17) by the Institutional Ethical Committee of the Faculty of Pharmacy, The University of Lahore.

Acute oral toxicity

The OECD 425 guidelines were followed for assessing acute oral toxicity. Healthy female albino rats were fasted overnight but had free access to water (OECD, 2001). Initially, fenchone was administered at 2000 mg/kg dose orally for the limit test to a single rat according to body weight, and the animal was closely observed for 30 min and then for next 4 h and 24 h. If there were no mortality rates, the same dose was administered to four other rats, and the rats were monitored for any alteration in general behavior, allergic reactions, body weight, and mortality for 14 days. The same protocol was followed for the normal control, which received only .5% carboxymethylcellulose (CMC) as a vehicle according to their body weight (Anwar et al., 2021).

Estimation of hematological and biochemical parameters

The rats were anesthetized by administering 3%–4% isoflurane by diluting it with oxygen, and blood was withdrawn by cardiac puncture after 14 days. The hematological parameters encompassed hemoglobin (Hb), red blood cells (RBCs), packed cell volume (PCV), mean corpuscular volume (MCV), mean corpuscular hemoglobin (MCH), mean corpuscular hemoglobin concentration (MCHC), and white blood cells (WBCs), while blood was isolated in tubes having EDTA sodium, followed by centrifugation at 1,400 *g* for 10–15 min for the isolation of serum for measuring various biochemical parameters like AST, ALT, ALP, bilirubin, creatinine, uric acid, triglycerides, and cholesterol. All these parameters were assessed by utilizing their specific kits (Konan, Bacchi, Lincopan, Varela, and Varanda, 2007).

Estimation of oxidative stress parameters

Lastly, rats were killed by cervical dislocation, and vital organs like the heart, liver, kidney, and spleen were excised and weighed separately. The tissue homogenate was prepared by mixing 1 gm of tissue with 10 mL of phosphate buffer (.1 M, pH 7.4) followed by centrifugation. The supernatant was isolated for the measurement of

oxidative stress parameters like GSH, SOD, NO, and MDA (Saleem et al., 2017; Anwar et al., 2021). All the tests were executed in triplicate.

Superoxide dismutase (SOD) estimation

A volume of 2.8 mL of potassium phosphate buffer (.1 M, pH 7.4) was mixed with .1 mL of tissue homogenate, followed by .1 mL pyrogallol solution. Mixture absorbance was measured at 325 nm, and the following SOD standard cure regression line was drawn for estimating SOD values (Nazir et al., 2021):

$$Y = 0.0095X + 0.1939.$$

Nitrite (NO) level estimation

The supernatant of tissue homogenate and Griess reagent were taken in equal proportion and mixed thoroughly, and this mixture was allowed to incubate for 10 min, followed by the measurement of absorbance at 546 nm. A sodium nitrite regression line was used for estimating nitrite levels (Nazir et al., 2021) as follows:

$$Y = 0.003432X + 0.0366.$$

Glutathione (GSH) estimation

Tissue homogenate (1 mL) was precipitated with 10% trichloroacetic acid (1 mL) along with phosphate buffer (4 mL). The aliquot supernatant was separated after precipitation followed by the addition of .5 mL of 5, 5 dithiobis 2 nitrobenzoic acid (DNTB). Mixture absorbance was measured at 412 nm, and the following formula was utilized for estimating the amount of GSH in the tissue homogenate (Saeed, Saleem, Anwar, Ahmad, and Anwar, 2020):

$$Glutathione\,(GSH) = Y - \frac{0.00314}{0.034} \times \frac{DF}{BT} \times VU,$$

where Y is the absorbance at 412 nm, DF is the dilution factor, BT is the tissue homogenate, and VU is the volume of aliquot.

Malondialdehyde (MDA) estimation

Tissue homogenate (1 mL) was added to 3 mL of thiobarbituric acid (TBA) reagent. The resulting mixture was stirred and allowed to incubate for 15 min at room temperature, followed by cooling on an ice bath and centrifugation. The layer of supernatant was separated for measuring the absorbance at 532 nm. The following formula was utilized for estimating the concentration of MDA in tissue homogenate (Nazir et al., 2021):

$$\text{Conc of MDA} = \frac{\text{Abs } 532 \times 100 \times V_t}{1.56 \times 10^5 \times W_t \times V_u},$$

where V_t is the total volume mixture, 1.56×10^5 is the extinction coefficient, W_t is the weight of the dissected tissue, and V_u is the volume of aliquot.

TABLE 1 Behavioral changes after treatment with a single dose of fenchone (F) (2000 mg/kg) in the acute oral toxicity study when compared to those of the normal control.

Parameter	Normal control (NC)	Treatment group
Fur and skin	N	N
Eyes	N	N
Salivation	N	N
Respiration	N	N
Urination (color)	N	N
Feces consistency	N	N
Somatomotor activity and behavior pattern	N	N
Sleep	N	N
Mucous membrane	N	N
Convulsions and tremors	NF	NF
Itching	NF	P
Coma	NF	NF
Mortality	NF	NF

N, normal; NF, not found; P, present.

Histopathological evaluation

The excised organs including the heart, liver, kidney, and spleen were placed in paraformaldehyde (4%), fixed in paraffin, and cut into 5-μm sections, followed by staining with eosin and hematoxylin and observed using the microscope for any pathological changes (Anwar et al., 2021).

Assessment of acute diuretic activity of fenchone

Acute diuretic activity

The rats were placed in metabolic cages 7 days prior to the procedure to acclimatize them to the experimental conditions. The rats, weighing 150–250 gm, were divided into five groups, with five rats in each group. Initially, all the rats received 5 mL/100 gm (p.o) of .9% normal saline to ensure a uniform water and salt load (Younis et al., 2021). After 45 min, Group I, which was the normal control group, received only .5% CMC (1 mL/kg), while Group II was the reference standard and received 15 mg/kg furosemide by the oral route, and the test groups (III, IV, and V) were given 100, 200, and 400 mg/kg of fenchone, respectively, through oral gavage.

Animals were kept in metabolic cages, and urine sampling was carried out after 2, 4, and 6 h of treatment for analysis of Na^+, K^+, Ca^{++}, urinary creatinine, pH, and uric acid.

Electrolyte estimation

pH was measured using a pH meter, and Na^+, K^+, Ca^{++}, uric acid, and urinary creatinine were measured (Prathibhakumari and Prasad, 2014) using Bio-active Diagnostic System kits.

TABLE 2 Effects of treatment (F) on body weight of rats in the acute toxicity study.

Body weight	Normal control (NC)	Treatment group
0 day body weight (gm)	168 ± 7.90	165.2 ± 8.3
First day body weight (gm)	169 ± 7.90	166.5 ± 8.3
Seventh day body weight (gm)	169.5 ± 7.70	161.2 ± 11.3
Fourteenth day body weight (gm)	168.5 ± 6.61	161.5 ± 11.9*

Values are shown as mean ± SEM; N = 6, *$p < .05$ in comparison with the first day.

TABLE 3 Effects of F (2000 mg/kg) dose on organ weight in the acute toxicity study.

Organ	Normal control (gm)	Fenchone (2000 mg/kg)
Heart	.52 ± .021	.52 ± .035
Kidney	1.74 ± .02	1.71 ± .014
Liver	7.03 ± .02	7.02 ± .018
Spleen	.53 ± .02	.50 ± .028

Values are presented as mean ± SEM, N = 6.

Diuretic index, saluretic index, and Lipschitz value

Based on the urine volume and electrolyte concentrations, the diuretic index, saluretic index, and Lipschitz value were also calculated.

Diuretic index = urinary volume of the treatment group/urinary volume of the normal control group,

Saluretic index $Na^+(SI_{Na}^+)$ = urinary Na^+ concentration of the treatment group/urinary Na^+ concentration of the normal control group,

Saluretic index $K^+(SI_K^+)$ = urinary K^+ concentration of the treatment group/urinary K^+ concentration of the normal control group,
Saluretic index (SI) = $SI_{Na}^+ + SI_K^+$ of the treatment group/$SI_{Na}^+ + SI_K^+$ of the normal control group,
Lipschitz value = urinary volume of the treatment group/urinary volume of the standard group.

Statistical analysis

The results of the experiments were evaluated using GraphPad Prism version 5, and the data were presented as mean ± SEM. Both one-way ANOVA and two-way ANOVA were used for analyzing the data statistically, followed by the Tukey comparison test and Bonferroni and Dunnett's *post hoc* tests. $p < .05$ was considered significant. $p < .01$ and $p < .001$ indicated moderate and highly significant levels, respectively.

Results

Effect of treatment on the behavioral pattern in the acute toxicity study

Table 1 shows that no mortality or morbidity occurred during the acute toxicity study with fenchone (F) treatment (2000 mg/kg). No significant difference was noted in behavioral parameters when compared to the normal control group.

Effects of treatment on body weight and organ weight

The body weight of the treated animals was noted from the first day to the 14th day. The treatment group showed a parallel increase in body weight similar to the normal control group in the early days, but a significant decrease was observed on the 14th day in comparison with the first day as shown in Tables 2, 3. A non-significant difference was observed in all organ weights when compared with the control group.

Treatment effect on complete blood count in the acute toxicity study

On the 14th day, blood was withdrawn by cardiac puncture from the treated animals. A significant rise in the RBC count and Hb level was observed in animals treated with fenchone (2000 mg/kg) when compared with those of the control group as shown in Table 4. However, other parameters are parallel to the normal control group.

Analysis of biochemical markers in treatment groups in the acute toxicity study

Table 5 illustrates that animals treated with fenchone (2,000 mg/kg) showed a significant decrease in the triglyceride and cholesterol levels in comparison with those of the control group. However, hepatic functioning markers were significantly higher than those of the control group. Surprisingly, fenchone significantly decreased the uric acid levels in the treated animals when compared with the control.

Oxidative stress marker analysis in the acute toxicity study

Figure 1 shows the results of oxidative stress biomarker analysis in the chosen organs of the treated animals. The results showed that in the kidneys of the Fenchone-treated animals, there was a significant decrease in SOD, NO, and GSH when compared to those of the normal control group. A highly significant increase in

TABLE 4 Analysis of complete blood count in animals treated with fenchone (2000 mg/kg) in the acute toxicity study.

Parameter	Unit	Normal control (NC)	Fenchone (2000 mg/kg)
Hb	G/dL	10.74 ± .01	15.2 ± .15*
RBCs	$\times 10^6/\mu L$	3.64 ± .02	8.1 ± .05*
PCV	%	43.0 ± .57	41 ± .57
MCV	f/L	101.66 ± .38	52.6 ± 1.45
MCH	pg/L	25.52 ± .27	19.7 ± .23
MCHC	G/dL	25.35 ± 0.1	37.6 ± .63
WBCs	$\times 10^3/\mu L$	7.3 ± .10	7.0 ± .05

Values are presented as mean ± SEM, N = 6. *$p < .05$ in comparison with the control group.

TABLE 5 Effect of treatment on biochemical parameters.

Biochemical marker		Unit	Normal control	Fenchone (2000 mg/kg)
Lipid profile	Triglycerides	mg/dL	197 ± 1.15	135 ± 1.15**
	Cholesterol	mg/dL	223 ± 1.45	192 ± 1.152**
	HDL	mg/dL	22.5 ± .65	27.5 ± 1.23
Renal function test	Creatinine	mg/dL	23.7 ± .176	22.4 ± .127
	Uric acid	mg/dL	23.5 ± .213	.379 ± .001*
Liver function test	ALP	U/L	186 ± 1.87	192 ± 1.9
	ALT	U/L	45 ± .34	58 ± .63*
	AST	U/L	72 ± 1.42	81 ± 2.1*
	Bilirubin	mg/dL	.95 ± .032	1.310 ± .017

Data are presented as mean ± SEM, N = 6; *$p < .05$, **$p < .01$, and ***$p < .001$ vs. normal control.

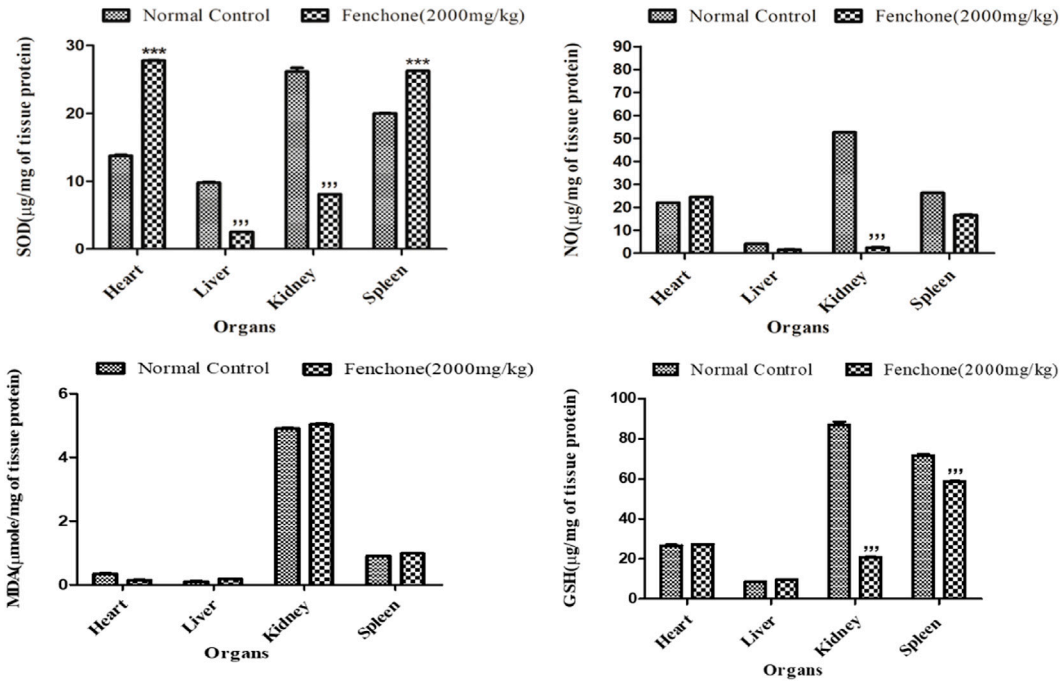

FIGURE 1
Oxidative stress marker analysis in treated animals in the acute toxicity study. Data are stated as mean ± SEM, N = 3. ***$p < .001$ represents a significant increase, while '''$p < .001$ represents a significant decrease vs. normal control.

SOD levels was observed in the heart. Lipid peroxidation did not show any significant difference in all chosen organs when compared to that of the normal control group.

Histopathological analysis

Histopathological analysis showed no remarkable change in the architecture of cells (Figure 2).

Effect of different doses of fenchone on urinary electrolytes (Na^+ and K^+) and Na^+/K^+ ratio in acute diuretic activity

The effects of different doses of fenchone (100, 200, and 400 mg/kg) and furosemide (15 mg/kg) on sodium and potassium are shown in Figure 3. Fenchone (200 mg/kg and 400 mg/kg) resulted in a significant increase in sodium and potassium excretion. Na^+ and K^+ excretion rates induced by

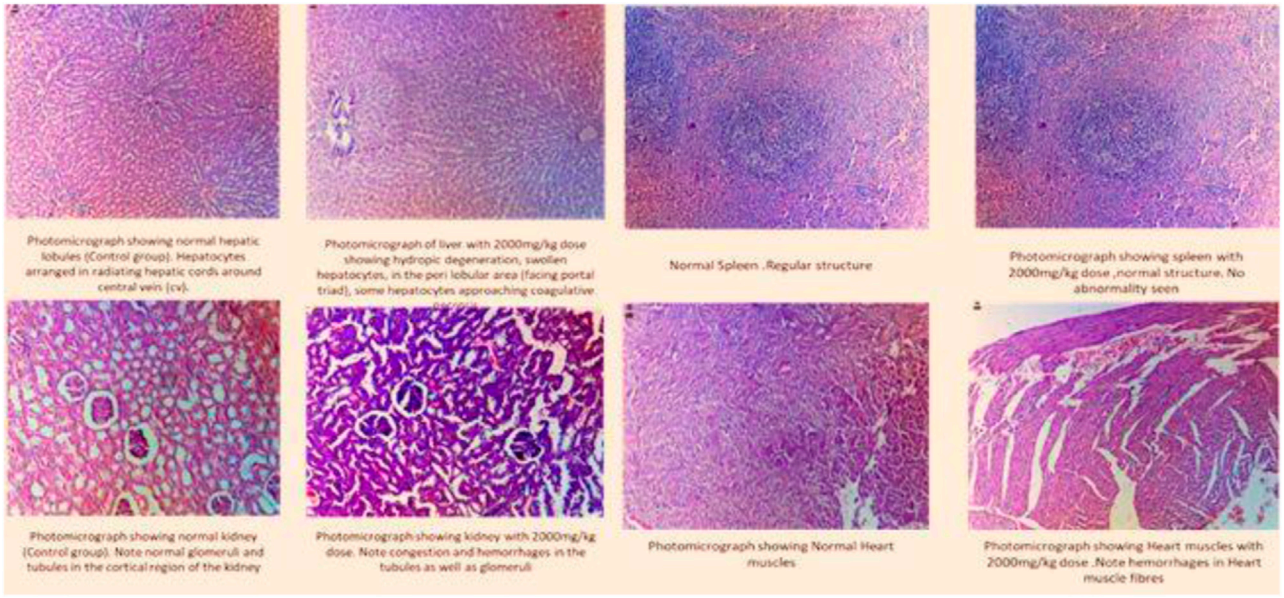

FIGURE 2
Histogram of the selected organs treated with fenchone (2000 mg/kg) in the acute toxicity study.

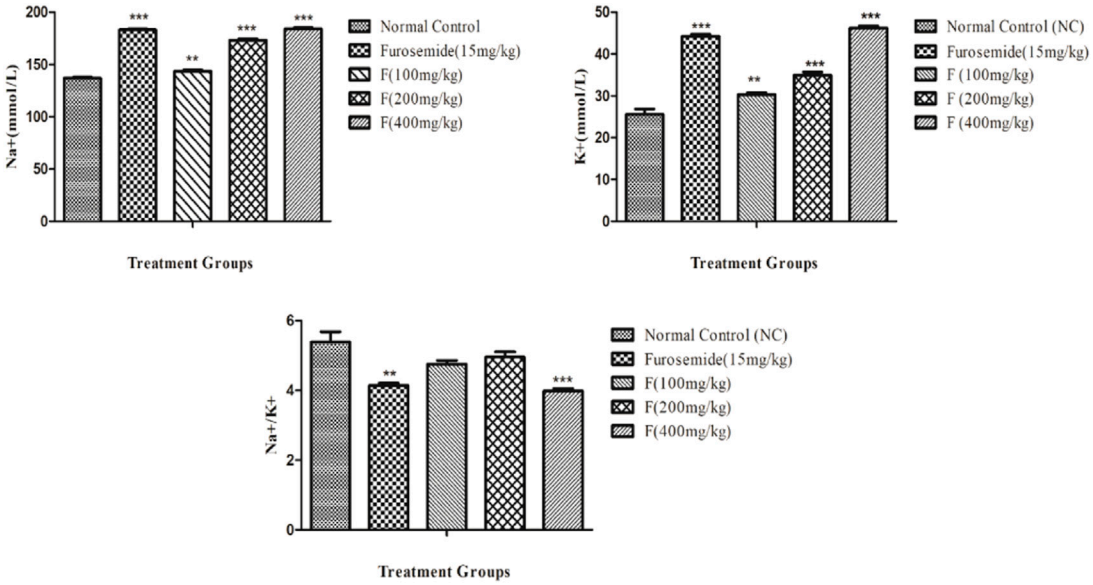

FIGURE 3
Effect of different doses of fenchone on urinary electrolytes (Na^+ and K^+) where furosemide was taken as the standard drug. Data are stated as mean ± SEM, N = 6. ***$p < .001$ represents a significant increase, while '''$p < .001$ represents a significant decrease vs. normal control.

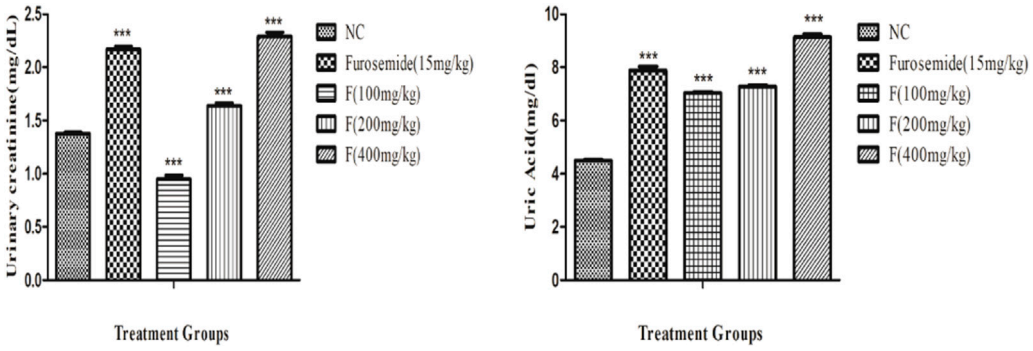

FIGURE 4
Effect of different doses of fenchone on urinary creatinine and uric acid excretion where furosemide was taken as the standard drug. Data are stated as mean ± SEM, N = 6. ***p < .001 represents a significant increase, while '''p < .001 represents a significant decrease vs. normal control.

fenchone (400 mg/kg) were 184.06 ± 1.21 and 46.21 ± .51, whereas in the normal control group the rates were 136.93 ± .95 and 25.53 ± 1.31 mmol/L, respectively. Moreover, fenchone (400 mg/kg) resulted in more electrolyte excretion of sodium and potassium than furosemide. Moreover, there was a significant increase in the Na^+/K^+ ratio at a dose of 400 mg/kg fenchone when compared with that of the control group.

Effect of different doses of fenchone on urinary creatinine and uric acid

The effects of different doses of fenchone (100, 200, and 400 mg/kg) and furosemide (15 mg/kg) on urinary creatinine and uric acid are shown in Figure 4. There was a significant increase in the excretion of creatinine in the urine, and it was the highest with fenchone (400 mg/kg) when compared to the control. Moreover, the concentration of uric acid in the urine also increased significantly with a higher dose of fenchone (400 mg/kg), which was 9.14 ± .10 when compared to that of the normal control group, which was 4.49 ± .02. Both urinary creatinine and uric acid excretion results were comparable to furosemide.

Effect of different doses of fenchone on urinary calcium

There was a significant increase in the urinary calcium excretion, and it was the highest with fenchone (400 mg/kg) when compared to the control. The urinary excretion of Ca^{++} with fenchone at 400 mg/kg was 22.08 ± .28 when compared to that of the normal control group which was 10.11 ± .33 as shown in Figure 5.

Effect of different doses of fenchone on urinary pH and urinary volume

The acute diuretic effect of different doses of fenchone (100, 200, and 400 mg/kg) is shown in Table 6. The fenchone

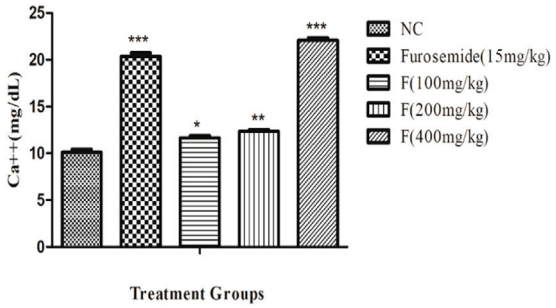

FIGURE 5
Effect of different doses of fenchone on urinary calcium where furosemide was taken as the standard drug. Data are stated as mean ± SEM, N = 6. ***p < .001 represents a significant increase, while '''p < .001 represents a significant decrease vs. normal control.

(400 mg/kg) dose resulted in increased urinary output at a 6-h interval following treatment. There was a dose-dependent increase in urinary volume measured at 6 h in 400 mg/kg fenchone-treated rats which was 5.22 ± .20 mL/100 gm, while the urinary volume was 2.23 ± .14 in the control. Moreover, the urinary output at 6 h in rats treated with fenchone (400 mg/kg) was comparable to the output in rats treated with furosemide, a standard diuretic drug. Urinary output data also suggested that the increase in urine load was due to the increased polarity resulting from this activity. Finally, the urine pH values showed a significant increase with fenchone (200 and 400 mg/kg) treatment when compared with those of the normal control group.

Effect of fenchone on the diuretic index, Lipschitz value, saluretic index of Na^+ and K^+, and saluretic index

By utilizing the excreted concentration of electrolytes (Na^+ and K^+) and urinary output in the control, standard, and treatment groups, the diuretic index, Lipschitz value, and saluretic index were calculated as shown in Table 7, and the results were quite significant at a dose of 400 mg/kg F.

Discussion

Toxicity profiling of newer molecules has gained attention and interest since it helps provide future directions to researchers, manufacturers, and distributors. The rules and regulations for toxicity studies of newer compounds help in regulating and ensuring their safety for further use in human beings. The procedure involves administration of the test compound followed by examination and investigation of biochemical parameters in animal models (Rand and Petrocelli, 1985), since the main purpose of the toxicity study is to administer the single highest dose that could result in inducing toxic effects (Klaassen, 2013).

The acute toxicity study involved the oral administration of a single dose of fenchone (2000 mg/kg) to female rats since female rats are more responsive to any biochemical change than male rats (OECD, 2001). Until the 14th day, no mortality or fatal toxicity was noted, indicating that the LD_{50} of F is significantly greater than 2000 mg/kg. Generally, it has been observed that variations in the behavior pattern and body weight are the primary indicators of toxicity (Variya, Bakrania, Madan, and Patel, 2019), and the results indicated no change in the behavioral pattern of the animals. However, there was a significant decrease in the body weight on day 14 when compared to that of the normal control group, whereas a non-significant difference was observed in the organ weights. Fenchone, an important constituent of fennel seeds, causes weight loss by boosting metabolism (Yamini, Sefidkon, and Pourmortazavi, 2002), so the decrease in weight loss due to fenchone treatment might be attributed to this.

Both biochemical evaluation and hematological evaluation provide a genuine overview regarding toxicity along with organ dysfunction. Pluripotent stem cells give rise to white blood cells (WBCs), red blood cells (RBCs), and platelets after maturation and differentiation (Ugwah-Oguejiofor et al., 2019). The Hb level and RBC count were observed to be increased in the acute toxicity study in contrast to the control group owing to the antioxidant properties that helped in stabilizing the RBC membrane and raising the level of RBCs by influencing the kidneys and liver, thereby increasing the level of erythropoietin (Mansouri et al., 2015). All the remaining parameters were normal when compared to those of the control group.

Dyslipidemia is linked with obesity since it may cause insulin resistance in the periphery by increasing the hepatic output of fats from the diet and raising triglyceride hydrolysis (Klop, Elte, and Castro Cabezas, 2013). Triglyceride and cholesterol levels were significantly reduced in the acute toxicity study that might be attributed to altered expression of the leptin receptor (Zakernezhad et al., 2021).

Estimating biochemical parameters in the liver and kidney is of primary importance since both these organs play a vital role in drug metabolism and excretion, respectively (Bariweni, Yibala, and Ozolua, 2018), and any variation in either liver or kidney function tests shows toxicity (Abdelkader et al., 2020). Liver enzymes including ALT and AST were increased at a dose of 2000 mg/kg F that might have resulted from cell damage to the liver since ALT and AST are the enzymes present in the cytosol and mitochondria of hepatocytes (Samadi-Noshahr, Hadjzadeh, Moradi-Marjaneh, and Khajavi-Rad, 2021), whereas there was a significant decrease in the uric acid levels.

Uninterrupted exposure or formation of free oxidative radicals in living organisms can lead to disturbances in redox homeostasis, resulting in damage to cellular nucleic acids, proteins, and lipids (Jones, 2006; Zhang et al., 2020). If the interrupting stimulus is not removed, irreversible cell damage will ensue, resulting in responses of numerous defensive cascades including gene regulatory cycle, repair, and various antioxidant routes to protect against oxidative stress (Nair et al., 2015). Endogenous oxidants and antioxidants were measured in the specific organs of rats to assess any change or cellular stress induced by F dosing. The results showed that there was a significant increase in SOD levels in the heart and spleen that might be attributed to the immunomodulatory effect of the drug (Anwar et al., 2021), whereas a significant decrease was observed in the liver and kidney. Similarly, there was a significant decrease in NO and GSH levels in the kidney showing that it might have been excreted from the kidney, indicating a decline in oxidative stress markers, and these results can be correlated to the histopathological slides.

It has been established that diuretics are the mainstay for treating hypertension and edematous conditions, which are expressed as excessive extracellular fluid. In general, diuretics are known to increase the excessive salt and water excretion from the body, thus reducing blood flow resistance by decreasing blood pressure and volume (Younis et al., 2021). Even though diuretics are available abundantly for human use, the side effects pose a need for newer agents from plants or their constituents (Wright, Van-Buren, Kroner, and Koning, 2007), displaying numerous pharmacological effects on renal physiology and acting on distinct and well-established targets like nitric oxide-cGMP, carbonic anhydrase, renin–angiotensin system, and renal carriers (Aparecida Livero, Vergutz Menetrier, Luiz Botelho Lourenco, and Gasparotto Junior, 2017). In the present research, fenchone resulted in a significant dose-dependent increase in diuretic activity, with a maximum response at 400 mg/kg dose. A single dose of fenchone significantly increased the urinary output from the second hour and increased with time, and the effect was the highest with F 400 mg/kg (5.22 ± .20) after 8 h. This effect was significantly higher than that of the standard drug furosemide (15 mg/kg) which was 4.83 ± .29, but the onset time was less with fenchone. The time difference in

TABLE 6 Effect of different doses of fenchone on pH and urinary volume.

Treatment group	pH	Urine volume mL/100 gm at 8 h
Normal control (NC)	7.17 ± .04	2.23 ± .14
Furosemide (15 mg/kg)	7.76 ± .08***	4.83 ± .29 ***
F (100 mg/kg)	7.69 ± .09 *	2.93 ± .08
F (200 mg/kg)	7.83 ± .03 ***	3.44 ± .18 **
F (400 mg/kg)	7.88 ± .05 ***	5.22 ± .20 ***

Results are stated as mean ± SEM, where *$p < .05$, **$p < .01$, and ***$p < .001$, when compared to the normal control group. NC, normal control group; Na^+/K^+, urinary concentration of sodium/urinary concentration of potassium.

TABLE 7 Effect of fenchone on the diuretic index, Lipschitz value, saluretic index of Na^+ and K^+, and saluretic index.

Treatment group	Diuretic index (DI)	Lipschitz value (LV)	Saluretic index (SI)		Saluretic index (SI)
			SI_{Na^+}	SI_{K^+}	
Normal control (NC)	1.00	.46 ± .04	.97 ± .01	1.00	1.00
Furosemide (15 mg/kg)	2.18 ± .23 ***	1.00***	1.33 ± .02***	1.74 ± .11***	1.40
F (100 mg/kg)	1.32 ± .12	.60 ± .03	1.04 ± .01	1.19 ± .07	1.07
F (200 mg/kg)	1.54 ± .06	.71 ± .04*	1.25 ± .01***	1.37 ± .10*	1.28
F (400 mg/kg)	2.18 ± .19 ***	1.1 ± .11***	1.33 ± .01***	1.81 ± .10***	1.41

Results are stated as mean ± SEM, where *$p < .05$, **$p < .01$, and ***$p < .001$, when compared to the normal control group.

the onset of diuretic action can be related to the absorption profiles of fenchone. The increase in the urinary output of F can be attributed to the increase in compound polarity that might have increased the renal circulation along with glomerular filtration and thus increased the formation of urine (Chen et al., 2014).

The current study also revealed that F 400 mg/kg dose also resulted in inducing a significant increase in urinary electrolytes Na^+ (184.06 ± 1.21) and K^+ (46.21 ± .51) when compared to those of furosemide which were 183.06 ± 1.24 for Na^+ and 44.23 ± .49 for K^+, showing both saluretic and kaliuretic activities that might be due to their interaction with polar groups (Martín-Herrera, Abdala, Benjumea, and Pérez-Paz, 2007). Similarly, there was an increase in the Na^+/K^+ ratio at F 400 mg/kg dose that might be attributed to an increase in sodium loss along with potassium retention (Feng et al., 2013), which is an essential feature of a good diuretic that produces reduced hyperkalemic effects (Ghelani, Chapala, and Jadav, 2016).

Creatinine is a reliable marker for assessing kidney function (Prathibhakumari and Prasad, 2014). Urinary creatinine was significantly increased at both 200 mg/kg and 400 mg/kg doses, but a higher effect was observed with fenchone (400 mg/kg) in a dose-dependent manner, so its use can be considered safe in patients with renal insufficiencies.

Uric acid is the end-product of nucleic acid metabolism in the human body, and this homeostasis is attained by either modulating the formation, breakdown, or excretion of uric acid. Hyperuricemia is generally characterized by an elevation in the levels of uric acid and is considered a risk factor for causing cardiovascular disease, diabetes, hypertension, chronic kidney disease, and gout (Zhang et al., 2018). The current research revealed that the F (200 and 400 mg/kg) dose resulted in a significant increase in the excretion of uric acid in the urine with much higher results at 400 mg/kg dose, and thus it can be used in treating gout.

Conclusion

The current study showed that the LD_{50} of fenchone is greater than 2,000 mg/kg, no mortality or signs of toxicity were reported, and it has a remarkable diuretic potential comparable to furosemide. Moreover, oral treatment with F resulted in increased excretion of sodium and potassium in the urine, along with increases in the Na^+/K^+ ratio, diuretic index, Lipschitz value, and saluretic index. The results suggest that fenchone (F) may be considered a safe therapeutic agent in patients with cardiovascular and renal insufficiencies, but further mechanistic studies would be essential before introducing it into clinical trials.

Data availability statement

The raw data supporting the conclusion of this article will be made available by the authors, without undue reservation.

Ethics statement

The animal study was reviewed and approved by the Institutional Ethical Committee of the Faculty of Pharmacy, The University of Lahore, with Approval No. IREC-2022-17.

Author contributions

AB carried out the research and drafted the manuscript, MM and WY designed the project, and IA carried out the statistical analysis.

Acknowledgments

The authors thank The University of Lahore for providing research facilities to carry out the research.

Conflict of Interest

The authors declare that the research was conducted in the absence of any commercial or financial relationships that could be construed as a potential conflict of interest.

Publisher's note

All claims expressed in this article are solely those of the authors and do not necessarily represent those of their affiliated organizations, or those of the publisher, the editors, and the reviewers. Any product that may be evaluated in this article, or claim that may be made by its manufacturer, is not guaranteed or endorsed by the publisher.

References

Arome, D., and Chinedu, E. (2013). The importance of toxicity testing. *J. Pharm. Biosci.* 4, 146–148.

Abdelkader, N. F., Elyamany, M., Gad, A. M., Assaf, N., Fawzy, H. M., and Elesawy, W. H. (2020). Ellagic acid attenuates liver toxicity induced by valproic acid in rats. *J. Pharmacol. Sci.* 143 (1), 23–29. doi:10.1016/j.jphs.2020.01.007

Agarwal, R., Gupta, S. K., Agrawal, S. S., Srivastava, S., and Saxena, R. (2008). Oculohypotensive effects of Foeniculum vulgare in experimental models of glaucoma. *Indian J. Physiol. Pharmacol.* 52 (1), 77–83.

Aneela, S., De, S., Kanthal, L., Choudhury, N., Das, B., and Sagar, K. (2011). Acute oral toxicity studies of Pongamia Pinnata and Annona squamosa on albino wister rats. *Int. J. Res. Pharm. Chem.* 1 (4), 820–824.

Anwar, F., Saleem, U., Rehman, A.-U., Ahmad, B., Froeyen, M., Mirza, M. U., et al. (2021). Toxicity evaluation of the naphthalen-2-yl 3, 5-dinitrobenzoate: A drug candidate for alzheimer disease. *Front. Pharmacol.* 12, 607026. doi:10.3389/fphar.2021.607026

Aparecida Livero, F., Vergutz Menetrier, J., Luiz Botelho Lourenco, E., and Gasparotto Junior, A. (2017). Cellular and molecular mechanisms of diuretic plants: An overview. *Curr. Pharm. Des.* 23 (8), 1247–1252. doi:10.2174/1381612822666161014114437

Balunas, M. J., and Kinghorn, A. D. (2005). Drug discovery from medicinal plants. *Life Sci.* 78 (5), 431–441. doi:10.1016/j.lfs.2005.09.012

Bariweni, M. W., Yibala, O. I., and Ozolua, R. I. (2018). Toxicological studies on the aqueous leaf extract of Pavetta crassipes (K. Schum) in rodents. *J. Pharm. Pharmacogn. Res.* 6 (1), 1–16.

Chen, D.-Q., Feng, Y.-L., Tian, T., Chen, H., Yin, L., Zhao, Y.-Y., et al. (2014). Diuretic and anti-diuretic activities of fractions of Alismatis rhizoma. *J. Ethnopharmacol.* 157, 114–118. doi:10.1016/j.jep.2014.09.022

Dandekar, P., Dhumal, R., Jain, R., Tiwari, D., Vanage, G., and Patravale, V. (2010). Toxicological evaluation of pH-sensitive nanoparticles of curcumin: Acute, sub-acute and genotoxicity studies. *Food Chem. Toxicol.* 48 (8-9), 2073–2089. doi:10.1016/j.fct.2010.05.008

de Souza Pessoa, M. L., Silva, L. M. O., Araruna, M. E. C., de Lima Serafim, C. A., Júnior, E. B. A., Silva, A. O., et al. (2020). Antifungal activity and antidiarrheal activity via antimotility mechanisms of (-)-fenchone in experimental models. *World J. Gastroenterology* 26 (43), 6795–6809. doi:10.3748/wjg.v26.i43.6795

Feng, Y.-L., Lei, P., Tian, T., Yin, L., Chen, D.-Q., Chen, H., et al. (2013). Diuretic activity of some fractions of the epidermis of Poria cocos. *J. Ethnopharmacol.* 150 (3), 1114–1118. doi:10.1016/j.jep.2013.10.043

Ghelani, H., Chapala, M., and Jadav, P. (2016). Diuretic and antiurolithiatic activities of an ethanolic extract of Acorus calamus L. rhizome in experimental animal models. *J. traditional complementary Med.* 6 (4), 431–436. doi:10.1016/j.jtcme.2015.12.004

Him, A., Ozbek, H., Turel, I., and Oner, A. C. (2008). Antinociceptive activity of alpha-pinene and fenchone. *Pharmacologyonline* 3, 363–369.

Jones, D. P. (2006). Redefining oxidative stress. *Antioxidants redox Signal.* 8 (9-10), 1865–1879. doi:10.1089/ars.2006.8.1865

Jothy, S. L., Zakaria, Z., Chen, Y., Lau, Y. L., Latha, L. Y., and Sasidharan, S. (2011). Acute oral toxicity of methanolic seed extract of Cassia fistula in mice. *Molecules* 16 (6), 5268–5282. doi:10.3390/molecules16065268

Keskin, I., Gunal, Y., Ayla, S., Kolbasi, B., Sakul, A., Kilic, U., et al. (2017). Effects of Foeniculum vulgare essential oil compounds, fenchone and limonene, on experimental wound healing. *Biotech. Histochem.* 92 (4), 274–282. doi:10.1080/10520295.2017.1306882

Kim, T., Song, B., Cho, K. S., and Lee, I.-S. (2020). Therapeutic potential of volatile terpenes and terpenoids from forests for inflammatory diseases. *Int. J. Mol. Sci.* 21 (6), 2187. doi:10.3390/ijms21062187

Klaassen, C. D. (2013). *Casarett and doull's toxicology: The basic science of poisons*, 1236. New York, NY, USA: McGraw-Hill.

Klop, B., Elte, J. W. F., and Castro Cabezas, M. (2013). Dyslipidemia in obesity: Mechanisms and potential targets. *Nutrients* 5 (4), 1218–1240. doi:10.3390/nu5041218

Konan, N. A., Bacchi, E. M., Lincopan, N., Varela, S. D., and Varanda, E. A. (2007). Acute, subacute toxicity and genotoxic effect of a hydroethanolic extract of the cashew (Anacardium occidentale L.). *J. Ethnopharmacol.* 110 (1), 30–38. doi:10.1016/j.jep.2006.08.033

Krum, H., and Pellizzer, A.-M. (1998). New and emerging drug treatments for hypertension. *Aust. Fam. physician* 27 (4), 235–240.

Lahlou, S., Tahraoui, A., Israili, Z., and Lyoussi, B. (2007). Diuretic activity of the aqueous extracts of Carum carvi and Tanacetum vulgare in normal rats. *J. Ethnopharmacol.* 110 (3), 458–463. doi:10.1016/j.jep.2006.10.005

Lewis, R. W., Billington, R., Debryune, E., Gamer, A., Lang, B., and Carpanini, F. (2002). Recognition of adverse and nonadverse effects in toxicity studies. *Toxicol. Pathol.* 30 (1), 66–74. doi:10.1080/01926230252824725

Mansouri, E., Kooti, W., Bazvand, M., Boroon, M. G., Amirzargar, A., Afrisham, R., et al. (2015). The effect of hydro-alcoholic extract of Foeniculum vulgare Mill on leukocytes and hematological tests in male rats. *Jundishapur J. Nat. Pharm. Prod.* 10 (1), e18396. doi:10.17795/jjnpp-18396

Martín-Herrera, D., Abdala, S., Benjumea, D., and Pérez-Paz, P. (2007). Diuretic activity of Withania aristata: An endemic Canary Island species. *J. Ethnopharmacol.* 113 (3), 487–491. doi:10.1016/j.jep.2007.07.005

Morton, D. M. (1998). Importance of species selection in drug toxicity testing. *Toxicol. Lett.* 102, 545–550. doi:10.1016/s0378-4274(98)00263-x

Nair, A. R., Lee, W.-K., Smeets, K., Swennen, Q., Sanchez, A., Thévenod, F., et al. (2015). Glutathione and mitochondria determine acute defense responses and adaptive processes in cadmium-induced oxidative stress and toxicity of the kidney. *Archives Toxicol.* 89 (12), 2273–2289. doi:10.1007/s00204-014-1401-9

Nazir, S., Anwar, F., Saleem, U., Ahmad, B., Raza, Z., Sanawar, M., et al. (2021). Drotaverine inhibitor of PDE4: Reverses the streptozotocin induced alzheimer's disease in mice. *Neurochem. Res.* 46 (7), 1814–1829. doi:10.1007/s11064-021-03327-9

Oecd (2001). *OECD guideline 425: Acute oral toxicity—up-and-down procedure*. France: OECD Guidelines for the Testing of Chemicals: Organization for Economic Cooperation and Development Paris.

Prathibhakumari, P., and Prasad, G. (2014). Pharmacological investigation on the diuretic activity of the aqueous fruit extract of Neolamarckia cadamba (Roxb) Bosser. *J. Pharm. Res.* 8 (2), 130–135.

Rand, G. M., and Petrocelli, S. R. (1985). *Fundamentals of aquatic toxicology: Methods and applications*. Washington, D.C, USA: U.S. Department of Energy.

Rather, M. A., Dar, B. A., Sofi, S. N., Bhat, B. A., and Qurishi, M. A. (2016). Foeniculum vulgare: A comprehensive review of its traditional use, phytochemistry, pharmacology, and safety. *Arabian J. Chem.* 9, S1574–S1583. doi:10.1016/j.arabjc.2012.04.011

Rehman, N. U., Ansari, M. N., Samad, A., and Ahmad, W. (2022). *In silico*, *ex vivo* and *in vivo* studies of roflumilast as a potential antidiarrheal and antispasmodic agent: Inhibition of the PDE-4 enzyme and voltage-gated Ca++ ion channels. *Molecules* 27 (4), 1008. doi:10.3390/molecules25041008

Saeed, M., Saleem, U., Anwar, F., Ahmad, B., and Anwar, A. (2020). Inhibition of valproic acid-induced prenatal developmental abnormalities with antioxidants in rats. *ACS omega* 5 (10), 4953–4961. doi:10.1021/acsomega.9b03792

Saleem, U., Amin, S., Ahmad, B., Azeem, H., Anwar, F., and Mary, S. (2017). Acute oral toxicity evaluation of aqueous ethanolic extract of Saccharum munja Roxb. roots in albino mice as per OECD 425 TG. *Toxicol. Rep.* 4, 580–585. doi:10.1016/j.toxrep.2017.10.005

Samadi Noshahr, Z., Hadjzadeh, M. A. R., Moradi-Marjaneh, R., and Khajavi Rad, A. (2021). The hepatoprotective effects of fennel seeds extract and trans-Anethole in streptozotocin induced liver injury in rats. *Food Sci. Nutr.* 9 (2), 1121–1131. doi:10.1002/fsn3.2090

Schlickmann, F., Boeing, T., Mariano, L. N. B., da Silva, R. d. C. M. V. d., Fonseca, A., da Silva, L. M., et al. (2018). Gallic acid, a phenolic compound isolated from Mimosa bimucronata (DC.) Kuntze leaves, induces diuresis and saluresis in rats. *Naunyn-Schmiedeberg's Archives Pharmacol.* 391 (6), 649–655. doi:10.1007/s00210-018-1502-8

Shen, B. (2015). A new golden age of natural products drug discovery. *Cell* 163 (6), 1297–1300. doi:10.1016/j.cell.2015.11.031

Slavchev, I., Dobrikov, G. M., Valcheva, V., Ugrinova, I., Pasheva, E., and Dimitrov, V. (2014). Antimycobacterial activity generated by the amide coupling of (−)-fenchone derived aminoalcohol with cinnamic acids and analogues. *Bioorg. Med. Chem. Lett.* 24 (21), 5030–5033. doi:10.1016/j.bmcl.2014.09.021

Ugwah-Oguejiofor, C. J., Okoli, C. O., Ugwah, M. O., Umaru, M. L., Ogbulie, C. S., Mshelia, H. E., et al. (2019). Acute and sub-acute toxicity of aqueous extract of aerial parts of Caralluma dalzielii NE Brown in mice and rats. *Heliyon* 5 (1), e01179. doi:10.1016/j.heliyon.2019.e01179

Variya, B. C., Bakrania, A. K., Madan, P., and Patel, S. S. (2019). Acute and 28-days repeated dose sub-acute toxicity study of gallic acid in albino mice. *Regul. Toxicol. Pharmacol.* 101, 71–78. doi:10.1016/j.yrtph.2018.11.010

Wright, C., Van-Buren, L., Kroner, C., and Koning, M. (2007). Herbal medicines as diuretics: A review of the scientific evidence. *J. Ethnopharmacol.* 114 (1), 1–31. doi:10.1016/j.jep.2007.07.023

Wright, G. D. (2019). Unlocking the potential of natural products in drug discovery. *Microb. Biotechnol.* 12 (1), 55–57. doi:10.1111/1751-7915.13351

Yamini, Y., Sefidkon, F., and Pourmortazavi, S. (2002). Comparison of essential oil composition of Iranian fennel (Foeniculum vulgare) obtained by supercritical carbon dioxide extraction and hydrodistillation methods. *Flavour Fragr. J.* 17 (5), 345–348. doi:10.1002/ffj.1117

Younis, W., Schini-Kerth, V., Nocchi, S. R., Silva, D. B., de Souza, P., Bukhari, I. A., et al. (2021). Involvement of muscarinic receptors in hypotensive and diuretic effects of aqueous soluble fraction from Asphodelus tenuifolius cav. *Evidence-Based Complementary Altern. Med.* 2021, 1–15. doi:10.1155/2021/6653270

Zakernezhad, F., Barati, M., Sanadgol, N., Movahhedi, M., Majd, A., and Golab, F. (2021). The association between fennel extract, serum lipid profile, and leptin receptor expression. *Basic Clin. Neurosci.* 12 (6), 711–720. doi:10.32598/bcn.2021.998.2

Zhang, C., Zhang, J., Zhu, L., Du, Z., Wang, J., Wang, J., et al. (2020). Fluoxastrobin-induced effects on acute toxicity, development toxicity, oxidative stress, and DNA damage in *Danio rerio* embryos. *Sci. Total Environ.* 715, 137069. doi:10.1016/j.scitotenv.2020.137069

Zhang, Y., Jin, L., Liu, J., Wang, W., Yu, H., Li, J., et al. (2018). Effect and mechanism of dioscin from Dioscorea spongiosa on uric acid excretion in animal model of hyperuricemia. *J. Ethnopharmacol.* 214, 29–36. doi:10.1016/j.jep.2017.12.004

frontiers | Frontiers in Pharmacology

TYPE Original Research
PUBLISHED 02 February 2023
DOI 10.3389/fphar.2023.1111915

Check for updates

OPEN ACCESS

EDITED BY
Arshad Mahmood,
Al Ain University, United Arab Emirates

REVIEWED BY
Syed Shams Ul Hassan,
Shanghai Jiao Tong University, China
Aamir Mushtaq,
Government College University Lahore, Pakistan

*CORRESPONDENCE
Qurat Ul Ain,
quratkhawaja2@gmail.com
Uzma Saleem,
uzma95@gmail.com

SPECIALTY SECTION
This article was submitted to Predictive Toxicology, a section of the journal Frontiers in Pharmacology

RECEIVED 30 November 2022
ACCEPTED 11 January 2023
PUBLISHED 02 February 2023

CITATION
Ain QU, Saleem U, Ahmad B and Khalid I (2023), Pharmacological screening of silibinin for antischizophrenic activity along with its acute toxicity evaluation in experimental animals.
Front. Pharmacol. 14:1111915.
doi: 10.3389/fphar.2023.1111915

COPYRIGHT
© 2023 Ain, Saleem, Ahmad and Khalid. This is an open-access article distributed under the terms of the Creative Commons Attribution License (CC BY). The use, distribution or reproduction in other forums is permitted, provided the original author(s) and the copyright owner(s) are credited and that the original publication in this journal is cited, in accordance with accepted academic practice. No use, distribution or reproduction is permitted which does not comply with these terms.

Pharmacological screening of silibinin for antischizophrenic activity along with its acute toxicity evaluation in experimental animals

Qurat Ul Ain[1]*, Uzma Saleem[1]*, Bashir Ahmad[2] and Iqra Khalid[1]

[1]Department of Pharmacology, Faculty of Pharmaceutical Sciences, Government College University, Faisalabad, Pakistan, [2]Hamza College of Pharmaceutical and Allied Health Sciences, Lahore, Pakistan

Silibinin (SIL), a flavolignan extracted from the medicinal plant "silybum marianum (milk thistle)", has traditionally been used to treat liver disease. This phytochemical has displayed neuroprotective properties, its activity against schizophrenia is not elucidated. The present study was designed to evaluate the antipsychotic potential of silibinin and probe its toxic potential. The acute oral toxicity study was assessed as per OECD 425 guidelines. Animals were divided into two groups of female rats (n = 6): one group served as the normal control and the other group received a 2,000 mg/kg dose of SIL. We also evaluated the antipsychotic potential of SIL. To this end, animals were divided into six groups (n = 10) of mice for both the preventive and curative protocols. Group I (CMC 1 mL/kg) served as the normal control and received CMC 1 mL/kg; group II was the diseased group treated with ketamine (10 mg/kg) i.p; group III was the standard group treated with clozapine 1 mg/kg; groups IV, V, and VI served as the treatment groups, receiving SIL 50, 100, and 200 mg/kg, respectively, orally for both protocols. Improvement in positive symptoms of the disease was evaluated by stereotypy and hyperlocomotion, while negative symptoms (behavioral despair) were determined by a forced swim test and a tail suspension test in the mice models. The results suggested that the LD_{50} of SIL was greater than 2,000 mg/kg. Moreover, SIL prevented and reversed ketamine-induced increase in stereotypy ($p < 0.001$) and behavioral despair in the forced swim and tail suspension tests ($p < 0.001$). Taken together, the findings suggest that silibinin is a safe drug with low toxicity which demonstrates significant antipsychotic activity against the positive and negative symptoms of schizophrenia.

KEYWORDS

silibinin, acute oral toxicity, schizophrenia, ketamine, oxidative stress

1 Introduction

Phytochemicals derived from plant, animals, and marine sources have played a vital role in alleviating major human suffering. They have demonstrated therapeutic potential in reducing the risk of major health problems such as cancers, cardiovascular diseases, and different central nervous system (CNS) disorders (Kumar and Khanum, 2012). Phytochemicals have gained attention due to their therapeutic value and the fact that they have fewer adverse effects. Most people seem to believe that natural products are free of any kind of adverse properties, Paracelsus, known as the father of toxicology, stated that "all substances are poisons; it is the right dose that differentiates remedy and poison." Hence, assessing the toxic potential of natural products is of vital importance (Newman and Cragg, 2012).

Schizophrenia is a severely debilitating disease that affects patients' thoughts, behavior, perception, and memory (Faludi et al., 2011). The disease affects 1%–1.5% of the global population (Mcgrath et al., 2008) and is rated seventh among the most costly diseases (Ross and Margolis, 2005). Symptoms of schizophrenia cluster into three groups: positive symptoms include hallucination, thought disorder, and delusion; negative symptoms include lack of interest and pleasure and low social interaction; cognitive symptoms include memory and thinking problems (Tandon et al., 2013). The etiology of this disease is still unclear, although the dopamine hypothesis remains its mainstay. After 1980, the glutamate hypothesis was proposed as the establishing basis of schizophrenia (Yadav et al., 2019).

Pharmacotherapeutic agents for schizophrenia were introduced in 1950s and have been active for positive symptoms but ineffective against negative symptoms and cognitive deficits (Purdon et al., 2001). Typical antipsychotics have been dopamine (D2) receptor antagonists such as haloperidol and prochlorperazine. Second generation drugs (clozapine and quetiapine) were then approved for negative symptoms and cognitive impairments (Wang et al., 2019). These antipsychotic drugs are the mainstay of treatment but are unsuccessful at counteracting the symptoms and progression of the disease. Some serious adverse effects as extrapyramidal symptoms, dyslipidemia, diabetes, and hypertension are related to antipsychotic drug use (Brown, 2012; Fell et al., 2012). Therefore, there is a need to investigate new and more effective therapeutic alternatives with fewer adverse effects to increase adherence and therapeutic outcomes.

Silibinin (SIL) is a flavolignan derived from silymarin, a compound that is extracted from the seeds and fruit of the milk thistle herb (*Silybum marianum*). This plant belongs to the Asteraceae family and its fruit has been famous for use in medicines for centuries. Silybin A and Silybin B are two stereoisomers of silibinin (Mashhadi Akbar Boojar et al., 2020). Flavonoids are known for their antioxidant antiviral, anti-inflammatory, and neuroprotective effects (Hassan et al., 2022). According to previous findings, SIL acts as an antioxidant, anti-inflammatory, anticarcinogenic, and growth promoting agent and is used as a hepatoprotective agent—especially for liver cirrhosis (Chu et al., 2004; Shanmugam et al., 2008; Yin et al., 2011). Moreover, it is also useful for dermatological conditions and skin aging and can act as an antiviral and protective agent against retinal diseases (Singh and Agarwal, 2009; Ahmed-Belkacem et al., 2010). Furthermore, SIL is a neuroprotective agent against neural damage, ethanol-induced brain damage, Aβ-induced memory impairment, and neurotoxicity associated with lipopolysaccharide. Its antidepressant activity is also established (Mazzio et al., 1998; Yan et al., 2015), but its antipsychotic property has not been investigated. Acute toxicity study is basic and preliminary to evaluating the general safety and toxicity of a substance (Baig et al., 2022); however, despite its wide usage, toxicity data is not yet available for SIL (Kennedy et al., 1986).

Hence, the present study aims to evaluate the acute oral toxicity of SIL and determine its antipsychotic potential.

2 Materials and methods

2.1 Drug and chemicals

This study used silibinin (CAS # 22888-70-6), ketamine (CAS # 1867-66-9), clozapine (CAS # 5786-21-0), sodium hydroxide (CAS # 1310-73-2), sodium carboxymethyl cellulose, isoflurane (CAS # 26675-46-7), pyrogallol (CAS # 87-66-1), DTNB (5, 5-dithiobis-(2-nitrobenzoic acid) (CAS # 2516-96-3), Folin-Ciocalteu (CAS # F9252), potassium phosphate monobasic, and sodium phosphate monobasic. All chemicals were of analytical grade and were purchased from Sigma Aldrich (China).

2.2 Animals

Adult Wister female rats weighing 200–300 g were used to examine acute toxicity. Male and female Swiss albino mice (approximately 30 g) were purchased from Government College University Faisalabad, Pakistan, and were used for behavioral studies of schizophrenia. The animals were kept in the department's animal house at 22 ± 2□C with a relative humidity of 44%–56% and a 12 h light–dark cycle. They were provided with a standard rodent pellet diet and water. The animals were acclimatized to handling and the room and apparatus before experimentation commenced. Ethical approval for the animal studies was obtained from the Animal Ethics Committee of Government College University Faisalabad, reference number GCUF/ERC/2015.

2.3 Acute oral toxicity studies

The OECD's (Organization for Economic Co-operation and Development) 425 Guidelines were followed for performing an acute oral toxicity study. In this study, two groups of healthy adult Wister rats were used (n = 6). The animals were fasted overnight but were allowed access to water. Group I received 0.5% carboxy methyl cellulose (CMC) (1 mL/100 g) and was designated as normal control. Group II, the treatment group, received 2000 mg/kg of SIL orally. Initially, only one animal received SIL (2000 mg/kg) by a single oral dose and observations were made for 24 h. If the animal survived, four further animals were administered single oral doses of SIL (2,000 mg/kg). The animals were observed for mortality, changes in general behavior, weight change, and any kind of allergies for 14 days (Choi et al., 2021).

2.4 Hematological and biochemical analysis

After 14 days, animals were anesthetized with 3%–5% isoflurane diluted with oxygen. Blood samples were collected after anesthesia by cardiac puncture, and hematological and biochemical parameters were evaluated. Hematological parameters included WBC, RBC, Hb, platelet count, hematocrit (HCT) value, mean corpuscular hemoglobin concentration (MCHC), mean corpuscular volume (MCV), and mean corpuscular hemoglobin (MCH) using a hematology analyzer (Norma, USA). For biochemical tests, plasma and serum were separated and biochemical parameters were estimated. The lipid profiling of cholesterol and triglycerides was measured using their specific kits (CC1132, and CC1302 by MTD Diagnostic, Italy, respectively). Liver function tests for alanine transaminase (ALT) and aspartate transaminase (AST) were performed using their appropriate kits (CC1223, CC1213 by MTD Diagnostic, Italy, respectively) (Steinberg et al., 2019).

2.5 Determination of oxidative stress markers

2.5.1 Preparation of organ tissue homogenates

After euthanasia with 3%–5% isoflurane anesthesia diluted with oxygen, the mice brains were collected from all animals in each group with scarification; the brains were washed in a cold solution of normal saline. Brain tissue homogenates were prepared by adding a 0.1 M phosphate buffer of pH 7.4 in a 1:10 ratio. Homogenates were then centrifuged at 6,000 rpm at 4□C for a period of 10 min. Supernatants were then separated for performing different biochemical tests. Organs such as the heart, kidney, lung, liver, and spleen were also collected and weighed separately. Tissue homogenates were prepared similarly to brain homogenate.

2.5.2 Estimation of glutathione level

In 1 mL of tissue homogenate of each of the above organs (heart, brain, kidney, liver, and spleen), 10% trichloroacetic acid (1 mL) was added for precipitation of protein. In 4 mL of phosphate solution, supernatant and 5,5-dithiobis-2-nitrobenzoic acid (DTNB) reagent (0.5 mL) were added and absorbance was measured at 412 nm. The level of GSH is expressed in μg or level of glutathione per mg of protein. GSH level was then measured using the formula (Bhangale and Acharya, 2016):

$$GSH\ level = Y - 0.00314 \div 0.0314 \times DF \div Bt \times Vu$$

where Y is the absorbance at 412 nm, Bt is homogenate of brain tissue, DF is dilution factor, and Vu is the aliquot volume (1 mL).

2.5.3 Estimation of the catalase level

Mixed into 0.05 mL of supernatant (tissue homogenate of each organ—heart, brain, kidney, liver, and spleen) was 1.95 mL of phosphate buffer (50mM, pH 7.0). The above solution was mixed with 1 mL of 30 mM hydrogen peroxide (H_2O_2) and absorbance was recorded at 240 nm. Values were expressed in micromoles of H_2O_2 oxidized/min/mg of protein. The catalase level was determined by formula (Anwar et al., 2021).

$$CAT\ activity = O.D \div E \times vol.\ of\ sample \times mg\ of\ protein$$

where $O.D$ is the change in absorbance/minute while E is the extinction coefficient (0.071 $mmol^4$/cm) of H_2O_2.

2.5.4 Estimation of superoxide dismutase level

Tissue homogenates (0.1 mL) of heart, brain, kidney, liver, and spleen were added to 2.8 mL of 0.1 M potassium phosphate buffer (pH 7.4) and 0.1 mL pyrogallol solution. The absorbance of the mixture was measured on a UV spectrophotometer at 325 nm (X. Li, 2012).

By using a regression line equation, SOD level was thus determined:

$$Y = 0.0095\,x + 0.1939$$

2.5.5 Determination of malnodialdehyde level

The supernatant of 1 mL of each organ (heart, brain, kidney, liver, and spleen) and 1 mL of thiobarbituric acid (4.0 mM) were mixed in 100 mL of glacial acetic acid. A mixture of 3 mL of sample was shaken and set aside for 15 min and kept for cooling. Centrifugation was done at 35,000 rpm for 10 min. Absorbance was taken at 532 nm.

Group I	Vehicle control group (0.5% CMC 1 mL/kg i.p)
Group II	Negative control group (ketamine 10 mg/kg i.p)
Group III	Positive control group (clozapine 1 mg/kg i.p)
Group IV	SIL 50 mg/kg
Group V	SIL 100 mg/kg
Group VI	SIL 200 mg/kg orally

Malnodialdehyde was quantified as micromole per mg of protein. The following formula was used for MDA quantification:

$$Conc.\ of\ MDA = Abs532 \times 100 \times Vt \div \left(1.56 \times 10^5\right) \times wt \times Vu$$

where Abs_{532} is absorbance, Vt is mixture volume (4 mL), 1.56×10^5 is the molar extinction coefficient, wt is the weight of brain, and Vu is the volume of aliquot (1 mL) (Bhangale and Acharya, 2016).

2.5.6 Estimation of nitrite level

Griess reagent was used to determine nitrite level by spectrophotometer. A mixture was made by adding equal quantities of Griess reagent and tissue homogenate of each organ (heart, brain, kidney, liver, and spleen). Incubation was done for 10 min and then absorbance was taken at 546 nm. Nitrite level was calculated by the following regression line equation for sodium nitrite (Anwar et al., 2021):

$$Y = 0.003432x + 0.0366$$

2.5.7 Estimation of protein content

Three solutions were prepared. A) 1% NaK tartrate in H_2O; B) 0.5% $CuSO_4.5H_2O$; C) 2% Na_2CO_3 dissolved in 0.1 N NaOH in water. Reagent 1 was formed by mixing Solutions A (48 mL), B (1 mL), and C (1 mL). Reagent 2 was prepared in 2:1 part (one part folin-phenol [2 N]: one part H_2O). For protein content determination, we added 0.2 mL tissue homogenate of each organ (heart, brain, kidney, liver, and spleen) to 4.5 mL of reagent and then incubated it for 10 min. Reagent 2 (0.5 mL) was then added to the mixture and incubated again for 30 min. The absorbance of the mixture was noted at 660 nm. The protein contents were determined by the following regression line equation of BSA and expressed in μg/mL (Lowry et al., 1951):

$$Y = 0.00007571x + 0.0000476$$

2.6 Evaluation of antipsychotic potential

2.6.1 Study protocol

The effect of SIL on ketamine-induced schizophrenia-like behavioral alterations was evaluated by a procedure following Ben-Azu et al. (2018) with modifications for both the preventive and treatment protocols. Animals were grouped in two phases, with six groups for the preventive study and six groups for the curative tests (n = 10).

Ketamine was given to all groups except group I1; group III received clozapine; groups IV, V, and VI received SIL with a 30 min interval after ketamine. In the preventive protocol, SIL was

administered 30 min before ketamine in groups IV, V, and VI while, in the curative protocol, SIL was given to these groups after 30 min of ketamine administration.

2.7 Behavioral tests

2.7.1 Ketamine-induced stereotypy

The effect of SIL on stereotypy induced by ketamine was assessed by any repetitive, functionless activity of mice in a transparent observation cage (23 × 20 × 20 cm). Stereotypical behavior was counted as head movement, intermittent sniffing, licking, and chewing for 2 min after 5, 10, 15, 30, and 60-min intervals. After each observation, the chamber was cleaned with 70% ethanol to remove any odor.

Initially, animals were individually placed in cylindrical metal cages for 15 min prior to the test to acclimatize to the environment. After ketamine administration, the mice were immediately placed in a cage at the base. Scoring for stereotypy was set as:

0 = no stereotypy,
1 = head movements,
2 = intermittent sniffing,
3 = chewing,
4 = licking intensely (Eneni et al., 2020).

2.7.2 Ketamine-induced hyperlocomotion

Locomotor activity was measured by an activity meter. An acclimatization time of 10 min was given to each animal before testing. After acclimatization, animals were individually placed in an actophotometer, and total locomotor activity was counted for 5 min. Before and after ketamine administration, animals were placed in the actophotometer. Observations were made in a square closed arena of 30 cm that was equipped with infrared-light-sensitive photocells. The total number of crossings was automatically calculated for 5 min. After each test session, the chamber was cleaned with 70% ethanol (Bishnoi et al., 2008).

2.7.3 Ketamine-induced immobility

2.7.3.1 Immobility in forced swim test

The mice were acclimatized in a glass cylinder of 33 cm height and 20.5 cm diameter that contained water 20 cm deep at 25☐C. They were removed after 15 min and returned to the cage. This was referred to as "training day". The next day, the mice were again placed in a cylinder for 6 min. Their swimming activity was recorded after the initial first 2-min period. Their duration of immobility was determined where "immobility" refers to a condition when no other activity was present despite that needed to keep the animal`s head above the water. The animals were then dried with a towel after the test was completed (Chen et al., 2021).

2.7.3.2 Immobility in tail suspension test

To determine immobility, a tail suspension test was performed. The mice were suspended from a tail hanger with adhesive tape that was wrapped around their tails from about 2 to 3 cm from the tip, and about 30 cm above the floor in a box (25 × 25×30 cm). The animals were observed for 6 min and the duration of their immobility was measured manually. Immobility was determined when the animal hung passively and remained motionless (Arruda et al., 2008).

TABLE 1 Estimation of mice body weights during acute oral toxicity study.

Groups		Body weights g)	
Treatments	Day 1	Day 7	Day 14
Normal control	228.5 ± 3.86	233.83 ± 3.80	238.50 ± 3.86
SIL (2,000 mg/kg)	239.3 ± 5.50	253.50 ± 6.92*	264.50 ± 7.28**

Values expressed as mean ± SEM; n = 6, where *p < 0.05, **p < 0.01 compared to Day 1.

TABLE 2 Estimation of organ weight in treatment groups during acute oral toxicity study.

Organs	Weights g)	
	Normal control	SIL (2000 mg/kg)
Liver	3.31 ± 0.38	3.30 ± 0.12
Heart	0.31 ± 0.13	0.33 ± 0.21
Lung	0.74 ± 0.11	0.80 ± 0.45
Spleen	0.28 ± 0.13	0.31 ± 0.08
Kidney	0.82 ± 0.27	0.83 ± 0.31

Data presented as mean ± SEM, n = 6.

2.8 Statistical analysis

All results were presented as mean ± SEM. Statistical significance difference was analyzed by one-way ANOVA followed by Dunnett`s $t$-test and two-way ANOVA followed by Bonferroin`s multiple comparison test. *p < 0.05, **p < 0.01, and ***p < 0.001 denoted mild, moderate, and high levels of significance.

3 Results

3.1 Acute toxicity studies

3.1.1 Effect of treatments on body and organ weight

The body weights of the treatment groups were measured daily until the 14th day. Significant increases in body weight were seen in group (SIL 2,000 mg/kg) treated animals compared with Day 1 (Table 1). There was no significant difference in the weights of the selected organs compared with the normal control group (Table 2).

3.1.2 Treatment effect on hematology parameters

On the 14th day, blood was collected from each group through cardiac puncture. Table 3 showed that, except for the platelet and WBCs count, all parameters show a non-significant difference compared to the control group. The platelet count significantly decreased and the WBCs count was significantly increased compared to the control group.

3.1.3 Effect of treatments on biochemical markers in the acute oral toxicity study

The SIL (2,000 mg/kg) treated group showed a significant increase in all biochemical markers (renal, hepatic, and lipid profile) compared with the normal control group. Uric acid and protein levels had parallel values as compared to control (Table 4).

TABLE 3 Estimation of hematological parameters in acute oral toxicity.

Parameters	Control	SIL (2000 mg/kg)
Hb (g/dL)	12.33 ± 0.42	14.25 ± 0.44
Total RBC's (x10^6/ml)	05.93 ± 0.15	06.26 ± 0.09
HCT (%)	31.53 ± 0.84	34.88 ± 1.04
MCV (fL)	54.81 ± 0.35	56.51 ± 0.46
MCH (pg)	20.04 ± 0.88	21.69 ± 0.96
MCHC (g/dL)	37.50 ± 0.92	40.00 ± 1.21
W.B.C (X10^3/ml)	03.63 ± 0.06	09.60 ± 0.18*
Platelet count (X10^3/ml)	819.16 ± 1.95	547.3 ± 6.85ˆ

Data represented as mean ± SEM; n = 6, *$p < 0.05$ significant increase, ˆ$p < 0.05$ significant decrease vs. control group.

TABLE 4 Estimation of biochemical markers in acute oral toxicity.

Biochemical markers	Normal control	SIL (2000 mg/kg)
Cholesterol (mg/dL)	57.93 ± 1.20	79.23 ± 1.63***
Triglycerides (mg/dL)	56.1 ± 1.43	81.08 ± 1.54***
ALT (U/L)	39.33 ± 1.60	55.17 ± 2.28***
AST (U/L)	63.33 ± 1.56	77.5 ± 1.76***
Uric acid (mg/dL)	05.2 ± 1.62	3.45 ± 1.23
Protein (g/dL)	07.12 ± 2.13	7.93 ± 2.02
Creatinine (mg/dL)	1.16 ± 1.23	2.13 ± 1.18*
Bilirubin (mg/dL)	1.5 ± 1.21	2.74 ± 1.13*

Data represented as mean ± SEM; n = 6, *$p < 0.05$ significant increase, ***$p < 0.001$ high significant increase vs. control group.

3.1.4 Oxidative stress markers in acute toxicity studies

Oxidative stress biomarkers were estimated in selected organs (heart, brain, kidney, liver, and spleen) to identify signs of toxicity and cellular destruction. A significant reduction in endogenous antioxidants (SOD, GSH, and CAT) was observed in the kidney while MDA levels in the kidney had risen when compared to the control group. The spleen and liver displayed a significant rise in SOD and CAT *versus* control. MDA and nitrite levels were significantly reduced in the brain and heart compared to normal control groups (Figure 1).

3.1.5 Histopathological analysis

Histopathological analysis showed normal cellular architecture, and no significant change was observed in selected organs after treatment compared to the normal control group (Figure 2).

3.2 Behavioral observations

3.2.1 Effect of SIL on ketamine-induced stereotypy in preventive and treatment protocols

Stereotypy (in minutes) was counted in all treatment groups in both the preventive and treatment protocols. Animals treated with ketamine showed significant stereotypic behaviors compared to the control group. Observations were made between 10 and 30 min in both the treatment and preventive protocols. SIL at all dose levels reduced the stereotypy counts compared to the ketamine group in the treatment protocol, and hence, there was a highly significant ($p < 0.001$) and dose-dependent response to decreasing stereotypy (Figure 3B). In the preventive protocol, SIL at 100 mg/kg showed a significant ($p < 0.01$) reduction in stereotypy while SIL (200 mg/kg) and clozapine showed highly significant ($p < 0.001$) decreases in the stereotypy score (Figure 3A).

3.2.2 Effect of SIL on ketamine-induced hyperlocomotion in preventive and treatment protocols

In the open field test, locomotor activity was significantly increased in the ketamine group when compared with control in both the preventive and curative treatment protocols. While the results showed SIL at all doses and clozapine significantly ($p < 0.001$) reduced the hyperlocomotion induced by ketamine in both protocols. Moreover, in the preventive protocol, SIL at 100 mg/kg showed a significant reduction ($p < 0.01$) in the number of crossings. Hence SIL represented a dose-dependent decrease in hyperlocomotion in comparison to the ketamine group (Figures 4A, B).

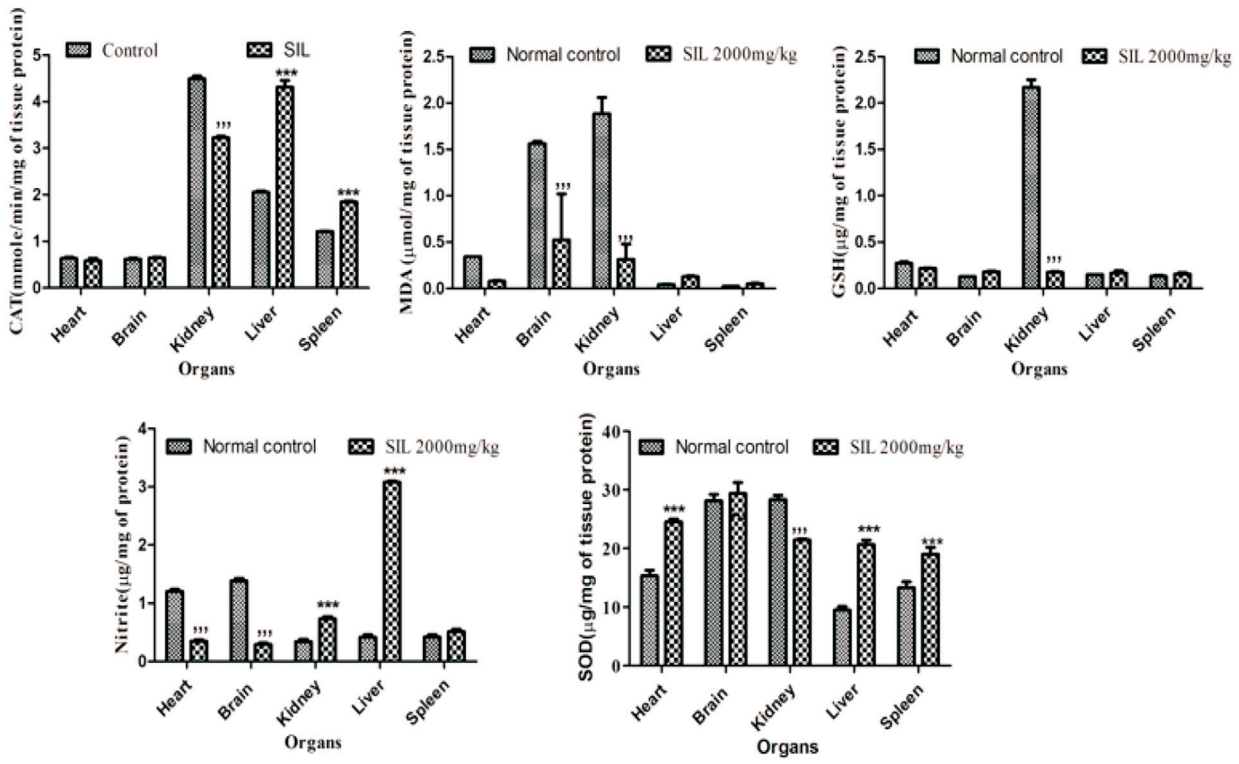

FIGURE 1
Effect of normal control and SIL treatment on oxidative stress markers. Data presented as mean ± SEM. n = 6. Here, ***$p < 0.001$ high significant increase vs. the control group, and ***$p < 0.001$ significant decrease compared with the normal control group.

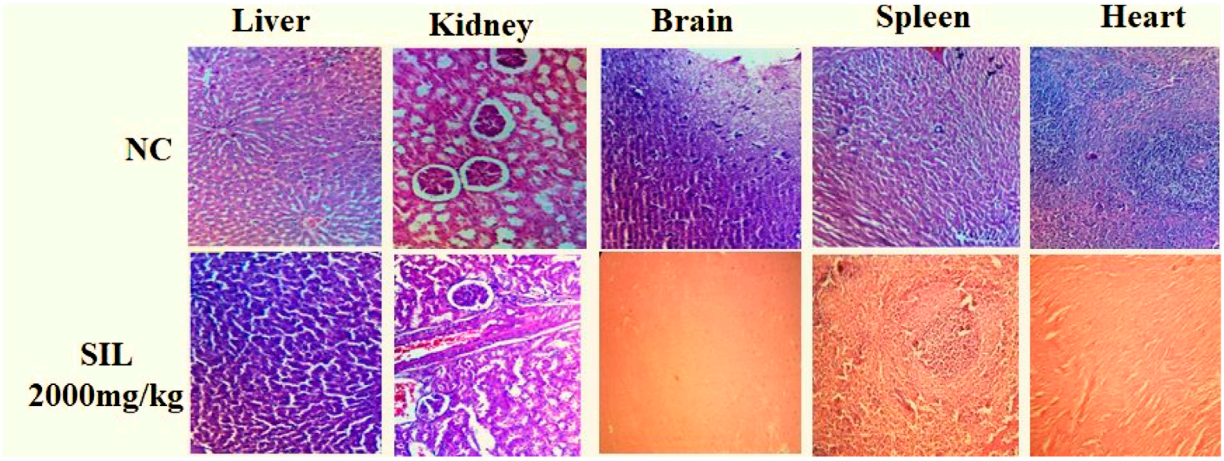

FIGURE 2
Histogram of selected organs in treated groups in acute toxicity study.

3.2.3 Effect of SIL on ketamine-induced immobility by forced swim test in preventive and treatment protocols

Behavioral despair was evaluated by immobility time in the forced swim test in all treatment groups in the preventive as well as treatment protocols. Ketamine injection produced a marked increase in immobility time that connotes behavioral despair when compared with the saline group. SIL showed a significant ($p < 0.001$) and dose-dependent reduction in immobility in all treatment groups in the treatment protocol. In the preventive protocol, only the highest dose group of 200 mg/kg exhibited a significant reduction in immobility time (Figures 5A, B).

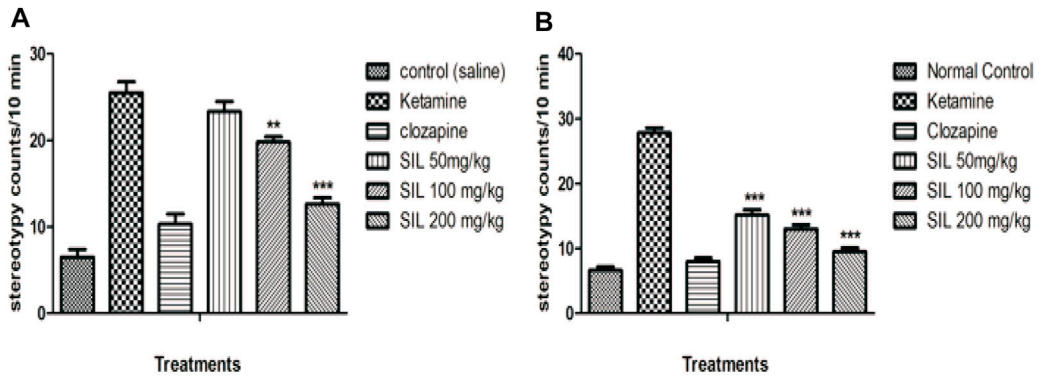

FIGURE 3
Effect of SIL on ketamine-induced stereotypy in preventive **(A)** and curative **(B)** protocols. Values expressed here as mean ± SEM; n = 10, where $^{**}p < 0.01$, $^{***}p < 0.001$ compared to the ketamine group.

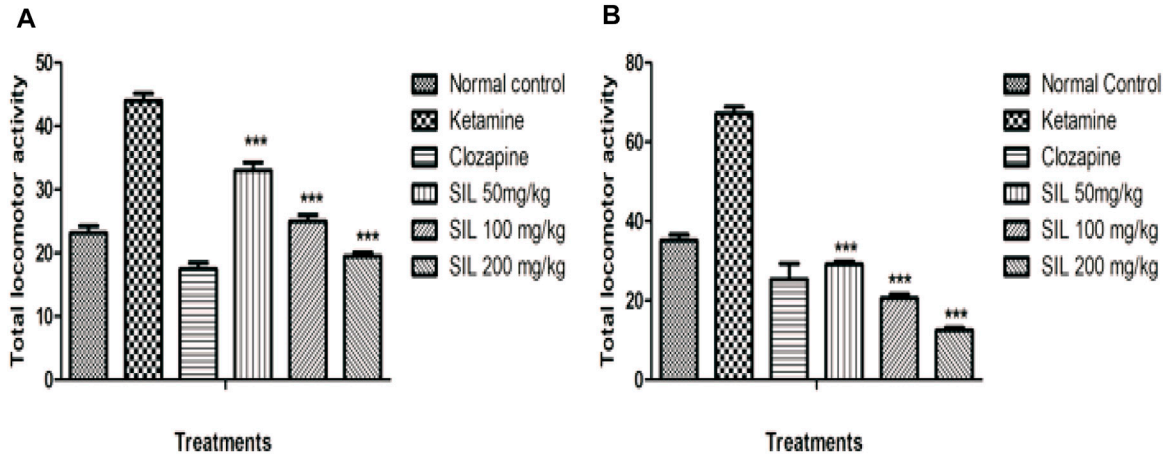

FIGURE 4
Effect of SIL on ketamine-induced hyperlocomotion in preventive **(A)** and curative **(B)** protocols. Values are expressed as mean ± SEM; n = 10, $^{***}p < 0.001$ as compared to the ketamine group.

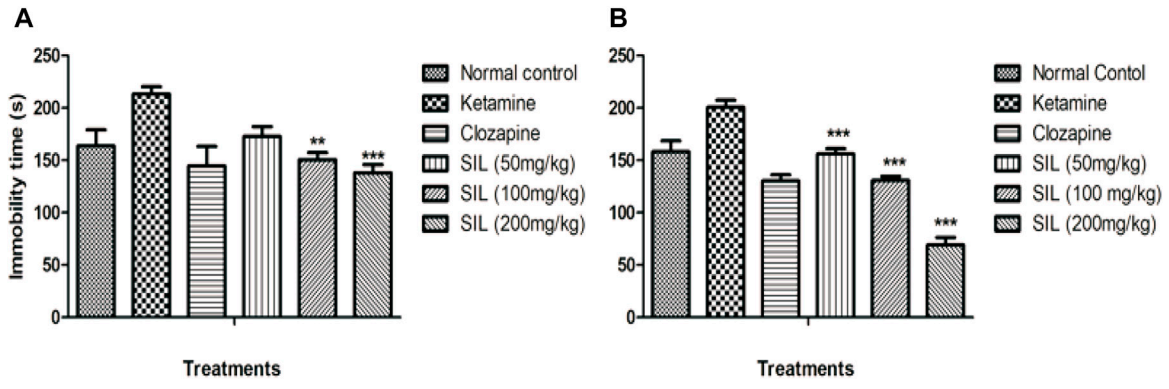

FIGURE 5
Effect of SIL on ketamine-induced immobility in forced swim test in preventive **(A)** and treatment **(B)** protocols. Values are represented here as mean ± SEM; n = 10, where $^{**}p < 0.01$, $^{***}p < 0.001$ compared to the ketamine group.

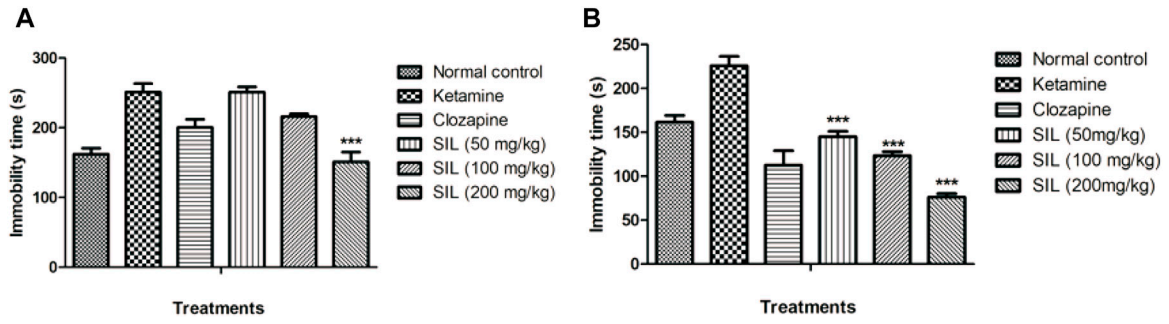

FIGURE 6
Effect of SIL on ketamine-induced immobility by tail suspension test in preventive **(A)** and treatment **(B)** protocols. Values expressed as mean ± SEM; n=10, ***p<0.001 compared to the ketamine group.

3.2.4 Effect of SIL on ketamine-induced behavioral despair by tail suspension test in preventive and treatment protocols

Behavioral despair was also evaluated by the tail suspension test in treatment and preventive protocols (Figures 6A, B). Ketamine (10 mg/kg) significantly induced immobility and behavioral despair compared with the control group. In the curative protocol, SIL significantly ($p < 0.001$) and dose dependently reduced immobility time in mice. Only clozapine and SIL 200 mg/kg showed a highly significant ($p < 0.001$) reduction in ketamine-induced immobility (Figures 6A, B).

4 Discussion

Phytochemicals are derived from natural origins and provide cost-effective, valuable, and relatively safe alternatives for allopathic medicines (Saleem et al., 2022; Datta et al., 2021). The WHO and FDA have emphasized the validation of safe and effective uses of natural chemicals by conducting scientific studies (Saleem et al., 2017) and preliminary toxicity studies are important for the safe use of phytochemicals. Silibinin is known for its various pharmacological properties, like treating diabetes, hypertension, dyslipidemia; it has been utilized in China, the USA, and Europe for thousands of years for its folkloric properties against liver diseases and its hepatoprotective properties (Mazzio et al., 1998; Takke and Shende, 2019). However, comprehensive knowledge about its safety and toxicity is still lacking. Hence, this study was designed to evaluate the LD_{50} of SIL by following OECD guidelines in an animal model which will help to determine the safe dose range for managing its adverse effects in clinical practice (Anwar et al., 2021). The main purpose of this study was to observe animals after a single high-dose administration for any life-threatening toxicities or adverse effects. The results of this study provide evidence that SIL, according to the globally harmonized classification system, can be placed in the fifth group where LD_{50} > 2000 mg/kg in a lower toxicity class (Saleem et al., 2017). Undeniably, hematological and biochemical estimations remain the hallmarks of the health status of the body, as these are sensitive to changes produced by chemical toxins. Platelets are known to play an important role in coagulation (Li et al., 2008); results have revealed a decrease in the level of platelet counts, which might be linked to the hemostatic property of SIL. Moreover, the elevated WBC count is suggestive of the immunopotentiation property of SIL by endogenous defense system to the adverse effects of silibinin. As the liver and kidney are primary organs for the metabolism and elimination of chemicals, alterations in the liver's function parameters and renal function tests are known to be connected to the toxicity of said organs (Moses et al., 2018). Moreover, an increase in cholesterol and triglyceride showed the hyperlipidemic effect of SIL, while elevation in ALT and AST might show some hepatic injury. Liver damage may cause increased permeability of cell membranes that could result in a release of aminotransferases into the blood (Ogunlana et al., 2013). These findings also demonstrate that elevated renal function parameters may also be related to mild renal injury. Moreover, histopathological findings appear quite normal, and no significant change appeared in the selected organs studied.

Continuous exposure to reactive oxygen species in the living system causes oxidative stress damage, adversely affecting proteins, lipids, nucleic acid, and whole-body systems. Necrosis, apoptosis, and irreversible cellular damage are linked with oxidative stress (Jones and Libert, 2006; Nair et al., 2015). The current studies estimated the endogenous levels of oxidants and antioxidants in the major organs of animals' bodies after treatment with SIL. There was a significant reduction in antioxidants (GSH, CAT, and SOD) in the kidney and an increase in the oxidant MDA. SIL as a lipophilic compound might be excreted through the kidney, indicative of a decrease in its antioxidant parameters. Moreover, an increase in the level of antioxidants (SOD and CAT) in the liver and spleen and a reduction in MDA and nitrite in the brain and heart shows the increased antioxidant property of SIL in these respective organs.

Another aim of the present study is to demonstrate the efficacy of SIL in protecting and reversing ketamine-induced psychosis-like behavioral manifestations. In recent research on schizophrenia, the use of animal models that can present different symptoms of schizophrenia (positive, negative, and cognitive) has become more popular (Chatterjee et al., 2012b). Schizophrenia, being a complex neuropsychiatric disease, involves different neurochemical alterations, including the effect of dopamine, gamma amino butyric acid (GABA), and glutamate on motor neuron function (Vasconcelos et al., 2015). Our results support previous findings that ketamine (an NMDA blocker) can induce multifarious behavioral alterations (i.e., stereotypy, hyperlocomotion, and behavioral despair) that are relevant to the positive and the negative symptoms of the disease. Ketamine-induced stereotypy and hyperlocomotion have remained

important measures of positive symptoms (Ben-Azu et al., 2016). These symptoms have been previously linked with the NMDA receptor blockade that is present in inhibitory GABA neurons in the mesolimbic region of the brain. This inhibition causes behavioral alterations called stereotypy that are characterized by aimless and repetitive motor activity (Chatterjee et al., 2012b). Furthermore, ketamine may act as an indirect dopamine agonist, which might also explain its valuable role in behavioral stimulations (Irifune et al., 1991). Clozapine is a widely used drug for schizophrenia patients in clinical settings as well as a reference drug for researchers on schizophrenia (Vasconcelos et al., 2015). Thus, our study demonstrated the effect of SIL to prevent and reverse ketamine-induced stereotypy (as evidenced through decreased stereotypic head movements, intermittent sniffing, intense licking, and chewing in mice) and hyperlocomotions (number of crossings), revealing its antipsychotic potential against positive symptoms (Ben-Azu et al., 2018).

Furthermore, SIL was also evaluated for its effect on negative symptoms of schizophrenia by ketamine-induced immobility duration by a forced swim test and tail suspension test. Both models represented behavioral despair and a lack of motivational behavior suggestive of the negative symptoms of disease (Chatterjee et al., 2012a). Our findings are in line with previous research as intraperitoneal injection of a sub-anesthetic dose of ketamine demonstrates behavioral despair related to negative symptoms of schizophrenia represented by increased immobility in the forced swim and tail suspension tests (Eneni et al., 2020). The administration of SIL reduced the immobility period in these tests comparable with clozapine. This and other antipsychotic drugs act to manage the negative symptoms of schizophrenia, generally acting as antagonists on 5HT2 receptors (Glatt et al., 1995; George et al., 2020). Accordingly, our findings imply that SIL can act as antipsychotic drug and may attenuate the positive and negative symptoms of schizophrenia, warranting further investigation of its mechanism of action.

Conclusion

From the findings of this acute toxicity study, it can be concluded that the LD_{50} of SIL is more than 2000 mg/kg, and there was no sign of morbidity and mortality seen in animals, except for some alterations in renal function test parameters and lipid profile. More importantly, this study revealed that SIL can attenuate positive and negative symptoms of schizophrenia and can act like an atypical antipsychotic. However, the results suggest that it must be evaluated in future chronic and repeated administration of silibinin to completely ensure its safety. Antipsychotic potential can be determined in more detail by long-term studies. Furthermore, a more scientific approach can further identify the mechanistic study of silibinin as an antipsychotic drug.

Data availability statement

The raw data supporting the conclusions of this article will be made available by the authors, without undue reservation.

Ethics statement

Ethical approval for the animal studies was obtained from the Animal Ethics Committee of Government College University Faisalabad with reference number GCUF/ERC/2015.

Author contributions

US and BA supervised the project; QA and IK performed all the research work and drafted the manuscript.

Acknowledgments

The authors are thankful to Government College University Faisalabad for providing research facilities to carry out the research.

Conflict of interest

The authors declare that the research was conducted in the absence of any commercial or financial relationships that could be construed as a potential conflict of interest.

Publisher's note

All claims expressed in this article are solely those of the authors and do not necessarily represent those of their affiliated organizations, or those of the publisher, the editors, and the reviewers. Any product that may be evaluated in this article, or claim that may be made by its manufacturer, is not guaranteed or endorsed by the publisher.

References

Ahmed-Belkacem, A., Ahnou, N., Barbotte, L., Wychowski, C., Pallier, C., Brillet, R., et al. (2010). Silibinin and related compounds are direct inhibitors of hepatitis C virus RNA-dependent RNA polymerase. *Gastroenterology* 138 (3), 1112–1122. doi:10.1053/j.gastro.2009.11.053

Anwar, F., Saleem, U., Rehman, A., Ahmad, B., Froeyen, M., Mirza, M. U., et al. (2021). Toxicity evaluation of the naphthalen-2-yl 3,5-dinitrobenzoate: A drug candidate for alzheimer disease. *Front. Pharmacol.* 12, 607026. doi:10.3389/fphar.2021.607026

Arruda, M., Soures, P., Honorio, J., Lima, R., Chaves, E., Lobato, R., et al. (2008). Activities of the antipsychotic drugs haloperidol and risperidone on behavioural effects induced by ketamine in mice. *Sci. Pharm.* 76, 673–687. doi:10.3797/scipharm.0810-11

Baig, M. W., Majid, M., Nasir, B., Hassan, S. S. U., Bungau, S., and Haq, I. U. (2022). Toxicity evaluation induced by single and 28-days repeated exposure of withametelin and daturaolone in Sprague Dawley rats. *Front. Pharmacol.* 13, 999078. doi:10.3389/fphar.2022.999078

Ben-Azu, B., Aderibigbe, A. O., Ajayi, A. M., Eneni, A. E. O., Umukoro, S., and Iwalewa, E. O. (2018). Involvement of GABAergic, BDNF and Nox-2 mechanisms in the prevention and reversal of ketamine-induced schizophrenia-like behavior by morin in mice. *Brain Res. Bull.* 139, 292–306. doi:10.1016/j.brainresbull.2018.03.006

Ben-Azu, B., Aderibigbe, A. O., Ajayi, A. M., and Iwalewa, E. O. (2016). Neuroprotective effects of the ethanol stem bark extracts of Terminalia ivorensis in ketamine-induced schizophrenia-like behaviors and oxidative damage in mice. *Pharm. Biol.* 54 (12), 2871–2879. doi:10.1080/13880209.2016.1190382

Bhangale, J. O., and Acharya, S. R. (2016). Anti-Parkinson activity of petroleum ether extract of Ficus religiosa (L.) leaves. *Adv. Pharmacol. Sci.* 2016, 9436106. doi:10.1155/2016/9436106

Bishnoi, M., Chopra, K., and Kulkarni, S. K. (2008). Protective effect of Curcumin, the active principle of turmeric (Curcuma longa) in haloperidol-induced orofacial dyskinesia and associated behavioural, biochemical and neurochemical changes in rat brain. *Pharmacol. Biochem. Behav.* 88 (4), 511–522. doi:10.1016/j.pbb.2007.10.009

Brown, A. S. (2012). Epidemiologic studies of exposure to prenatal infection and risk of schizophrenia and autism. *Dev. Neurobiol.* 72 (10), 1272–1276. doi:10.1002/dneu.22024

Chatterjee, M., Jaiswal, M., and Palit, G. (2012a). Comparative evaluation of forced swim test and tail suspension test as models of negative symptom of schizophrenia in rodents. *ISRN Psychiatry* 2012, 595141. doi:10.5402/2012/595141

Chatterjee, M., Verma, R., Ganguly, S., and Palit, G. (2012b). Neurochemical and molecular characterization of ketamine-induced experimental psychosis model in mice. *Neuropharmacology* 63 (6), 1161–1171. doi:10.1016/j.neuropharm.2012.05.041

Chen, S. T., Hsieh, C. P., Lee, M. Y., Chen, L. C., Huang, C. M., Chen, H. H., et al. (2021). Betaine prevents and reverses the behavioral deficits and synaptic dysfunction induced by repeated ketamine exposure in mice. *Biomed. Pharmacother.* 144, 112369. doi:10.1016/j.biopha.2021.112369

Choi, H. J., Yun, J. W., Kim, Y. H., Kwon, E., Hyon, M. K., Kim, J. Y., et al. (2021). Evaluation of acute and subacute toxicity of sodium taurodeoxycholate in rats. *Drug Chem. Toxicol.* 44 (3), 268–276. doi:10.1080/01480545.2019.1609493

Chu, S. C., Chiou, H. L., Chen, P. H., Yang, S. F., and Hsieh, Y. S. (2004). Silibinin inhibits the invasion of human lung cancer cells via decreased productions of urokinase-plasminogen activator and matrix metalloproteinase-2. *Mol. Carcinog.* 40 (3), 143–149. doi:10.1002/mc.20018

Datta, S., Ramamurthy, P. C., Anand, U., Singh, S., Singh, A., Dhanjal, D. S., et al. (2021). Wonder or evil?: Multifaceted health hazards and health benefits of Cannabis sativa and its phytochemicals. *Saudi J. Biol. Sci.* 28 (12), 7290–7313. doi:10.1016/j.sjbs.2021.08.036

Eneni, A. O., Ben-azu, B., Ajayi, A. M., and Aderibigbe, A. O. (2020). Diosmin attenuates schizophrenia-like behavior, oxidative stress, and acetylcholinesterase activity in mice. *Drug metabolism pesonalised Ther.* 35 (4). doi:10.1515/dmpt-2020-0119

Faludi, G., Dome, P., and Lazary, J. (2011). Origins and perspectives of schizophrenia research. *Neuropsychopharmacol. Hung* 13 (4), 185–192. doi:10.5706/nph201112001

Fell, M. J., McKinzie, D. L., Monn, J. A., and Svensson, K. A. (2012). Group II metabotropic glutamate receptor agonists and positive allosteric modulators as novel treatments for schizophrenia. *Neuropharmacology* 62 (3), 1473–1483. doi:10.1016/j.neuropharm.2011.06.007

George, M. Y., Menze, E. T., Esmat, A., Tadros, M. G., and El-Demerdash, E. (2020). Potential therapeutic antipsychotic effects of Naringin against ketamine-induced deficits in rats: Involvement of Akt/GSK-3β and Wnt/β-catenin signaling pathways. *Life Sci.* 249, 117535. doi:10.1016/j.lfs.2020.117535

Glatt, C. E., Snowman, A. M., Sibley, D. R., and Snyder, S. H. (1995). Clozapine: Selective labeling of sites resembling 5HT6 serotonin receptors may reflect psychoactive profile. *Mol. Med. Camb. Mass* 1 (4), 398–406. doi:10.1007/bf03401577

Hassan, S. S. U., Samanta, S., Dash, R., Karpinski, T. M., Habibi, E., Sadiq, A., et al. (2022). The neuroprotective effects of fisetin, a natural flavonoid in neurodegenerative diseases: Focus on the role of oxidative stress. *Front. Pharmacol.* 1313 (10), 1015835. doi:10.3389/fphar.2022.1015835

Irifune, M., Shimizu, T., and Nomoto, M. (1991). Ketamine-induced hyperlocomotion associated with alteration of presynaptic components of dopamine neurons in the nucleus accumbens of mice. *Pharmacol. Biochem. Behav.* 40 (2), 399–407. doi:10.1016/0091-3057(91)90571-I

Jones, D., and Libert, M. (2006). Antioxidants and Redox signaling. *Redefining oxidative stress* 8 (9), 1865–1879.

Kennedy, G. L., Ferenz, R. L., and Burgess, B. A. (1986). Estimation of acute oral toxicity in rats by determination of the approximate lethal dose rather than the LD50. *J. Appl. Toxicol.* 6 (3), 145–148. doi:10.1002/jat.2550060302

Kumar, G. P., and Khanum, F. (2012). Neuroprotective potential of phytochemicals. *Pharmacogn. Rev.* 6 (12), 81–90. doi:10.4103/0973-7847.99898

Li, M., Jia, Z., Hu, Z., Zhang, R., and Shen, T. (2008). Experimental study on the hemostatic activity of the Tibetan medicinal herb lamiophlomis rotata. *Phytother. Res.* 765, 759–765. doi:10.1002/ptr.2359

Li, X. (2012). Improved pyrogallol autoxidation method: A reliable and cheap superoxide-scavenging assay suitable for all antioxidants. *J. Agric. Food Chem.* 60 (25), 6418–6424. doi:10.1021/jf204970r

Lowry, O. H., Rosebrough, N. J., Farr, A. L., and Randall, R. J. (1951). Protein measurement with the Folin phenol reagent. *J. Biol. Chem.* 193 (1), 265–275. doi:10.1016/s0021-9258(19)52451-6

Mashhadi Akbar Boojar, M., Mashhadi Akbar Boojar, M., and Golmohammad, S. (2020). Overview of Silibinin anti-tumor effects. *J. Herb. Med.* 23, 100375. doi:10.1016/j.hermed.2020.100375

Mazzio, E. A., Harris, N., and Soliman, K. F. A. (1998). Food constituents attenuate monoamine oxidase activity and peroxide levels in C6 astrocyte cells. *Planta Medica* 64 (7), 603–606. doi:10.1055/s-2006-957530

Mcgrath, J., Saha, S., Chant, D., and Welham, J. (2008). Schizophrenia: A concise overview of incidence, prevalence, and mortality. *Epidemiol. Rev.* 30, 67–76. doi:10.1093/epirev/mxn001

Moses, W., Oboma, I., and Raymond, I. (2018). *Toxicological studies on the aqueous leaf extract of Pavetta crassipes (K. Schum) in rodents*.

Nair, A. R., Lee, W. K., Smeets, K., Swennen, Q., Sanchez, A., Thévenod, F., et al. (2015). Glutathione and mitochondria determine acute defense responses and adaptive processes in cadmium-induced oxidative stress and toxicity of the kidney. *Archives Toxicol.* 89 (12), 2273–2289. doi:10.1007/s00204-014-1401-9

Newman, D. J., and Cragg, G. M. (2012). Natural products as sources of new drugs over the 30 years from 1981 to 2010. *J. Nat. Prod.* 75 (3), 311–335. doi:10.1021/np200906s

Ogunlana, O. O., Ogunlana, O. E., Adeneye, A. A., Udo-Chijioke, O., Dare-Olipede, T., Olagunju, J. A., et al. (2013). Evaluation of the toxicological profile of the leaves and young twigs of Caesalpinia bonduc (Linn) roxb. *Afr. J. Traditional, Complementary, Altern. Med. AJTCAM/Afr. Netw. Ethnomedicines* 10 (6), 504–512. doi:10.4314/ajtcam.v10i6.20

Purdon, S. E., Malla, A., Labelle, A., and Lit, W. (2001). Neuropsychological change in patients with schizophrenia after treatment with quetiapine or haloperidol. *J. Psychiatry Neurosci.* 26 (2), 137–149.

Ross, C. A., and Margolis, R. L. (2005). Neurogenetics: Insights into degenerative diseases and approaches to schizophrenia. *Clin. Neurosci. Res.* 5, 3–14. doi:10.1016/j.cnr.2005.07.001

Saleem, A., ul-Ain, Q., and Akhtar, M. F. (2022). Alternative therapy of psychosis: Potential phytochemicals and drug targets in the management of schizophrenia. *Front. Pharmacol.* 13, 895668. doi:10.3389/fphar.2022.895668

Saleem, U., Amin, S., Ahmad, B., Azeem, H., Anwar, F., and Mary, S. (2017). Acute oral toxicity evaluation of aqueous ethanolic extract of Saccharum munja Roxb. roots in albino mice as per OECD 425 TG. *Toxicol. Rep.* 4, 580–585. doi:10.1016/j.toxrep.2017.10.005

Shanmugam, K., Holmquist, L., Steele, M., Stuchbury, G., Berbaum, K., Schulz, O., et al. (2008). Plant-derived polyphenols attenuate lipopolysaccharide-induced nitric oxide and tumour necrosis factor production in murine microglia and macrophages. *Mol. Nutr. Food Res.* 52 (4), 427–438. doi:10.1002/mnfr.200700180

Singh, R. P., and Agarwal, R. (2009). Cosmeceuticals and silibinin. *Clin. Dermatology* 27 (5), 479–484. doi:10.1016/j.clindermatol.2009.05.012

Steinberg, P., van der Voet, H., Goedhart, P. W., Kleter, G., Kok, E. J., Pla, M., et al. (2019). Lack of adverse effects in subchronic and chronic toxicity/carcinogenicity studies on the glyphosate-resistant genetically modified maize NK603 in Wistar Han RCC rats. *Archives Toxicol.* 93, 1095–1139. doi:10.1007/s00204-019-02400-1

Takke, A., and Shende, P. (2019). Nanotherapeutic silibinin: An insight of phytomedicine in healthcare reformation. *Nanomedicine Nanotechnol. Biol. Med.* 21, 102057. doi:10.1016/j.nano.2019.102057

Tandon, R., Gaebel, W., Barch, D. M., Bustillo, J., Gur, R. E., Heckers, S., et al. (2013). De fi nition and description of schizophrenia in the DSM-5. *Schizophrenia Res.* 150, 3–10. doi:10.1016/j.schres.2013.05.028

Vasconcelos, G. S., Ximenes, N. C., de Sousa, C. N. S., Oliveira, T. de Q., Lima, L. L. L., de Lucena, D. F., et al. (2015). Alpha-lipoic acid alone and combined with clozapine reverses schizophrenia-like symptoms induced by ketamine in mice: Participation of antioxidant, nitrergic and neurotrophic mechanisms. *Schizophrenia Res.* 165 (2–3), 163–170. doi:10.1016/j.schres.2015.04.017

Wang, L., Zhang, Y., Wang, C., Zhang, X., Wang, Z., Liang, X., et al. (2019). A natural product with high affinity to Sigma and 5-HT7 receptors as novel therapeutic drug for negative and cognitive symptoms of schizophrenia. *Neurochem. Res.* 44 (11), 2536–2545. doi:10.1007/s11064-019-02873-7

Yadav, M., Jindal, D. K., Parle, M., Kumar, A., and Dhingra, S. (2019). Targeting oxidative stress, acetylcholinesterase, proinflammatory cytokine, dopamine and GABA by eucalyptus oil (Eucalyptus globulus) to alleviate ketamine-induced psychosis in rats. *Inflammopharmacology* 27 (2), 301–311. doi:10.1007/s10787-018-0455-3

Yan, W. J., Tan, Y. C., Xu, J. C., Tang, X. P., Zhang, C., Zhang, P. B., et al. (2015). Protective effects of silibinin and its possible mechanism of action in mice exposed to chronic unpredictable mild stress. *Biomol. Ther.* 23 (3), 245–250. doi:10.4062/biomolther.2014.138

Yin, F., Liu, J., Ji, X., Wang, Y., Zidichouski, J., and Zhang, J. (2011). Silibinin: A novel inhibitor of Aβ aggregation. *Neurochem. Int.* 58 (3), 399–403. doi:10.1016/j.neuint.2010.12.017

Frontiers in Pharmacology

Explores the interactions between chemicals and living beings

The most cited journal in its field, which advances access to pharmacological discoveries to prevent and treat human disease.

Discover the latest Research Topics

See more →

Frontiers

Avenue du Tribunal-Fédéral 34
1005 Lausanne, Switzerland
frontiersin.org

Contact us

+41 (0)21 510 17 00
frontiersin.org/about/contact